SUPPLEMENTO
AL VOLUME VIII, SERIE X, DEL
NUOVO CIMENTO
A CURA DELLA SOCIETÀ ITALIANA DI FISICA

1958 — 2° Trimestre — N. 2

CONVEGNO INTERNAZIONALE SUI RAGGI COSMICI

ORGANIZZATO

DALL'UNIONE INTERNAZIONALE DI FISICA

CON LA COLLABORAZIONE DELLA SOCIETÀ ITALIANA DI FISICA

VILLA MONASTERO

VARENNA, SUL LAGO DI COMO

21-26 GIUGNO 1957

RENDICONTI

SUPPLEMENTO AL VOLUME VIII, SERIE X
DEL NUOVO CIMENTO

N. 2, 1958
2° Trimestre

INDICE SISTEMATICO

(A pag. 131 è dato l'Indice Alfabetico degli Autori)

PART I – Solar and geomagnetic effects on cosmic rays.

SECTION A: Solar flare effects . . . . . pag. 133

J. A. SIMPSON – Solar flare cosmic rays and their propagation . . » 133
G. COCCONI, K. GREISEN, P. MORRISON, T. GOLD and S. HAYAKAWA – The cosmic ray flare effect . . . . . » 161
K. KAWABATA, I. KONDÒ, K. MURAKAMI and M. WADA – On the unusual increase and the modulation of cosmic rays . . . . . » 169
R. LÜST – Impact zones for solar cosmic ray particles . . . . . » 176
G. PFOTZER – On the separation of direct and indirect fractions of solar cosmic radiation on February 23, 1956 and on the difference in steepness of momentum spectrum of these two components . » 180
P. A. SWEET – The production of high energy particles in solar flares » 188
S. F. SINGER – A model for solar flare increases of cosmic rays based on hydromagnetic turbolence . . . . . » 197
D. ECKHARTT – The electro-magnetic state in interplanetary space during the flare of Feb. 23, 1956 . . . . . » 202
H. ALFVÉN – Electro-magnetic state of interplanetary space . . . » 209
J. F. DENISSE – Courte discussion des observations radioastronomiques associées à l'ejection de matière du soleil. . . . . » 212
D. H. MENZEL – Solar activity and cosmic radiation . . . . . » 214
K. O. KIEPENHEUER – On the origin of the solar component of cosmic radiation . . . . . » 218
G. PFOTZER – Latitude effect of solar cosmic radiation on Feb. 23, 1956 with respect to the problem of effective geomagnetic co-ordinate system . . . . . » 220
P. L. MARSDEN and J. G. WILSON – Determination of latitude equivalents for second phase solar flare particles. . . . . » 228

SECTION B: Geomagnetic effects . . . . . pag. 233

P. MEYER and J. A. SIMPSON – New changes in the low-energy particle cut-off and spectrum of the primary cosmic radiation . . . » 233
E. Å. BRUNBERG – Directional properties of cosmic ray telescopes . » 237

Y. Miyazaki – Comparison of the cosmic-ray intensity observed at different altitudes . . . . . pag. 244
P. Rothwell and J. Quenby – Cosmic rays in the earth's magnetic field » 249
M. A. Pomerantz, A. E. Sandström and D. C. Rose – Shipboard neutron monitor determination of cosmic-ray equator . . . . . » 257
A. E. Sandström – Cosmic ray soft component measurements during a flight from Scandinavia across the North Pole and around Asia and Europe . . . . . » 263
L. Katz, P. Meyer and J. A. Simpson – Further experiments concerning the geomagnetic field effective for cosmic rays . . . . . » 277
M. Kodama – Latitude effect of cosmic ray nucleon and meson component at sea level . . . . . » 283

Section C: Cosmic ray variation . . . . . pag. 285

D. Venkatesan – The 27-day variation on cosmic ray intensity . . » 285
N. V. Neher – Cosmic-ray changes near the North geomagnetic Pole from 1954 to 1956 . . . . . » 298
V. Sarabhai and P. D. Bhavsar – Changes of solar anisotropy and of the intensity of cosmic radiation . . . . . » 299
N. R. Parsons and A. G. Fenton – Solar daily cosmic ray variations observed with meson telescopes at high southern latitudes . . . » 313
A. Ehmert – Variations of nuclear and mesonic component . . . . » 318
S. F. Singer – Observation of cosmic ray decreases at the pole . . » 326
S. F. Singer – Cosmic ray time variations produced by deceleration interplanetary space . . . . . » 334
S. F. Singer – On the low energy cut-off of the cosmic radiation . » 342
A. Schlüter – Störmer orbits of low energy . . . . . » 349
L. I. Dorman and E. L. Feinberg – True primary energy spectrum variations and solar activity . . . . . » 358
L. I. Dorman and E. L. Feinberg – Solar corpuscolar streams and cosmic ray variations . . . . . » 379
L. I. Dorman – The generation and propagation of solar cosmic rays » 391

Part II – **Origin problem.**

G. R. Burbidge – The origin of cosmic rays: some astrophysical problems . . . . . pag. 403
I. S. Šklovskij – Some problems of radioastronomical theory of the origin of cosmic rays . . . . . » 421
V. L. Ginzburg – On the origin of cosmic rays . . . . . » 430
V. I. Krassovskij and I. S. Šklovskij – Variation of the intensity of cosmic radiation during earth's geological history and their possible influence on life's evolution . . . . . » 440
L. Davis, Jr. – An examination of the Fermi mechanism . . . . . » 444
C. Y. Fan – Galactic origin of cosmic radiation . . . . . » 457
F. J. M. Farley – Cosmic rays in intergalactic space . . . . . » 466
G. Cocconi – The exterior ballistics of the cosmic radiation . . . . » 472
K. Sitte – Extragalactic cosmic radiation . . . . . » 478

Y. Sekido, S. Yoshida, Y. Kamiya, H. Ueno and K. Nagashima – A point source of cosmic rays and its time variation . . . . . pag. 482
J. Heidmann – Continuous creation of cosmic rays . . . . . » 486
H. Alfvén – General observation on the origin problem . . . . . » 491

Part III – Composition of the primary radiation.

P. Fowler, P. S. Freier and E. P. Ney – The primary α particle spectrum over North America and geomagnetic cut-off energies . pag. 492
F. B. McDonald – Study of primary cosmic ray α and proton energy spectra, geomagnetic cut-off energies and temporal variations . . » 500
M. Koshiba, G. Schultz and M. Schein – The charge spectrum of the cosmic radiation at 41 °N . . . . . » 508
M. M. Shapiro, B. Stiller and F. W. O'Dell – Flux of primary helium near the geomagnetic equator . . . . . » 509
C. J. Waddington – The light and medium nuclei in the cosmic radiation . . . . . » 513
C. J. Waddington – The flux of medium and heavy nuclei in the cosmic radiation near the equator . . . . . » 518
R. R. Hillier and V. J. Rajopadhye – The heavy nuclei in the cosmic radiation . . . . . » 520
R. Cester, A. De Benedetti, C. M. Garelli, B. Quassiati, L. Tallone and M. Vigone – On the charge and energy spectrum of heavy primaries . . . . . » 523
B. J. O'Brien, A. J. Herz and J. H. Noon – The charge spectrum of light elements at 41 °N geomagnetic latitude . . . . . » 524
W. R. Webber – The charge composition and energy spectra of primary cosmic rays and the energy balance problem . . . . . » 532
S. F. Singer – Energy spectra of primary cosmic rays and the interpretation of their origin . . . . . » 546
S. F. Singer – On the origin of the charge spectrum of the primary cosmic radiation . . . . . » 549
B. Peters – General observation on the composition of the primary radiation . . . . . » 556

Part IV – Air showers.

Section A: General introduction . . . . . pag. 560

G. Cocconi – Introductory remarks about air showers . . . . . » 560

Section B: Harwell air shower experiments . . . . . pag. 567

T. E. Cranshaw, W. Galbraith, N. A. Porter, J. de Beer and M. Hillas – Harwell air shower experiment . . . . . » 567
J. V. Jelley – Čerenkov radiation in the atmosphere and its application to the study of extensive air showers . . . . . » 578

Section C: Soviet Union air shower experiments . . . . . pag. 585

G. T. Zacepin – Brief survey of some work on extensive air showers conducted in the Soviet Union . . . . . » 585
V. A. Dmitriev, G. B. Hristiansen and G. V. Kulikov – The high-energy nuclear active component of extensive air showers. . . . » 587
G. B. Hristiansen – On the lateral distribution of electrons and mesons in extensive air showers . . . . . » 598
A. E. Čudakov and N. M. Nesterova – Čerenkov radiation of extensive air showers . . . . . » 606
N. A. Dobrotin, O. Dovženko, V. Zacepin, E. Murzina, S. I. Nikols'kij, I. Rakobolskaja and E. Tukiš – Combined method of investigation of the extensive air showers. . . . . » 612

Section D: M.I.T. air shower experiments . . . . . pag. 623

G. Clark, J. Earl, W. Kraushaar, J. Linsley, B. Rossi and F. Scherb – The M.I.T. air shower program . . . . . » 623

Section E: Sydney air shower experiments. . . . . . pag. 653

M. H. Brennan, J. A. Lehane, J. Malos, D. D. Millar, C. S. Wallace and M. M. Winn – The Sydney air shower experiment . . » 653
M. H. Brennan, J. Malos, D. D. Millar and C. S. Wallace – Čerenkov light from air showers . . . . . » 662

Section F: Tokyo air shower research . . . . . pag. 665

M. Oda – Underground studies of μ-meson component in extensive air showers . . . . . » 665
T. Matano, I. Miura, M. Oda, K. Suga, G. Tanahashi and Y. Tanaka – A measurement of energy flow in the extensive air showers » 668
J. Nishimura – Lateral distribution of energy flow of cascade showers » 672

Section G: Other air shower experiments . . . . . pag. 675

A. Citron and G. Stiller – Time variations of extensive air showers » 675
K. Greisen – Further measurements on extensive air showers . . . » 681
K. Sitte, I. L. Kofsky, D. L. Stierwalt, S. Lehrer, K. Tausk and A. Wataghin – Air shower observation between 5 200 m and 3 260 m altitude . . . . . » 684
L. Jánossy, T. Sándor and A. Somogyi – The temperature effect of extensive air showers . . . . . » 701

Part V – Interactions of cosmic radiation.

M. Schein and D. M. Haskin – Nucleon-nucleon interactions at energies greater than 10^{12} eV . . . . . pag. 710
I. M. Gramenizkij, G. B. Ždanov, E. A. Zamčalova, M. I. Tretjakova and M. N. Ščerbakova – One case of nuclear interaction in photoemulsion at the energy of $\sim 5 \cdot 10^{13}$ eV/nucleon . . . . . » 714

B. Edwards, J. Losty, D. Perkins and J. Reynolds – Nuclear interactions between 10^3 and 10^5 GeV . . . . . pag. 722
P. Fowler, P. S. Freier, C. Lattes, E. P. Ney and P. H. Perkins – A cosmic ray jet in the 10^{12} electron volt energy range . . . » 725
G. B. Ždanov, E. A. Zamčalova, M. I. Tretjakova and M. N. Ščerbakova – Two interesting cases of secondary high-energy interactions in photographic emulsion . . . . . » 726
N. L. Grigorov, V. Y. Šestoperov, V. A. Sobinjakov and A. V. Podgurskaja – Large bursts investigation and high-energy particles ($10^{12} \div 10^{13}$) eV interaction with light nuclei . . . . . » 730
S. I. Brikker, N. L. Grigorov, M. A. Kondrateva, A. V. Podgurskaja, A. I. Saveleva, A. V. Sobinjakov and V. Y. Šestoperov – Photographic plate investigation of the high-energy particles interaction with lead nuclei . . . . . » 733
A. E. Čudakov, N. A. Dobrotin, N. L. Grigorov, G. N. Vernov and G. T. Zacepin – Investigation of interaction at extremely high-energies using the analysis of extensive air showers . . . . » 737
G. B. Hristiansen and G. V. Kulikov – On the number of particle spectrum of extensive air showers . . . . . » 742
G. T. Zacepin – On the multiple production of particles in weak interaction of nucleons by means of their excitation . . . . . » 746
V. V. Gužavin and I. P. Ivanenko – On the three-dimensional development of an electron-photon cascade shower . . . . . » 749
Co-operative emulsion Group in Japan – Studies on transverse momenta of high-energy jets with emulsion cloud chambers . . » 761
G. A. Milečin and I. L. Rozental′ – On some interaction characteristics of very high-energy particles and their interpretation from the view point of the hydrodynamical theory of multiple particle production . . . . . » 770
D. S. Černavskij – Multiple production of particles in jets . . . . » 775
I. I. Gurevič, A. P. Mišakova, B. A. Nikol′skij and L. V. Surkova – Explosive showers produced by high-energy cosmic-ray particles » 786
G. Wataghin – Theoretical interpretation of multiple production of particles in high-energy collisions. . . . . » 793
S. A. Korff – Cosmic ray neutron studies. . . . . » 796
P. S. Goel, D. P. Kharkar, D. Lal, N. Narsappaya, B. Peters and V. Yatirajam – Prehistoric cosmic ray intensity . . . . . » 801

INDICE ALFABETICO DEGLI AUTORI

Alfvén H., 209, 491.

Bhavsar P. D., 299.
Brennan M. H., 653, 662.
Brikker S. I., 733.
Brunberg E. Å., 237.
Burbidge G. R., 403.

Cester R., 523.
Černavsky D. S., 775.
Čudakov A. E., 606, 737.
Citron A., 675.
Clark G., 623.
Cocconi G., 161, 472, 560.
Co-operative Group Japan, 761.
Cranshaw T. E., 567.

Davis L. Jr., 444.
de Beer J., 567.
Debenedetti A., 523.
Denisse J. F., 212.
Dmitriev V. A., 587.
Dobrotin N. A., 612, 737.
Dorman L. I., 358, 379, 391.
Dovženko O., 612.

Earl J., 623.
Eckhartt D., 202.
Edwards B., 722.
Ehmert A., 318.

Fan C. Y., 457.
Farley F. J. M., 466.
Feinberg E. L., 358, 379.
Fenton A. G., 313.
Fowler P., 492, 725.
Freier P. S., 492, 725.

Galbraith W., 567.
Garelli C. M., 523.
Ginzburg V. L., 430.
Goel P. S., 801.
Gold T., 161.
Gramenizkij I. M., 714.
Greisen K., 161, 681.
Grigorov N. L., 730, 733, 737.
Gurevič I. I., 786.
Gužavin V. V., 749.

Haskin D. M., 710.
Hayakawa S., 161.
Heidmann J., 486.
Herz A. J., 524.
Hillas M., 567.
Hillier R. R., 520.
Hristiansen G. B., 587, 598, 742.

Ivanenko I. P., 749.

Jánossy L., 701.
Jelley J. V., 578.

Kamiya Y., 482.
Kawabata K., 169.
Katz L., 277.
Kharkar D. P., 801.
Kiepenheuer K. O., 218.
Kodama M., 283.
Kofsky I. L., 684.
Kondò I., 169.
Kondratieva M. A., 733.
Korff S. A., 796.
Koshiba M., 508.
Krassovsky V. I., 440.
Kraushaar W., 623.
Kulikov G. V., 587, 742.

Lal D., 801.
Lattes C., 725.
Lehane I. A., 653.
Lehrer S., 684.
Linsley J., 623.
Losty J., 722.
Lüst R., 176.

Malos J., 653, 662.
Marsden P. L., 228.
Matano T., 668.
McDonald F. B., 500.
Menzel D. H., 214.
Meyer P., 233, 277.
Milečin G. A., 770.
Millar D. D., 653, 662.
Mišakova A. P., 786.
Miyazaki Y., 244.
Miura I., 668.
Morrison P., 161.
Murakami K., 169.
Murzina E., 612.

Nagashima K., 482.
Narsappaya N., 801.
Neher H. V., 298.
Nesterova N. M., 606.
Ney E. P., 492, 725.
Nicol'skij B. A., 786.
Nicol'skij S. I., 612.
Nishimura J., 672.
Noon J. H., 524.

O'Brien B. J., 524.
Oda M., 665, 668.
O'Dell F. W., 509.

Parsons N. R., 313.
Perkins D., 722.
Peters B., 556, 801.
Pfotzer G., 180, 220.
Podgurskaja A. V., 730, 733.
Pomerantz M. A., 257.
Porter N. A., 567.

Quassiati B., 523.
Quenby J., 249.

Rakobolskaja I., 612.
Rajopadhye V. I., 520.
Reynolds J., 722.
Rose D. C., 257.
Rossi B., 623.
Rothwell P., 249.
Rozental' I. L., 770.

Sándor T., 701.
Sandström A. E., 257, 263.

Sarabhai V., 299.
Saveleva A. I., 733.
Sekido Y., 482.
Shapiro M. M., 509.
Schein M., 508, 710.
Scherb F., 623.
Ščerbakova M. N., 714, 726.
Schlüter A., 349.
Schultz G., 508.
Šestoperov V. Y., 730, 733.
Šklovskij I. S., 421, 440.
Simpson J. A., 133, 233, 277.
Singer S. F., 197, 326, 334, 342, 546, 549.
Sitte K., 478, 684.
Sobinjakov V. A., 730, 733.
Somogyi A., 701.
Stierwalt D. L., 684.
Stiller B., 509.
Stiller G., 675.
Suga K., 668.
Surkova L. V., 786.
Sweet P. A., 188.

Tallone L., 523.
Tanahashi G., 668.
Tanaka Y., 668.
Tausk K., 684.
Tretjakova M. I., 714, 726.
Tukiš E., 612.

Ueno H., 482.

Vigone M., 523.
Venkatesan D., 285.
Vernov G. N., 737.

Wada M., 169.
Waddington C. J., 513, 518.
Wallace C. S., 653, 662.
Wataghin A., 684.
Wataghin G., 793.
Webber W. R., 532.
Wilson J. G., 228.
Winn M. M., 653.

Yatirajam V., 801.
Yoshida S., 482.

Zamčalova E. A., 714, 726.
Zacepin G. T., 585, 737, 746.
Zacepin V., 612.
Ždanov G. B., 714, 726.

La Direzione del Nuovo Cimento *ringrazia vivamente il prof.* Giampiero Puppi, *i dott.* Menotti Galli, Sergio Ratti *e la dott.* Luisa Vercesi Basilico *per l'efficace collaborazione data nel preparare questo fascicolo.*

PART I

Solar and Geomagnetic Effects on Cosmic Rays

SECTION A: Solar Flare Effects

Solar Flare Cosmic Rays and Their Propagation.

J. A. SIMPSON

Enrico Fermi Institute for Nuclear Studies
The University of Chicago - Chicago, Ill.

1. – Introduction.

Of the five large increases of cosmic ray intensity, the event of 23 February, 1956, was the most outstanding for quantitative study. It provided direct evidence for the occasional production of particles with energies up to $20 \div 30$ GeV for protons, evidence for important interplanetary magnetic fields, and evidence on the mode of charged particle propagation from the solar source to the earth. During a solar flare in which cosmic rays are produced, the entire solar system becomes a laboratory in which extensive quantitative measurements can be carried out from the position of the earth. In this paper we shall be concerned with:

a) the propagation of particles from the source,

b) the initial anisotropy of the radiation at the earth,

c) the approach to isotropic incidence,

d) the storage of particles by interplanetary magnetic fields,

e) the mode of particle escape from the solar system,

Thus, we are directly concerned with the physics of particle propagation, storage and the spectrum, from which studies we may place limiting conditions on the acceleration mechanism. Since this paper is to provide a general intro-

duction to the topic of the solar flare effect, and this is the first of a series of papers on this subject at the Conference, we shall review some of the important experimental results from over the world; but in the matter on interpretation we shall emphasize our work at the Institute in Chicago, comparing some of these ideas with extremely different ideas that will be discussed more fully in other papers. The recent results concerning the initial stages in the propagation of flare particles (Sect. 3-9) are discussed in more detail elsewhere [1].

2. – General features of an increase of cosmic ray intensity.

Fig. 1 represents the increase of cosmic ray intensity observed at Chicago, along with the times of important developments in the progress of the flare [2]. The most notable features include the rapid rise to maximum intensity and

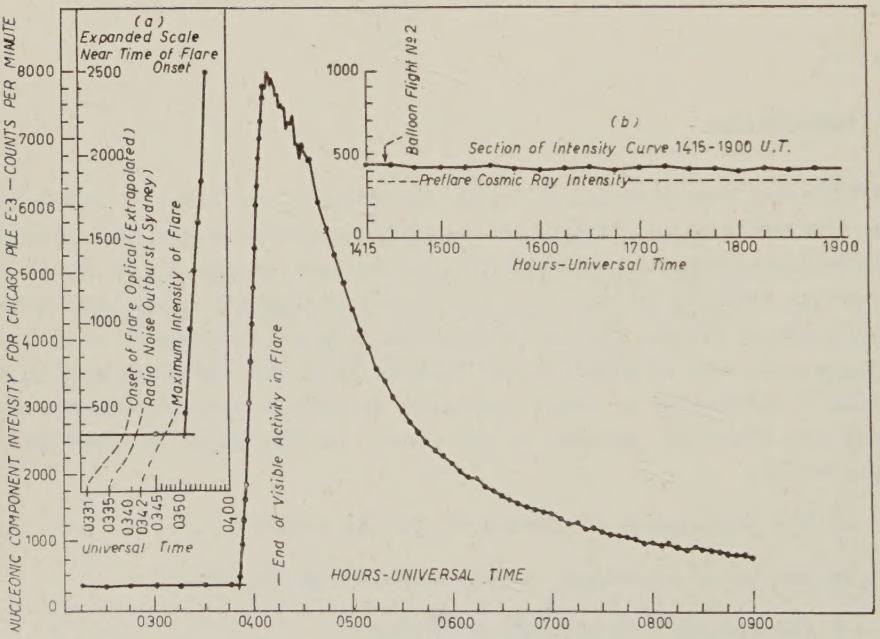

Fig. 1. – The increase of cosmic ray intensity following the optical flare of 23 February 1956 at Chicago, Illinois.

the gradual decline of intensity over a period of many hours. We shall be concerned with the characteristics of this increase at early times, namely, the time up to the maximum intensity, and the late times, namely, beyond the

time of maximum intensity. In order to compare the data from the many stations throughout the world it is necessary to define certain parameters which are common to all the data. In Fig. 2 we show the definition for the time of onset t_0, the time when particles are first detected t_0^*, namely, pre-onset, and the time of maximum t_m.

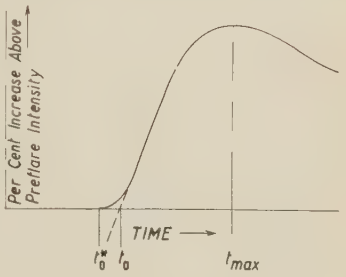

Fig. 2. – Several cosmic ray recorders display intensity as a function of time in sufficient detail to reveal a small increase leading into the sharp rise of intensity. This is identified as a « foot » on the intensity curve. We define this foot as the pre-onset increase and specify the beginning of this pre-onset as t_0^*. The steep slope of the intensity increase when extrapolated to the time axis defines the onset time t_0. These are times observed at the earth.

3. – The delayed arrival of low energy particles [1].

The onset times can be rather accurately determined for about 18 to 20 detectors throughout the world. These onset times and their distribution are shown in Fig. 3. It is clear that a range of nine minutes or more exists

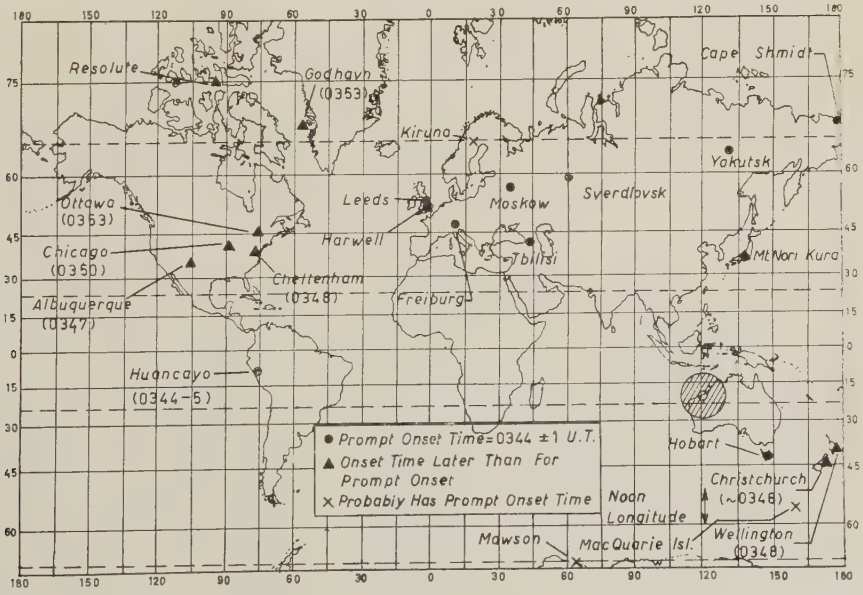

Fig. 3. – The world-wide distribution of cosmic ray detectors for which the onset time has been established.

which cannot be accounted for by timing, or other experimental errors. The earliest onset times are spread out in longitude from Cape Shmidt [3] to Freiburg [4], and perhaps as far west as the British stations. This is a longitude range of over 160° in the northern hemisphere, extending from early morning to early afternoon hours local time.

We shall now investigate the meaning which this range of onset times and their distribution over the earth have for understanding the propagation of solar cosmic rays during the first minutes of the intensity increase.

The observations reported in Fig. 3 were obtained with either ion chambers, counter telescopes or neutron intensity monitors. If a beam of solar particles arrives at the top of the atmosphere containing a mixture of high and low energy particles, then all three types of detectors would respond to the secondaries from the high energies and at least the neutron monitor would respond to the secondaries from the low energy particles (> 1 GeV). It is clear, therefore, that if the first arriving solar cosmic rays particles have a wide spread in energy, there should be a unique value for the onset time throughout the world for all kinds of detectors. But from Fig. 3 we see that for the flare of 23 February 1956 not all detectors responded to the arrival of particles with the prompt onset time near 0344 U.T. For example, the observations from the Asia-Europe area are compared with Chicago (USA) [2] and Ottawa (Canada) [5] in Fig. 4. Here we find no evidence for particles arriving before 0349 U.T. at Chicago and before 0350 at Ottawa (the respective onset times are 0350 and 0353), whereas the detectors in Europa and Asia experience a sharp increase at (0344 $\pm$ 1) U.T. for both charged particle and neutron detectors (*). Since in the minutes following prompt onset, the

(*) S. N. Vernov (Dorman, Feinberg, Glokova, Grigorov, Kopilov, Sanin, Shafer and Vernov: Private communication, June 22, 1957) has recently provided us with a re-evaluation of all the data from the cosmic ray intensity increases recorded in the U.S.S.R. Using our criterion for onset times, we list below the revised onset times for the Soviet stations:

Station	Geomagnetic coordinates		t_0
	Lat.	Long.	
Tbilisi	36° N	122°	0341
Sverdlovsk	48° N	141°	0341-2
Moscow	51° N	120°	0342-3
Yakutsk	51° N	193°	0343-4
Cape Shmidt	63° N	227°	0344-5

According to this report an over-all error of about $\pm$ 1 minute is to be assigned to each of the above values for t_0.

primary particle intensity over Europe exceeded background by a factor 25 ÷ 50 without a detectable increase appearing at Chicago or Ottawa, the mechanism preventing the arrival of solar produced particles at Chicago and Ottawa under

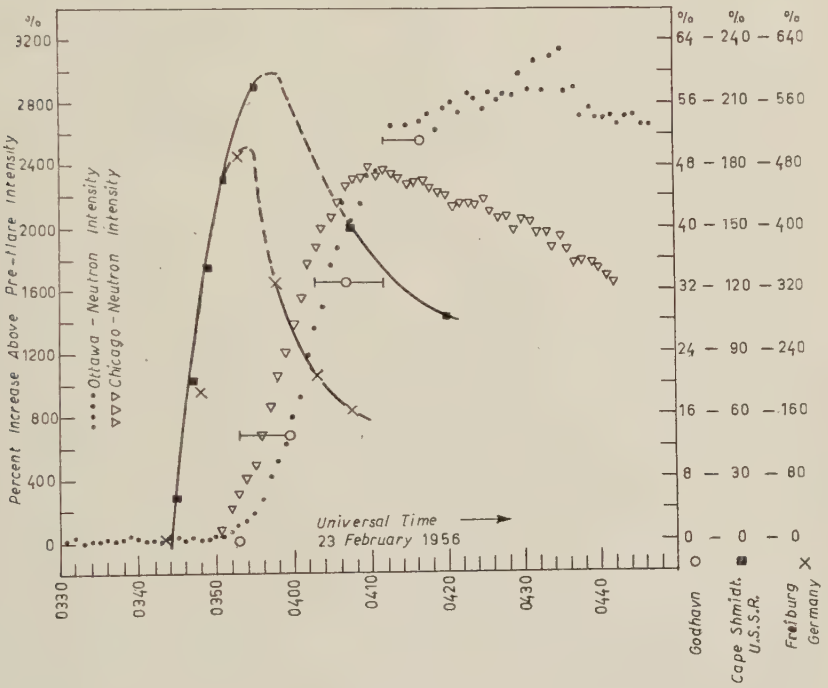

Fig. 4. — The delayed intensity increases in the western hemisphere are shown for the neutron monitors at Chicago and Ottawa. Note the absence of any increase of intensity at Ottawa before 0349 U.T.

We wish to make two comments regarding these new data: First, even taking into account the assigned errors in timing, there appears be to a systematic delay in onset time with increasing geomagnetic latitude. It is well established that within any given impact zone the magnetic rigidity of arriving particles decreases with increasing geomagnetic latitude. Consequently, this small and systematic spread in onset times is explained if we assume that the highest energy particles arrive first, i.e., that there is a small dispersion effect within an impact zone similar to the large dispersion effect (Fig. 7) we find between the « 0900 » and the « 2000 » hour impact zones. Second, though this small effect may be real, it is small compared with the observed time differences of 9 ÷ 10 minutes, and represents a small spread of particle energies. Therefore, the assumption we have made in this paper, namely, that the onset time in Europe and Asia is represented by a unique, prompt onset at (0344 ± 1) U.T. is still satisfactory for studying the initial phases of propagation and does not change appreciably the results shown in Fig. 7.

these circumstances must have been exceedingly effective and depended upon factors other than the response characteristic of the detectors.

We now examine the behavior of the primary beam in the geomagnetic field. If we make the assumption that the solar cosmic rays are arriving roughly isotropically at this time then we apply the classical Lemaitre-Vallarta theory. Since, from Fig. 3, promptly arriving radiation appears within the geomagnetic latitude range 0° up to 55°, then particles of the same energy range would have access to Chicago and Ottawa if the cosmic rays were isotropic. But, since no effect appears at these latter stations, we must conclude that the cosmic rays did not arrive isotropically, and the source as seen at the earth was limited in size.

The problem of determining at what positions inside the terrestrial magnetic field particles arrive as a function of their energy, if the source at infinity is of finite size, has been treated extensively recently. The allowed regions of impact on the earth are called impact zones. From the above general arguments we conclude that impact zones of some kind existed during at least the first 10 minutes of solar particle arrival at the earth. On the other hand for later times (later than 1 hour) it should be emphasized that the experimental evidence strongly indicates isotropic incidence.

Fortunately, the magnitude of the cosmic ray effect was sufficiently large to obtain a measure of the effectiveness in excluding particles from some regions of the earth. An increase of intensity as small as $(15 \div 20)\,\%$ beginning at 0344 U.T. would have been readily detected at Ottawa, but no effect was observed even though the intensity of promptly arriving particles outside the terrestrial field was $> 5\,000$ percent. Therefore, less than one solar produced particle in a hundred was able to reach Ottawa before 0349 U.T. Let us assume tentatively that this promptly arriving beam of solar particles contained particles over the energy range found to exist for later times ($1 \leqslant E \leqslant 30$ GeV for protons). Then this discrimination factor 10^2 for exclusion of particles must apply to particles of *all* energies in order to account for no early increase of intensity being observed at some stations.

However, it was shown in earlier papers [6-8] from this laboratory that, although the exclusion of high energy particles from regions outside the main impact zones may be complete, there is a background region extending over all longitudes which arises from connecting orbits of low energy particles —energies near the geomagnetic cut-off for the observing position in the background zone. Thus, even though we can account for the exclusion of high energy particles outside the main impact zones, we cannot argue that low energy particles are similarly excluded. It then follows that the observations at Chicago and Ottawa are inconsistent with the assumption that the promptly arriving beam contains particles of both low and high energies.

However, if we assume that the first high energy particles arrive several

minutes ahead of the first low energy radiation, then we shall be able to account for the delayed cosmic ray increases at Chicago and Ottawa as we shall show later. With the assumptions that impact zones existed during the first $10 \div 15$ minutes of the cosmic ray increase, and that the low energy cosmic rays arrive late in this time interval, we are led to the following alternative explanations for the late arriving particles:

a) either the late arriving particles come from directions other than the limited source so that they have access to regions of the earth otherwise forbidden for a source at the sun, or

b) they arrive from the same source as the prompt particles but with lower energy so they may enter the background zone inaccessible to high energy particles.

For alternative *a*), two extreme possibilities have been proposed, both of which involve the question of how magnetic fields are distributed in the interplanetary medium. If disordered magnetic fields exist beyond the orbit of the earth, as suggested by the study of the flare event at late times [2], then cosmic ray particles might be back-scattered from this barrier to arrive late with respect to the high energy particles. This idea rests upon the erroneous assumption that Chicago and Ottawa were in highly forbidden zones for particles of *all* energies; we discard this possibility to account for the delayed onsets. The opposite extreme assumes a uniform field throughout the space between the sun and the earth, its direction being inclined with respect to the sun-earth line so that only high energy particles can arrive promptly [9]. We shall later show that this suggestion does not agree with experimental evidence for early or late times in the history of the flare.

We, therefore, explore alternative *b*) wherein the particles of all energies during the first $10 \div 15$ minutes come from the source direction, but only the high energies arrive promptly at the earth. The time delay in transit as a function of particle energy arising from particle velocity distribution does not account for more than 10% of the time delay effect reported in Fig. 4. Before investigating further the origin of the assumed time delays as a function of energy, we shall briefly discuss the properties of the impact and background regions on the earth at the time of the giant flare.

4. – Sun-earth orbits and the intensity of cosmic radiation at the top of the atmosphere.

We know that the earth is not a perfect dipole, that important irregularities exist in the outer portions of the terrestrial field, and that there may be stray magnetic fields in the nearby interplanetary medium. Nevertheless,

from our discussion in the previous section we know that these defects in the magnetic field were insufficient to destroy pronounced anisotropies produced by a source of finite size. Consequently, we have extended the early orbit calculations using the AVIDAC computer at the Argonne National Laboratory, Chicago. This work was done by Dr. REIMAR LÜST, who reports on the details of the orbit calculations elsewhere in this Journal. The calculations assist in drawing conclusions on the behavior of impact and background zones.

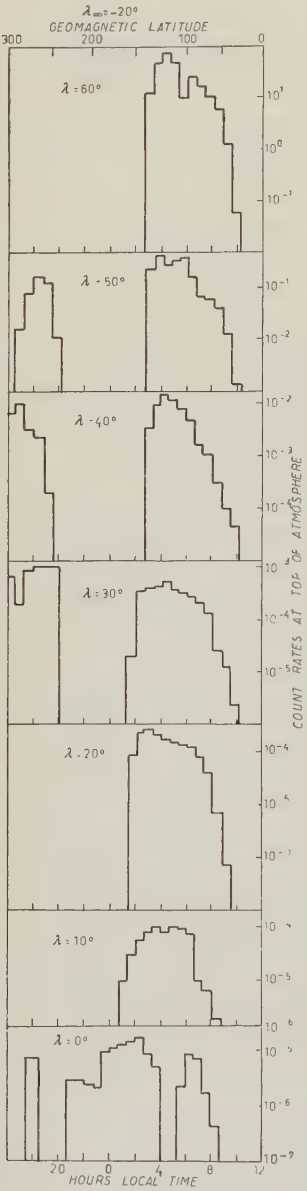

Using a spectrum $(pc/Ze)^{-6}$ for the production spectrum, assuming that the particles extend in energy out to 30 GeV, and taking for purposes of calculation the solid angle of the source as $\pm 15°$ in latitude and $\pm 10°$ in longitude, it has been possible to determine whether there exist distinct impact zones for a finite source. The details of the calculation appear in a paper published elsewhere [1]. At the time of the flare, the sun was located about 20° south of the geomagnetic equator. For the northern hemisphere, we show in Fig. 5 the expected cosmic ray intensities at the top of the atmosphere. The « 2000 » hour impact zone is as important as the first impact zone due to the very steep energy spectrum contributing particles of low energy preferentially to the third impact zone rather than the first impact zone.

If the solid angle of the source is increased, the impact zones will extend over a wider range of longitudes than shown in Fig. 5. It is clear from Fig. 3 that since the prompt onset time associated with the combined «0900 » and « 0300 » impact zones is observed over a 160° longitude

Fig. 5. – The calculated counting rates at the top of the atmosphere have been determined using the results of the sun - earth orbit calculations and steep differential particle rigidity spectrum. Since the sun was approximately 20° south of the geomagnetic equator at the time of the flare, these results are for the *northern* hemisphere. (For details see Reference [1] and the paper by R. LÜST in this issue, pag. 176).

band, the effective source at the time of the flare must have had a larger solid angle than the source used for our calculations. We shall discuss this matter later.

The relationship between source latitude, and latitude for arrival is shown graphically in Fig. 6 for 2 GeV and 10 GeV rigidity particles. We observe that for a given source latitude and particle rigidity the impact points approach asymptotically the geomagnetic cut-off latitude for that rigidity. Therefore, outside the two major impact zones the incoming particles are restricted to a small spread in rigidity near the value of the geomagnetic cut-off prevailing at the location of the observer. In the vicinity of the « 2000 » hour zone, this effect forbids higher energy particles from arriving at intermediate and high geomagnetic latitudes.

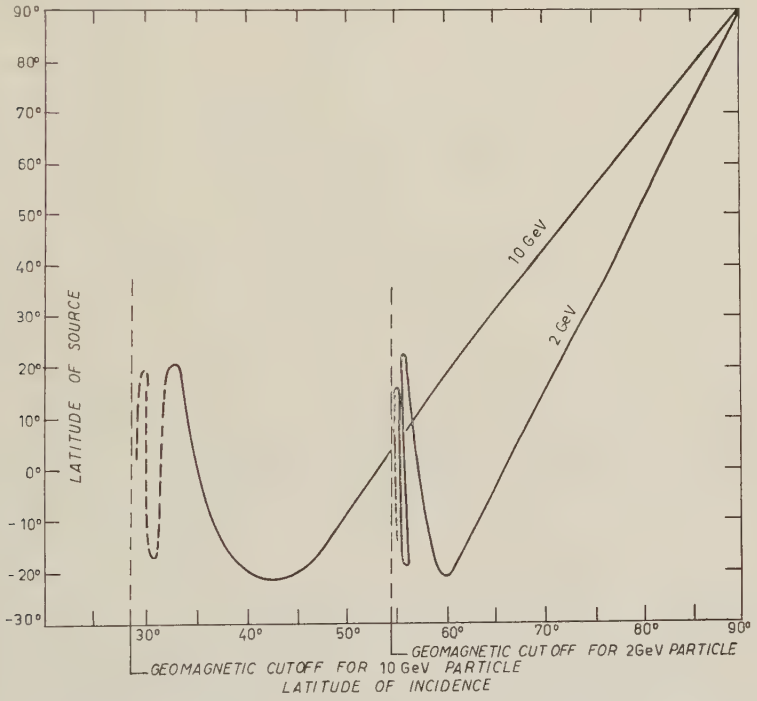

Fig. 6. – The particles admitted to the « 2000 » hour impact zone have a low magnetic rigidity which is close to the geomagnetic cut-off rigidity,

The steep energy spectrum results in the « 2000 » hour impact zone displaying an intensity almost as great as that in the first impact zone. This is in agreement with the observations in Europe and North America (*).

(*) G. Pfotzer (in this issue, pag. 180). Finds a spectrum near $[pc/Ze]^{-4}$ from his analysis of the anisotropic radiation. This spectral form will change the computed cosmic ray intensities in the various impact zones which we report here, but does not change the results of our analysis.

From the above results it is clear that if a burst of particles from the source contained particles of *all* magnetic rigidities, then the prompt onset time observed in the « 0900-0300 » hour regions would also have been obtained in the spread out « 2000 » hour zone, which includes Chicago and Ottawa. Since

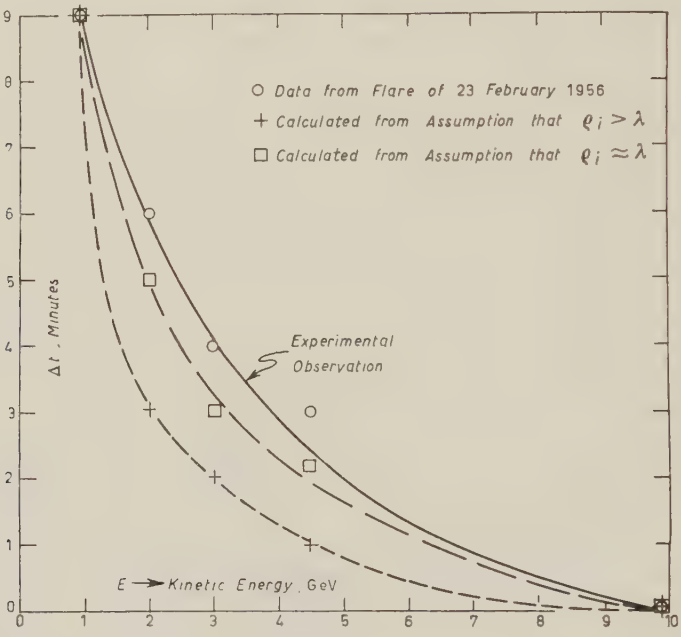

Fig. 7. – The time delays for the first arriving particles as a function of energy. This is called the dispersion effect.

this did not occur (Fig. 4), we conclude that the radiation of high magnetic rigidity reaches earth first. Hence, the prompt onset time will only be observed in the merged « 0900-0300 » hour zone in the northern hemisphere, and the « 0900 » hour zone in the southern hemisphere, whereas, the delayed onset times in the « 2000 » hour region and background zone will critically depend upon the magnetic rigidity of the arriving particles. For the longitude band centered on « 2000 » hour the delay in onset time, Δt, with respect to prompt onset, for the experimental observations over a wide range of geomagnetic cut-off rigidities is shown in Fig. 7. We have expressed the time delay over a particle energy range of $(1 \div 10)$ GeV, assuming that the incoming particles are principally protons [2]. The delay in onset time appears to be a smooth function of primary particle energy.

5. Origin of the delays in onset times for the arrival of solar cosmic rays.

If the impact zones at the earth during the early portion of the flare event are even approximately correct, then the first high energy particles arrive ahead of successively lower energy particles so that the time difference Δt depends upon particle energy, and may be as large as $\Delta t = 9$ minutes for particles differing in energy by an order of magnitude. We therefore seek a physical explanation for this effect and the phenomenon associated with it.

Differences in transit time arising from the range of β for the particles accounts for less than 10% of the effect. Also the time spent in the geomagnetic field, even for complicated orbits belonging to higher order impact zones, is less than 0.1 seconds. We are then led to either *a*) possible differences in the production time for cosmic ray particles within the flare, or *b*) mechanisms operative during the propagation of the particle between the flare region and the geomagnetic field. There are not, at present, any arguments for delayed production of the low energy particles in the visible flare region (*); indeed, it is likely that even for a rapid acceleration process the low energy particles will tend to appear in the source first, or at the same time as high energy particles. If we tentatively discard time delays in the flare region, we then consider mechanisms which may produce the effect after cosmic ray production.

In addition to the differences of onset time Δt for cosmic ray increases observed at the earth, there exists the elapsed time between production and first detection of particles which may be even larger than for the difference in onset times. We define the elapsed time from the beginning of production at the sun to the first arrival at the earth as the *initial transit time* t'. It is clear from the four earlier large cosmic ray flares that this time may be many-fold the value of the transit time for electromagnetic radiation and this transit delay has frequently been noted in the literature. Thus, Δt is the « dispersion » arising from the time delay in transit t' and is a function of particle energy as shown in Fig. 7. (Dispersion may also be a function of t'.)

The value of t' for particles of a given energy depends upon our assumptions regarding the time of solar production. In this paper we shall consider the time of maximum energy output per unit volume of the flare as the time when

---

(*) We have already shown that the kinetic energy stored in solar cosmic ray particles exceeds $3 \cdot 10^{31}$ ergs for the flare of 23 February 1956 [2]. This would imply that if the efficiency for cosmic ray production were as high as 1%, as seems improbable, the total flare energy exceeds $3 \cdot 10^{33}$ ergs. We know that the flare was seen in white light and hence was of comparable intensity to the photospheric background [10]; these observations are consistent with the total flare energy being confined to the visible flare region.

cosmic ray production begins (*). For the February 1956 flare this would correspond to maximum light output and to the time approximately 0342 U.T. If solar radio emission should turn out to be the dominant mechanism for cosmic ray production, it would be necessary to specify the time for initial production as 0335 U.T., thus increasing t' so that it would be approximately equal to the dispersion time.

We shall now discuss possible explanations for the time delays and begin by considering the dispersion effect in time, Δt.

The alternatives are not numerous. Assuming prompt production of all particle energies within the flare volume, we are left with the problem of invoking suitable magnetic fields in order to increase the effective lengths of the low energy particle trajectories relative to the high energy particles. We also require temporary storage of the short burst of radiation, since the observed arrival of solar flare particles for more than $(16 \div 18)$ hours is difficult to attribute to continuous production in the flare region. Interplanetary magnetic fields appear to be the most likely means for charged particle storage. The question then arises: do the magnetic fields invoked for storage also introduce the observed spread in onset times at the earth? There is the possibility, that the interplanetary volume is pervaded by a uniform magnetic field [9, 11, 12*a*] which may introduce some spread in the arrival times of particles, but arguments given in Sect. 9 indicate that a uniform or diverging magnetic field does not satisfy the experimental observations. A second possibility is the assumption of disordered magnetic fields located outside the orbit of the earth in the form of an enclosing barrier to provide temporary storage—a model which appears to fulfil some of the requirements for the late development of the cosmic ray flare event [2].

Although we have shown that « reflection » of charged particles from the inner boundary of such a barrier field cannot be the origin of the onset time delay Δt, we shall consider other ways by which the spread of onset times may be produced by particle diffusion through irregular magnetic fields.

If we make the tentative assumption that irregular fields are extended throughout the region within the earth's orbit, we see that a burst of radiation at the sun containing particles of all energies will diffuse outward through the field and that, since the diffusion mean-free-path will in general be a function of particle energy, there may develop significant differences in the arrival time between the first high energy and low energy particles.

However, continuous diffusion throughout the region between sun and earth cannot represent the physical conditions at the time of onset on 23 Feb-

(*) The total energy output of the flare in non-radio emission is at least of the order 10^{33} ergs, whereas the total energy emitted in the radio spectrum is of the order 10^{25} ergs.

ruary 1956. Enough diffusion to produce the observed time delays leads to the smearing out of impact zones and, contrary to observations, a unique onset time would follow for all observed intensity increases. We, therefore, discard uniform diffusion between the sun and the earth.

The remaining possibilities for using diffusion to produce the time delays require that the diffusion be restricted to either a region around the sun or around the earth. Even though some diffusion near the earth is likely, and is a possible way to account for the large Forbush type decrease of total intensity underway prior to the onset of the flare event [2], the earth would have to be immersed in a much larger volume of disordered fields to produce the observed diffusion time differences $\Delta t = 9$ minutes than for the volume to produce the observed Forbush decrease. Also, the requirements on the scale size of the disordered magnetic field region and the retention of observed impact zones at the earth are mutually exclusive.

The flare of 19 November 1949 provides an independent argument against the time difference arising from disordered fields in the vicinity of the earth. At that time there was no evidence for a Forbush decrease having occurred prior to the flare. (The Carnegie Institution ionization chambers displayed a 1% decrease in intensity below the average for the period.) Even so, the time delay between high and low energy particles was approximately 11 minutes as we shall indicate in Sect. 6.

Consequently we explore solar particle diffusion in the vicinity of the sun.

6. – Diffusion of solar cosmic ray out of the general solar magnetic field.

Babcock has demonstrated beyond doubt that the sun possesses a general magnetic field [13]. He has shown that the field intensity near the photospheric surface is of the order 1 gauss. However, irregularities in the general field are certain. From the Babcock data there are obvious irregularities, and eclipse pictures taken at various phases of the solar cycle emphasize the changing distortion of the general field in the solar corona throughout the solar activity cycle. From independent solar-terrestrial observations there is extensive evidence that ionized matter in the form of streams and clouds emanate from deep in the solar atmosphere—these bursts of ionized matter inevitably squeeze and spread the general field in such a way as to produce small scale irregularities.

In view of these arguments we shall assume as a working model that, although when observed as a large scale phenomenon the general solar field is roughly coherent, it is not a « good » dipole field—it is a general field containing more or less random small scale irregularities extending from photospheric level out to $(50 \div 100)$ solar radii. We now ask how cosmic ray particles

in the energy range (1 : 30) GeV will propagate out of this solar field from the visible flare region. Trapping orbits will have very short life times because the magnetic field irregularities will scatter the particles into everchanging orbits. Indeed, if the general solar field were sufficiently perfect to sustain trapping orbits, it is difficult to see how low energy cosmic rays could ever escape from the vicinity of the sun (*), without invoking special effects [14]: the fact that a high yield of low energy cosmic rays exists is a strong argument that the field is not a perfect dipole. Furthermore, the flare itself produces an enormous outburst of radiation and matter which may extend one solar radius, or more, above the photosphere. Cosmic rays may then be carried in this outburst to the higher corona where the general solar field is weaker, *before* the diffusion we discuss here becomes effective.

If the magnetic field irregularities are distributed throughout the solar corona they may be considered to be scattering centers for charged particles of cosmic ray energy with successive scatterings leading to more or less isotropic diffusion of particles in the general solar field. In the following discussion we shall assume that the propagation of charged cosmic ray particles away from the solar flare region may be treated as particle diffusion out of the general solar magnetic field. The time required for a low energy particle to travel through a diffusing medium is in general longer than for a high energy particle, and it is this possibility that we invoke to generate the delay in arrival time of the flare particles at the earth.

Sekido and Murakami [15] have proposed that the magnetic field around the sun be a trapping field for flare particles in order to account for the initial transit time t' defined earlier. We wish to point out that from our preceding arguments it would be difficult to sustain trapping orbits because of field imperfections and that, in addition to the bulk time delay t' we must explain the dispersion time difference Δt. For these reasons we prefer to try exploring diffusion rather than trapping as the dominant mechanism in the vicinity of the sun (+).

From the observed spread of the main impact zones we assume that the source, or diffusing region, centered at the sun extends out at least 50 solar radii. To simplify the calculations the diffusing region shall be represented as a spherical envelope of radius r' concentric with the sun. If the photospheric radius is r_0, then $r_0 \ll r'$. All particles that enter the volume defined by

(*) For a proton of 2 GeV/c in a field of 10^{-2} gauss, the Larmor radius is $7 \cdot 10^8$ cm which is 10^{-2} solar radius.

(+) *Note added in proof.* - L. I. Dorman and, independently, G. Pfotzer, in this issue, pag. 180. Have also suggested that there may be a diffusing region in the vicinity of the sun. The magnetic clouds near the sun which Dorman invokes to produce his « scatter » radiation could be used equally well in place of our model to explain the dispersion effect, if the clouds are sufficiently dense around the sun.

$r < r_0$ are absorbed. In addition to the symmetry of the model, we also assume that the diffusion coefficient $K(\varepsilon)$ throughout the envelope is constant and non-zero, i.e. $\partial K(\varepsilon)/\partial r = 0$. The particle density $J(\varepsilon)$ is represented in the diffusion equation as:

$$\frac{\partial J(\varepsilon)}{\partial t} = \frac{cL(\varepsilon)}{3} \nabla^2 J(\varepsilon) , \qquad \text{where } K(\varepsilon) = \frac{cL(\varepsilon)}{3} ; \tag{1}$$

$L(\varepsilon)$ being the scattering mean-free-path.

The solutions of the spherically symmetric diffusion equation have already been considered in an earlier paper for several cases [2].

Since the scale size of the flare region is r_f, where (cosmic radiation carried by the large outburst of energy may modify this somewhat) we may assume that the particles are injected instantaneously at $t = 0$ into the solar envelope at $r \approx 0$. Then the particle density, at the time $t > 0$ and at $r \gg r_0$, is

$$J(\varepsilon) = \frac{A}{(\pi K t)^{\frac{3}{2}}} \exp\left[-\frac{r^2}{\pi K t}\right] . \tag{2}$$

From the exponential factor we see that $(Kt)^{\frac{1}{2}}$ is proportional and comparable to the distance l beyond r_0 to which particles of a given energy have diffused in the time t.

If the relative distances that particles of energies ε_1, ε_2 travel in the times τ_1, τ_2 are represented as lengths l_1, l_2 then

$$\frac{l_1}{l_2} = \left(\frac{K_1 \tau_1}{K_2 \tau_2}\right)^{\frac{1}{2}} = \left(\frac{L(\varepsilon_1)\tau_1}{L(\varepsilon_2)\tau_2}\right)^{\frac{1}{2}} . \tag{3}$$

To understand the dependence of $L(\varepsilon)$ upon particle energy we must consider the problem of scattering charged particles in magnetic fields. If we call λ the scale size for an irregularity capable of deflecting a particle of relativistic energy, then $\lambda \ll r_0 = 7 \cdot 10^{10}$ cm. If ϱ_i is the Larmor radius of the particle inside a scattering region, the scattering process will depend upon the relative magnitudes of ϱ_i and λ. For a sufficiently high energy particle $\varrho_i > \lambda$ under all conditions; for a sufficiently low energy particle $\varrho_i < \lambda$ under all solar conditions. The energies to be considered here are within the range $(1 \div 20)$ GeV. As one possible case the irregularities in magnetic field intensity may be treated as concentrations of strong fields interspersed with regions of very weak fields. Then for sufficiently large and dense concentrations $\varrho_i < \lambda$ and $\varrho_i \ll \varrho_0$ (where ϱ_0 is the Larmor radius in the average field at radius r) so that the particles over a wide range of energies will undergo wide angle deflections in collisions with these irregularities. Under these conditions $L(\varepsilon)$ depends very little, if at all, upon particle energy. But if this diffusion is the

main process which leads to the differences in onset time at the earth, we know from Fig. 7 that the process *is* strongly energy dependent and the limiting case $\varrho_i < \lambda$ does not apply to solar conditions at the time of the February 1956 flare. We are led to the conclusion that $\varrho_i \geqslant \lambda$.

A detailed discussion of the function $L(\varepsilon)$ and the explicit form used for the calculations appears in reference [1], and will not be discussed further here.

If we call τ' the transit time, assumed independent of particle energy, from the outer boundary of the solar diffusing envelope to the orbit of the earth, and Δt the difference in the observed onset times for particles of energy ε_1, ε_2 we may write

$$\tau_2 + \Delta t + \tau_2' = \tau_1 + \tau_1' \,. \tag{8}$$

All particles have relativistic energy, and we assume they travel with velocity c. Since we have assumed that the envelope radius r' will be independent of particle energy, then $\tau_1' = \tau_2'$ and $\tau_2 + \Delta t = \tau_1$

$$\text{If} \quad R = \frac{\tau_2}{\tau_1} \,, \qquad \text{then} \qquad \tau_1 = \frac{R}{1 - R} \Delta t \,. \tag{9}$$

From experimental observations we have the time of onset as a function of geomagnetic cut-off energy for five different geomagnetic latitudes all in the region of the spread-out « 2000 » hour zone as shown in Fig. 7.

The ratio R is best determined for a wide spread in Δt and particle energy; the Ottawa and Huancayo [16] data are, therefore, used to obtain the value τ_2 for the diffusion time out of the solar envelope for particles of energy 10 GeV or greater. It then follows that using the two end points of the curve in Fig. 7 we can calculate the values for Δt under the alternate assumptions $\varrho_i > \lambda$ or $\varrho_i \approx \lambda$. The results are shown in Fig. 7 where it appears that $\varrho_i \approx \lambda$ is the better assumption. The errors of $\Delta t = \pm 1$ minute do not justify further approximations in the calculations, especially in view of the fact that the effective solar envelope radius must be a function of particle energy.

An order of magnitude estimate can now be obtained for the radius of the solar diffusing envelope from the high energy particles $\varepsilon \geqslant 10$ GeV which have prompt onset at the earth: $\tau = 2.6$ minutes for these particles: ... $r' \leqslant \tau c$ and $r' \approx 0.3$ A.U. This represents a $\sim 35^\circ$ source in the sky. Independent estimates of the source size from the width of the « 0900-0300 » hour impact zone require a source of at least this size as noted in Sect. 8.

If diffusion through the general solar magnetic field accounts for the dispersion in onset times Δt, then there are two consequences which follow for the behavior of the cosmic ray intensity during the first minutes of the increase of intensity. First, the rate of rise of cosmic ray intensity following t_0 must be a function of the lateness of onset time over the entire energy range. The

time required for the intensity to rise to 50% of maximum intensity is given in Table I for each station. These results are in the right direction and of the

TABLE I. – *Rate of cosmic ray intensity increase following* t_0.

	t_0	Time for intensity to increase to 50% t_m
Prompt arrival . . .	0344	4 minutes
Cheltenham	0348	6 minutes
Chicago	0349	8 minutes
Ottawa	0353	11 minutes

correct magnitude for agreement with the diffusion hypothesis. Second, for any given energy, the growth of intensity at the outer boundary of the envelope will at first be gradual; the increase of intensity everywhere at the earth should, therefore, have an exponential « foot » on the intensity curves. This is observed in some cases and has been defined here as the gradual pre-onset increase t_j^*. For example the preflare increase began about 0341 U.T. and amounted to 20% (ionization) at Hobart, Tasmania [17] and was 10% (ionization) at Freiburg [4]. For low energies and late onset the foot is also evident in the Ottawa neutron intensity data, Fig. 4.

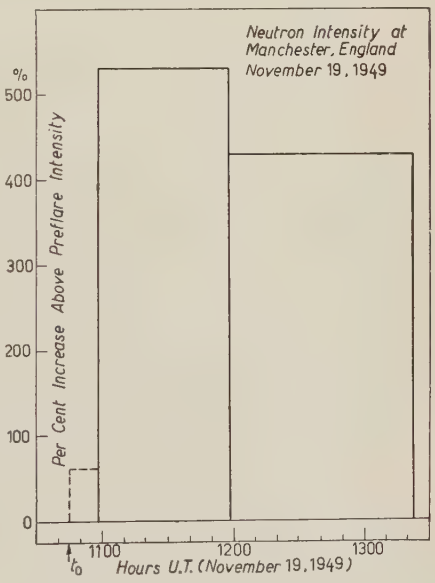

Fig. 8. – The cosmic ray intensity at Manchester, England, 19 November 1949.

If this explanation for the observed dispersion in arrival times of particles is correct then these dispersion effects must have occurred at the time of previous cosmic ray intensity increases. For example, on November 19, 1949, the ion chamber at Climax, Colorado, was in an impact zone with onset time t_0=1045 U.T. [18] whereas the neutron detector at Manchester, England (*) was in a higher order region. For Manchester we see from Fig. 8 it is unlikely that the onset was earlier than about to $t_0 \approx 1055$; hence $\Delta t \approx 10$ minutes.

(*) We are grateful to Dr. H. J. J. BRADDICK and Dr. N. ADAMS for providing us with more accurate data on the neutron intensity increase at Manchester (Nov. 19, 1949) than has heretofore been published.

The model for a solar diffusing envelope which we presented here to account for the dispersion effect is undoubtedly in nature a mixture of magnetic field regions, since not only are there the field irregularities in the envelope, but also radially stretched magnetic fields in the equatorial regions, in addition to the enormous radial channel of disordered fields produced by the giant solar flare itself. Hence, each flare event may display some differences in the energy dependence of Δt and apparent source size. The differences in t' and Δt for the five flares may depend upon how far out into the corona the flare burst carries the cosmic ray production before diffusion outward through the envelope takes place.

Because of diffusion, cosmic ray particles reach the back side of the solar envelope and escape. There is, at present, therefore, a difficulty with the model since few increases of cosmic ray intensity have occurred without any observed solar flare. Perhaps the outward diffusion is limited more to a radial diffusion channel than we suspect at present.

7. – The cosmic ray intensity in the polar regions.

The flare of February 1956 was the first for which cosmic ray detectors were operating in both polar regions. Data on the detectors in polar regions (defined as the limiting latitudes greater than $\pm 60°$) are given in Table II.

TABLE II. – *Polar stations.*

	Estimated geomagnetic latitude (revised co-ordinates) in brackets)	Geographic longitude	Time of onset	Time of maximum intensity	Detector and absorber
Mawson	−73° (−71°)	65° E	Est. 0344-50	< 0358	Vertical; 10 cm Pb
Macquarie Island	−61° (−56°)	160° E	Est. 0344	< 0400	Vertical; 10 cm Pb
Cape Shmidt . .	+63° (+68°)	180° E	0344	0358	Ionization; 12 cm Pb
Kiruna	+68° (+63°)	20° E	Est. 0344	0400	Vertical; no absorber
Godhavn . . .	+80° (~ 75°)	55° W	0353-4	~ 0420	Ionization; 12 cm Pb
Resolute	+83°	100° W	0353	~ 0415	Vertical; 14 cm Pb

We have recently analyzed the experimental data for the polar regions [1] and find that some detectors displayed increases consistent with a prompt onset time and, therefore, were in impact zones, whereas other polar stations appear to have had no connecting orbits with the source direction; we shall here only summarize some of the conclusions.

There were impact zones extending into the lower Polar regions for the promptly arriving particles, and after about 0353, the kind of radiation arriving at Ottawa extended throughout the North Polar, and probably the South Polar regions. At late times, especially after 0500 hour U.T., the highest total particle intensities are found in the polar regions. The polar radiation at late times is composed of the entire radiation which has access to the earth. The four previous large cosmic ray increases support this view since the intensity at Godhavn at late times is always farther above pre-flare intensity than any other comparable ion chamber anywhere in the world.

8. – The time of transition from anisotropy to isotropy.

Since Godhavn and Resolute are located at latitudes inaccessible to the solar source, the polar observations support the view that the radiation reaching Ottawa and Godhavn was beginning to come from directions other than the sun after 0353 U.T. During the following hours there was no further evidence that the incoming radiation arrived from a preferred source position except for small anisotropies measured at high energies in Stockholm [19] and Rome [20]. We favor the view that this anistropic effect after the first hour may arise from the north and south telescopes observing particles of different energies. If so, the observed steep particle spectrum will produce appreciable differences in intensity between the two telescopes. Also, the telescope anisotropy persisted for more than a quarter revolution of the earth which suggests that there was not a unique position for the apparent source.

We argue, therefore, that the period following 0353 U.T. represents the transition from a preferred source direction to isotropic incidence.

In Sect. 6 we made the simplifying assumption that the source size was constant, and independent of particle energy. However, it is clear that if our calculations of the impact zone locations are even approximately correct, then the solar cosmic rays came from a region which included the position of the sun. The size of this diffusion source for different particle energies may be estimated, both from the longitude spread of the merged first and second zones in Asia and Europe, and from the time for particles to diffuse out of the source. At the time of prompt onset (0344 U.T.) the source as observed at the earth was less than 1 radian in solid angle. However, for approximately 1 GeV magnetic rigidity particles first arriving about 0353 U.T. the source would appear to occupy an exceedingly large solid angle. It is at this time we believe that the transition from particle arrival in impact zones to more or less isotropic incidence begins.

9. Propagation in uniform or uniformly diverging magnetic fields as an explanation for the dispersion effect and impact zones.

It has recently been suggested, principally by EHMERT [9], HAYAKAWA [11], GOLD and others [12], that the region including the sun and the earth was pervaded at the time of the flare by a more or less uniform magnetic field along which the solar cosmic rays may propagate to the earth. We shall consider here briefly the implications which *a*) the existence of impact zones and *b*) the dispersion effect have upon this hypothesis during the early stages of the cosmic ray intensity increase.

The first step is to show how particles moving in a uniform field will be distributed just outside the influence of the terrestrial magnetic field near the time of prompt onset, t_0 and at later times, $t_0+\Delta t$. The second step is to find out what distribution the particles will have within the magnetic field and at the top of the atmosphere for these respective times. We shall give here only the main features and principal effects.

Call φ the angle between the direction of the magnetic field lines of force and the sun-earth line, l. Charged particles with a wide range of magnetic rigidities are assumed to be emitted isotropically by the flare into this magnetic field; we define α as the angle which a particle trajectory makes with respect to the field lines. We also assume that all particles are relativistic and travel at the same velocity. Then the time to travel along the field in the sun-earth direction is $t=(l\cos\varphi)/(\beta c\cos\alpha)$. Clearly, if $\varphi=0$, particles of *all* energies traveling along the line will reach the earth. But if $\varphi\neq 0$, then only particles above a lower rigidity limit N' may reach the earth, and only at late times. If we define ϱ to be the radius of curvature of the trajectory projected on the plane perpendicular to l, then there is a value $\varrho'(=l\sin\varphi)$ determined by φ which establishes the lower rigidity limit N' for solar particles observed at the earth. Particle trajectories with a radius of curvature less than ϱ' will not reach the earth at any time.

To account for the prompt onset time t_0, high energy particles are required to move along a small spread of orbits about l. As time elapses, $t>t_0$, particles will begin to approach the earth with $\alpha\to 90^\circ$ to form an apparent particle source in the sky which lies in a plane approximately 90° with respect to the sun-earth direction, depending upon the bending of the field lines between the sun and earth. The apparent source is practically concentrated in the plane perpendicular to the uniform magnetic field. Thus, the apparent source moves from a position coincident with the sun at t_0 to a position approximately 90° away from the sun by approximately $t=0353$ U.T., if the arrival of particles in forbidden zones is to be explained by this model.

We have investigated the distribution of impact points at the top of the

atmosphere for this line source. The results are shown in Fig. 9 for half the sky. It is clear that the impact zones are remarkably well defined, and, since the line source must persist for as long as there are solar cosmic ray particles stored in the uniform field, the impact zone effect at the earth as shown in Fig. 9 will remain for many hours after its initial formation.

We believe that the experimental observations argue against a uniform magnetic field pervading the sun-earth regions at the time of the flare.

First, the uniform field model does not produce delays in onset times of the kind shown in Fig. 4. The time delays arise in a uniform field from the spiral trajectories of the particles, rather than from the difference in velocities of the particles, since this latter effect is less than 10% of the observed dispersion. Then, for the initial burst of solar cosmic rays, the first arriving particles are those of all energies which travel along the field direction, i.e. for $\alpha \approx 0°$. Since the transit time is $t' = l/(\beta c \cos \alpha)$ for small values of φ, the radiation first reaching the earth contains particles of *both* low and high energies. Similar conditions will exist for a slowly diverging or radial magnetic field. On the other hand, EHMERT [9] has suggested that the time delay comes about by making φ large and by invoking the progressive shift of the apparent source from the sun direction to a position in the sky far from the sun—as we have noted above. This requires that the impact zones be well defined at all times during the shift of the apparent source, and for later times. It also requires that very low energy particles ($\lesssim$ 6 GeV for protons) have no access to the earth at any time during the intensity increase. Neither of these requirements appear to be fulfilled by the observations.

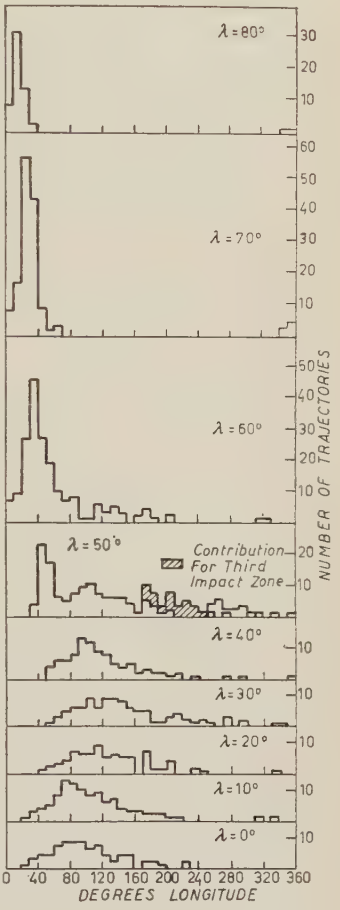

Fig. 9. – The locations of impact zones inside the terrestrial field obtained by assuming a line source of particles extending over half the sky. For particles arriving from directions in a plane, a second set of zones displaced 180° would be expected.

Second, for times in excess of $t_0 = 0.353$ U.T. the uniform field model requires the presence of a line source which produces impact zones distributed as shown in Fig. 9. During the rotation of the earth, many stations on the earth have access to the main impact zone at some time during the decline of

solar C.R. intensity. At these times the intensity is predicted to be substantially greater than at other times. No effects of this kind have been reported, and we conclude that the intensity was almost completely isotropic in the vicinity of the earth at later times.

Once the transition to nearly isotropic conditions occurs, the storage mechanism takes over the further propagation of the solar produced particles.

10. – The storage and escape of cosmic ray particles at late times.

The optical and radio emission data provide convincing evidence that the solar flare of 23 February 1956 terminated within an hour or so of its onset On the other hand, we know that radiation of solar flare origin in the multi-GeV energy range continued to arrive at the earth for more than 15 hours. Continuous production at the sun over this period appears extremely unlikely—especially in view of the required integrated energy output and the optical evidence—and we conclude that the radiation was produced in a short burst followed by storage in interplanetary magnetic fields.

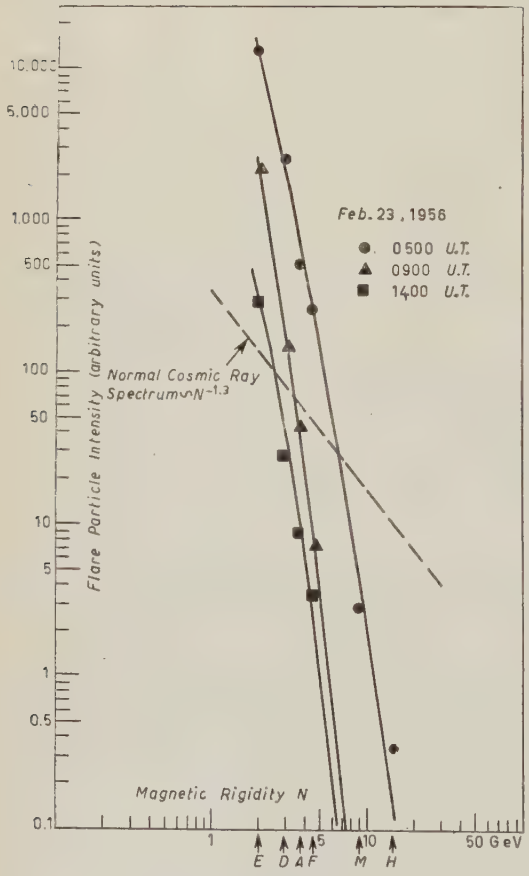

Fig. 10. – The primary cosmic ray spectrum at late times [2].

The previous discussions emphasized that the incident radiation at late times approached a high degree of isotropy; indeed, the spectrum is remarkably constant in time over this period, as shown in Fig. 10. Thus the model for the storage magnetic fields must not only permit the radiation to propagate from the sun to the earth without destroying impact zones during the first (10 ÷ 15) minutes of the event, but also bring about isotropy of the radiation within an hour. The subsequent escape of the particles from the solar system determines the decline of intensity observed at the cosmic ray station, placing an additional restriction upon the form of storage fields.

This leads us to the important question: What configuration of storage magnetic fields in interplanetary space is required at the time of the flare to satisfy these conditions? To examine this question we shall roughly separate into two distinct and mutually exclusive groups the models proposed by various authors. One group of models requires ordered magnetic fields of solar origin extending outward from the sun which are either uniform or diverging. The earth is assumed to lie in or near the field distribution. The alternate group of models depends upon disordered magnetic fields distributed in space so as to require solar cosmic ray particle diffusion into the galaxy. In the following discussion we shall call these extreme classes of models the *ordered* and the *disordered* magnetic field models, respectively.

a) *Ordered fields.* Introducing a uniform field to form an arc between the sun and the earth appears attractive for the storage of particles and for the introduction of a large transit time delay t'. If the lines of force were parallel it is clear that most of the stored particles with access to the earth at late times will be those with velocity vectors making a large angle α (alpha) with respect to the sun-earth line. As this condition for parallel lines of force is relaxed the field becomes more divergent and the population of stored particles for α near 90° decreases sharply. A magnetic field diverging by more than $(5 \div 10)\%$ in the sun-earth distance will not store particles sufficiently long to account for observations. On the other hand, parallel lines of force lead to a plane source near the earth with impact zones on the earth at late times.

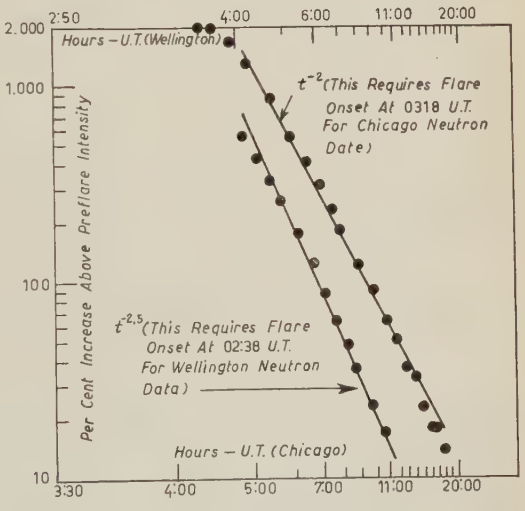

Fig. 11. – Experimental data fitted to the power law dependence expected from the hypothesis of storage in a uniform magnetic field.

The difficulties with ordered fields may be approached from another point of view. The cosmic ray intensity decreases according to $\sim t^{-2}$ for particles spiralling in a uniform field [9, 13]. Since we know that this requires injection into the field *at* the sun, the zero time for the power law plot must correspond to this time of injection. R. Vogt, in our laboratory, has determined the time for injection required to produce a t^{-2} power law dependence. From Fig. 11 we find an excellent fit with the Chicago data, for example, but

with the unattainable requirement that the flare region inject cosmic rays more than 10 minutes *before* the flare existed.

Because of the enormous energy requirement for forming a uniform field distribution of solar origin, any model requiring its existence must assume that the proper fields were present long before the flare event. This raises the physical question that since ionized matter carries the field into the interplanetary medium, how can the field retain its uniform character in space, even temporarily, in view of the motions of the ionized medium? We do not exclude the existence of a radial magnetic field, but we do not believe it can account for storage.

b) Disordered interplanetary magnetic fields. We now turn to the opposite point of view and examine the possibilities and difficulties associated with disordered or tangled fields. In this case the fields may be of solar origin, being plasma clouds ejected from the sun and containing magnetic fields, or the disordered fields might be a consequence of a galactic arm field whose boundary with the inner volume of the solar system has been made irregular by plasma clouds and ion beams. These possibilities have been discussed elsewhere [2, 21, 22]. In general, we assume that, although there is a diffusive region in the vicinity of the sun forming the source region, this inner region only accounts for the impact zone and dispersion effects—and is probably not the main storage region for cosmic rays. As a consequence of the observed impact zone effects the region between the source and the orbit of the earth should be relatively free of extensive scattering and deflecting magnetic fields other than a uniform or radial field. For this reason we have called the region inside the orbit of the earth, but beyond the source, a « field free » region, that is, $B \lesssim \leqslant 10^{-6}$ gauss in this region if the fields are disordered, and $B \lesssim 10^{-5}$ gauss if the magnetic field is radial. Therefore, we suggest that the main magnetic field effects for retaining solar cosmic rays begin beyond one astronomical unit and extend outward to considerable depth in the solar system. This dispersed distribution of scattering centers may be called a barrier region of disordered magnetic fields, since it only allows the escape of solar cosmic rays by diffusion or holes in the barrier. If the mean-free-path between the scattering centers is of the same order of magnitude as the sun-earth distance, then this barrier will not be greatly different from the region enclosed within the orbit of the earth. Earlier we have discussed the properties of such a model requiring diffusion and a $t^{\frac{3}{2}}$ law dependence during early phases of the storage, and we shall not repeat these arguments here [2]. Recently R. Vogt has calculated the shape of the intensity curve using the expansion of terms in Appendix I, reference [2], with the assumption that the depth of the diffusion region, or barrier, is approximately 5 astronomical units, i.e., ($a = 1$, $b = 6$) and that the coefficient of diffusion is energy dependent for this

model. It is obvious that the onset time for storage occurs at the same time as the beginning of isotropy at the earth. 0358 U.T. was selected for the commencement of the diffusion with the results for Chicago and Wellington shown in Fig. 12. This agreement between observation and calculation is in itself not an argument for the correctness of the model—however, this feature of the storage process may be explained by the model.

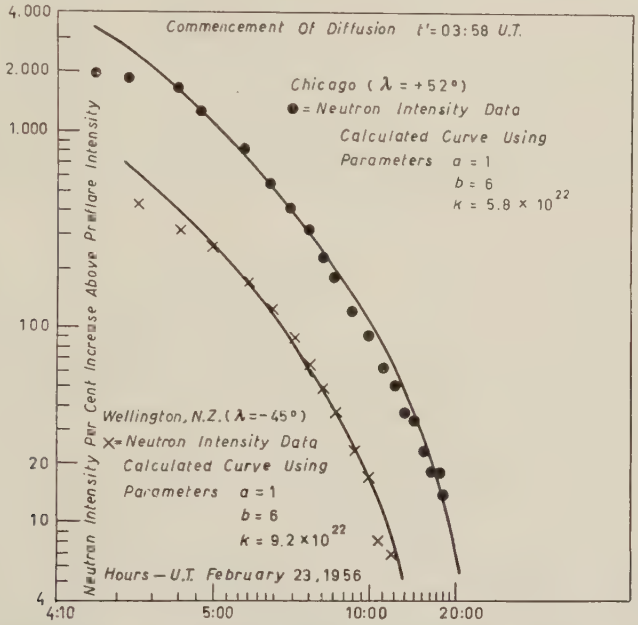

Fig. 12. – Experimental data compared with the theoretical curve for particle storage in disordered magnetic fields.

Now, to consider the difficulties with the diffusion model.

First, we have invoked an inner diffusing region at the source to obtain not only the bulk transit time delay t' but also the dispersion Δt and, for storage, extensive scattering regions beyond the earth. Thus, two magnetic field configurations are required, although one may be the consequence of the other.

Second, the rate of rise of cosmic ray intensity during the first minutes of the flare appears to be too steep for a simple diffusing effect. Here, however, we are dealing with a range of energies admitted to a given detector and this fact, along with the imperfections of diffusion, may give more nearly a linear rate of rise.

Third, perhaps the most serious and general criticism against the diffusion storage mechanism is the fact that occasionally we should expect the inner region of the solar system to be filled with solar cosmic rays from a flare

occurring on the back side of the sun, as discussed in reference [2]. Certainly no events of the magnitude observed in the 1956 flare have been detected under these circumstances, but there is increasing evidence for smaller increases to be observed (especially using the low energy sensitive neutron monitor) when no flares are present on the visible side of the sun. For example, an

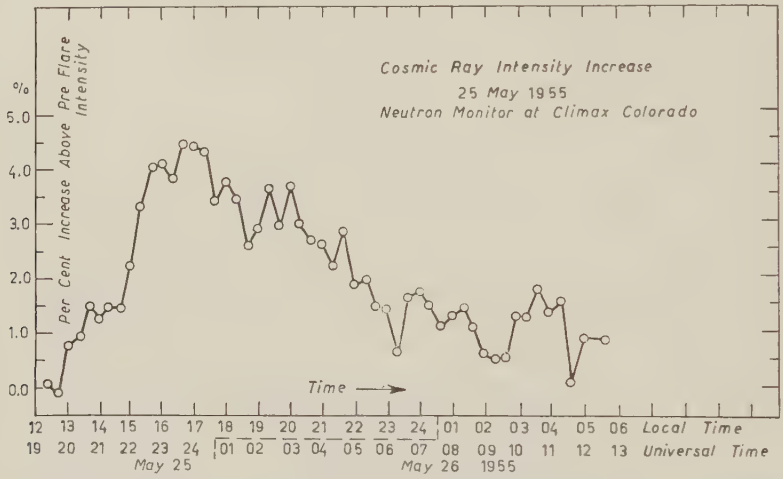
Cosmic Ray Intensity Increase
25 May 1955
Neutron Monitor at Climax Colorado
Per Cent Increase Above Pre Flare Intensity
%
5.0
4.0
3.0
2.0
1.0
0.0
Time
12 13 14 15 16 17 18 19 20 21 22 23 24 01 02 03 04 05 06 Local Time
19 20 21 22 23 24 01 02 03 04 05 06 07 08 09 10 11 12 13 Universal Time
May 25
May 26
1955

Fig. 13. – An increase of cosmic ray intensity not associated with an observed solar flare. A coincident, but smaller, increase was observed at Sacramento Peak.

intensity increase of 4.5% occurred at Climax on 25 May 1955, with a smaller, but coincident, increase at Sacramento Peak. The radiation producing this increase has a steeper spectrum than the non-solar radiation. The increase at Climax is shown in Fig. 13. A search for a solar event at that time has led to a negative result. Two additional but larger increases have also been observed in the Antarctic. We cannot prove that these increases arise from backside solar flares, but this is a reasonable possibility.

11. – Concluding remarks.

Even though the solar conditions and the distribution of interplanetary fields may differ in detail for each of the five great cosmic flare events, it is likely that the dominant mode of propagation in the solar system is the same for all five events. If so, this raises the question of why some great flares produce cosmic rays and others do not appear to do so.

There are at least two possibilities:

1) the onset of the flare with its sudden release of energy from a small

volume is fundamentally a non-linear process which may require the attainment of special conditions before the particles are accelerated and ejected at cosmic ray energies, or

2) the mode of propagation from the region of production may allow particles to reach the earth from great flares at some times but not at other times.

At present we cannot decide conclusively between these, or other alternatives.

Although the discussion in this paper has been concerned with physical behavior of radiation after production, it is obvious that these studies lead us to estimates of important parameters [2] (such as energy densities in the flare, energy and composition spectra of the particles at production, etc.) concerned with the unsolved problem of particle acceleration at the sun.

* * *

The author is particularly indebted to Dr. D. C. Rose (National Research Council, Ottawa, Canada) for permission to use the one minute interval recording of neutron intensity data at Ottawa. The compilation of data on the February 1956 flare prepared by Dr. H. Elliot and Dr. T. Gold was extremely valuable.

REFERENCES

[1] R. Lüst and J. A. Simpson: *Phys. Rev.* **108**, 1563 (1957).
[2] P. Meyer, E. N. Parker and J. A. Simpson: *Phys. Rev.*, **104**, 768 (1956). This paper is mainly concerned with the cosmic ray effects at late times, i.e. isotropy, spectrum, storage mechanism.
[3] L. I. Dorman, N. S. Kaminer, V. K. Koiava, Ju. G. Shafer and B. F. Schwarzman: *Nuclear Physics*, **1**, 585 (1956).
[4] A. Sittkus, W. Kühn and E. Andrich: *Zeits. f. Naturf.*, **11***a*, 325 (1956).
[5] D. C. Rose and J. Katzman: *Can. Journ. Phys.*, **34**, 884 (1956).
[6] J. Firor: *Phys. Rev.*, **94**, 1017 (1954).
[7] F. S. Jory: *Phys. Rev.*, **103**, 1068 (1956).
[8] R. Lüst: *Phys. Rev.*, **105**, 1827 (1957).
[9] A. Ehmert: *Proceedings of the Conference on Cosmical Electrodynamics*. Stockholm, Sweden, September 1956.
[10] M. Notuki, T. Hatanaka and W. Unno: *Pub. Astro. Soc. Jap.*, **8**, 52 (1956).
[11] S. Hayakawa: private communication.
[12] G. Cocconi, K. Greisen, P. Morrison, T. Gold and S. Hayakawa: in this issue, p. 161; and private communication by G. Cocconi, T. Gold, K. Greisen S. Hayakawa and P. Morrison: received 18 September 1957.

[13] H. W. Babcock and H. D. Babcock: *Astrophys. Journ.*, **121**, 349 (1955).
[14] S. E. Forbush, P. S. Gill and M. S. Vallarta: *Rev. Mod. Phys.*, **21**, 44 (1949).
[15] J. Sekido and K. Murakami: *Proceedings of the International Conference on Cosmic Rays*, Guanajuato, Mexico, 1955.
[16] S. E. Forbush: private communication.
[17] A. G. Fenton, K. G. McCracken, N. R. Parson and P. A. Trost: *Nature*, **177**, 1173 (1956). We are indebted to Dr. Fenton for his review of his ionization data.
[18] S. E. Forbush, T. B. Stinchcomb and M. Schein: *Phys. Rev.*, **79**, 501 (1950).
[19] D. Eckartt: *Proceedings of the Conference on Cosmical Electrodynamics*, Stockholm, Sweden (1956); E. A. Brunberg and D. Eckartt: *Tellus*, **8**, 508 (1956).
[20] F. Bachelet and A. M. Conforto: *Nuovo Cimento*, **3**, 1153 (1956).
[21] L. Davis: *Phys. Rev.*, **100**, 1440 (1955).
[22] K. Kawabata, I. Kondo, K. Murakami and M. Wada: in this issue, p. 169.

INTERVENTI E DISCUSSIONI

— L. Biermann:

Around a rotating celestial body, which is the seat of a magnetic field, there must be a region which rotates as the surface of the star or planet in question. That is to say, the interplanetary or interstellar gas in this co-rotating region belongs in a sense to the star, in spite of the fact, that it will in general extend far beyond the ordinary outer atmosphere; in the case of the sun the corona extends to approximately five or ten solar radii, whereas according to an estimate by Lüst the co-rotating sphere should extend to perhaps the orbit of Mercury.

In connection with the interpretation of the observation on February 23, 1956, it seems suggestive to regard this co-rotating region as the place, where the low energy part of the solar « cosmic » radiation has been stored during the first about 8 minutes after the outburst. Since the magnetic lines of force must be assumed to close within this region, the magnetic field which might have the character of one of the force-free models studied by Lüst and Schlüter (*Zeits. f. Astrophys.*, **34**, 263 (1954)) should well be able to act in this way.

On the other hand, the work on the comets, referred to in another connection, leads also to the conclusion, that the co-rotating sphere around the sun, does not extend to the neighbourhood of the earth, since then the comets' tail should behave quite differently than it is observed.

SUPPLEMENTO AL VOLUME VIII, SERIE X
DEL NUOVO CIMENTO

N. 2, 1958
2° Trimestre

The Cosmic Ray Flare Effect.

G. Cocconi, K. Greisen and P. Morrison

Laboratory of Nuclear Studies, Cornell University - Ithaca, N. Y.

T. Gold

Harvard College Observatory - Cambridge, Mass.

S. Hayakawa

Research Institute of Fundamental Physics, Kyoto University - Kyoto

1. – General considerations.

In trying to devise a model to explain the sudden increases of cosmic rays observed on the earth following some solar flares, one has to face two major difficulties. Firstly, the magnetic fields which one has reason to suppose exist in the vicinity of the flare in the chromosphere of the sun and that extend out through the corona are of such a strength that one would suppose them to maintain the cosmic ray particles in a comparatively small volume and allow them to diffuse out only at a very low rate. For the energies of the particles and the field strengths in question, one might estimate that Larmor radii might range from 50 km in the chromosphere or inner corona to 50 000 km at three or four solar radii above the surface. One is neither entitled to assume that a magnetic path exists that to a sufficient precision links the earth with a point near the sun where the cosmic rays were produced, nor is one entitled to assume a sufficient rate of drift of particles out of such fields to produce an onset that rises to a maximum at the earth within a few minutes. It is thus necessary to find a mechanism by which the cosmic rays can be quickly liberated or quickly distributed through a large volume near the sun so that a magnetic path to the earth is no longer extremely unlikely.

The second major problem concerns the magnetic fields that must exist at distances from the sun as great as or greater than the earth's distance in order to account for the arrival of particles in the late stages of the flare effect from all or at any rate a great variety of directions. The magnetic guidance of the particles must be such as to allow them to arrive here quickly in the first place, but to give later the appearance of being diffused.

The first problem we think has to be overcome by the assumption of a co-operative propagation mechanism for cosmic rays. Whilst any single particle might be constrained by the field, it is clear thet there is a limit on the constraining force that the fields can exert. At too high a cosmic ray pressure, the cosmic ray flux will itself alter the magnetic fields and cause motions of the ordinary gas whose currents produce these fields. We suppose that when in certain circumstances the total cosmic ray flux exceeds a certain amount, the containment of the particles becomes unstable and they can suddenly leak out from the front of the region in which they were contained into all or a great number of directions. Perhaps this problem is analogous to the Taylor instability in hydrodynamics and perhaps the instability leads to channels being established in the ordinary gas where gas and the fields that it carried are removed to the sides and the pressure replaced by cosmic ray particle pressure within. Such channels could be of small diameter, namely of the order of magnitude of Larmor radii, and very many of them might be set up so that essentially the cosmic rays can now propagate through the fields. Such a process would not only explain how the particles get out from the strong solar fields, but it would also explain the essential threshold nature of the flare effect. All the cosmic ray flare effects that have been seen have been very well above the threshold of measurement, and by comparison with any other properties of flares, one would have expected a very great number of weaker effects that would still have been easily measurable in the same interval of time. The absence of this very large number of slightly weaker effects certainly requires an explanation in terms of some threshold in the phenomenon. We would thus suppose that a great many flares, if not all, produce cosmic ray particles, but that only those that produce a sufficient total flux to burst through the containing fields can show up on earth as a sudden increase in the cosmic ray rate. (There may, of course, be a different effect, namely that associated with the small flares which might allow a slow diffusion out, and therefore a very gradual contribution to the cosmic ray flux.) This instability would tend to allow particles to escape only into a hemisphere above the surface of the sun, or even a smaller region, and this might account for the absence of any large flare effects from the flares that must have occurred on the back of the sun; for there is good reason to identify all five observed cosmic ray effects with phenomena on the near side of the sun.

2. – Idealized cases of cosmic ray propagation.

We assume a burst of cosmic rays, idealized as a δ function in time for each momentum interval, propagating toward the earth in a space where a general magnetic field pre-exists, with an overall direction sun-earth, diverging

away from the sun, and trailing the sun's rotation. This is discussed again in Part III.

The problem now consists in determining the time and the space distribution of cosmic rays reaching the earth. In order to take one step at a time, consider an oversimplified case: the cosmic ray source is an infinite plane, the front up to which co-operative propagation has been effective, of intensity *constant* in time (not a δ-function now), monoenergetic, and isotropic,

$$i(\theta, \varphi, t) = I_0 \quad (\mathrm{m^{-2}\ s^{-1}\ sr^{-1}})$$

and that a homogeneous field, H, perpendicular to it, extends from the sun to the earth (Fig. 1). Then at the earth the intensity is:

$$i(\theta, \varphi, t) = I_0 = \text{constant} \qquad (\theta \leqslant \pi/2)$$

because, according to the Liouville theorem, any direction for which $\theta \leqslant \pi/2$ is an allowed direction for cosmic rays to reach the earth, and, at the source, i is independent of θ. Note, however, that:

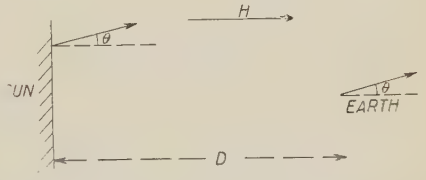

Fig. 1 – Geometry of the idealized case.

a) To each direction (θ, φ) with $\theta < \pi/2$ at the earth, there corresponds a unique point on the source plane.

b) H being homogeneous, the orbits that connect the earth to the source plane terminate all on the plane inside a circle of radius

$$R = 2\varrho = 2\left(\frac{pc}{ZeH}\right)$$

(ϱ = radius of curvature of a particle moving perpendicularly to the field). It follows that the source plane need not be infinite in order to supply at the earth orbits with $\theta < \pi/2$, but must only be of dimensions of the order of R around the foot of the straightest path sun-earth. A representative value for R is ($H = 10^{-4}$ gauss, $pc = 5 \cdot 10^9$ eV, $Z = 1$) $R = 3 \cdot 10^{11}$ cm = 2 solar diameters.

c) The pitch angle θ of the trajectory is a constant along the whole path from sun to earth.

d) The time spent by a particle in going from the source to the earth is

$$t = \frac{D}{v \cos\theta} = \frac{t_0}{\cos\theta}, \qquad \text{where } t_0 = \frac{D}{v} \approx 8 \text{ min.}$$

If now cosmic rays are emitted from the same plane but only for a short period, which we approximate as a δ-function, their intensity on the earth can be found. At the source:

$$i(\theta, \varphi, t)\,\mathrm{d}t\,\mathrm{d}\Omega = I_0 \delta\left(\frac{t}{t_0} - \frac{1}{\cos\theta}\right)\mathrm{d}t\,\mathrm{d}\Omega\,. \tag{1}$$

At the zenith angle, θ, on earth the radiation arrives at time $t = t_0/\cos\theta$, with an average intensity which can be obtained by integrating the differential intensity i over the finite solid angle $\Delta\Omega$ of the detector on earth. Neglecting effects of the earth's magnetic field,

$$i(t, \Delta\Omega) = \frac{\int\limits_{\Delta\Omega} i(\theta, \varphi, t)\,\mathrm{d}\Omega}{\int\limits_{\Delta\Omega}\mathrm{d}\Omega}\,.$$

Using (1), and setting $\cos\theta = \mu = 1/w$ for the integration,

$$i = \frac{I_0}{\Delta\mu}\int \delta(w - t/t_0)\,\frac{\mathrm{d}w}{w^2}\,,$$

$$= \frac{I_0}{\Delta\mu}\,(t_0/t)^2 \qquad \text{after } t = t_0,$$

$$= 0 \qquad \text{before } t = t_0;$$

this function is plotted in Fig. 2.

In order to interpret the general observations more realistically, the following features must be considered:

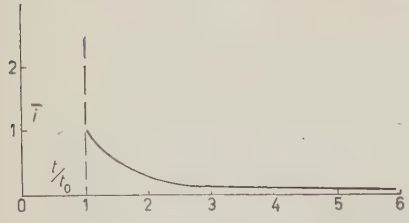

Fig. 2. – Behaviour of the C. R. intensity in the idealized case.

1) The field between sun and earth is not homogeneous, but of decreasing intensity the farther one goes from the sun. Indeed, this is required by the model, for a small area, of solar size, must be connected by lines of force to a much larger area near the earth's orbit. In this case the large θ's will be missing at the earth, and the intensity will decrease faster than in the model of constant H.

2) Particles of various momenta, pc, can appear on the front of the region to which co-operative propagation has been effective at slightly different times, and consequently the intensity at the earth may be the sum of many curves similar to that of the figure, but slightly displaced in time.

3) In order to evaluate the intensity of cosmic rays *observed* in the lower earth atmosphere, one has to consider that, at $t \approx t_0$, only particles with $\theta \approx 0$ arrive on the earth; these particles arrive vertically only in the impact zones. Later, θ increases and the regions that can be hit vertically change position on the earth, forming rings that correspond to the impact zones of particles arriving at angle θ from the sun and with various azimuths (at a given time cosmic rays arrive from all φ's with the same intensity).

4) Not all flares give rise to an emitting front, as its formation depends on the density of energy in the plasma. Nor do all the flares which have an emitting front give cosmic rays that invest directly the earth. This happens only when there is a magnetic field connecting the front with the earth. The last condition probably explains why the few flares observed to produce cosmic ray increases on the earth are grouped toward western longitudes on the sun; the rotation of the sun favors the formation of fields bent in that direction.

5) The existence of flares with emitting fronts, not magnetically connected with the earth, can possibly explain the correlation between flares and small cosmic ray increases. These flares inject cosmic rays which reach the earth only through diffusion; no sharp, high peaks of cosmic ray intensity are thus observed.

3. – The magnetic field between the earth and the sun.

The cosmic ray evidence during the solar flare events is probably the best available for judging the structure of magnetic fields in the earth-sun region. In the great flare event of February 23, 1956, there is no doubt that the stream of particles first reached the vicinity of the earth from some common direction which was, as near as can be judged, that to the sun, whilst the incoming particles later, after half an hour, came in, as near as could be judged, isotropically. This fact alone provides the most definite indication that one has at present of the existence of magnetic fields in large regions that are of sufficient strength to deflect particles coming from the sun at energies of several GeV by angles of at least 90° before approaching the earth's own magnetic field. If such fields have the structure of turbulent eddies, each small compared with the earth-sun distance, and dispersed at sufficient density to account for the gradual decay of the cosmic ray intensity after the event, and for the isotropic arrival, then such clouds would make it impossible to account for the sudden steep onset in the initial phase of the event. It is clearly necessary to suppose the fields to be so shaped as not to impede much the initial particles that we may assume to have started out in a favorable direction to reach the

earth, but at the same time to trap for longer periods of time a sufficient portion of the particles to make up the decaying part of the intensity curve. Such trapping must occur in a region that contains the sun and the earth; it cannot be confined to the neighborhood of the sun, for then the isotropy in the late phase could not be accounted for. SIMPSON *et al.* have for this purpose suggested that the field between the earth and the sun is weak enough to allow a more or less unimpeded transmission of particles, but that at short distance beyond the earth there occurs a magnetic reflecting screen so that the particles remain trapped for some time within this screen. It may not be necessary, however, to go to a model which is, from the astronomical point of view, very artificial, and which requires a high factor in the magnetic field strengths between the inner and the outer regions, in the opposite sense from that which would be expected, as well as a very particular position of the reflecting screen and a high reflectivity of it in order to account for the rather simple shape of the intensity time curve.

We have seen that an elongated field between the sun and the earth would not interfere with the initial phase. If this elongated field were, in fact, parallel, the shape of the intensity time graph could be accounted for. But no such accurate parallelism as would be required can reasonably be assumed. A small divergence of the field would rapidly steepen the flat spirals of the trajectories, and thereby greatly reduce the number of particles that will arrive with a long delay. We therefore propose a model in which elongated tongues of mag-

Fig. 3. – The shape of a solar magnetic tongue, viewed in the Sun's meridian plane.

netic field extend out from the sun to some region beyond the earth, which are capable of the rapid transmission as well as the trapping of particles, as sketched in Fig. 3.

An outburst of gas from the sun of the sort that causes magnetic storms on the earth and very likely, in some geometrical conditions, the « Forbush decreases » of cosmic rays, must originate from some regions on the sun that contain significant magnetic fields. Whatever the local shape of the fields might be at the beginning, they will be drawn out into an elongated tongue. In the solar corona, such shapes are frequently recognized and are evidently common. No indications appear in any of the visible parts of the solar corona of any turbulent or ill-organized motion, but on the contrary, all shapes seen indicate smooth, non-turbulent patterns of flow. Do these rather regular patterns that can sometimes be seen out to eight solar radii in fact extend out

to the vicinity of the earth, or must they be expected to break up into turbulent eddies in between?

To understand this, it would be necessary to formulate the theorem that defines the smallest scale of turbulent eddies in a tenuous magnetized gas. The organizing length in a non-magnetic gas would be assumed to be the mean free path at the molecular impact velocities that are occurring. Eddies that are so small that they are only a few mean free path across would decay very rapidly, and therefore below a certain size the transfer of turbulent energy by viscosity into heat will occur directly and without the generation of smaller eddies.

In the case of a magnetized gas, a shorter mean free path becomes the organizing length in some cases, namely the mean free path measured along the particle orbits. For motions normal to the magnetic field, the straight measure will thus be of the order of the Larmor radius, whilst it will be the ordinary mean free path for motion along the field. The viscous dissipation of an arbitrary eddy would thus be impeded by the magnetic field only in some directions and not in others, and thus the smallest possible scale of eddies of a pattern resembling that of isotropic turbulence is not likely to be much diminished by the presence of the field. (This, of course, does not imply that smaller patterns may not exist where particular conditions of motions and fields are satisfied by which the viscous dissipation is very greatly reduced. Presumably somewhat special conditions are required to set up these shapes.)

As the earth-sun region corresponds to only a small number of mean free paths at the gas velocities in question, one may well expect that no general turbulence is established by a solar stream on this scale. In that case, there would be no reason to expect any different shapes of the magnetic fields from the type of patterns seen in the corona, with the exception of the possibility that the fields may not be strong enough to enforce rigid body rotation of such a tongue out to the distance of the earth. The tongue may thus be bent so that the outer part lags behind the inner, as suggested in Fig. 4.

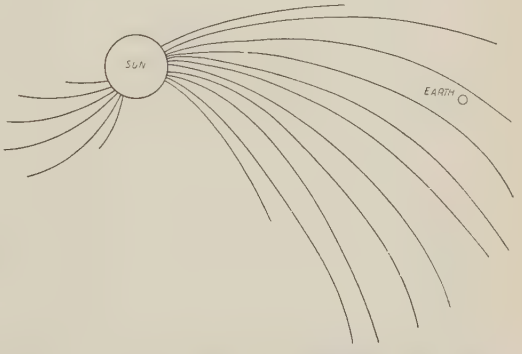

Fig. 4. – Distortion of magnetic tongues by solar rotation.

The indications from pictures of the corona are that tongues like this may exist over a wide range of latitude on the sun, but that they are much more common in the equatorial regions. At some distance from the sun, the preponderance of equatorial

zone tongue should become much enhanced by the centrifugal force. This would assist in providing a force to draw out the magnetic field in the equatorial plane, as well as to bend tongues originating at other latitudes toward the equatorial plane. It is suggested that this is the reason for the very high precision with which, in the 1954 eclipse, the equatorial extensions of the corona were found to be aligned. At the earth, effects have also been noted which may be explained in terms of a very sharp concentration in the equatorial plane. Magnetic storm activity is greatly enhanced at certain periods, which unfortunately cannot be sufficiently sharply defined to make the distinction between the equinoxes and the time of crossing the sun's equatorial plane. No reason has ever been found for ascribing this marked enhancement to any effect connected with the equinoxes themselves.

That at the 1956 flare the earth should have been in such a tongue is made more likely by the observation that the effect occurred in the midst of a Forbush decrease; for this may be interpreted as the result of the earth's position in a rapidly expanding mass of gas into whose magnetic fields the external cosmic ray flux has not yet fully penetrated.

The propagation of cosmic ray particles liberated at the base of such a tongue can be described approximately. In detail it would, of course, be a formidable task of orbit calculation. The fact that the field is much elongated radially will allow a rapid propagation outwards for all the particles that started in approximately the outward direction. The fact that the field is diverging will turn particles more nearly in this direction. On the other hand, if the field strengths are adequate, the whole tongue can eventually get filled with cosmic rays proceeding with widely varying pitch angles relative to the field. The process should be approximately represented by the idealized model discussed earlier in the paper. The co-operative propagation mechanism that must have been present at the time of injection of particles into this « magnetic bottle » will have ceased at a later stage, and there is no reason why the converging field near the sun should not act as an efficient reflector. The « bottle » is then shut except for particles of very steep pitch, and except for the drift across the curved parts of the field. There is now no very particular position of magnetic screens required to explain the intensity-time curve of the phenomenon, for the earth may be placed almost anywhere within this tongue and still one could expect to see (i) a rapid initial rise as the region filled with cosmic rays initially spiralling with a steep pitch around a line from the solar direction, (ii) a later decay with a good approximation to isotropy, as the full bottle slowly empties.

SUPPLEMENTO AL VOLUME VIII, SERIE X
DEL NUOVO CIMENTO

N. 2, 1958
2° Trimestre

On the Unusual Increase and the Modulation of Cosmic Rays.

K. KAWABATA

Tokyo Astronomical Observatory - Tokyo

I. KONDÒ, K. MURAKAMI and M. WADA

Scientific Research Institute - Tokyo

1. – Introduction.

The intensity variations at the time of the unusual increases had been explained by one of the authors as follows [1] (Fig. 1).

1) Acceleration of the particles up to the cosmic-ray energies takes place in the vicinity of the solar flare.

2) These particles are first trapped in a volume of radius of 0.2∼0.4 A.U., then emitted from this sphere to the interplanetary space. These particles arrive at the earth through a fairly straight line and cause the increase at the impact zone.

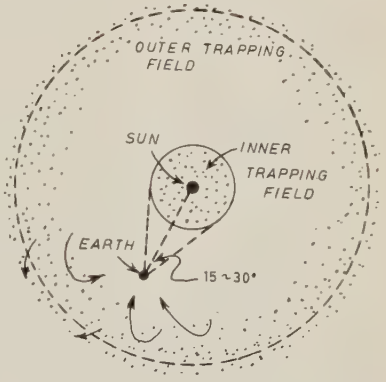

Fig. 1. – The model for the unusual increases proposed by SEKIDO and MURAKAMI [1].

3) Another trapping field, which has a dimension of the order of several A.U., scatter back and store these particles for several hours. These scattered back particles make the increase in the background and the polar regions.

At a first glance, the increase of February 23, 1956, seems difficult to be explained by the above mentioned model. Because:

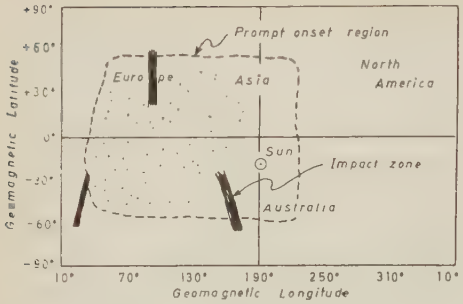

Fig. 2. – The observed region of prompt onset and the position of the impact zone calculated from the orbits.

The prompt onset zone (where the increase started at about 0345 U.T.) extends over a fairly wide longitudinal region, and this may not be explained in terms of the inner trapping field (Fig. 2).

In order to investigate the phenomena, however, one must consider the influence of the electromagnetic conditions in the interplanetary space at the time of the increase, since the cosmic-ray intensity suffered a large modulation for a week or two before the commencement of the increase.

This large intensity decrease was a typical example of cosmic-ray storm. In the previous paper [2], the authors tried to explain these cosmic-ray storms as the results of the modulation of cosmic-ray particles caused directly or indirectly by the magnetic clouds emitted from the sunspot groups. From the fact that the cosmic-ray intensity suffered a large decrease already before the flare, it is likely to suppose that the sunspot groups which were responsible for the large solar flare of February 23, already emitted a number of the magnetic clouds which were permeating in the interplanetary space at the time of the increase. From the observed cosmic-ray variation (Fig. 3), one can estimate the scale of the region which was occupied by these magnetic clouds. As can be seen from Fig. 3, the disturbed region might have a large extension. If one assumes that the sunspots emit these clouds in a 45° semiangle cone, with velocities of 400∼1000 km/s, the envelope of the disturbed region may have a shape as shown in Fig. 4.

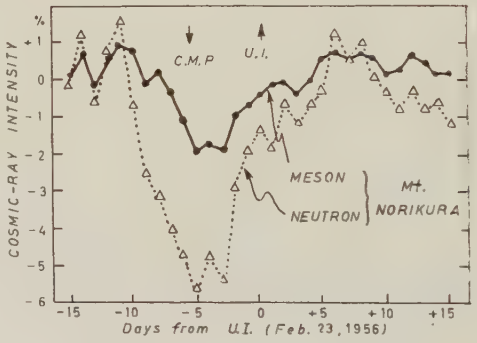

Fig. 3. – The variation of cosmic-ray intensity and its relation to the central meridian passage (C.M.P.) of the sunspost groups and the unusual increase (U.I.) of Feb. 23, 1956.

To explain these experimental facts, the following arguments were suggested by BROWN [3]:

1) The cosmic-ray particles which travel through the outer region of he stream in fairly straight orbits may form the prompt onset zone.

2) The cosmic-ray particles which travel through the disturbed region suffering many collisions with clouds, may reach the earth from all directions at the later time.

To test his hypothesis, we calculated the intensity variation at the earth, assuming a conical shape diffusing medium which has the apex at the sun. It was found from the calculation, however, that this model does not fit with the experimental results because, assuming a reasonable aperture of the cone, one may find that the intensity decays as $t^{-\frac{5}{2}} \sim t^{-\frac{7}{2}}$ which contradicts the observed value $t^{-\frac{3}{2}}$ [4].

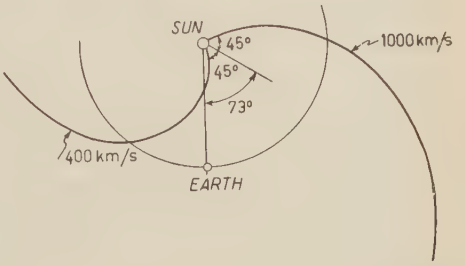

Fig. 4. – The envelope of the region occupied by the magnetic clouds emitted from the sun, assuming the velocities of the cloud to be 400∼1000 km/s.

This results suggest that the particles are diffused out very quickly from the boundary and cannot travel through the cone for a large distance (say 1 A.U.) without being scattered out.

2. – A model for the increase on Feb. 23.

It was postulated by the authors that the particles which travel through the outer region may be injected into the disturbed region from the boundary and these particles cause the increase at the prompt onset zone. Also these particles are trapped in the disturbed region and scatter back to the earth to form the late onset zone. In this case, the intensity maximum at the late onset zone will occur when the injection of the particles is almost ended. Or in other words, when the number of particles which are injected from the boundary and are scattered out become the same.

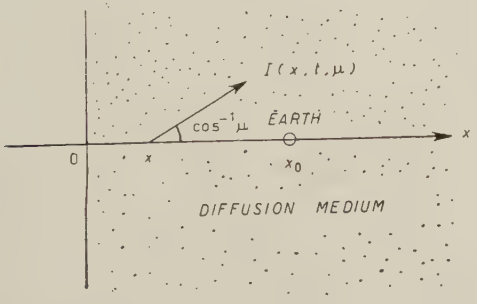

Fig. 5.
The model used in the calculation.

So if one assumes that the incident intensity decreases as exp $[-t/\tau]$ after passing its maximum, the intensity at the late onset zone will reach its maximum at $t \approx \tau$. In order to confirm this picture, the authors made calculations using the following model.

1) As the earth lies near the boundary (Fig. 4), and at least at

the early stage of the increase the injected particles may be confined in a region not far from the boundary, the approximation of a infinitely wide plane boundary can be used (Fig. 5).

2) The distance of the earth from the boundary can be estimated from Fig. 4 as 0.3∼0.5 A.U.

The calculation was carried out as follows:

$$\frac{1}{c}\frac{\partial I}{\partial t}+\mu\frac{\partial I}{\partial x}=-\varkappa I+\frac{\varkappa}{2}\int_{-1}^{+1}I(x,t,\mu)\,d\mu;$$

putting

$$I=\begin{cases} I_+(x,t) & \text{for} \quad \mu>0 \quad \text{so} \quad \bar{\mu}=\dfrac{1}{\sqrt{3}}, \\ I\ (x,t) & \text{for} \quad \mu<0 \quad \text{so} \quad \bar{\mu}=-\dfrac{1}{\sqrt{3}}, \end{cases}$$

using the boundary condition

$$I_+(0,t)\begin{cases} =0 & \text{for} \quad t<0\,, \\ =\exp\left[-t/\tau\right] & \text{for} \quad t\geqslant 0\,, \end{cases}$$

and the initial condition

$$I_+(x,0)=I_-(x,0)=0 \qquad \text{for} \quad x\neq 0,$$

I_+ and I_- were calculated for $x=x_0=0.3$ A.U., $\tau=20$, 40 min, the diffusion mean free path $\lambda=1/\varkappa=0.52$, 0.26, 0.13 A.U. as the function of t.

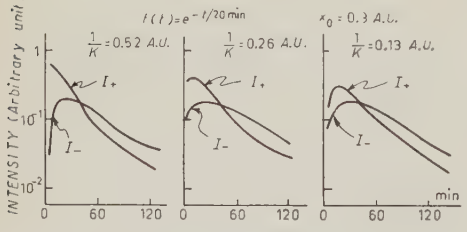

Fig. 6. – The intensity variations calculated from the model for $\tau=20$ min.

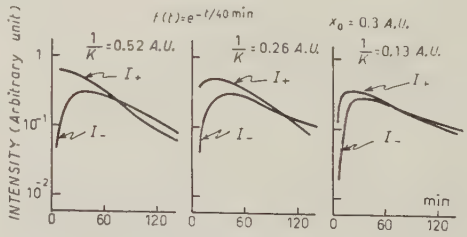

Fig. 7. – The intensity variations calculated from the model for $\tau=40$ min

The results are plotted in Fig. 6 and 7. The asymptotic solution of this transfer equation has a form $t^{-\frac{3}{2}}$. The case for $\tau=20$ min may fit the increase on February 23, 1956.

3. – Discussion.

The model presented in the preceding section suggests the following points.

1) By carefully examining the intensity-variations for the time intervals which include the unusual increases (Fig. 8), it can be suggested that on each occasion, the earth was situated in the disturbed region, regardless of the amount of disturbances by the magnetic clouds. This leads us to conclude that the scattering and the storage of the particles might have occured by the presence of these clouds. If one assumes $\int_{\text{sun}}^{\text{earth}} \varkappa \, dr \approx 1$ in all cases, the prompt onset was caused by the particles which came directly from the sun, and the late onset was caused by the trapped particles. After the emission has ceased the trapped particles are gradually diffused out. The end of the $t^{-\frac{3}{2}}$ decay of the intensity depends on the depth of the diffusing medium measured by λ.

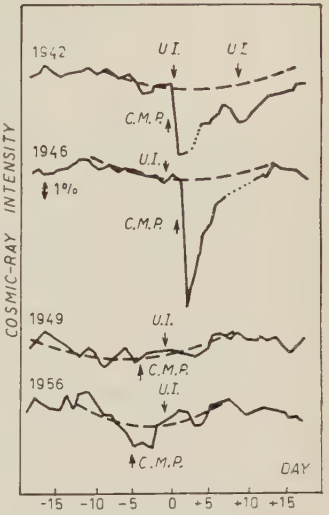

Fig. 8. - The intensity variations for the time intervals which include the unusual increases. The data are from LANGE and FORBUSH [6] and from the record at the Scientific Research Institute, Tokyo.

2) The difference in the delay of the maximum time at the late onset zone from that of the prompt onset zone can be explained by assuming different τ for different flares and τ may be determined from the intensity curve of the flare (Fig. 9).

3) The experimental fact that the prompt onset zone extends to the east but not to the west from the impact zone which is calculated from the orbits directly connecting the sun and the earth (Fig. 2), would be explained by this model, because the boundary is not parallel to the earth's orbit but facing to the eastern side of the sun.

4) If the earth is not situated in the disturbed region, the increase may be observed only at the impact zone of a narrow longitudinal width, so the world wide increase does not occur. This condition may be satisfied when the flare occurs at the eastern limb or in the backside of the sun. Also if the disturbed region has a too small diffusion m.f.p., the observed increase will be smaller for all directions. These facts may explain the rarity of the unusual increase.

5) The inner trapping field which was assumed before, may not be needed in order to explain the width of the prompt onset zone.

6) From the calculated intensity variation, the following features may

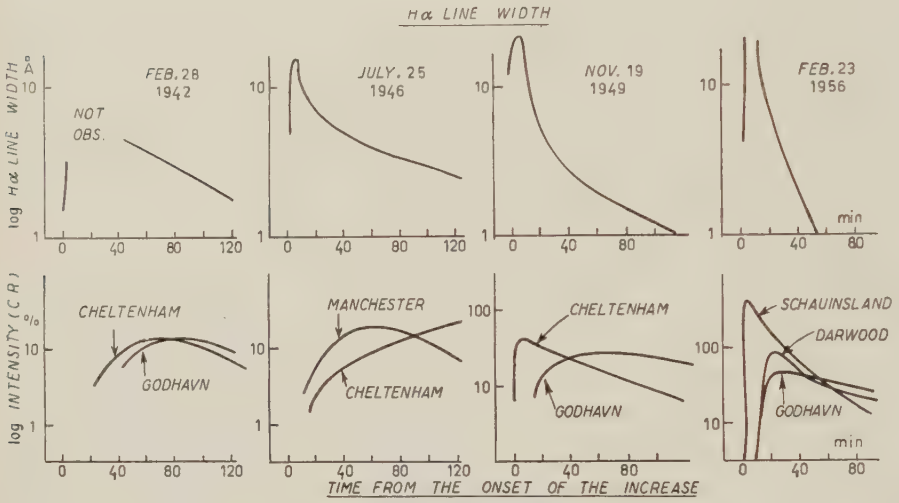

Fig. 9. – The intensity curves for the flare and the unusual increases. The data for the flares are from Ellison [7, 8], Ellison and Conway [9] and Notuki [10]. The data for cosmic ray intensity are from Forbush, Stinchcomb and Schein [11], Dolbear and Elliot [12], Forbush [13], and Sittkus [14].

be suggested for the shape of the energy spectrum of the particles observed at the earth:

a) The energy spectrum of the particles which falls in the prompt onset zone may be less steeper than that at the emission from the sun.

b) The energy spectrum at the late onset zone is rather similar to that at the emission.

c) The energy spectrum at the decaying portion of the intensity variation is steeper than that at the emission.

7) The diffusion m.f.p. λ must be comparable to x_0 in order to explain the observed intensity variation. This fact rejects the hypothesis that these clouds reduce the intensity of the preexisting cosmic ray particles for a long time interval [5].

REFERENCES

[1] Y. Sekido and K. Murakami: *Report at Mexico Meeting* (1955).
[2] Y. Sekido, M. Wada, I. Kondò and K. Kawataba: *Rep. Ionosphere Res. Jap.*, **9**, 174 (1955).
[3] R. R. Brown: *Journ. Geophys. Res.*, **62**, 147 (1957).
[4] P. Meyer, E. N. Parker and J. A. Simpson: *Phys. Rev.*, **104**, 768 (1956)l
[5] P. Morrison: *Phys. Rev.*, **101**, 1397 (1956).
[6] I. Lange and S. E. Forbush: Pub. 175, Vol. XIV of Carnegie Institution of Washington (1948).
[7] M. A. Ellison: *Month. Not. Roy. Astr. Soc.*, **103**, 3 (1943).
[8] M. A. Ellison: *Month. Not. Roy. Astr. Soc.*, **109**, 3 (1949).
[9] M. A. Ellison and M. Conway: *Observatory*, **70**, 77 (1950).
[10] N. Notuki: private communication.
[11] S. E. Forbush, T. E. Stinchcomb and M. Schein: *Phys. Rev.*, **79**, 501 (1950).
[12] D. W. N. Dolbear and M. Elliot: *Nature*, **159**, 58 (1947).
[13] S. E. Forbush: private communication.
[14] A. Sittkus: *Zeits. f. Naturf.*, **11***a*, 325 (1956).

SUPPLEMENTO AL VOLUME VIII, SERIE X
DEL NUOVO CIMENTO

N. 2, 1958
2° Trimestre

Impact Zones for Solar Cosmic Ray Particles (*).

R. LÜST (**)

The Enrico Fermi Institute for Nuclear Studies
The University of Chicago - Chicago, Ill.

Earlier calculations of sun-earth orbits show that cosmic-ray particles coming from the sun arrive at different impact zones on the earth because of their deflection in the geomagnetic field. The first zone is at 0900 hours local solar time for positively charged particles starting at the geomagnetic equator, the next one is at 0300 hours, and further zones are located at 2000 and 1300 hours. There are an infinite number of such zones, but only the first three impact zones are of major importance. The other zones cause the so-called « background radiation ».

For a better understanding of the observations of the flare event on February 23, 1956—especially of the observations during the first half hour of the cosmic ray increase—the orbit calculations were extended both in number of orbits and in their rigidity range [1], using the AVIDAC computer of the Argonne National Laboratory, Chicago.

Together with prior calculated orbits [2, 3] it was possible to determine the primary particle rigidities and the relative counting rates at the top of the atmosphere for different geomagnetic latitudes and longitudes at the earth, under the assumption that the particles, after leaving the sun are deflected only by the geomagnetic dipole field.

The counting rates at the top of the atmosphere depend essentially on the allowed opening angles in which particles arrive, on the range of allowed rigidities, and on the form of the differential rigidity spectrum at the source.

(*) Assisted in part by the Office of Scientific Research and the Geophysics Research Directorate, Air Force Cambridge Research Center, Air Research and Development Command, U.S. Air Force.

(**) Permanent adress: Max-Planck-Institut für Physik, Göttingen.

Since the observations were carried out deep within the atmosphere the principal contributions from primary particles coming from those arriving within 30° from the vertical and only orbits with zenith angles smaller than 32° were selected. Since the intensity increase was observed also at the geomagnetic equator, the particles must have had rigidities exceeding 10 GeV. It seems reasonable that the rigidity of the particles was not much above 30 GeV. Particles with rigidities below 1 GeV should not be able to contribute to an increase at sea level. Therefore, a rigidity range from 1 to 30 GeV was chosen in order to compute the counting rates.

The Chicago cosmic ray measurements [4] gave a differential rigidity spectrum proportional to N^{-8} (N = rigidity) near the earth for late times during the intensity increase. The source spectrum may have been quite steep, and therefore, the calculations of the counting rates were based on a rigidity spectrum proportional to N^{-6}. The observations indicate that the apparent size of the source was not very small, and therefore, the solid angle of the solar source was selected as $\pm 15°$ in latitude and $\pm 10°$ in longitude.

In Fig. 1 the relative counting rates at the top of the atmosphere are given as a function of the geomagnetic longitude or local time, for different geomagnetic latitudes. Here it was assumed that the position of the sun is at the geomagnetic equator and that the differential rigidity spectrum is a flat spectrum. Even with the very large solid angle of the solar source there still exist distinct impact zones. The magnetic rigidities of particles arriving close to the vertical

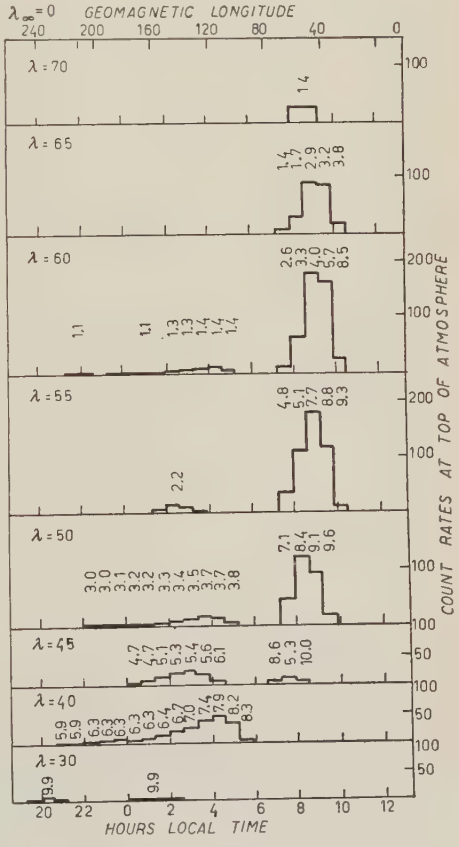
λ_M = 0 GEOMAGNETIC LONGITUDE
240 200 160 120 80 40 0
λ = 70
λ = 65
λ = 60
λ = 55
λ = 50
λ = 45
λ = 40
λ = 30
COUNT RATES AT TOP OF ATMOSPHERE
20 22 0 2 4 6 8 10 12
HOURS LOCAL TIME

Fig. 1. – The calculated counting rates expected at the top of the atmosphere as a function of the geomagnetic longitude or local time for different geomagnetic latitudes using a differential flat rigidity spectrum and assuming the sun at the geomagnetic equator. The numbers in the histograms refer to the mean rigidity (in GeV) of the particles arriving at the top of the atmosphere.

Fig. 2. – The calculated counting rates expected at the top of the atmosphere as function of the geomagnetic longitude or local time for different geomagnetic latitudes at the time of the February 1956 flare using a differential rigidity spectrum $\propto (pc/Ze)^{-6}$. These results are for the *Northern* hemisphere.

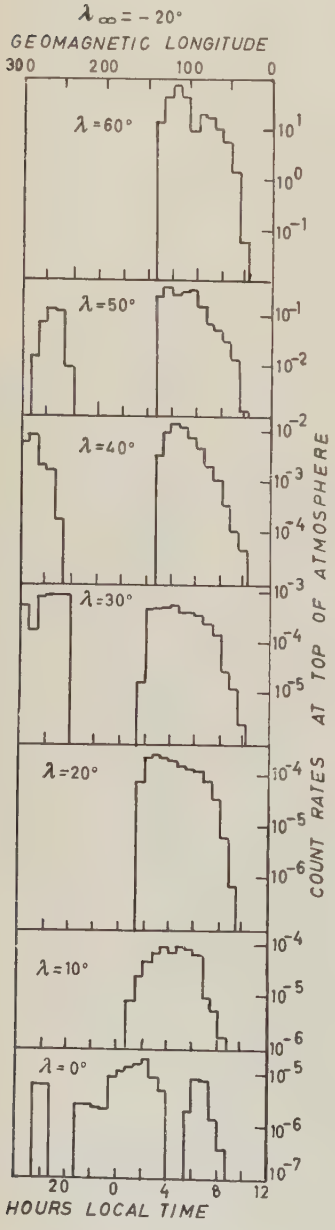

Fig. 3. – The counting rates at the top of the atmosphere (see Fig. 2). These results are for the *Southern* hemisphere.

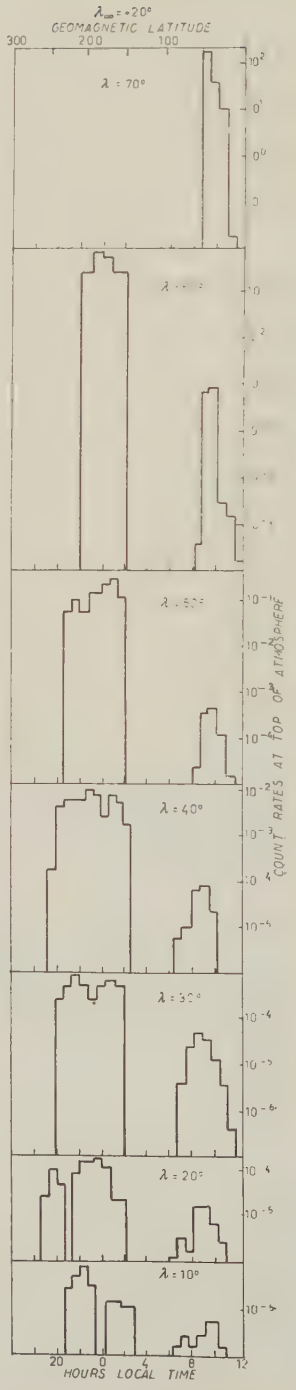

are different in different impact zones. For a fixed latitude, particles with highest rigidity arrive in the 900 hour zone, whereas particles of successively lower rigidity arrive in the 0300 and 2000 hour zones. Particles with rigidities very close to the geomagnetic cut-off rigidity at a given latitude produce background radiation for that latitude distributed over all geomagnetic longitudes.

The position of the sun at the time of flare onset was about 20° south of the geomagnetic equator. Fig. 2 and Fig. 3 show the relative counting rates at the top of the atmosphere for the northern hemisphere and southern hemisphere respectively. Here the steep rigidity spectrum was taken into account. Since the sun was south of the geomagnetic equator, the 0900 and 0300 impact zones merge into one broad impact zone in the northern hemisphere. The European and Russian stations were located in this zone, the stations of Chicago and Ottawa were located in the spread-out 2000 hour zone and are only able to receive particles of low rigidity. In the southern hemisphere the 0900 hour zone remains apart while the 0300 and 2000 hour zones merge. Since the rigidity spectrum is so steep, most of the radiation is of low rigidity, and contributes strongly to the spread-out 2000 hour zone. In this case the counting rates are much higher in this zone as compared to the results of the flat spectrum (Fig. 1) and are of the same order of magnitude as in the 0900-0300 hour zone. This is in agreement with the observation that maximum intensities for nucleonic component increases in Europe and North American are of the same order of magnitude.

From these results one must conclude that the particles which were the first to arrive on the earth during the flare onset on February 23 were those of high magnetic rigidity, while those of low rigidity only arrived later, because the prompt onset time was observed only in the merged 0900 to 0300 hour zone in the northern hemisphere and in the 0900 hour zone in the southern hemisphere.

REFERENCES

[1] R. Lüst and J. A. Simpson: *Phys. Rev.*, **108**, 1563 (1957).
[2] F. S. Jory: *Phys. Rev.*, **103**, 1068 (1956).
[3] R. Lüst: *Phys. Rev.*, **105**, 1827 (1957).
[4] P. Meyer, E. N. Parker and J. A. Simpson: *Phys. Rev.*, **104**, 768 (1956).

SUPPLEMENTO AL VOLUME VIII, SERIE X
DEL NUOVO CIMENTO

N. 2, 1958
2° Trimestre

On the Separation of Direct and Indirect Fractions of Solar Cosmic Radiation on February 23, 1956 and on the Difference in Steepness of Momentum Spectrum of These Two Components.

G. PFOTZER

Max-Planck-Institut für Physik der Stratosphäre - Weissenau

1. – Direct and deflected radiation.

It may be considered as a matter of fact that Solar Cosmic Radiation (S.C.R.) which was recorded as the hitherto observed five big flare effects partially entered the earth magnetic field in the direction from the sun, partially from widely distributed directions. The first kind of radiation, which may be defined as « direct fraction » will be received in the so called « impact zones », the second kind, the « deflected fraction » by other stations too.

This firstly was pointed out by SCHLÜTER [1] with respect to the flare effects between 1942 and 1949 in order to explain that besides stations in the impact zones also stations in forbidden zones, especially the polar stations, recorded intensity increases in the mentioned cases. Detailed analysis of the same events by FIROR [2] and SEKIDO and MURAKAMI [3] further confirmed this suggestion.

2. – Isotropy of deflected radiation.

If there were no distinct local deflection centers in planetary space which could act as secondary local sources and therefore no limited secondary impact zones could be expressed one has to assume that the stations in solar impact zones for some time interval recorded a mixture of derivatives from direct and also from irregulary deflected S.C.R.

With respect to the most important outburst hitherto observed on February 23, 1956, it was stated by MEYER, PARKER and SIMPSON [4] and in-

dependently by EHMERT and PFOTZER [5], that the components recorded in the decay phase of intensity increase should be attributed to an isotropic radiation outside the earth magnetic field.

This follows from the unique and practically undisturbed time law of intensity decrease recorded by all monitoring stations in the decay phase of the event.

3. Method of separation of direct and deflected fractions.

If we consider the isotropy of deflected radiation as true, than for this fraction usual Störmer theory holds. It follows that all stations to which the same effective geomagnetic cut-off rigidity can be attributed should have recorded the same intensity in the decay phase and vice versa. This offers a method to separate direct and deflected fractions in the impact zones.

For this purpose we have to find out for each station in the impact zone an adaquate station outside the impact zone with the same intensity record in the decay phase, precisely a station with the same cut-off magnetic rigidity.

If we subtract now the outside-impact-intensity from the impact intensity for all times than the difference will show the intensity time relation of direct radiation.

With the restriction, that we consider the assumed inner trapping field as part of the source we are able to determine evidently the duration of particle emission from the source.

4. – Duration of emission at the source, storage of deflected radiation.

Fig. 1 shows as example the results of the comparison of neutron counting rates in Weissenau [6] and Wellington Harbour [4] resp. Leeds [7] and Chicago [4]. The first station of each pair is located in the 5 h local time impact zone the second outside the impact zone. The practically equal counting rates in the decay phase besides may be considered as a criterium that the same geomagnetic cut-off is to be attributed to the corresponding stations. As according to Störmers theory the intensity of normal C.R. should be the same for each pair of stations, relative intensities $\Delta N/N$ of solar radiation measure the intensity of secondary neutrons in the same units N. Time and relative intensities both are plotted in a logarithmic scale.

From the difference of the two records resp. we recognize what is already well known that the earliest particles of direct radiation reached the earth roughly to the time of maximum development of the flare ($H_{\alpha\,\mathrm{max}}$). But we see further that the flux decreases rapidly at the end of the flare ($H_{\alpha\,\mathrm{normal}}$).

This may be considered as an evident proof, that the emission from the source did not exceed the duration of the optical phenomenon of the flare.

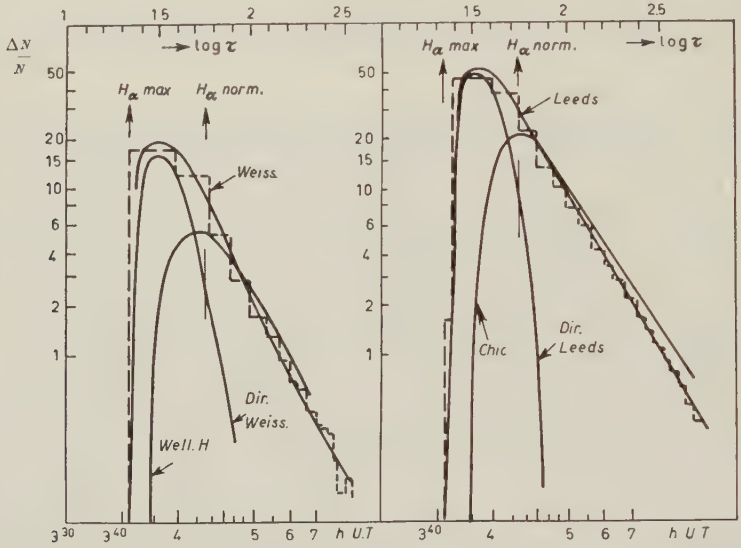

Fig. 1. – Examples for separation of neutron counting-rates attributed to direct and deflected fractions of solar C.R. on February 23, 1956.

It implies further, that the particles which produced the neutrons observed in the decay phase of the record on the earth did not only suffer deflection with insignificant path prolongation, but indeed were stored for several hours in the solar system.

5. – Estimation of momentum-spectrum.

As Sekido and Murakami [3] already pointed out, the spectrum of magnetic rigidy of the deflected resp. stored radiation should be much steeper than the spectrum of direct radiation. With respect to the production mechanism the spectrum of the radiation as it escapes from the source is of higher principal interest, than that of the deflected fraction. Reckoning the presumed inner trapping field [2, 3] as belonging to the source we may assume that the distribution of magnetic rigidity of the direct radiation was identical with the distribution near the source.

If now the intensity of direct radiation is known for several stations in the impact zones located in different geomagnetic latitudes, than the steepness of the magnetic rigidity spectrum approximately may be determined.

Assuming that the proton component was predominant we measure rigidity by proton momentum p. According to FIROR, SIMPSON and TREIMAN [8] the counting rate of solar protons of the station in geomagnetic latitude Φ_i, longitude Λ_i, atmospheric depth x_i, may be expressed by

$$\Delta N_i = C_i \int_{P_i + \Delta p_i/2}^{P_i - \Delta p_i/2} f(p) S(p, x_i) \Omega_i(p) \, \mathrm{d}p , \tag{1}$$

where C_i is an apparative constant, $f(p)$ the momentum spectrum of solar protons, p_i the center value of the recorded momentum band; Δp_i the bandwidth for the i-th station depending from the angular width of the source, $\Omega_i(p)$ the solid angle of incidence which is filled with allowed trajectories of protons of momentum p at the i-th station and $S(p, x_i)$ the yield function for neutrons produced by solar particles of rigidity p in atmospheric depth x_i.

As the counting rate of neutrons from isotropic normal C.R. N_i in this connection can be expressed by:

$$N_i = C_i \cdot V_i , \tag{2}$$

where V_i is the latitude factor of neutron intensity at the station i related to the intensity at an equator station in the same depth x_i the apparative constant C_i in (1) may be eliminated by combining (1) and (2).

It is now further established, that the momentum bandwith Δp_i covers a narrow range of p, so we can write:

$$\Delta N_i / N_i = \frac{1}{V_i} f(p_i) S(x_i, p_i) \Omega_i(p_i) \Delta p_i . \tag{3}$$

Writing now the same espression for a station k we find for the proportion of relative intensities or $(\Delta N_i/N_i)/(\Delta N_k/N_k)$

$$\frac{\Delta N_i / N_i}{\Delta N_k / N_k} = \frac{V_k f(p_i) S(x_i, p_i)}{V_i f(p_k) S(x_k, p_k)} \frac{\Omega_i(p_i)}{\Omega_k(p_k)} \frac{\Delta p_i}{\Delta p_k} . \tag{4}$$

In our special case we consider only stations in the same impact zone within the relatively narrow range of latitudes between 50° and 60°. Therefore it may be allowed to assume that the focussing effect in this latitude region may not vary strongly.

That means

$$\frac{\Omega_i(p_i)}{\Omega_k(p_k)} \approx 1,$$

$\Delta p_i / \Delta p_k$ then exclusively determines the proportion of counting rates between the stations i and k for a flat spectrum ($f(p) = \text{const.}$). (This procedure may

be justified by comparing the results of an elaborate calculation of counting rates for the flat spectrum by LÜST [9] with our approximation).

We now approximate the momentum spectrum by a power law $f(p) \sim p^{-\gamma}$ and introduce the yield function according to FONGER (*)

$$S(p_i) = C p_i (1 + p_i^2)^{-\frac{1}{2}} \ln \frac{1 + p_i^2}{1 + p_{th}^2}, \tag{5}$$

where C is a constant and $p_{th} \approx 1.5$ GeV/c the threshold momentum for neutron production.

Thus combining (4), and (5) we finally get:

$$\frac{\Delta N_i / N_i}{\Delta N_k / N_k} = \frac{V_i}{V_k} \left(\frac{p_k}{p_i}\right)^{\gamma} \frac{(1 + p_k^2)^{-\frac{1}{2}} \ln \{(1 + p_i^2)/(1 + p_{th}^2)\}}{(1 + p_i^2)^{-\frac{1}{2}} \ln \{(1 + p_k^2)/(1 + p_{th}^2)\}} \frac{\Delta p_i}{\Delta p_k}. \tag{4'}$$

By comparing now the measured relative intensities of two stations in the impact zone we are able to determine a mean γ in the energy range $p_i \leqslant p \leqslant p_k$ by equation (4').

p_i and p_k, the central values of momentum for mainly vertical incident radiation are to be determined by the position of the sun in the allowed source directions for stations i and k in the impact zone. Δp_i and Δp_k depend from the fractions of solid angle $\Delta\Omega_{si}$ resp $\Delta\Omega_{sk}$ of the real source which cover allowed source directions for the stations i and k.

Therefore we can write approximately

$$\frac{\Delta p_i}{\Delta p_k} = \frac{\mathrm{d}P_i/\mathrm{d}\Omega_s}{\mathrm{d}P_k/\mathrm{d}\Omega_s} \frac{\Delta\Omega_{si}}{\Delta\Omega_{sk}}.$$

It is now to be seen, that for vertically incident particles this proportion becomes nearly independent from the source width Ω_s because with increasing Ω_s gradually $\Delta\Omega_{si}/\Delta\Omega_{sk} \approx 1$ is fullfilled. In our special case this will be reeached for angular source diameters between 20° and 30°. These are values assumed as reasonable according to the analysis of FIROR [2]. If we now consider this proportion as representative for zenith-angles of incidence inside of about 30°, than equation (4') can be solved for γ.

We now compare the relative intensities of neutrons from direct radiation at the 4 stations Stockholm [10] Leeds [8], Göttingen [11] and Weissenau [6], located in the impact zone. We use the integral values measured till 4 h U.T., because the ends of recording intervals coincide at this time.

(*) This function was derived by FONGER [12] and reproduces the latitude effect for the neutron-component of the primary distribution of rigidities of the normal C.R., it is valid for atmospheric depths $\leqslant 600$ g/cm². We only transformed the original function of the argument E (kinetic energy) into the function of argument p.

Table I contains the data needed for solving eq. (4'). There we find the geomagnetical longitudes Λ_s and latitude Φ_s for the different stations in the centred dipole system resp. in the excentric dipole system (marked by *),

TABLE I. – *Geomagnetic co-ordinates of four stations in the 5' impact zone; center values of momentum p, bandwiths of momentum Δp for vertically incident protons, related to angular source diameters of 15° resp. 30° and recorded relative counting rates of neutrons produced by direct radiation of February 23, 1956.*

Station	Λ^0_{st} E	Φ_t N	p (GeV/c)	Δp (GeV/c) $D_s =$ 15°	30°	Φ^*_{st} N	p^* (GeV/c)	ΔP^* (GeV/c) $D_s = 30°$	$\overline{\Delta N}/N$
Stockholm	105.5	58	2.3	0.36	0.66	56	2.7	0.82	733
Leeds	83.5	57	2.0	0.19	0.48	54	2.5	0.72	663
Göttingen	93.7	52.5	3.6	0.42	1.00	50	4.5	1.15	—362
Weissenau	91.5	49	5.0	0.45	1.20	47	6.2	1.65	≦265

further the corresponding central values of momentum, momentum widths for angular source diameter of 15° resp. 30° and finally the neutron counting rates in arbitrary units. The momentum values were determined graphically from diagrams of which an example is shown by Fig. 2, for Weissenau. These diagrams were drawn according to interpolations of allowed source directions calculated by JORY [13]. They show the allowed source directions related to the four stations for vertically incident particles and the corresponding momenta for the centered and the excentric dipole system together with the position of the sun relative to the allowed source directions (center of the circles). The circles round the sun correspond to angular source diameter of 15° resp. 30°.

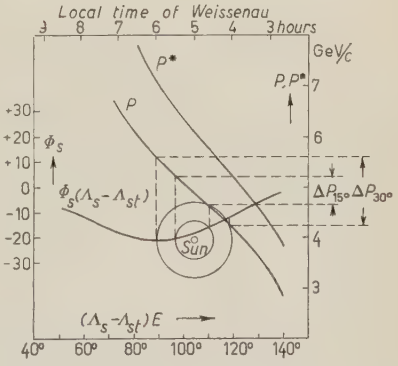

Fig. 2. – Directions to a source $\varphi_s(\Lambda_s - \Lambda_{st})$ for protons incident vertically at Weissenau at various local times. Further: central values of rigidities and bandwidths of rigidity for angular source diameters of 15° resp. 30°, where p is related to the centred dipole geomagnetic system and p^* to the excentric dipole system. (Curves are interpolated by using the calculation results of JORY).

In Table II we inserted the calculated values of γ corresponding to the different assumptions on source widths and dipole systems.

We first state, that the value of γ calculated by comparison of the counting rates between Stockholm and Göttingen resp. Leeds and Göttingen should be the

TABLE II. – *Exponent γ estimated under various assumptions for source width, resp. magnetic dipole location D=angular diameter of the source p in* GeV/c *for protons.*

Comparison of count. r. of neutr. between	Central dipole			Excentric dipole	
	$p_i \div p_x$	γ		$p_i^* \div p_k^*$	γ
		$D_s = 15°$	$D_s = 30°$		$D_s = 30°$
Stockholm Göttingen	2.0 ÷ 3.6	3.9	4.5	2.5 ÷ 4,5	3.6
Göttingen Leeds	2.0 ÷ 3.6	4.7	4.6	2.5 ÷ 4.5	3.6
Göttingen Weissenau	3.6 ÷ 5.0	2.3	2.7	4.5 ÷ 6.2	3.2

same. This is the case only for source widths which exceed 15°. We further see, that a nearly unique value for the entire momentum intervall is found after correction for the excentricity of magnetic dipol location. Thus our considerations lead to the result

$$f(p)\,\mathrm{d}p \sim p^{-3,4}\,\mathrm{d}p\ ; \qquad 2.5 \leqslant p \leqslant 6\ \mathrm{GeV/c}\ ,$$

for the direct fraction of solar C.R.

This figure is to be compared with the value γ' estimated independently by MEYER, PARKER and SIMPSON [4] and by the author [14] for the deflected radiation.

It was found

$$\gamma' \to 6 \text{ to } 7\ .$$

This difference between γ and γ' seems to be a reasonable result as it confirms, that the momentum spectrum of the deflected and in interplanetary space stored radiation was much steeper than the spectrum of direct radiation.

A more detailed report will appear in *Ann. der Phys*, **20** (1957.)

* * *

The author is indebted to the Deutsche Forschungsgemeinschaft for supporting the work on C.R.-time variations.

REFERENCES

[1] A. Schlüter: *Zeits. f. Naturf.*, **6***a*, 592 (1951).
[2] J. Firor: *Phys. Rev.*, **103**, 1068 (1956).
[3] Y. Sekido and K. Murakami: *Proceedings of the Guanajato Conf. Mexico*, 1956.
[4] P. Meyer, E. N. Parker and J. A. Simpson: *Phys. Rev.*, **104**, 768 (1956).
[5] A. Ehmert and G. Pfotzer: *Mitt. a.d. Max-Planck-Institut f. Phys. d. Stratosphäre, Weissenau*, No. 6 (1956).
[6] A. Ehmert and G. Pfotzer: *Zeits. f. Naturf.*, **11***a*, 322 (1956).
[7] T. E. Cranshaw, W. Galbraith and N. A. Porter: *Journ. Atm. Terr. Phys.*, **8**, 274 (1956).
[8] J. W. Firor, J. A. Simpson and S. B. Treiman: *Phys. Rev.*, **95**, 1015 (1954).
[9] R. Lüst: *Phys. Rev.*, **105**, 1827 (1957).
[10] A. E. Sandström: private communication.
[11] P. Meyer: *Zeits. f. Naturf.*, **11***a*, 326 (1956).
[12] W. H. Fonger: *Thesis University of Chicago*, 1953), communicated by J. A. Simpson and W. C. Fagot: *Phys. Rev.*, **90**, 1068 (9153).
[13] F. S. Jory. *Phys. Rev.*, **103**, 1068 (1956).
[14] G. Pfotzer. *Mitt. a.d. Max-Planck-Inst. f. Physik der Stratosphäre, Weissenau*, No. 7 (1956).

SUPPLEMENTO AL VOLUME VIII, SERIE X
DEL NUOVO CIMENTO

N. 2, 1958
2° Trimestre

The Production of High Energy Particles in Solar Flares.

P. A. SWEET

University of London Observatory

The topology of the magnetic field above a complex sunspot group with four components arising from flux tubes protruding through the photosphere from below is examined. It is shown that two neutral points must occur, and that the field divides into four topologically distinct systems with a line of magnetic force in common which passes through both neutral points.

The above topology is typical of all intersecting flux tubes.

Two properties of the field are established: *a*) without Joule dissipation of magnetic energy, magnetohydrostatic equilibrium is impossible when the components of the spot are given arbitrary relative displacements or twists; *b*) during the resulting interpenetration of the flux systems the voltage drop down the line of force between the neutral points is proportional to the rate of exchange of flux between the systems.

Relative velocities of order 10 km/s between the components would be required in order to explain the production of cosmic ray particles of the highest energies. Such motions could arise from transverse or torsional hydromagnetic waves travelling upwards along the flux tubes below the photosphere.

Such a mechanism is consistent with the point-like nature of a flare at its onset, but does not satisfactorily explain the positions of flares relative to the components of the spot group.

1. – Introduction.

MEYER, PARKER and SIMPSON [1] have shown that particles with energies up to order 10 GeV were produced in the solar flare of 23 February 1956, all the cosmic-rays being produced within half an hour. Of the electromagnetic theories of flares, the neutral point theory proposed by GIOVANELLI [2] and

later developed by HOYLE [3], DUNGEY [4] and SWEET [5], and the Fermi mechanism as suggested by PIDDINGTON [6] and PARKER [7] offer possible explanations of the production of cosmic-rays.

In the present paper the potentialities of the neutral point mechanism are explored in relation to the production of cosmic-rays. The discussion is based on the rather restrictive assumption that sunspots arise when flux tubes, normally lying below the photosphere are made to protrude through it into the chromosphere.

2. – The topology of the magnetic field above a complex spot.

Consider a flux tube emerging from the solar surface as in Fig. 1, ignoring a possible general field. Below the photosphere the tube has a well-defined cylindrical boundary outside which the field vanishes. At higher levels the tube splays out and follows roughly the surface. It connects up with similar flux systems returning into the Sun. The entire field in the atmosphere is therefore bounded by a surface Σ_0 of which LXM, PYQ in Fig. 1 represent a part. Surfaces such as XY in Fig. 1 may be introduced cutting off the flux tubes in the Sun's interior from the field in the atmosphere. A surface Σ is thereby defined, of which $LXYQ$ in Fig. 1 represents a part. This surface is mapped on to a plane in Fig. 2. It will be referred to as the photosphere, and the region above it will be referred to as the atmosphere. A four com-

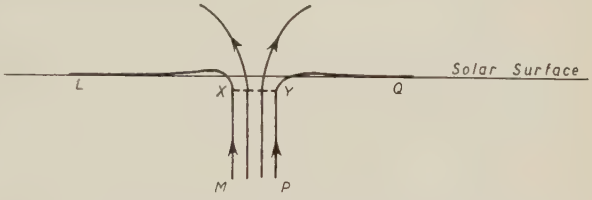

Fig. 1. – Emergent flux tube and defining boundary.

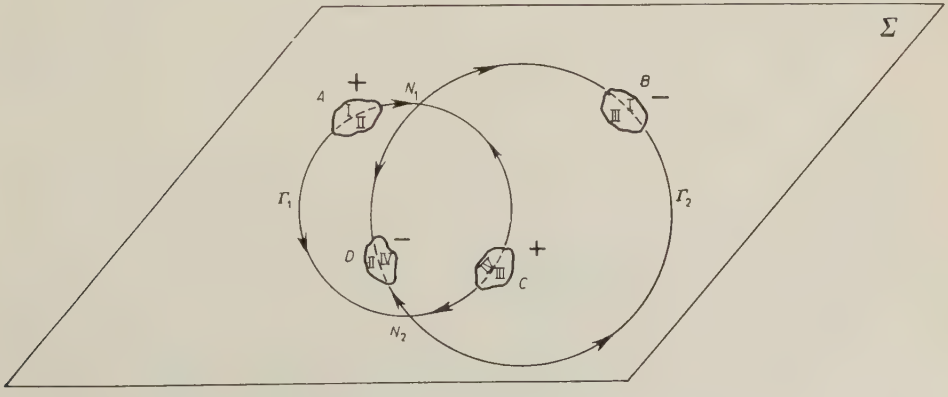

Fig. 2. – Typical connectivity of a complex spot in the solar surface.

ponent spot group is examined in which magnetic flux emerges from regions A and C and returns into the Sun through B and D. Each region has a definite boundary, and the remainder of the photosphere is covered by the limiting lines of force running in it. When the four regions are connected by these lines, at least two points must occur in which two lines intersect (one or both of these points may be at infinity in singular cases). These are the neutral points in the magnetic field. Fig. 2 illustrates a type of connectivity; the neutral points are N_1 and N_2. The flux from A does not return wholly to either B or D but is shared between them. The other regions share their flux likewise; thus flux from AI returns to BI and the remainder, from AII, returns to DII, etc. The field in the atmosphere is therefore divided into four separate systems I, II, III and IV, the amounts of flux running through each depending on the strengths and relative positions of A, B, C and D and on the electric currents in the atmosphere. A displacement of the components A and D, as a pair, away from the pair B and C tends to transfer flux from systems I and IV to systems II and III, while a displacement of A and B from C and D transfers flux from systems II and III to systems I and IV.

The lines of magnetic force which enter the atmosphere from AI return into the interior through BI, and the lines from AII return through DII. The lines which enter the atmosphere along the boundary between AI and AII cannot return into the interior through either component B or D. They must therefore return either to the neutral points N_1 or N_2 or through component B. Component B has the same magnetic polarity as A, so that in the latter case the lines would first have to pass through neutral points. In general there are no neutral points in the system other than N_1 and N_2, hence the latter alternative does not occur. Further, the lines in question must all return through the same neutral point for, if not, there would be a limiting line passing through neither neutral point. These lines of force, together with

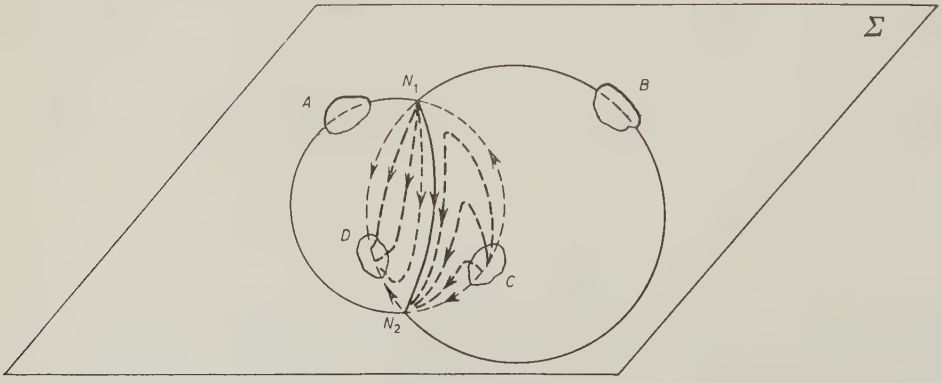

Fig. 3*a*. – Lines of force in the surfaces separating the four flux systems.

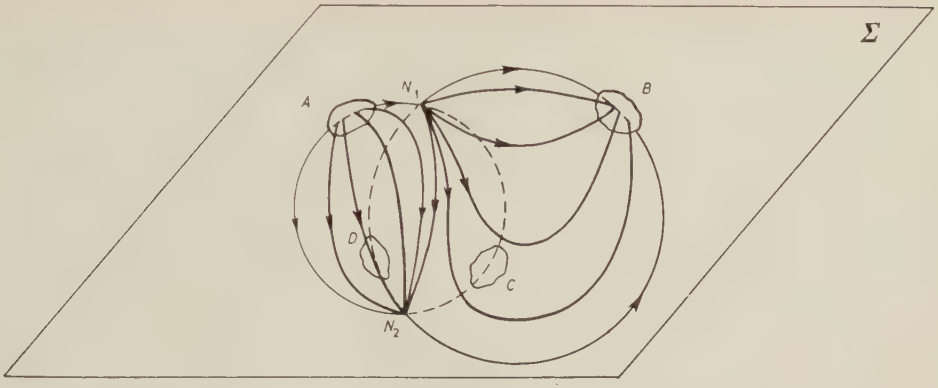

Fig. 3*b*. – Lines of force in the surfaces separating the four flux systems.

the lines from the other three boundaries (*B*I, *B*III), (*C*III, *C*IV) and (*D*II, *D*IV) define four surfaces. These surfaces intersect the photosphere in the four lines joining the neutral points in Fig. 2. They divide the atmosphere into four regions defined by the flux systems I, II, III and IV, and must therefore intersect each other in a single line of force Γ passing through the neutral points. The field in the atmosphere is therefore of the form illustrated in Fig. 3-*a* and 3-*b*.

3. – Application to intersecting flux tubes.

The above topology must obtain when any two flux tubes, or two distinct sections of the same tube, are made to intersect. This can be established by taking four surfaces of cross-section across the tubes, one on each side of the region of intersection, for both tubes. These surfaces, together with the bounding surfaces of the tubes, define a simply-connected surface which can be represented on a plane Σ. The four surfaces of cross-section are then represented by the components A, B, C and D in Fig. 2.

4. – Magnetohydrostatic equilibrium above Σ.

Electric currents must flow in a layer immediately above Σ. These will normally be restricted to a thin layer of the atmosphere where the available mechanical forces are strong enough to support them. They can, for certain purposes, therefore be regarded as surface currents in Σ.

Suppose that the field is initially potential above Σ, and consider the effect of giving the components A, B, C and D relative displacements. If the medium

above Σ is a perfect conductor the total flux in each of the regions AI, etc., must remain constant. In general the equivalent potential field corresponding to the new positions of the components will involve different flux sharing. This equivalent potential field is unique; the actual field cannot therefore be potential, and electric currents must flow above Σ. These exert mechanical forces $jH \sin\theta/c$ on the medium, where H is the resultant field strength, j is the electric current density and θ is the angle between the two. For definiteness the displacements of the components are taken to be of the same order of magnitude as the typical linear dimensions L of the system. Hence

$$j = O(cH_0/4\pi L)\,, \tag{1}$$

where H_0 is a typical field strength. Further, there are no neutral points above Σ, so that $H = O(H_0)$, hence

$$jH \sin\theta/c = O(H_0^2 \sin\theta/4\pi L). \tag{2}$$

In the solar atmosphere above a sunspot the mechanical forces are small compared with $H_0^2/4\pi L$. If magnetohydrostatic equilibrium exists then θ must be small. The field in the atmosphere then assumes a nearly « force-free » configuration, where $\boldsymbol{j}$ is nearly parallel to $\boldsymbol{H}$.

In such a system the mapping of CIV, say, on to DIV must, at interior points, contain appreciable rotation relative to its original mapping in the initial potential field configuration. Since the conductivity is perfect this could only be achieved by the right amount of rotation of the material in the flux tubes below Σ. In general this cannot immediately occur owing to the inertia of the material below Σ. The required electric currents therefore cannot occur immediately along lines of force arising from interior points of any of the regions AI, etc. The necessary currents would be required to flow along the lines of force in the neighbourhood of the four surfaces separating the four flux systems I, II, III and IV. It must therefore converge on the neutral points N_1 and N_2. The effect of this on magnetohydrostatic equilibrium at these points is considered in the next section.

5. – Magnetohydrostatic equilibrium at a neutral point.

Consider a neutral point at which the field vanishes only to the zero order in its neighbourhood, but at which an electric current is present. Take rectangular axes $N(x, y, z)$, then at points near the origin the field is given by

$$H_\lambda = a_{\lambda\mu} x_\mu\,, \tag{3}$$

where the $a_{\lambda\mu}$ are constants. The axes can always be orientated so that

$$[a_{\lambda\mu}] = \begin{vmatrix} a & \gamma & -\beta \\ -\gamma & b & \alpha \\ \beta & -\alpha & c \end{vmatrix} . \tag{4}$$

The condition $\operatorname{div} \boldsymbol{H} = 0$ requires that

$$a + b + c = 0 . \tag{5}$$

Hence

$$\operatorname{curl} (\operatorname{curl} \boldsymbol{H} \wedge \boldsymbol{H}) = 2(\alpha a, \beta b, \gamma c) . \tag{6}$$

In hydrostatic equilibrium

$$\frac{\operatorname{curl} \boldsymbol{H} \wedge \boldsymbol{H}}{4\pi} - \operatorname{grad} P + \varrho \boldsymbol{g} = 0 , \tag{7}$$

where P is the gas pressure and $\boldsymbol{g}$ is the acceleration of gravity. Consider the case of an isothermal atmosphere in which $\varrho = \mu P / \Re T$ and where $T = \text{const}$. On taking the curl of (7) and eliminating grad P between the resulting equation and (7),

$$\operatorname{curl} (\operatorname{curl} \boldsymbol{H} \wedge \boldsymbol{H}) + \frac{\mu}{\Re T} (\operatorname{curl} \boldsymbol{H} \wedge \boldsymbol{H}) \wedge \boldsymbol{g} = 0 . \tag{8}$$

By hypothesis the first term in (8) is of zero order, and the second term is first order. Hence at the origin

$$\operatorname{curl} (\operatorname{curl} \boldsymbol{H} \wedge \boldsymbol{H}) = 0 . \tag{9}$$

Therefore, from (6)

$$\alpha a = \beta b = \gamma c = 0 . \tag{10}$$

If any two of the quantities (a, b, c) vanish, then the third must also vanish, by (5); the neutral point will then be a rotational [8] one. By hypothesis the quantities (α, β, γ), which are proportional to the components of the electric current, do not all vanish, hence at least one of (a, b, c) vanishes. Let it be c, then if $a \neq 0$, we have $\alpha = \beta = 0$, $b = -a$ and the field can be written

$$\boldsymbol{H} = (ax + \gamma y, -\gamma x - ay, 0) . \tag{11}$$

If $\gamma > a$ the field is of the rotational type with its neutral line along the z-axis. If $\gamma < a$ it is of the deformation type [8] with a neutral line again along the z-axis.

Hence magnetohydrostatic equilibrium is impossible at a deformation neutral point which is not on a neutral line, and at which an electric current flows. An extension of this theorem to neutral points in neutral surfaces, as in the case of N_1 and N_2 in Fig. 3, where the field vanishes to the first order, shows that equilibrium would be impossible if the electric current had a component perpendicular to Σ. In the situation described in the previous section the electric currents near N_1 and N_2 must have components perpendicular to Σ; equilibrium is therefore impossible.

The flux systems must consequently interpenetrate. The extent of the interpenetration due to classical diffusion in a conducting medium would be negligible during the lifetime of a solar flare. The work of PARKER [9] and SWEET [5], however, shows that the rate of interpenetration depends not only on the conductivity but also on the inertia of the gas at the neutral points, and that it could well be fast enough to effect a significant interpenetration during the lifetime of a flare.

6. - The induced electric intensity in interpenetrating flux systems.

Suppose the components A, B, C and D are in relative motion. Consider the surface S defined by the lines of force entering the atmosphere across the boundary ($CIII$, CIV), as in Fig. 3-b, together with the area CIV. Denote by Γ_3 the curve which bounds S. Then from Maxwell's equation

$$\operatorname{curl} \boldsymbol{E} = -\frac{1}{c}\frac{\partial \boldsymbol{H}}{\partial t}\,, \tag{12}$$

we have

$$\int_{\Gamma_3} \boldsymbol{E}\cdot \mathrm{d}\boldsymbol{s} = \int_S \operatorname{curl} \boldsymbol{E}\cdot \mathrm{d}\boldsymbol{S} = -\frac{1}{c}\int_S \frac{\partial \boldsymbol{H}}{\partial t}\cdot \mathrm{d}\boldsymbol{S}\,. \tag{13}$$

Let $\boldsymbol{v}$ be the velocities of points on the moving curve Γ_3. Then

$$\int_S \frac{\partial \boldsymbol{H}}{\partial t}\cdot \mathrm{d}\boldsymbol{S} = \frac{D}{Dt}\int_S \boldsymbol{H}\cdot \mathrm{d}\boldsymbol{S} + \int_{\Gamma_3} (\boldsymbol{v}\wedge \boldsymbol{H})\cdot \mathrm{d}\boldsymbol{s}\,. \tag{14}$$

The first term on the R.H.S. of (14) is the rate of change of magnetic flux through CIV; the second term vanishes since $\boldsymbol{H}$ is parallel to $\mathrm{d}\boldsymbol{s}$ on Γ and $\boldsymbol{H} = 0$ in Σ. Further, since $\boldsymbol{E} = 0$ in Σ (strictly $\boldsymbol{E}$ does not vanish exactly,

but it is negligible owing to high conductivity),

$$\int_{\Gamma_3} \boldsymbol{E}\cdot\mathrm{d}\boldsymbol{s} = \int_{\Gamma} \boldsymbol{E}\cdot\mathrm{d}\boldsymbol{s}\,. \tag{15}$$

Hence

$$\int_{\Gamma} \boldsymbol{E}\cdot\mathrm{d}\boldsymbol{s} = -\frac{1}{c}\frac{D}{Dt}\int_{C\mathrm{IV}} \boldsymbol{H}\cdot\mathrm{d}\boldsymbol{\Sigma}\,. \tag{16}$$

(16) expresses the fact that the voltage drop V down Γ, passing from N_1 to N_2, is equal to $(1/c)\times$ rate of decrease of flux through CIV, i.e.,

$$V = -\frac{1}{c}\frac{D}{Dt}\int_{C\mathrm{IV}} \boldsymbol{H}\cdot\mathrm{d}\boldsymbol{\Sigma}\,. \tag{17}$$

Suppose now that the velocity of displacement of the components is of order v and, through the mechanical weakness at the neutral points established in Sect. 5, is able to adjust itself continually to nearly the equivalent potential configuration. The rate of decrease of magnetic flux through CIV is then of of order vLH_0. With $L = 10^9$ cm and $H_0 = 10^3$ gauss, $V = O(10^4 v)$V, where v is in cm/s.

Cosmic ray particles of 10^{10} eV could therefore be produced with velocities v of order 10 km/s. Horizontal relative velocities of this order of magnitude are not normally to be expected among the components of a spot group. The author had at first supposed [5] that this difficulty could be overcome if free interpenetration were prevented through the maintenance of magnetohydrostatic equilibrium as the component moved. The energy stored thereby would be released when equilibrium finally broke down. The work of Sect. 5 in the present paper shows that this might have been achieved if neutral lines were present, but would be impossible at neutral points.

It is not inconceivable that velocities of the right order of magnitude could arise from hydromagnetic waves travelling from below the photosphere upwards along the flux tube of one of the components of the spot group.

7. – Gas dynamics near the neutral points.

These must be studied in order to determine the rate of interpenetration of the flux systems for given displacements of the components of the spot group. The analysis required seems prohibitive at the present time since the process depends on non-linear equations. A dynamical analogy based on the

forcing together of two parallel plates [5] indicates that the rate of interpenetration would be high enough to account for the observed cosmic ray energies. A more refined analysis by PARKER [9], however, shows that velocities v of only 0.01 km/s could be expected. A fuller examination of this mechanism is required.

8. – Conclusions.

A neutral point theory of solar flares might be tenable if sunspots were formed from flux tubes protruding through the photosphere. Such a mechanism is consistent with the point-like nature of a flare at its onset, but does not satisfactorily explain the positions of flares relative to the components of the spot group.

As PARKER [9] has pointed out, the conversion of magnetic energy into Joule heat and high energy particles at neutral points would be of general interest apart from its possible significance for solar flares.

REFERENCES

[1] P. MEYER, E. N. PARKER and J. A. SIMPSON: *Phys. Rev.*, **104**, 768 (1956).
[2] R. G. GIOVANELLI: *Month. Not. Roy. Astr. Soc.* **108**, 163 (1948).
[3] F. HOYLE: *Recent Researches in Solar Physics*, (Cambridge, 1949), p. 93.
[4] J. W. DUNGEY: *Phil. Mag.*, **44**, 725 (1953).
[5] P. A. SWEET: *Trans. Int. Astr. Un., Stockholm*, 1956 (in press.)
[6] J. H. PIDDINGTON: *Trans. Int. Astr. Un., Stockholm*, 1956 (in press).
[7] E. N. PARKER: *Phys. Rev.*, **107**, 830 (1957).
[8] Notation of K. L. MACDONALD: *Amer. Journ. Phys.*, **22**, 586 (1954).
[9] E. N. PARKER: *Journ. Geophys. Res.* **62**, 509 (1957).

SUPPLEMENTO AL VOLUME VIII, SERIE X
DEL NUOVO CIMENTO

N. 2, 1958
2° Trimestre

A Model for Solar Flare Increases of Cosmic Rays Based on Hydromagnetic Turbulence (*).

S. F. SINGER

University of Maryland - College Park, Maryland

1. – Experimental problems concerning solar flare increases.

This short note is intended to describe qualitatively a mechanism for accelerating cosmic ray particles in solar flares. It is intended at this stage mainly for discussion purposes since many of the features involved are too complicated to be treated in a quantitative way except by rather far-fetched approximations. The note is divided into three parts, the first discussing certain facts about solar flare increases and raising questions *which can be answered by experiments*. The second part describes a physical picture of the solar atmosphere during a flare which produces conditions suitable for cosmic ray acceleration. The third part indicates how a selection mechanism may be established which accelerates only a small number of particles to high energies and how the geometry of the region determines the steepness of the energy spectrum.

1) *Why do only certain flares produce cosmic ray increases?* The present model would indicate that this is not the case. *All* flares accelerate particles to a greater or lesser extent. However, (we hypothesize) the spectrum exponent could be so steep as to make the number of high energy cosmic rays practically undetectable except with equipment having very high counting rate and, therefore, good statistical accuracy. It is proposed, therefore, that experimentally one might pick up very small increases with equipment having a high counting rate, located in the *auroral* zone at *high altitudes*. Furthermore,

(*) This work has been supported in part by the Air Force Office of Scientific Research under Contract AF No. 18(600)-1038.

rocket experiments during solar flares might indicate increases, again at high latitudes, whereas the usual sealevel equipment might show no effects. (*)

2) *What is the form of the spectrum of the solar flare particles?* Present indications are that the spectrum is extremely steep (EHMERT, SEKIDO, SIMPSON), a fact which has to be explained by any acceleration model. Nothing is known at present concerning a low energy cut-off or « knee » for these solar flare particles. From our present model one would expect *no* low energy cut-off but this fact again requires experimental verification.

3) *What is the chemical composition of the solar flare cosmic rays?* This is an important question and cannot be answered at present. It is generally assumed that the charge distribution resembles that of the ambient cosmic radiation. However, the present model would favor heavy nuclei and protons over electrons; we might therefore expect to observe a higher Fe/H ratio than in the normal primary radiation. This problem again can be settled by experiments on the primary radiation during a solar flare.

2. – Physical picture flare region.

The physical picture which underlies our cosmic ray acceleration model is the following. Above the flare, solar gas is ejected with hypersonic velocities, probably in the form of a jet. From aerodynamic experiments (Pai) it is well known that between the jet and the ambient gas there exists a transition zone in which hydrodynamic turbulence is produced. This turbulence builds up rapidly and is fed by the kinetic energy of the jet. It is reasonable to assume that the density of the turbulence energy increases, i.e. that the turbulent region expands but not rapidly enough to overcome the increase in total turbulent energy.

(*) *Note added in proof.* – Short duration increases in cosmic ray intensity following a small solar flare were found by a detector designed to follow very rapid intensity changes ($\sim$ a few seconds). The high counting rate telescope is sensitive to low energy cosmic rays whose effect would be small at low altitudes. The detector was therefore unshielded and flown at 25000 feet near the auroral zone. A 3 h flight was made on 9 August 1957. Two 30% increases were observed ar 1349 UT and 1433 UT; they lasted for 2 min, 41 s and 1 min, 58 s, respectively. A class 1 west limb flare started at 1330 UT, according to data supplied by Dr. W. O. ROBERTS (Climax, Colorado). This observation indicates that small solar flares can at times produce short increases of *low energy* cosmic rays which might be missed by low altitude detectors.

J. DENISSE (Meudon, Paris) has informed us that an unusual radio noise storm followed this particular flare.

Now the gas in the corona and beyond is an extremely good conductor so that concurrently with the build-up of hydrodynamic turbulence, we have a build-up of magnetic turbulence. This leads to equipartition, first in the smaller scales of turbulence and gradually in the larger scales of turbulence. It is not certain that equipartition is reached within the short time duration of the flare but it is probable that the magnetic turbulent energy density must increase exponentially until the ponderomotive reactions of the magnetic field on the gas motion become appreciable (see Fig. 1).

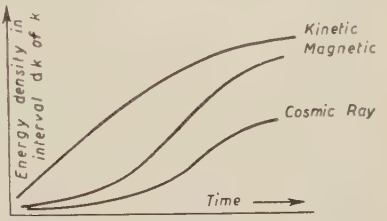

Fig. 1. – Schematic diagram showing increase of energy densities for non-stationary turbulence.

In the buildup of the smaller scales of turbulence which is so important for increasing the magnetic field, an important consideration is the production of cosmic rays which acts as an energy dissipative factor (since the cosmic rays escape from the system); this should speed up the development of the magnetic turbulence since the time scale is

$$\sim \frac{\overline{B}^2}{8\pi} \cdot [\text{energy dissipated per s}]^{-1}.$$

Once cosmic rays are produced, the process builds up rapidly. In this way we can account for the delay of several minutes between the flare and the onset of the cosmic ray increase.

3. – Cosmic ray acceleration (qualitative).

To accelerate cosmic rays under these conditions, we need a means of selecting certain particles to be accelerated since otherwise all of the gas tends to become accelerated and, therefore, effectively acts as a dissipation on the turbulence and keeps it from building up. The selection mechanism proposed is the following. It is reasonable to assume that out of the central jet moving with velocity $V \sim 10^9$ cm/s particles diffuse into the turbulent region by magnetic field gradients or by scattering (*). Those particles which have a radius of curvature $\varrho = MV/e\overline{B}$ greater than some scale distance L can then traverse a streamlet of a turbulent element. Each streamlet will carry an electric polarization voltage given by $(\boldsymbol{v} \times \boldsymbol{b})L$. While the gas which moves with velo-

(*) Since all the particles in the jet have the same speed, the injection mechanism favors high atomic masses (i.e. heavy ions) which will then have a larger radius of curvature. It discriminates definitely against electrons.

city v and produces the polarization is not affected by it, the injected particle which crosses (+) the streamlet can be accelerated or decelerated, depending on the direction in which it crosses. Since the turbulence and the magnetic energy densities are increasing (with reflecting centers in some cases moving closer together), the particle will tend to gain energy *on the average* and will try to approach equipartition (see Fig. 1) (*).

In fact this acceleration mechanism will not persist long enough to allow the particle to reach equipartition. Since the turbulent region is small, the diffusion of particles out of the region is quite important; for after diffusing out of the region, they will no longer be accelerated. Leaking out by diffusion is an important process for a *high energy* particle since its radius of curvature is larger; hence the geometry of the turbulent region sets an upper limit to the particle energy. Only those particles which remain a long time, preferably by diffusion parallel to the jet, can gain much energy. This picture explains qualitatively the very steep spectrum observed: the spectrum exponent as in the Morrison-Olbert-Rossi picture of galactic acceleration is given by the competition between acceleration and diffusion outward (see Fig. 2).

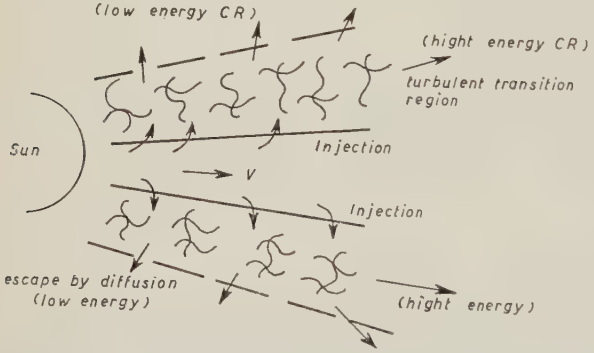

Fig. 2. – A picture of the turbulent region where acceleration takes place.

From Fig. 2 it is also evident that the emission of particles is generally *not* isotropic, with lower energy particles emitted with larger angles to the sun-earth line. This fact may explain the later arrival of lower energy primaries (noted by SIMPSON) in the flare increase of February 1956.

(+) Since the question is often raised whether such voltages would not be short circuited by the highly conducting surrounding gas, it should be remarked that the polarization will not persist for very long since the plasma outside of the streamlet will adjust itself to remove the electric field. However, this takes a certain amount of time: the plasma has inertia. These fluctuating electric fields accelerate particles which can traverse them rapidly enough.

(*) The mechanism resembles that of FERMI and that of SWANN, but differs in the following respects. In the Fermi mechanism $L \gg \varrho$, so that the particle experiences short elastic collisions after drifting for a long time L/V. Here $L \sim \varrho$. In the Fermi mechanism the magnetic field merely couples the particle with the moving cloud and is otherwise not important. Here the field increases on the average so that the particle energy is increased by induction also, as in Swann's mechanism.

4 – Conclusions.

The present model for cosmic ray acceleration in flares is merely a special example of the following mechanism: statistical acceleration of charged particles in a conducting gas where turbulence is *increasing*; the acceleration being due in part to induction, in part to elastic collisions with elements of the gas, the whole system tending to equipartition; incorporating a selection mechanism which allows only a few particles to be accelerated.

It seems likely that there are other examples of this mechanism existing.

(i) Cosmic ray acceleration in the envelopes of supernovae and novae (GINZBURG, HAYAKAWA), this mechanism to give energies up to 10^{15} eV for protons. It is possible that these spectra (as in the solar case) are quite steep and that the familiar $\gamma = 1.8$ exponent expresses the fact that there are many more cases with steeper spectra than with flatter ones and is the result of superposition.

(ii) The acceleration of solar low energy protons to auroral energies in the auroral zone (SINGER).

(iii) The production of high velocity particles in the Russian thermonuclear experiments (ARCIMOVIČ), caused by instability and resulting turbulence as the shockwave collapses near the center of the discharge tube.

SUPPLEMENTO AL VOLUME VIII, SERIE X
DEL NUOVO CIMENTO

N. 2, 1958
2° Trimestre

The Electro-Magnetic State in Interplanetary Space During the Flare of Feb. 23, 1956.

D. ECKHARTT

The Royal Institute of Technology - Stockholm

1. The increase in cosmic ray intensity in connection with the solar flare of February 23, 1956, was observed at different places around the earth to have started at different times. This means that cosmic ray particles which have been produced in the vicinity of the sun must have travelled along orbits of different length before reaching the earth. We have investigated the observed differences in onset times [1]. After correction for the deflection in the geomagnetic field, it is possible to connect the onset time observed at a particular cosmic ray station with certain directions outside the geomagnetic field. A relation between the time delays and the directions from which the flare cosmic ray particles entered the geomagnetic field, is expected to give some information about the electromagnetic state in interplanetary space.

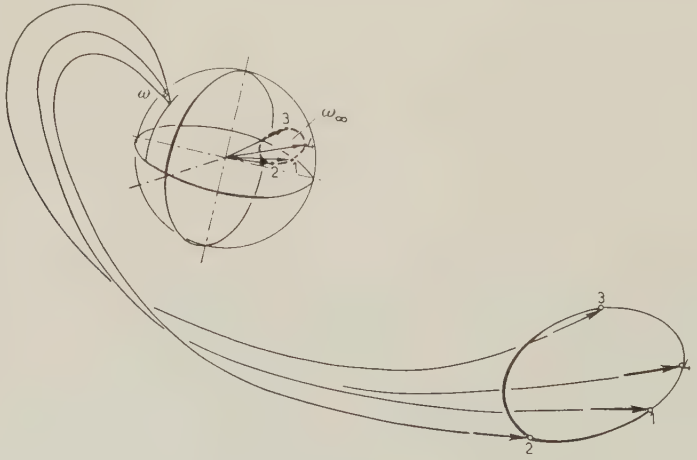

Fig. 1.

In Fig. 1 the deflection of cosmic ray particles in the geomagnetic field is visualized. A cosmic ray detector above the atmosphere measures particles

from certain directions outside the geomagnetic field which depend upon the position of the detector, the angle of incidence at the detector and the momenta of the cosmic ray particles. We denote these directions outside the geomagnetic field as asymptotic directions. Each asymptotic direction is defined by two angles. It is convenient to refer to these angles in the geographic system of the earth. This is illustrated in Fig. 1 by drawing through the centre of the terrestrial globe a line which is parallel to the asymptotic direction and intersects the surface of the globe at a point defined by a longitude and a latitude angle [2]. As seen from Fig. 1, the solid angle of the detector outside the geomagnetic field appears as an area, ω_∞, on the globe. In the two-dimensional figures which we are going to present here, we use a polar projection of the globe looking upon it in the direction of the north pole.

In this two-dimensional representation, Fig. 2 gives the areas of asymptotic directions for a number of ionization chamber stations where the onset times have been measured accurately [1]. These areas refer to primary protons of momentum 3.5 to 15 GeV/c which arrive at the chosen stations within an angle of 32° around the zenith direction. Protons of this momentum range are considered to be responsible for the observed increase in cosmic ray intensity at the chosen stations [3]. It can be shown that, when increasing the zenith angle of impact from 32° to 60°, the corresponding areas of asymptotic directions should be enlarged by an amount corresponding to about 10° for a station near the geomagnetic pole, and to about 15° for a station lying above 50° geomagnetic latitude [1].

The directions towards the sun at the beginning of the flare are indicated by the dotted line figures at the top of Fig. 2 and 3. The solar cosmic ray source is assumed to have an angular diameter of 15° and 30° resp. Those stations for which the areas of asymptotic directions cover these dotted line regions, lie inside one of Firor's impact zones [4].

The observed onset times are written next to the name of each station. In Fig. 2, those stations are shown which measured the increase to have started after 3^{41} U.T. From the connection between onset times and asymptotic directions the following conclusions can be drawn.

Asymptotic directions close to the direction towards the sun are

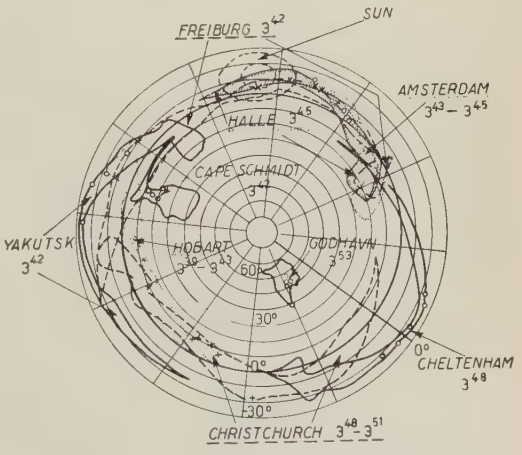

Fig. 2.

connected with earlier onset times than those pointing away from the sun. Asymptotic directions lying in the equatorial plane are connected with earlier onset times than those pointing perpendicular to it. It should be pointed out that Hobart and Christchurch, which measured the earliest and latest onset times resp., have their areas of asymptotic directions lying very close to each other.

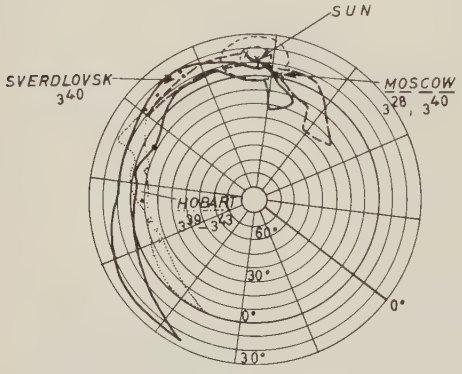

Fig. 3.

The connection between onset times and asymptotic directions does not show a symmetrical distribution with respect to the direction towards the sun. There are stations inside the impact zones, like Halle and Amsterdam, which observed relatively late onset times. On the other hand, Hobart, lying completely outside the impact zones, measured one of the earliest onset times.

The earliest onset times seem to be connected with asymptotic directions that point somewhat to the left with respect to the direction towards the sun in our figures. This conclusion is supported when looking upon Fig. 3 where we show the asymptotic direction for stations with onset times earlier than 3^{41} U.T.

These results indicate that those particles which arrived first at the earth did not travel along straight lines from the sun. This proves the existence of deflecting fields between the sun and the earth.

On February 25, two days after the flare increase, a heavy magnetic storm was registered [5]. According to ALFVÉN [6], magnetic storms are caused by the electric field set up in a beam of ionized gas which is emitted from the sun. The solar magnetic field lines within such a beam should be dragged outwards from the sun. Outside the beam there should be an inflow of magnetic flux towards the sun.

We assume that the magnetic storm of February 25, was caused by such a beam. The 27-day recurrences of high values of the daily K_p-sums following this event and lasting for several solar rotations, gives strong support to the assumption that this beam was already present when the solar flare occurred on February 23. On the other hand, the relatively long time delay between the flare cosmic ray increase and the magnetic storm, together with the relative positions of the beam and the flare on the sun, as

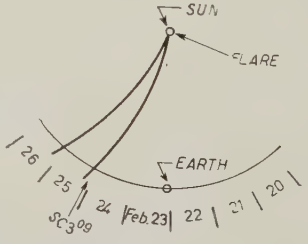

Fig. 4.

seen from Fig. 1, makes a connection between the two events very improbable.

Comparing Fig. 1 with Fig. 2 and 3, it is seen that the asymptotic directions of earliest onset times point towards this beam. We suggest, therefore, that the earliest cosmic ray particles escaped from the vicinity of the sun through the regions inside the beam where they follow the dragged-out field lines [7]. We assume that there exist small regions containing disordered magnetic fields besides the rather regular fields of Alfvén's model, especially in the transition regions near the edge of the beam. These irregularities in the magnetic field scatter the cosmic ray particles out of the beam. They enter the geomagnetic field from directions pointing towards the beam.

The quantitative treatment of a model based on these ideas will be presented in the evening session. The calculated onset times show, at least, the same trend as the observed ones show.

2. I have shown that the first solar flare cosmic ray particles arriving at the earth do not seem to have travelled along straight lines from the sun to the earth. On the other hand, the registration of a magnetic storm two days after the flare increase followed by recurrent occurrences of high values for K_p during several periods of solar rotation, suggests the presence of a solar beam, as is shown in Fig. 4. It is expected that the magnetic fields within such a beam should have a decisive influence upon the propagation of the flare cosmic ray particles through interplanetary space.

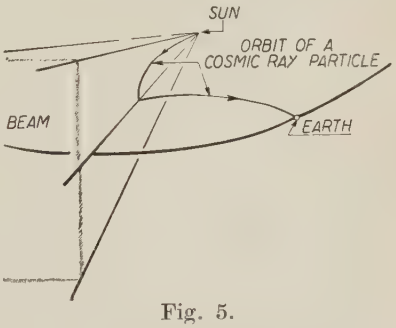

Fig. 5.

We have made an attempt to explain the observed differences in onset times by adapting the concepts of the general solar magnetic field suggested by ALFVÉN [7] to the particular situation around February 23. In our model, similar configurations of magnetic fields within and outside the beam are used, for which calculated cosmic ray orbits have just been presented by Prof. ALFVÉN.

Going into details, we assume that the solar flare cosmic ray particles cannot escape from the vicinity of the sun until they have entered the beam. This takes place during a negligibly short time. Within the beam the cosmic ray particles travel along the dragged-out magnetic field lines. We assume that near the edge of the beam there exist small regions containing disordered magnetic fields and probably originating from irregularities in the flow pattern of the gaseous stream. These regions of disordered magnetic fields scatter the cosmic ray particles out of the beam. We are interested in those particles

the velocity vectors of which lie in the ecliptic plane after they have been scattered out from the beam. The magnetic field outside the beam which is perpendicular to the ecliptic plane, determines the further part of their orbits. This is illustrated in Fig. 5. The first part of the orbit lies in a meridional plane at the edge of the beam and has the shape of a magnetic field-line within the beam.

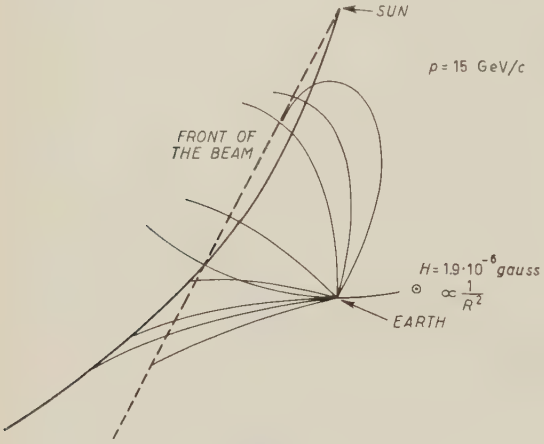

Fig. 6.

The second part of the orbit lies in the ecliptic plane and can be graphically determined. Fig. 6 gives some examples of these constructed orbits. The value of the magnetic field at the earth's orbit which we have used here is somewhat lower than in Alfvén's model where equilibrium between outflow and inflow of magnetic flux within the beam and outside the beam, respectively was presumed.

In the idealized orbits of Fig. 5 and 6, we have treated the scattering as if it would take place at one point. In reality the particle changes its direction gradually when passing through the regions of disordered magnetic fields. The difference in length between the real orbit and the idealized one is probably of the order of the sum of the diameters of all the scattering regions which the particle has to pass in order to be deflected by 90°, that means, to be scattered out from the beam. This difference in length is small compared to the total length of the orbit provided that certain conditions are fulfilled concerning the diameter and the magnetic field of each individual scattering region. For example, near the orbit of the earth and in the equatorial region, the magnetic field within the beam can reach a value of $50 \cdot 10^{-6}$ G [7]. If the diameter of a

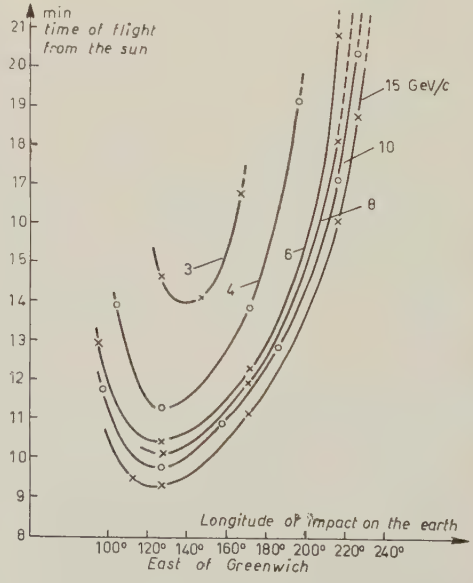

Fig. 7.

scattering region is around one hundredth of the breadth of the beam and its magnetic field three times larger than within the beam, a cosmic ray particle of 10 GeV/c needs about one minute to be deflected by 90°.

We have constructed a number of orbits for different momentum values in the range 3 to 15 GeV/c. After dividing the total length of the orbit from the sun to the earth by the velocity of light we arrive at a time-table, which gives a relation between the times of flight from the sun and the longitude of impact on the earth in the ecliptic plane. This is shown in Fig. 7. It is seen that there exists a minimum value of the times of flight which happens to lie in the direction towards the sun. This is a particularity of the relative positions of the beam and the earth.

Now, Fig. 2 and 3 are combined with Fig. 7: for each station and for each momentum value the longitude angles of those asymptotic directions are determined which lie in the ecliptic plane. By means of Fig. 7, these asymptotic directions are connected with certain values of the time of flight. The shortest time of flight for all momentum values gives the onset time for a particular station. A comparison between the observed onset times and the calculated ones is given in the Table I. The relative time scale of Fig. 7 is adjusted to the absolute one using the onset time observed at Sverdlovsk as a reference, because our model predicts the shortest distance from the sun for this station.

TABLE I.

Station	Observed onset times (UT)	Calculated onset time		
		Particle orbit follows magnetic field lines inside the beam	Particle orbit lies completely in the ecliptic plane	
		Straight beam	Straight beam	Curved beam
Sverdlovsk	3^{40}	3^{40} (*)	3^{40} (*)	3^{40} (*)
Moscow	3^{38}, 3^{40}	3^{41}	3^{41}	3^{41}
Hobart	$3^{39} - 3^{43}$	3^{42}	3^{41}	3^{42}
Yakutsk	3^{42}	3^{41}	3^{40}	3^{41}
Freiburg	$3^{41} - 3^{43}$	3^{41}	3^{41}	3^{41}
Cape Schmidt	3^{42}	3^{42}	3^{41}	3^{42}
Amsterdam	$3^{43} - 3^{45}$	3^{43}	3^{43}	3^{42}
Halle	3^{45}	3^{42}	3^{41}	3^{41}
Cheltenham	3^{48}	—	3^{50} (+)	3^{47} (+)
Christchurch	$3^{48} - 3^{51}$	3^{48}	3^{46}	3^{51}

(*) The relative time scale has been adjusted to the absolute one.

(+) No asymptotic direction for arrival lies in the ecliptic plane inside the range of allowed impact longitudes of the model. For an angle α between an asymptotic direction and the ecliptic plane, the time of flight has been enlarged by a factor $(1 + \mathrm{tg}\,\alpha)$.

Three different cases have been considered. The first one is that just described. In case 2 the orbit lies completely in the ecliptic plane, which means, that within the beam the cosmic ray particles move along radius vectors from the sun. Case 3 is similar to case 2 but a curved beam has been used.

As mentioned above, the accuracy of the calculated onset times is one to two minutes. As seen from the Table the model gives the same large difference in onset times between Hobart and Christchurch as was observed. It fails to explain the relatively late onset time observed at Halle.

As seen from Fig. 6, in this strongly simplified model only a limited range of longitudes on the earth is allowed for cosmic ray particles coming directly from the beam. The occurance of moderate geomagnetic disturbances during the days preceding February 23, suggests the presence of an other beam on the opposite side of the earth. Evidently this beam did not have the same properties of guiding the cosmic ray particles from the sun to the earth, but may reflect the particles which have been emitted from the first beam.

REFERENCES

[1] D. Eckhartt: Study in greater detail awaiting publication in the December issue, of *Tellus* (1957).
[2] E. Å Brunberg: *Tellus*, **8**, 215 (1956).
[3] P. Meyer, E. N. Parker and J. A. Simpson: *Phys. Rev.*, **104**, 772 (1956).
[4] J. Firor: *Phys. Rev.*, **94**, 1017 (1954).
[5] J. Bartels: *The Solar Cosmic Ray Outburst, 1956, February 23.* Collection of Cosmic Ray, Solar, Ionospheric and Magnetic Data Relating to the Event, by H. Elliot and T. Gold (private communication).
[6] H. Alfvén: *Cosmical Electrodynamics*, Chapter VI (Oxford, 1950).
[7] H. Alfvén: *Tellus*, **8**, 1 (1956).

SUPPLEMENTO AL VOLUME VIII, SERIE X
DEL NUOVO CIMENTO

N. 2, 1958
2° Trimestre

Electro-Magnetic State of Interplanetary Space.

H. ALFVÉN

The Royal Institute of Technology - Stockholm

For the understanding of the time variations of Cosmic Radiation it is essential to have a model of the magnetic field in interplanetary space.

The first model which was proposed was the dipole model, according to which the interplanetary field is an extension of a solar dipole field. This model was used by JÁNOSSY [1] and VALLARTA [2] in order to explain the low energy cut-off in Cosmic Radiation. This effect, however, requires a magnetic field which is much more regular than we could possibly assume (ALFVÉN [15] and KANE, SHANLEY and WHEELER [16] and it is now obvious that another explanation must be found for the absense of low-energy particles.

DAVIS [3] and MEYER, PARKER and SIMPSON [4] have proposed a model according to which there is a field-free cavity around the sun out to beyond the earth's orbit. EHMERT [5] has suggested that a fairly homogeneous galactic magnetic field is of decisive importance even inside the earth's orbit. The results by ECKHARTT [6] and VENKATESAN [7] demonstrate in a convincing way the difficulties associated with both of these models.

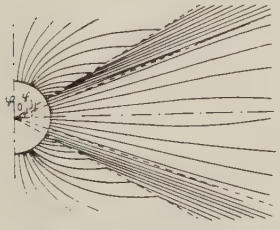

Fig. 1.

I shall here discuss a tentative model which is essentially a dipole field, modified by storm-producing beams emitted from the sun. The model is similar to a model independently proposed by GOLD [8]. The properties of the model have been discussed earlier [9]. Compare Fig. 1 and 2. The model is reconcilable with the following phenomena, which any model of the interplanetary magnetic field must take account of:

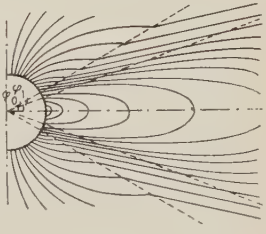

Fig. 2.

1) The visual structure of the corona. This has been shown by GOLD.

2) The 27-day variation. This has just been discussed by VENKATESAN.

3) The flare effect. As ECKHARTT has shown the first particles from the flare of February 23, 1956, reached the earth not from the direction of the sun but from other directions which are reconcilable with the model. The essentially radial field of the model explains why the particles often but not always seem to come from the sun, as shown by FIROR and others [10].

4) The diurnal variation. The results from different stations are still somewhat conflicting probably in part due to the differences in the measuring equipments. Investigations by SANDSTRÖM [11] seem to indicate that there is a possibility to reconcile the empirical results with our model, but the field calls for further investigations.

5) Magnetic storms and aurorae. The model gives the electric field which is essential in the theory of magnetic storms and aurorae [12].

6) The generation of Cosmic Radiation. The model generates Cosmic Radiation, especially during years of decreasing solar activity [13]. During years of increasing solar activity it decelerates Cosmic Radiation in a way which is reconcilable with the long-time variation in Cosmic Radiation.

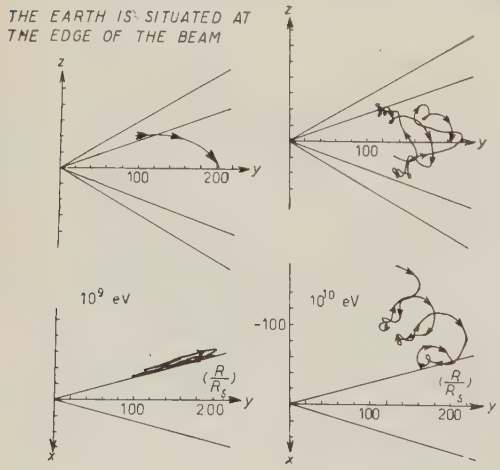

Fig. 3.

It should be stressed that our tentative model aims to demonstrate only the general type of field which is likely to be present in interplanetary space. Of course the beams are usually not so symmetrical as in the figures. Moreover, during years of low solar activity the field is somewhat more similar to a dipole field, whereas it is more extended when the solar activity is high. The limit between the blown-up solar field and a galactic field—or I should prefer to call it a trapping field—occurs normally outside the earth's orbit. During the extreme minimum of solar activity 1952-1954, the limit may have receded to inside the earth's orbit, which may explain a series of unusual phenomena during these years.

A few hundred Cosmic Ray orbits in the field of this model have been calculated by BLOCK [14]. A few samples of these are shown in Fig. 3. It is hoped that the discussion of a number of characteristic orbits will give a good survey of possible Cosmic Ray phenomena in interplanetary space.

REFERENCES

[1] L. JÁNOSSY: *Zeits. f. Phys.*, **104**, 430 (1937).
[2] M. S. VALLARTA: *Nature*, **139**, 839 (1937).
[3] L. DAVIS: *Phys. Rev.*, **100**, 1440 (1955).
[4] P. MEYER, E. N. PARKER and J. A. SIMPSON: *Phys. Rev.*, **104**, 768 (1956).
[5] A. EHMERT: *Proc. of International Astronomical Union Symposium. Electro-magnetic Phenomena in Cosmical Physics* (1956).
[6] D. ECKHARTT: in this issue, p. 202.
[7] D. VENKATESAN: in this issue, p. 285.
[8] T. GOLD: *IUPAP Conference in Guanajuato* (1955).
[9] H. ALFVÉN: *Tellus*, **8**, 1 (1956).
[10] J. FIROR: *Phys. Rev.*, **94**, 1017 (1954).
[11] A. E. SANDSTRÖM: *Tellus*, **8**, 18 (1956).
[12] H. ALFVÉN: *Tellus*, **7**, 50 (1955).
[13] H. ALFVÉN: *Tellus*, **6**, 232 (1954).
[14] L. BLOCK: Manuscript under preparation.
[15] H. ALFVÉN: *Phys. Rev.*, **72**, 88, (1947).
[16] E. O. KANE, T. J. B. SHANLEY and J. A. WHEELER: *Rev. Modern Phys.*, **21**, 51 (1949),

SUPPLEMENTO AL VOLUME VIII, SERIE X
DEL NUOVO CIMENTO

N. 2, 1958
2° Trimestre

Courte discussion des observations radio-astronomiques associées à l'éjection de matière du soleil.

J. F. Denisse

Observatoire de Paris

On décrit deux aspects de l'activité solaire qui se manifestent par des émissions radioélectriques très intenses et dont les propriétés ont été précisées par des observations effectuées avec le Grand Interféromètre de Nancy qui permet d'obtenir une définition angulaire de l'ordre de la minute d'arc sur la longueur d'onde 177 cm [1].

1. – *Emission du type IV.* Généralement associés aux éruptions chromosphériques, on a caractérisé jusqu'à présent deux types de sursauts, le sursaut isolé (burst type II) et le grand sursaut (outburst type III) dont les propriétés sont bien connues. Miss Dodson avait signalé [3] que certains sursauts de type III (major ou minor +) paraissaient dédoublés. A. Boischot [2] a pu caractériser sans ambiguité ce double comme un type d'émission nouveau (type IV), toujours associé à une éruption optique. Sur la longueur d'onde de 177 cm, ce sursaut se manifeste souvent quelques dizaines de minutes après l'éruption optique et peut durer de une à plusieurs heures. L'émission est plus intense que la plupart de celles qui se manifestent dans d'autres circonstances. La région émissive occupe une très vaste étendue de la couronne qui peut dépasser 10′ d'arc. L'altitude de la région émissive peut atteindre plusieurs rayons solaires.

Le rayonnement émis se caractérise principalement par une remarquable stabilité; il est complètement dépourvu de sursauts brefs (type I) qui accompagnent les orages radioélectriques; il est complètement polarisé circulairement.

Seules quelques éruptions (une dizaine en un an pour 2 heures d'observation journalières) présentent une émission de type IV.

Etant donné sa très grande intensité, il est exclu que cette émission soit d'origine thermique; d'autre part sa stabilité indique qu'elle n'est sans doute

pas émise par un processus d'oscillations macroscopiques du type oscillations de plasma; l'origine la plus probable semble être une émission par rayonnement synchrotron d'électrons de haute énergie.

2. – A la suite d'une année complète d'observations, on a pu préciser certaines propriétés des sources des orages radioélectriques (enhanced radiation) [4] qui représentent une forme d'activité du soleil assez permanente plus ou moins associée aux taches solaires.

Diamètre apparent: quelques minutes d'arc.

Altitude (sur $\lambda = 177$ cm): 300 à 400 000 km.

Durée de vie maximum: une semaine.

Il est très difficile de rattacher sans ambiguité ces centres d'émission aux taches solaires optiques: en particulier, leurs changements de position d'un jour à l'autre ne correspondent pas à un mouvement de rotation uniforme. Aucun type de tache optique ne paraît plus particulièrement susceptible d'être associé à un centre radio. Ces centres ne présentent pas de récurrence à 27 jours. Leur passage au méridien central du Soleil s'accompagne en moyenne quelques jours après d'une recrudescence d'activité géomagnétiques.

Une propriété paraît particulièrement importante: plusieurs centres apparaissent souvent en même temps avec de longitudes héliographiques très différentes: cette propriété qui n'a pas d'équivalence en optique fait apparaître ces émissions comme une forme de l'activité solaire entièrement nouvelle.

RÉFÉRENCES

[1] E. J. Blum, A. Boischot et M. Ginat: *Compt. Rend.*, **243**, 19 (1956).
[2] A. Boischot: *Compt. Rend.*, **244**, 1326 (1957).
[3] H. W. Dodson, E. R. Hedeman et L. Owren: *Astrophys. Journ.*, **118**, 169 (1953).
[4] Y. Avignon, E. J. Blum, A. Boischot, R. Charvin, M. Ginat et P. Simon: *Compt. Rend.*, **244**, 1460 (1957).

SUPPLEMENTO AL VOLUME VIII, SERIE X
DEL NUOVO CIMENTO

N. 2, 1958
2° Trimestre

Solar Activity and Cosmic Radiation (*).

D. H. MENZEL

Harvard College Observatory - Cambridge, Mass.

Nine years ago, W. W. SALISBURY and I [1] suggested that the sun might be responsible for the softer component of cosmic radiation. We further noted that an extremely low-frequency electromagnetic radiation, whose existence we had detected and which we supposed to be of solar origin, might cause the cosmic radiation. E. MCMILLAN [2] examined our theory in detail and showed that it was at least tenable.

After ten years, some modifications of the original concept are necessary. A short-time periodic fluctuation of the fundamental spot field seems unreasonable. These fields, however, extend into the solar chromosphere and corona, where they play an important role in controlling the form and flow of the ionized gas. Observations of solar activity reveal the existence of occasional shock waves, sometimes associated with solar flares, which undoubtedly cause rapid changes in the magnetic field, with consequent production of an electric field, in accord with Maxwell's equations.

The electromagnetic radiation resulting from such a process will consist of pulses or damped oscillations rather than uniform waves as postulated in the original theory. This change of view is not a major one, however, since the charged particle was supposed to receive its acceleration during just one-half of a cycle, riding the wave crest in a manner that may graphically be described as « surf boarding ». And, in this respect, a single pulse is just as effective as a succession of them.

Most workers have taken for granted that the solar cosmic rays originate simultaneously with the H_α flare phenomenon. Since the rays tend to arrive some minutes after the flare, and since there is no obvious method of origin,

(*) This research was supported in part by the Air Force Cambridge Research Center, Geophysics Research Directorate, through Contract AF19(604)-146 with Harvard University.

the argument for simultaneous production, at best, depends on circumstantial evidence. Indeed, scientists have had to postulate the existence of interplanetary magnetic fields, to account for the delay. Such fields are by no means improbable. But the lack of observed simultaneity allows us to consider an origin related to but later than the visual flare itself.

Solar observations coupled with theoretical considerations give some insight into the physical nature of a flare. BIERMANN [3] has noted that the intense magnetic field of a sunspot tends to inhibit the normal convection arising from the ionization of hydrogen in surface layers. Hence, as KROOK, MENZEL, and WILD [4, 5] have shown, the decreased radiation from the spot itself requires a compensating enhancement of convection in the layers immediately around the spot. At lower levels and higher densities, the convective flow is subsonic, but the speed increases as the disturbance moves into regions of lower and lower density, until it finally becomes supersonic. At the higher altitudes some of the kinetic energy goes toward heating the corona, which attains a temperature in the range from 1 000 000 to 5 000 000 °K. The velocity of sound in ionized hydrogen, the dominating constituent of the solar atmosphere, is

$$v_s = \sqrt{\gamma \frac{kT}{m}}\,, \tag{1}$$

where γ is the ratio of specific heats and m the mean atomic mass, which corresponds to an atomic weight of $\frac{1}{2}$ for ionized hydrogen. With $\gamma = \frac{5}{3}$, and $T = 2 \cdot 10^6$, as a representative value, we have

$$v_s = 2.3 \cdot 10^7 \text{ cm/s} = 230 \text{ km/s}\,.$$

Although the observed speeds of most prominences fall below this figure, occasional jets or surges have been observed with speeds well above this mark. A few violent ejections have velocities in excess of 100 km/s. Even higher speeds have been inferred from radio observations. However—and this is the significant point—as violent as the flares are, the energies of the individual atoms are small. The production of cosmic rays requires some physical process capable of imparting high energy to a few atoms. This sort of process can occur only in regions of relatively low density. The low-level coronal or flare regions, which contain from 10^9 to 10^{11} protons per cubic centimeter, do not appear likely places for a process of this sort to occur.

Evidence from the coronagraph, supplementing that from eclipses, strongly indicates that the corona consists of a series of « petals », broad at the base and tapering to a point at high levels. The term « petal » is used to describe the appearance of a region whose true shape must—if its extension in the third dimension is comparable to that in the other two—somewhat resemble

a lamp chimney or a bottle with gracefully curved sides. The exact shape will depend upon the pattern of the surface disturbance, which sends pulsing jets of gas into the volume.

This activity spins out the lines of magnetic force, compressing them toward the outer boundary and « combing » them into long streamers extending radially from the sun. At a given height above the solar surface we may expect the gas pressure, p_g, and H, the magnetic field, to be governed by an equation of the form:

$$p_g + H^2/8\pi = \text{const} .$$

The gas pressure is lowest, therefore, in regions where the field intensity is greatest.

Motion picture records of flare and coronal activity provide confirmation of the above model. (*) In one specific example, a low-level flare observed in H_α is invisible in the coronal line, 5303, of thirteen-times ionized iron. Nevertheless, subsequent coronal pictures clearly show what appears to be a shock wave, spreading out from the initial flare with a speed of some 300 km per second. The force of the explosion expands the elastic magnetic shell, further compressing the lines of force in the boundary zones. As the bottleneck expands, the magnetic lines of force, as revealed by the ionized matter clinging to them, wave back and forth with a whip-like action.

Fig. 1 symbolizes the electromagnetic features of the model. A and A' represent the bottle-shaped regions of high gas pressure and weak field, and B the boundary regions where the gas density is low and the field strong. Now suppose that a flare occurs within the region A, distorting it progressively as the shock wave speeds upward. The compression of the lines of force within B induces a sort of « betatron » action on the ions within the region. I have sometimes called this phenomenon the « watermelon seed effect », because the materials tends to squirt out like a watermelon seed pinched between the fingers. This model here proposed resembles one independently suggested by Krook, who has noted that a magnetic disturbance progressing through the gas could accelerate the ionized gas just ahead of the moving field.

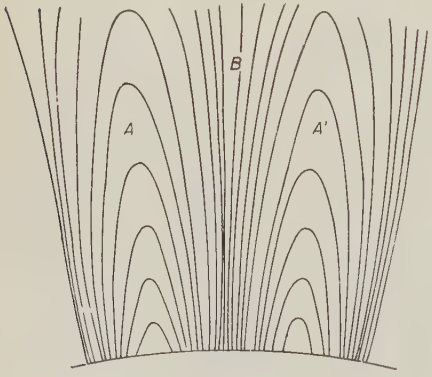

Fig. 1.

(*) The Author showed during the session a motion picture film of solar activity, from records taken at Sacramento Peak Observatory.

At high densities the forces are of magnetohydrodynamic character. The slight outward divergence and the progressive constriction of the field force the accelerated particles outward, something like toothpaste squeezed from a tube. As the wave moves into the upper corona, it takes on the character of an ordinary electromagnetic pulse and thus bears some sort of resemblance to waves discussed by SALISBURY and MENZEL.

REFERENCES

[1] W. W. SALISBURY and D. H. MENZEL: *Nucleonics*, **2**, 67 (1948).
[2] E. MCMILLAN: *Phys. Rev.*, **79**, 498 (1950).
[3] L. BIERMANN: *Vierteljahresschrift Astron. Gesell.*, **76**, 194 (1941).
[4] M. KROOK and P. WILD: *Astr. Journ.*, **62**, 22 (1957).
[5] M. KROOK and D. H. MENZEL: *Astr. Journ.*, **62**, 21 (1957).

SUPPLEMENTO AL VOLUME VIII, SERIE X
DEL NUOVO CIMENTO

N. 2, 1958
2° Trimestre

On the Origin of the Solar Component of Cosmic Radiation.

K. O. KIEPENHEUER

Fraunhofer Institute - Freiburg im Breisgau.

Ascending prominences in the outer corona often reach velocities above 600 km/s, which is 3 times the thermal velocity of coronal protons. It is hardly imaginable that such prominences move through the corona. Because of the high viscosity of coronal matter [1] and because of the fact, that ascending prominences mostly show a positive acceleration it seems much more probable that prominences and the surrounding corona are lifted together by the same force. Also Dunn's coronal film taken at Sacramento Peak observatory gives some evidence in this direction.

There can be no doubt, that the acceleration force is of magnetic nature. It can be assumed that these forces originate in magnetic disturbances which are transported into the corona by magnetized volumes of chromospheric matter (surges) which act on the induction currents in the surrounding corona [2].

Under such circumstances the coronal density below regions with expanding velocities exceeding sensibly the thermal velocity of coronal protons will show for simple hydrodynamic reasons a considerable decrease in density, thus forming a kind of hollow cavity. According to the shape of prominences these cavities seem to have the form of bubbles. From theoretical considerations however a more filamentary shape of the cavities is to be expected.

Such low density cavities represent very favorable conditions for the acceleration of cosmic ray particles, conditions which do not exist in the undisturbed corona because of high density of electrons, and in the interplanetary space because of unsufficient variation of magnetic flux.

It can be shown that only densities of a few electrons cm^{-3} are allowed in order to avoid a disturbing reaction of the accelerated charges on the primary field. A potential difference of 10^9 to 10^{10} volts along the inner wall

of the coronal cavity is obtained without difficulty by inserting plausible values for the magnetic field and the dimensions of the current system.

This type of mechanism has the advantage to explain in a natural way the observed delay between the beginning of the flare and the terrestrial onset of the cosmic ray burst. It explains also more easily why cosmic ray particles can leave the magnetic field of the associated active region of the sun and why even particles in connection with flares close to the solar limb can reach the earth.

REFERENCES

[1] A. Unsöld: *Physik der Sternatmosphären*, (Berlin, 1955), p. 702.
[2] K. O. Kiepenheuer: *Jodrell Bank Symposium on Radio Astronomy*, 1955, p. 65.

SUPPLEMENTO AL VOLUME VIII, SERIE X
DEL NUOVO CIMENTO

N. 2. 1958
2° Trimestre

Latitude Effect of Solar Cosmic Radiation on February 23, 1956 with Respect to the Problem of Effective Geomagnetic Coordinate System (*).

G. Pfotzer

Max-Planck-Institut für Physik der Stratosphäre - Weissenau

1. – Problem.

In recent papers the problem of effective geomagnetic co-ordinate system for Cosmic Radiation has been discussed by Simpson *et al.* and Rose *et al.* [1, 2].

It was stated that measurements of minimum intensity of the low energetic nuclear component near the geomagnetic equator and studies of geomagnetic effects of the α-particles [3] and the heavier components [4] seem to indicate that the conventional geomagnetic co-ordinate system is improper for applying to cosmic ray phenomena.

By analysis of the available data Simpson *et al.* and Rose *et al.* [1, 2] concluded that the effective geomagnetic equator plane could be explained by a westward shift of the inclined magnetic dipole of the earth by about $40° \div 50°$, whereas the inclination of the dipole axis towards the rotational axis of the earth should be retained.

2. – Latitude effect of solar cosmic ray in the decay-phase of the outburst on February 23, 1956.

If such remarkable discrepancies arise by considering the latitude effect of normal cosmic radiation with respect to the conventional geomagnetic co-ordinate system they should be much more striking for particles with a steeper spectrum of magnetic rigidity than for the normal cosmic radiation.

(*) A more detailed report appeared in *Mitteilungen a. d. Max-Planck-Institut für Physik der Stratosphäre Weissenau*, no. 9, 1956.

As now has been stated independently by MEYER, PARKER and SIMPSON [5] and by the author [6] the differential spectrum of magnetic rigidity, which could be attributed to the additional radiation from solar flare on February 23, 1956, is to be described by a power law of the shape

$$f(p)\,\mathrm{d}p \sim p^{-\gamma},$$

with γ between 6 to 7 and p, = magnetic rigidity, measured in GeV/Ze. As we restrict ourselves to the proton component which is assumed to be predominant p may be understood as proton momentum.

This holds for the decay phase of solar particle intensity observed at the top of the atmosphere. It has been derived under the assumption, that the directions of motion of the incoming particles were isotropically distributed before entering the earth's magnetic field.

This is a consequence of the undisturbed monotone decrease of intensity, which seems to have been a world-wide behaviour of the solar cosmic radiation in the end phase of the flare effect.

According to EHMERT and PFOTZER [7] the intensity of the measured secondary component at the earth surface in the decay phase of the flare effect decreases with an inverse time square-law. So if we define $(\Delta N_i\, \Phi_i, t)$ as the fraction of the considered secondary component at a station i in geomagnetic latitude Φ_i at time t, which can be attributed to solar cosmic radiation we can write

$$\Delta N_i(\Phi_i, t) = C_i(\Phi_i) t^{-2}\,, \tag{1}$$

where $t = 0$ is fixed to 330^{h} U.T. and C_i is a chararacteristic constant for the station i.

It follows from (1) that the latitude factor $V_{i)}^{**}$ between a station i and a standard station 0, which may be defined by:

$$\frac{\Delta N_{i,n}}{\Delta N_{0,n}} = \frac{C_i}{C_0} = V_{i0}^{**}\,, \tag{2}$$

is independent of time. Similarly we define the latitude factor of normal cosmic rays by

$$\frac{N_{i,n}}{N_{0,n}} = V_{i0}\,, \tag{3}$$

where $N_{i,n}$ resp. $N_{0\,n}$ are the intensities of the considered secondary component of normal cosmic radiation at the stations i and 0 reduced to a normalized depth x_n (g/cm²).

If the stations are located in atmospheric depths x_i resp. x_0 we can write

$$N_{i,n} = N_i \exp\left[(x_i - x_n)/L_1\right] \tag{4}$$

and

$$\Delta N_{i,n} = \Delta N_i \exp\left[(x_i - x_n)/L_2\right] \tag{5}$$

a.s.o., where L_1 is the absorption length of the measured component of normal cosmic radiation and L_2 the absorption length of the solar fraction. Writing the same expressions for the station 0 and combining (2), (3), (4), (5) one gets from measured relative intensities and known qualities the latitude factor of the solar fraction,

$$\left(\frac{\Delta N_i}{N_i} \Big/ \frac{\Delta N_0}{N_0}\right) V_{i0} \exp\left[\frac{(x_i - x_0)(L_1 - L_2)}{L_1 L_2}\right] \begin{cases} = V_{i0}^{**} & \text{for } L_1 \neq L_2 \\ = V_{i0}^{*} & \text{for } L_1 = L_2 \end{cases} . \tag{6}$$

As we assume, that the solar radiation in the decay phase was isotropic, Störmer's theory holds and it is to be expected that plotting V_{i0}^{**} versus the cut-off rigidity p_i of the different stations the points more or less close should fit in a unique trend. But this would be the case only if we calculate the cut-off rigidities in the appropriate effective system.

3 – Latitude effect of solar C.R. related to different dipole-orientations.

What is now the appropriate effective system? In Table I we find the geographic co-ordinates of different stations, where the low energetic nuclear component was recorded. (This component is to be preferred because its intensity excess was impressively higher than that of the observed charged components and secondly because it is related to primary particles by a unique yield function).

Further we find there the geomagnetic co-ordinates in the conventional system of centred dipole ($\lambda_0 = 290°.9$ E is the geographic longitude, where the centred dipole axis in northern hemisphere points the earth surface) and in two other systems, where the tilted dipole axis is shifted westward by angles of 15° resp. 45°, without changing its inclination towards the rotational axis of the earth ($\lambda_0 = 275°$ E, resp. 245° E).

We state, that according to the analysis of the Chicago and Ottawa groups the « effective system » for cosmic ray phenomena should be represented by the system correlated to $\lambda_0 = 245°$ E.

In Table II we find the values of cut-off rigidities related to protons only and measured as proton-momentum in GeV/c. In the first column for each

TABLE I. – *Geomagnetic coordinates for neutron monitoring stations in three systems, related to various dipole orientations.*

Station	Height above sea level	Atm. depth (g/cm²)	Geogr. system		Convent. geom. syst. $\lambda_0 = 290°.9$ E		$\lambda_0 = 275°$ E		CR eff. ? system $\lambda_0 = 245°$ E	
			$\lambda°$ E	$\varphi°$	$\Lambda°$ E	$\Phi°$	$\Lambda°$ E	$\Phi°$	$\Lambda°$ E	$\Phi°$
Stockholm	0	1030	18	59	105	57.3	120	55	142	49.6
Leeds	0	1030	358	53	84	57	98	53	125	47.5
Ottawa	0	1030	284	45	354	56.8	01.5	56.3	48.7	53.7
Durham	0	1030	289	42	0	54	18.5	53	52	49.7
Chicago	240	1000	272	42	338	53	0	53	30	53
Göttingen	275	1000	10	51.5	93.7	52.3	109	50	134.8	44.2
Weissenau	445	975	9.5	47.8	91.5	49	107	46.5	133.2	40.5
Climax	3610	645	254	39	319	48	334	49.7	12	50.3
Wellingt H.	0	1030	175	— 41	253	— 45.6	273	— 43.3	296	— 36.4
Berkely	100 (*)	1180	238	38	300	44	316	47	353	49.5
Albuquerque	1575	860	254	35.5	318	43	334	46	13	47
Sacram. P.	3210	680	255	33	319	42	336	43.5	357	44.3
Mexiko C.	2490	760	261	19.5	327	29	344	30.5	19	30.5
Norikura	2800	725	137	36.1	203	25.4	218	27	244	31.6
Huancayo	3600	645	258	— 12	354	— 1	10.5	— 1	39	— 3.6

(*) + 160 light material

TABLE II. – *Cut-off rigidities (proton momenta) for neutron monitoring stations in the conventional and in two westward shifted systems; p_{ik} and p^*_{ik} in GeV/c; Δp_{ik} in percent of p_{ik}.*

Station	$\lambda_0 = 290°.9$ E			$\lambda_0 = 275°$ E			$\lambda_0 = 245°$ E			lg	lg
	p_{i1}	Δp_{i1}%	p^*_{i1}	p_{i2}	Δp_{i2}%	p^*_{i2}	p_{i3}	Δp_{i3}%	p^*_{i3}	V^*_{i0}	V^{**}_{i0}
Stockholm	1.17	+18.1	1.38	1.62	+17.0	1.90	2.62	+14	3.00	3.10	3.13
Leeds	1.30	+22.4	1.59	1.96	+20.0	2.35	3.09	+15	3.55	2.81	2.84
Ottawa	1.40	+21.8	1.69	1.40	+20.9	1.68	1.84	+21	2.23	3.07	3.10
Durham	1.78	+18.5	2.12	1.98	+17.9	2.34	2.62	+16	3.05	3.18	3.21
Chicago	1.98	+12.9	2.23	1.98	+13.6	2.25	1.94	+15	2.24	2.93	2.93
Göttingen	2.09	+14.9	2.40	2.56	+15.2	2.96	3.85	+17	4.50	2.38	2.36
Weissenau	2.76	+11.9	3.08	3.36	+12.0	3.76	5.00	+ 7	5.35	2.13	2.10
Climax	2.96	+ 9.25	3.24	2.58	+ 5.1	2.71	2.46	+ 9.5	2.70	2.76	2.32
Wellingt. H.	3.58	—11.6	3.16	4.18	— 6.14	3.92	6.30	— 6.2	5.90	2.17	2.20
Berkeley	3.95	+ 1.8	4.20	3.24	+ 1.05	3.28	2.64	+ 6.1	2.66	1.63	1.85
Albuquerque	4.24	+ 4.2	4.44	3.45	+ 4.0	3.60	3.24	+ 8.2	3.50	1.88	1.70
Sacram. P.	4.50	+ 3.6	4.66	4.10	+ 4.7	4.30	3.90	+ 6.3	4.16	1.83	1.43
Mexiko C.	8.70	+ 0.8	8.75	8.20	+ 2.6	8.40	8.20	+ 2.5	8.4	0.54	0.24
(+)	10.9		11.8	10.2		10.5	10.2		10.4		
Norikura	10.0	+ 6.9	10.7	9.30	+ 4.6	9.70	7.8	+ 7.4	8.4	0.20	— 0.11
(+)	12.0		12.8	11.5		12.0	10.0		10.7		
Huancayo	14.9	— 8.8	13.6	14.9	— 7.9	13.7	14.9	+ 7.8	13.8	0	— 0.44

(+) Upper figure related to the Störmer cone, the lower one to the main cone.

system there is inscribed the cut-off momentum for a centered dipole field, the second column shows the corrections for the excentric dipole location, according to the magnetic survey of VESTINE and LANGE [8] with respect to the epoch 1945, the third column gives the corrected momentum for the excentric dipole in the different systems. Finally lg V_{i0}^{*} and lg V_{i0}^{**} are inscribed in the last column, where V_{i0}^{*} is related to the assumption $L_1 = L_2$, and V_{i0}^{**} to $L_1 = 140$ g/cm² and $L_2 = 100$ g/cm².

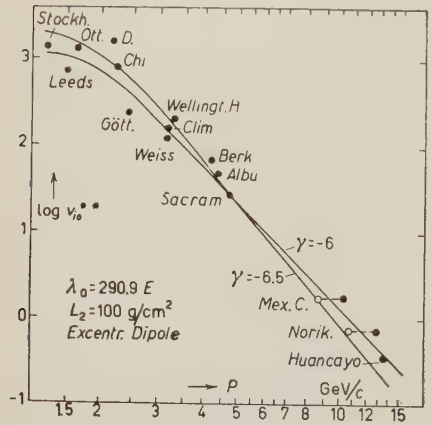

Fig. 1. – $\log V_{i0}^{**} - \log p_i$ plot related to the conventional geomagnetic co-ordinate system but corrected for excentricity of magnetic dipole location ($L_2 \neq L_1$).

The foregoing is then straightforward. We only need to find out in which of the three systems (the conventional, the presumably effective system or in a system intermediate between the two extreme locations of the dipole) the $V_{i0}^{**} - p_i$ plot shows the closest trend of points.

Plotting the points in a logarithmic scale we get the results of Fig. 1 for the conventional system corrected for excentricity of dipole location. (For L_1 we assumed 140 g/cm², for L_2 according to the result of a balloon flight with a neutron recording apparatus, reported by MEYER, PARKER and SIMPSON [5] we introduced 100 g/cm²). For Mexico-City and Norikura in low latitudes the open circles correspond to the Störmer forbidden cone, the full circles to the main (allowed) cone. The effective location may be assumed between the two extreme cases. The main cone is decisive for the equator station Huancayo and the Störmer cone for the remaining stations.

It is to be seen, that the points in the conventional system show a fairly good unique and close trend. The drawn curves are calculated, assuming a pover law $f(p)\,dp \sim p^{-\gamma}$, with $\gamma = 6$ and $\gamma = 6.5$ resp. and using the yield function for the neutron component according to FONGER [9].

But if one considers the location of the points for Leeds, Chicago, Ottawa and Stockholm, and assumes, that they deviate in a systematical manner from the close trend, than indeed for this stations a westward shift of the co-ordinate system would improve the picture.

But considering Fig. 2, where the points are plotted in the « presumable effective » system we observe a very pronounced splitting up of the trend. The two plots are related to $L_1 = 140$ g/cm², $L_2 = 100$ g/cm² and $L_1 = L_2 = 140$ g/cm² respectively in order to see what may be the influence of different assumptions for the absorption length of the neutron component related to solar cosmic rays.

In any case this system does not seem to be appropriate for solar cosmic radiation if the assumption of isotropy in the decay phase is approximately correct.

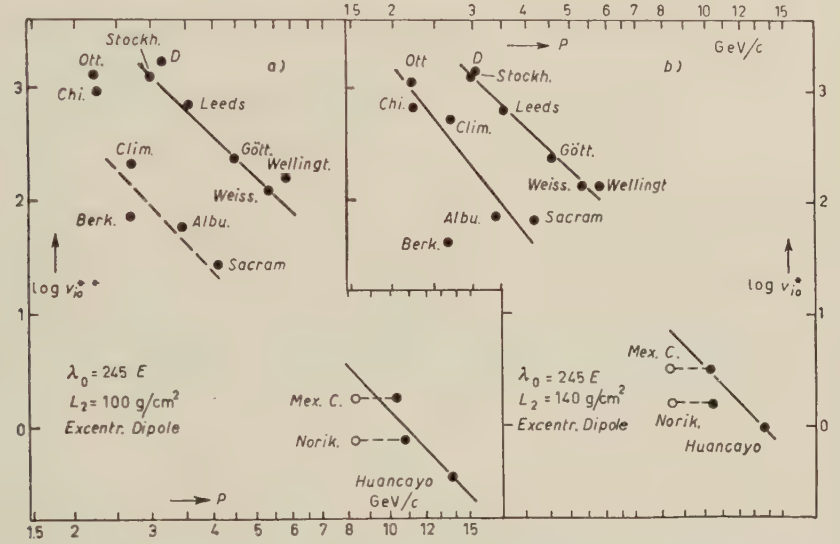

Fig. 2. – log V_{i0}^* resp. log V_{i0}^{**} — log p_i plot in a geomagnetic co-ordinate system where the tilted dipole is shifted 45° westward. (Effective dipole system for normal CR?).

At first sight Fig. 3 seems to indicate that the trend is closest for the westward shift of 15° and for $L_1 = L_2$. But there are strong objections against this assumption. Firstly there are decisive deviations of the points of Berkeley

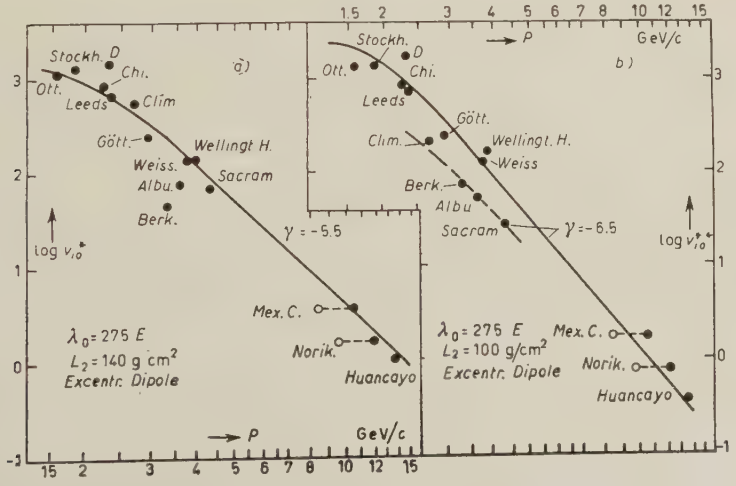

Fig. 3. – log V_{i0}^* — resp. log V_{i0}^{**} — log p_i plot in a geomagnetic co-ordinate system where the tilted dipole is shifted 15° westward.

and Albuquerque, which cannot be explained by quite different recording conditions with respect to other stations. Secondly neighbouring stations at mountain hights and at sea level show distinctly different percentage increases. This could not be if $L_1 = L_2$. So we have to exclude $L_1 = L_2$. And if we assume the most probable value for $L_2 = 100$ g/cm^2 one recognizes that the points for Climax, Berkeley, Albuquerque and Sacramento in Western USA in every case follow distinctly a close trend which distinguishes itself clearly from trends of the remaining points.

4. – Conclusions.

According to the results of our considerations we state, that the best approximation to a unique mean trend of points for solar cosmic rays is reached if we use the conventional geomagnetic system as base and apply corrections for excentric dipole location. Though the points for some european and american stations are better aligned in the intermediate westward shifted system, there are observed at least two different trends.

If further measurements of the normal cosmic radiation latitude cut-off finally should confirm that a westward shifted system is more suitable to explain the data one would be obliged to assume that the solar cosmic rays in the decay phase of the event were not distributed isotropically. But as we used time independent data based on the world-wide unique time law of intensity decrease, the splitting up of the trend in the westward shifted systems could only be explained by assuming that a special anisotropic distribution of deflecting centers rotates rigidly with the earth.

As till now no reason is known for such a behaviour we conclude that the influencies on cosmic ray particle trajectories cannot be described in details in terms of a simple dipole model alone.

Though the measured intensities in the conventional « excentric dipole » system fit clearly better in a unique trend than in the westward shifted systems also in this case discrepancies between the data of the eastern american stations and the european stations cannot be overseen.

It seems to us that the discrepancies cannot at all be entirely eliminated by choosing an adequate location and orientation only of one field producing dipole because they inherently may arise on account of the very deviations of the effective field from a dipole field and its symmetry qualities.

* * *

The author wishes to express his gratitude to all colleagues who kindly interchanged their records with those of the Max-Planck-Institut für Physik der Stratosphäre, Weissenau. He is further indebted to the Deutsche Forschungsgemeinschaft for supporting the work on time variations of Cosmic Radiation.

REFERENCES

[1] J. A. Simpson, F. Jory and M. Pyko: *Journ. Geophys. Res.*, **61**, 11 (1956).
[2] J. A. Simpson, K. B. Fenton, I. Katzmann and D. C. Rose: *Phys. Rev.*, **102**, 1648 (1956).
[3] C. J. Waddington: *Nuovo Cimento*, **3**, 930 (1956).
[4] R. E. Danielson, P. S. Freier, J. E. Naugle and E. P. Ney: *Phys. Rev.*, **103**, 1075 (1956).
[5] P. Meyer, E. N. Parker and J. A. Simpson: *Phys. Rev.*, **104**, 768 (1956).
[6] G. Pfotzer: *Mitteilungen a. d. Max-Planck-Institut für Physik der Stratosphäre, Weissenau*, no. 7, 1956.
[7] A. Ehmert and G. Pfotzer: *Mitteilungen a. d. Max-Planck-Institut für Physik der Stratosphäre, Weissenau*, no. 6, 1956.
[8] E. H. Vestine and L. Lange: Carnegie Inst. Wash. Publ. 578, 1949 und 580.
[9] W. H. Fonger: *Thesis University of Chicago* (1953) communicated by J. A. Simpson and W. C. Fagot: *Phys. Rev.*, **30**, 1068 (1953).

SUPPLEMENTO AL VOLUME VIII, SERIE X
DEL NUOVO CIMENTO

N. 2, 1958
2° Trimestre

Determination of Latitude Equivalents for Second Phase Solar Flare Particles.

P. L. MARSDEN and J. G. WILSON

The Physical Laboratories of the University of Leeds - Leeds

1. – Introduction.

The cosmic ray disturbance following the solar flare of 23 February 1956 showed, after an initial phase exhibiting strong impact zone phenomena, a long period during which the earth may be considered to have been in an isotropic « atmosphere » of cosmic particles. The extent of the region occupied by this atmosphere, and the details of the constraint by which it was contained, are matters about which there is not yet agreement, but it is common ground that the density of particles diminished with time by a leakage process and that the more energetic particles were the first to leak away. The rigidity spectrum of the particles over a period of many hours after flare-activity had ceased was such that the response of neutron monitors at sea-level exhibited a very strong latitude effect in the middle latitudes, and this feature provides a further powerful approach to the problems which have already been revealed by other methods of the relationship of the effective geomagnetic field, as it controls particle trajectories near the earth, with the conventional dipole field (C.D.F.) deduced from surface measurements. It will be recognized that this approach arose only in a preliminary way for the event of 1956, and that at subsequent flare disturbances a considerably wider and more effective cover of stations will be in operation.

In this note we examine the response during this second phase of neutron monitors as reported from two groups of stations, one in eastern North America and the other in Western Europe. These are characterised by a relatively close grouping of stations in regions between which there is clear evi-

dence of a discrepancy in the conventional geomagnetic description. They also contain stations which differ in altitude by an amount which is small in terms of the attenuation length of the nucleonic component in the atmosphere and for which, therefore, any uncertainty as to the appropriate value of this attenuation coefficient for flare particles is not important.

2. – Ratios of proportional increase.

In Table I, we summarize the proportional increase $\Delta N/N_0$ as a function of time at Leeds and Chicago which, in the grouping of stations already referred to are those, one from each group, in which the proportional increases are most closely similar. The fourth column of the Table, and see also Fig. 1, gives the ratio of proportional increases at the two stations, $(\Delta N/N_0)_{\text{Leeds}}/(\Delta N/N_0)_{\text{Chicago}}$ and shows that over the fifteen hours 0500-2000 U.T. this ratio remains constant within the limits set by the statistical uncertainty of the measured counts. It is not useful to continue this comparison after 2000 h U.T., for not only is it for any part of this period statistically much weaker, but the increases are becoming sensitive to the precise assumptions made about the variation of the background intensity N_0. The records over a period of days around the time of the flare event leave little doubt that N_0 is in fact increasing during the period covered in Table I, and for the purpose of the Table N_0 has been assumed to be increasing linearly as indicated at the foot of Table I. This assumption is not so strongly established, however, as to be of value under conditions where its application amounts to more than a small correction. It is the uniformity of this ratio of proportional increases over a period of more than twelve hours that provides direct evidence of the effective isotropy of the atmosphere of cosmic particles giving rise to the second phase of the flare records. Analyses corresponding to that of Table I have been made between all stations lying within each of the geographical groups already referred to: these are summarized in Table II.

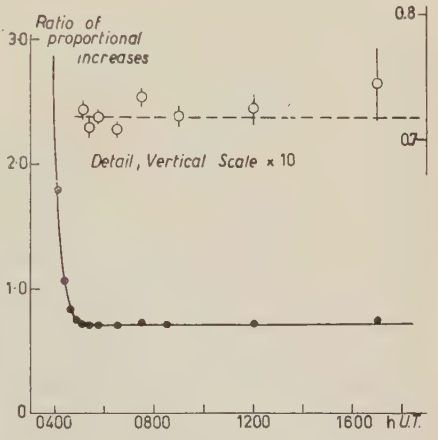

Fig. 1 – Time variation of the ratio of the proportional increases in the cosmic ray intensity recorded by neutron monitors at Leeds and Chicago.

TABLE I. – *Proportional increase at Leeds and at Chicago* [1], *23 February, 1956.*

Time Interval (h U.T.)	$(\Delta N/N_0)_{\text{Leeds}}$	$(\Delta N/N_0)_{\text{Chicago}}$	$(\Delta N/N_0)_{\text{Leeds}}/(\Delta N/N_0)_{\text{Chicago}}$
0400 - 0415	35.47	19.79	1.79 ± 0.01
0415 - 0430	29.94	19.70	1.063 ± 0.007
0430 - 0445	13.75	16.47	0.835 ± 0.006
0445 - 0500	9.73	12.90	0.754 ± 0.007
0500 - 0515	7.25	10.02	0.724 ± 0.007
0515 - 0530	5.68	8.01	0.710 ± 0.008
0530 - 0600	4.27	5.94	0.718 ± 0.006
0600 - 0700	2.67	3.76	0.708 ± 0.006
0700 - 0800	1.61	2.19	0.734 ± 0.008
0800 - 1000	0.85	1.19	0.719 ± 0.009
1000 - 1400	0.345	0.476	0.725 ± 0.013
1400 - 2000	0.112	0.150	0.745 ± 0.03

N_0 (Leeds) = 3152/15 min at 0000 h on 23-2-56, rising to 3309/15 min at 0200 h on 24-2-56.
N_0 (Chicago) = 5199/15 min at 0000 h on 23-2-56, rising to 5381/15 min at 0200 h on 24-2-56.

TABLE II. – *Relative values of the proportional increase for the second phase of activity.*

Reference station	Second station	Relative proportional increase
Leeds	(Chicago)	(1.395 ± 0.009)
	Gronigen [3]	0.65 (*)
	Göttingen [4]	0.403 ± 0.008
	Weissenau [5]	0.250 ± 0.008
Chicago	(Leeds)	(0.718 ± 0.005)
	Durham (N. H.) [6]	1.48 ± 0.05
	Ottawa [7]	1.83 ± 0.027

(*) Based on one time only (0720 h U.T.).

3. – Relative proportional increases as functions of geomagnetic co-ordinates.

In Fig. 2 (*a*, *b*) the relative proportional increases listed in Table II are plotted against the C.D.F. geomagnetic latitudes of the stations as derived from the data of VESTINE, LAPORTE and LANGE [2]. Among themselves, the data for each geographic region are not inconsistent, the proportional increase being relatively larger at the higher geomagnetic latitudes. It is apparent that actual values of latitudes are displaced as between the two groups however, and both curves indicate that the effective difference of magnetic latitude between Leeds and Chicago is rather more than one degree, Chicago being in the higher latitude. This result is in general accord with other

data (WADDINGTON [8]) on limiting particle trajectories as between North America and Western Europe, and leads to a rather precise evaluation of the difference between these two regions.

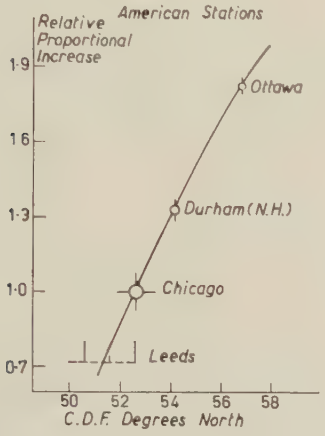

Fig. 2*a*. – Ratios of relative responses for the European stations as a function of C.D.F. geomagnetic latitude.

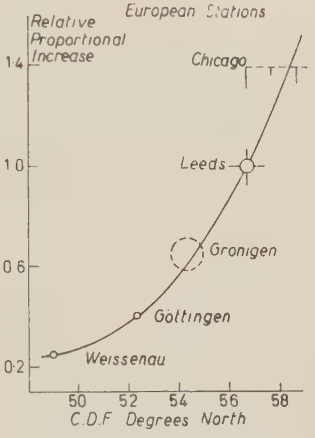

Fig. 2*b*. – Ratios of relative responses for the American stations as a function of C.D.F. geomagnetic latitude.

The second-order approximation in which the centred dipole is replaced by one located eccentrically has long been recognized: in recent years variations in this approximation from the model originally proposed have been made in an attempt to fit more accurately particular features of the cosmic ray data. The tendency has been for this improved fit of restricted data to be gained at the expense of accurate representation of other features. For the relatively small geographic regions we discuss here, it is not helpful to initiate any new variant of this model, but we note one or two points arising from existing proposals.

From a world-wide study of neutron-monitor data for the 1956 event, PFOTZER [9] has concluded that the overall best fit is obtained using and eccentric dipole model in which the pole is located at (275° E, 78°.5 N) with the magnetic centre lying at a distance from the centre of the earth of 0.0087 of the earth's radius in the direction (243° E, 8° N). Our emphasis has been placed rather differently, for we have drawn attention to restricted geographical regions in which quite precise evaluations of the relative proportional responses have been shown to be obtainable. Among our stations three—Chicago, Durham (N.H.), Leeds—are placed on the Pfotzer model in the same latitude. The relative values of the proportional increases at these stations, which are respectively 1.00, 1.48 and 0.72 must then be interpreted as a longitude effect ($\Delta E = 0°$ (Chicago), 18°.5 (Durham), 98° (Leeds)), with a large amplitude and with a maximum which must be placed in longitude 20°-40° E.

At the proposed latitude (53°) so large a longitude effect is extremely difficult to accept, while the model further indicates a longitude maximum well to the west of that indicated above.

It has been supposed that deviations between the magnetic field which best describes the surface situation and that which determines the motion of field-sensitive cosmic ray particles are probably to be related to the rotation of the inclined terrestrial dipole in the surrounding conducting medium.

At the present time further experimental data are essential for any detailed analysis of this behaviour, and we draw attention to the relevance of comparisons such as that made in Table I.

1) The constancy of the ratio of proportional increases shown in the Table indicates that over short times the latitude difference between the two well-separated stations does not change by amounts greater than of the order 0°.1. While a comparison of our result with the conclusions at other times from work by different methods [8, 10, 11] suggests that there is long-term stability to within perhaps 1°, it seems likely that stability between successive flare events, which may happen against very different background conditions, will be tested to much closer limits.

2) It seems likely to be some considerable time before cosmic ray equivalents of latitude are made over more than a very few regions. A comparison of the type of that in Table I over the relatively closely spaced stations in, for example, Western Europe, may be expected to allow lines of constant proportional response to be drawn. The 1956 data suggest that these lines are not greatly inclined to those of the conventional field, but with an increased number of stations more precise conclusions will become possible.

REFERENCES

[1] P. Meyer, E. N. Parker and J. A. Simpson: *Phys. Rev.*, **104**, 768 (1956).
[2] E. H. Vestine, L. Laporte and I. Lange: Carnegie Institution of Washington, Publication 580 (1947).
[3] H. L. de Vries: *Physica*, **22**, 357 (1956).
[4] B. Meyer: *Zeits. f. Naturf.*, **11***a*, 326 (1956).
[5] A. Ehmert and G. Pfotzer: *Zeits. f. Naturf.*, **11***a*, 322 (1956).
[6] J. A. Lockwood, H. E. Yingst, A. R. Calawa and G. Sarmaniote: *Phys. Rev.*, **103**, 247 (1956).
[7] D. C. Rose: private communication.
[8] C. J. Waddington: *Nuovo Cimento*, **3**, 930 (1956).
[9] G. Pfotzer: *Mitt. a. d. Max-Planck-Inst. Phys. der Stratosphäre, Weissenau*, no. 9, 1 (1956).
[10] R. E. Danielson, P. S. Freier, J. E. Naugle and E. P. Ney: *Phys. Rev.*, **103**, 1075 (1956).
[11] J. A. Simpson, K. B. Fenton, J. Katzman and D. C. Rose: *Phys. Rev.*, **102**, 1648 (1956).

PART I.

SECTION B: Geomagnetic Effects.

New Changes in the Low-Energy Particle Cut-Off and Spectrum of the Primary Cosmic Radiation (*).

P. MEYER and J. A. SIMPSON

Enrico Fermi Institute for Nuclear Studies
The University of Chicago - Chicago, Ill.

At the time of the Guanajuato Conference on Cosmic Radiation we have reported some experiments that showed that the primary cosmic ray energy spectrum as well as the low energy cut-off are not permanent features of the cosmic radiation but undergo remarkable changes with time [1]. The rapid changes in these properties of the primary radiation—rapid compared to galactic time scales—let us conclude that the mechanism responsible for the low energy cut-off is operating within or in the vicinity of the solar system. It was suggested at that time that the observed phenomena may be solar controlled and related to the activity cycle of the sun. In order to settle the question whether solar activity is the dominating factor for the observed changes we have extended the experiment of 1954 and have carried out additional measurements in the fall of 1956, when the level of solar activity had again appreciably increased [2].

The information on the changes in spectrum and cut-off was obtained by measuring the nucleonic component intensity as a function of geomagnetic latitude at high altitude. In each measurement a neutron monitor was installed in an aircraft and carried between approximately 40° and 60° N geomagnetic latitude. All data were collected along identical paths and for the same atmospheric depth, namely 22.5 cm Hg (30 000 ft pressure altitude). Hence, the results obtained in the years 1948, 1951, 1954 and 1956 are directly comparable.

(*) Assisted in part by the Office of Scientific Research and the Geophysics Research Directorate, Air Force Cambridge Research Center, Air Research and Development Command, U.S. Air Force.

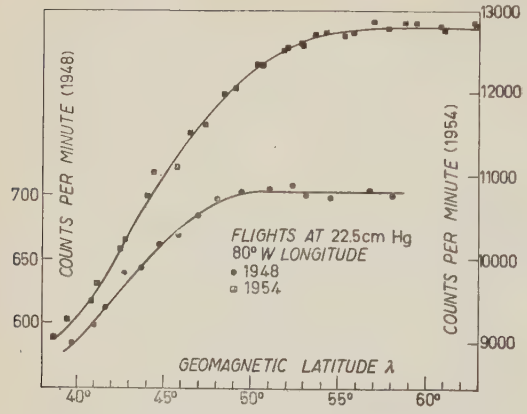

Fig. 1. – The nucleonic component latitude curves for 1948 and 1954 at 80° West longitude and 310 g/cm² atmospheric depth.

The 1948 and 1954 latitude curves are shown in Fig. 1. Three important points are easily noticed:

a) the slope of the latitude curve is appreciably steeper in 1954 than in 1948;

b) the knee has shifted northward;

c) the intensity of the low energy particles has increased.

Since NEHER [3] could show with the help of balloon-borne equipment that the cut-off in 1954 occured at much higher geomagnetic latitudes than we observed, we conclude that the presence of a knee in our 1954 curve is due to atmospheric absorption at aircraft altitudes.

The corresponding latitude curve for 1956 is shown in Fig. 2 and the 1954 curve has been included as a dashed line. Further changes in the slopes, in the position of the knee, and in the intensity of the low energy particles can clearly seen and it can be noted that the direction of the changes has reversed be since 1954.

A more detailed analysis of the slopes of the latitude curves reveals the changes of the primary spectrum within the rigidity range from ~1 GeV to 4.4 GeV. If we represent the primary differential spectrum of 1948 by the power law $j = C/(p/Z)^{\gamma}$, with γ=2, according to WINCKLER, than we obtain for the exponent of the 1954 spectrum $\gamma = 2.7$ and for 1956 an exponent $\gamma = 2.5$.

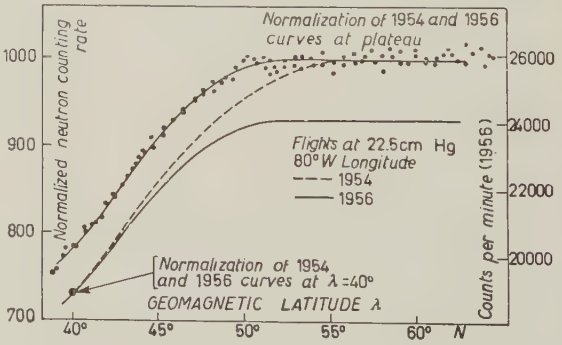

Fig. 2. – The nucleonic component latitude curves for 1956 at 80° West longitude and 310 g/cm² atmospheric depth. For comparison the 80° W latitude curve for 1954 is shown as a dashed line.

These spectra are drawn in Fig. 3. A summary of the changes in the latitude curves for the years 1948 through 1956 is given in Fig. 4. All the latitude curves were normalized at the plateau in order to clearly show the relative motion of the knee.

From these results we are again led to the conclusion that the cut-off mechanism is solar controlled and must operate within or near the solar system. We also conclude that solar activity is the dominating factor in producing the cut-off, the changes in the primary spectrum, and the changes in total intensity of the primary particles. There exists a close correlation between these properties of the primary cosmic radiation and the 11 years activity cycle of the sun (Fig. 5). Obviously, the changes in intensity are the same effect that was originally discovered by FORBUSH [4].

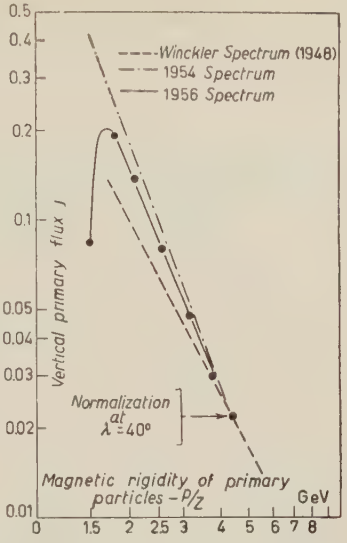

Fig. 3. – The primary particle rigidity spectrum for 1956 deduced from the latitude intensity measurements shown in Fig. 1 and 2. If we assume that the differential spectrum in 1948 was represented by $j=C/(p/Z)^{\gamma}$, with $\gamma=2$, then the 1956 spectrum requires $\gamma=2.5$.

Experiments that were carried out over the past few years indicate that we are dealing with the modulation of pre-existent galactic cosmic radiation. Specific mechanisms to account for the experimental evidence have been proposed recently by MORRISON [5] and PARKER [6]. These models use the diffusion of cosmic ray particles through disordered interplanetary magnetic fields of solar origin. Parker's model in particular would be able to account for variations with a period as long as 11 years. Any of these modulating mechanisms depress the density of the prevailing galactic cosmic radiation in the vicinity of the earth and one is therefore led to the conclusion that the only time

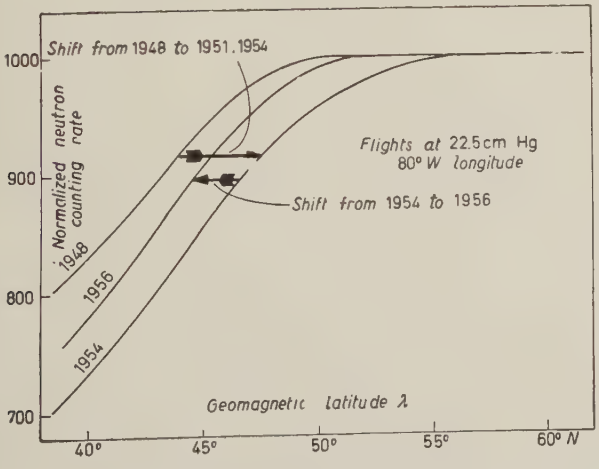

Fig. 4. – The nucleonic component latitude curves for 1948, 1954 and 1956 arbitrarily normalized at latitudes $> 58°$ N in order to display the magnitude of the shifts in the low rigidity cut-off of the cosmic ray spectrum.

an observer on the earth may have access to the true galactic cosmic ray spectrum is the brief period of minimum solar activity.

It remains to be shown whether one single mechanism may be responsible not only for the 11 year variation but also for fluctuations of much shorter time like the 27 day variation and the sudden decreases of the Forbush type. Further experiments of a similar type as those described may help to answer this question.

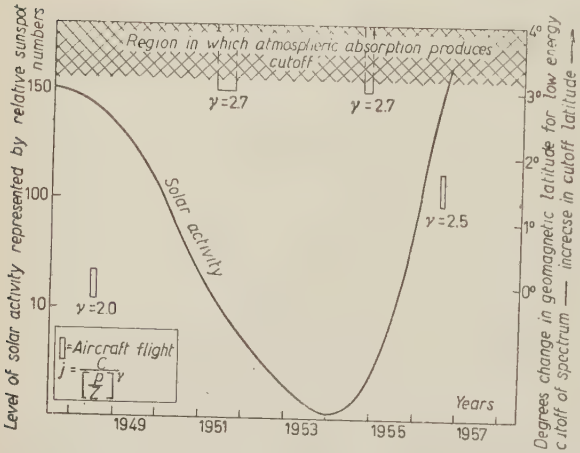

Fig. 5. – The changes in cut-off latitude and exponent γ of the primary spectrum as a function of time. For comparison the level of solar activity as measured by relative sunspot number is shown over the period of the experiments.

REFERENCES

[1] P. MEYER and J. A. SIMPSON: *Phys. Rev.*, **99**, 1517 (1955).
[2] For a more detailed description of the experiment see: P. MEYER and J. A. SIMPSON: *Phys. Rev.*, **106**, 568 (1957).
[3] H. V. NEHER: *Phys. Rev.*, **103**, 228 (1956).
[4] S. E. FORBUSH: *Journ. Geophys. Res.*, **59**, 525 (1954).
[5] P. MORRISON: *Phys. Rev.*, **101**, 1397 (1956).
[6] E. N. PARKER: *Phys. Rev.*, **103**, 1518 (1956).

SUPPLEMENTO AL VOLUME VIII, SERIE X
DEL NUOVO CIMENTO

N. 2, 1958
2° Trimestre

Directional Properties of Cosmic Ray Telescopes.

E. Å. Brunberg

The Royal Institute of Technology - Stockholm

During the study of the cosmic ray intensity and its time variations different kinds of recording apparatus have been used as for instance ionization chambers and Geiger-Müller tube telescopes of different aperture and pointing in different directions. In this way different time variations are observed. Our knowledge of that part of the variation which is induced by the atmosphere seems now to be fairly well established (see *Progress in Elementary Particle and Cosmic Ray Physics*, Vol. 4 (Amsterdam, 1958) Dorman and Feinberg, Trefall, Maeda and Wada and many others) but the mechanism of the extraterrestrial variations is the subject of several theories. These are compared with by measurements carried out with instruments, the measuring properties of which we know little about. The aim of the present paper is to show how this problem can be treated by introducing the optics of cosmic ray telescopes.

The problem is as follows: given a cosmic ray source with known spectrum, located in a given direction far away from the earth, what is the counting rate of a telescope on the earth pointing in a given direction?

As in ordinary optics we start by treatifhe casen of a point source (in this case a cosmic ray point source) infinitely ar away from the earth and find the image given by the telescope. By image we mean the intensity recorded by the apparatus during one day. Using this result it is then possible to deduce the image of any finite cosmic ray source.

The problem is divided into two main parts, namely a study of the deflection in the geomagnetic field of the primary particles and the spread in the atmosphere of the secondaries. In connection with solar flares Firor, Jory and during this conference, Lüst, have discussed the counting rate of an omnidirectional detector outside the atmosphere. Sandström has pointed out the importance of taking into account the spread in the atmosphere when designing counter telescopes.

1. – Geomagnetic effects.

We consider the state of affairs in the six-dimensional phase space and look at particles with momenta in the momentum interval between p and $p+\mathrm{d}p$ in the divergent beam from the source. The cross-section of the beam is large compared to the cross-section of the earth. Using Liouville's theorem it can be shown that the density of the corresponding flow in phase space is constant and the same in all parts of phase space where we have the flow.

A telescope with a solid angle $\mathrm{d}\Omega$ and surface a is represented in phase space by a six-dimensional element when considering particles in the small momentum interval $\mathrm{d}p$. The element moves about in phase space as the earth rotates. When it happens to lie completely inside the flow, as regards both its momentum and space parts, the telescope measures the same intensity as another telescope pointing towards the source would measure outside the magnetic field, provided the products of the solid angles and the surfaces of the two telescopes are equal.

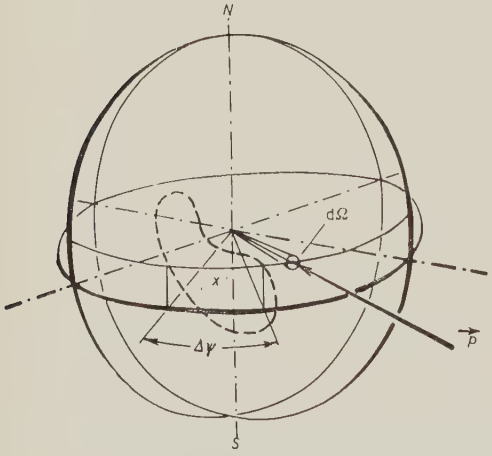

Fig. 1.

The projection of solid angle and surface is carried out along the particle orbits in the geomagnetic field. The directions of the particle orbits far away from the earth are called asymptotic directions. They are represented by vectors, the endpoints of which coincide with the center of a globe. The foot points describe on the surface of the globe a curve, which is the projected solid angle of the telescope as in Fig. 1.

It can be shown that the condition for the element of the telescope being completely inside the flow in phase space is fulfilled when the projected solid angle of the telescope is within the solid angle, subtended by the beam from the source. If this is not so, the intensity measured by the telescope at a certain moment is reduced and given by

$$i_a = I(p)\,\mathrm{d}p \cdot \Delta\varepsilon \int_a \mathrm{d}a \cdot \cos u \qquad \text{particles/s}\,,$$

where $I(p)\,\mathrm{d}p$ is the number of particles in the momentum interval $\mathrm{d}p$, $\Delta\varepsilon$ is the solid angle, which is common to the projected solid angle of the telescope

and the solid angle, subtended by the primary beam. The integral finally, is the effective measuring surface of the telescope.

If the telescope has a finite solid angle and the solid angle of the source is infinitely small, $\Delta\varepsilon$ is either equal to the solid angle of the source or zero. This case is considered in Fig. 1, where the angular position of a source is given by the vector $\boldsymbol{p}$ and the source subtends the solid angle $d\Omega$. When the earth is rotating $d\Omega$ moves along a circle on the globe. During the angular interval $\Delta\Psi$ the telescope records full intensity given by the primary effective spectrum in the chosen momentum interval.

The image of a given source can now be calculated by summing up the contribution from all momentum intervals of the effective spectrum. Fig. 2

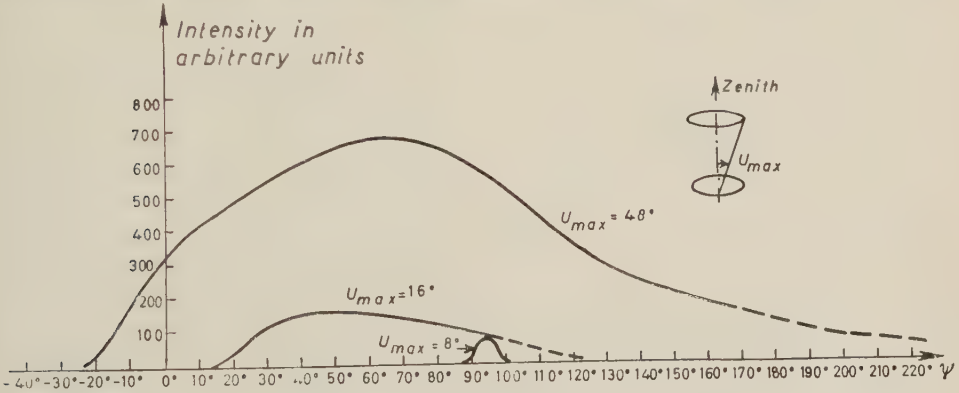

Fig. 2.

shows the result for telescopes with different apertures pointing in the zenith direction at Huancayo. The source lies in the equatorial plane and the isotropic background is neglected. It seems reasonable in this first approach to use the same source spectrum as that of the isotropic background. The effective primary spectrum of an ionization chamber assuming only protons is known up to 13 GeV. FONGER has deduced a spectrum above this point of the form $(1+E)^{-1.2}$, which has been used a source spectrum.

The curves show that the image of the source depends very much on the aperture of the telescope. The next problem is now to determine the effect of the spread of secondaries in the atmosphere.

2 – The spread in the atmosphere.

The problem can be expressed by the following question: given a cosmic ray source with known spectrum, located in a given direction far away from the earth, what is the counting rate of a telescope on the earth, pointing in a given direction if the geomagnetic deflection is neglected?

The problem is divided into three parts:

1) the path of a primary particle, before it interacts in a nucleon-nucleon collision;

2) the intensity and energy distributions of mesons created in the nucleon-nucleon collision;

3) the behaviour of the mesons on their way towards the telescope.

We consider a parallel beam of particles entering the atmosphere from a direction $\alpha'\beta'$ (Fig. 3). At a certain height z there are nucleon-nucleon collisions and mesons, going out in a direction making the angle Θ to the primary direction, are recorded by the telescope, which is pointing in a direction $\alpha\beta$.

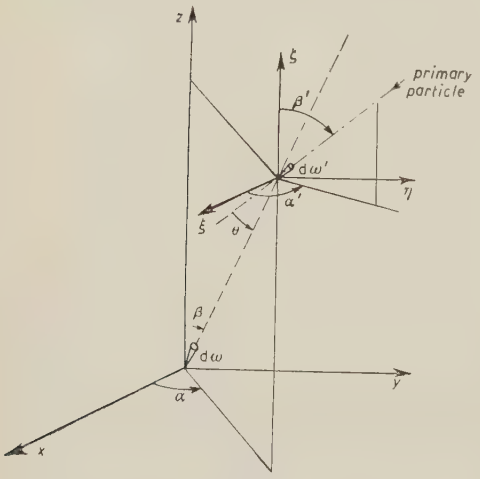

Fig. 3.

The rate of nucleon-nucleon collisions at different heights in the atmosphere is important in the following and has been calculated, assuming an atmosphere in equilibrium and that the mean cross-section for interaction is 120 g/cm². The calculations are done for protons of 20 GeV/c as an example.

In the center of mass system of the nucleon-nucleon collision the produced mesons are assumed to have an isotropic intensity distribution. The energy distribution of the mesons in the center of mass system has been taken into account by using the energy spectrum of mesons, obtained by CAMERINI *et al.* (*Progress in Cosmic Ray Physics*, Vol. 1 (Amsterdam, 1952), p. 22). Under these assumptions the intensity and energy distribution of π-mesons in the laboratory system have been calculated.

Let us consider π-mesons going out in the direction towards the telescope. The influence of $\pi \rightarrow \mu$ decay upon the intensity distribution of the μ-mesons is neglected. On their way towards the telescope the μ-mesons lose energy due to ionization and they also decay. Mesons starting at large angles Θ have smaller energies and will consequently decay more rapidly seen from the laboratory system than those starting from directions which deviate little from the primary direction. Further they are more likely to be absorbed before they reach the telescope. These effects have a sharpening influence on the angular intensity distribution recorded by a telescope deeper in the

atmosphere compared to the distribution just below the point of a nucleon-nucleon collision. An estimate of the Coulomb scattering of the μ-mesons has been done and shows that it has a negligible influence on the angular distribution.

The intensity measured by a telescope with an infinitely small solid angle has been numerically integrated for different measuring directions of the telescope in zenith as well as in azimuth. In Fig. 4 are plotted the image of the

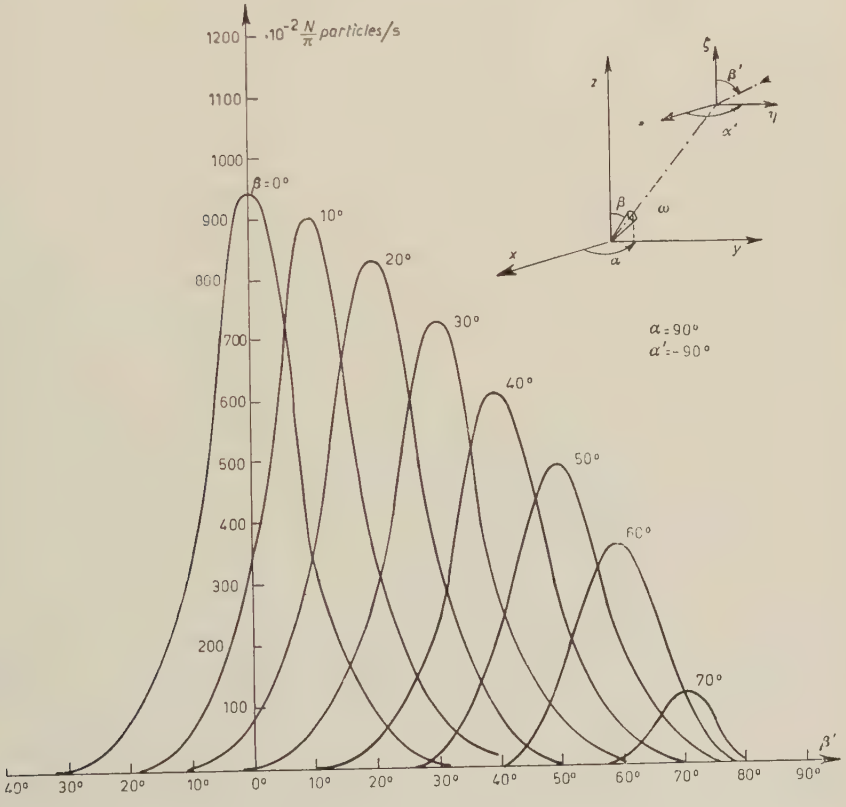

Fig. 4.

source obtained with the telescope oriented in the plane of the source but with different zenith angles. It must be pointed out that what we measure is the ratio between source intensity and background and in Fig. 5 is plotted the image of the source seen with telescopes of different apertures assuming a $\cos^2\beta$ law for the zenith dependence of the isotropic background. If we measure an amplitude of 1% with an infinitely narrow telescope, a broad angle telescope measures a much smaller amplitude as seen from this figure.

Amplitudes of the order of 1% in the daily intensity variation have been observed with narrow angle telescopes (SARABHAI). This could be understood

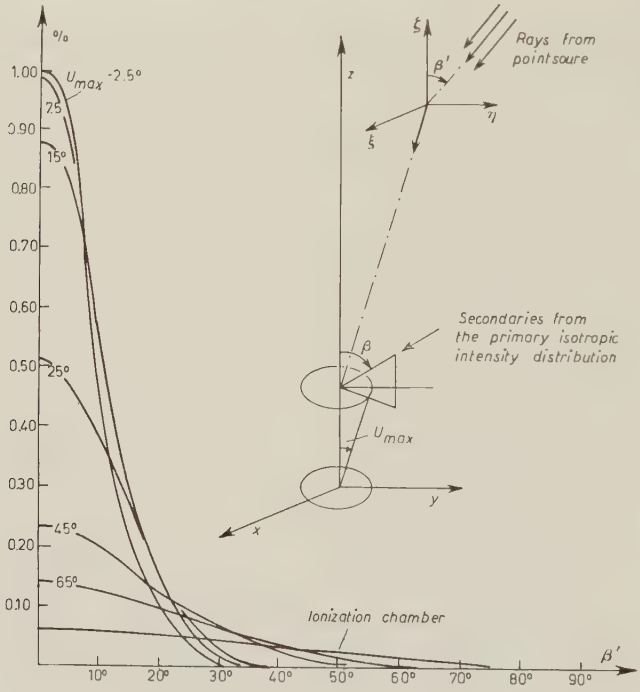

Fig. 5.

if there are cosmic ray sources in space of rather limited extension. Such sources could give rise to larger amplitudes in the daily variation observed by narrow angle telescopes than by broad angle telescopes or ionization chambers.

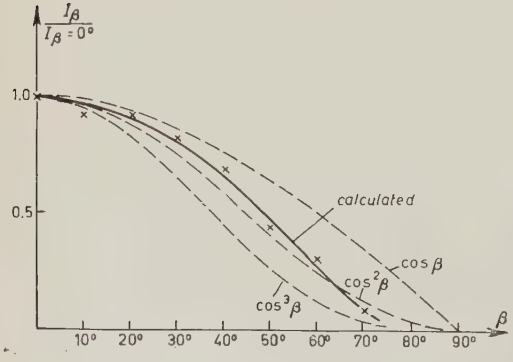

Fig. 6.

A valuable check of the calculations as regards the atmospheric part can be obtained by deducing the zenith angle dependence of the radiation, which experimentally is found to be approximately a $\cos^2\beta$ curve (JOHNSON, GREISEN and many others, see e.g. MONTGOMERY, 1949). This has been done for a narrow angle telescope assuming isotropic distribution of point sources over the hemisphere using the described

calculations. The whole spectrum has not been taken into account, the calculations are carried out for 20 GeV/c protons. The result is shown in Fig. 6 where the $\cos\beta$, $\cos^2\beta$ and $\cos^3\beta$ curves have been drawn for comparison. The calculated curve agrees rather well with the $\cos^2\beta$ curve. The rather good agreement between the calculated curve and the $\cos^2\beta$ curve indicates that the assumptions regarding the meson production and the primary energy of 20 GeV give an essentially representative picture of the phenomena in the atmosphere.

BIBLIOGRAPHY

E. Å. Brunberg: *Tellus*, **8**, No. 2 (1956).

U. Camerini, W. O. Lock and D. H. Perkins: *Progress in Cosmic Ray Physics*, Vol. 1 (Amsterdam, 1952), p. 22.

L. I. Dorman and E. L. Feinberg: *On the Nature of the Cosmic Ray Variations.* Awaiting publication in *Proceedings of the Guanajuato Conference.*

J. Firor, *Phys. Rev.*, **94**, 1017 (1954).

W. Fonger: *Phys. Rev.*, **91**, 351 (1953).

K. Greisen: *Phys. Rev.*, **61**, 212 (1942).

T. Johnson: *Rev. Mod. Phys.*, **10**, 205 (1938).

F. S. Jory: *Phys. Rev.*, **103**, 1068 (1956).

K. Maeda and M. Wada: *Journ. Sci. Res. Inst., Tokyo*, **48**, No. 1350 (1954).

D. J. X. Montgomery: *Cosmic Ray Physics*, (Princeton, 1949), p. 169.

A. E. Sandström: Awaiting publication in *Proceedings of the Guanajuato Conference.*

V. Sarabhai and N. W. Nerurkar: Awaiting publication in *Proceedings of the Guanajuato Conference.*

SUPPLEMENTO AL VOLUME VIII, SERIE X
DEL NUOVO CIMENTO

N. 2, 1958
2° Trimestre

Comparison of the Cosmic-Ray Intensity Variations Observed at Different Altitudes (*).

Y. MIYAZAKI

Cosmic-Ray Laboratory, Scientific Research Institute - Tokyo

1. – Introduction.

Continuous observations of the cosmic-ray meson component have been made by means of a Nishina type ionization chamber during these ten years at the Scientific Research Institute, Tokyo (Geomagn. Lat. $+25° 40'$ N, Long. $206° 32'$ E, sea level) [1].

Since August, 1955, measurements of the meson component have also been made continyuousl at Mt. Norikura (Geomagn Lat. $+25° 49'$ N, Long. $204° 31'$ E, Alt. 2840 m above sea level) by means of a ionization chamber identical wiht the one used at sea level.

Simultaneous registration of cosmic-ray intensity at different altitudes have already been performed by several workers using an identical equipment, however, the comparison of the intensity obtained by these kinds of observations has not yet been tried up to now.

The aim of this study is to find out the time variations of comparatively low energy primary cosmic rays by the comparison of the results obtained at different latitudes but at almost the same geomagnetic longitude and latitude.

2. – Comparison of the meson component observed at different altitudes.

Since the over-all multiplicity of μ-mesons observed at mountain and at sea level is different, especially in the low energy regions, then the μ-mesons observed at mountain and at sea level correspond to the primary cosmic rays

(*) This work was supported by the Ministry of Education and the Japanese National Committee for the IGY.

of different energy. Obviously the difference of the meson intensity observed at different altitudes reflects the intensity variation of the low energy primary particles.

It is well known that the meson intensity is affected not only by the time variation of primary particles but also by the temperature variation of the atmosphere above the stations. These features can be expressed by equations taking into account the partial temperature effect [2],

$$\frac{\Delta M_s}{M_s} = \eta_2 + \alpha' \Delta T_1' + \alpha_2 \Delta T_2 \,, \tag{1}$$

$$\varepsilon \frac{\Delta M_m}{M_m} = (\varepsilon - 1)\eta_1 + \eta_2 + (\varepsilon - 1)\alpha_1 \Delta T_1 + \alpha_1'' \Delta T_1'' \,, \tag{2}$$

where $\Delta M_s/M_s$, $\Delta M_m/M_m$ mean the variational fraction of mesons observed at sea and at mountain level, respectively, η_2 means the variational fraction of primary cosmic rays corresponding to the meson component which can reach sea level, η_1 the variational fraction of primary cosmic rays corresponding to the meson component which can be observed only at mountain level, $\alpha' \Delta T_1'$ the variation caused by the temperature change above the mountain, $\alpha_2 \Delta T_2$ the variation caused by the temperature change below the mountain, $(\varepsilon - 1)\alpha_1 \Delta T_1$ the variation of the meson component which can not reach sea level by the temperature change above the mountain, $\varepsilon = M_m/M_s$.

From (1) and (2), we get

$$\frac{\Delta M_\Delta}{M_s} = \varepsilon \frac{\Delta M_m}{M_m} - \frac{\Delta M_s}{M_s} = (\varepsilon - 1)\eta_1 + (\varepsilon - 1)\alpha_1 \Delta T_1 - \alpha_2 \Delta T_2 \,. \tag{3}$$

Since the momentum of μ-mesons observed only at mountain level is very low, the effective depth of the mean temperature T_1 is situated only little above the mountain. Further, the variation of temperature above and below the mountain is approximately the same. Thus we may put $\Delta T_1 = \Delta T_2$. Then we get

$$\eta_1 = \frac{1}{\varepsilon - 1}\left(\frac{\Delta M_\Delta}{M_s} - \alpha \Delta T_2\right). \tag{4}$$

In order to check the equation (4), the relation between

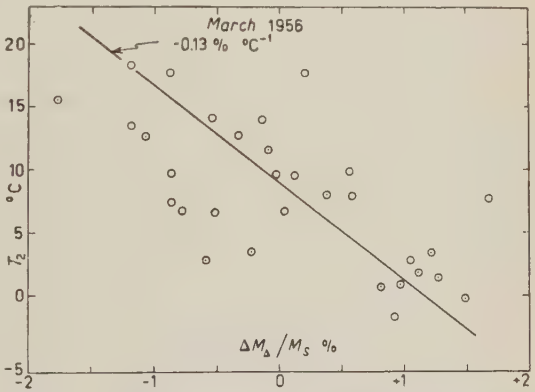

Fig. 1. – The correlation between the difference of the meson intensities observed at Mt. Norikura and at sea level corrected for the barometer effect Δ and the mean atmospheric temperature between mountain and sea level T_2.

$\Delta M_\Delta/M_s$ and T_2 is plotted in Fig. 1 using the data for the period when $\eta_1 \approx 0$. Coefficient α was obtained from Fig. 1 [3],

$$\alpha = -0.13\,\%\ ^\circ\mathrm{C}^{-1}. \tag{5}$$

From the statistical analysis [3], α_1 is $-0.279\,\%\ ^\circ\mathrm{C}^{-1}$ and α_2 is $-0.065\,\%\ ^\circ\mathrm{C}^{-1}$. Then α is obtained by the relation $\alpha = (\varepsilon - 1)\alpha_1 - \alpha_2$, using $\varepsilon = 1.7$ as $-0.13\,\%\ ^\circ\mathrm{C}^{-1}$. This value is just identical with the one obtained by the difference method mentioned above. Thus the assumption that the temperature effect of $\Delta M_\Delta/M_s$ is mainly caused by T_2 is justified.

3. – Comparison of the daily variation.

The mean daily variation of the meson component observed at mountain (m) and at sea level (s) is shown in Fig. 2 together with $\Delta M_\Delta/M_s$ ($=\Delta$). These values were corrected only for the pressure of the atmosphere, however, the corrections for the temperature must be applied on them, as mentioned above. The upper atmospheric temperature obtained by radio sonde observation is not accurate enough to correct for the temperature effect of cosmic-ray intensity variations.

As mentioned in Sect. 2, the atmospheric effect on Δ depend mainly

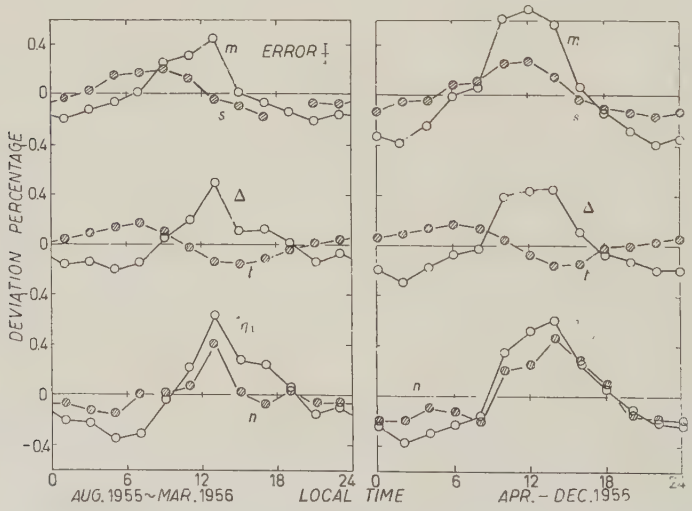

Fig. 2. – The mean diurnal variation of m, s, n, Δ, t and η_1. m, meson intensity observed at Mt. Norikura; s, meson intensity observed at Tokyo; n, neutron intensity observed at Mr. Norikura; Δ, difference of the meson intensities observed at Mt. Norikura and at Tokyo; t, mean atmospheric temperature effect to Δ, calculated from the atmospheric pressure observed at Mt. Norikura and at Tokyo; η_1, difference of the meson intensities corrected for the temperature effect.

upon the variation of T_2. The mean temperature of atmosphere is related by the Laplacian formula with height and pressure. Then from the atmospheric pressure variation at mountain and at sea level, the variation of temperature between mountain and sea level can be estimated. The estimated temperature t is shown in Fig. 2. The fact that the curves Δ and t run not parallel means the presence of a diurnal variation not caused by the atmospheric temperature variation.

4. – Comparison of the daily variation of the meson and neutron components.

$\Delta M_\Delta / M_s$ was corrected for the temperature variation (ΔT_2) using the method mentioned in Sect. 3 and it is shown in Fig. 2 as η_1.

Cosmic-ray neutrons have been continuously measured at Mt. Norikura since August, 1955, by a standard neutron monitor of Simpson's type [4]. η_1 is compared with the pressure corrected neutron intensity (n). It is clear from the figure that the two curves agree quite well.

In order to see the daily variations of (m), (s), (t), (η_1), and (n) more accurately, the amplitude and the maximum times of the first harmonics of the daily variation of each component were calculated. It is shown in Fig. 3. Vectors n and η_1 almost coincide. This fact shows that the neutron intensity and the difference of the meson intensity observed at mountain and at sea level correspond almost equally to the low energy side of the primary spectrum.

The intensity variations of the primary cosmic rays at the time of cosmic-ray storms were also examined using the method mentioned above. It was found that the variation of η_1 is almost the same as that of the neutron component. The method is available for the study of cosmic-ray storms.

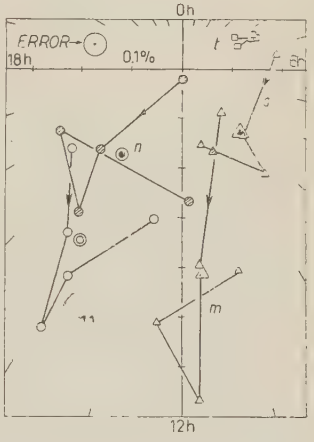

Fig. 3.– Harmonic dial of the first harmonics for the diurnal variations of m, s, n, t and η_1. Four points correspond to the first harmonics of the mean diurnal variations for the periods Aug.-Nov. 1944, Dec. 1955-Mar. 1956, Apr.-Jul. 1956 and Aug.-Dec. 1956, respectively.

5. – Conclusions.

The time variation of comparatively low energy primary cosmic rays could be derived by the comparison of simultaneous observation of the meson component at different altitudes.

The method is also available for the detailed study of cosmic-ray storms.

* * *

The author would like to express his deep appreciation to all members of the Cosmic-Ray Laboratory, Scientific Research Institute, both for the operation of the apparatus and for the preparation of the study, especially to Messers M. WADA and I. KONDO.

The observations at mountain level were made possible through the arrangement of Mt. Norikura Cosmic-Ray Laboratory, Tokyo University. He offers his sincere thanks to Prof. KIKUCHI the president of the mountain laboratory.

REFERENCES

[1] Y. MIYAZAKI: *Journ. Sci. Res. Inst. Tokyo*, **48**, 80 (1954); **49**, 268 (1955).
[2] K. MAEDA and M. WADA: *Journ. Sci. Res. Inst. Tokyo*, **48**, 71 (1954).
[3] M. WADA and S. KUDO: *Journ. Sci. Res. Inst. Tokyo*, **50**, 1 (1956).
[4] M. KODAMA K. MURAKAMI and Y. SEKIDO: *Journ. Sci. Res. Inst. Tokyo*, **51**, 37 (1957); *Journ. Phys. Soc. Japan*, **12**, 122 (1957).

SUPPLEMENTO AL VOLUME VIII, SERIE X
DEL NUOVO CIMENTO

N. 2, 1958
2° Trimestre

Cosmic Rays in the Earth's Magnetic Field.

P. Rothwell and J. Quenby

Imperial College - London

1. – Introduction.

The intensities of cosmic ray particles observed at various latitudes and longitudes are often not in good agreement with the intensities predicted from Lemaitre-Vallarta theory for the motion of charged particles in the earth's dipole field. A suggestion has been made recently that this is because the earth's outer magnetic field, with which cosmic ray particles interact, is distorted by the motion of ionized interplanetary matter in the field (Rose *et al.*, 1956). However, it seems possible that differences between the earth's real field, and the eccentric dipole approximation to it, may be sufficient to explain the differences between observed and calculated cosmic ray intensities. A simple experimental test of this point can be made by measuring cosmic ray intensities in places where it is known that there are large differences between the earth's measured field and the eccentric dipole field. If the earth's outer field is much distorted at distances where it interacts with the incoming cosmic ray particles, then no particular correlation between surface magnetic field anomalies and cosmic ray intensity discrepancies would be expected. On the other hand, if the outer field is not appreciably distorted at such distances, it would be reasonable to expect cosmic ray intensity and surface magnetic measurements to indicate similar field anomalies.

A neutron intensity monitor is particularly suitable for recording changes in cosmic ray intensity with latitude and longitude, because it is sensitive to the low energy end of the cosmic ray spectrum which is most affected by the earth's magnetic field, and because it is not subject to atmospheric temperature variations.

The main shipping route between England and South Africa crosses two regions where differences between the earth's real field and the dipole approximation to it are well marked.

a) The measured position of zero magnetic dip—the dip equator—lies at 7° N, 14° W, while the dipole (or geomagnetic) equator lies at 5° S, 5° W on this route.

b) The horizontal component of the earth's magnteic field in the South Atlantic near Cape Town is anomalously low ($\sim$ .13 G, instead of $\sim$ .27 G).

In a dipole field, the position of minimum cosmic ray intensity and the position of zero magnetic dip should both lie at the geomagnetic equator, and cosmic ray intensities near 30° N and 30° S geomagnetic latitude should be about the same. A neutron monitor installed on a ship making the journey from England to South Africa could determine:

a) The position of minimum cosmic ray intensity, to within a degree or two of latitude, and show whether it lies nearer the geomagnetic equator, the dip equator, or some other « cosmic ray » equator, and

b) The cosmic ray intensity in the region of low horizontal magnetic intensity in the South Atlantic (near Cape Town), and show how it compares with the intensity at a similar geomagnetic latitude in the North Atlantic (near the Canary Islands) where it is known that the dipole field and the earth's measured surface field are similar (BARTELS, 1936).

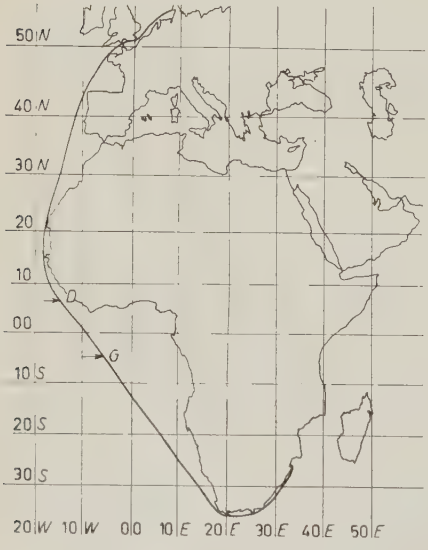

Fig. 1.

In this way, it could be seen whether there is any connection between surface magnetic field and cosmic ray intensity anomalies.

2. – Experimental arrangement.

The neutron monitor used in this experiment was of the standard Simpson type and consisted of five BF_3 proportional counters surrounded by lead and paraffin wax. It was housed in a thermostatically controlled hut, placed on the top deck of M/V Roxburgh Castle, travelling from London to Cape Town, Lourenço Marques and back (see Fig. 1). Cosmic ray intensities scaled by 100, were printed every hour. Barometer readings were taken every two hours, and a pressure correction was made to the counting rate of .75% per millibar. A similar monitor operated in London over the same period and percentage

corrections for small changes in the mean daily intensity recorded there were made to the cosmic ray intensities recorded on board. The counting rate of the monitor in London was ~ 14000 counts per hour.

3. – Results.

The corrected cosmic ray intensities (6 hourly averages) recorded on two voyages are shown in Fig. 2, plotted against

a) geographic latitude,

b) geomagnetic latitude,

c) angle of magnetic dip.

The position of minimum intensity lies at

a) $7 \pm 1°$ N geographic latitude,

b) $12 \pm 1°$ N geomagnetic latitude,

c) $0 \pm 2°$ magnetic dip.

The ship crossed the «cosmic ray» equator proposed by SIMPSON *et al.* (1956) at $\sim 3°$ N, 11° W, geographic co-ordinates, i.e. 4° S of the position of minimum intensity found in this experiment.

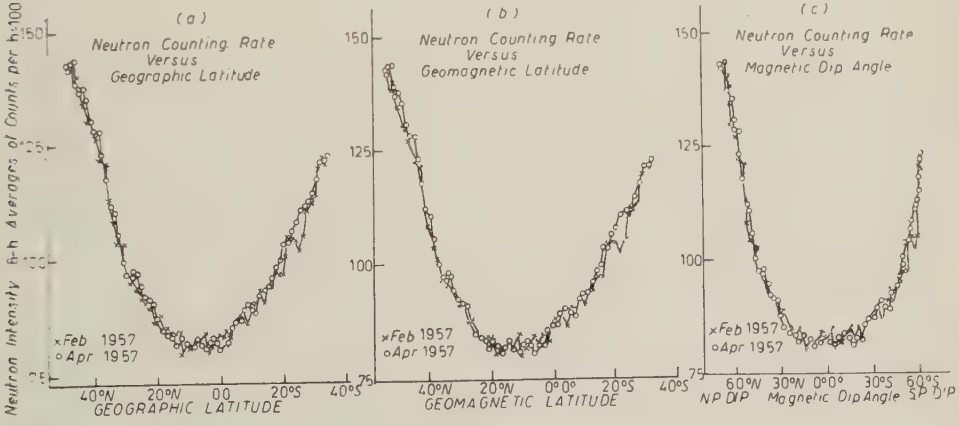

Fig. 2.

Table I gives for comparison *a*) the cosmic ray intensities at 30° N and 30° S geomagnetic latitudes together with the horizontal magnetic intensities in the earth's field and in the eccentric dipole field, and *b*) cosmic ray intensities at angles of magnetic dip in the northern and southern hemisphere, similar to those found at 30° S and 30° N.

TABLE I.

Geomagnetic latitude		Angle of dip	Horizontal magnetic intensity (earth's field)	Horizontal magnetic intensity (dipole field)	Couting rate per hour × 100
(*a*)	30° N	35° N	.29 G	.27 G	92 ± .4
	30° S	64° S	.13 G	.27 G	123 ± .5
(*b*)	7° S	35° S	.23 G	.31 G	91 ± .4
	52° N	64° N	.20 G	.19 G	130 ± .5

It is seen that, at 30° S geomagnetic latitude, where the horizontal component of magnetic intensity in the earth's field is much lower than in the eccentric dipole field, the cosmic ray intensity is $\sim 30\,\%$ higher than at 30° N, where the horizontal magnetic intensity is similar in the earth's field and the dipole field. Intensities at similar angles of magnetic dip in the northern and southern hemisphere are comparable, however.

4. - Discussion.

The results of this experiment show that there does exist a connection between surface magnetic field and cosmic ray intensity anomalies. Previous observations of cosmic ray intensity anomalies, which gave rise to the suggestion that the earth's outer magnetic field differs in distribution from that expected from the surface field, may also be explained in terms of the difference between the earth's real field and the eccentric dipole approximation to it.

a) The positions of minimum cosmic ray intensity at various longitudes do not coincide with the geomagnetic equator (SIMPSON *et al.*, 1956). Fig. 3 shows the position of the geomagnetic equator and the magnetic dip-equator (1955 survey), together with experimentally observed positions of minimum cosmic ray intensities at various longitudes, measured with neutron monitors, and counters, telescopes or ionization chambers (also see Table II). The positions of minimum cosmic ray intensity lie nearer the dip

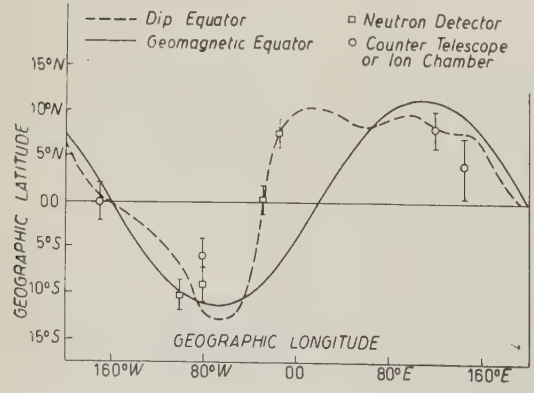

Fig. 3.

equator than the geomagnetic equator in nearly every case; this is particularly noticeable at longitudes where there is a considerable distance between dip and geomagnetic equator.

TABLE II.

Type of measurement	Longitude	Geomagnetic equator	Dip equator	Minimum cosmic ray intensity	Reference
Neutron monitor, sea level, 2 equatorial crossings	14° W	7° S	7° N	7° ± 1° N	ROTHWELL and QUENBY (1957)
Neutron monitor, sea level, 1 equatorial crossing	30° W	9° S	1° S	0° ± 1° N	SIMPSON, FENTON, KATZMAN and ROSE (1956)
Neutron monitor, 8 aeroplane flights to 11° S and back	80° W	11° S	12° S	9° ± 2° S	SIMPSON (1951)
Counter telescope, sea level, 6 equatorial crossings	80° W	11° S	12° S	6° ± 2° S	JOHNSON and REED (1937)
Neutron monitor, sea level, 1 equatorial crossing	100° W	10° S	8° S	11° ± 1° S	SIMPSON, FENTON, KATZMAN and ROSE (1956)
Ionization chamber, sea level, 11 equatorial crossings	170° W	2° N	0°	2° ± 1° S	COMPTON and TURNER (1937)
Counter telescope, sea level, 1 equatorial crossing	145° E	9° N	7° N	4° ± 3° N	LAW, MCKENZIE and RATHGEBER (1949)
Ionization chamber, sea level, 8 equatorial crossings	121° E	11° N	8° N	9° ± 1° N	SEKIDO, ASANO and MASUDA (1943)

b) Measurements of α-particle cut-off energies in the earth's field give values that are higher than predicted on dipole theory over Europe, and lower over North America (WADDINGTON, 1956). A new calculation of the eccentric dipole field, based on the 1955 magnetic survey (WEBBER, 1957) and some re-measurements of the α-particle cut-off energies (WADDINGTON, 1957), show

that discrepancies between the observed and calculated energies are smaller than was thought at first (WEBBER, 1957). The horizontal component of the earth's surface field at geographic latitudes $\sim 40^\circ$ N to $\sim 60^\circ$ N is lower than that of the dipole field over North America, and slightly higher over Europe; this could explain the remaining discrepancy between European and American α-particle measurements.

c) The longitude effect is not negligible at 30°-35° geomagnetic latitude, contrary to the predictions of dipole theory (ROSE *et al.*, 1956). The anomalously high cosmic ray counting rate found in this experiment in the region of low horizontal magnetic intensity near 30° S, 20° E would produce a large longitude effect at this latitude. The longitude effect found by ROSE in the northern hemisphere could, similarly, be ascribed to local field anomalies.

5. – Conclusion.

Observations of cosmic ray intensities at places where there are large surface magnetic field anomalies suggest that discrepancies between measured cosmic ray intensities and intensities predicted by Lemaitre-Vallarta theory for the motion of charged particles in a dipole field, arise because of differences between the earth's real field and the eccentric dipole approximation to it, rather than because of a distortion of the earth's outer magnetic field.

* * *

The authors wish to thank the Union Castle Line for their generosity and co-operation in this experiment, and in particular, Captain N. WILLCOCK for making all arrangements for the installation and transport of the equipment, and an observer, on M/V Roxburgh Castle.

APPENDIX

Further measurements on the position of minimum cosmic ray intensity at various longitudes, using neutron monitors, were reported during the conference by SIMPSON (12 equatorial crossings) and by ODA and POMERANTZ (one equatorial crossing each).

These results are shown in Fig. 4, together with the results reported previously by SIMPSON *et al.* (1956).

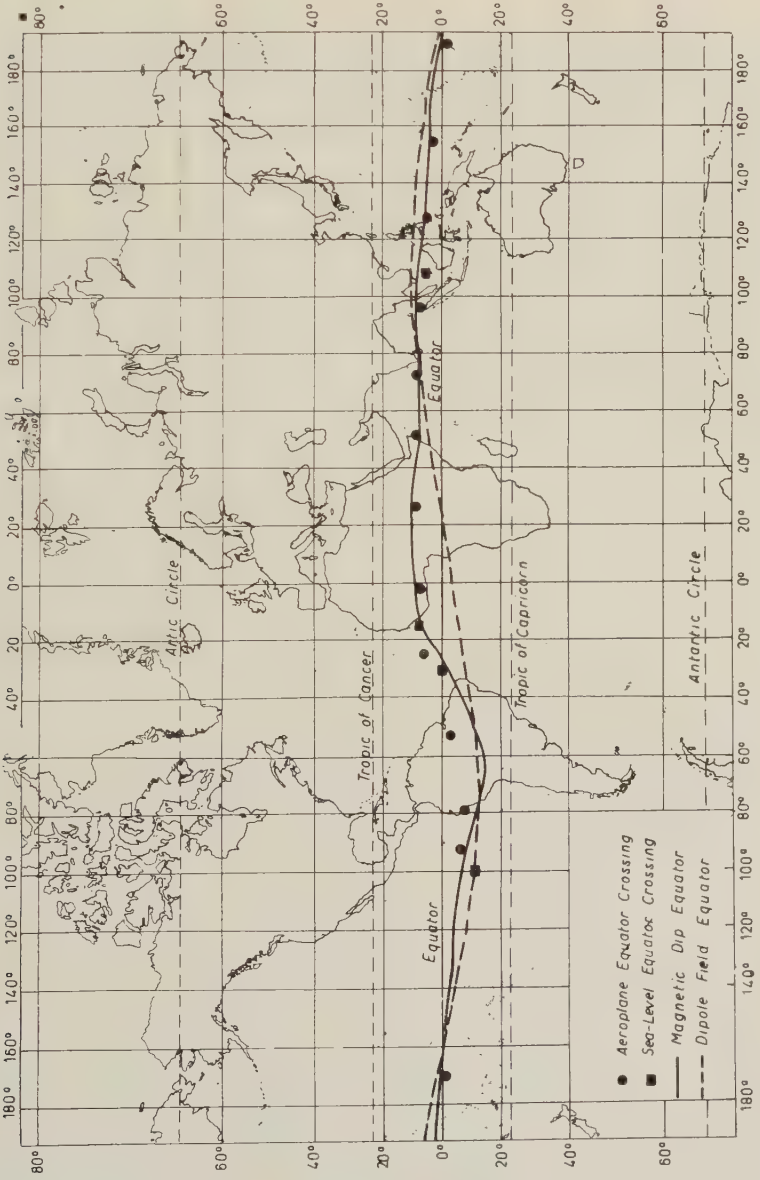

Fig. 4.

It can be seen that all the positions of minimum cosmic ray intensity lie very near to the magnetic dip equator (1955 survey).

BIBLIOGRAPHY

D. C. Rose, K. B. Fenton, J. Katzman and J. A. Simpson: *Canad. Journ. Phys.*, **34**, 968 (1956).
J. Bartels: *Terr. Mag.*, **41**, No. 3, 225 (1936).
J. A. Simpson, K. B. Fenton, J. Katzman and D. C. Rose: *Phys. Rev.*, **102**, No. 6, 1648 (1956).
J. A. Simpson: *Phys. Rev.*, **83**, 1175 (1951).
T. H. Johnson and D. N. Reed: *Phys. Rev.*, **51**, 557 (1937).
A. H. Compton and R. Turner: *Phys. Rev.*, **52**, 799 (1937).
P. G. Law, C. D. McKenzie and H. D. Rathgeber: *Austr. Journ. Sci. Research*, A **2**, No. 4, 493 (1949).
Y. Sekido, Y. Asano and T. Masuda: *Sci. Papers Inst. Phys. Chem. Research* (*Tokyo*), **40**, 439 (1943).
C. J. Waddington: *Nuovo Cimento*, **3**, 930 (1956).
W. Webber: in this issue, p. 532.
H. H. Aly and C. J. Waddington: *Nuovo Cimento*, **5**, 1679 (1957).

SUPPLEMENTO AL VOLUME VIII, SERIE X
DEL NUOVO CIMENTO

N. 2, 1958
2° Trimestre

Shipboard Neutron Monitor Determination of Cosmic-Ray Equator.

M. A. POMERANTZ

Bartol Research Foundation of the Franklin Institute - Swarthmore, Penn.

A. E. SANDSTRÖM

Fysiska Institutionen, Uppsala Universitet - Uppsala

D. C. ROSE

Division of Pure Physics, National Research Council of Canada - Ottawa

1. – Introduction.

It has been recognized for many years that the dipole approximation to the earth's magnetic field derived from surface measurements does not invariably provide the appropriate geomagnetic co-ordinates for describing the observed spatial distribution of cosmic ray intensities. Recent neutron monitor measurements [1] supported by other lines of evidence, such as comparisons of α-particle cut-off energies [2], have unambiguously demonstrated the existence of appreciable discrepancies. Although the available data appeared to indicate that the equator derived from the position of intensity minima (the so-called *cosmic-ray equator*) could be simulated by a westward shift of the inclined magnetic dipole of the earth by about 40°-45° without requiring an appreciable change in the angle of inclination [3], drastic anomalies at high latitudes were still apparent [1].

To facilitate a detailed analysis of this problem, it appeared to be extremely desirable to obtain with neutron monitors as complete a global map as possible of the contours of equal cosmic ray intensity (*isocosms*). This method of detection of the nucleonic component possesses unique advantages over the techniques employed in earlier world-wide surveys in being free from atmospheric temperature effects, and in displaying much larger variations with latitude as a consequence of its sensitivity to the low energy band of the cosmic ray spectrum, which is so greatly influenced by magnetic fields in the vicinity of the earth. Since extensive observations at sea level had already

been obtained recently with shipboard instruments [1], a program to extend these measurements to regions of the earth not previously traversed was therefore undertaken. A prime objective of the present investigations is to continue making measurements along a selected route over a long period of time, thereby permitting the detection of even relatively small time variations which, should they occur, could significantly affect the conclusions derived from this type of experiment.

In view of the fact that the program is still in progress, we shall not attempt in this preliminary report either to present all of the results obtained thus far or to discuss the implications in detail. Rather, attention will be confined to a brief description of the determination of the cosmic-ray minimum off the west coast of Africa, in a heretofore unexplored region which was selected for the initial phase of the investigations because it is quite crucial in the comparison of various possible representations of the cosmic ray equator.

2. – Experimental procedure.

A detailed description of the pile geometry, which is identical in every respect with that utilized previously during cruises of HMCS Labrador and USS Atka, has already been published [4]. Although the present circuit arrangements, methods of recording, and other details [5] differ somewhat, absolute counting rates are in fact directly comparable within a relatively small uncertainty.

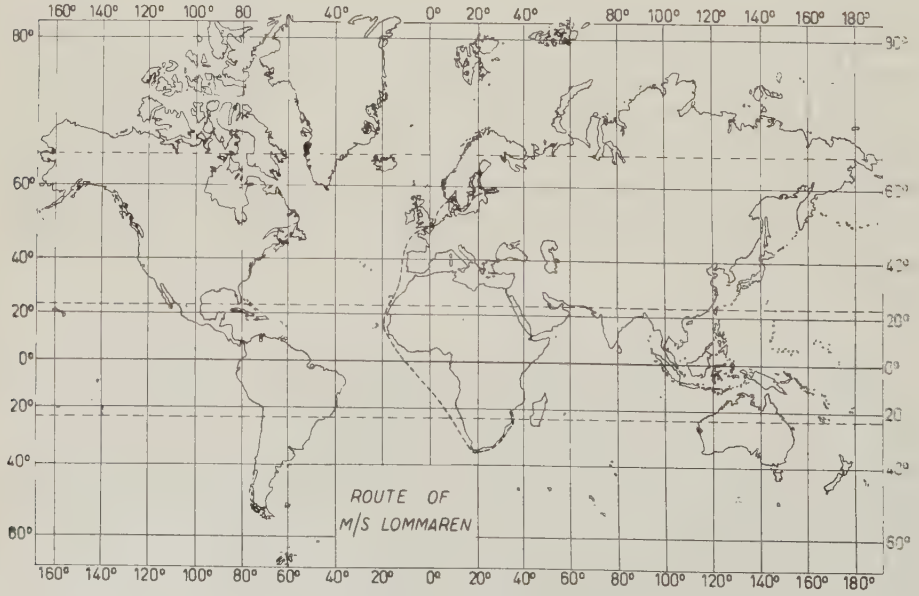

Fig. 1. – Route of the M/S Lommaren.

The pile and all associated equipment are installed in a thermostatically-controlled air-conditioned hut on the boat-deck of the M/S Lommaren. The route is shown in Fig. 1.

3. – Results and discussion.

Although the third voyage to South Africa is currently in progress, the results from the first round-trip only are available at present. The pressure-corrected nucleonic component intensity plotted as a function of geographic latitude is shown in Fig. 2 for the southbound voyage from Göteborg, Sweden, to Capetown, South Africa (Nov. 2, 1956 - Nov. 20, 1956) and in Fig. 3 for the northbound voyage (Dec. 30, 1956 - Jan. 19, 1957).

While the ship was traveling southward, a large Forbush-type decrease occurred on Nov. 10. The location of the cosmic ray minimum is significantly influenced by this event, and the importance of such considerations is apparent in Fig. 2. Here are indicated the data uncorrected for this world-wide variation, as well as the results of normalization with respect to the neutron-monitor records from Huancayo [6] and Upsala respectively. Obviously neither of the latter represents the true curve, although the positions of the minimum are in approximate agreement and differ appreciably from that of the uncorrected curve.

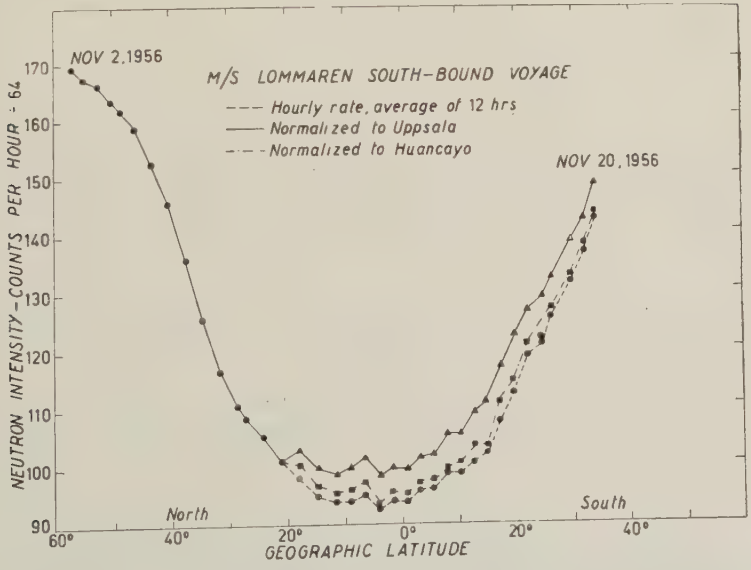

Fig. 2. – Intensity of the nucleonic component at sea level plotted as a function of geographic latitude. First southbound voyage, Göteborg, Sweden, to Capetown, South Africa.

Fortunately fluctuations during the return voyage were much less drastic, and the position of the minimum is quite unambiguous. However, the base level of cosmic ray intensity was low during this entire period, and Fig. 3 shows the result of applying a correction for this effect on the basis of the Upsala neutron monitor records. In general, the absolute counting rates during the northbound and southbound voyage are brought into agreement by this procedure, although some discrepancies are certain to result from any normalization which does not take into account the fact that the amplitude of world-wide variations is dependent upon both particle rigidity and geographic position.

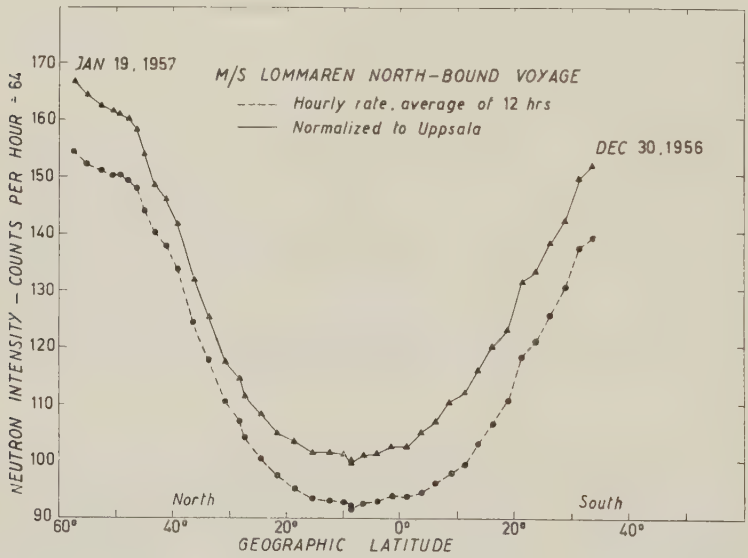

Fig. 3. – Intensity of the nucleonic component at sea level plotted as a function of geographic latitude. First northbound voyage, Capetown, South Africa, to Göteborg, Sweden.

The results of the first voyage yield as the position of the cosmic-ray equator, expressed in geographical co-ordinates:

$$(8 \pm 1)^\circ \text{ N}, \qquad 14^\circ \text{ W}.$$

For purposes of comparison, Table I lists the geomagnetic latitudes of this point corresponding to a simple dipole field with polar co-ordinates consistent with the particular observation cited. It is clear that the position of the cosmic ray equator off the west coast of Africa is inconsistent even with the prediction

TABLE I. – *Geomagnetic latitude of observed position of cosmic ray intensity minimum corresponding to dipole approximation and polar co-ordinates consistent with other observations.*

Reference	Nature of observation	Polar co-ordinates	Geomagnetic Latitude of cosmic-ray equator
[7]	Surface Magnetic Field Measurements	78°.6 N 70°.1 W	15° N
[3]	Cosmic Ray Intensity Minima	80°.2 N 113°.2 W	6° N
[8]	α-Particle Cut-off	75°.5 N 90°.0 W	12° N

based upon similar measurements of cosmic ray intensity minima in the western hemisphere if a simple dipole representation of the earth's magnetic field is assumed. It is interesting to note, on the other hand, that the minimum actually lies very close to the isoclinic equator representing a surface measurement of the inclination of the earth's magnetic field equal to 0°.

* * *

It is a pleasure to thank the Transatlantic Company of Sweden for their very generous co-operation in making the facilities of the ship available for these experiments. In particular, we are grateful to Capt. A. LAGERWALL for making the many necessary arrangements, and to Capt. GUNNAR RUNSTEN, master of the M/S Lommaren for his help and hospitality. Appreciation is also expressed to the National Geographic Society for sponsoring the field operation. Support from the U. S. National Committee for the International Geophysical Year, as well as the U. S. Office of Naval Research has aided this project. Finally, we wish to thank Mr. LARS ERICSON who served as observer aboard the ship, Mr LAMBERT VÄLI, who calculated the ship's positions for every two hours, and Dr. V. R. POTNIS, who assisted in the reduction of the data.

REFERENCES

[1] D. C. Rose, K. B. Fenton, J. Katzman and J. A. Simpson: *Can. Journ. Phys.*, **34**, 968 (1956).
[2] C. J. Waddington: *Nuovo Cimento*, **3**, 930 (1956).
[3] J. A. Simpson, K. B. Fenton, J. Katzman and D. C. Rose: *Phys. Rev.*, **102**, 1648 (1956).
[4] D. C. Rose and J. Katzman: *Can. Journ. Phys.*, **34**, 1 (1956).
[5] M. A. Pomerantz: *Journ. Frank. Inst.*, **263**, 153 (1957).
[5] Kindly supplied by Dr. J. A. Simpson.
[7] E. H. Vestine, L. Laporte, I. Lange and W. E. Scott: *Pub. Carnegie Institution of Washington*, **580** (1947).
[8] P. Freier, P. F. Fowler and E. P. Ney: *Bull. Am. Phys. Soc.*, **2**, 191 (1957).

SUPPLEMENTO AL VOLUME VIII, SERIE X
DEL NUOVO CIMENTO

N. 2, 1958
2° Trimestre

Cosmic Ray Soft Component Measurements During a Flight from Scandinavia Across the North Pole and Around Asia and Europe.

A. E. Sandström

Fysiska Institutionen, Uppsala Universitet - Uppsala

1. – Introduction.

During the international geophysical year cosmic ray measurements, including such with neutron monitors, will be made at at a number of stations in the northern polar region and its vicinity. Therefore it was supposed to be of interest to collect some knowledge as to the cosmic ray soft component variations across this region along at least two meridians as opposite to each other as possible. With the aid of the Scandinavian Airlines System this enterprise could be undertaken, the neutron monitor being returned along the usual commercial flight routes over the southern parts of Asia and Europe. The survey included several regions inaccessible by shipborne instruments. Considering the risk for time variations of the rigidity of the primary particles it was especially convenient that the flight could be completed within a comparatively short period.

2. – Experimental equipment.

The small neutron monitor was originally intended for preliminary studies, although it played a part in connection with the solar flare effect of February 23, 1956 [1]. For the flight expedition it had to be partly rebuilt.

The arrangement of the lead core is principally the same as that of the transportable monitors designed by Simpson *et al.* [2]. As the two proportional counters are short, the length of the lead core is only 28 cm. The counters, lent by the Swedish Atomic Energy Co., have an effective length

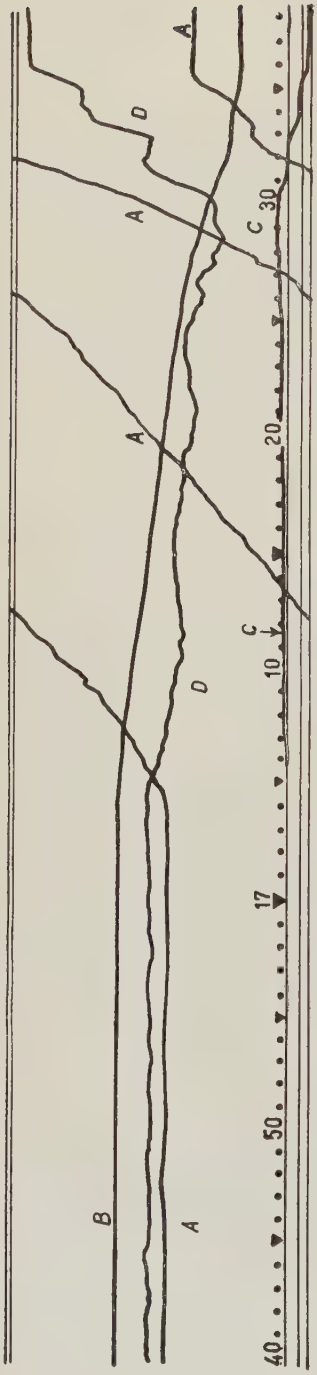

Fig. 1. – Part of a flight record showing to the left a flight on an isobaric surface and to the right a descent to ground. Compare text.

of 200 mm. Their diameter is 29 mm. They are filled with $^{10}BF_3$ of 95 % enrichment to a pressure of 700 mm Hg.

The paraffin shield had to be dimensioned according to the space and weight limits agreed upon by the SAS Company. The whole monitor is enclosed in a wooden box, the minimum distance from the lead core to the outer surface of the shielding being 12.2 cm.

The stabilized high voltage for the proportional counters was supplied by an E.H.T. unit, Type 532, from the Isotope Developments Co., England. The pulses from the counters pass a preamplifier, at the same time serving as connector box. From the preamplifier the pulses are fed to a main amplifier with discriminator. From the latter the pulses can be fed either to a scale of four or to a Philips decade counter with five digits. A printing counter can be connected in series either with the scale of four or with the first digit of the decade counter. It is also possible to connect the latter in series with the scale of four. Thus the printing counter will receive either every fourth, tenth, or fortieth pulse. When the mechanical counter is in series with the scale of four the complete five digit decade is in parallel with the latter. This arrangement provides, for all the three possible cases, the means of reading the number of pulses visually, thus safeguarding the continuous recording of data should a break-down of the printing counter occur.

The 220 volt AC power for the electronic equipment was provided by a rotating transformer fed from the 24 volt DC mains of the aircraft. The essential parts of the equipment can be seen in Photo 1 (*a* and *b*).

The pulses were counted during 6 minutes intervals. The pulses triggering the printing

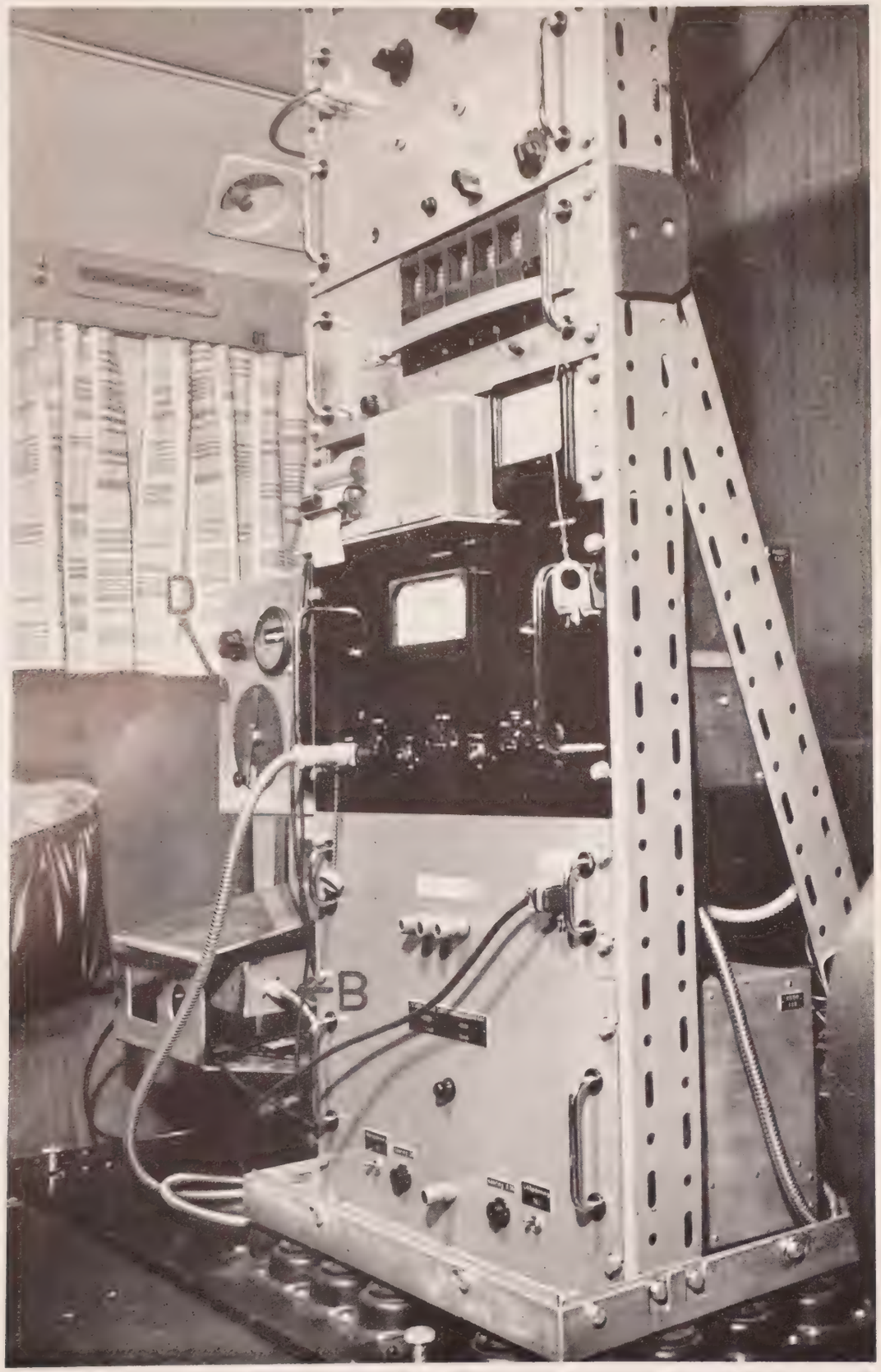

Photo 1-*a*.

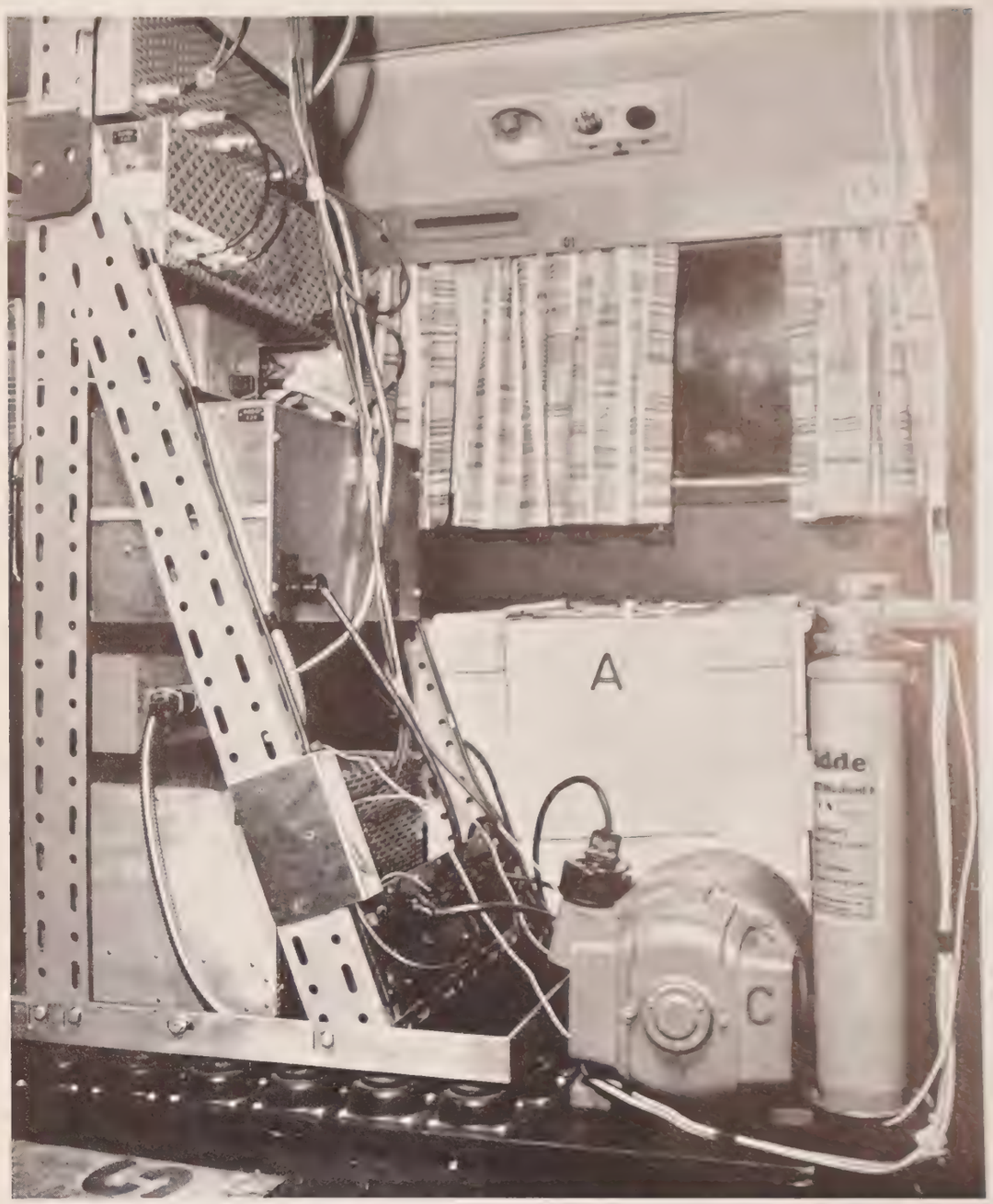

Photo 1-*b*.

Photo 1-*a*,*b*. – The neutron monitor as installed in a DC7C aircraft. *A* is the neutron pile monitor proper. The connector box (*B*) with preamplifier can be seen in the picture to the left. *C* (in the picture to the right) is the rotating transformer. The performance of the latter was hand-regulated by means of resistors and a variac (*D*). The electronics from top to bottom: main amplifier, discriminator with scale of four, decade scale, printing counter, E.H.T. unit, and the stabilized unit for anode voltages. The device for the 6 min pulses is at the top of the rack and cannot be seen in either one of the photographs. The mounting of the rack was shockproof. The monitor box rested on thick rubber matting.

counter every sixth minute were obtained from a contactor controlled by the signals from a master clock.

Immediately after each ascent and frequently during the flight the time correction of the contactor was determined by comparison with the chronometers of the aircraft.

The pulses from the contactor were also fed to one of the signal detectors of the flight recorder providing the means of synchronizing the records of this instrument with the monitor registrations. The flight recorder, manufactured by Societé de Fabrication d'Instruments de Mesure, also includes a chronometer. Combined with the times of take-off it furnishes an easy identification of the individual contact times. The recording is made photographically on a strip of paper.

Part of one of the records is reproduced in Fig. 1. A barograph arrangement measures the atmospheric pressure outside the plane. It can be computed from two curves, one (B) giving a rough value, only, the precision values being read from curve A. As regards the rest of the curves, C is the rough record and D the precision record of the speed of the aircraft relative to the surrounding air. The numbered dots constitute the time reference. Tiny indications between these dots correspond to the pulses received by the signal detector from the contactor belonging to the monitor equipment. These indications mark the beginning and end of each 6 minutes counting interval.

3. – The route.

The route (Fig. 2) was mainly determined by the points of stops.

The polar part of the flight started from Stockholm (59°.4 N, 18°.0 E) with a fuelling stop at Kallax airfield (65°.5 N, 22°.1 E) before the long distance flight over Tromsö and the North Pole to Alaska. From Tromsö (69°.7 N, 19°.0 E) the route followed the meridian 19° E to the North Pole and thereafter the meridian 144°.0 W with a slight deviation to the east. In the vicinity of Barter Island (70°.2 N, 143°.6 W) it turned to Fairbanks (64°.9 N, 147°.7 E) and Anchorage (61°.2 N, 150°.0 W). The whole flight, including fuelling at Kallax and Fairbanks, took only 19.6 hours.

After an interval of 35 hours the second part of the flight started from Anchorage to Shemya (52°.7 N, 174°.0 E) and after refuelling at the latter place it went straight on to Tokyo (35°.5 N, 139°.7 E). The deviations from the great circles between these three places were small and took place mainly after Anchorage and in the vicinity of Japan. Including the stop at Shemya this part of the flight took 15.5 hours.

In Tokyo the monitor was taken off the first DC7C aircraft and seven days later (Febr. 26) it was mounted in another one.

The return flight was marked by more frequent visits to airports and air-

fields although without any major stops. It followed the shortest distances from Tokyo over Okinawa (26°.5 N, 128°.0 E) to Manila (14°.5 N, 121°.0 E), Bangkok (13°.8 N, 100°.6 E), and Karachi (23°.3 N, 69°.9 E), the small deviations being due to flight route regulations only. Between Karachi and Athen, major changes of direction took place abeam Sharjak (25°.3 N, 55°.9 E), Bagdad West (33°.3 N, 44°.3 E), Damaskus (33°.4 N, 36°.3 E), and Nicosia (35°.2 N, 33°.4 E). From Athen the route went over a point 38.9° N, 16.5° E in Calabria to Rome. The plane then visited Geneve, Frankfurt a/M, and Köpenhamn following the ordinary flight routes through Europe. Including eight stops the whole flight from Tokyo to Stockholm took 52.5 hours.

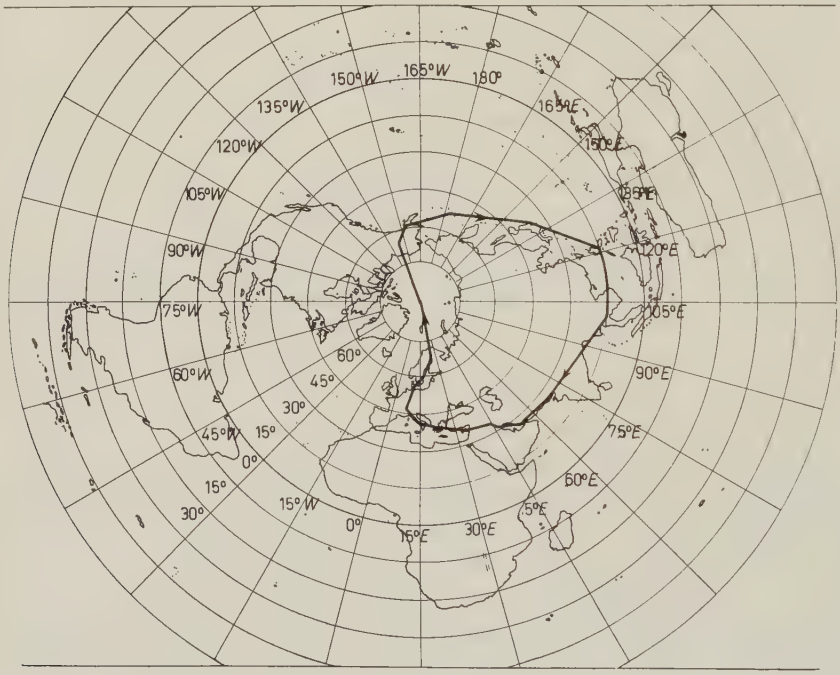

Fig. 2. – Routes of the aircrafts carrying the neutron pile monitor.

The flight can be followed in detail by means of the time intervals and positions listed in Table I.

Most of the data were collected while the flying height was controlled by the automatic pilot of the aircraft. On most distances the height was remarkably constant. In some cases the variations were below the resolving power of the flight recorder even during very long runs. While crossing the polar sea the plane followed the same isobaric level for nearly 900 nautical miles with a maximum deviation of 1.5 mb. The *average* pressures are listed in Table I.

TABLE I.

Date	Time interval (GMT)	Average pressure (mb)	Geographical		Pressure corrected counting rate for (48÷100) min
			Lat.	Long.	
16.2	1241 - 1335	560.4	62°.4 N	19°.1 E	106.3
	1611 - 1653	668.8	68°.2 N	19°.9 E	105.7
	1705 - 1729	590.1	71°.3 N	19°.0 E	101.5
	1729 - 1817	590.1	74°.0 N	19°.0 E	102.7
	1817 - 1905	591.1	77°.3 N	19°.0 E	101.3
	1905 - 1953	590.6	80°.5 N	19°.0 E	100.1
	1953 - 2041	590.3	83°.7 N	19°.0 E	100.0
	2041 - 2129	590.3	86°.9 N	19°.0 E	99.1
	2129 - 2217	590.8	89°.8 N	144°.0 W	98.5
	2217 - 2305	591.8	86°.8 N	144°.0 W	98.6
	2305 - 2353	591.7	83°.5 N	144°.0 W	99.5
	2353 - 0041	590.4	80°.3 N	144°.0 W	99.4
17.2	0041 - 0129	592.3	77°.0 N	143°.8 W	99.3
	0129 - 0217	590.7	73°.6 N	142°.8 W	100.4
	0217 - 0305	606.1	70°.8 N	143°.4 W	99.4
	0305 - 0405	608.6	67°.7 N	145°.6 W	98.1
	0648 - 0724	596.9	63°.3 N	149°.4 W	97.1
18.2	1850 - 1938	606.7	59°.4 N	153°.9 W	97.0
	1938 - 2026	601.5	58°.5 N	160°.0 W	96.4
	2026 - 2114	594.5	57°.7 N	166°.8 W	96.0
	2114 - 2202	594.9	56°.5 N	172°.9 W	95.2
	2202 - 2250	594.1	54°.9 N	178°.4 W	93.8
	2250 - 2320	582.5	53°.8 N	177°.1 E	91.4
19.2	0223 - 0311	592.2	51°.7 N	170°.0 E	88.6
	0311 - 0359	593.3	50°.3 N	165°.2 E	84.9
	0359 - 0447	593.0	48°.6 N	160°.8 E	79.3
	0447 - 0535	593.0	46°.9 N	157°.2 E	73.8
	0535 - 0623	593.0	45°.2 N	154°.1 E	67.1
	0623 - 0711	593.2	43°.6 N	151°.0 E	59.3
	0711 - 0759	594.0	42°.0 N	148°.4 E	58.2
	0759 - 0847	594.0	39°.4 N	146°.3 E	55.5
	0847 - 0947	591.5	37°.0 N	143°.2 E	51.2
26.2	0613 - 0701	592.6	34°.8 N	138°.1 E	46.9
	0701 - 0749	592.4	31°.9 N	135°.5 E	43.9
	0749 - 0837	592.1	30°.0 N	132°.8 E	44.8
	0837 - 0925	591.6	28°.1 N	130°.0 E	42.4
	0925 - 1013	591.4	25°.9 N	127°.7 E	41.4
	1013 - 1101	590.0	23°.0 N	126°.2 E	39.3
	1101 - 1149	590.0	19°.9 N	124°.7 E	38.7
	1149 - 1243	590.1	16°.6 N	123°.2 E	38.2
	1623 - 1711	505.5	13°.9 N	111°.3 E	39.9
	1711 - 1759	505.5	14°.0 N	107°.4 E	37.1
	1759 - 1847	505.9	14°.0 N	103°.8 E	35.2

TABLE I (*continued*).

Date	Time interval (GMT)	Average pressure (mb)	Geographical		Pressure corrected counting rate for (48÷100) min
			Lat.	Long.	
26.2	2150 - 2238	495.5	16°.8 N	95°.5 E	37.9
	2238 - 2326	495.5	17°.6 N	92°.3 E	36.6
	2326 - 0014	495.5	18°.4 N	88°.9 E	36.0
27.2	0014 - 0102	494.8	19°.3 N	86°.2 E	32.9
	0102 - 0150	495.7	20°.1 N	83°.0 E	34.7
	0150 - 0238	495.5	20°.6 N	80°.2 E	34.0
	0238 - 0326	495.5	21°.5 N	77°.2 E	34.8
	0326 - 0414	495.5	22°.6 N	73°.8 E	35.0
	0414 - 0456	495.5	23°.3 N	70°.4 E	35.9
	0745 - 0833	537.1	25°.2 N	62°.9 E	37.7
	0833 - 0921	538.0	25°.2 N	59°.7 E	37.9
	0921 - 1009	535.2	25°.5 N	56°.4 E	38.7
	1009 - 1057	534.0	26°.7 N	53°.1 E	40.3
	1057 - 1145	533.5	28°.9 N	50°.1 E	40.8
	1145 - 1233	533.0	31°.0 N	47°.4 E	46.9
	1233 - 1321	538.2	32°.9 N	44°.4 E	48.5
	1321 - 1409	545.3	33°.4 N	40°.8 E	49.3
	1409 - 1457	542.7	33°.6 N	37°.0 E	51.9
	1457 - 1545	533.3	35°.0 N	33°.8 E	51.5
	1545 - 1633	533.3	36°.0 N	30°.1 E	54.9
	1633 - 1709	533.3	37°.7 N	26°.5 E	57.0
	1946 - 2034	585.0	38°.3 N	20°.5 E	65.5
	2034 - 2122	585.0	39°.1 N	16°.6 E	68.8
	2122 - 2146	585.2	40°.7 N	14°.5 E	72.4
28.2	0000 - 0036	459.3	43°.3 N	9°.8 E	76.4
	0036 - 0112	461.0	45°.0 N	7°.8 E	80.5
	0237 - 0319	585.6	47°.6 N	8°.9 E	89.4
	0447 - 0529	683.6	51°.9 N	9°.2 E	93.3
	0529 - 0605	682.5	53°.8 N	10°.3 E	94.5
	0915 - 1009	742.9	57°.6 N	15°.3 E	100.9

By arrangement navigators and pilots reported changes of course or height as soon as possible thus providing the means for the observers to verify if a sudden change of counting rate was to be regarded as natural or as the result of a break-down of some part of the monitor equipment.

4. – The measurements.

The intensity data were collected principally by means of the printing counter. The electronics were started as soon as in the usual course of proceedings an auxiliary generator was connected to the DC mains of the aicraft.

During this procedure and while all air traffic routine tests were being performed the electronics of the monitor usually had ample time to attain its normal temperature. Measurements began at the take-off. During the ascent as well as during descents the number of counts during 1 minute intervals were read from the decade counter. As soon as the plane had reached its marching level the visual 1 minute observations were exchanged for such of 30 minutes' duration. These readings were performed as a precaution against a break-down of the mechanical counter. In such a case the visual 30 minute readings would immediately have been exchanged for 6 minute readings.

The performance of the decade counter was followed closely, all the time making it possible to observe, without too serious a loss of time, any trouble which might develop. These precautions were followed throughout the whole flight although it soon became apparent that the performance of the monitor and its electronics was good during all prevailing flight conditions. Trouble developed only twice. In the first instance it was of small importance. Before the start from Anchorage the low temperature in the aircraft had caused some dimensional changes in the mechanical counter with the result that it had got stuck. Thanks to the general increase in temperature this trouble was overcome before the plane reached its marching level.

The second trouble was of a more serious kind. It was caused by moist tropical air entering the plane during the descent at Manila. Moisture then condensed on the insulators of the connector box, resulting in the loss of a dozen 6 minutes intervals. In Bangkok the same trouble started once again but in this place it was possible to procure some hygroscopic material to keep the moisture at bay.

The paper strips from the flight recorder were developed in Stockholm at the laboratories of the Scandinavian Airlines System. They were read by means of calibration diagrams provided by the manufacturer.

The performance of the neutron monitor itself was tested by means of a RaBe-source. The first test was made after mounting the monitor in the aircraft on the evening before the start. The second test was undertaken immediately after its arrival in Stockholm on the return flight. Both tests agreed within the statistical fluctuations of the 6 minutes registration intervals.

5. – The barometer coefficient.

To determine the barometer coefficient of the monitor two flights were undertaken over the middle of Sweden. The records from both these flights show the logarithm of the counting rate to be a rectilinear function of the atmospheric pressure (Fig. 3). The first flight (May 8, 1956) resulted in a comparatively high value, — 0.007 86. The second flight (Jan. 9, 1957) gave

a value of -0.00738. The latter value has to be considered as the most reliable one, as at that time the new neutron monitor in Uppsala provided facilities for verifying that no single events interfered with the measurements. However, the difference between the two sets of measurements depends mainly on three observations made at comparatively low altitudes during the first flight (pressure > 700 mb). The statistical fluctuations are big. Disregarding the corresponding three points in Fig. 3 it becomes natural to draw the dotted line through the remaining five. Evidently, this line is parallel, or nearly parallel, to that resulting from the second flight. Thus both the flights seem to yield a value which is practically equal to that generally accepted.

During the flight around Asia and Europe few opportunities offered themselves for determination of the barometer coefficient, the aircraft keeping to the same height during each section of the flight. However, before the descent to Kallax airfield (65°.5 N, 22°.1 E) the plane flew along a pressure surface of (561.1 $\pm$1.5) mb and between Kallax and Tromsö (69°.7 N, 19°.0 E) it flew along another pressure surface of (668.8 $\pm$1,2) mb. Combining these

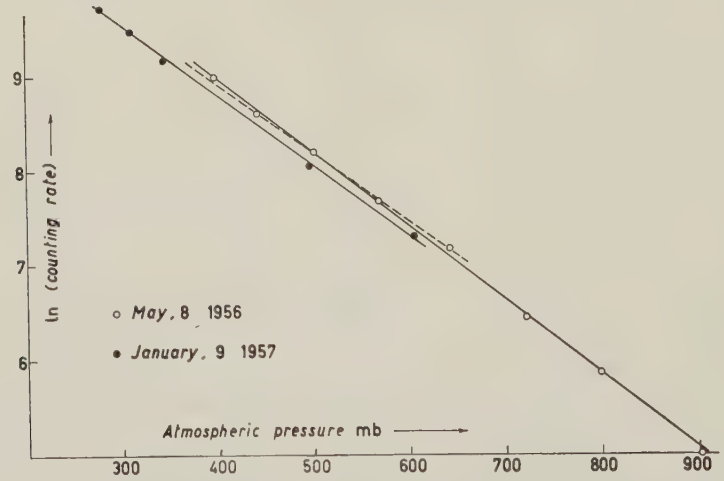

Fig. 3. – The counting rates as functions of the atmospheric pressures during two flights over the middle of Sweden.

values with the corresponding counting rates a coefficient of $-(0.00751 \pm \pm 0.00028)$ is found.

An attempt was made to correlate the counting rate with the atmospheric pressure during descents and ascents, the counting rate being read visually, as already mentioned, during 1 minute intervals. For the transit from Scandinavia to Japan the separate values are comparatively consistent, giving an average of $-(0.0073 \pm 0.0003)$. In many other instances the correlation between counting rate and pressure is comparatively good although

the value of the coefficient varies considerably from case to case even at the same latitude.

Everything considered it was decided that the generally accepted value of — 0.737 per cent/mb should be used in the calculations.

It is perhaps unnecessary to remark that owing to the magnitude of some of the pressure differences the exponential formula has been used exclusively for correcting the observed values.

6. – Numerical treatment.

The number of counts for every single 6 minutes period was corrected separately for variations in atmospheric pressure. 590 mb was selected as the normal pressure level as this offers comparatively small corrections for the major number of measurements. In the polar region the sum of eight 6 minutes intervals was found to correspond to positions spaced approximately 3° apart. The same division into 48 minutes intervals was then followed throughout the whole investigation. In some cases, however, it turned out to be inconvenient to group the 6 minutes intervals in numbers of eight. Then, for the sake of standardization, the total number of counts has been converted into that of a 48 minutes interval.

The geographical position was calculated for the center of each 6 minutes intervals. The positions listed in Table I are the means of those of the 6 minutes intervals constituting each 48 minutes period. This way of averaging is quite satisfactory considering the accuracy with which aircraft positions can be determined on long transocean flights as well as compared to the statistical fluctuations.

The barometer readings from the flight recorder were carefully averaged for each 6 minutes interval. There are some cases of rather large pressure variations within such an interval. However, comparisons within adjacent intervals having very small pressure variations do not indicate any decrease of accuracy due to the averaging in cases of large variations.

The statistical fluctuations amount to 1.0% in the polar region and increase to 1.8% for latitudes with a minimum counting rate. The maximum error introduced by the barometer reading is perhaps 0.4% for single 6 minutes intervals. As it decreases through the summation of intervals it will usually be considerably less than 0.4%. However, in cases of pressures differing very much from 590 mb an error of unknown magnitude might be introduced through the assumption that the barometer coefficient is independent of latitude. Thus, in the polar region the limit of errors can be put at 1.5%, increasing to 2% in the region of minimum counting rate.

In case of major variations in the number of incoming primaries corrections could be computed by comparison with the registrations from two neutron

monitors on the ground. One of them is the new monitor in Uppsala, Sweden. The other one is that at the corona observatory on Mt. Norikura, Japan. According to the latter the variations in primary intensity are negligible, being less than one per cent during the whole flight. As compared to the statistical fluctuation of the airborne monitor the Uppsala values also indicate a constant inflow of primaries during each one of the periods February 16-19 and February 26-28 separately. However, the average counting level of the latter of these two periods is 2.7% higher than that of the former.

At present the difference between the two monitors is a riddle. Owing to the considerable altitude the counting rate of the Mt. Norikura monitor is more than four times that of the Uppsala monitor. This turns the former into a first order reference instrument. However, the variation indicated by the Uppsala monitor is five times the statistical fluctuations and it cannot be disregarded. Anyhow, corrections are apparently not to be applied to any values except those of the later part of the return flight. Neglect of such a correction increases the uncertainty of these values from 1.5 to approximately 4%. Not knowing the reason for the difference displayed by the two monitors the latter course has been followed.

7. – The results.

Considering the general interest shown all determinations of the latitude effect the counting rates corrected for barometer effect are listed in Table I together with time intervals, average pressures, and positions. Figs. 4-7 offer a more comprehensible material for discussion. They are drawn so as to cover every point during the whole flight. Figs. 4-6 overlap to some extent.

Fig. 4 describes the variations during the flight over the polar region including Northern Europe and Alaska. It is drawn in an unorthodox way, the latitudes being plotted for eastern and western longitudes separately. This has been done to simplify comparisons between the two halves of the transit. The unexpectedly high counting rate over Scandinavia catches the eye immediately. One would expect the fairly constant counting rate characteristic of the polar region slowly to develop into a slope towards the well-known knee of the latitude effect. It is therefore necessary to discuss the possibility of any systematic error being present.

From the table we find that the most extreme counting rate was found during the first part of the flight at an altitude exceeding that over the polar sea. It is therefore natural to suppose that an error has been introduced through an inaccurate value of the barometer coefficient. However, the next run of the aircraft flown at an altitude considerably lower than that over the polar sea resulted in as extreme a counting rate as in the former case. Moreover,

as already mentioned, from the two runs at different altitudes a value of the barometer coefficient can be calculated which is not at variance with that generally accepted. Turning to the counting rate at latitude 57°.6 N we find it higher than ought to be expected for this altitude. Nevertheless the value fits very well into the general tendency displayed by the values corresponding to latitudes 51°.9 N and 53°.8 N as well as with the high counting rate measured 12 days earlier ove the northern part of Scandinavia. It would certainly have been far better to have several more points to define this part of the curve, but owing to the frequent visits to airports most of the distances flown at a constant altitude became too short for yielding more than one point of measurement.

It has also to be taken into consideration that the airborne monitor has too small a paraffin shield for a complete protection against external neutrons. Therefore, neutrons produced in the fuel of the aircraft would account for an excess counting rate during the early stages of a flight. Later on the number of external neutrons would decrease with the consumption of fuel. However, the effect ought to reappear after every refuelling. It should have been as prominent after the departure from Anchorage as after the departure from Stockholm. Accordingly, this explanation has to be abandoned.

It becomes necessary once again to take up the question of the difference in counting rate shown by the Uppsala monitor. If a correction is introduced for this change in counting level it would not in any way diminish the « hump » in the curve of Fig. 5. The three points below 60° recorded during the return flight would only be displaced so as to increase the gradient of the slope.

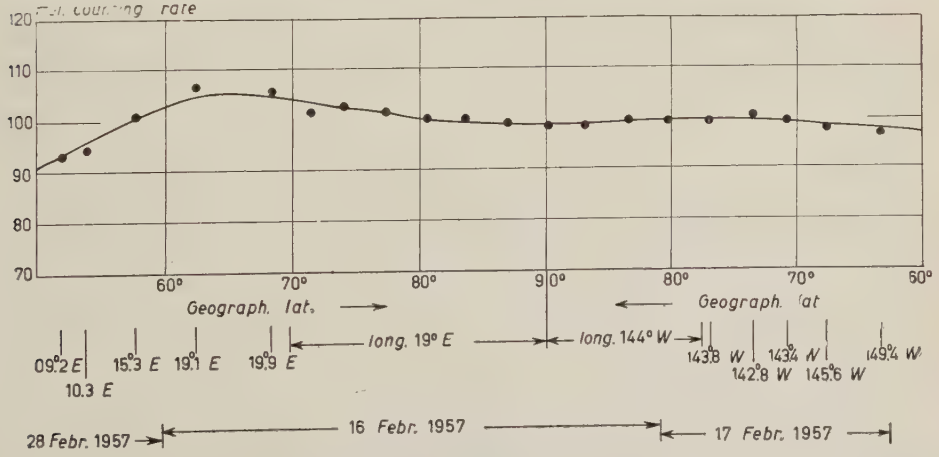

Fig. 4. – Diagram showing relative counting rates over the polar cap and adjacent regions.

Thus, at the moment no explanation can be given of the high counting rate over Northern Europe. Further investigations are indicated.

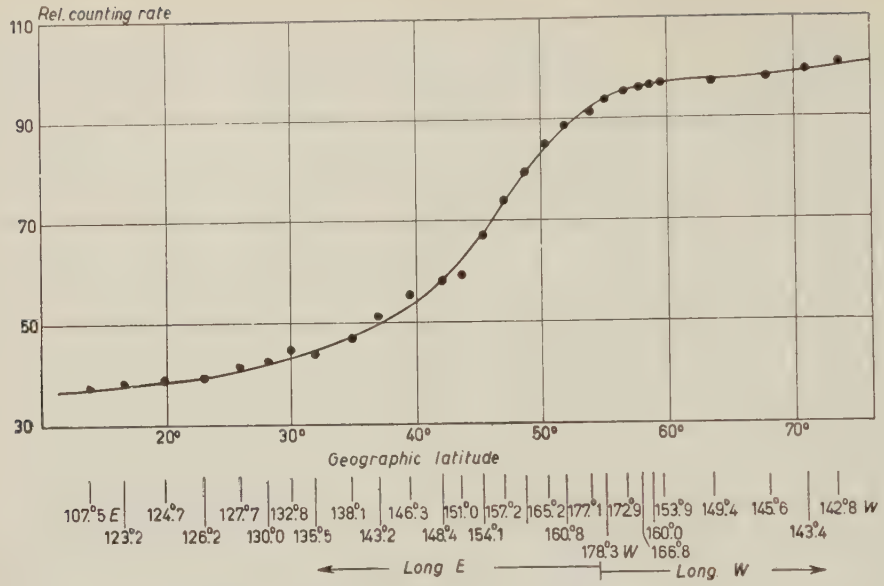

Fig. 5. – The relative counting rates during the eastern part of the flight.

Figs. 5 and 6 show the shape of the knees at longitudes 9° E and 177° E. The former is very well developed while the latter exhibits the meeting of two slopes which do not differ very much as to angular coefficients. As is to be

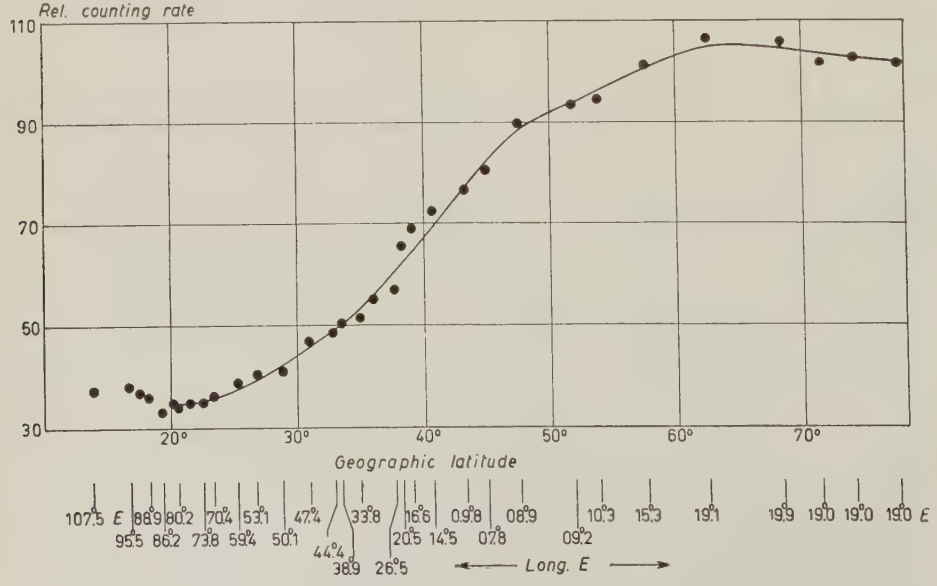

Fig. 6. – The relative counting rates during the western part of the flight.

expected the geographic latitudes of the two knees show a considerable difference, the knee at longitude 9° E falling at latitude 47° N and that at 177° E falling at 54° N.

Owing to variations in the rigidity of the primary particles the latitude of the knee varies with time. Despite this a comparison can be made between the positions of the two knees as in the present case the lapse of time between the two measurements is very short. In addition the registrations from both the stationary monitors show sufficiently constant values to make such a comparison permissible. For that purpose the points of measurement have been referred to geomagnetic co-ordinates. It is an open question if in this case the new cosmic ray magnetic co-ordinates as recommended by Rose *et al.* [3] should be preferred to conventional geomagnetic co-ordinates. However, for a first survey the latter will suffice as a first approximation.

In Fig. 7 the counting rate has been plotted versus geomagnetic latitude. In such a diagram the longitude ought not to play any part regarding the position of the points of measurement. Nevertheless all the points of the « western » part of the flight are definitely displaced relative to those of the « eastern » part. This is a further indication that the conventional geomagnetic co-ordinates constitute only a first approximation where cosmic rays are concerned. Once more considering the discrepancy between the two reference monitors it has to be noted that a correction according to the Uppsala monitor should emphasize the shift between the two curves of Fig. 7.

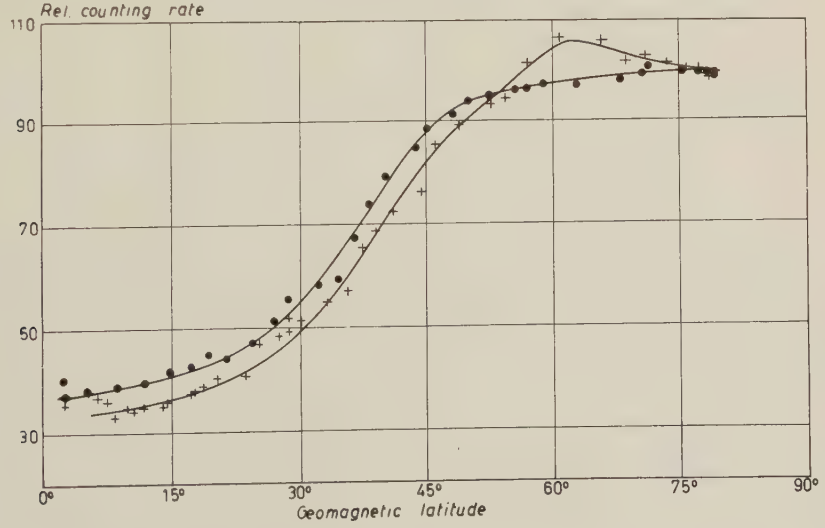

Fig. 7. – The relative counting rates referred to conventional geomagnetic co-ordinates.

As is to be expected the two knees coincide far better as to latitude, the knee at 9° E geograph. long. being located at 46° geomagn. lat. and that at

177 E geograph. long. being located at 47° geomagn. lat. It has to be noted, also, that the first one of these two knees is changed in a remarkable way by the transformation to geomagnetic co-ordinates. It becomes so faintly developed as to seem to be on the verge of disappearing. At the same time the region of abnormally high counting rate appears still more pronounced.

* * *

I am deeply indebted to the Scandinavian Airlines System and its directors for making it possible to carry out this investigation.

My thanks are extended to the technicians of the SAS workshops and to the pilots and navigators for their never-failing interest and help.

I also welcome the opportunity to thank my two untiring comrades on the flight: Mr. Ole Edvardsen, who had the responsibility of trimming the electronics and shared with me the task of supervising the performance of the equipment; Mr. Sten Lyholm of the SAS company, who took care of the power supply and the flight recorder.

I am also indebted to Dr. C. T. Elvey, Fairbanks, Mr. Steve Barnes, Anchorage, and Professor Y. Miyazaki, Tokyo, for preparing repair facilities in case anything serious should have happened to the monitor equipment.

The investigation presented here is part of a cosmic ray project sponsored by the Swedish Natural Science Research Council and the Swedish National Committee for Geophysics.

REFERENCES

[1] D. Eckhartt: *Tellus*, **8**, 281 (1956): letter to the editor.

[2] J. A. Simpson, W. Fonger and S. B. Treiman: *Phys. Rev.*, **90**, 934 (1953), Fig. 9.

[3] D. C. Rose, K. B. Fenton, J. Katzman and J. A. Simpson: *Can. Journ. Phys.*, **34**, 968 (1956).

SUPPLEMENTO AL VOLUME VIII, SERIE X
DEL NUOVO CIMENTO

N. 2, 1958
2° Trimestre

Further Experiments Concerning the Geomagnetic Field Effective for Cosmic Rays (*).

L. Katz

Geophysics Research Directorate - Cambridge Mass.

P. Meyer and J. A. Simpson

Enrico Fermi Institute for Nuclear Studies
The University of Chicago - Chicago, Ill.

1. – Since cosmic ray particles begin to interact with the terrestrial magnetic field at considerable distances from the earth, these particles provide important information concerning the description of the magnetic field extending beyond the surface of the earth. In earlier publications we have discussed the unique properties of the relationship between magnetic fields and cosmic ray intensity measurements in the equatorial zone. We have defined the line of minimum cosmic ray intensity around the earth as the effective geomagnetic field equator for cosmic ray particles (The « cosmic ray equator »). Experiments initiated in 1954 were concerned with the following basic questions regarding the terrestrial field. Is the magnetic field which interacts with cosmic ray particles adequately represented by:

a) the centered, or eccentric dipole approximation derived from the spherical harmonic analysis of surface magnetic field data? (+) or

b) the Local measured fields at the surface of the earth, or

c) for example, partly by a distribution above the earth's surface which arises from the interaction of the rotating permanent field with the ionized medium around the earth?

The first of these questions was clearly answered at Guanajuato by showing

(*) Assisted in part by the Office of Scientific Research and the Geophysics Research Directorate, Air Force Cambridge Research Center, Air Research and Development Command, U. S. Air Force.

(+) See, for example, the analysis of Gauss, Chapman and Bartels, etc.

that the effective equator for cosmic rays was not represented by the classical equator derived from geomagnetic dipole field analysis [1] and that these differences extended to intermediate latitudes as shown by the longitude effect. At that time we used a sine curve on a Mercator projection to represent the available data. The answers to questions *b*) and *c*) remain, and to investigate the matter further we have recently undertaken additional experiments. The analysis of the data is not yet complete but, because of current interest in these questions, we give here some preliminary results of the measurements.

2. – A nucleonic component monitor composed of two separate detectors and recording circuits was transported by aircraft at constant pressure altitude (corresponding to 18000 feet altitude) around the equator according to the route described in Fig. 1.

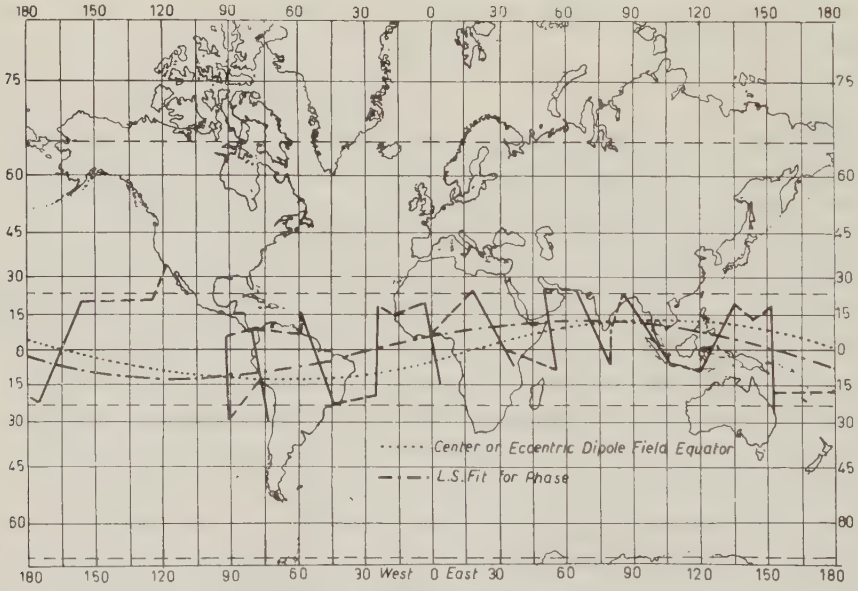

Fig. 1. – Route of aircraft carrying neutron intensity monitor at 18000 feet pressure altitude. The solid line portions of the route correspond to the latitude curves shown in Fig. 2.

The elapsed time for the 12 equatorial crossings was 45 days, during which time there were only small primary cosmic ray intensity variations. Corrections for these variations were provided by the neutron monitor data at Huancayo, Peru. Preliminary latitude curves derived from the 12 equatorial crossings are given in Fig. 2. From these data both the equatorial longitude effect and the position of the minimum cosmic ray intensity as a function of longitude may be investigated.

A) The longitude effect at the equator. – The intensity at the minimum of each latitude curve in Fig. 2 was measured for 12 longitudes. The deviations from mean intensity around the earth are shown in Fig. 3. This is the longitude effect at the effective geomagnetic equator. The following points are of special interest.

1) There is a remarkable symmetry in the curve. The maximum and minimum intensities are nearly 180 degrees apart and the areas under the two halves of the curve are approximately equal. There are no large contributions from functions which have a period different from 2π.

2) The peak to peak amplitude is 25%. This demonstrates that the equivalent magnetic center of the earth is eccentric with respect to the axis of rotation. A preliminary calculation gives approximately 300 km as the separation of the magnetic and geoid centers.

3) The peaks of the curve are displaced approximately 40 degrees west of the longitude curve predicted from the dipole terms of the harmonic analysis and in the direction of the maximum and minimum surface magnetic fields.

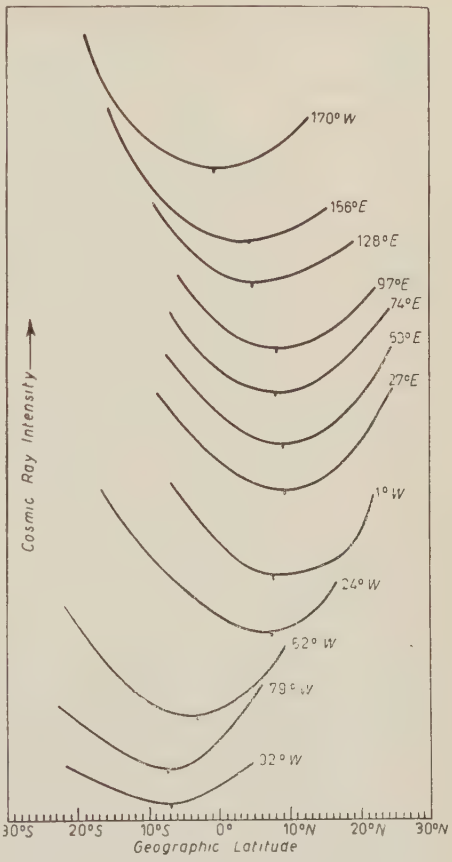

Fig. 2. – Latitude curves for the 12 equatorial crossings shown in Fig. 1. These curves have not yet been corrected for the longitude effect.

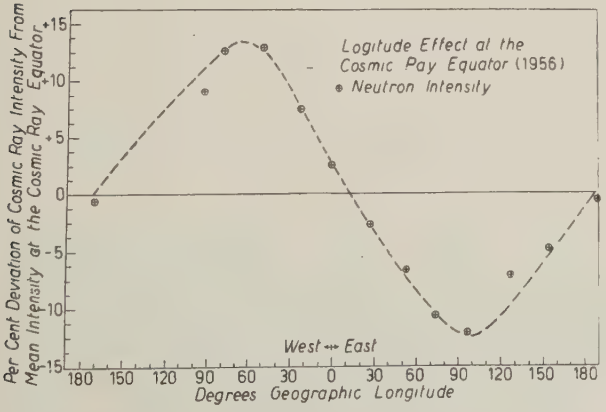

Fig. 3. – The longitude effect for the nucleonic component at the cosmic ray equator.

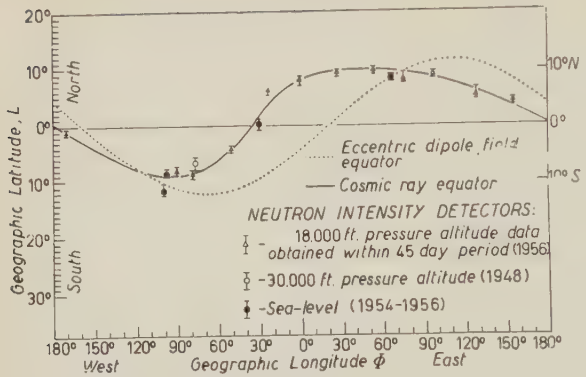

Fig. 4. – The smooth curve represents the cosmic ray equator. Experimental points have not been corrected for the longitude effect.

B) The effective equator for cosmic rays. – Measurement of the location of the minimum intensity depends to some extent upon the slopes of the latitude curves in Fig. 2. The slopes are generally different in the two hemispheres; part of this asymetry arises from the longitude effect introduced by obliquely crossing the equator. (See Fig. 1). Atlhough we have not yet corrected for this effect, the tentative location of minima shown in Fig. 2 is plotted in Fig. 4. A smooth curve was drawn to represent the principal features of the «cosmic ray» equator derived from the new data. The amplitude shown in Fig. 4 is substantially less than given by the geomagnetic dipole approximation The intersections of the curve with the geographic equator are not 180 degrees apart. If this curve were to represent the surface points common to a plane intersecting the earth, then the results shown here imply that the equatorial plane of the magnetic field does not pass through the geoid center. In Fig. 3 we show how this asymmetry in the Mercator projection in Fig. 4 might be represented. Of course, the representation of the data by a plane is rough, and Fig. 5 is not to scale.

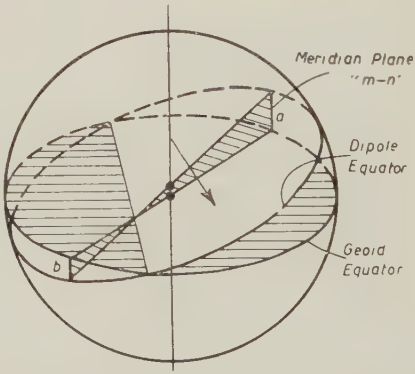

Fig. 5. – This figure is not to scale.

At Guanajuato we showed how the cosmic ray results compared with both the eccentric dipole field equator and the magnetic dip equator for the 1945 magnetic survey [1]. In Fig. 6 the same curves are shown for comparison with the new data.

Returning to the three questions raised in Sect. **1**, the new experimental results reported here illustrate conclusively that the traditional description of the geomagnetic field by spherical harmonic analysis does not represent the field distribution important for cosmic ray particles. It also appears that the observed surface fields—although in much closer agreement with the location of

the « cosmic ray » equator—do not completely describe the effective field distribution. If so, there remains the question of how important are external fields which might be derived, for example, from the rotation of the earth in an ionized medium.

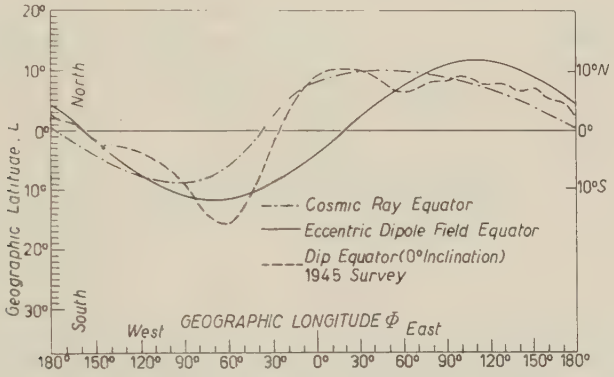

Fig. 6. – A comparison of the cosmic ray, dipole and dip equators.

The preliminary character of the results shown in Fig. 2 and 4 should be emphasized. A full account of these measurements and their interpretation will be published later.

* * *

It is a pleasure to thank Mr. JOHN BUTLER for undertaking the installation and maintenance of the apparatus, and for assisting in the measurements during the flights. The support of the Strategic Air Command, U.S.A.F., was most impressive, and the organization of the expedition by Major GEORGE OTT and his staff was deeply appreciated. We are furthermore indebted to the officers and men of the Strategic Air Command for the excellent execution of the flight program.

* * *

Note added in proof.

P. ROTHWELL has suggested [2] that the cosmic ray intensity distribution is determined only by the surface magnetic fields, taking into account the new 1955 magnetic equator instead of the 1945 dip equator [1]. In order to compare our new « cosmic ray » equator curve from Fig. 4 with the 1955 dip equator, we have plotted this dip equator

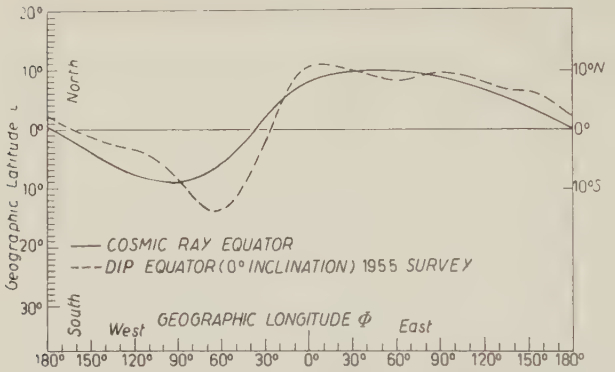

Fig. 7. – A comparison of the preliminary cosmic ray equator with the 1955 dip equator.

using co-ordinates published by the Hydrographic Office, U. S. Navy, which are almost identical with the Admiralty Charts used by ROTHWELL. The curves are compared in Fig. 7.

REFERENCES

[1] J. A. SIMPSON, K. B. FENTON, J. KATZMAN and D. C. ROSE: *Phys. Rev.*, **102**, 1648 (1956).

[2] P. ROTHWELL and J. QUENBY: in this issue, p. 249.

SUPPLEMENTO AL VOLUME VIII, SERIE X
DEL NUOVO CIMENTO

N. 2, 1958
2° Trimestre

Latitude Effect of Cosmic Ray Nucleon and Meson Components at Sea Level.

M. KODAMA

Scientific Research Institute - Tokyo

During the period from November 1956 to April 1957, measurements of cosmic-ray nucleon and meson components were made on the ice breaker Soya throughout the voyage to and from the Antarctic. Go and return routes of Soya were nearly the same as shown in Fig. 1.

Absolute intensity of the neutrons observed at the high latitude was about

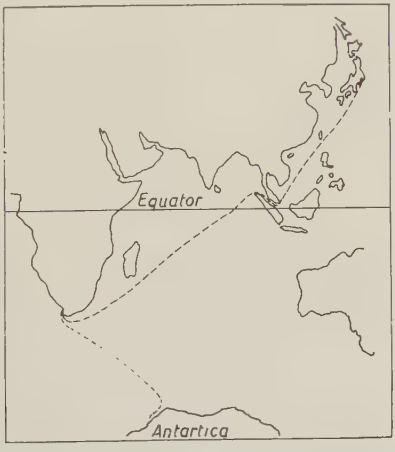

Fig. 1. – The voyage course where cosmic-ray measurements were carried out.

8000 counts per hour. The meson component was observed by Neher type ionization chamber. Day to day variations of neutron intensity are shown in Fig. 2.

The data obtained were reduced to the relative intensity using the natural logarithmic representations and were corrected for the barometric pressure

by the coefficient of -0.77%/mb. Then the correction for the world-wide intensity variations was made using the neutron data of Huancayo (*), Mt.

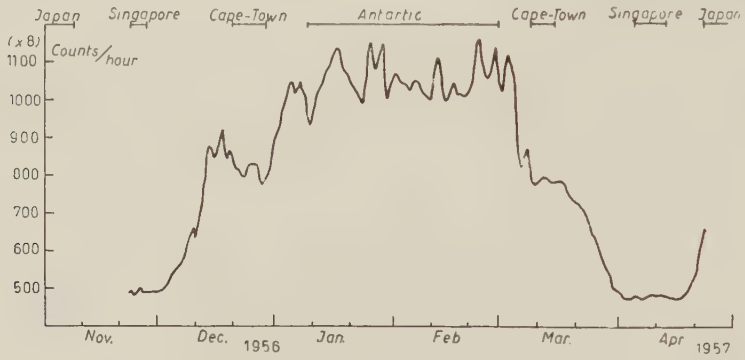

Fig. 2. – Day-to-day variations of neutron intensity.

Norikura, Mexico (*) and Chicago (*), but only by the data of Mt. Norikura after Mar. 22, 1957.

The latitude effect thus obtained was 59% as shown in Fig. 3.

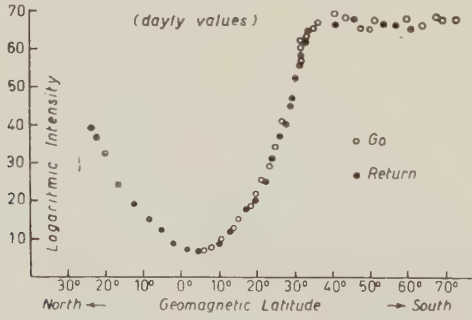

Fig. 3. – Variations of cosmic-ray intensity against the geomagnetic latitude.

Detailed analysis of this curve and the results of the meson component measurements will be reported in near future.

(*) Kindly furnished by Prof. J. A. Simpson of Chicago University.

PART I.

SECTION C: **Cosmic Ray Variation**

The 27-Day Variation in Cosmic Ray Intensity.

D. VENKATESAN

The Royal Institute of Technology - Stockholm

1. – The correlation between cosmic radiation and geomagnetic activity.

1 1. *Introduction.* – The study of electromagnetic phenomena like the magnetic storms, aurorae and certain types of cosmic ray effects like the 27-day variation in intensity are of importance for the proper understanding of the interplanetary electromagnetic state. Solar activity appears to influence the electromagnetic conditions in interplanetary space to a considerable extent. Hence changes in solar activity during its eleven year cycle would be revealed in the above effects attributed to the interplanetary beams or clouds.

The relation between the transient behaviour of the geomagnetic field and cosmic ray intensity has been engaging the attention of a number of people. It is clear from all these studies that the connection between the two is rather complicated. The extensive work of FORBUSH [1], HESS and DEMMELMAIR [2], HOGG [3], SEKIDO [4], YOSHIDA [5] and others reveals that there is a relationship between the two. On the other hand the careful studies of SIMPSON [6] and CHASSON [7] show cases where there seems to be a lack of association between the two. The lack of a detailed correspondence between the two phenomena has been pointed out by DOLBEAR and ELLIOT [8] and TRUMPY [9].

Moreover while SIMPSON [6] and KANE [10] find that the K_p maximum (or minimum) follows the corresponding one in cosmic ray intensity by about 4-6 days, VAN HEERDAN-THAMBYAH PILLAY [11] observe that it precedes the cosmic ray intensity maximum (or minimum) by about 5 days. The author from a study [12] of the Carnegie Institution data [13] for about 20 months during 1945-46, obtained results agreeing with the former two. The studies cover different periods and so it is an open question whether a change in the relationship of the K_p maximum (or minimum) and cosmic ray one occurs during the solar cycle. It is the purpose of this paper to study this as well

as the connection between cosmic ray activity and geomagnetic activity at least during one complete solar cycle.

The beam model: ALFVÉN has invoked beams emitted from the solar surface, with a magnetic field frozen in the beam and an electric field arising from polarization effects. The field frozen in the beam derives from the solar field. The direction of the electric field is in the direction of rotation of the sun. The electric field according to him is the most important property of the beams and on this basis has explained the essential features of magnetic storms and aurorae. He has further pointed out that the cosmic rays could be decelarated in the electric field of the beams and the relative decrease in intensity per day could be expressed in terms of this electric field. Hence it would be reasonable to expect a certain measure of similarity between the changes in this relative decrease and the changes in electric field as revealed by the geomagnetic disturbance. (The latter could be expressed in terms of the international planetary index K_p). This would be completely true provided the deceleration in the electric field of the beams is the only important effect in cosmic rays. But there seem to be two other effects connected with cosmic rays as pointed out by ALFVÉN [13-*d*].

The international planetary index K_p, a reliable but arbitrary standard could be used as a measure of geomagnetic activity. Eight three hourly values of K_p are available for each day. One could either use the sum of these eight values or the highest of these eight as a measure of the geomagnetic disturbance for any day. In general the two reveal very good correspondence. The latter has been used in the present analysis.

1 2. *Analysis and results.* – The well known Chree method of analysis has been adopted. This consists in superposing data of days exhibiting a maximum (or minimum) value. One could choose, say, five days for each month. The method is free from any preconceived ideas about the length and significance of the recurrence tendency. The analyses have been carried out for each year during the period 1937-55, using the daily mean cosmic ray intensity as recorded by the ionization chamber at Huancayo. The analyses for each year have been done corresponding to both five maximum and five minimum intensity days per month, and the difference determined. This method of taking the difference curve removes any seasonal effects as well as any errors due to systematic instrumental drift, which are expected to be of the same order in both the analyses. The same « zero days » or chosen maximum (or minimum) intensity days for cosmic rays are used for the analyses of the geomagnetic material.

Only data involving major breaks of five days or more have been neglected. Otherwise interpolation has been made to obtain values for the missing days. Table I gives the number of days chosen for each year. The analyses have

been carried out for 60 days on either side of the zero days. In the final curve, each point corresponding to the average of three days is plotted as is usually done in these analyses.

TABLE I. – *Periode used for Chree analysis in each year with the number of zero days in each year.*

Year	Period	N. of zero days with period from which the days are chosen	Year	Period	N. of zero days with period from which the days are chosen
1937	Jan.-Dec.	50. March-Dec.	1947	Jan.-Dec.	60. Jan.-Dec.
1938	»	60. Jan.-Dec.	1948	Jan.-Dec.	60. »
1939	»	60. »	1949	»	60. »
1940	»	60. »	1950	»	60. »
1941	»	60. »	1951	»	60. »
1942	»	60. »	1952	»	60. »
1943	Jan.-Sept.	35. Jan.-Jul.	1953	»	60. »
1944	»	35. »	1954	»	60. »
1945	Jan.-Dec.	60. Jan. Dec.	1955	»	50. Jan.-Oct.
1946	»	60. »			

The correlation coefficient, $\gamma_{I.K.}$ between the cosmic ray intensity, I, and the index of geomagnetic activity, K_p is calculated. Similarly the correlation coefficient, $\gamma_{\Delta I.K}$ between the relative decrease in intensity per day, $-\Delta I/I \cdot \Delta t$, and K_p is also determined. Both these correlation coefficients reveal changes during the solar cycle.

It is observed that there are cases during the solar cycle when K_p precedes the cosmic ray peak, and cases when K_p follows the cosmic ray peak. The results for the entire period is summarized in Table II. It can be seen from the same that for the period 1950-1954, K_p has been consistently earlier than the correspondingly cosmic ray peak. The only year when it is not uniquely clear, is 1951, since there are two peaks, one before and one after. But even here, the predominant one is earlier agreeing with the general conclusions reached.

It could be summed up that during the rising part of the solar cycle and possibly during the earlier part of the fall in solar activity, the K_p maximum (or minimum) follows the cosmic ray one after about 4-6 days. These cases would correspond to cases of deceleration in the electric field of the beams causing the geomagnetic disturbances.

The years when K_p precedes could mean that the electric field involved is in the opposite direction, thereby producting an acceleration instead of deceleration. The question of a reverse electric field has to be confirmed from

TABLE II. – *Occurrence of K_p peaks with respect to cosmic ray peaks.*

Year	K_p peaks
1955	Not clear. One peak 3 days after and one 6 days before.
1954	6 days before.
1953	6 days before.
1952	5-6 days before.
1951	One predominant 9 days before and one 9 days after.
1950	6 days before.
1949	4 days after.
1948	5-6 days after.
1947	3-4 days after.
1946	5-6 days after.
1945	4 days after.
1944	One 12 days before and one 10 days after.
1943	One 6 days before and one 6 days after.
1942	One 9 days before and one 9 days after.
1941	One 6 days before and one 6 days after and 15 days before and one 15 days after.
1940	One 15 days before and one 15 days after.
1939	6 days after.
1938	One 12 days after and one 14 days before.
1937	6 days after.

other evidence as well, say geomagnetic disturbances and aurorae. This work is being taken up. It should be mentioned that the whole phenomenon could be complicated by two other effects, viz. the magnetic field effect and the capture effect as pointed out by ALFVÉN [13-*d*].

Fig. 1 shows the results of the analysis by the author [15] for a limited period in 1946, February to October, when there was a series of heavy FORBUSH

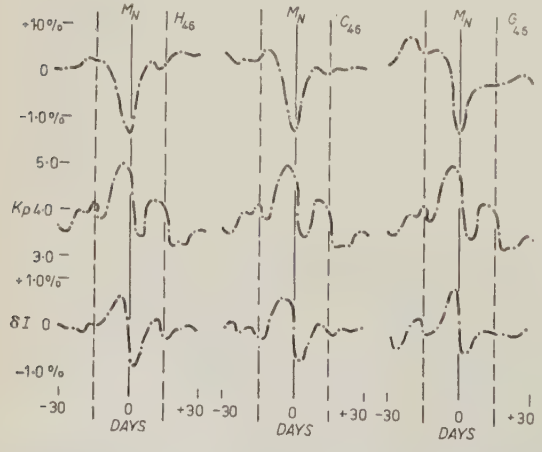

Fig. 1. – Chree analysis for the period Febr. to Oct., 1946, for the cosmic ray intensity as recorded by the ionization chambers at Huancayo, Cheltenham and Godhavn, and the international planetary, index, K_p. The top curve refers to the cosmic ray intensity, I, the middle curve to K_p, and the bottom one to the relative decrease in intensity, $-\Delta I/I \cdot \Delta t$ per day.

decreases. The top curve corresponds to I, the cosmic ray intensity, the middle one to K_p, and the bottom one to $-\Delta I/I \cdot \Delta t$, the relative decrease in intensity per day. The bottom curve is reversed and plotted to show the correlation with K_p better. The analysis corresponds to minimum intensity days, for Huancayo (H), Cheltenham (C) and Godhavn (G), the days for all the analyses including the geomagnetic data, being chosen from Huancayo. The negative correlation between I and K_p, and the positive correlation between $-\Delta I/I \cdot \Delta t$ and K_p is easily seen. The present analyses have been done to study these correlations over each year for at least one solar cycle, to see whether these results are observed over long periods.

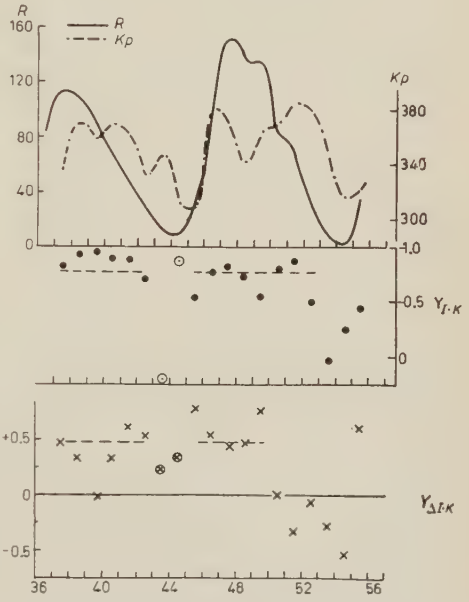

Fig. 2. – Changes in the correlation $\gamma_{I,K}$ between I, the cosmic ray intensity and K_p, the correlation $\gamma_{\Delta I,K}$ between $-\Delta I/I \cdot \Delta t$, the relative decrease in cosmic ray intensity per day and K_p, during the solar cycle. R represents the annual mean sunspot number. On the same figure are also plotted the sum of the K_p maximum values corresponding to 60 most disturbed days, for each year.

Fig. 2 shows the variation of solar activity over the years as revealed by R, the annual mean sunspot number, a measure of the variation of the geomagnetic disturbances each year as revealed by the sum of the K_p maximum corresponding to the 60 most disturbed days for each year, the correlation $\gamma_{I,K}$, between I and K_p and the correlation $\gamma_{\Delta I,K}$ between $-\Delta I/I \cdot \Delta t$ and K_p. The correlation is carried out corresponding to 15 days on either side of the « zero days », which are the chosen days exhibiting maximum (or minimum) intensity values. This restriction to ± 15 days is done in order to avoid the disturbance due to secondary 27-day sequences which are often observed separated by about 14 days from the previous sequence. But it should be pointed out that even if the correlation is carried out corresponding to ± 54 days, the general nature of the results is not essentially altered.

The years 1943 and 1944 have data missing during the whole month of October, which restricts the analyses to seven months instead of twelve months as in other years. Hence a circle has been put around the values for these years.

It can be seen that the geomagnetic disturbance does not follow the solar activity always and shows a departure during 1946-52. This would be con-

sidered later. The correlation between I and K_p is in general high and negative, being about — 0.8 for the period 1937-55, omitting 1943 and 1944 for reasons mentioned earlier, and the years 1952-55. The lowering of the correlation appears around the minimum solar activity period. If one observes into greater details, it seems that this correlation follows the measure of the geomagnetic disturbance.

The correlation between $-\Delta I/I \cdot \Delta t$ and K_p, which gives a measure of the correspondence between the deceleration effect of cosmic rays in the electric field and geomagnetic disturbance, is in general positive and about + 0.5 for the period except for the years 1949-54. Its sign is even reversed for 1951-54. These are the years when K_p was observed to be consistently earlier than cosmic rays, pointing out a possible acceleration instead of deceleration. These need further study. But it appears that the deceleration in the electric field seems to be predominant in most of the years, altough there could be exceptions.

2. – Amplitude of the 27-day variation in cosmic ray intensity: (*)

Since the recurrence phenomena are attributed to the beams, it would be natural to look for a relation between the amplitude of the 27 day variation and solar activity. Meyer and Simpson [16] have reported a progressive decline of the amplitude of the neutron intensity over the years 1951-53, which would be expected from the decreasing solar activity. From an analysis of the Carnegie Institution data from 1937 to 46 and neutron data from the latter half of 1951 to 1953, they have pointed out that the amplitude appears to follow the solar cycle, as revealed by the sunspot number.

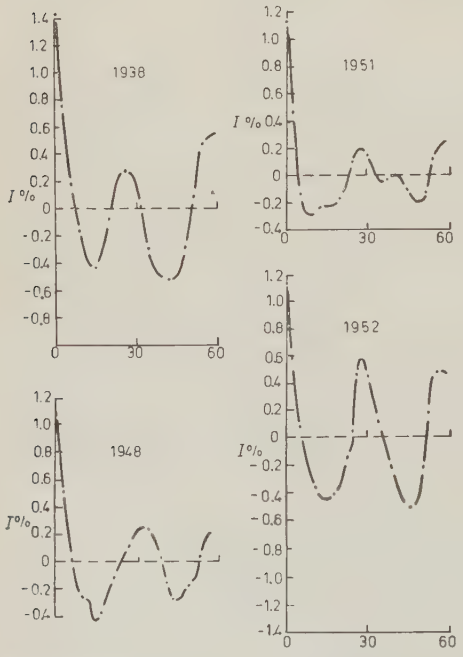

Fig. 3. – Recurrence tendency in cosmic ray intensity at Huancayo as revealed by Chree analysis for the years 1938, 48, 51 and 52. The ordinates represent the intensity in percent and the abscissae the interval in days.

(*) This part of the manuscript dealing with the amplitude of the 27-day variation is awaiting publication in a detailed form in *Tellus*.

The following features emerge from the present study. The recurrence tendency undergoes changes during the solar cycle and there seems to be consistent changes even in the period of the recurrence tendency from 30 to 27 days. The recurrence tendency near the 27 day is most pronounced in the years 1938, 1948, 1951 and 1952. While the former two years correspond to periods of high solar activity, the latter two correspond to epochs near the end of the solar cycle. The minimum solar activity was during the year 1954. It can be seen from Fig. 3 that 1952 reveals the most prominent recurrence tendency about the 27-th day.

A comparison is made in Fig. 4, between the changes in solar activity as revealed by R the mean sunspot number, A, which is half the difference between the 0-th day and 14-th day, and which could be taken as a measure of the amplitude. On the same figure is plot ted σ (tracking), defined by MEYER and SIMPSON [16] as a measure of the worldwide 27 day variation. In their analysis, MEYER and SIMPSON remove some periods from the data, namely those containing temporary increases due to solar flares, and Forbush decreases, which they consider to be different from the 27 day variation. In this analysis, since only data from Huancayo are used, where no flare increases are observed on 28-th February 1942, and 26-th July, 1946, no data have been deleted. Since we consider that the Forbush decreases differ only in the matter of degree, we have not deleted this either. There is close agreement between the results of this analysis and the analysis of MEYER and SIMPSON in spite of differences in the method of choosing data and analysis, for the period for which their analysis is available. So we expect that the same agreement is likely to be there if their analysis had been available for the intermediate period.

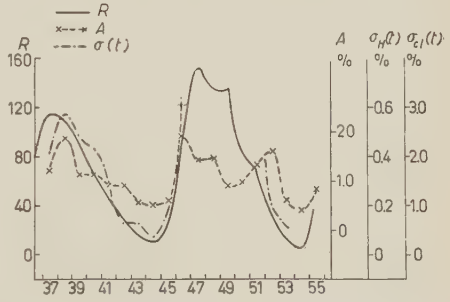

Fig. 4. – Comparison of the amplitude of the 27-day variation in cosmic ray intensity during the solar cycle. R refers to the mean annual sunspot number, A, which is a measure of the amplitude of the 27-day variation as determined in this analysis and $\sigma(t)$, a measure of the world wide 27-day variation as defined by MEYER and SIMPSON [16].

The good agreement between solar activity as revealed by sunspot number and the amplitude of the 27 day variation in cosmic ray intensity for the periods 1937-46 and 1952-55, breaks down during the intervening period. While the solar activity goes further up after 1946, the amplitude decreases, so that we have a minimum in the amplitude for the year 1948 when solar activity is almost at its highest.

It would be extremely interesting to find out whether this breakdown in the relationship during 1946-52, is reflected in any other effects attributed to the beams, say, geomagnetic disturbances. The sum of the K_p maximum values for the 60 most disturbed days in each year could be taken as a measure of the geomagnetic disturbance in each year. This is shown in Fig. 5 along with solar activity and the amplitude of the 27 day intensity variation in cosmic rays. It is clearly seen that they show essentially the same sort of departure from solar activity as exhibited by cosmic rays. The period 1946-52 needs a careful study from various viewpoints, viz., cosmic rays, geomagnetic storms, aurorae, etc. *This result draws the attention that the amplitude of the 27 day variation in cosmic ray intensity is more closely connected with geomagnetic activity rather than with solar activity.*

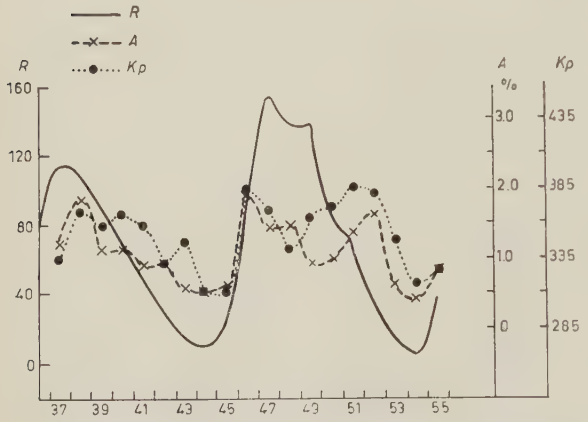

Fig. 5. – Changes in A, the amplitude of the 27-day variation in cosmic ray intensity and geomagnetic disturbances as represented by the sum of K_p maximum on the 60 most disturbed days during the solar cycle. The solar activity is represented by R, the mean annual sunspot number.

As a tentative explanation for the departure from solar activity, it may be suggested that there is some sort of saturation of the electromagnetic conditions in interplanetary space. It is possible that the beams, to which could be attributed the unusually heavy activity in 1946 lasting for about six months, have transported the major quantity of the available flux. Hence, although the solar activity goes up, further emission of beams would have a comparatively weaker field to transport. The electric field would therefore be weaker and so it seems reasonable that immediately

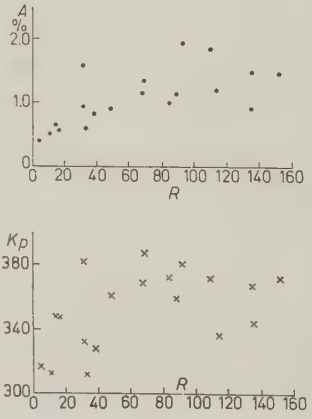

Fig. 6. – Relation between the amplitude of the 27-day variation in cosmic ray intensity and the geomagnetic disturbances as represented by the sum of K_p maximum on 60 most disturbed days on one hand and the solar activity as represented by R, the mean annual sunspot number, on the other.

after 1946, there is a decrease in the geomagnetic disturbances. The gradual resetting of the disturbed solar field starts, so that after 1948, the electric field becomes stronger and this is reflected in the increase in the amplitude of the 27 day variation in cosmic ray intensity and in the geomagnetic disturbances. From 1952 onwards it again follows the solar activity. It would be interesting to look into the auroral disturbances during this period.

Fig. 6 shows the amplitude of the 27-day variation of cosmic ray intensity and the K_p sums for the 60 disturbed days for each year against the solar activity as revealed by R, the annual mean sunspot number. It appears that both reach a maximum corresponding to a value of the sunspot number in about the range $80 \div 100$, and then appear to decline for further rise in solar activity. This points to some sort of saturation of the electromagnetic state.

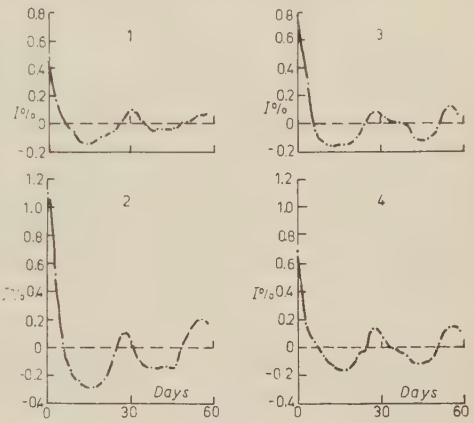

Fig. 7. – Systematic changes in the periodicity of the recurrence tendency as revealed by the Chree analysis for years grouped according to solar activity. 1) refers to years corresponding to the beginning of the solar cycle, 2) to years when activity is maximum, 3) to years when the solar activity is decreasing, and 4) to years corresponding to end of cycle.

A study of the recurrence period from cosmic ray evidence appears to indicate a certain systematic variation with solar activity. It would therefore be

TABLE III. – *Recurrence period for years grouped according to solar activity.*

No.	Group corresponding to	Years combined	Recurrence interval (days)
1	Beginning of new cycle	1944, 1945 1954, 1955	30
2	Maximum of activity	1937, 1938 1946, 1947 1948, 1949	Between 27 and 30
3	Fall of activity	1939, 1940 1941 1950, 1951	Between 27 and 30
4	End of cycle	1942, 1943 1952, 1953	27

worthwhile to secure evidence from geomagnetic side also. The period 1937 ÷ 55 is divided into four groups: *a*) rising part of the solar cycle, *b*) maximum solar activity, *c*) fall of activity, and *d*) end of the cycle. It can be seen from Fig. 7 that the recurrence period is greater for the first group than for the others. Table III shows the grouping of the years as well as the period for each group. The systematic decrease in the period suggests that the region of production of beams changes in a systematic way with solar activity. The butterfly pattern of the distribution of sunspots is well known. If the region of production of the beams gradually proceeds downwards from a higher to the equatorial latitudes, then the periodicity should reveal some systematic variation of this type.

3. – Daily variation of cosmic ray intensity on disturbed days.

It has been pointed out earlier that a measure of the geomagnetic disturbance of a year could be obtained from the K_p sums corresponding to the 60 most disturbed days in each year. The daily variation of cosmic ray intensity at Huancayo corresponding to these 60 most disturbed days in each year has been determined for the period 1937 ÷ 55. Fig. 8 shows the solar activity as represented by R, the sunspot number, the measure of the geomagnetic disturbance for each year as represented by the K_p sums referred above, M^D, $M\Phi^D$, M^S and $M\Phi^S$, the amplitudes and time of maximum of the diurnal and semi-diurnal components of the daily variation of cosmic ray intensity corresponding to these 60 most disturbed days.

It can be seen that the time of diurnal maximum, $M\Phi^D$ essentially follows

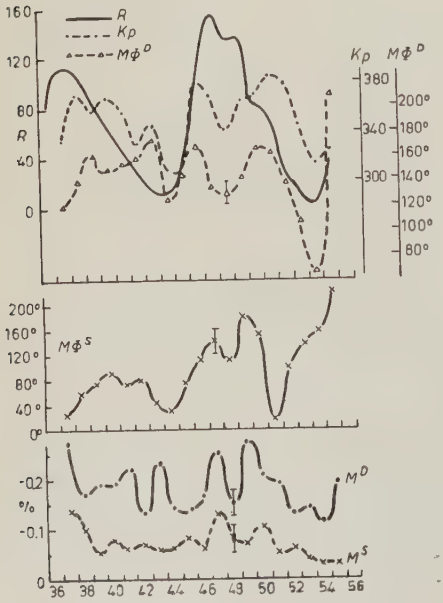

Fig. 8. – Changes in the daily variation of the cosmic ray intensity corresponding to the 60 most disturbed days during the solar cycle. R refers to the mean annual sunspot number, K_I, to the sum of the K_p maximum values corresponding to the 60 most disturbed days, $M\Phi^D$ and $M\Phi^S$ to the times ot maximum of the diurnal and semidiurnal components of the daily variation of cosmic ray intensity corresponding to the above mentioned 60 days, and M^D and M^S to the diurnal and semidiurnal amplitudes of the daily variation of cosmic ray intensity.

the changes in geomagnetic activity, thereby stressing the close connection between the two. It is not possible to say anything so definitely about the time of maximum of the semidiurnal variation, $M\Phi^s$. But it appears that $M\Phi^s$, the semidiurnal time of maximum follows the solar activity better than the geomagnetic activity, except that it reaches a minimum a couple of years earlier. It is to be noted that in spite of the good general agreement between $M\Phi^D$ and geomagnetic activity, the change in the former from 1954 to 1955 is much more rapid than for the latter. It is not possible to say anything definite about the amplitude of the daily variation.

It has been pointed out by Sarabhai, Desai and Venkatesan [17], that the time series of the mean annual diurnal time of maximum roughly follows the solar cycle. This can be seen from Fig. 9. This shows that the annual mean diurnal variation masks the diurnal variation of the disturbed days, which deviates from the solar activity curve. The correlation between the diurnal times of maximum at Huancayo and Cheltenham has been shown to

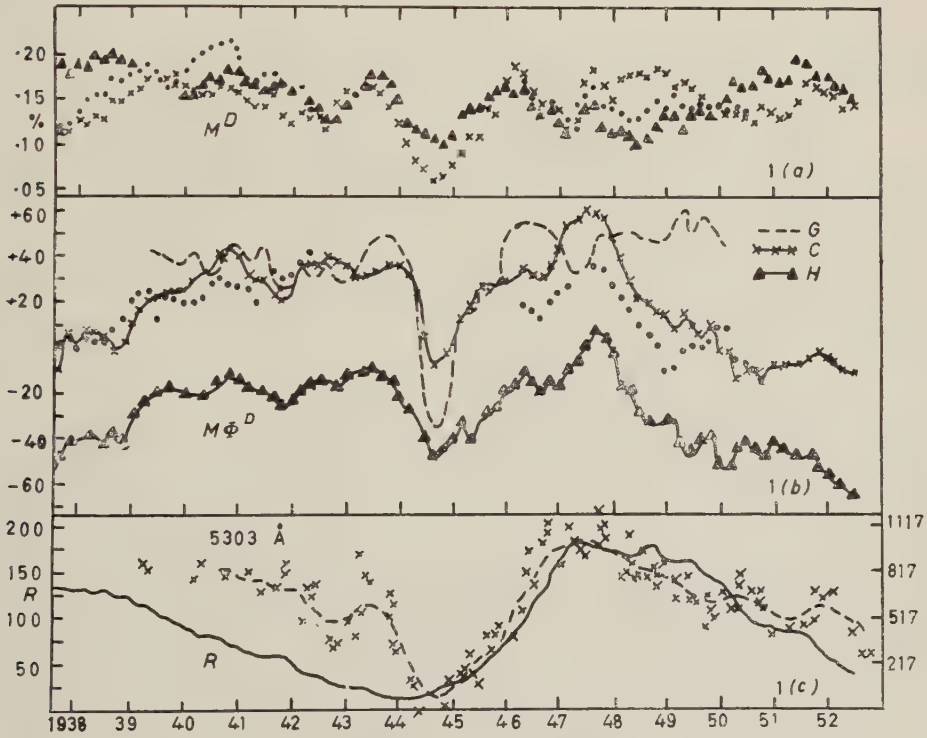

Fig. 9. – Changes in the daily variation of cosmic ray intensity during the solar cycle taken from the figure in paper by Sarabhai, Desai and Venkatesan [17]. On the same are also shown the changes in the time of maximum of the diurnal component of the daily variation in cosmic ray intensity at Godhavn, during 1939-50. It is the time series of annual means shifted by every two months.

be $+0.93$. It is therefore reasonable to expect the same behaviour in the diurnal time of maximum on disturbed days at Cheltenham also. In Fig. 9 the time series of the diurnal time of maximum at Godhavn is also shown. This shows good positive correlation with the stations Huancayo and Cheltenham only for the period 1939-46 and shows negative correlation from 1946 to 1950 up to which the data are available. Therefore it is not possible to say anything about the disturbance daily variation at Godhavn.

It has been pointed out by the same authors that the correlation between the diurnal amplitudes at Huancayo and Cheltenham for 1940-46 breaks down thereafter. In view of all these large changes being observed atfer 1946, it is necessary to use caution in drawing any general conclusion about the period. The period needs special study from all viewpoints.

4. – Conclusions.

The following facts emerge from the study:

1) In general there is a negative correlation between I, the cosmic ray intensity, and K_p the planetary index, although there are exceptions.

2) There is a positive correlation between the relative decrease in intensity, $-\Delta I/I \cdot \Delta t$ and the planetary index, K_p. There are exceptions during the low sunspot activity period of $1949 \div 54$.

3) The K_p minimum (or maximum) is observed to precede the corresponding cosmic ray one in some years and follow in other years. But it appears that the latter case is generally found during the rising part of the solar cycle and possibly during the early fall.

4) There is clear evidence that the amplitude of the 27 day variation in cosmic ray intensity follows the geomagnetic disturbance better than the solar activity. Both of them exhibit similar departure from solar activity during $1946 \div 52$.

5) The time of maximum of the diurnal variation of cosmic ray intensity on disturbed days follows the geomagnetic disturbance better than the solar activity. The semidiurnal time of maximum on disturbed days appears to follow the solar activity in a rough measure.

* * *

The author wishes to thank Dr. Forbush for unpublished data after 1946 which have enabled this study to be made.

REFERENCES

[1] S. Forbush: *Phys. Rev.*, **52**, 1254 (1937).
[2] V. F. Hess and A. Demmelmair: *Nature*, **140**, 316 (1937).
[3] A. R. Hogg: *Memoirs of the Commonwealth Observatory, Canberra*, No. 10 (1949).
[4] Y. Sekido, M. Wada, I. Kondò and K. Kawabata: *Rep. Ion. Res. Japan*, **9**, 174 (1956).
[5] S. Yoshida: *Nuovo Cimento*, **4**, 1410 (1956).
[6] J. A. Simpson: *Phys. Rev.*, **94**, 426 (1954).
[7] R. L. Chasson: *Phys. Rev.*, **96**, 1117.
[8] D. W. N. Dolbear and H. Elliot: *Nature*, **159**, 58 (1947).
[9] B. Trumpy: *Physica*, **19**, 645 (1953).
[10] R. P. Kane: *Phys. Rev.*, **98**, 130 (1955).
[11] V. Heerdan and Thambyah Pillai: *Phil. Mag.*, **46**, 1238 (1955).
[12] D. Venkatesan: *International Astronomical Union Conference on Electromagnetic Phenomena in Cosmical Physics* (1956).
[13] Carnegie Institution Publication: *Cosmic Ray Results from Huancayo Observatory*, Publication 175 (1948).
[14] H. Alfvén: *a*) *Cosmical Electrodynamics* (Oxford, 1950), Chap. VI; *b*) *Tellus*, **6**, 232 (1954); *c*) *Tellus*, **7**, 50 (1955); *d*) *International Astronomical Union Conference on Electromagnetic Phenomena in Cosmical Physics* (1956).
[15] D. Venkatesan: *Tellus*, Awaiting publication (1957).
[16] P. Meyer and J. A. Simpson: *Phys. Rev.*, **96**, 1085 (1954).
[17] V. Sarabhai, U. D. Desai and D. Venkatesan: *Phys. Rev.*, **96**, 469 (1954).

SUPPLEMENTO AL VOLUME VIII, SERIE X
DEL NUOVO CIMENTO

N. 2, 1958
2° Trimestre

Cosmic-Ray Changes near the North Geomagnetic Pole from 1954 to 1956.

H. V. Neher

California Institute of Technology - Pasadena, Cal.

Summary (*). — Since the summer of 1954, when the sun was at a very low state of activity, the intensity of cosmic rays at high altitudes near the poles has been decreasing in accordance with Forbush's relationship. The decrease in the numbers of primaries from the summer of 1954 to 1955 was only a few percent, but the decrease was approximately a factor of two between 1955 and 1956. At the middle altitudes the intensity was even less in 1956 than in 1937 when the sun was at a maximum of activity. However the ionization at balloon altitudes did not pass through a maximum in 1956 as it did in 1937. The shape of the ionization-depth curve at atmospheric pressures of 10 to 100 g cm^{-2} is quite sensitive to the relative numbers of low-energy particles in the primaries. If protons, such particles have energies in the range 100 to 500 MeV. By comparing the shapes of such curves taken near the geomagnetic poles at different times, the presence or absence of a « knee » at very high altitudes may be predicted for it is just the absence or presence of such low-energy particles that causes the presence or absence of the « knee ». The relative numbers of low-energy (100 to 500 MeV protons) particles to those of higher energy do not always bear the same relationship to each other. Thus, on some days the numbers of low-energy particles will be higher than on some other days, but the numbers of those of higher energy may be less. The reverse situation may also be true. As to the nature of the primaries that change so radically with time, there is some evidence that they may be almost all protons. Thus, the latitude effect at high altitudes is certainly consistent with this assumption. Also, the experiments of the Minnesota group show an absence of low-energy α-particles even during the low period of solar activity in 1954.

(*) The complete paper has appeared in the *Phys. Rev.*, **107**, 588 (1957).

SUPPLEMENTO AL VOLUME VIII, SERIE X
DEL NUOVO CIMENTO

N. 2, 1958
2° Trimestre

Changes of Solar Anisotropy and of the Intensity of Cosmic Radiation.

V. Sarabhai and P. D. Bhavsar

Physical Research Laboratory - Ahmedabad

1 – Introduction.

Realization has grown in recent years that the solar anisotropy of cosmic radiation which is detected by the measurement of the solar daily variation of meson intensity corrected for atmospheric influence, is of a highly variable character [1-8]. The solar and terrestrial relationships of the changes of anisotropy have been studied and theories have been advanced [9-11], to explain the creation of the anisotropy by a modulation of the cosmic ray intensity incident in particular directions. A confirmation of these experimental observations and tests of the proposed models for the modulation of cosmic rays are of crucial significance to the theories of the origin of cosmic rays and of the electromagnetic state of interplanetary space.

To undertake this task we want firstly an experimental technique which permits us to select days on which significant daily variations of different types occur. It has been shown earlier [6] that days on which the daily variation has a significant amplitude, can broadly be classified into three groups. On the so called « *d* » type days, the daily variation has one maximum near noon, on « *n* » type days it has one maximum early morning and on « *s* » type days it has two maxima instead of one. It is also known that the 3 different types of daily variations are more clearly revealed in observations with vertical narrow angle telescopes, having semiangles of about 5°, than with ionization chambers or wide angle telescopes. Not only is the amplitude of the variation larger, but the separation of maxima of « *d* » and « *n* » types is greater for narrow angle observations than for omnidirectional studies. However, since the magnitude of the solar anisotropy and the consequent amplitude of the daily variations changes from day-to-day, it is important to have

an instrument with as high a counting rate as possible so that even days on which the amplitude is small can be significantly classified. Therefore the experimental technique should involve the use of narrow angle telescopes of as large aperture as is possible.

The second aspect of the study should relate to the examination of the worldwide character of the changes in anisotropy. While it has been shown that some aspects of changes in the 12-month mean anisotropy are correlated for a station at the equator (Huancayo) and at stations in the middle latitudes (Cheltenham or Christchurch) it has also been noticed [8] that day-to-day changes which are correlated for Ahmedabad, Freiburg and Amsterdam are not correlated with the day-to-day changes in the equatorial station of Kodaikanal. Classification of days according to the nature and magnitude of the anisotropy occurring on each day is an important task which is meaningful only if changes of the daily variation exhibit certain global characteristics.

Finally, having classified days in terms of the character of the anisotropy, it is worthwhile to study the solar and terrestrial relationships of the changes of anisotropy. For this, we can examine the values of physical quantities such as I, the mean cosmic ray intensity, C_p the daily planetary magnetic character figure and the indices for solar activity on the solar disc on days of different classifications.

We present here the first results of an investigation being conducted since July 1955 at Ahmedabad (Lat. 23°01′ N, Long. 72°36′ E, Geomagn. Lat. 13° N, Alt. 180 ft.).

2 – Experimental technique.

A cubical meson telescope conforming to the specifications of the standard instrument to be used during the International Geophysical Year has been modified to provide additional data. The instrument has three counter trays of area 85 cm × 85 cm, each tray made up of 20 Geiger counters. The vertical separation of the extreme trays is 85 cm and 96.5 g/cm² of iron are kept between the two lower trays. In each tray, pairs of adjoining counters are operated with a common electronic quenching unit. 10 vertical triple coincidence telescopes ^{5}T of semiangle 5° in the E-W plane are formed by using separately each pair of counters in a tray. The output of five such pairs is also combined and used to provide 2 vertical triple coincidence telescopes ^{26}T of semiangle 26° in the E-W plane. Finally, the triple coincidences of the complete trays provide the standard telescope ^{45}T of semiangle 45° in the E-W plane. The semiangle in the N-S plane of all telescopes is 45°. The characteristics of the different telescopes are indicated in Table I.

In practice, the records of the 10 narrow angle telescopes ^{5}T are not sepa-

rately registered, but they are combined into 4 groups, 2 of 3 telescopes each, and 2 of 2 telescopes each. While on a large number of days data from all 10 telescopes are available, there are a number of days when due to instrumental failures some of the telescopes are not in operation. When this happens the useful data on any particular day relate to fewer than 10 narrow angle telescopes and to one or to none of the two 26° telescopes ^{26}T.

TABLE I.

Semi-angles		Number of telescopes available	Bihourly counting rate per telescope	Total bihourly counting rate N	% standard deviation for bihourly rate $100/(N)^{\frac{1}{2}}$
E-W	N-S				
5°	45°	10	1300	13000	± 0.9 %
25°	45°	2	29000	58000	± 0.4 %
45°	45°	1	100000	100000	± 0.3 %

The satisfactory functioning of the telescopes is verified by comparison of the changes in their daily mean rates. For each day, a daily variation and a daily mean intensity for ^{5}T and ^{26}T telescopes is derived by averaging the data of similar telescopes that are satisfactorily in operation on that particular day. The standard deviation of the data varies according to the number of telescopes in operation on each day. Therefore, in considering the significance of a variation measured on a day, we have to relate it to the standard deviation appropriate to the number of similar telescopes which are in operation.

The daily variation data on each day are first corrected for the influence of the daily variation of barometric pressure using a coefficient of -2.2% per cm of Hg. The appropriateness of using this coefficient has been discussed by SARABHAI *et al.* [4, 16]. The data are then harmonically analysed and the amplitudes and times of maxima of the diurnal and the semidiurnal components of ^{5}T and ^{26}T are calculated.

3 – Types of daily variations.

In the present study, a 2σ level of significance has been adopted when examining the types of daily variations that occur on different days. The amplitude and time of maximum of the diurnal component are physically meaningful only on days on which the daily variation curve is essentially diurnal in character and exhibits one principal maximum during 24 hours. Similarly the amplitude and the time of maximum of the second harmonic are physically meaningful when the daily variation is semi-diurnal in character with two maxima in 24 hours. By examining the daily variation formed by super-

position of diurnal and semidiurnal components having a ratio of amplitudes M^D/M^S ranging from 0.2 to 2.0, it is clear that when this ratio is less than 0.75 the final curve always exhibits two pronounced maxima in 24 hours. On the other hand when the ratio is larger than 1.5 the daily variation exhibits only one maximum.

For ^{5}T, in Fig. 1*a* is given the histogram showing the frequency of occurrence of the diurnal maximum for each of 12 bihourly intervals of a day for 103 days on which the diurnal amplitude $M^D \geqslant 2\sigma$. If we now impose the condition that $M^D/M^S \geqslant 1.5$, the resulting histogram is shown in Fig. 1 *b*. This relates to 71 days on which we can conclude from the ratio of the amplitudes of the diurnal and the semidiurnal components that the daily variation has one maximum only. It is observed that by restricting attention to significant days which have only one maximum during 24 hours, the histogram clearly reveals the tendency for the diurnal maximum to occur in one of two preferred periods of the day, at 0700 and at 1500 hours IST. We can therefore distinguish days on which the maximum of the diurnal variation occurs between midnight and noon from those on which the maximum occurs between noon and midnight. A similar classification into « *n* » and « *d* » type days was undertaken by SARABHAI and NERURKAR [6] who observed during an investigation in 1954-55, the tendency for narrow angle telescopes to exhibit daily variations with one of two preferred times of maxima for the diurnal component, when the semidiurnal component was small compared to it. However, at that time, the maxima occurred at 0300 hours and at 1100 hours instead of at 0700 hours and at 1500 hours respectively, during 1956. The shift to later hours of both maxima during the period of about two years from 1954 to 1956 is probably connected with the shift to later hours observed in the time of maximum of the diurnal component of the 12 month mean daily variation since the last minimum of solar activity in 1954.

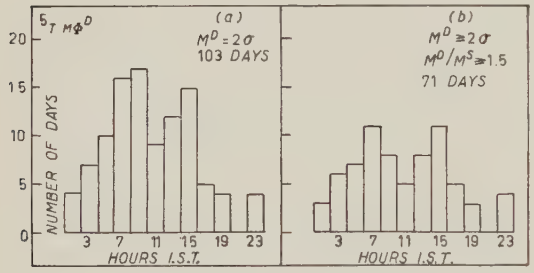

Fig. 1. – The distribution of occurrence of the diurnal maximum for ^{5}T for each of 12 bihours of a day, (*a*) when $M^D \geqslant 2\sigma$, and (*b*) when $M^D \geqslant 2\sigma$ and $M^D/M^S \geqslant 1.5$. M^D and M^S are the per cent amplitudes of the diurnal and the semidiurnal components of the daily variation.

On days when the ratio $M^D/M^S \leqslant 0.75$ and $M^S \geqslant 2\sigma$, we have a daily variation which has a significant semi-diurnal component, predominating over the diurnal component. On such days, the daily variation exhibits two maxima instead of one and we can classify the day as an « *s* » type day.

In order to study the nature of the daily variation on days when the diurnal and the semidiurnal components are of comparable amplitude, i.e. $1.5 > M^D/M^S > 0.75$, and the diurnal component is significant at the 2σ level, we can consider separately the harmonic components of the mean daily variation on such days when the diurnal component has a maximum occurring between midnight and noon, and between noon and midnight.

In Table II are indicated the amplitude and time of maximum of the diurnal and the semidiurnal components for the mean daily variations during

Table II.

No.	Character of the variation on each day	Average percentage amplitudes and the times of maxima (expressed in degrees) for the 1st and the 2nd harmonic components of the daily variation.				
		M^D	$M\Phi^D$	M^S	$M\Phi^S$	M^D/M^S
1	$1.5 > M^D/M^S > 0.75$ and $0° < M\Phi^D < 180°$	0.8 ±0.2	120°	0.3 ±0.2	— 24°	2.7
2	$M^D/M^S \geqslant 1.5$ and $0° < M\Phi^D < 180°$	0.98±0.15	100°	0.12±0.15	56°	8.2
3	1+2 combined	0.92±0.10	107°	0.06±0.10	18°	15.1
4	$1.5 > M^D/M^S > 0.75$ and $180° < M\Phi^D < 360°$	1.0 ±0.3	180°+27°	0.4 ±0.3	38°	2.5
5	$M^D/M^S \geqslant 1.5$ and $180° < M\Phi^D < 360°$	0.90±0.18	18°+59°	0.04±0.18	— 9°	22.2
6	4+5 combined	0.92±0.15	180°+52°	0.11±0.15	+ 27°	8.4
7	$M^S \geqslant 2\sigma$ and $M^D/M^S < 0.5$	0.16±0.15	110°	0.23±0.15	48°	0.7

the two groups of days. Also indicated in the table for comparison are the characteristics of the diurnal and the semidiurnal components of the « *n* » and « *d* » type days when $M^D/M^S \geqslant 1.5$ and M^D is significant at the 2σ level. It is observed that even for days on which individually M^D/M^S is between 1.5 and 0.75, the average daily variation has a ratio much larger than 1.5. This indicates that while on individual days we have a semidiurnal component

which is comparable to the diurnal component, there is no strongly preferred time of maximum of the semidiurnal component. In consequence, the resultant average daily variation for the 2 groups of days is diurnal in character. Moreover, the time of maximum and amplitude of the diurnal component of the average for the two groups do not differ significantly from those of the « *d* » and « *n* » type days respectively where even on individual days the ratio $M^D/M^S > 1.5$. The days relating to the two groups can therefore be grouped with « *n* » and « *d* » type days respectively. In effect therefore classification of days can be undertaken on the following criteria:

a) « *n* » type days are those days on which the daily variation has $M^D \geqslant 2\sigma$, $M^D/M^S > 0.75$ and the diurnal maximum occurs between midnight and noon.

b) « *d* » type days are those days on which the daily variation has $M^D \geqslant 2\sigma$, $M^D/M^S > 0.75$ and the diurnal maximum occurs between noon and midnight.

c) « *s* » type days are those days on which $M^S \geqslant 2\sigma$, M^D/M^S 0.75.

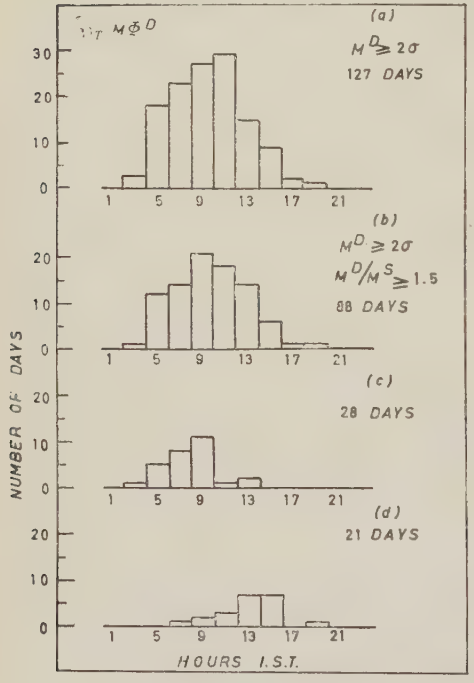

Fig. 2. – The distribution of occurrence of the diurnal maximum for ^{26}T for each of 12 bihours of a day: (*a*) when $M^D \geqslant 2\sigma$, (*b*) when $M^D \geqslant 2\sigma$ and $M^D/M^S \geqslant 1.5$, (*c*) for days on which ^{5}T has a daily variation of « *n* » type, and (*d*) for days on which ^{5}T has a daily variation of « *d* » type.

Fig. 2-*a* and 2-*b* show histograms for ^{26}T corresponding to the histograms shown in Fig. 1-*a* and 1-*b* for the ^{5}T telescopes. It will be observed that the separation of groups of days on which the daily variation is a maximum in the morning or in the afternoon is not as distinct in ^{26}T as for the narrow angle telescope ^{5}T. However, the reality of the occurrence of the daily variation with a diurnal maximum at one of two preferred times of maxima even in ^{26}T is seen by separating the days included in Fig. 2-*a* according to the type recorded by ^{5}T. Thus the histograms of occurrence of time of maximum of the diurnal component of ^{26}T on days on which ^{5}T has a maximum before noon or in the afternoon are shown in Fig. 2 *c*) and 2 *d*) respectively. It is clear that days on which

there is a morning maximum in ^{5}T are associated with an earlier time of maximum in ^{26}T than days on which ^{5}T has a maximum in the afternoon. The separation of the two groups in ^{26}T is however only by about four hours in place of about 8 hours for ^{5}T.

In Fig. 3 we show separately the daily variations for ^{5}T and ^{26}T averaged for all days on which

a) there is a significant « *n* » type of variation,

b) there is a significant « *d* » type of variation,

c) there is a significant « *s* » type of variation, and

d) there is any one of the above three types i.e. at least one of the harmonic component is significant but there is no other criterion to separate the days.

It is observed from the Fig. 3 *d*) that if all days with significant variation are considered, but no classification is undertaken, the average daily variations of ^{5}T and ^{26}T are not significantly different from each other. The amplitude of variation recorded by narrow angle telescopes ^{5}T is no greater than the amplitude from the wider angle telescopes ^{26}T. However, if we classify the variations into the « *d* », « *n* » and « *s* » types there is marked difference in the results from, ^{5}T and ^{6}T telescopes. The amplitude of the daily variation in narrow angle telescopes is much greater than in telescopes with wider angles. It has been pointed out by EHMERT [12] and by SARABHAI and NERURKAR [6] that the ratio of amplitudes of variations measured by narrow and wide angle telescopes is not constant. However, the average ratio of amplitudes of the diurnal components of ^{5}T and ^{26}T is 1.8 for the « *d* » type and 1.7 for the « *n* » type. The ratio of amplitudes for the semidiurnal components of narrow and wide angle telescopes is 2.9 for « *s* » type days. These ratios may be compared to the average ratios of 3.0, 2.0 and 1.0 reported by NERURKAR [13] for ^{5}T and ^{15}T telescopes for the period 1954÷55.

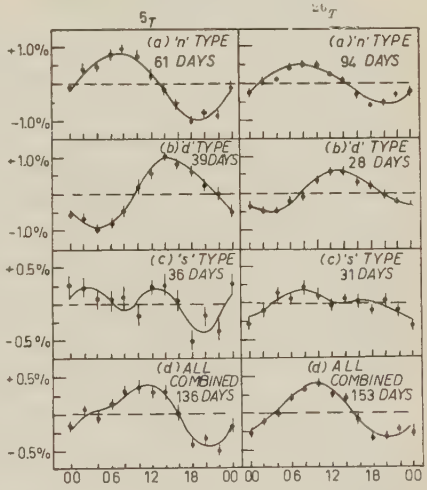

Fig. 3. – Average daily variation for « *n* », « *d* » and « *s* » type days for ^{5}T and ^{26}T telescopes and the average daily variation for all these types of days taken together.

By the side of the curves in Fig. 3 the number of days are indicated on which daily variations of significant amplitude of each type are observed by

^{5}T and ^{26}T telescopes during the period February 1956 to December 1956. Of the total number of days on which data are available, a significant daily variation is observed on 44.7% of days for ^{5}T and on 58.6% of days for ^{26}T. The « *n* » type of daily variation occurs most frequently. It accounts for 44.8% of the days of significant variation for ^{5}T and 61.4% for ^{26}T. The corresponding percentages for « *d* » type days are 28.7% and 18.3% respectively; while for « *s* » type days they are 26.5% and 20.3% respectively. The percentages given here do not indicate directly the relative frequency of occurrence of the daily variations of different types. This is because the amplitudes of « *n* », « *d* » and « *s* » type variations for the same telescopes are not equal, as can be seen from Fig. 3. The level of significance which establishes a lower limit of amplitude below which we disregard data for the purpose of classification, thus acts differentially in respect of the dsitribution of amplitude of each type of variation.

4 – Classification of days according to the character of the daily variation.

It has been demonstrated in the preceding section that there is a tendency for « *n* » and « *d* » type days records selected according to ^{5}T telescope to be respectively associated with earlier and later times of maxima of the diurnal component of ^{26}T telescopes. The validity of classification of days into « *n* » and « *d* » types is more clearly indicated in Fig. 4 where the time of maximum of the diurnal component of ^{5}T is plotted against the time of maximum of the diurnal component of ^{26}T on each day on which both the diurnal components are significant at their respective 2σ levels.

There are 49 such days, and it is clear that there is a remarkable association of the time of diurnal maxima recorded by the ^{5}T and ^{26}T telescopes. The correlation between the pairs of values in Fig. 4 relating to each day is $+0.86 \pm 0.04$. The regression lines indicate that narrow angle telescopes reveal larger changes than the wider angle telescopes, in confirmity with the observ-

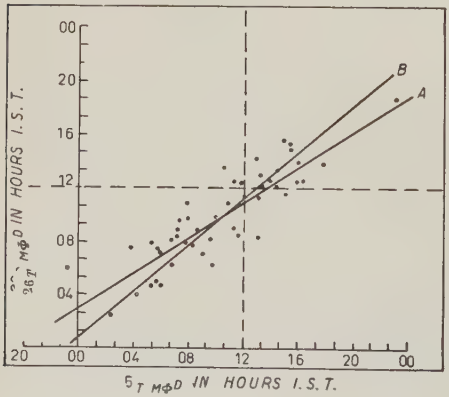

Fig. 4. – Diagram showing the relation between the times of maxima of the diurnal components of the daily variations measured on individual days by ^{5}T and ^{26}T telescopes. The line of regression *A* is of ^{26}T $M\Phi^{D}$ on ^{5}T $M\Phi^{D}$, and line *B* is of ^{5}T $M\Phi^{D}$ on ^{26}T $M\Phi^{D}$.

ation made by SARABHAI *et al.* [4] from a comparison of Huancayo ion chamber and Ahmedabad counter telescope data. The grouping of times of maxima around two epochs, one before noon and the other after noon, is clearly seen, as in the histograms of Fig. 1. The horizontal and vertical lines corresponding to noon indicate the boundary for the classification into « *n* » and « *d* » type days. There are only two points out of 49 where there is substantial disagreement between ^{5}T and ^{26}T telescopes in classifying according to « *n* » and « *d* » types. There are eleven days on which ^{5}T and ^{26}T telescopes simultaneously register significant « *s* » type daily variations. As against this, there are 20 days on which either ^{5}T or ^{26}T has a « *d* » or an « *n* » type variation, and the other has an « *s* » type variation. If we, therefore, consider all classifications, we have a total of 58 days on which both types of telescopes are in agreement. As against this, there are 22 cases of disagreement, most of them involving an « *s* » type classification. When one realises that a large semidiurnal component, significant at the 2σ level, can arise either as an adjunct to a main diurnal component, or by itself because the variation is truly semidiurnal in character, it is clear that the present system of classification into « *s* » type days requires further refinement.

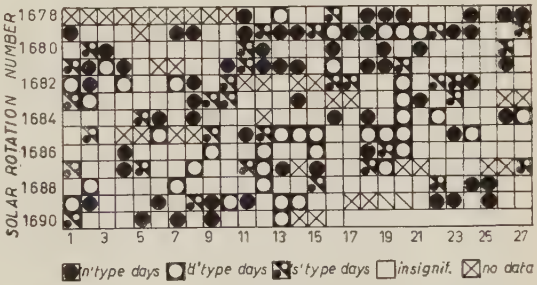

Fig. 5. – Bartel's diagram showing the dates of occurrence of « *n* », « *d* » and « *s* » type of daily variation. Days on which ^{5}T is inoperative are indicated as « no data » days.

In Fig. 5 we show on a Bartel's diagram, days classified as « *n* », « *d* » and « *s* » according to the daily variation recorded by ^{5}T telescopes. Also indicated on the diagram are those days on which no data are available for evaluating daily variation. It will be observed that there is a tendency for at least the « *n* » and « *d* » type days to occur in groups of 2 to 3 days. There is also evidence of a 27 day recurrence tendency, particularly for « *d* » type days.

5. – Correlated changes of anisotropy, mean intensity and C_p, the daily magnetic planetary character figure.

For studying correlated changes it is convenient to use the method of superposed epochs. We consider as an epoch each day when a particular type of daily variation occurs, and compute the average of daily mean intensity I and C_p on days of epoch as well as on 5 days on either side of epoch.

Such analysis is conducted separately for « *u* » type, « *d* » type and « *s* » type days indicated in the Bartel's diagram in Fig. 5.

In studying the correlated changes of the daily variation and of the daily mean intensity I, the latter is first corrected for the influence of change of daily mean barometric pressure using a coefficient $\alpha_B = -1.8\%$ per cm Hg, derived experimentally from the present data. The corrected daily mean intensity still exhibits changes of a long term character due to seasonal and other factors. The long term changes are next removed, without eliminating short time fluctuations of I over periods of 5 to 10 days, by taking moving averages of I over a period of 13 days and applying correction for the variation of the moving averages. In Fig. 6 *a*), *b*) and *c*) are indicated the values of I

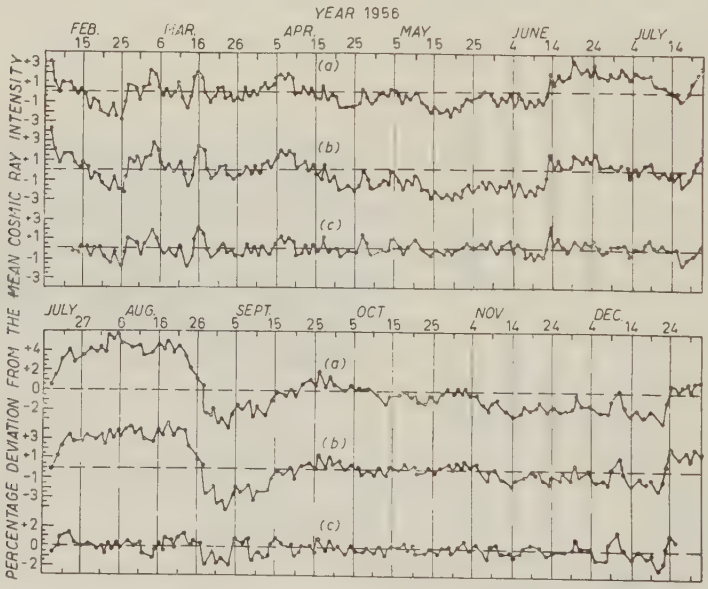

Fig. 6. – The day to day change of the daily mean intensity I of cosmic rays as observed by ^{5}T, (*a*) uncorrected intensity, (*b*) corrected for the day to day changes in barometric pressure, and (*c*) corrected for long term changes (see text).

before applying pressure correction, after applying pressure correction and after removing long period variations respectively. The latter values of I are used in the analysis of correlated changes.

The result of this analysis for the daily mean intensity measured by ^{5}T is shown separately in Fig. 7 *a*), *b*) and *c*) for « *u* », « *d* » and « *s* » type days respectively. The change of C_p in each case is also shown.

A remarkable result of this analysis is that « *u* » type days are accompanied by an increase of intensity of about $0.16 \pm 0.03\%$ from 3 days prior to epoch.

The intensity is normal on epoch, but decreases significantly after epoch to reach, 2 days later, a minimum value about (0.27 ± 0.03%) less than the average daily mean intensity for the entire period of observation. « *d* » type days on the other hand are associated with increase of mean intensity which remains about (0.17 ± 0.04%) above the average from epoch to +2 days. A slight decrease in intensity before epoch is not significant. For « *s* » type days, the mean intensity is nearly normal during the epoch period and on 3 days before and after it. For C_p, the values are high compared to the mean of the entire period, from −3 to +1 days of the « *n* » type epochs. For « *d* » type epochs this is also true for +1 and +2 days after the epoch day, but there is a C_p minimum in the interval 0 to −1 days before the epoch. For « *s* » type epochs, C_p values show a minimum near about the epoch day and an increase 4 days after the epoch.

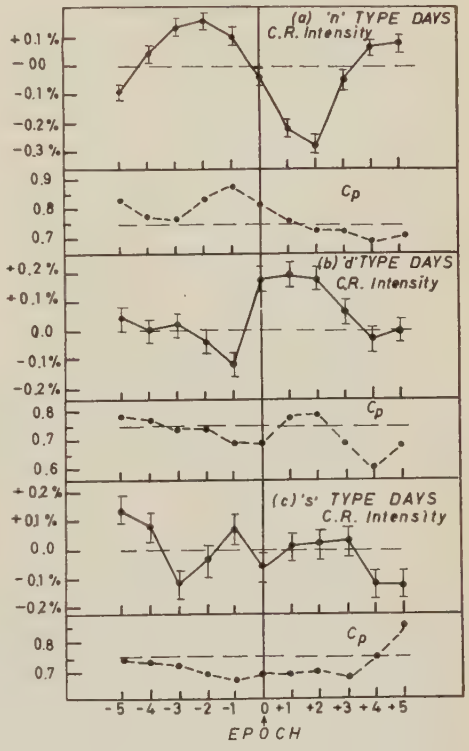

Fig. 7. – Average daily mean cosmic ray intensity changes on −5 to +5 days, (*a*) for « *n* » type days as epochs, (*b*) for « *d* » type days as epochs and (*c*) for « s » type days as epochs. The corresponding average change of magnetic character figure C_p in each case, is also shown.

6. – Discussion.

The results presented here are of a preliminary character and indicate certain tentative conclusion which can be drawn from the analysis of data from narrow angle telescopes operated over a period of 11 months in 1956.

It is seen that on a majority of days, which have a daily variation of significant amplitude, the variation can be designated as belonging to the « *n* », the « *d* » or the « *s* » type. The experimental technique at present does not permit a variation to be established at the 2σ level of significance unless it has a harmonic component of amplitude greater than 0.74% for ^{5}T and 0.34% for ^{26}T telescopes. With an improvement of technique involving a larger ef-

fective aperture of narrow angle telescopes than at present, it would be possible to extend the study to variations of smaller amplitude than is now possible. It is not known what characteristics would be shown by the daily variations of small amplitude.

The difference between « *d* » and « *n* » types of variations is more marked for narrow angle telescopes than for wide angle instruments. Thus in deriving an average of the daily variation over an extended period of days, the reduction of amplitude for ^{5}T is much greater than for ^{26}T. If we wish to compare the amplitudes of daily variations recorded by narrow and wide angle telescopes, the comparison should be made separately for each type of variation and not for an average variation having a combination of all types of variations. This point requires to be borne in mind when considering the results of other workers who have compared the amplitudes of the daily variations of narrow and wide angle telescopes without attempting to classify the different types of variations.

The shift towards later hours, by about four hours, from 1954 to 1956, of the time of maximum of « *n* » as well as of « *d* » type of variations seems to indicate that the striking changes observed in the 12 month mean daily variation can be due not only to the change of frequency of occurrence of days of each type, but to an intrinsic shift of time of maximum and of the anisotropy. Close study over an extended period with narrow angle telescopes is required to understand better the nature of the changes that occur.

The classification of days according to the character of the observed daily variation requires to be further refined so that when the classification is made, it relates to a characteristic of the anisotropy, and is therefore detectable on a global basis. In the present study the validity of the characterisation is tested only by comparison made of two types of telescopes operating at one station. It is important to extend this comparison to other instruments at the same station and at different stations.

One of the most important conclusions that can tentatively be drawn from the present study is the one concerning correlated day to day changes of anisotropy and the daily mean intensity. The main weakness in the evidence that is presented lies in the absence of upper air meteorological data with which the daily mean intensity could properly be reduced to standard atmospheric conditions. We have been unable to evaluate the extent of error which can be introduced on this account in our analysis. At low latitudes however, day to day changes are not as important as at high latitudes, and it is believed therefore that a more accurate correction for meteorological changes than we have been able to apply to our values of daily mean intensity, would not alter our conclusions substantially.

The observation that « *n* » type days are associated with decreases of intensity and « *d* » type days with increases of daily mean intensity after the

respective epochs is one of great significance in the interpretation of processes responsible for the anisotropy and changes of cosmic ray intensity. An increase of intensity can result either by the presence of a source of cosmic rays within the solar system, or what is more likely, by a modulation process involving the increase of energy of cosmic rays incident from certain directions. In the latter case one would require the creation of an ordered electric field in appropriate regions of interplanetary space as viewed from the earth. Since the space is believed to be often filled with clouds of ionized solar matter, it would be difficult to sustain the field in the absence of trapped coherent magnetic fields within the ionized streams.

The present evidence, along with that of SIMPSON *et al.* [14], are the only ones in support of the existence of variations of intensity which represent not just decreases, as shown by HEERDAN and THAMBYAHPILLAI [15], but increases of intensity as well. Since, as discussed above, they are indicative of the existence of coherent magnetic fields and not just turbulent fields in interplanetary space, it is of great importance to confirm experimentally these findings with a large number of independent investigations extending over a long period of time. Our present study relates to only 11 months of observations and it is therefore necessary to take the present conclusions as tentative for the time being.

* * *

We are grateful to Dr. N. W. NERURKAR and to Dr. R. P. KANE for many helpful suggestions and discussions. Mr. VISWANATHAN and Mr. THAKORE have rendered very valuable computational assistance. We are indebted to the Department of Atomic Energy of the Government of India for generous assistance.

REFERENCES

[1] V. SARABHAI and R. P. KANE: *Phys. Rev.*, **90**, 204 (1953).
[2] T. THAMBYAHPILLAI and H. ELLIOT: *Nature*, **171**, 918 (1953).
[3] V. SARABHAI, U. D. DESAI and D. VENKATESAN: *Phys. Rev.*, **96**, 469 (1954).
[4] V. SARABHAI, U. D. DESAI and D. VENKATESAN: *Phys. Rev.*, **99**, 1490 (1955).
[5] J. W. FIROR, W. H. FONGER and J. A. SIMPSON: *Phys. Rev.*, **94**, 1031 (1954).
[6] V. SARABHAI and N. W. NERURKAR: *Proc. of the Guanajuato Conf.* (1955), in press.
[7] E. REMY and A. SITTKUS: *Zeits. f. Naturf.*, **10***a*, 172 (1955); **11***a*, 556 (1956).

[8] V. Sarabhai, N. W. Nerurkar, S. P. Duggal and T. S. G. Sastry: *Proceedings of a Symposium on Electromagnetic Phenomena in Cosmical Physics*, Stockholm, (1956) in press.
[9] E. Å. Brunberg and A. Dattner: *Tellus*, **6**, 254 (1954).
[10] H. Alfvén: *Tellus*, **6**, 232 (1954).
[11] N. W. Nerurkar: *Proc. Ind. Acad. Sci.*, A **45**, 341 (1957).
[12] A. Ehmert: *Zeits. f. Naturf.*, **6***a*, 622 (1951).
[13] N. W. Nerurkar: *Doctoral Thesis*, Gujarat University (unpublished).
[14] J. A. Simpson, W. H. Fonger and L. Wilcox: *Phys. Rev.*, **85**, 366 (1952); J. A. Simpson, H. W. Babcock and H. D. Babcock: *Phys. Rev.*, **98**, 1402 (1955).
[15] I. J. Van Heerden and T. Thambyahpillai: *Phil. Mag.*, **46**, 1238 (1955).
[16] V. Sarabhai, U. D. Desai and R. P. Kane: *Proc. Ind. Acad. Sci.*, A **38**, 327 (1953).

SUPPLEMENTO AL VOLUME VIII, SERIE X
DEL NUOVO CIMENTO

N. 2, 1958
2° Trimestre

Solar Daily Cosmic Ray Variations Observed with Meson Telescopes at High Southern Latitudes.

N. R. Parsons and A. G. Fenton

Physics Department, University of Tasmania - Hobart

Solar daily variations in meson intensity have been recorded at Hobart, Tasmania ($\lambda = 52°$ S) and at the Australian National Antarctic Research Expedition's station at Mawson, Antarctica ($\lambda = 73°$ S). The telescope geometry used in all measurements reported here was (1 m × 1 m) × 1.5 m, with 10 cm of lead absorber.

The brief discussion below will cover two aspects of the records:

1) A comparison of the phase of the daily variation recorded by vertical telescopes at Hobart and Mawson and a comparison of long term phase changes at Hobart, Mawson and some northern stations.

2) A comparison of the daily variations recorded simultaneously at Mawson by telescopes directed vertically, 45° N, 45° E, 45° S and 45° W of the zenith respectively.

1. – Vertical telescope measurements at Hobart and Mawson.

Fig. 1 shows the manner in which the bimonthly mean amplitudes and times of maximum of the pressure-corrected 24 hour component vary for vertically-directed telescopes at Hobart and Mawson. The figure also shows the phase changes reported from some northern stations. The long-term phase changes are broadly similar, confirming the world-wide nature of this phenomenon.

There is a consistent phase lag in local time of 3 to 4 hours at Mawson relative to Hobart. This is also evident in the 12 hour component, and it is found very difficult to explain this in terms of residual atmospheric influences. An explanation has been sought in terms of a primary particle anisotropy

outside the earth's field region and the different deflections suffered by particles arriving at the two stations. The usual dipole field configuration has been assumed and use made of the trajectory data of BRUNBERG and DATTNER [1].

Accurate values of the expected phase difference in solar time at the two stations have been calculated for several assumed values of the mean energy of the anisotropic primaries in the range 1.5 to $5.0 \cdot 10^{10}$ eV. (There is much evidence suggesting that the mean energy of the anisotropy, if it exists, lies within this range). It is found that the maximum phase lag at Mawson which can be accounted for in this way is about 1 hour (for mean energies near the bottom of the range).

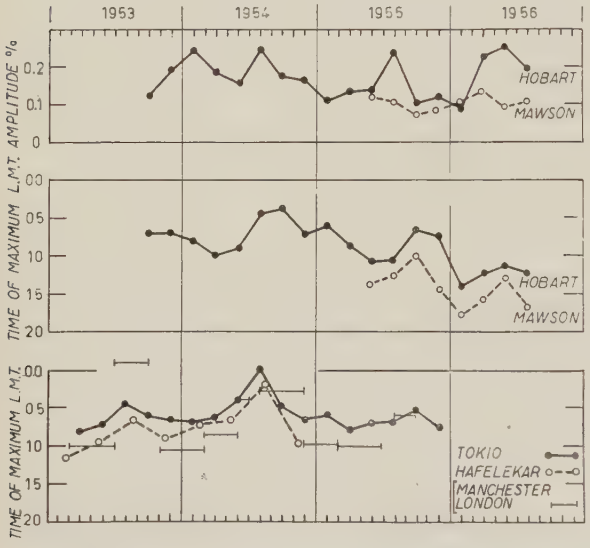

Fig. 1. – The 24 hour component of the daily variation of vertical meson intensity, showing changes in amplitude and phase at Hobart and Mawson, and changes in phase observed at northern stations.

In view of recent evidence that the effective field of the earth may be more adequately described by a 45° westward rotation of the inclined dipole, the expected phase differences have been recalculated using the appropriate modified system of geomagnetic co-ordinates in which Hobart is effectively 9° further north and Mawson 5° further south. It is found that the expected phase differences for particular energies are substantially increased, but that only for primary particle energies up to $2.0 \cdot 10^{10}$ eV is the predicted phase difference approximately 3 hours, close to the observed value.

We conclude then that the results are not consistent with an explanation of the daily variation in terms of an external anisotropy and its interaction with a « normal » dipole field, but that they could be consistent with this interpretation if the field has the suggested modified orientation and if the mean energy of the primary particles involved is close to $1.5 \cdot 10^{10}$ eV.

In a recent paper, ELLIOT and ROTHWELL [2] suggested that the whole of the daily variations probably arise from some modulation mechanism operating within the region occupied by the earth's field. If this is so, it is possible that times of maximum may be related basically to the local geomagnetic

time scale and not to solar time. This alone could explain a mean phase lag of about $2\frac{1}{2}$ hours in solar time at Mawson relative to Hobart—nearly that observed. Such a dependence on local geomagnetic time offers an alternative explanation of the observed results, and if it could be substantiated, it would be very difficult to avoid the conclusion of ELLIOT and ROTHWELL that the daily variations do indeed originate locally within the field region.

2. – Directional telescope measurements at Mawson.

Fig. 2 shows the mean solar daily variations recorded at Mawson over the 10 months period May 1955-February 1956 in each of five different telescope headings, namely vertical, and at an inclination of 45° to the north, east, south and west. There are significant differences in both phase and amplitude, whilst the most striking feature is the absence of any significant diurnal variation in the south direction.

If these results are to be explained in terms of an anisotropic distribution of primary particles outside the earth's field region, then we should be able to determine an initial direction of approach of the excess radiation and a mean energy for the particles involved which together would be simultaneously consistent with all the observed directional daily variations.

In examining the plausibility of this interpretation we have considered both the « normal » and modified dipole field orientations mentioned in Sect. 1 above.

For a chosen primary particle energy and direction of arrival at Mawson, we may find a fixed point P on the earth's surface through which the earth's radius is parallel to the initial direction of approach of the particles. Thus it can be shown that each telescope at Mawson effectively scans a different celestial latitude belt as the earth rotates and that if the daily variations are due to an anisotropy outside the field region, then we would expect the order of occurrence of observed maxima and the observed phase differences to be

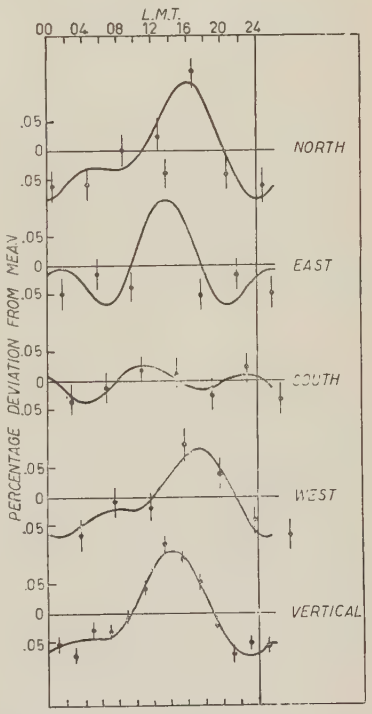

Fig. 2. – The solar daily variations in meson intensity observed with directional telescopes at Mawson, averaged over the period May 1955 to February 1956. Standard errors are indicated with the observational points.

predicted by the geographic longitude differences between the points P appropriate to each directional telescope.

For the « normal » dipole orientation, Fig. 3 A) shows schematically the geographic latitudes of the points P, and thus the celestial latitudes scanned by the telescopes for three different values of primary particle energy. Fig. 3 B) shows the positions in geographic longitude of the points, again for three values of primary particle energy.

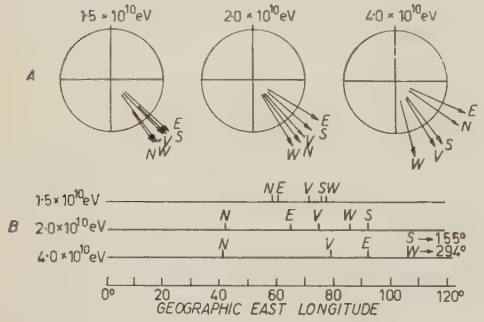

Fig. 3. – A) Schematic representation of the geographic south latitudes of the points P (refer text) appropriate to each direction of particle arrival at Mawson, and to three values of primary particle energy. The diagram indicates the celestial latitudes scanned by the directional telescopes. B) Schematic representation of the geographic east longitudes of the points P. The expected order of occurrence of maxima in the daily variations is that of decreasing east longitude, with phase differences as indicated.

Fig. 4 contains the results of similar calculations, but assuming the dipole field to be rotated westward through 45° as discussed in Sect. **1**.

Examination of these two diagrams shows clearly that for both field orientations and for the range of energies considered the south-pointing telescope in all cases scans a south celestial latitude belt close to and intermediate between those scanned by the other telescopes. In most cases the vertical and south-pointing telescopes scan very close belts. It is therefore very difficult to explain the virtual absence of a diurnal variation in the south-pointing telescope, when all the others show substantial and broadly similar variations. Further the order of occurrence of maxima and phase differences predicted by Fig. 3 B) and 4 B) in no case bear any similarity with those actually observed (Fig. 2).

It is clear then that the observed directional daily variations cannot be satisfactorily explained on the assumption of an external anisotropy interacting with a dipole field.

Further consideration of the evidence suggests strongly that

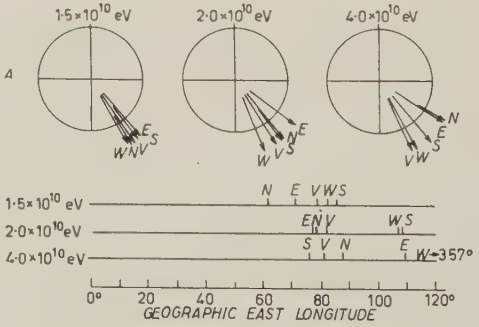

Fig. 4. – A) and B), as in Fig. 3, but calculated by assuming a 45° westward rotation of the inclined dipole field.

the assumption of a simple dipole field configuration may be incorrect, and that use of trajectory data calculated on this assumption could be seriously misleading.

To explain the results we need either external anisotropies interacting with a suitably distorted field, or, if this is not the case, we must conclude, with ELLIOT and ROTHWELL, that the daily variations are probably produced locally by intensity-modulating mechanisms operating within the region occupied by the earth's field.

More detailed accounts of this work have been submitted for publication n the *Australian Journal of Physics*.

REFERENCES

[1] E. Å. BRUNBERG and A. DATTNER: *Tellus*, **5**, 135, 269 (1953).
[2] H. ELLIOT and P. ROTHWELL: *Phil. Mag.*, (8), **1**, 669 (1956).

SUPPLEMENTO AL VOLUME VIII, SERIE X
DEL NUOVO CIMENTO

N. 2, 1958
2° Trimestre

Variations of Nuclear and Mesonic Component.

A. EHMERT

Max Planck-Institut für Physik der Stratosphäre - Weissenau

Since May 1956 we recorded in Weissenau (420 m above sea level, geographic co-ordinates: 47°.8 N, 9°.5 E; geomagnetic co-ordinates: 49° N, 91°.5 E) with six telescopes:

2 cubical telescopes with 10 cm lead between the counter trays
each giving 55 000 coincidences per 2 hours = $\overline{K}_{10}$

2 cubical telescopes without lead
each giving 68 000 coincidences per 2 hours = $\overline{K}_0$

2 twofold telescopes with wide angle
each giving 182 000 coincidences per 2 hours = $\overline{K}_{2f}$

The latter ones form a part of the other telescopes. Fig. 1 shows the arrangement. Recorded are coincidences of the trays,

1-2-3 , 2-3-4 , 2-3 , – – , 5-6-7 , 6-7-8 , 6-7 .

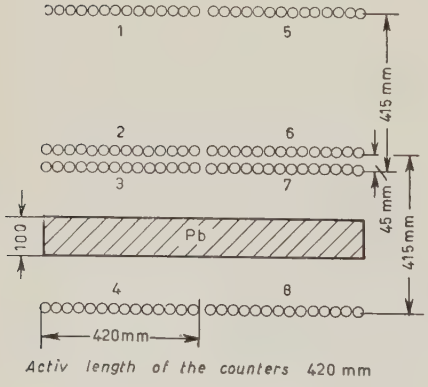

Since October 1956 in the same room a neutron monitor with 12 counters is operated with geometrical arrangement

Fig. 1. – The arrangement of the Geiger counters. All counters of one tray (1, 2, 3 etc., are connected in parallel) coincidences are recorded: 1-2-3 and 5-6-7 = cubical telescope without lead K_0; 2-3-4 and 6-7-8 = cubical telescope with 10 cm lead K_{10}; 2-3 and 6-7 = wide angle telescope K_2 .

according to SIMPSON's proposal [1] (*). Two separate electronic equipments are used. Each records the neutron captures in 6 counters. Each half gives 2800 counts per 2 hours $= \overline{N}$.

Coefficients of air pressure are evaluated to be

$$(1)\quad \begin{cases} \dfrac{\Delta K_{10}}{\Delta K_{10}\cdot\Delta P} = -\dfrac{0.0255}{\text{cm Hg}}, & \dfrac{\Delta K_{0}}{\Delta K_{0}\cdot\Delta P} = -\dfrac{0.0295}{\text{cm Hg}}, \\ \dfrac{\Delta K_{2}}{K_{2f}\cdot\Delta P} = -\dfrac{0.0276}{\text{cm Hg}}, & \dfrac{\Delta N}{N\cdot\Delta P} = -\dfrac{0.1035}{\text{cm Hg}}. \end{cases}$$

Evaluation of air temperature coefficients from meson records alone is commonly seriously troubled by variations of magnetic origin.

As the neutron number is free from influences on μ-meson decay we tried to introduce it as a correction for the meson number to find better correlation with atmospheric temperature influence. But the found coefficients change from month to month and this indicates a systematic further influence. To describe this influence is one purpose of this paper. For briefness we restrict here for the details on the wide angle telescope without lead, having a greater influence of μ-meson decay than the cubic telescopes.

The anomalous interdiurnal variations (2) during times of constant atmospheric temperature provide a distinct regression between the variations of the neutron number and that of the coincidence numbers of the different telescopes.

Plotting the *air pressure corrected* values K_{2f}, K_0, K_{10} against N we found that all three regression lines cut at the same value $\overline{N}$ of N. We call the corresponding values $\overline{K}_{2f}$, $\overline{K}_0$ and $\overline{K}_{10}$. They are given above for 9.25 km height of the 300 mb level and for 72 cm Hg air pressure. According to this fact we introduce

$$(2)\quad \begin{cases} K'_{10} = \dfrac{1}{1.82}\dfrac{(K_{10}-\overline{K}_{10})}{\overline{K}_{10}}, & K'_{0} = \dfrac{1}{1.47}\dfrac{(K_{0}-\overline{K}_{0})}{\overline{K}_{0}}, \\ K'_{2f} = \dfrac{1}{1.10}\dfrac{(K_{2f}-\overline{K}_{2f})}{\overline{K}_{2}}, & N' = \dfrac{1}{3.57}\dfrac{(N-\overline{N})}{\overline{N}}, \end{cases}$$

giving the same scale for 1.82% of K_{10}, 1.47% of K_0, 1.10% of K_{2f} and 3.57% of N and get nearly identical interdiurnal variation curves for K'_{10}, K'_0, K'_{2f} and N'

(*) The author is indebted to his colleague DR. G. PFOTZER for lending his unpublished corrected neutron records for this comparison.

in some cases or with constant differences (related to atmospheric temperature) in others. Fig. 2 gives an example for 12/13.3.57.

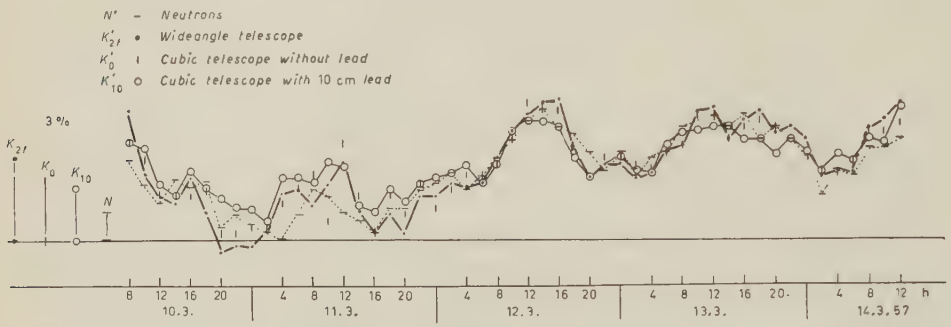
N' – Neutrons
K'2f • Wideangle telescope
K'0 I Cubic telescope without lead
K'10 O Cubic telescope with 10 cm lead
3 %
K2f
K0
K10
N
8 12 16 20 4 8 12 16 20 4 8 12 16 20 4 8 12 16 20 4 8 12 h
10.3. 11.3. 12.3. 13.3. 14.3.57

Fig. 2. – Variations of neutrons and of the different coincidence numbers. The different scale values are given on the left side.

The corresponding scale values for K_{2f}, K_0, K_{10} and N are given on the left side in Fig. 2.

For monthly averages (without December 1956) the same relation was found.

So it was hopeful to use this relation to calculate the expected variations of meson numbers for constant atmospheric conditions from the variation of neutron numbers and to compare the difference against the real meson number with the atmospheric data.

As there are no more sounding ascents near Weissenau, we used the height of 300 mb level as given by the weather chart for 2^{00} GMT and used only the records from 0^{00} till 4^{00} GMT every day for the comparison.

In Fig. 3 these dayly night values of the neutrons N' = (open circles) and of the wide angle coincidences $= K'_{2f}$ ($= M'$ = full circles) are plotted. The given scale values correspond to relation (2). It is immediately seen that during the first half of October, in the midth of November 1956 and during parts of March and April 1957 the relation holds fairly well.

The differences between the two upper curves of Fig. 3 are plotted below as open circles ($N' - M'$) together with the height of 300 mb level. The scale is adjusted to best correlation with a coefficient:

$$\frac{\Delta K_{2f}}{K_{2f} \cdot \Delta H_{300}} = -\frac{2.2\%}{km} \tag{3}$$

corresponding ln 0.08% per °C for even change in all heights.

The difference of the circles against this curve is once more given as $(N' - M')_{corr}$. The variations of this curve show that relation (2) did not hold

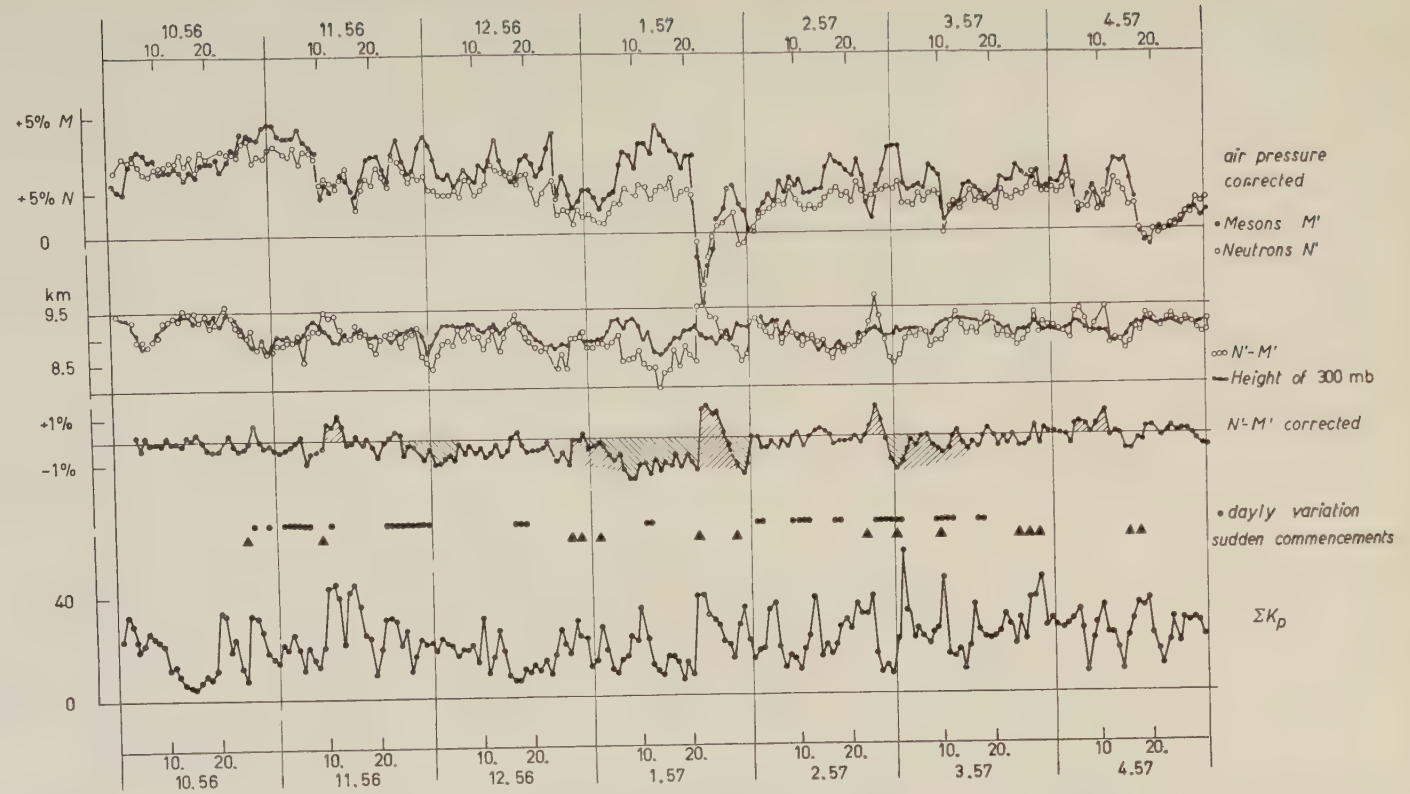

Fig. 3. – Variations of the dayly night values 0^{00}–4^{00} GMT. *Upper curves*: meson number and neutron number corrected for fix air pressure. *Second curves*: the difference of the two upper curves N'— M' and the height of 300 mb level at these times. *Third curve*: the difference of the two second curves, it gives the difference of neutron variation and corrected meson variation. *Follows*: indication of days with abnormal dayly variation and sudden commencements of magnetic disturbances. *Lowest curve*: dayly sums of threehourly K_p indices as indication of magnetic situation.

for all the time. But there is no further relation to weather in this curve. Especially no correlation to high-level or tropospheric temperature.

During the magnetic storm effect from January 21 to 26 the deficit in mesons was higher than that expected from relation (2) and the neutron deficit, though the percent deficit in neutrons is larger than the percent deficit in mesons: $\Delta M/M < \Delta N/N$, $\Delta M' > \Delta N'$.

Severe magnetic storms affect higher primary energies than the other modulation effects [2].

A similar effect is seen at the smaller storm effects of November 10, February 25, April 6, but not at April 13.

The times of sudden commencement are signed in Fig. 3. They show a narrow connection of these events with the start of deviations of $(N' - M')_{corr}$ from normal values. The final curve in Fig. 3 shows the dayly sums of the 3-hour-range-magnetic indices [3], giving a logarithmic mass of the field variations by the impact of solar corpuscular radiation on the earth. This is a measure for solar clouds in the near of the earth, but no direct measure for their action on cosmic rays.

We regret not yet to be able to compare magnetic ring current fields. The material of equatorial magnetic stations is not yet available.

The most surprising fact is the deficit of the corrected values of $(N' - M')$ in January before the magnetic storm and a similar smaller effect at the end of November and beginning of December 1956 and on 1-st March. As the highest amount is only 1.5% of K_{2f}, at first we suspected an experimental error, as possible by a change of sensitivity of the telescopes. But this proved to be improbable as all records show this effect in an amount corresponding to the general relations between the corrected results of these records. Examining the variations of N' and $K'_{2f\,corr.}$ one can see, that in all these cases meson intensity was recovered to a higher extent than neutron intensity. But a further more general aspect is found:

A plot of all values of K'_{2f} (after correction for the same height of the 300 mb of 9.25 km and for 72 cm Hg air pressure) against N' (that is corrected for 72 cm Hg) is given in Fig. 4 and 5 and a separation into several sections of time is introduced in the following manner:

		K'_{2f}/N	$\frac{\Delta K_2 \cdot N}{\Delta N \cdot K_{2f}}$
1.10.56 – 15.11.56 full dots	Fig. 5	1.30	0.40
17.11.56 – 24.12.56 circles	Fig. 5	1.45	0.90
26.12.56 – 22. 3.57 full dots	Fig. 4	2.10	0.66
23. 2.57 – 2. 3.57 circles	Fig. 4	1.45	0.90
12. 4.57 – 26. 4.57 crosses	Fig. 5	1.45	0.90

It is seen, that there exist distinct regression lines. The coefficients are given in the table as well for K'_f/N' as for the relation of the percentual variations.

During the magnetic storm of January 23/24 K'_{2f}/N' passes over from 2.1 to 1.45 and falls then back to the prestorm value.

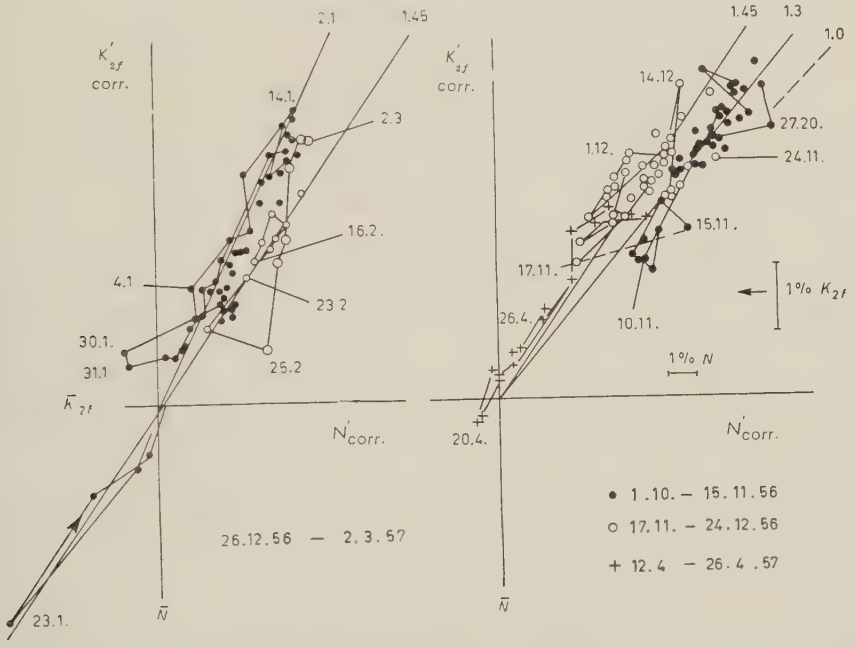

Fig. 4 and 5. – The fully corrected coincidence numbers of the wide angle telescope are plotted against the corrected neutron number to show variation of the relation.

The distortion of mesons at February 25/26 is unic as there is no change of the neutron number. It is restricted to 10 hours and is common to all our meson records.

At least three of the well distinguished regression-lines in Fig. 4 and 5 cut the point $N' = 0$, $K'_{2f} = 0$ as also does the line for anomalous interdiurnal variations, that were used above to define $\overline{N}$ and $\overline{K}_{2f}$, corresponding to $N' = 0$ and $K'_{2f} = 0$. The further distinction of this point for this long period variations is not induced by the procedure. It was expected, that for the regression lines in Fig. 4 and 5 different intersection points might result so far, as regression lines are defined. But the result shows a distinction of the same point for different times. The same holds also (what is not shown here) for $\overline{K}_0$ and $\overline{K}_{10}$.

(Only the distortion of February 25 to 28 does not fit, being obviously of a different nature).

A very similar result we had found [4] at earlier comparisons of our coincidence record with that of the ionization record of SITTKUS [5] from July to October 1951. The intersection point of the regression lines for different times was 2% below the mean of the coincidence number, as the new point does for K_{2f}.

As for the same time in 1951 FONGER [6] had found a very good correlation between this ionization and the neutrons, recorded by SIMPSON, FONGER and WILCOX [7] with 5-fold percentage variation of the neutrons, we can say, that in this time (1951) the percentage variations of our coincidence were between 1/5, 1/2.5 fold that of the neutrons, whilst we found today for the K_{2f} 1/2.5 to 1/1.1 and for the cubical telescope 1/3.3 to 1/1.5. This telescope is more similar to that which we formerly used. So we find a direct confirmation of these earlier results.

The percentage variations get the smaller, the more particles from high zenit angles are recorded. The absolute number of the particles forming the same variation of K_0' and K_{2f}' is for the twofold coincidence arrangement twice that of the cubical arrangement. This shows with respect to geometry, that particles with zenith angle up to at least 40° are involved. It is surprising that the corrected ionization chamber records of SITTKUS, in August and September 1951 resemble in their general trend more the Chicago neutron records than our coincidence record though showing all characteristics of our record. This may indicate a variation of the ionization by nuclear particles that is slightly higher than the variation of ionization by μ-meson variation.

$\overline{K}$,$\overline{K}_{2f}$ (also $\overline{K}_0$ and $\overline{K}_{10}$) are natural normalization values and it is useful to publish the corrected values in percent of them. They depend on the chosen standard air pressure and the meson values also on standard atmospheric height. Their dependence on latitude and height of the station is not yet known.

The variation of the steepness $\Delta K_{2f}'/\Delta N'$ means probably a greater or lesser suppression of primary low energy particles. The higher $\Delta K_{2f}'/\Delta N'$, the higher is the extent of this suppression which may be due to very extended magnetic clouds.

The variation within the periods of constant $\Delta K'/\Delta N'$ show the nature of magnetic storm effects [8] as is seen evidently once more from $N' - M_{\text{corr.}}$ in Fig. 3, Fig. 4 and Fig. 5 show that these variations do not change the steepness $\Delta K_{2f}'/\Delta N'$ at least so far as intensities do not get lower than $\overline{K}_{2f}$ and $\overline{N}$. We think that is an indication, that these magnetic storm effect affects all energies like any shadow effect. The same conclusion was drawn by us from the fact, that severe magnetic storms like those of July 27, 1946 or March 1, 1942, are composed of two different effects. The one of them beeing narrowly correlated to the magnetic « ring current field » as measured at equatorial stations [9] and having the same percentual effect on particle numbers in tele-

scopes and on ionization in chambers ad Godhavn, Cheltenham and Huancayo. That is not possible with a strong energy dependent selection of the effect.

For the main phase of the storm there exists a further decrease-effect, that is much more pronounced in telescope measurements and at mountain stations. This indicates a stronger energy dependence of this effect. that ended in all cases very abruptly after half a day or more.

In FORBUSH's records in Cheltenham on March 1, 1942, this part of the storm effect reached $\sim 3\%$, on our coincidence record in Friedrichshafen $\sim 8\%$ at this date. On January 21, 1957, the effect in our K_2, number reached 6.3% in our K_0 (cubus) 8.5%, that in the ionization in Kühlungsborn [10] reached 3.3%. That is quite the same relation. We see from this, that the same energy region is affected as in the main phase effect in severe storms.

The more it is interesting, that even in this case of energy dependent influence we deal often with an energy dependence that is not induced by the storm itself but was ruling in the prestorm time with recovering intensity. Probably it is determined by conditions in a space much larger than that occupied by the cloud causing the magnetic storm and affecting cosmic rays. The detection of this effect from neutron- or meson-records alone seems impossible.

* * *

The author is indebted to the Deutsche Forschungsgemeinschaft for financial help that enabled the different records.

REFERENCES

[1] J. A. SIMPSON: *Cosmic Ray Studies*. The Institute for Nuclear Studies, The University of Chicago, March 1953.
[2] A. EHMERT and A. SITTKUS: *Zeits. f. Naturf.*, **6***a*, 618 (1951); A. EHMERT: *Zeits. f. Naturf.*, **6***a*, 625 (1951).
[3] J. BARTELS: *Geophysikalisches Institut der Universität Göttingen*, monthly issue.
[4] A. EHMERT: *Bagnères Conference*, 1953, *Recueil des Travaux du Laboratoire du Pic du Midi, Rayonnement Cosmique*, p. 15 (1953).
[5] A. SITTKUS: *Sonnenzirkular* of the Fraunhofer-Institut at Freiburg.
[6] W. H. FONGER: *Cosmic Ray Studies*. The Institute for Nuclear Studies, The University of Chicago, March 1953.
[7] J. A. SIMPSON, W. FONGER and L. WILCOX: *Phys. Rev.*, **85**, 366 (1952).
[8] A. EHMERT: *Guanajuato Conference*, 1955.
[9] A. EHMERT: *Die Naturwissenschaften*, **41**, 317 (1954).
[10] E. A. LAUTER: *Geophysikalische Meßreihen des Observatoriums Kühlungsborn*.

SUPPLEMENTO AL VOLUME VIII, SERIE X
DEL NUOVO CIMENTO

N. 2, 1958
2° Trimestre

Observation of Cosmic Ray Decreases at the Pole (*).

S. F. SINGER

University of Maryland-College Park, Maryland

1. – Introduction.

The world-wide decreases of cosmic ray intensity at sea level which were first described by FORBUSH [1] are quite striking and in some cases as large as 10%. While they are often associated with magnetic storms there are examples where the decreases occur without magnetic storms and conversely, magnetic storms occur without cosmic ray decreases (for a recent review see [2, 3]). This suggests that the connection between magnetic storms and Forbush type decreases is not an immediate one but goes back to a common cause, presumably the emission of corpuscular matter from the sun.

On the other hand there are smaller cosmic ray variations associated with small magnetic disturbances which have a recurrence of about 27 days, the solar rotation period. They are generally considered as distinct from the Forbush decreases, but as will be shown in this paper they are probably different only n d egree.

2. – Observations.

Fig. 1 shows the intensity of the cosmic radiation at four stations during the period May and June of 1951. All data are corrected for barometric pressure. Observations were made during the same period by many other groups who find similar variations. For the purpose of the present discussion the data

---

(*) Presented at the American Physical Society Meeting, Washington, 1954, (*Phys. Rev.*, **95**, 647 (1954)) and at the Cosmic Ray Congress, Guanajuato, Mexico in September 1955 (unpublished). This work has been supported in part by the Air Force Office of Scientific Research under Contract AF No. 18(600)-1038.

in Fig. 1 will be sufficient to establish the world-wide character of the variations.

Our measurements at the polar station were obtained by means of a vertical Geiger counter telescope. These represent the first measurements of cosmic storm decreases at the geomagnetic pole.

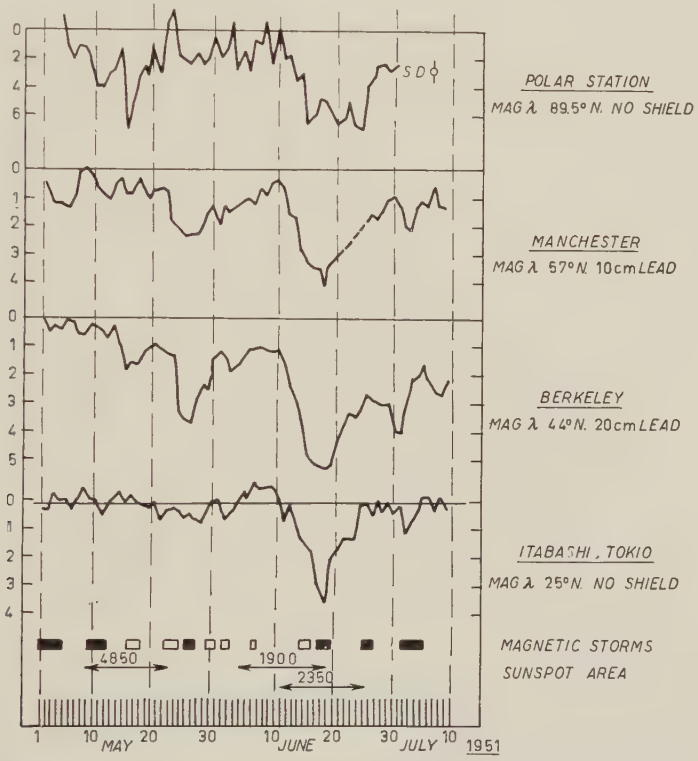

Fig. 1. – Forbush decreases during May-July, 1951 (Note that polar station variations are drawn to half-scale).

The cosmic ray telescope was operated at the Danish-American weather station at Thule, Greenland from August 1950 to July 1951. The telescope was completely unshielded; the total thickness of material including counter walls was 3.5 g/cm². The light roof overhead had a thickness of about 0.5 g/cm². The telescope was originally used and brought up to Greenland to serve as a calibration device for small balloon-borne telescopes and then left in Thule in August 1950. The telescope consisted of three counter trays, each of effective area 6×6 inches. The vertical separation between the two extreme trays was 16 inches, the third tray was in the center position. The number of triple coincidences and the barometric pressure were recorded every hour; the rate was about 1000 per hour.

3. – Relation to ring current.

These observations present further evidence of the fact that the Forbush decreases cannot be caused by the Störmer ring current flowing around the earth's equator. This ring current has been hypothesized to explain the magnetic storms and is assumed to flow several earth radii out. However, it has already been pointed out by T. H JOHNSON [4], and later by HAYAKAWA *et al.* [5] and TREIMAN [6], that the ring current cannot very well account for the decreases observed at medium latitudes and the equator, and could in fact lead to increases depending on its position. It is clear that the vertical intensity at the pole cannot be influenced by a ring current, or in fact by any change of the earth's dipole field, since vertically incident cosmic ray particles at the pole are not affected by the earth's field. It seems reasonable therefore to assume that the simultaneous decreases at the other latitudes are not due to ring currents either. This does not exclude the existence of a ring current [7]; rather the evidence suggests that the ring current which produces the magnetic storm and the agency which produces the cosmic ray storm are both a *consequence* of a common primary effect. This common primary effect is certainly of solar origin and has been identified by ALFVÉN [8] with a corpuscular beam or the emission from the sun of clouds of ionized gas. It is interesting to note that the decreases at the pole cannot be explained either by an electric polarization due to a ring current. The effect, as has been pointed out by NAGASHIMA [9] who has discussed it in detail, is still too small to account for the observed decreases.

4. – Relation to magnetic storms

We now wish to interpret in detail some of the features of the observed decreases: (i) their recurrence, (ii) their widening and variation of onset time, (iii) the larger size of the polar decreases. It has been stated in the literature that the relation between cosmic storms and magnetic storms is an occasional one, in the sense that sometimes magnetic storms and cosmic storms parallel each other very closely, sometimes we have magnetic storms without cosmic storms, and sometimes cosmic storms without magnetic storms. Attempts have been made to account for these phenomena on the basis of different mechanisms on the sun for producing associated events and separate events. For example, SEKIDO *et al* [10] have introduced a classification of *S* and *M*-type of storms depending on whether they accompany the decrease in cosmic ray intensity or not; he has assumed that *S*-type storms are caused by the corpuscular emission from sun spot groups and the *M*-type storms by the corpuscular emission from the so-called *M*-regions.

Also it is generally believed that the cosmic storms do not show a recur-

rence tendency and are thus distinct from the 27-day recurrent variations of the cosmic radiation.

The data in Fig. 1 and Table I, however, seem to contradict this assumption. There is a very clear recurrence with a period of about 27 days shown by Forbush decreases, all associated with meridian passage of solar active regions. (This recurrence is particularly prominent in the case of the Manchester data.) We note also from Fig. 1 that the recurring storms become larger, i.e. the decreases become greater and wider at all latitudes.

TABLE I. – *Active solar regions and associated geomagnetic activity during May-June 1951* (*) *(under each region is given the time of meridian passage, passage number, and coronal and flare data).*

51-F	51-H	51-G	51-A	51-E	51-D
May 1; No. 2 Low activity (4 flares)	May 2; No. 2 (1 flare)	May 10; No. 1 Low activity (2 flares)	May 15; No. 5 Very great activity (61 flares) Yellow coronal line Ionospheric storm Low geomagn. activity	May 21; No. 3 Low activity (7 flares) Low geomagn. activity	May 22; No. 3 Moderate activity (12 flares) No appreciable geomagnetic activity
High geomagn. activity Ionosph. storm (May 1-5)					
May 28; No. 3 Low activity (2 flares)	May 29; No. 3	June 2 Low activity (2 flares) Ionospheric storm	June 12; No. 6 Great activity (22 flares) No yellow line No ionospheric storms No appreciable geomagnetic activity	June 16; No. 4 Moderate activity (11 flares) Ionospheric storm (June 18-19)	June 18; No. 4 Low activity (2 flares)
Moderate geom. activity Moderate ionosph. storm				Moderate geom. activity	

(*) D. E. TROTTER and W. O. ROBERTS: *High Alt. Obs. Rept. on Solar Activity* No. 6.

At the same time the accompanying magnetic storms become weaker. (This information has been obtained from magnetic observatory data (see also Table I); the first storm shown on May 1 is very intense, May 28 is of medium intensity; June 18 quite weak). We also note that the Forbush decrease precedes the magnetic storm in some cases by two or three days when the decrease is very wide but not when the decrease is very narrow.

These observations may be explained in the following manner. The common cause of magnetic and cosmic storms is the emission of corpuscular radiation

from the sun, in the form of a beam («à la Alfvén») or in the form of a turbulent cloud («à la Morrison»). Whichever it is, after some time it will expand and diffuse into the interplanetary space. A young beam of high particle density can produce a large magnetic storm but does not extend over a sufficient volume to produce a large cosmic ray decrease. As the beam gets older, its intensity will decrease but its dimension may increase. It will therefore be less effective in producing a magnetic storm but more effective in producing a cosmic storm. Finally, as the density becomes quite small the magnetic storm can only be produced when the earth is in the center of the beam, i.e. at the highest particle density. Hence, the time difference between the onset of the cosmic storm and the occurrence of the magnetic storm measures in a manner of speaking the extension of the beam. From a series of observations one might be able to obtain the rate of spreading of the beam.

The above hypothesis has a consequence which looks very attractive. An initial beam, very young, is likely to produce a strong magnetic storm without an accompanying cosmic storm while a diffused beam can produce a cosmic storm without a magnetic storm. Thus the same phenomenon could explain all the intermediate cases of cosmic and magnetic storm events. The intensity of magnetic storms as compared to cosmic storms depends on the density and extension of the beam or cloud.

This is of course a phenomenological picture designed to explain a particular set of observations. We may picture that the emitting region on the sun changes as it gets older so that the corpuscular emission becomes less dense, and at the same time more diffuse. Hence, we have here in principle a method for investigating the change with time in the nature of the corpuscular emission from the sun.

5. – Relation to 27 day variation

Another aspect of this hypothesis is that the 27 day variation is similar to the Forbush decrease, the difference being more in degree than in kind. The cause of the 27 day variation is certainly not settled: the Chicago group [12] considers them to be *increases* and quite distinct from the Forbush decreases, whereas the London group [13] has produced evidence to show that they are intensity decreases (*).

(*) Brown [18] also interprets the 27-day events as decreases produced in a manner similar to the Forbush decreases, while Kodama and Murakami [19] adduce evidence for solar emission (i.e. production) of particles by studying the concurrent diurnal variation.

6. – Special value of polar observations.

We now consider why the polar decreases are both larger and wider than the decreases observed at other latitudes. (Note that the scale used in Fig. 1 for the polar station is one-half that of the stations at other latitudes.). We must take into account that the instruments used for cosmic ray observations are not monochromatic detectors but measure the effects of primaries from about 3 GeV on up to the very highest energies. As has been shown by the work of BRUNBERG and DATTNER [14], the asymptotic velocity vectors of such primaries will cover a very wide region because of their dispersal by the earth's magnetic field. It is quite clear however that at the pole in the vertical direction the velocity vectors of all primaries will stay together, no matter what their energy, since they are parallel to the magnetic field. In fact, ÅSTRÖM [15] has shown that even at quite large zenith angles, a focusing effect occurs at the pole due to the form of the magnetic field (Fig. 2). Evidently, the radiation which enters into a vertical telescope at the pole has stayed together up to a distance of about forty earth radii. Somewhere in that region the earth's magnetic field becomes of the order of magnitude of the general interplanetary field. From this point on, the path of the cosmic rays depends on the type of model one assumes for the interplanetary magnetic field. In any case, whatever the cause of the cosmic storm decrease, it also exists some distance from the earth perpendicular to the plane of the ecliptic. If it existed throughout the space surrounding the earth, then the decreases at lower latitudes would be as large as at the pole. The localized extent of the mechanism responsible for the cosmic ray decrease can also be deduced from the enhanced diurnal variation of cosmic ray intensity, which is observed during the cosmic ray storm (by SEKIDO and YOSHIDA [16]). If it were possible to construct a monoenergetic directional detector, this diurnal variation should be very much larger.

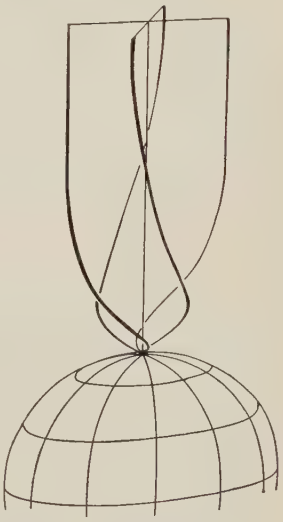

Fig. 2. – Asymptotic orbits of particles entering a polar telescope under different zenith angles. This figure illustrates focussing effect of magnetic field at high altitudes (ÅSTRÖM).

This points up the usefulness of a polar station to probe deep into the interplanetary space. Very likely the character of the interplanetary field differs during different parts of the solar cycle. This can be judged by the fact that the shape of the corona of the sun as observed in eclipses differs very

much during the solar cycle and depends very strongly on solar activity. When the interplanetary field is quite regular, cosmic rays coming up from the pole would all be led away into a particular region of space; if the decelerating mechanism exists there, then of course we will observe a decrease. On the other hand, during high solar activity when the interplanetary field is quite turbulent, cosmic rays as they come up into it (tracing back from the polar telescope) will be dispersed according to their energy; the decrease which we observe may then be smaller because the decelerating mechanism may act only in limited portions of space and thus will affect only primaries which traverse these regions.

It is possible therefore that two polar stations, one at the South pole and one at the North pole will not always give the same results. They may also give results different from those of middle latitude stations, depending on the phase of the solar cycle that we are in. We hope to obtain information on this point during the International Geophysical Year when recording telescopes will be set up at both polar locations.

7. – Conclusion.

We find it possible to give a reasonably satisfactory picture which explains (i) the recurrence of cosmic ray decreases, (ii) their increase in amplitude while the corresponding magnetic storms decrease, and (iii) the larger size of the polar decreases. The latter suggests that the mechanism which produces the Forbush decreases operates at large distances from the earth. It would be difficult to explain otherwise why the polar decreases are larger.

The present paper attempts no detailed explanation for the Forbush decreases (see following paper). Clearly however, the cause must be (i) a decrease in the number of primary cosmic rays, e.g. screening by a magnetic field, or (ii) a deceleration of the particles before entering the earth's atmosphere, or (iii) screening and deceleration.

These possibilities can be discriminated against by observing the energy spectrum of primary cosmic rays during a Forbush decrease. In the absence of such observations however, we must hypothesize a reasonable mechanism for producing the decreases. We favor a « diffusive deceleration » mechanism [17] which produces a deceleration and therefore an intensity decrease as the cosmic rays are reflected back and forth in the *expanding* cloud of magnetically turbulent gas which the sun has emitted.

* * *

The experimental work was performed while I was associated with the Applied Physics Laboratory of Johns Hopkins University. I thank Mr. R. Ostrander for his active help, and Dr. J. A. Van allen and Dr. R. E. Gibson

for support of the work; Mr. GLENN DYER and Mr. JOHN HUGHES of the U.S. Weather Bureau Arctic Section and personnel of the Danish Meteorological Office for supporting the experiment at Thule, Greenland. Many of my colleagues made data available to me concerning their observations: S. FORBUSH (Huancajo and Cheltenham), D. C. ROSE (Resolute, Canada), H. TERFALL, (Bergen, Norway), J. JACKA (Macquarie Island, Australia), J. A. SIMPSON (Chicago and Climax), R. L. CHASSON (Berkeley), Y. SEKIDO (Tokyo), D. I. DAWTON (Manchester). Solar data wery kindly furnished by Dr. W. O. ROBERTS.

I am particularly grateful to Dr. H. ELLIOT who called my attention to the events in the summer of 1951 and induced me to undertake the analysis of the records. Fig. 1 of the paper was prepared by DAWTON and ELLIOT who assembled the cosmic ray and magnetic data.

REFERENCES

[1] S. E. FORBUSH: *Terr. Mag.*, **43**, 207 (1938).
[2] H. E. ELLIOT, in *Progress in Cosmic Ray Physics*, Vol. I (Amsterdam, 1952); also B. TRUMPY: *Physica*, **19**, 645 (1953); A. EHMERT: *Naturwissenschaften*, **41**, 317 (1954).
[3] S. F. SINGER, in *Progress in Elementary Particle and Cosmic Ray Physics*, Vol. IV (Amsterdam, 1958).
[4] T. H. JOHNSON: *Terr. Mag. Atmos. Elec.*, **43**, 1 (1938).
[5] S. HAYAKAWA, J. NISHIMURA, O. NAGATA and Z. SUGIURA: *Journ. Sci. Res. Inst. Tokyo*, **44**, 121 (1950).
[6] S. B. TREIMAN: *Phys. Rev.*, **89**, 130 (1953).
[7] The actual distribution of the ring current around the earth has been calculated on the basis of a new model of magnetic storms (S. F. SINGER: *Trans. Amer. Geophys. Union*, **38**, 175 (1957)); however its effect on cosmic ray orbits has not yet been investigated.
[8] H. ALFVÉN: *Nature*, **158**, 618 (1946).
[9] K. NAGASHIMA: *Journ. Geomag. Geoelectr.*, **3**, 100 (1951); **5**, 141 (1953).
[10] Y. SEKIDO, M. WADA, I. KONDO and K. KATAWABA: *Rep. Ionosph. Res. Japan*, **9**, 174 (1955); Y. SEKIDO: *Rep. Ionosph. Res. Japan*, **9**, 182 (1955).
[11] P. MORRISON: *Phys. Rev.*, **101**, 1397 (1956).
[12] P. MEYER and J. A. SIMPSON: *Phys. Rev.*, **96**, 1085 (1954); J. A. SIMPSON, H. W. SIMPSON, H. W. BABCOCK and H. D. BABCOCK: *Phys. Rev.*, **98**, 1402 (1955).
[13] I. J. VAN HEERDEN and T, THAMBYAHPILLAI: *Phil. Mag.*, **46**, 1238 (1955).
[14] E. A. BRUNBERG and A. DATTNER: *Tellus*, **6**, 73 (1954).
[15] E. ÅSTROM: *Tellus*, **8**, 239 (1956).
[16] S. YOSHIDA: *Nuovo Cimento*, **4**, 1410 (1956).
[17] S. F. SINGER: *Bull. Am. Phys. Soc.*, II, **2**, 192 (1957); also in this issue, p. 209.
[18] R. R. BROWN: *Journ. Geophys. Res.*, **61**, 639 (1956).
[19] M. KODAMA and K. MURAKAMI: *Journ. Geomag. Geoelectr.*, **8**, 71 (1956).

SUPPLEMENTO AL VOLUME VIII, SERIE X
DEL NUOVO CIMENTO

N. 2, 1958
2° Trimestre

Cosmic Ray Time Variations Produced by Deceleration in Interplanetary Space (*).

S. F. SINGER

University of Maryland - College Park, Maryland

1. – Introduction.

The world-wide decreases of the cosmic radiation which accompany magnetic storms, first described by FORBUSH [1], are quite striking and in some cases as large as 10%. While they are often associated with magnetic storms, there are many examples where the decreases occur without magnetic storms, and conversely magnetic storms occur without cosmic ray decreases [2]. This suggests that the correlation between magnetic storms and Forbush-type decreases is not an immediate one, but goes back to a common cause. ALFVÉN [3] first suggested that the emission of corpuscular matter from the sun, which is responsible for magnetic storms, is also directly responsible for the cosmic ray decrease.

Previously, the view was held that the cosmic ray decrease is due to a redistribution of cosmic rays by the magnetic effects of the magnetic-storm producing ring current around the earth's equator. But this would lead to a detailed correspondence between Forbush events and magnetic storms. For this reason a number of authors, T. H. JOHNSON [4], HAYAKAWA *et al.* [5], and most recently TREIMAN [6], have examined this proposal theoretically. On the basis of their work the ring current effect appears too small; depending on its position it could even give the reverse effect and lead to a cosmic ray increase.

A very interesting proposal has been made by NAGASHIMA [7], who has considered the effect of the electric polarization field which is thought to

(*) This work has been supported in part by the Air Force Office of Scientific Research under Contract AF No. 18(600)-1038.

stabilize the ring current. This electric field would decelerate the cosmic rays and would therefore decrease their intensity; however, the other objections to the ring current hypothesis still remain. Furthermore, on the experimental side there has been a recent observation by SINGER [8] which rules out the ring current hypothesis: a magnetic strom decrease was found at Thule, Greenland, near the geomagnetic pole. Clearly, no symmetric ring current or any other change in the earth's dipole field could account for this decrease. We can conclude, therefore, that the cause of the Forbush decrease must lie at some distance from the earth, and that it is probably tied up more directly with the solar corpuscular beam, as originally suggested by ALFVÉN [3].

2. – Theories of the Forbush decrease.

2·1. *Beam deceleration.* – A general class of explanations for the cosmic-ray effect has to do with electric fields, set up presumably by polarization of the neutral but ionized solar beams. Here it is not the change in magnetic cut-off at the earth, but the deceleration of cosmic-ray particles passing through the electric fields, which is supposed to account for the intensity variations. Under the ALFVÉN [9] model the energy lost by a particle crossing the beam is $(v \times H)b$, where v is the beam velocity, H the frozen-in field carried by the beam, and b the breadth of the beam.

This Alfvén model has been discussed in greater detail recently by BRUNBERG and DATTNER [10]. It depends critically on the assumption that there is a magnetic field carried by the corpuscular beam so that an electric polarization is produced, and that there exists also a general, although weak magnetic field between the sun and the earth which deflects cosmic ray sufficiently to prevent their acceleration by the same polarization field. The authors, however, neglect the deflection of cosmic rays within the beam itself, as well as refraction effects at the edge of the beam. As a consequence, it is not easy to see how one can obtain the rather good *isotropy* (small diurnal variations) which is observed at all latitudes.

Another consequence of the Alfvén model is that the change of energy of a cosmic ray particle passing through the electric field is independent of initial particle energy: that is, the *percentage* change in energy is a decreasing function of energy. One would expect, then, to find a fairly marked latitude dependence, which, however, is not observed.

2·2. *Magnetic screening.* – More recently, MORRISON [11] has put forth the following picture of magnetic storm phenomena. Along with others, MORRISON supposes that clouds of ionized, magnetized matter are emitted from the sun during active solar periods. However, in contrast to ALFVÉN's view of an

ordered magnetic field associated with the beam, MORRISON assumes a situation of magnetic turbulence within the clouds. Now Liouville's theorem prescribes that in equilibrium conditions, the cosmic ray intensity must be the same inside the cloud as outside. By starting with a cloud empty of cosmic rays one is dealing with a non-equilibrium situation, and if the magnetic field is large enough, the diffusion time into the cloud may be made as long as a day or so, if one is willing to accept fields of the order $5 \cdot 10^{-3}$ G. So for this period of time the cosmic ray intensity within the cloud will be below the normal value: and when such a cloud envelops the earth one will observe a cosmic-ray decrease, along with magnetic effects associated with the cloud (via the formations of ring currents, for example).

MORRISON's suggestion is a very interesting one. The main difficulties with his picture are the large magnetic fields required to affect cosmic rays of the relevant energies, about 30 GeV. Also, since the diffusion time must depend on the particle energy, his model should lead to a large latitude dependence of the Forbush decrease which has as yet not been observed. On the contrary, the observed latitude effect is small; the variations observed by neutron counters [12] are only a few times larger than those of ion chambers or meson telescopes, much less than during solar flare increases.

Morrison's model has been critically discussed by PARKER [13], who has added the following modification: he assumes that a turbulent magnetic cloud can be captured and held to the earth by the gravitational field. In this geocentric model the earth acts as a very effective absorber of cosmic rays and this lessens considerably the requirements put on the screening ability of the cloud. Clearly the rate of leakage through the cloud can be much higher if there exists a removal mechanism. PARKER also uses this barrier cloud to explain the knee of the cosmic radiation. It is not clear as yet to what extent this model is ad hoc and whether it is reconcilable with other geophysical phenomena.

Also it seems difficult to explain *polar* Forbush decreases by a geocentric gas cloud. Further, the observations that the polar decreases are larger than those at moderate latitudes [8] can be interpreted most directly in terms of the low dispersion in direction of cosmic rays which enter into a polar telescope and therefore in terms of a mechanism (deceleration or screening) which operates at *some considerable distance* from the earth [8].

2·3. *Diffusive deceleration model.* – The model we wish to discuss here to explain the storm decrease makes use of a turbulent cloud also, but it does not rely on the Morrison diffusion mechanism. Instead, we consider that the cloud is expanding and that the cosmic rays are reflected back and forth in a region where the turbulent energy is decreasing. We are dealing here, therefore, with an « inverse Fermi » mechanism in which particles are decelerated.

This model does not require high fields: it should lead to a reasonably small latitude effect, since low energy particles will be able to diffuse towards the earth without losing too much energy (cf. below). Here we neglect the ionization loss; for very low energy particles it is of far greater importance and produces the « knee » (low energy cut-off of primary spectrum) [14].

We will now discuss the physical picture in somewhat greater detail. The emission of high-speed jets of gas or « puffs » of gas from the sun with supersonic velocity will set up turbulence at the boundary between the jet and the ambient interplanetary gas. The field strength which results due to the large amount of twisting can be quite large. We will take values of 10^{-4} G as a very conservative estimate, even though they could be much higher. We now picture these vortices spreading out into space from the beam and expanding slowly, while at the same time the intensity of the field decreases see Fig. 1). At first, to estimate the

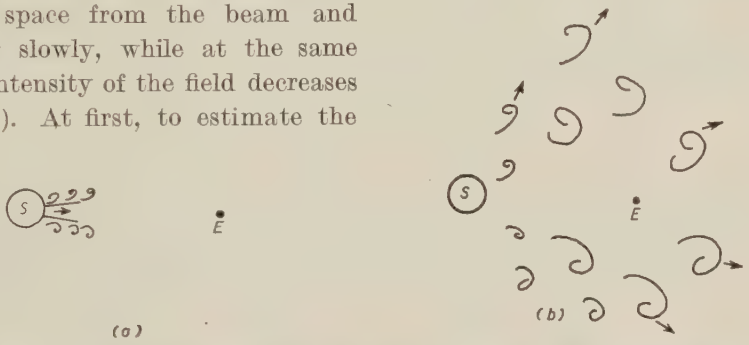

Fig. 1 *a*) and *b*). · Schematic diagram showing the production and spreading out of hydromagnetic turbulence from the vicinity of the sun into interplanetary space. (*a*) shows the situation after a solar eruption; (*b*) about a day later. Cosmic rays which are trapped in this region share in the expansion, hence lose energy.

expansion, we will take a distance of one astronomical unit, about 10^{13} cm, and a time of the order of a day, about 10^5 s (*). We will now examine the variation of energy density with time. Starting with field values of the order of 10^{-4} G, we have:

$$\text{Energy density } w = \mu \overline{H}^2 / 8\pi \sim 4 \cdot 10^{-10} \text{ erg/cm}^3 .$$

After 10^5 s and expansion of roughly a factor of 2, the energy density, according to BATCHELOR [15], has decreased by 2^{-4} and is therefore $0.25 \cdot 10^{-10}$.

(*) The above figures can be made plausible by considering experimental evidence. The fact that the decreases are observable at the pole [8] shows the large extension of the phenomenon. The time constant is also apparent from the experimental observations.

The average decrease in energy density therefore is:

$$\frac{dw}{dt} = 4 \cdot 10^{-15} \text{ erg/cm}^3 \text{ s} .$$

A 30 GeV proton has a radius of curvature of 10^{12} cm if $H = 10^{-4}$ G. We estimate, therefore, an average time of 100 s in the turbulent region, and therefore an energy loss of $4 \cdot 10^{-13}$ erg/cm^3. We note that this figure is of the same order as the energy density of cosmic rays in the vicinity of the earth, which is 10^{-12} erg/cm^3. The rough equality of the two figures makes it plausible that decaying turbulent magnetic fields will « pump » energy out of cosmic rays.

It is possible also to consider the particles as being reflected from centers having high magnetic fields which recede from each other due to the expansion. This view corresponds to an inverse Fermi effect, since it is similar in principle to the acceleration mechanism considered by FERMI [16] to take place in galactic space. The fractional energy loss per collision α is:

$$\alpha = \delta U/U \approx \tfrac{4}{3}(V/c)^2 \approx 10^{-4} ,$$

where $V \geqslant$ the average expansion velocity (about $1.5 \cdot 10^{13}$ cm/10^5 s). But in the diffusion model the number of collision $N \approx (L/\lambda)^2 \approx (1.5 \cdot 10^{13}/10^{12})^2 \approx 200$. With $U \sim 30$ GeV, $\Delta U = UN\alpha$ and is more than adequate to give the necessary deceleration, about $3 \cdot 10^8$ eV, to account for the observed decrease (*).

3. – 27-day variation.

We consider the 27-day variations closely related to the Forbush decreases and produced essentially by the same mechanism, but on a smaller scale [8]. It is well known that the sun has centers of activity (so-called M-regions) which emit corpuscular radiation for many solar rotations. In our view, the emission is weaker than during the large magnetic storms, resulting in a weaker turbulence generation and smaller cosmic ray effect.

4. – Solar cycle variations.

FORBUSH [17] has recently published the remarkable records obtained with lead-shielded ion chambers at various stations throughout the world. There are many irregular fluctuations observed simultaneously at all stations. Overriding all of these irregular, though by no means small time variations, there exists a pronounced trend apparently associated with the solar cycle. The peak-to-peak variation is nearly 4%. The intensity is clearly inversely correlated with sun-spot number.

(*) Or since $\Delta U/U \sim \Delta p/p \sim 2\%$, then from Liouville's theorem the intensity $j = Dp^2\beta$ decreases by $\sim 4\%$.

4·1. *Solar origin of cosmic rays.* – ALFVÉN [9] has given an interpretation of this effect in terms of a model in which the bulk of the cosmic radiation is accelerated by field variations in the vicinity of the sun. His model also explains the diurnal variation observed during the solar cycle.

4·2. *Galactic origin of cosmic rays.* – MORRISON [11], on the other hand, has tried to account for the solar cycle variation by assuming that his diffusion process operates over a much larger volume, of the order of 100 times the sun-earth distance. Similarly, PARKER [13] assumes that his geocentric clouds lead to a depression in intensity near the earth of the galactic cosmic radiation.

Our view is similar, namely, that the decreases are due to the cumulative effect of solar corpuscular emission which is at its maximum when the cosmic ray intensity is at a minimum. We are dealing here with effects which are too small to be detected as individual Forbush decreases, but add up to cause a general lowering of the cosmic ray intensity. A striking example was the 6-months decrease which started in February, 1946 [17]. This change in intensity implies a change in the spectrum with solar cycle. In fact, a steepening of the low energy portion of the primary spectrum has been found by MEYER and SIMPSON [18]. In addition, it appears that the very low energy portion of the cosmic ray spectrum, below about 500 MeV, is present during the period of the minimum of the solar cycle [19].

5. – Experimental tests.

Our most important lack of information is with regard to the *primary* radiation, since all continuous measurements so far have been carried out at sea level and mountain altitudes. Changes, if any, in the composition of the primaries are of interest; but for the interpretation of the Forbush decreases the energy spectrum of the primary radiation is of particular importance. Theories of the type discussed by ALFVÉN [9], NAGASHIMA [7], or in the present paper would lead to a deceleration of particles, and therefore to a *shift* in the *position of the knee*; while the pure decrease, such as assumed by MORRISON [11], would simply reduce the number of incident particles and therefore show a different type of latitude effect, but without disturbing the position of the knee for protons (nor for *heavy primaries*).

From an experimental point of view, the different theories will lead to different types of variations of the primary intensity with latitude; hence it would be very rewarding to measure the primary spectrum during the Forbush decrease. In order to establish a shift in the position of the knee, we must use either time-correlated high-altitude balloon flights, or time-correlated rocket flights, or observations of the primary radiations by means of an artificial

earth satellite [20]. A schematic presentation of the types of latitude effects is shown in Fig. 2.

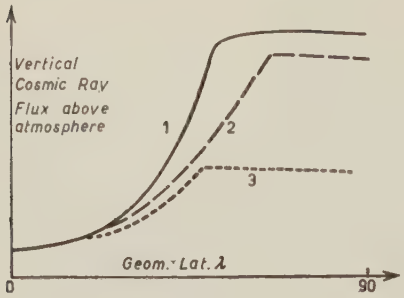

Fig. 2*a*.

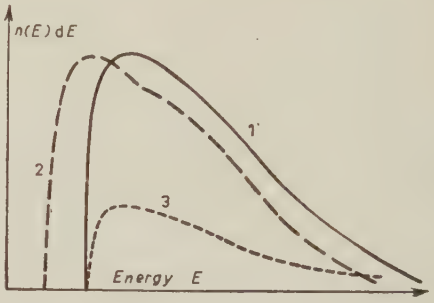

Fig. 2*b*.

Fig. 2. – Schematic diagrams of latitude curves obtained by means of a satellite; 1) for a normal cosmic ray spectrum; during a FORBUSH decrease; for a decelerated spectrum (2), and for an attenuated spectrum (3). (The decelerated spectrum is shown unattenuated for sake of clarity) (Ref. [20]).

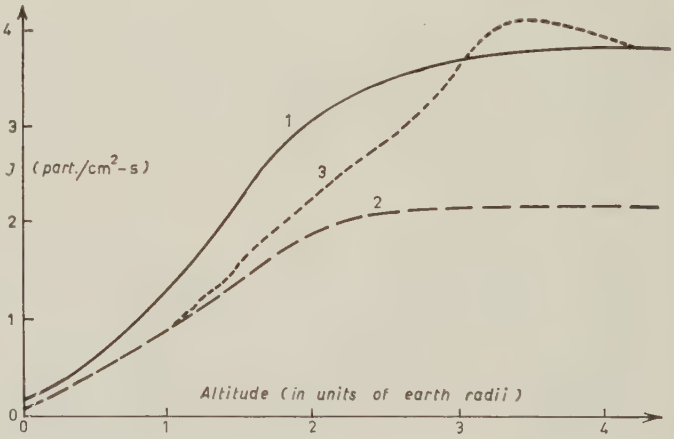

Fig. 3. – Schematic diagrams showing the increase in total flux as a function of altitude at the geomagnetic equator. The abscissa is given in terms of earth radii. The solid line (1) shows the normally expected variation calculated from the primary spectrum and geomagnetic theory. The dash line (2) shows the flux variation during a FORBUSH decrease; the cosmic ray intensity is supposed to be depressed at large distances from the earth as well. The dotted curve (3) shows the flux variation expected from the geocentric theory of Parker; it may be possible even to observe an additional increase due to cosmic rays which are reflected by the geocentric barrier.

A clear-cut experimental test seems possible with respect to Parker's geocentric theory. Since his barrier extends out to ~ 3 earth radii, rocket experiments to extreme altitudes could establish whether the Forbush decrease is local or exists also at large distances away from the earth, as would be expected from the model described in the present paper. Fig. 3 shows the altitude dependence which may be obtained for the two different cases.

REFERENCES

[1] S. E. FORBUSH: *Terr. Mag.*, **43**, 207 (1938).

[2] For a recent review see H. E. ELLIOT: *Progress in Cosmic Ray Physics* (Amsterdam, 1952); also B. TRUMPY: *Physica*, **19**, 645 (1953); A. EHMERT: *Naturwissenschaften*, **41**, 317 (1954).

[3] H. ALFVÉN: *Nature*, **158**, 618 (1946).

[4] T. H. JOHNSON: *Terr. Mag. Atmos. Elec.*, **43**, 1 (1938).

[5] S. HAYAKAWA, J. NISHIMURA, T. NAGATA and M. SUGIURA: *Journ. Sci. Res. Inst. Tokyo*, **44**, 121 (1950).

[6] S. B. TREIMAN: *Phys. Rev.*, **89**, 130 (1953).

[7] K. NAGASHIMA: *Journ. Geomag. Geoelectr.*, **3**, 100 (1591); **5**, 141 (1953).

[8] S. F. SINGER: *Phys. Rev.*, **95**, 647 (1954) (A); also in this issue, p. 334.

[9] H. ALFVÉN: *Tellus*, **6**, 232 (1954).

[10] E. A. BRUNBERG and A. DATTNER: *Tellus*, **6**, 73 (1954).

[11] P. MORRISON: *Phys. Rev.*, **101**, 1397 (1956).

[12] J. A. SIMPSON: *Phys. Rev.*, **94**, 426 (1954).

[13] E. N. PARKER: *Phys. Rev.*, **103**, 1518 (1956).

[14] S. F. SINGER: in this issue, p. 342.

[15] G. K. BATCHELOR: *Gas Dynamics of Cosmic Clouds* (New York, 1955), p. 119.

[16] E. FERMI: *Astrophys. Journ.*, **119**, 1 (1954).

[17] S. E. FORBUSH: *Journ. Geophys. Res.*, **59**, 525 (1954).

[18] P. MEYER and J. A. SIMPSON: *Phys. Rev.*, **99**, 1517 (1955).

[19] H. V. NEHER and E. A. STERN: *Phys. Rev.*, **98**, 854 (1955).

[20] S. F. SINGER: *Rocket Exploration of the Upper Atmosphere* (London, 1954), p. 369.

SUPPLEMENTO AL VOLUME VIII, SERIE X
DEL NUOVO CIMENTO

N. 2, 1958
2° Trimestre

On the Low Energy Cut-Off of the Cosmic Radiation (*).

S. F. SINGER

University of Maryland - College Park, Maryland

1. – Introduction.

The existence of a latitude cut-off in flux («Knee») due to the absence of low energy primaries has been established near 58° in rocket experiments by VAN ALLEN and SINGER [1], MEREDITH, VAN ALLEN and GOTTLIEB [2], and balloon experiments conducted by NEHER, PETERSEN and STERN [3]. These measurements were carried out in the period of 1950-1952. In more recent flights, however, during 1954, NEHER and STERN [4] found that the latitude cut-off did not exist and deduced from the observed increase between latitudes 58° and 68° that the proton spectrum extended down to 150 MeV.

Some questions are raised in the interpretation of the low energy cut-off in the primary radiation and of its apparent shift with time. In 1954 we reached the minimum of the solar cycle, as judged by sun spot number; apparently, the presence of the knee or at least its position is correlated with the sun spot number [4]. This possibility had been suggested also by POMERANTZ and VALLARTA [5].

A very important approach to the study of the very low energy spectrum has been made by ELLIS *et al.* [6]. In order to establish whether the cut-off is due to a magnetic field, they have investigated the cut-off rigidity for heavy primaries as well as for protons at the *same magnetic rigidity*. However, recent experiments [7] with photographic emulsions in extremely high altitude balloon flights give a contradictory result, showing a differential α-spectrum with a peak at 300 MeV per nucleon and a peak at a higher energy per nucleon for very heavy primaries.

(*) This work has been supported in part by the Air Force Office of Scientific Research under Contract AF No. 18(600)-1038.

In view of the latter result, and for reasons listed below, we can no longer assume that the cut-off (at ~ 560 MeV for protons) is due to a solar dipole field, as suggested earlier [8]. We must take into account:

(i) The negative results of measurements of the surface field of the sun [9].

(ii) The absence of the expected diurnal variation [10].

(iii) The analysis of solar flare increases of cosmic rays, and of the maximum deviation of the particles in their travel between the sun and the earth which places an upper limit of $5 \cdot 10^{32}$ G cm^3 on the solar dipole moment, about 1/10 of the value necessary to explain the cut-off [11].

No alternative explanation has as yet found general acceptance. In principle, the cut-off could be inherent in the *source* and indicate a deficiency of low energy particles coming from the acceleration process. The presence of low energy primaries during periods of little solar activity would then be difficult to reconcile with a theory of *galactic* origin.

Another possibility is that the knee is caused by an effect between the source and the earth. It is very suggestive that the cut-off (at least in 1950-52) occurred at an energy where protons begin to be non-relativistic and the ionization loss begins to rise rapidly (*). If one adopts a simple model in which the radiation passes through a *fixed* absorber, it is possible to remove the very low energy primaries, but impossible to produce a sharp cut-off near 500 MeV (+).

2. – « Lumpy » field model.

The picture favored here is that of a « guillotine effect » which does not violate Liouville's theorem. We adopt a model of interplanetary space where there are large fluctuations of gas density which are associated, because of the high conductivity, with similar fluctuations in magnetic field. High rigidity, high energy particles will traverse these regions without difficulty. Low rigidity particles will undergo a much more complicated motion. In the steady-state, no-energy-loss case, this would not affect their intensity (because of Liouville's theorem); they would merely spend more time in the high magnetic field regions. However, the non-uniform density implies that non-relativistic particles will lose energy at a faster rate; this will lower their intensity con-

(*) Professor B. Rossi called attention to this point some years ago.

(+) This was done independently by J. A. Van Allen (private communication), by the writer (unpublished), and probably by others as well. These attempts had two things in common: (i) the absorber thickness was the same for all particles regardless of energy, (ii) the Liouville factor was not taken into account.

siderably (because of the Liouville factor) (*). They will eventually lose enough energy to be caught in a high field region and not escape; this will reduce their intensity to nearly zero. Fig. 1 schematically represents this effect produced by introducing a non-uniform density.

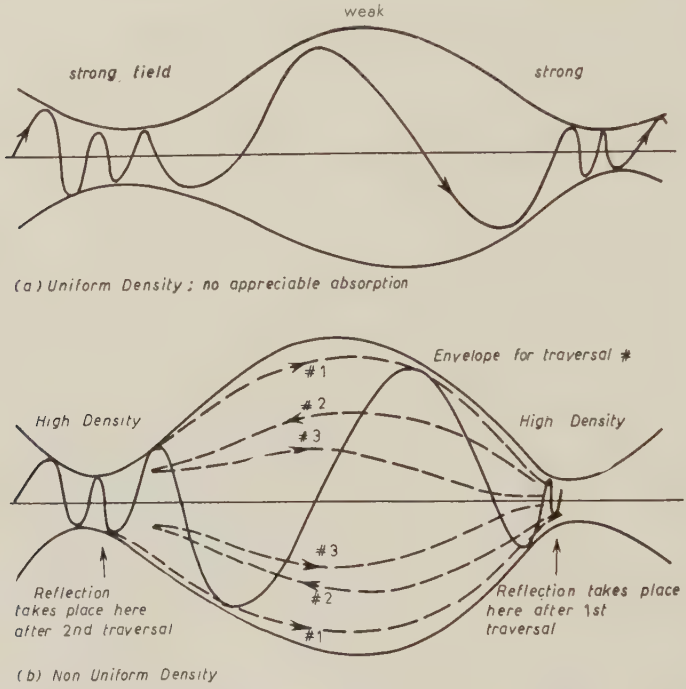

Fig. 1. – Schematic diagram showing how a « trap » is created for a non-relativistic particle when high density and high field are coupled. (*a*) uniform density; no appreciable absorption; (*b*) non-uniform density.

In order to treat the effect of a decaying and expanding turbulent field on low energy cosmic rays, we must examine more carefully our previous model [12] developed to account for Forbush decreases. The energy loss there takes place on a statistical basis, i.e., a particle may lose or gain energy. Now on the average the losses outweigh the gains in an expanding turbulent region [12]; but this by itself does not produce a « knee ». However, when an energy loss becomes of the order of magnitude of the total energy of the part-

(*) A generalized treatment of Liouville's theorem yields for the differential intensity $j = Dp^2\beta c$, here D is particle density in phase space. When the relative change in the momentum p is small, the flux is hardly affected; but when, for example, p is cut in half by a deceleration, the flux is reduced to $\frac{1}{4}$ of its former value. In the *non-relativistic* region the reduction is even greater, since now β is affected; effectively, then, j varies as p^3.

icle, then the particle has a strong chance of disappearing; once it has been decelerated into the non-relativistic region, it will lose energy very rapidly due to ionization and can no longer recover and regain energy. This process is seen plausible when we examine the energy decrease according to Fermi's [13] model. The fractional energy loss per collision $\alpha = \Delta U/U$ is of the order of $\frac{4}{3}(V/c)^2$. To be conservative, we will adopt the low value of 100 km/s for V, about 10 times less than its value following a solar outburst [12]. We find then $\alpha \sim 10^{-7}$. The number of collisions N is given as $(L/\lambda)^2$, about 10^5. L is $\sim 10^{13}$ cm, $\lambda = 3 \cdot 10^{10}$ cm corresponding to $H = 10^{-4}$ G. (We must adopt a rather low value for λ, since the particle, because of its lower rigidity, can now be reflected by lower magnetic fields which one would expect to find spaced closer together (+)). The energy loss is seen to be a substantial fraction of the particle's *kinetic* energy when the particle becomes non-relativistic, since $\Delta U/U \sim 1\%$ where U is the *total* energy; at the same time since the ionization loss rises rapidly, proportional to Z^2/β^2.

3. The « Knee » as an indicator of interplanetary turbulence.

The picture we have, therefore, is the following: Periods of high activity in the solar cycle (given by a suitable index of solar activity, e.g. sunspot number) lead to increasing lumpiness (turbulence) of the interplanetary gas and magnetic field. The general cosmic ray intensity (average energy 30 GeV) is then lowered by the deceleration produced by the expansion and decay of turbulent interplanetary magnetic fields [12]. For very low energy primaries (around 1 GeV) this deceleration can be catastrophic, since it involves a large fraction of their kinetic energy. Once a particle by chance slips into the non-relativistic region, the ionization loss becomes dominant; the particle cannot escape from a high field region once it is trapped in it. These regions, therefore, become effective sinks for non-relativistic particles and remove them rapidly from the cosmic radiation near the earth. During periods of low solar activity the interplanetary field structure is smooth; the « traps » are now reduced and the position of the energy cut-off (and knee) is found to be lowered. Superimposed on the general slow shift of the cut-off energy during the solar cycle, we may expect to find more rapid fluctuations, a study of which would indicate the effectiveness of the process described in the present paper. For example, a particularly appropriate time for observation would be following an extended period of low activity during which the cut-off energy might be lowered to a value which depends on the efficiency of our process; after the commencement of high activity one could then study the time-constant with which the cut-off energy moves upward towards the relativistic limit. The

(+) Such a reflecting center would have $Hl \sim 3 \cdot 10^6$; typically $H \sim 10^{-3}$ gauss and l the dimension of the center $\sim 3 \cdot 10^9$ cm.

cut-off energy for primary protons thus becomes an indicator for the average degree of turbulence of the interplanetary medium. A detailed study of the position of the energy cut-off with time can therefore be used to study the degree of turbulence in the interplanetary gas.

The considerations presented must be treated with some reservation, since they are intimately tied up with the way in which the low energy cosmic radiation is produced. In a theory of solar origin, as for example proposed by ALFVÉN [14], one cannot discuss the absorption effects apart from the production of cosmic rays; we must combine them in an appropriate manner.

4. – Experimental tests.

In principle there are two experimental methods for measuring the position of the energy cut-off; one depends on the earth's magnetic field to analyze momenta, in other the energy of the particles is measured directly, e.g. in a photographic plate. The first method is generally carried out by measuring intensity of cosmic rays as a function of geomagnetic latitude; it can be carried to the logical extreme by mounting a Geiger counter into an artificial earth satellite vehicle to give a continuous indication of the form of the energy spectrum and the position of the cut-off. A different approach consists of projecting a Geiger counter from the equator upward to several earth radii [15]. This method eliminates uncertainties arising at high latitudes from the imperfect knowledge of the shadow cone, effects of quadrupole field and atmospheric currents. Fig. 2 shows

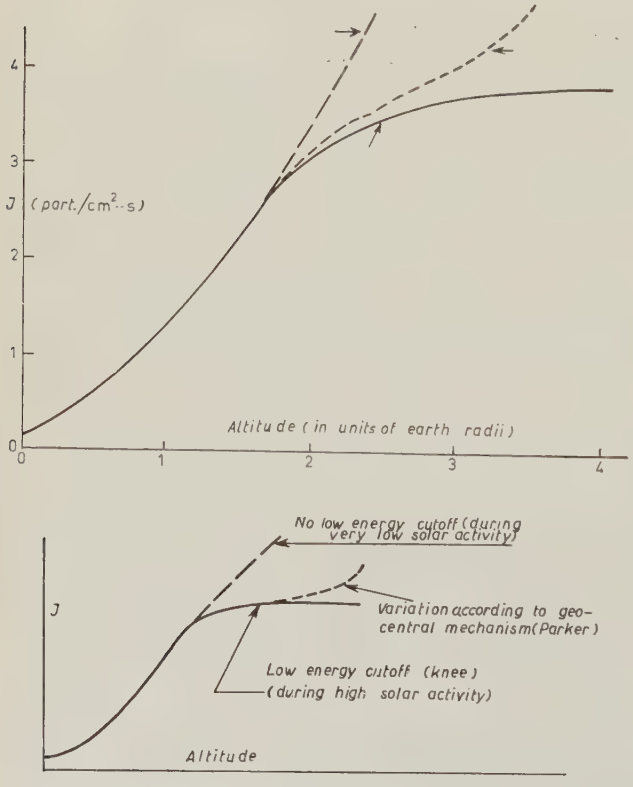

Fig. 2. – Variation of omnidirectional cosmic ray flux vs. altitude at geomagnetic equator.

the counting rate to be expected as a function of altitude. It has been computed for a momentum spectrum $n(p) \sim 0.48 p^{1.1}$. In this calculation the geomagnetic (rather than geometric) shadow effect of the earth was taken into account (*).

The direct method is particularly appropriate to measure the energy of α-particles and heavy primaries. According to the model presented here one would expect the cut-off to be *not* sharp, i.e. the existence of some particles of energy below cut-off. Also, the cut-off should occur at higher rigidities for primaries of higher charge, since there the ionization loss is more important (Fig. 3). Experiments of the type carried on by the Bristol and Minnesota [7] groups should be very important in this connection.

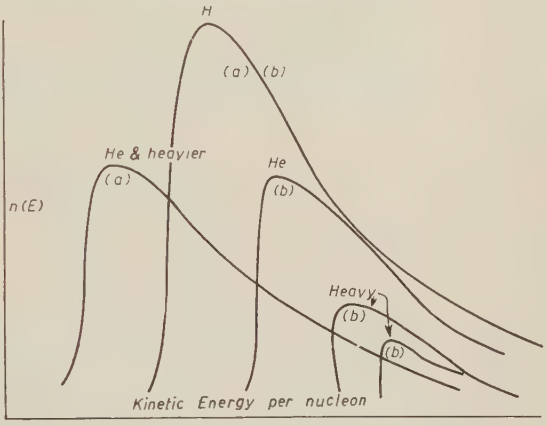

Fig. 3. – Schematic diagram showing the position of the energy cut-off for primaries of different charge under two different theories: (*a*) magnetic screening; (*b*) diffusive deceleration plus ionization loss.

(*) This measurement could also discriminate between the mechanism proposed in the present paper (in which the low energy cut-off exists throughout at least the inner part of the solar system), and the geocentric mechanism proposed by PARKER [16] in which the cut-off is local, produced by a cloud of turbulent gas within 1-2 earth radii.

REFERENCES

[1] J. A. VAN ALLEN and S. F. SINGER: *Nature*, **170**, 62 (1952).
[2] L. H. MEREDITH, J. A. VAN ALLEN and M. B. GOTTLIEB: *Phys. Rev.*, **99**, 198 (1955).
[3] H. V. NEHER, V. Z. PETERSEN and E. A. STERN: *Phys. Rev.*, **90**, 655 (1953).
[4] H. V. NEHER and E. A. STERN: *Phys. Rev.*, **98**, 854 (1955)
[5] M. A. POMERANTZ and M. S. VALLARTA: *Phys. Rev.*, **76**, 1889 (1949).
[6] R. A. ELLIS, M. B. GOTTLIEB and J. A. VAN ALLEN: *Phys. Rev.*, **95**, 147 (1954).
[7] P. H. FOWLER, C. J. WADDINGTON, P. S. FREIER, J. NAUGLE and E. P. NEY: *Phil. Mag.*, **2**, 157 (1957).
[8] L. JÁNOSSY: *Zeits. f. Phys.*, **104**, 430 (1937).

[9] H. v. KLÜBER: *Month. Not. Roy. Astr. Soc.*, **111**, 2 (1951); G. THIESSEN: *Nature*, **169**, 147 (1952).
[10] J. FIROR, F. S. JORY and S. B. TREIMAN: *Phys. Rev.*, **93**, 551 (1954).
[11] S. B. TREIMAN: *Phys. Rev.*, **95**, 1029 (1954).
[12] S. F. SINGER: in this issue, pp. 326, 334.
[13] E. FERMI: *Astrophys. Journ.*, **119**, 1 (1954).
[14] H. ALFVÉN: *Tellus*, **6**, 232 (1954).
[15] S. F. SINGER: *Phys. Rev.*, **98**, 1547 (1955) (A).
[16] E. N. PARKER: *Phys. Rev.*, **103**, 1518 (1956).

SUPPLEMENTO AL VOLUME VIII, SERIE X
DEL NUOVO CIMENTO

N. 2, 1958
2° Trimestre

Störmer Orbits of Low Energy.

A. SCHLÜTER

Max-Planck-Institut für Physik, Göttingen

The equation of motion of a charged particle in the field of a magnetic dipole allows for a similarity transformation as has been found by C. STÖRMER. Instead of considering particles of different rigidity in a fixed field one needs only consider the trajectories of a fixed rigidity and finds the trajectories corresponding to all other rigidities by a change of the linear scale. This is most conveniently done by introducing the Störmer unit of length, so that the radius of the earth expressed in this unit (which will be denoted by 1) is a measure of the rigidity. Table I gives the relation between this quantities according to momentum $P = 59 \cdot 10^9 A^2$ [eV · Z c].

TABLE I.

A	P in 10^9 eV · Z/c	Regime
infinite	infinite	small deflection
1.0	59	large deflection
0.4	9.5	large deflection
0.1	0.59	spiralling (ALFVÉN)

Inspection of numerically calculated trajectories shows that one has, depending on A, three relatively distinct regions of different behaviour of the trajectories.

a) For $A > 1$ the magnetic field exerts only a minor influence, shifting the points of impact somewhat, mainly in the direction of earlier hours (for positively charged particles).

b) For $1 \gtrsim A \gtrsim 0.4$ large deflections occur—the particles may greatly change their longitude and may alternate between northern and southern latitudes.

c) For $A < 0.4$ the particles behave according to what one might call the Alfvén regime. They spiral around the line of force with increasing pitch angle ϑ (= angle between the velocity vector and the local line of force) as A decreases until they are reflected, where ϑ reaches 90°, and return—except for that set of trajectories (of measure zero) which finally reach the point $A = 0$ and which we call « Nullbahnen ». At the same time not all latitudes remain accessible to particles coming from infinity, but for decreasing A (starting at $A = 0.5$) a belt of increasing width around the equator forms a forbidden region.

It is this last regime we are here concerned with. Consider now a certain line of force and the particles of fixed rigidity spiralling around it. Assume that the number of those particles having a certain pitch angle ϑ (as defined before; $\vartheta < 90°$) at a certain distance A_1 from the centre, can be described by a distribution function

$$Q\{\sin\vartheta\,;\,A\}\,\mathrm{d}\sin\vartheta\,, \qquad \vartheta < 90°$$

(by using $\sin\vartheta$ as the argument, an isotropic distribution corresponds to Q being independent of $\sin\vartheta$).

As the particles approach the central dipole, the magnetic field H increases and the pitch angle ϑ of every individual particle increases so that along a trajectory

$$(\sin^2\vartheta)/H = \text{const}\,.$$

Since every line of force gets closer to the axisas A decreases, the latitude dependence of the strength of the magnetic field may be neglected and H is proportional to A^{-3}. Therefore the distribution at a distance $A_2 < A_1$ follows from that at a distance A_1, as

$$Q\{\sin\vartheta, A_2\} = \left(\frac{A_2}{A_1}\right)^3 Q\left\{\sin\left(\vartheta\left(\frac{A_2}{A_1}\right)^3\right), A_1\right\}\,.$$

If now $A_2 \to 0$, it is only the vicinity of $\vartheta \to 0$ in the original distribution (that is in $Q\{\sin\vartheta, A_1\}$) which matters, and if we now assume that this distribution shows no singularity at $\vartheta = 0$, the distribution will become more and more isotropic (i.e. independent of $\sin\vartheta$ for $\vartheta < 90°$) as A decreases, regardless of its form at larger distances. At the same time the total number of particles associated with a given line of force decreases as A^{-3}.

Thus, once we know the number of particles spiralling at a given A_1 around every line of force (A_1 sufficiently small so that the Alfvén regime applies)

we possess as well all possible information about the particles at all smaller values of A, (or of smaller rigidity P when we make use of the inverse Störmer transformation). We know the points of impact since the particles follow the lines of force (with a maximum relative deviation $\propto A^2$), we know their intensity since it varies as A^{-3}, and we know their angular distribution, which is isotropic (strictly only for $\vartheta < 90°$ and neglecting the shadow effect of the earth. This is of no consequence in the limit $A \to 0$ since the lines of force in the allowed region there approach the vertical).

It therefore remains only to determine the number of particles associated with all lines of force (outside the forbidden belt), given a distribution of sources in infinity. To do this we reserve the argument and follow the trajectories form some small distance backwards to large distances and eventually to infinity. If we start at a very small $A = A_2$ where the pitch angle of a certain particle is ϑ ($< 90°$), we know that at a larger $A = A_1 \gg A_2$ (A_1 in the Alfvén region) the pitch angle had been smaller by $(A_2/A_1)^2$; therefore for large A (but still in the Alfvén region) the trajectory must have been very closely parallel to a line of force and therefore also to a Nullbahn, since in this region the Nullbahnen make a contact of high order with the lines of force (up to A^4 for the dependence of the latitude on A). Therefore all particles found at the same small A to be circulating around the same line of force —including the Nullbahn osculating that line of force—must have come from an infinitesimal vicinity of a point in phase space at infinity—infinitesimal, if A can be considered infinitesimal.

To find that point it is only necessary to follow any one of these trajectories back to infinity. This has to be done by numerical integration. The natural choice is to select for this purpose the Nullbahn osculating the line of force considered. By calculating all Nullbahnen, one then knows where every particle has come from that reaches the earth at a small A (i.e. with a momentum well below $10\ \mathrm{GeV} \cdot Z/c$). Since the assumed dipole field possesses an axis of symmetry, it is only necessary to calculate the one-parametric set of Nullbahnen which have at infinity (or alternatively at $A \to 0$) a certain longitude (which can be assumed to be zero). In continuation of earlier numerical work by C. Störmer, and using his methods, this has been done by R. Lüst and A. Schlüter to a sufficient extent for our present purpose. The Fig. 1 and 2 give a graphical representation of their results (*).

As parameter which uniquely determines the individual Nullbahn, the quantity 2γ ($0 \leqslant 2\gamma \leqslant 2$) has been used; 2γ is defined as the angular momentum component around the axis of symmetry in the non-dimensional units of Störmer and has as such been introduced by Störmer (however with the

(*) The present author wishes to express his thanks to these authors for their kind permission to use their results prior to publication.

opposite sign). The upper part of Fig. 1 gives the latitude (more precisely the distance u from the south-pole) at infinity as a function of 2γ. The middle part gives the change in longitude between infinity and $A \to 0$. The indicated local time holds for positively charged particles starting at infinity on

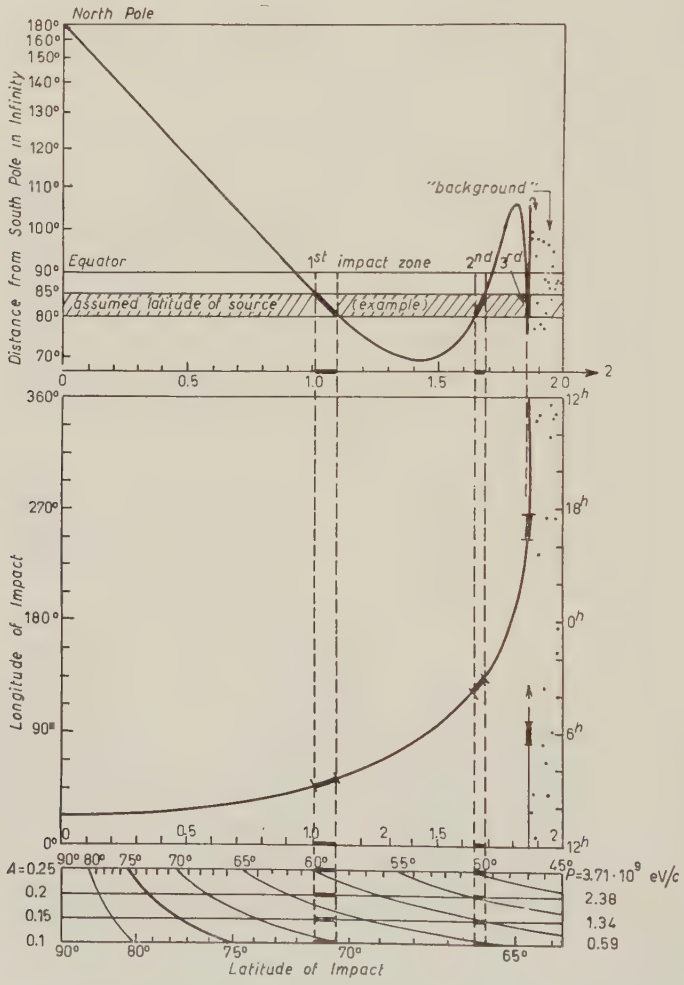

Fig. 1.

the 1200 hour-meridian. In the lower part of Fig. 1 the latitude ε is given at which the Nullbahnen of different 2γ and of the four different energies indicated intersect the surface of the earth. The figure refers only to Nullbahnen impinging on the northern hemisphere. For 2γ approaching 2 the Nullbahnen become more and more complicated, and it was not possible to

draw continuous lines in this region. Fig. 2 is a blow up of the region $1.8 \leqslant 2\gamma \leqslant 2$. For $2\gamma > 1.863$ the values of n and v are indicated by points which are equally spaced in 2γ at intervals of 0.005, except for a few Nullbahnen (indicated by x) which were too complicated even for the electric computer employed. In the upper part of Fig. 2 the points scatter around the equator not deviating from it by more than 14 degrees. The points of impact are distributed almost at random in longitude (middle part of Fig. 2) while they occupy for a fixed rigidity only a very narrow belt in latitude (lower part of Fig. 1) which is close to the forbidden belt around the equator.

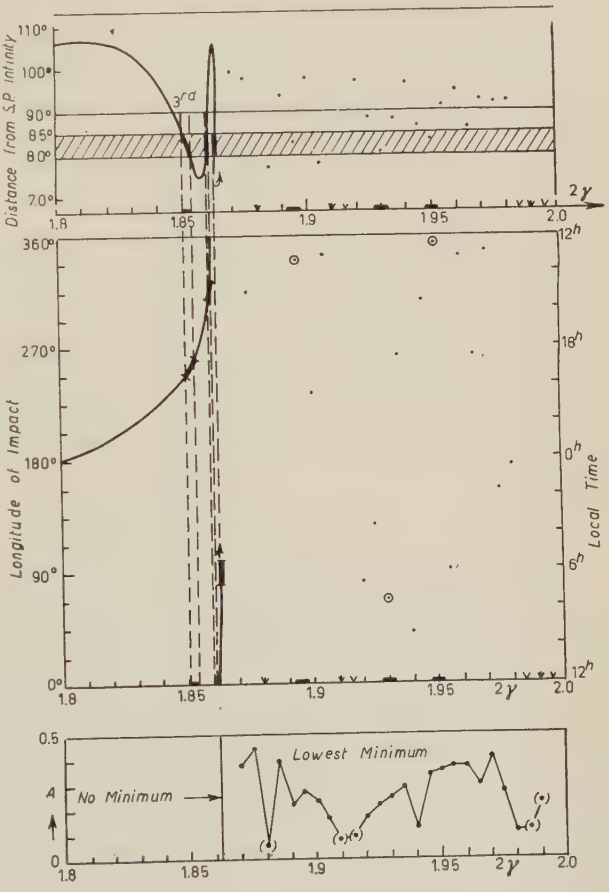

Fig. 2.

The use of these graphs may be illustrated by an example. Assume a source of particles at infinity at 5° to 10° south of the equator ($n = 85° \div 80°$). Particles from this source can travel along groups of Nullbahnen around distinct values of 2γ which intersect the earth at different locations, in the vicinity of which then *all* particles of low momentum have to arrive, forming impact zones on the earth as first described by the author. The impact zone of lowest 2γ (1-st impact zone) corresponds in this example to $2\gamma \approx 1.05$, the particles arrive at $\lambda \approx 8$ hours (positive particles, source at noon) and at a latitude of, for example, $r \approx 64°$ N if their momentum $P = 2.4 \cdot 10^9 \text{ eV} \cdot Z/c$. The second impact zone corresponds to $2\gamma \approx 1.67$; $\lambda \approx 3$ hours; and $v \approx 55°$ N. For the third: $2\gamma \approx 1.85$; $\lambda = 19$ hours; and $r \approx 53°$ N. Then follows an infinite series of Nullbahnen at almost the same γ (and therefore almost the same r) having widely different

deflections in longitude. Finally out of the 28 trajectories calculated in the completely confused region $2\gamma > 1.863$, three contribute to the Nullbahnen in the range considered in this example.

We are now in the possession of all information to answer a question of the following kind: At a certain location on the earth, particles of a certain energy (in the Alfvén region) have been observed—where on the sky outside the earth's magnetic field have they come from? We can however not yet answer the following additional question: The observed intensity of these particles was such and such—what was the intensity at the source? Nor can we answer the opposite question: Given a distribution of sources at infinity, what will be the distribution of the intensity for the different impact zones on the earth?

To answer these questions we must find in addition to the information contained in the Fig. 1 and 2, a relation between the intensities at infinity:

$$S\{P, \cos n, \lambda\}\, \mathrm{d}P\, \mathrm{d}\cos n\, \mathrm{d}\lambda \qquad \text{(source-function)}$$

and the occupation function for the different Nullbahnen

$$C\{P, 2\gamma, \lambda\}\, \mathrm{d}P\, \mathrm{d}(2\gamma)\, \mathrm{d}\lambda \qquad \text{(occupation-function)}.$$

We define precisely: $S\,\mathrm{d}P\,\mathrm{d}\,(\cos n)\,\mathrm{d}\lambda$ is the number of particles per steradian emitted by the surface element of the sky $\mathrm{d}(\cos n)\,\mathrm{d}\lambda$ in the momentum range $\mathrm{d}P$ into the solid angle occupied by the earth as seen from the source, making the obvious assumption that S is constant over this infinitesimal solid angle. Furthermore: $C\,\mathrm{d}P\,\mathrm{d}2\gamma\,\mathrm{d}\lambda$ is the number of particles per steradian of momentum $P \ldots P+\mathrm{d}P$, associated with the Nullbahnen arriving in the longitude range $\mathrm{d}\lambda$ and in the latitude range corresponding to $2\gamma \ldots 2\gamma + \mathrm{d}(2\gamma)$. We recall that the distribution over the angle ϑ may be assumed to be isotropic. Because of the axial symmetry of the magnetic field, the elements of longitude $\mathrm{d}\lambda$ transform between source and receiver as 1:1, the value of the deflection in longitude being known (cfr. the middle parts of the figures). We therefore drop the explicit reference to the dependence on λ. As I shall show the desired relation is then simply

$$C(P, 2\gamma)\,\frac{AR^2}{2}\,S(P, \cos n)\,,$$

where values of 2γ and the latitude of the source $n - 90°$ corresponding to one another have to be taken (cf. the upper parts of the figures), and where

R = radius of the earth and

$$A = (P/59 \cdot 10^9 \text{ eV}(Z/c))^{\frac{1}{2}},$$

as before.

Before proceeding to prove this theorem let us illustrate its use. Consider again the example studied before: The source-function is known and equal to a constant (say = 1 in some units) in the range $80° \leqslant n \leqslant 85°$, and zero outside as indicated in the Figures. Let P be $2.4 \text{ GeV} \cdot Z/c$ so that $A = 0.2$. Then $C = 0.1 R^2$ for all values of 2γ such that $80° \leqslant n(2\gamma) \leqslant 85°$, ($n$ as a function of 2γ is plotted in the upper parts of Fig. 1 and 2) and $C = 0$ for all other 2γ. That is: C is different from 0 for the intervals of 2γ indicated by thick lines on the 2γ-axis of the plots.

The total intensity in a certain impact zone is then proportional to the width of these intervals. In the confused region $2\gamma > 1.863$, each calculated point may be considered as representative for an interval of 2γ equal to the spacing of the points. Since three points fall into the strip in n considered, a weight of 0.015 has to be ascribed to this background in this case. Table II gives some numerical information for the example con-

Table II.

$80° \leqslant n \leqslant 85°$ zone of impact	2γ	Longitude (local time)	Latitude at $A = 0.2$	Width in 2γ
1-st	1.05	8 h	62°.7 N	0.090
2-nd	1.66	3 h	54°.8	0.040
3-rd	1.852	19 h	51°.3	0.0030
4-th	1.861	15 h	51°.22	0.0005
5-th	1.863	6 h	51°.20	0.00002
« background »	$1.863 \div 2.00$	random	$51.2 \div 50.8$	≈ 0.015

sidered. The smallness of the contribution of the higher impact zones is particularly obvious in this case. In a similar fashion the distribution on the earth of the particles coming from a more general distribution of sources can be determined.

Now a preparatory remark to the promised proof of the relation between S and C. As has been said before the Nullbahnen follow very closely the lines of force in the Alfvén region. The equation of the line of force in a given meridional plane is $\cos^2 v/r = \text{const}$, where v is the latitude and r the distance from the dipole. It is easily proven that the particular line of force

to which a Nullbahn of given 2γ approaches, is simply given by

$$\cos^2 v/A = 2\lambda \qquad \text{(Störmer units)}.$$

If now $C\{P, 2\gamma\}$ is a continuous function of 2γ, the intensity of the particles I per surface element of the earth $\mathrm{d}^2F = R^2\,\mathrm{d}\sin r\,\mathrm{d}\lambda$ (R = earth's radius) follows as:

$$I\{P, \sin v\}\,\mathrm{d}^2F = C\{P, 2\gamma(P, \sin v)\}\,\frac{1}{R^2}\,\frac{\partial 2\gamma}{\partial \sin v}\,\mathrm{d}^2F\,,$$

where the λ-dependence has again been dropped and where the partial derivative has to be evaluated at constant P (i.e. constant A). According to the relation given, this derivative is

$$\frac{\partial 2\gamma}{\partial \sin v} = \frac{2}{A}\sqrt{1-2\gamma A}\,,$$

or to the lowest order in A to which we want to restrict ourselves:

$$\approx \frac{2}{A}\,.$$

Therefore

$$I\{P, \sin v\} = 2C\{P, 2\gamma\}/AR^2,$$

where $|\sin v| = \sqrt{1-2\gamma A} > \sqrt{1-2A}$; $P^{\frac{1}{2}} \propto A \ll 0.5$ as before. (I is closely related to Q introduced earlier, the latter refers to Störmer units however. The $A^{-1}\cdot R^{-2}$ dependence of I for fixed C corresponds to the A^{-3} dependence of Q along a line of force, i.e. for fixed 2γ).

Using now the intensity on the earth I, rather than the occupation function C the relation to be proved is simply

$$I\{P, \sin v\} = S\{P, \cos n\}\,,$$

where v and n have to be chosen so as to correspond to the same 2γ. For $|\sin v| < \sqrt{1-2A}$ to which $2\gamma > 2$ would correspond, $I \equiv 0$, since these latitudes correspond to the interior of the forbidden belt around the equator.

The proof of the identity $I = S$ now rests on Liouville's theorem. This states when applied to our problem that an isotropic distribution of sources at infinity leads to the same intensity everywhere on the earth where trajectories exist which connect the point of impact with infinity. Since now in our approximation only that part of the sky contributes to which the same 2γ corresponds (and which has a longitude corresponding to the calculated deflection in λ), the intensity in other parts of the sky does not matter and we arrive at the stated relation.

We have to add two remarks to this proof concerning the neglect of absorption in applying Liouville's theorem. Absorption of course occurs on the surface of the earth (or within its atmosphere which amounts to the same thing for the present argument). This affects the particles of a pitch angle close to 90° and larger than the angle between the line of force and the horizontal. This effect seems to be of no particular importance, since these particles of grazing incidence are rarely ever observed. It also disappears in the limit $A \to 0$.

Absorption also plays a rôle under the following circumstances: Assume a trajectory coming from infinity entering the Alfvén region spiralling around a line of force (or equivalently around a Nullbahn) returning at $A = 0.22$ (say) traversing again the large deflection region and re-entering the Alfvén region and finally reaching $A = 0$. This is a Nullbahn and it is necessary to account for the contribution made by the trajectories associated with it if we are interested in rigidities corresponding to $A < 0.22$. If however the rigidity is larger than this, then these particles would be absorbed before arriving at the impact zone corresponding to the eventual v and λ of this Nullbahn for $A \to 0$. At the first passage through the Alfvén region preceding the assumed minimum at $A = 0.22$ the particles including the Nullbahn are counted as belonging to the Nullbahn around which they are circulating in this region. We therefore arrive at the rule not to count the contribution of those Nullbahnen which have a minimum at an A which is smaller than that corresponding to the rigidity considered. The Nullbahnen of a $2\gamma < 1.863$ do not show a minimum (other than $A = 0$). Corresponding, this effect is restricted to the region contributing to the « background ». In the lower part of Fig. 2 the lowest minima along the calculated Nullbahnen are given. For the few unfinished Nullbahnen the lowest minimum encountered before breaking off has been given. It is seen that at $A \approx 0.2$ the diminution of the « background » due to this effect is quite noticeable.

In concluding, I should like to make a remark on the accuracy of the procedure employed. We have used Alfvén's method of treating the motion of a charged particle in an inhomogeneous magnetic field only in the simplest approximation by taking the particles as spiralling around a fixed line of force. In the next approximation the inhomogeneity of the field and particularly the curvature of its lines of force leads to a shift in longitude also in the Alfvén region, the amount depending on the rigidity and on the pitch angle. Consequently our results are more precise as to the latitudes rather than to the longitudes of impact derived.

* * *

I should like to thank R. LÜST for discussions on this subject and K. KATTERBACH for the preparation of the graphs.

SUPPLEMENTO AL VOLUME VIII, SERIE X
DEL NUOVO CIMENTO

N. 2, 1958
2° Trimestre

True Primary Energy Spectrum Variations and Solar Activity.

L. I. Dorman and E. L. Feinberg

Scientific Institute for Terrestrial Magnetism, Ionosphere and Propagation of Radio Waves - Moscow
P. N. Lebedev Physical Institute, USSR Academy of Sciences - Moscow

1. – The determination of true primary energy spectrum variations for high energies ($\sim 10^{10}$ eV) requires μ-meson variations data. Thus we must be able 1) to eliminate from the data the meteorological variations, and 2) to use the data subsequently in order to obtain the true primary variations from secondary ones.

A method for eliminating atmospheric effects had been proposed and developed in the Soviet Union in 1946-1951 [1-5] and extensively tested and applied. (Similar methods were lately developed by Olbert [6], Maeda and Wada [7] and others). It was briefly communicated in Guanajuato [5]. Here we report: 1) its extension to meteorological effects of the neutron and the soft components, etc.; 2) additional cases of its check; 3) its application to deduction of true variations, essential in connection with solar activity, namely, of long-term and seasonal changes of diurnal variations and for the determination of the direction to the source of diurnal variations. The results in many points differ from those of other investigators, who did not use this method. After elimination of atmospheric effects (which, in some cases are inessential) we obtain primary variations in a number of cases using the « coupling coefficient method », which is an extension of the Neher [8] and Simpson [9] procedure. We find the energy spectrum of the 23 February 1956 solar flare, and some more crude results for previous flares.

2. – It has been shown by the present authors [1, 2, 4] that the expected meteorological variations of μ-mesons are equal to a sum of a simple barometric effect and of an integral over the atmosphere

$$\frac{\delta N_\mu}{N_\mu} = \beta \delta h_0 + \int_0^{h_0} W_\mu(h') \, \delta T(h') \, \mathrm{d}h' \,. \tag{1}$$

Here enter: 1) the temperature coefficient density $W_\mu(h')$, which has been already tabulated for a variety of experimental conditions (various depths in the atmosphere and underground, various inclinations of telescopes, etc [2, 4, 5]). It differs somewhat from that found later by MAEDA and WADA [7]; 2) variation of temperature $\delta T(h')$ at various isobaric levels which is taken from radioballoon data. No arbitrary parameters enter the calculations. Let us demonstrate new cases of application of this method.

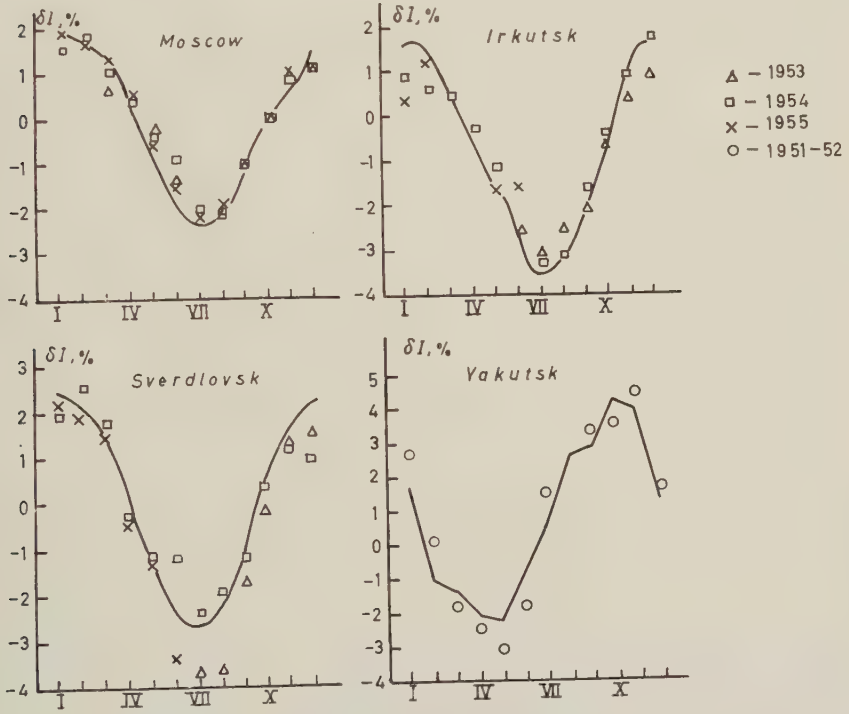

Fig. 1. – Seasonal variations of hard component intensity at four stations at sea level: Moscow, Irkutsk, Sverdlovsk, Yakutsk. Curve: calculated average meteorological variations; triangles: measured for 1953; squares: for 1954; crosses: for 1955; circles: IV-1951 – III-1952.

1) Take the seasonal variations. In Fig. 1 we give the results of a few years of ion chamber measurements at four Soviet sea level stations. It is seen that the observed seasonal variations almost completely reduce to the meteorological ones. The same conclusion was communicated by us in Guanajuato. It was recently drawn also by BACHELET and CONFORTO from their own measurements [10].

2) Now take the diurnal μ-mesons variations. Their amplitude is known to change from season to season. This, if true for primary variations, could lead to various important conclusions concerning their origin (for instance, to a conclusion on existence of sidereal variations). However, if meteorology is excluded properly, then the amplitude and the phase remain practically constant throughout the year. In Fig. 2 we see the harmonic dial where calculated meteorological variations explain almost completely the seasonal changes of phase and amplitude of diurnal variations [20].

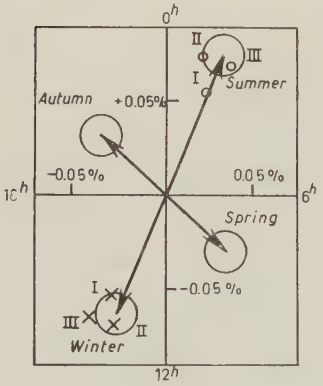

Fig. 2. – Excess of diurnal variations for various seasons over the average for the year in Moscow. Crosses and small circles: calculated meteorological excess; I: taking into account temperature variations up to 300 mb for the given station; II: the same as I, using the average data over various stations for several years; III: including upper levels according to a crude estimation. Arrows: measurements; large circles: probable error.

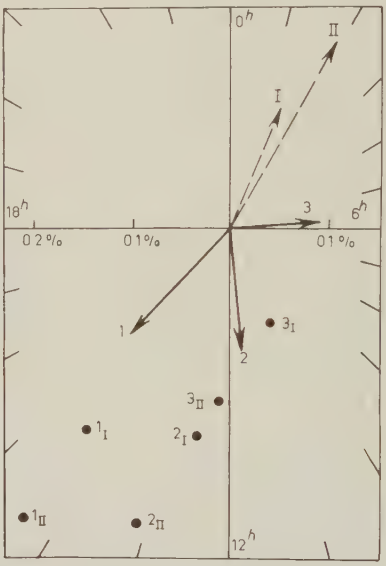

Fig. 3. – Diurnal variations measured: 1. Cheltenham, 1946; 2. Moscow, 1951-1952; 3. Moscow, 1953-1954 (arrows). Calculated temperature variations (dotted arrows). Black points: corresponding diurnal variations after temperature variations are excluded: I: variations of temperature up to 300 mb level are taken into account; II: a crude estimate of upper stratosphere included.

3) Take the long-term changes of diurnal variations, Fig. 3 [20]. Heavy arrows are vectors of observed variations: 1. Cheltenham, 1946; 2. Moscow, 1951-1952; 3. Moscow, 1953-1954. One could suppose that his vector is rapidly and systematically displaced during the period from 1946 (almost the maximum of solar activity) to 1954 (a minimum). However, if we subtract meteorological variations (dotted arrows), then we receive quite another

picture: points 1_I, 2_I, 3_I are received when we take into account variations of meteorological conditions in the atmosphere up to the level of 300 mb, points 1_{II}, 2_{II}, 3_{II} if we roughly include the upper stratosphere. The phases of maxima are now close to each other.

This method of eliminating meteorology is now limited only by the accuracy of temperature data. It is used sistematically at all Soviet stations for permanent recording of cosmic rays. Applied to underground measurements it enables, vice versa, to measure the temperature of the upper stratosphere. We give in the appendix the additional details of the method: formulas and graphs for meteorological correction in the cases of soft and neutron components. We would like to mention here merely that the results for the soft component explain quantitatively why its diurnal variations are so large and why the seasonal variations are so small, as well as why its barometric effect is so large.

3. – When the meteorological influences are thus eliminated all the data may be used for the determination of primary energy spectra of variations, since the observed variation of the i-th component at the latitude λ is [2*b*, 4, 5]:

$$\frac{\delta^j N_\lambda^i}{N_\lambda^i} = \int_{\varepsilon_\lambda^{\min}}^{\infty} \frac{\delta^j D(\varepsilon)}{D(\varepsilon)} W_\lambda^i(\varepsilon)\, \mathrm{d}\varepsilon \,. \tag{2}$$

$D(\varepsilon)$ is primary spectrum, $\delta^j D(\varepsilon)$ its variation (j means « diurnal », « seasonal », etc.); $W_\lambda^i(\varepsilon)$ is a « coupling coefficient », found from latitude effect. In some cases it was found when $\delta^j D(\varepsilon)$ was known from other data (in appendix we give $W_\lambda^i(\varepsilon)$ for soft μ-mesons found from $\delta^j D(\varepsilon)$ determined using neutron variations during the last solar flare). It is now tabulated for many cases (part of them was reported by us at the Guanajuato conference[5]; for the neutron component at sea level and 10 km altitude, for large air showers and large underground depth for μ-mesons, and for total ionization at 10 km

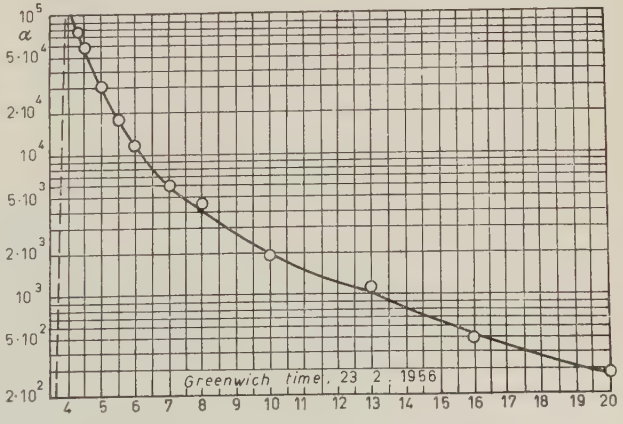

Fig. 4. – Temporal change of intensity factor a (see eq. (3)) during the solar flare 23.II.1956.

altitude we are giving them here). It has been realized by ALFVÉN, SIMPSON and others that neutron and μ-meson variations determine $\delta' D(\varepsilon)$ correspondingly for low and high ε. We use equation (2) to determine $\delta' D(\varepsilon)$, which fit all the data for variation $\delta' N$. Even now, when the data are rather scarce, the results deserve quotation.

1) For the solar flare 23 February 1956 we get for the period of isotropy:

$$\frac{\delta D(\varepsilon)}{D(\varepsilon)} = a(t)\varepsilon^{-5\pm0.5} . \tag{3}$$

The temporal change of $a(t)$ is shown in Fig. 4. This spectrum agrees with that found by SIMPSON *et al.* [11] for American stations. Determination of spectra for various moments of time was made using differences in intensities registered by various pairs of stations situated on different latitudes and approximately the same longitude. These spectra are shown in Fig. 5. It shows that spectra remain unchanged during almost 6 hours. Difference between intensities in Europe and America is easily established. It agrees with the difference in normal intensities if we pay due attention to the difference in energy spectra of the normal cosmic ray stream, on the one hand, and the solar flare variation spectra, on the other [4]. Therefore, it agrees with the results by SIMPSON *et al.* [11] and by WADDINGTON [12].

2) For previous large flares data are scarce. However, it seems likely that spectra for them were harder, possibly of the kind of $\delta D/D \sim \varepsilon^{-2} \div \varepsilon^{-3}$ (19 September 1949).

3) For diurnal variations $\delta D(\varepsilon)$ is found in the following way:

We assume various (five) forms of δD, calculate from (2) resulting $\delta N/N$ and compare it with data of observations (see Table I). For the beginning we leave aside the data for $\lambda = 80°$; due to the geomagnetic field, particles come here from the directions which form with the geomagnetic equator very large angles φ, $\varphi \sim \pi/2$. Then all other data clearly favour the spectrum:

$$\frac{\delta D(\varepsilon)}{D(\varepsilon)} = \begin{cases} 0 , & \varepsilon < \varepsilon_1 \approx 7 \text{ GeV} , \\ \dfrac{a}{\varepsilon} , & \varepsilon > \varepsilon_1 \approx 7 \text{ GeV} . \end{cases} \tag{4}$$

The spectrum thus found, we may approximately find a for large λ, i.e. for large φ (the intensity of the source depends on φ). It turns out that the best fit is given by

$$a(\varphi = 0°) \approx 0.17$$
$$a(\varphi = 26°) \approx 0.14 \qquad (\lambda = 50° \text{ for hard component})$$
$$a(\varphi = 75°) \approx 0.05 .$$

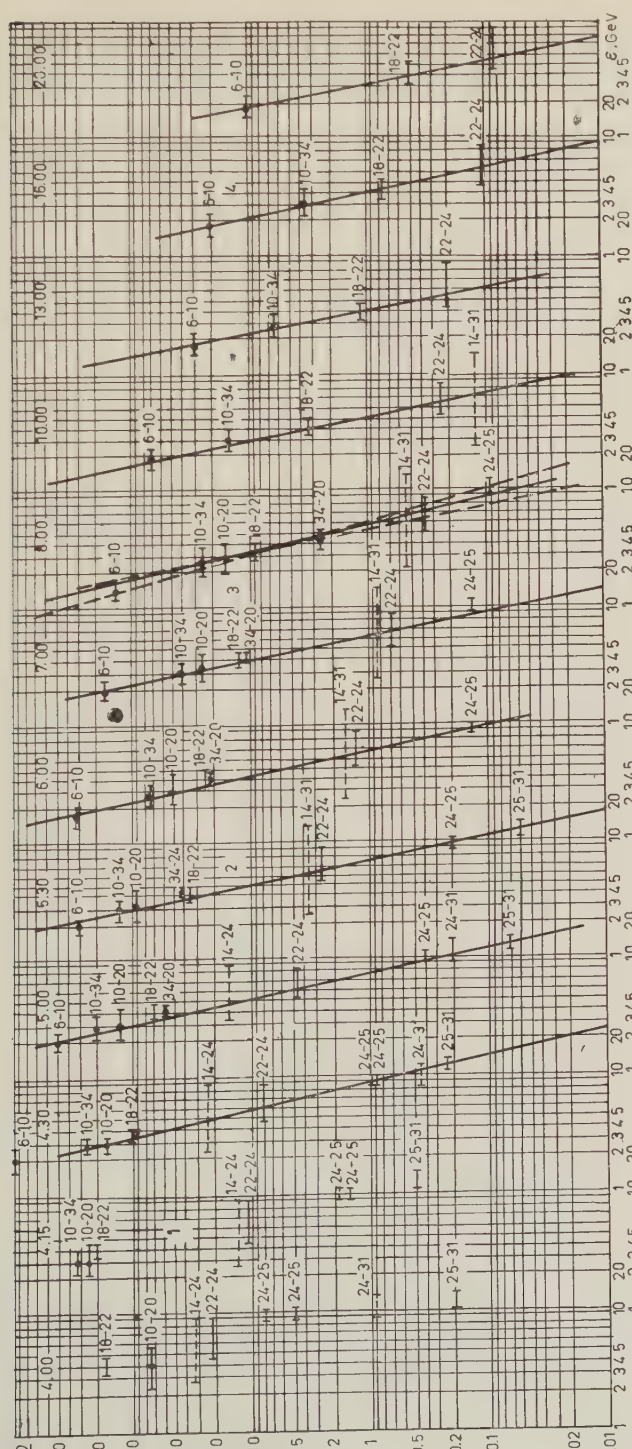

Fig. 5. – Energy spectra of additional cosmic ray streams in various moments (4 h, 4 h 15 m, 4 h 30 m, ..., 20 h) for the solar flare 23.II.1956. Pairs of numbers designate station numbers of used stations records according to the list in ref. [4].

TABLE I. – *Observed and calculated amplitudes of diurnal variations (meteorological effect eliminated).*

	Ionizing component $h_0 = 0$			Ionizing component $h_0 = 700$ g/cm²			Neutrons $h_0 = 700$ g/cm²			Hard component at sea level		
Latitude	0°	50°	80°	0°	50°	80°	0°	50°	80°	0°	50°	80°
Experiment	?	$\lesssim 1$	?	0.3 ± 0.1	?	?	0.43 ± 0.1	0.6 ± 0.1	?	0.3 ± 0.1	0.30	0.09 ± 0.03
Supposed spectra of variations												
I $\frac{\delta D}{D} = a$, $a = 0.003$	0.3	0.3	0.3	0.3	0.3	0.3	0.3	0.3	0.3	0.3	0.3	0.3
II $\frac{\delta D}{D} = \frac{a}{\varepsilon}$, $a = 0.14$	0.57	2.7	4.0	0.23	0.94	1.2	0.38	1.60	1.95	0.27	0.30	0.3
III $\frac{\delta D}{D} = \frac{a}{\varepsilon^2}$, $a = 2.95$	0.33	17	39	0.13	3.3	4.5	0.41	6	13	0.17	0.30	0.3
IV $\frac{\delta D}{D} = \begin{cases} 0 \text{ for } \varepsilon < \varepsilon_1 \\ a \text{ for } \varepsilon > \varepsilon_1 \end{cases}$	$\leqslant 0.3$	< 0.3	< 0.3	$\leqslant 0.3$	$\leqslant 0.3$	0.3	$\leqslant 0.3$	$\leqslant 0.3$	$\leqslant 0.3$	$\leqslant 0.3$	0.30	0.3
$a = 0.14$, ε_1 arbitrary												
V $\frac{\delta D}{D} = \begin{cases} 0 \text{ for } \varepsilon < \varepsilon_1 \\ \varepsilon \text{ for } \varepsilon > \varepsilon_1 \end{cases}$	0.57	0.48	0.32	0.23	0.46	0.44	0.38	0.60	0.56	0.27	0.30 Normalization point determining a	0.3
$a = 0.14$; $\varepsilon_1 = 7$ GeV												

Now, with this $\delta D(\varepsilon)$, we reconstructed the trajectories of particles in the field of Earth's magnetic dipole, using Brunberg's calculations. We receive thus for every diurnal effect the direction to the source of variations, given by two angles: χ formed by its projection on the ecliptics plane with the direction Earth-Sun, and q formed by it with the same plane. They are given in Table II for ten components (Instead of distribution, only some averages over E, χ_{eff} and q_{eff} are given). It follows from the table, that all components have the source of their variation to the left of the line Earth-Sun, $\chi_{\text{eff}} \approx \approx 82^\circ \pm 8^\circ$, although, due to the differences in energies of primaries, which are responsible for a given component, their observed times of maxima $t^i_{\max,\lambda}$ are scattered within ~ 4 hours $= 4^\circ.15 = 60^\circ$ $(\chi^i_\lambda = \psi^i_\lambda + 15^\circ$ $(t^i_{\max,\lambda} - 12))$.

TABLE II.

	Component	ψ^i_λ	χ^i_{eff}	Observed time of maximum	φ^i_{eff}
	Hard, global, sea level	62°	78° ± 8°	$13^h \pm 0.5$	0°
$\lambda = 0°$	Ionizing $h = 700$ g/cm²	69°	84° ± 8°	$13^h \pm 0.5$	0°
	Neutrons $h = 700$ g/cm²	91°	91° ± 15°	$12^h \pm 1$	0°
	Hard, global, sea level	38°	84° ± 8°	$15^h \pm 0.5$	26°
	Hard 32° to the south	23°	83° ± 8°	$16^h \pm 0.5$	14°
$\lambda = 50°$	Hard 32° to the north	61°	76° ± 8°	$13^h \pm 0.5$	17°
	Hard 48° to the east	52°	82° ± 8°	$14^h \pm 0.5$	− 9°
	Hard 48° to the west	9°	84° ± 8°	$17^h \pm 0.5$	39°
	Neutrons $h = 700$ g/cm²	45°	75° ± 8°	$14^h \pm 0.5$	− 1.4°
$\lambda = 80°$	Hard, sea level	24°	84° ± 15°	$16^h \pm 1$	75°
	Average:		82°		

This was found for the 1937-1946 observations. If, by a similar method, we look for χ_{eff} in other years, we find that it is displaced. Its variation during the last 24 years was earlier obtained by a number of investigators, who simply used the observed time of maximum $t_{\max}$ and supposed that all primaries have some effective energy, $\varepsilon_{\text{eff}} = 21$ GeV. Then the reconstruction gives χ_{eff} in Fig. 6. If in a similar manner we add points for 1953-1955 then this χ_{eff} varies drastically, from $+100°$ to $-60°$.

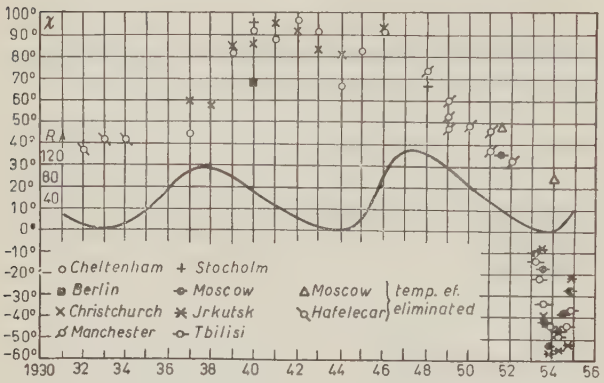

Fig. 6. – Effective angle χ showing the direction to the source of diurnal variations for the years 1930-1955. Curve: solar activity, measured by the Wolff number R.

However, here neither the meteorological variations were eliminated, nor was the whole spectrum of variations $\delta^j D(\varepsilon)$ known. Taking both of these facts into account we recalculate all the data and receive instead Fig. 7. It clearly shows that no such drastic change of χ_{eff} occurs. It changes only from $+90°$ to $+20°$, the source of extra cosmic rays flow remaining always to the left of the line Earth-Sun. The amplitude is almost constant and diminishes considerably exactly when χ is small. This long term displacement of the effective source is very important for the theory of origin of cosmic rays variations. It may be clarified by the fact discovered by SARABHAI *et al.* [13] who have recently shown that the diurnal variations split up into two waves, the location of their maxima differing by approximately 6 hours $\approx 90°$ and their relative

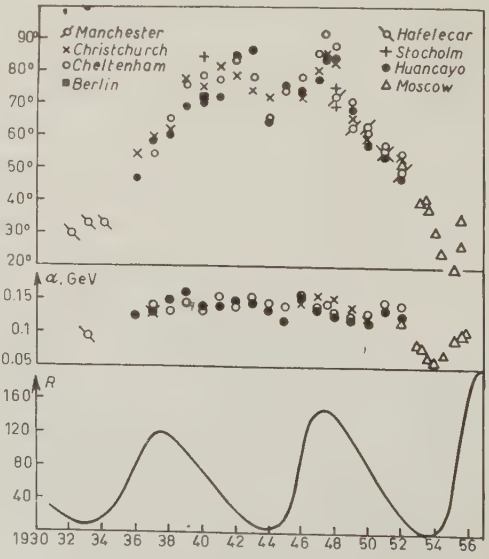

Fig. 7. – The same as Fig. 6, meteorological variations consistently eliminated, the energy spectrum of variations used for reconstruction of trajectories. a: amplitude of variation in energy spectrum.

intensities varying with a 22-years periodicity. This circumstance must play and outstanding rôle in the problem of the origin of cosmic rays variations.

Appendix

1. Meteorological effects of the soft and general components [14].

The soft component consists of equilibrium and non-equilibrium parts. The former, in turn, is composed of decay electrons from μ-mesons and of δ-electrons as well as of the products of their cascade multiplication in the atmosphere. If the soft component is separated with the aid of an absorber, then also soft μ-mesons and nucleons will incorporate therein.

1·1. *Variations of decay electrons.* – Let E^{dec} be the average energy transferred from μ-meson to decay electrons over one t unit, ε_0 the energy lost by the electrons on the same path. Then the total number n_e^{dec} of decay electrons together with the multiplication products may be found from the condition $n_e^{\mathrm{dec}}\varepsilon_0 = E^{\mathrm{dec}}$. Taking into account that the probability of μ-mesons disintegration per 1 cm is $m_\mu/\tau_\mu p_\mu$, we shall find the total number of decay electrons

$$N_e^{\mathrm{dec}} = \int_{m_\mu c^2}^{\infty} \frac{t m_\mu \varepsilon_\mu D(\varepsilon_\mu)\,\mathrm{d}\varepsilon_\mu}{3\varepsilon_0 \tau_\mu p_\mu}\,, \tag{1.1}$$

where m_μ and τ_μ are the mass and life time of μ-meson at rest, ε_μ and p_μ the full energy and the momentum of μ-mesons, and $D(\varepsilon_\mu)$ is the spectrum of μ-mesons at the observation level.

Varying (1.1) over t and $D(\varepsilon_\mu)$, we shall obtain

$$\frac{\delta N_e^{\mathrm{dec}}}{N_e^{\mathrm{dec}}} = \frac{\delta t}{t} + \frac{\displaystyle\int_{m_\mu c^2}^{\infty} \left(\frac{\varepsilon_\mu}{p_\mu}\right) \delta D(\varepsilon_\mu)\,\mathrm{d}\varepsilon_\mu}{\displaystyle\int_{m_\mu c^2}^{\infty} \left(\frac{\varepsilon_\mu}{p_\mu}\right) D(\varepsilon_\mu)\,\mathrm{d}\varepsilon_\mu}\,. \tag{1.2}$$

For the major part of μ-mesons (about 97 %), $\varepsilon_\mu/p_\mu \approx \mathrm{const} = C$. Taking into account that

$$t \sim \frac{1}{\varrho(h_0)} \sim \frac{T(h_0)}{h_0} \quad \text{and} \quad \frac{\delta t}{t} = -\frac{\delta h_0}{h_0} + \frac{\delta T(h_0)}{T(h_0)}\,,$$

we shall obtain

$$\frac{\delta N_e^{dec}}{N_e^{dec}} = -\frac{\delta h_0}{h_0} + \frac{\delta T(h_0)}{T(h_0)} + \frac{\delta N_\mu}{N_\mu},$$

where $\delta N_\mu / N_\mu$ is the variation of μ-meson intensity at the observation level.

1·2. *Variations of δ-electrons.* – The intensity of δ-electrons N_e^δ is approximately equal to $\int_{m_\mu c^2}^{\infty} A D(\varepsilon_\mu)\, d\varepsilon_\mu$, where A is a coefficient but slightly dependent on the energy of μ-mesons and independent of the atmospheric conditions. Hence we obtain

$$\frac{\delta N_e^\delta}{N_e^\delta} \approx \frac{\delta N_\mu}{N_\mu}. \tag{1.4}$$

1·3. *Variations of the non-equilibrium part.* – Since $N_e^{NE} \sim \exp[-h_0/L]$, we have:

$$\frac{\delta N_e^{NE}}{N_e^{NE}} = -\frac{\delta h_0}{L}, \tag{1.5}$$

where $L \approx 120$ g/cm².

1·4. *Net variations.* – If N_e is the total number of soft component electrons at a given level h_0 and

$$N_e^{dec} = \alpha N_e; \quad N_e^\delta = \beta N_e; \quad N_e^{NE} = \gamma N_e; \quad \alpha + \beta + \gamma = 1,$$

then

$$\frac{\delta N_e}{N_e} = \alpha \frac{\delta N_e^{dec}}{N_e^{dec}} + \beta \frac{\delta N_e^\delta}{N_e^\delta} + \gamma \frac{\delta N_e^{NE}}{N_e^{NE}}. \tag{1.6}$$

Hence on the basis of (1.3), (1.4), (1.5) and (1.6) we shall obtain for sea level ($h_0 = 1030$ g/cm²; $T(h_0) \approx 280$ °K; $\alpha \approx 0.5$; $\beta \approx 0.4$; $\gamma \approx 0.1$)

$$\frac{\delta N_e}{N_e} = -0.13 \frac{\%}{\text{mb}} \cdot \delta h_0 + 0.18 \frac{\%}{1\,^\circ\text{C}} \delta T(h_0) + 0.9 \frac{\delta N_\mu}{N_\mu}; \tag{1.7}$$

for mountain level ($h_0 = 650$ g/cm²; $T(h_0) \approx 250$ °K; $\alpha \approx 0{,}29$ $\beta \approx 0.14$; $\gamma - 0.57$)

$$\frac{\delta N_e}{N_e} = -0.53 \frac{\%}{\text{mb}} \cdot \delta h_0 + 0.12 \frac{\%}{1\,^\circ\text{C}} \cdot \delta T(h_0) + 0.43 \frac{\delta N_\mu}{N_\mu}; \tag{1.8}$$

and finally for the 10 km level ($h_0 \approx 300$ g/cm²; $T(h_0) \approx 225$ °K; $\alpha \approx 0.18$; $\beta \approx 0.04$; $\gamma \approx 0.78$)

$$\frac{\delta N_e}{N_e} = -0.72 \frac{\%}{\text{mb}} \cdot \delta h_0 + 0.08 \frac{\%}{1^\circ\,\text{C}} \cdot \delta T(h_0) + 0.22 \frac{\delta N_\mu}{N_\mu}; \tag{1.9}$$

Adding the variation of the μ-meson component, we shall obtain for the total component:—for sea level —

$$\frac{\delta N_{tot}}{N_{tot}} = -0.04\,\frac{\%}{\text{mb}}\cdot\delta h_0 + 0.05\,\frac{\%}{1\,^\circ\text{C}}\cdot\delta T\,(h_0) + 0.97\,\frac{\delta N_\mu}{N_\mu}\,; \tag{1.10}$$

for mountain level

$$\frac{\delta N_{tot}}{N_{tot}} = -0.38\,\frac{\%}{\text{mb}}\cdot\delta h_0 + 0.06\,\frac{\%}{1\,^\circ\text{C}}\cdot\delta T(h_0) + 0.70\,\frac{\delta N_\mu}{N_\mu}\,; \tag{1.11}$$

and for the 10 km level

$$\frac{\delta N_{tot}}{N_{tot}} = -0.57\,\frac{\%}{\text{mb}}\cdot\delta h_0 + 0.06\,\frac{\%}{1\,^\circ\text{C}}\cdot\delta T(h_0) + 0.38\,\frac{\delta N_\mu}{N_\mu}\,. \tag{1.12}$$

$\delta N_\mu/N_\mu$ in turn consists of barometric and temperature effects, the latter being determined by the change in distribution of the temperature over the whole atmosphere. Therefore variations for the general and soft components consist, of three effects:

a) The barometric one caused by decay electrons, by the electrons of the non-equilibrium part of the soft component and by μ-mesons.

b) The local temperature effect at observation level connected with decay electrons.

c) The temperature effect distributed over the atmosphere which is connected with μ-mesons.

In [15] where the soft component was investigated, it was found that it is closely connected with barometric pressure, the correlation coefficient reaching — 0.97. The barometric coefficient was found to be equal to $(-0.34 \pm 0.02)\%$/mb, while for the general component it proved to be only $(-0.18 \pm 0.01)\%$/mb and for the hard one $(-0.12 \pm 0.01)\%$/mb.

According to (1.7), the expected barometric coefficient (taking into account that μ-mesons generating the equilibrium part of the soft component are softer than those of the hard component) is equal to

$$-0.13\%/\text{mb} + 0.9(1 + 0.14)(-0.12 \pm 0.01)\%/\text{mb} = (-0.25 \pm 0.01)\%/\text{mb}\,.$$

In [15] the soft component contains soft μ-mesons which can be absorbed by Pb 10 cm thick. Since their barometric coefficient is about 1% (see [4], p. 126) and their share is about 10%, the expected barometric coefficient will be about $-0.25\cdot0.9 - 1.0\cdot1 \approx -0.33$ %/mb in good agreement with observations [15] $((-0.34 \pm 0.02)\%$/mb) and observations [16] $((-0.343 \pm 0.048)\%$/mb).

Somewhat peculiar should be the temperature effect of the soft component. The temperature effect distributed over the whole atmosphere and incorporated in $\delta N_\mu/N_\mu$ is negative. Bearing in mind the correlation between temperature distribution in the atmosphere and sea level temperature one should expect a certain correlation between $\delta N_\mu/N_\mu$ and the sea level temperature.

The method of unified temperature coefficient is based essentially on this circumstance. Its experimental values proved to be negative and equal to $-(0.1 \div 0.2)\,\%/^{\circ}C$. In the case of temperature variation of the soft component this effect will be, to some extent, compensated by the local positive temperature effect with coefficient $+0.18\%/^{\circ}C$; therefore the total temperature effect should be small and a certain effective net temperature coefficient should be close to zero. This is confirmed by the experimental data [15]. Since seasonal variations are mainly caused by the temperature effect which is small for the soft component, only correspondingly small seasonal variations of the soft component should be expected. This really takes place [15].

As was already mentioned previously, introduction of temperature corrections increases the amplitude of the 24 hours variation of the μ-meson component almost twice, up to the value of $(0.3 : 0.4)\%$. Since the influence of temperature variation on the intensity of the soft component is small, the observed 24 hours variations of this component should be close to the true 24 hours variations of μ-mesons with the amplitude $(0.3 \div 0.4)\%$. This really takes place [15].

2. – Temperature effect of the neutron component [14].

One of the advantages of measuring the intensity of neutrons by the method of their local generation in lead by fast neutrons coming from the air is that practically no effect due to the air density changes takes place and that only the barometric effect which can be easily taken into account is observed. This advantage, in turn, is due to the fact that chiefly stable particles, nucleons, participate in the process of neutron formation. However, a certain, though comparatively small, part of neutrons is generated by unstable particles. The maximum possible density effect which is connected with that part of neutrons was evaluated by Simpson *et al.* [9]. This evaluation was based on the method of considering the intensity of meteorological effects of μ-mesons [17] which as was shown in [2], proved to be erroneous. Taking into consideration the importance of considering even a small temperature effect when investigating certain variations in intensity of the neutron component of cosmic rays (especially annual and other variations) (*) we shall perform these evaluations more thoroughly.

The temperature effect of the intensity of the neutron component is caused by the participation of π- and μ-mesons in creation of nucleons. Now we consider each stage separately.

2·1. *The formation of neutrons by μ-mesons inside the monitor.* – We have to bear in mind two possibilities: the formation of neutrons by fast and slow μ-mesons. The fast μ-mesons, though with a very small probability, lead to nuclear transmutations with formation of neutrons. Since the intensity of μ-mesons is influenced by the temperature of the atmosphere to the extent

(*) Indeed, since seasonal temperature variations can attain 50 to 80 °C (for example, in Yakutsk) and since the value of the amplitude of expected annual variations of the extra atmospheric origin is of the order of one percent, effects of the order of 0.01% of 1 °C are essential.

determined by the density of the temperature coefficient $W_7^{\mu}(h)$, the neutron component should also be influenced by the temperature of the atmosphere, this influence will be determined by the coefficient $0.02\,W_7^{\mu}(h)$, since the neutrons generated by μ-mesons constitute about 0.02 of the whole number of neutrons recorded by the counter [9] (for sea level see curve 1 in Fig. 8, for mountain level the values quoted should be decreased approximatly 5 times).

When slowing down in the substance surrounding the counters the slow negative μ-mesons produce mesoatoms. The mesons in them are captured by the nuclei thus forming neutrons (in the average two neutrons per each captured μ-meson). The creation of about 3% of all recorded neutrons [9] is due to this process.

The slow μ-mesons are distinguished by a comparatively large temperature effect determined by the coefficient $W_T^{\mu}(h)_{\text{slow}}$. Therefore for the intensity of neutrons it is necessary to take into account the coefficient $0.03\,W_T^{\mu}(h)_{\text{slow}}$.

$W_T^{\mu}(h)_{\text{slow}}$ were calculated in [4] (see Fig. 11) for the μ-mesons absorbed by the lead screen with energy between 1.10^8 eV (μ-mesons at rest) and $4\cdot10^9$ eV (μ-mesons still remaining in the monitor). The curve 2 of Fig. 9 represents the temperature coefficient of neutrons at sea level connected with the effect under consideration (for mountain level the values given above should be decreased about 5 times).

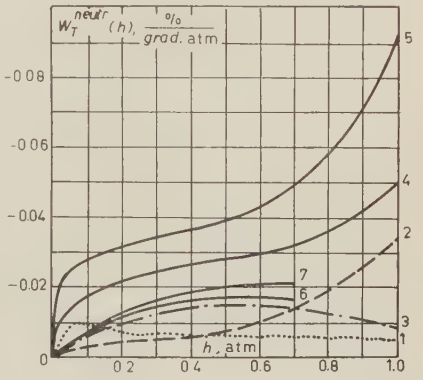

Fig. 8. – The temperature coefficient density for intensity of neutrons. 1 and 2: the contribution of fast and of slow μ-mesons for sea level, $\lambda = 50°$; 3: the contribution of π-mesons; 4 and 5: the net coefficients for sea level, $\lambda = 50°$ and 0° respectively; 6 and 7: the net coefficients for mountain level, $\lambda = 50°$ and 0° respectively.

2·2. *The effect of production of neutrons by π-mesons inside the monitor.* – Near the monitor π-mesons of low energy can be generated by the nucleon component. Some part of these π-mesons disintegrate while the rest cause nuclear disintegrations with generation of neutrons. The measurements by the method of photoemulsion show that π-mesons cause about 5% of all desintegrations [9].

The share of π-mesons captured by the nuclei is equal to

$$\varphi_{\text{abs}} = \frac{R_{\text{dec}}}{R_{\text{dec}} + R_{\text{abs}}} = \frac{p\tau_\pi \varrho}{p\tau_\pi \varrho + l m_\pi}, \tag{2.1}$$

where τ_π and m_π are the life time and the mass of a π-meson at rest, l the average path of π-mesons until the nuclear absorbtion, p the momentum of π-mesons and ϱ the density of the air. A respective change of this share induced by the change in density of the air at observation level h_0 is

$$\frac{\delta\varphi_{\text{abs}}}{\varphi_{\text{abs}}} = -\frac{\delta T(h_0)}{T(h_0)} \cdot \frac{l m_\pi}{p\tau_\pi \varrho + l m_\pi}. \tag{2.2}$$

Now we determine the local temperature coefficient of the intensity of neutrons representing the effect we consider; taking into account that about 5% of the registered neutrons are formed in this way and assuming in (2.2) $\varrho = 10^{-3}$ g cm^{-3}, $T(h_0) = 270$ °K, we see that, for $\bar{p} = 10^9$ eV/c, the temperature coefficient of local origin $\alpha_{\text{temp.}} = -0.016\,\%/\,^\circ\text{C}$ and, with $\bar{p} = 10^{10}$ eV/c, $\alpha_{\text{temp.}} = -0.008\,\%/\,^\circ\text{C}$.

2·3. *The effect of π-meson participation in the nucleon cascade.* – At present the process of formation of the nucleon component and the role of unstable particles in this process are not clear enough. We shall try to take approximately into account this role, using the results of ref. [18] and the coupling coefficients for the neutron component (Fig. 9)

According to ref. [18], primary protons with the energy $\lesssim 7\cdot10^9$ eV (average energy $\approx 3\cdot10^9$ eV) transfer about 60% of their energy to nucleons and only 25% to charged π-mesons; at the same time protons with the energy $\gtrsim 7\cdot10^9$ (average energy about $20\cdot10^9$ eV) transfer considerably larger part of their energy, about 50%, to charged π-mesons. It follows from the coupling coefficient for the neutron component that at sea level at the latitude of 50° about one third of the neutrons are produced by the primary particles with energy $\lesssim 7\cdot10^9$ eV and two thirds by the particles with energy exceeding $7\cdot10^9$ eV. Taking into account that part of the captured π-mesons is determined by expression (2.1) and the temperature effect by expression (2.2), we shall obtain

$$W^{\pi}_{T,\,\text{neutr.}}(h) = -\left\{\frac{1}{3}\,\frac{(lm_\pi/T(h))\cdot 0.25\,\bar{p}_1\tau_\pi\varrho}{(\bar{p}_1\tau_\pi\varrho + lm_\pi)^2} + \frac{2}{3}\,\frac{(lm_\pi/T(h))\cdot 0.5\,\bar{p}_2\tau_\pi\varrho}{(\bar{p}_2\tau_\pi\varrho + lm_\pi)^2}\right\}, \tag{2.3}$$

where $\bar{p}$ is the average momentum of π-mesons, $\bar{p}_1 \approx 10^9$ eV/c, $\bar{p}_2 \approx 5\cdot10^9$ eV/c. With these values the expression (2.3) may be approximately represented in the following form

$$W^{\pi}_{T,\,\text{neutr.}}(h) \approx -0.05\,h\ \%/\text{grad atm}\,, \tag{2.4}$$

where h is measured in atm.

Expressions (2.3) and (2.4) are true only for small h, i.e. for the upper layers of the atmosphere, where the energy distribution of nucleons is close to the initial one. As the nucleons propagate deeper into the atmosphere, their average energy becomes lower and here it would be more correct to consider that they transfer about $\frac{1}{4}$ of their energy to π-mesons, similarly to nucleons with the energy $\lesssim 7\cdot10^9$ eV. Therefore for such h (probably larger than several free paths of nucleons, i.e., larger than a certain h_1 of the order of 0.5 atm) we shall obtain

$$W^{\pi}_{T,\,\text{neutr.}}(h) \approx -\frac{(lm_\pi/T(h))\cdot 0.25\,\bar{p}_1\tau_\pi\varrho}{(\bar{p}_1\tau_\pi\varrho + lm_\pi)^2} \tag{2.5}$$

and approximately

$$W^{\pi}_{T,\,\text{neutr.}}(h) \approx -0.1\,h \quad \text{for} \quad h \gtrsim h_1 \approx 0.5\ \text{atm}\,. \tag{2.6}$$

For $h = 0.5$ atm, expression (2.4) gives -0.025%, while expression (2.6) gives 0.005%. Drawing a curve passing at $h = 0.5$ between these values, and at $h = 0$ using (2.4), at $h = 1$ using eq. (2.6), we shall obtain curve 3, Fig. 8, which, although very roughly, represents the dependence of $W^{\pi}_{T,\,\text{neutr.}}$ on h.

Since the life time of heavier mesons is smaller than that of π-mesons, their

contribution to the temperature effect may be neglected. Due to the very short life time of π^0-mesons it is also possible to neglect the formation of neutrons by γ-rays. Although the frequency of showers seems to involve a certain temperature effect, we shall neglect their influence because the contribution of neutrons generated in the showers is very small.

Since the contributions of slow and fast μ-mesons and of π-mesons have the same negative sign, no mutual cancellation can take place. We have:

$$\frac{\delta N_{\text{neutr.}}}{N_{\text{neutr.}}} = \alpha_{\text{temp.}} \cdot \delta T(h_0) + \int_0^{h_0} W_T^{\text{neutr.}}(h) \cdot \delta T(h)\, \mathrm{d}h \,, \tag{2.7}$$

where $\alpha_{\text{temp.}} = -(0.01 \div 0.02)\,\%/\,^\circ\text{C}$, while the total density of the temperature coefficient $W_T^{\text{neutr}}(h)$ for sea and mountain levels at the geomagnetic latitudes of 0° and 50° are given by curves 4-7 of Fig. 8.

Experimentally the temperature coefficient was determined in ref. [9] from the data of only two months recording. The values of the temperature coefficient found from the correlation between the intensity of neutrons and the air temperature are given with large errors: $(+0.10 \pm 0.12)\,\%/\,^\circ\text{C}$ and $(+0.03 \pm 0.15)\,\%/\,^\circ\text{C}$. It is impossible to draw any quantitative comparison with the above results. It is only possible to say that our results, within the limits of probable errors, do not contradict experimental data.

3. – New coupling coefficients.

For the neutron component at sea level and at the altitude of 10 km

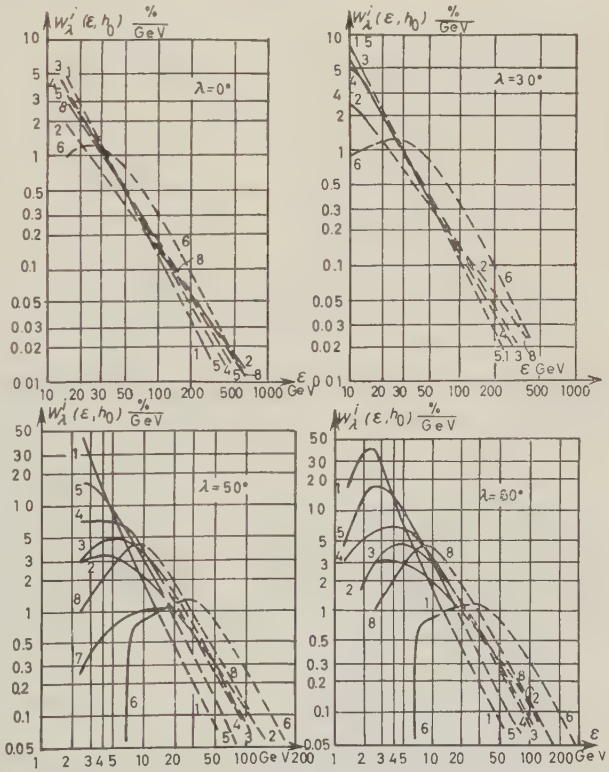

Fig. 9. – Coupling coefficient $W_\lambda^i(\varepsilon, h_0)$: 1 and 2 for the ionizing component at the boundary of the atmosphere and at the altitude 4 300 m; 3, 4 and 5: for the neutron component at sea level, at mountain level ($h_0 \approx 700$ mb) and at the altitude of 10 km ($h_0 \approx 300$ mb); 6 and 7: for the hard component at sea level according to the data corrected and not corrected for the influence of meteorological factors; 8: for the general ionizing component at the altitude of 10 km.

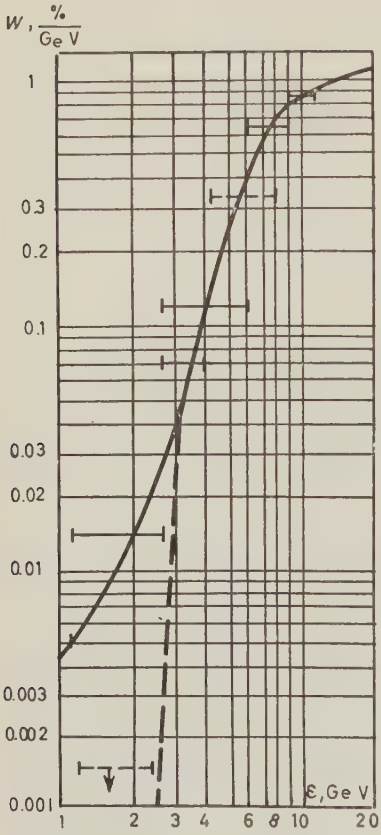

Fig. 10. – Coupling coefficients for an ion chamber (continuous curve) and for counter telescopes (dashed line) for the general ionizing component.

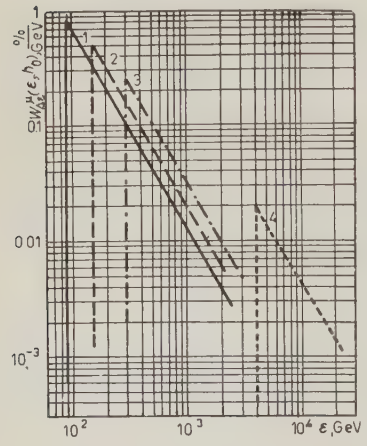

as well as for the general ionizing component at the altitude of 10 km the coupling coefficients were calculated from geomagnetic effects [4] and are shown in Fig. 9. The coupling coefficients in the region of low energies for ionizing chambers and counter telescopes were evaluated on the basis of the data concerning the outburst that took place on February 23, 1956 (see Fig. 10) [21].

In order to determine coupling coefficients for the underground observations we shall use the results for the μ-meson component at sea level and take into consideration that a given underground depth is reached only by μ-mesons with the energy exceeding certain $\Delta\varepsilon$. They are generated by the primary particles with energy exceeding $\alpha\Delta\varepsilon$, where according to [19], $\alpha \approx 10$. Coupling coefficients for the measurements underground at different depths (30, 60, 100 and 1000 m w.e.) are shown in Fig. 11.

Now we shall find coupling coefficients for extensive atmospheric showers.

In this case the method considered above does not fit, because the extensive atmospheric showers are caused by the primary particles of so high energies that they are not essentially influenced by the Earth's magnetic field. In this case a different way should be used.

In the essence we should find the probability of recording by a given counter of the showers formed by the primary particles with the energy ε. Normalization of this probability will give us the unknown coupling coefficient.

Two cases should be distinguished here: counter groups either not far (at a distance $d \lesssim 10$ m) or far from each other (several tens or hundreds meters). In the first case the dependence of the probability of shower

Fig. 11. – Coupling coefficients for underground measurements

1. $\alpha\Delta\varepsilon = 9 \cdot 10^{10}$ eV ($\approx$ 30 m w.e.)
2. $\alpha\Delta\varepsilon = 1.5 \cdot 10^{11}$ eV ($\approx$ 60 m w.e.)
3. $\alpha\Delta\varepsilon = 3 \cdot 10^{11}$ eV ($\approx$ 100 m w.e.)
4. $\alpha\Delta\varepsilon = 4 \cdot 10^{12}$ eV ($\approx$ 1000 m w.e.)

registration on d may be neglected, while in the second case the dependence on the distance between the counter groups will be essential.

Counters close to each other ($x \lesssim 10$ m). – If the spatial divergence of the electrons of the same pair in the electron-nuclear showers is much larger than the average distance between particles in the shower (which always takes place, except for very rare showers), it is possible to consider that particles trajectories are distributed at random. In this case, when a shower with density ϱ (average number of particles per 1 m^2) passes, the probability that at least one particle will pass through a group of counters (connected to each other in parallel) with a total effective area σ (in m^2) is $\omega = 1 - \exp[-\varrho\sigma]$. Let us consider a local installation consisting, say, of three groups of counters with the area σ. Let the shower axis pass through the point P remoted from the counter groups at a distance $r_1 = PA$; $r_2 = PB$ and $r_3 = PC$. The density at these points will be $\varrho(r_1)$, $\varrho(r_2)$ and $\varrho(r_3)$ respectively. According to measurements, ϱ may be represented in the form of a function

$$\varrho(r) = u(r)N ,$$

where N is the total number of particles in the shower at a given level, while the function $u(r)$ satisfying the normalization conditions

$$\int_0^\infty u(r)\cdot 2\pi r\,\mathrm{d}r = 1 ,$$

has approximately the form

$$u(r) = \begin{cases} ar^{-1}\exp[-r/R]/2 & \text{for } r \leqslant R , \\ b/r^{2.6} & \text{for } r \geqslant R . \end{cases}$$

Here R is the effective radius of the shower whose value depends on the pressure at the observation level. At mountain level ($h_0 \approx 700$ mb), $R = 80$ m, while at sea level $R = 55$ m. Coefficients a and b are found from the condition of normalization and from the continuity of the function $u(r)$ at the point $r = R$.

For mountain level ($R = 80$ m)

$$a = 2.37\cdot 10^{-3} ; \qquad b = 0.536 .$$

The probability that all three counter groups will be triggered by such a shower is

$$\omega_1\omega_2\omega_3 = \prod_{i=1}^{3} (1 - \exp[-u(r_i)x]) ,$$

where $x \equiv N\sigma$. The probability that the counter will record a shower with a number of particles N whose axis may pass through any point is found by integrating over the whole plane:

$$m_{\mathrm{loc}}^{\mathrm{sh}}(N) = \iint_\infty \prod_{i=1}^{3} (1 - \exp[-u(r_i)x])\,\mathrm{d}s . \tag{3.1}$$

The dependence of $m_{\mathrm{loc}}^{\mathrm{sh}}$ on N can be easily converted to the dependence on ε, if we take into account that

$$N \approx A\varepsilon^{s}, \tag{3.2}$$

where s is a slowly varying parameter which characterizes the age of the shower (before the shower maximum $s \lesssim 1$, at the maximum $s = 1$ and after the maximum $s \gtrsim 1$; at sea level $s \approx 1.2$), while $A \approx 0.3$ (if ε is mesured in GeV) is the constant coefficient.

The number of particles spectrum of showers can be represented in the form

$$D(N) \sim N^{-(\varkappa+1)}, \tag{3.3}$$

where $\varkappa$ is a constant very slowly varying with ε (when ε changes from 10^{14} eV to 10^{18} eV, $\varkappa$ changes only from 1.4 to 2.1). Taking into account (3.1) and (3.3) we shall obtain according to the definition of coupling coefficient

$$W_{\mathrm{loc}}^{\mathrm{sh}}(x) = Bx^{-(\varkappa+1)} \int\int_{\infty}^{3} \prod_{i=1} (1 - \exp[-u(r_i)x]\, \mathrm{d}\varrho\ ; \qquad x \equiv N\sigma, \tag{3.4}$$

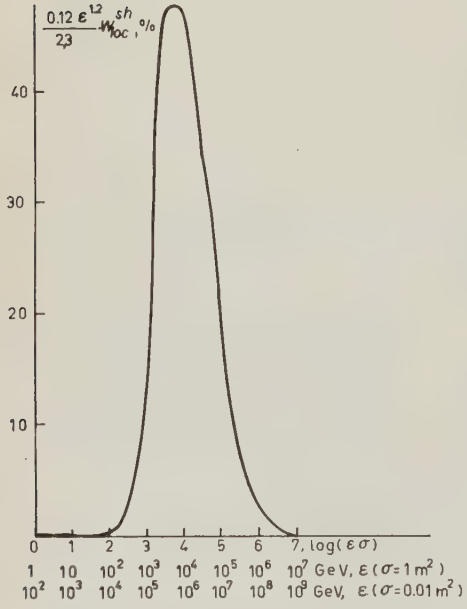

Fig. 12. – The function $\varepsilon^{1.2} W_{\mathrm{loc}}^{\mathrm{sh}}(\varepsilon)$ for sea level, $\varkappa = 1.4$, for $\sigma = 1\ \mathrm{m}^2$ and $\sigma = 0.01\ \mathrm{m}^2$. The values of ε should be multiplied by 0.3.

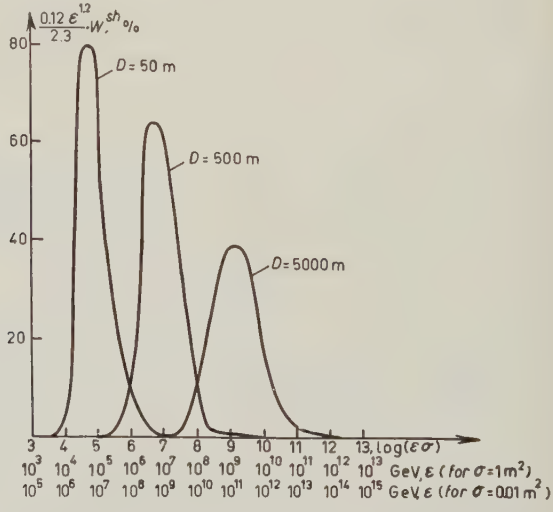

Fig. 13. – Coupling coefficients for a shower installation with counter groups at a distance D from each other. Effective area $\sigma = 1\ \mathrm{m}^2$ and $\sigma = 0.01\ \mathrm{m}^2$. The value of ε should be multiplied by 0.3.

where B is a certain coefficient found from the normalization condition

$$\int_0^\infty W_{\text{loc}}^{\text{sh}}(x)\,\mathrm{d}x = 100\ \%\ .$$

$W_{\text{loc}}^{\text{sh}}(x)$ can be easily converted to the dependence of ε.

Fig. 12 shows the values $\varepsilon^{1.2}W_{\text{loc}}^{\text{sh}}(\varepsilon)$ for $\sigma = 1\ \text{m}^2$. For any other value of σ the coupling coefficient may be found by displacing the scale along the abscissa. For example, the curve shown in Fig. 12 is also referred to the value $\sigma = 0.01\ \text{m}^2$, if the lower scale is used on the abscissa axis.

Counter groups far from each other. – By an analogous way it is possible to find coupling coefficients for any geometry of the installation. In particular, for the installation, selecting two-fold coincidences between two local installations described above and at a distance from each other of D meters,

$$W_D^{\text{sh}}(x) = B_1 x^{-(\alpha+1)} \iint_\infty \prod_{i=1}^{2} (1 - \exp[-u(r_i)x])^3\,\mathrm{d}s\ ; \qquad x \equiv N\sigma. \tag{3.5}$$

where for $D \gg d$ the distance between the shower axis and separate counter groups of each local installation are taken to be equal to the distance r_i $(i = 1, 2)$ between point P and the centres of corresponding local installation. The coupling coefficients for $\sigma = 1\ \text{m}^2$ and $\sigma = 0.01\ \text{m}^2$ are given in Fig. 13.

REFERENCES

[1] E. L. Feinberg: *Dokl. Akad. Nauk SSSR*, **53**, 421 (1946).
[2] L. I. Dorman: *a) Dokl. Akad. Nauk SSSR*, **94**, 433 (1954); *b) Izv. Akad. Nauk SSSR, Ser. Fiz.*, **20**, 24 (1956).
[3] L. I. Dorman, A. I. Kuzmin, G. V. Tjanutova, E. L. Feinberg and Yu. G. Šafer: *Žu. Éksper. Teor. Fiz.*, **26**, 537 (1954).
[4] L. I. Dorman: *Variations of Cosmic Rays* (Moscow, 1957; in Russian).
[5] L. I. Dorman and E. L. Feinberg: *Proceedings of the Guanajuato Conference*, 1955 (in press).
[6] S. Olbert: *Phys. Rev.*, **92**, 544 (1953).
[7] K. Maeda and M. Wada: *Journ. Sci. Rev. Instr.*, **48**, 71 (1954).
[8] H. Neher: in *Progress of Cosmic Rays*, Vol. 1 (Amsterdam, 1952).
[9] J. A. Simpson, W. H. Fonger and S. B. Treiman: *Phys. Rev.*, **90**, 934 (1953).
[10] K. Bachelet and A. M. Conforto: *Nuovo Cimento*, **12**, 923 (1954).
[11] P. Meyer, E. N. Parker and J. A. Simpson: *Phys. Rev.*, **104**, 768 (1956).
[12] G. J. Waddington: *Nuovo Cimento*, **3**, 930 (1956).

[13] V. Sarabhai, V. D. Dessai and D. Venkatesan: *Phys. Rev.*, **96**, 969 (1954).
[14] L. I. Dorman: *Trudy YaFAN, Ser. Fiz.*, issue 2 (1957).
[15] D. I. Dawton and H. Elliot: *Journ. Atm. Terr. Phys.*, **3**, 295 (1953).
[16] R. L. Chasson: *Phys. Rev.*, **96**, 1116 (1954).
[17] A. Duperier: *Journ. Atm. Terr. Phys.*, **1**, 296 (1951).
[18] N. L. Grigorov and V. C. Murzin: *Izv. Akad. Nauk SSSR, Ser. Fiz.*, **17**, 21 (1953).
[19] N. L. Grigorov: *Dissertation*, Moscow, *FIAN*, 1955.
[20] E. S. Glokova, N. S. Kaminer and N. A. Mišina: *Trudy YaFAN, Ser. Fiz.*, issue 2 (1957).
[21] L. I. Dorman and G. I. Freydman: *Trudy YaFAN, Ser. Fiz.*, issue 2 (1957).

SUPPLEMENTO AL VOLUME VIII, SERIE X
DEL NUOVO CIMENTO

N. 2, 1958
2° Trimestre

Solar Corpuscular Streams and Cosmic Ray Variations.

L. I. DORMAN and E. L. FEINBERG

Scientific Institute for Terrestrial Magnetism, Ionosphere and Propagation of Radio Waves - Moscow
P. N. Lebedev Physical Institute of the USSR Academy of Sciences - Moscow

1. – The idea that corpuscular streams of higly ionized neutral matter, ejected by the Sun, may lead to variations of cosmic rays of extrasolar origin is due to ALFVÉN [2]. Further developed by BRUNBERG [3], who encountered considerable difficulties, and by TRUMPY [4], and applied successfully to a particular case of crossed telescope observations by ELLIOT and DOLBEAR [5], this idea in its original form seems to lose considerably in its popularity. We reported in Guanajuata some encouraging results of investigation of this idea [6] (*). Further development of the idea and new experimental facts convinced us of the necessity of reporting the situation to this conference (+).

2. – Let us consider what, in fact, do we know about corpuscular streams:

a) We know that they exist, since thus we may reasonably explain geomagnetic disturbances.

b) We know their velocity, $u \sim 10^8$ cm/s from retardation of the geomagnetic disturbance as compared to solar events.

c) We know their widths at the terrestrial orbit from the duration of mag-

(*) Later we received the paper by NAGASHIMA [7]. In many points he expressed similar views and performed some calculations, similar to those performed by one of us (L. I. D. [8]). However his quantitative results disagree with experiment, since he used « effective energies » for primaries, while the complete true energy spectrum [1, 6, 8, 10] must be used.

(+) More detailed account see in [1].

netic storms (one or few days), $l \sim \delta R_\oplus$, $R_\oplus$ being the Sun-Earth distance, δ the vertex angle of the conic stream in the plane of the ecliptic, $\delta \sim 10 \div 30$.

d) We know that they originate mainly within the solar latitudes $10 \div 30°$, where the Sun spots are concentrated, and from their solar cycle variations we may estimate their vertical vertex angle—approximately $\delta_{vert} \lesssim 20°$.

e) We may try to estimate the density of particles in them N—basing on the shortest distance from the Earth, which is permissible for charged particles in geomagnetic field, and on the amount of geomagnetic perturbation observed [9]. And here the important specialization begins. It turns out that in the vicinity of the Earth $N \sim N_\oplus$ thus found is essentially different for small storms (which are usually smoother) and for large ones (usually more sudden). In one case $N_\oplus \sim 2$ cm^{-3}, in another $N_\oplus \sim 2 \cdot 10^2$ cm^{-3}. The intensity of magnetic perturbations is determined by $N_\oplus$ (and by u, which is almost always the same).

f) It seems that larger storms better correlate with the sunspot cycle and strongly depend upon it, their rate varying up to ~ 20 times within a cycle. On the contrary, smooth, moderate and weak storms depend upon it much less, their rate of variation being represented by a factor ~ 2. In this respect they are similar to such solar events, which (as, for example, protuberances) are not limited to the sun's equatorial region, and represent high latitude formations. We do not know the magnetic field within them, but it must exist, since both the general magnetic field of the sun and of local spots and other fields should be frozen up in such highly conducting matter. The field strength H will diminish while the stream is spreading. The component directed from the sun will probably diminish as R^{-2}, the perpendicular ones—presumably as R^{-1}.

At this point we pass from the region of facts to that of speculation. It is quite possible that turbulence within the stream will destroy the general systematical field. This fact can, in principle, be establised by using a moving probe charge, i.e., the cosmic rays. We shall attempt to show that cosmic rays serve to this purpose.

The above-listed information gives a hint that there exist two kinds of streams: 1) more rarified streams, connected with high latitudes formations, and 2) more dense ones, originating within the Sun's equatorial region and intimately connected with spots. We believe this idea may be supported by cosmic ray variations data.

2. – The passage of cosmic ray particles, having the spectrum $D(\varepsilon) \sim \varepsilon^{-(\gamma+1)}$, through the stream with magnetic field H has been studied by ALFVÉN [2]

and, more specifically, by NAGASHIMA [7] and by one of the present authors (L.D. [8]). Let the stream be conical (vertex angle δ, Fig. 1), its axis forming an angle α, with the line Earth-Sun. H within it we suppose to be uniform. This field scatters low energy cosmic ray particles, but if $\alpha > \delta/2$ (and if the stream does not sweep the Earth) due to isotropy of the initial cosmic rays this does not affect the intensity on the Earth. If, however, the particle energy ε exceeds some $\varepsilon_{\min}$, then it is accelerated or decelerated by the component $H^{\perp}$ of H normal to both the stream velocity u and to the particle's velocity. This $\varepsilon_{\min}$ we assume to be averaged over all possible passages through the given stream,

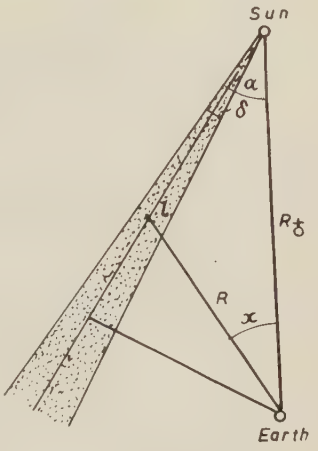

Fig. 1.

$$\varepsilon^{\pm}_{\odot\,\min} = 300\, H^{\perp}_{\odot} l_{\odot}$$

(if $H^{\perp}$ varies as R^{-1}; if it varies as R^{-2}, R being the distance from the sun, then enters a factor of the order of unity, but less than 1). If we average over all α and assume a pair of equal streams to the right and to the left of the Earth then the variation δD per one stream is

$$(1)\quad \frac{\delta D(\varepsilon)}{D(\varepsilon)} = \pm \frac{(1+\gamma)\Delta\varepsilon^{\pm}_{\odot}}{\varepsilon}\cdot\frac{\delta}{\pi^2}\left(1+\ln\frac{\pi}{\delta}\right), \quad \text{if } \varepsilon \gtrsim \sigma\varepsilon^{\pm}_{\odot\,\min}; \quad \frac{\delta D(\varepsilon)}{D(\varepsilon)} = 0, \text{ if } \varepsilon \lesssim \sigma\varepsilon^{\pm}_{\odot\,\min}.$$

Here $\Delta\varepsilon^{\pm}_{\odot} = (u/c)\varepsilon^{\pm}_{\odot\,\min}$ is the energy gain, σ is a factor depending on the law $H^{\perp}(R) \sim R^{-k}$. If $k=1$ (most probable), then $\sigma = 1$, if $k = 2, \sigma \gtrsim 1$. A pair of streams leads to an effective source to the left (if H is directed parallel to the geomagnetic dipole and we are in the northern hemisphere), situated under an angle $\chi = \pi/2$ with respect to the effectiveness of the line Earth-Sun. Moreover, various portions of a given stream may be expressed by introducing into (1) some factor $f_{1,2}(\chi)$, which is shown in Fig. 2, assuming various lengths $L = bR_{\odot}$ of streams ($b = 1, 2, 3, \infty$). It reflects the dependence upon solar time of this variation, when observed on the Earth (the geomagnetic field here is neglected).

Thus a passage of cosmic rays through an average stream actually gives variations on the Earth and, what is essential, exactly of the kind of spectrum necessary to explain quiet diurnal variations [6, 8]:

$$(2)\quad \frac{\delta D}{D} = \begin{cases} 0 & \varepsilon < \varepsilon_{\min} \approx 7 \text{ GeV} \\ \dfrac{a}{\varepsilon} & \varepsilon > \varepsilon_{\min}, \quad a = a(\varphi), \quad a(0) = 0.17. \end{cases}$$

Equation (1) was obtained from the known fact of the existence of solar streams with definite δ and u. The only assumption made was that they really possess H normal to the ecliptic plane. It is but natural to believe that it actually is so. From an experimental figure [6, 8, 10] $\varepsilon_{\min} \approx \varepsilon_{\min} \approx 7$ GeV we determine $H_{\overset{\circ}{+}}$

$$(3) \qquad H_{\overset{\circ}{+}} = \frac{\varepsilon^{\mp}_{\min}}{300\, l_{\overset{\circ}{+}}} \approx \approx \frac{7 \cdot 10^{9}}{300 \cdot 2 \cdot 10^{12}} \sim 10^{-5} \text{ gauss} .$$

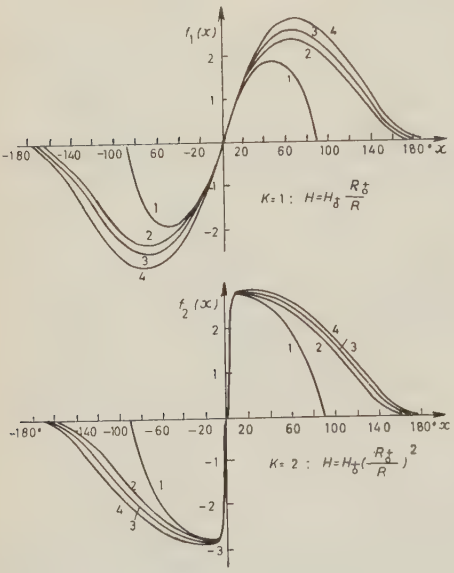

Fig. 2. – Intensity of a source of variations resulting from the existence of a pair of streams, versus an angle between the projection of direction to the source and the line Earth-Sun, for two possible cases of dependence of H upon the distance from the Sun, R.

This is the primary determination of the quantity, it cannot be compared with any other geophysical or astrophysical results. If $H \sim R^{-1}$ (most probable), it gives for the region on the sun where the field was frozen up $H \sim 2 \cdot 10^{-3}$, —a not unreasonable value for the supposition that this is the general solar field in the outer solar layers. The experimental value of a is to be compared with $(1+\gamma)\Delta\varepsilon_{\overset{\circ}{+}} \cdot \delta/\pi^2(1+\ln \pi/\delta)$, multiplied by the average number n of simultaneously existing streams. For $a \approx 0.15$ (for the period 1937 ÷ 1946 and $u \sim 10^8$ cm/s we get $n \sim 10 \div 20$ for various reasonable δ.

Further let us consider the dependence of a upon φ which, as may be shown (see ref. [1]), practically reflects the dependence of a number of streams on solar latitude Λ. It turns out that it decreases with φ and, therefore, with Λ too slowly for the supposition that they originate in the solar equatorial region to hold. Moreover, the calculation seems to show that these streams should be presumably high latitude formations. Thus they may not be directly associated with sunspots. In any case, future investigations may be very useful in this respect.

4. – Now we turn particularly to streams sweeping the Earth. The accelerating action of their vertical component has been already included in the previous calculation. But they should also scatter low energy particles and thus lead to decreases of intensities simultaneously with magnetic storms, namely,

they should cut-off all particles with energy $\varepsilon < \varepsilon_1$, where $\varepsilon_1 \approx \varepsilon_{\min}/3 \approx$ $\approx 2 \div 3$ GeV. This would not affect the sea level hard component and thus the whole conception might seem wrong.

In fact, we may in our usual manner determine the spectrum of variations during magnetic storms, although experimental data are scarce. Table I shows for very strong storms that the most suitable spectrum (assuming $\delta D/D$ identical for all latitudes from $\lambda = 0°$ up to $\lambda = 50°$; this is here not very safe,

TABLE I. – *Determination of the spectrum of variations during large magnetic storms.*

Tested spectrum	ε_1 (GeV)	$\frac{(\delta N_\mu/N_\mu)_{\text{sea level, } \lambda=50°}}{(\delta N_\mu/N_\mu)_{\text{sea level, } \lambda=0°}}$	$\frac{(\delta N/N)_{\text{stratosph., } \lambda=50°}}{(\delta N_\mu/N_\mu)_{\text{sea level, } \lambda=50°}}$	$\frac{(\delta N_\mu/N_\mu)_{\text{underegr., } \lambda=50°}}{(\delta N_\mu/N_\mu)_{\text{sea level, } \lambda=50°}}$
$\frac{\delta D}{D} = \begin{cases} -\frac{a}{\varepsilon}, & \varepsilon > \varepsilon_1 \\ 0, & \varepsilon > \varepsilon_1 \end{cases}$	15	—	24.5	0
	25	2.04	17.7	0
	63	1.39	12.2	0
	63	1.39	10.1	0
	100	1.33	9.3	0.01
	158	1.32	8.9	0.73
	250	1.30	8.8	0.94
	400	1.28	8.7	1.05
	630	1.28	8.7	1.17
$\frac{\delta D}{D} = \begin{cases} -a, & \varepsilon < \varepsilon_1 \\ 0, & \varepsilon > \varepsilon_1 \end{cases}$	15	—	11.5	0
	25	1.43	5.1	0
	40	1.12	2.75	0
	63	1.04	1.83	0
	100	1.01	1.46	0
	158	1.00	1.27	0.05
	250	0.97	1.18	0.38
	400	0.97	1.11	0.58
	630	9.09	1.06	0.70
$\frac{\delta D}{D} = \begin{cases} -a\varepsilon, & \varepsilon < \varepsilon_1 \\ 0, & \varepsilon > \varepsilon_1 \end{cases}$	15	—	5,75	0
	25	1.23	2.00	0
	40	0.97	0.87	0
	63	0.96	0.47	0
	100	0.92	0.32	0
	158	0.90	0.25	0
	250	1.04	0.17	0.96
	400	0.90	0.17	0.67
	630	0.93	0.15	2.07
Experiment		1.12 ± 0.06	2.8 ± 0.3	< 0.05

and this point is a weak one) is:

$$\left(\frac{\delta D}{D}\right)_{\text{storms}} \approx \begin{cases} -a & \text{for} \quad \varepsilon \lesssim 40 \text{ GeV}, \\ 0 & \text{for} \quad \varepsilon \gtrsim 40 \text{ GeV}. \end{cases} \tag{4}$$

For large decreases, $(\delta I/I)_{\text{hard comp., } \lambda=50^\circ} \approx 10\%$ we have $a = 0.3$.

This is similar to what we should expect due to screening by a stream, but the above theory [1, 8] gives, when the Earth is in the middle of an equatorial stream, if H is normal to the ecliptics,

$$\frac{\delta D}{D} = \begin{cases} -1 & \text{if} \quad \varepsilon < \varepsilon^{\pm}_{\odot\,\text{min}}/4 \\ -\dfrac{2}{\pi} \arcsin\left(\dfrac{\varepsilon^{\pm}_{\odot\,\text{min}}}{2\varepsilon} - 1\right) & \text{if} \quad \dfrac{\varepsilon^{\pm}_{\odot\,\text{min}}}{4} < \varepsilon < \dfrac{\varepsilon^{\pm}_{\odot\,\text{min}}}{2} \\ 0 & \text{if} \quad \varepsilon > \dfrac{\varepsilon^{\pm}_{\odot\,\text{min}}}{2}, \end{cases} \tag{5}$$

and if H is parallel to u (stream velocity):

$$\frac{\delta D}{D} = \begin{cases} -1 & \text{if} \quad \varepsilon > \dfrac{\varepsilon^{\pm}_{\odot\,\text{min}}}{4}; \\ 0 & \text{if} \quad \varepsilon > \dfrac{\varepsilon^{\pm}_{\odot\,\text{min}}}{4}; \end{cases} \qquad \varepsilon^{\pm}_{\odot\,\text{min}} = 300\, H_{\pm\odot} l_{\pm\odot}. \tag{6}$$

If we introduce a factor $f \lesssim 1$ in order to apply this to all particles (not only to those moving in the ecliptic plane), we find from (4) and (5) that $f \sim a$ and

$$\varepsilon^{\pm}_{\odot\,\text{min}} = 300\, H_{\pm\odot} l_{\pm\odot} \approx (3 \div 4) \cdot 40 \text{ GeV} \approx 120 \div 160 \text{ GeV}. \tag{7}$$

Therefore, fields of the order of $2 \cdot 10^{-4}$ Oe are necessary. The same value of $\varepsilon^{\pm}_{\odot\,\text{min}}$ may be deduced from other important facts. For instance, diurnal variations during storms are 1.5 ÷ 2 times larger for particles coming from the south than for those coming from the north ($\lambda \sim 50^\circ$). Therefore directions to the source given by the angles χ, φ must correspond to considerably different φ. Calculations using BRUNBERG and DATTNER'S results show that this is possible only if $\varepsilon > 40$ GeV (when φ will be respectively 16° and 38°; for $\varepsilon = 100$ GeV, $\varphi = 18^\circ$ and 67°, etc.). If δ is smaller than, say, 30°, this would secure considerable differences for southward and northward directions of the telescope (*). In view of this situation we turn to the hint from astrophysical researches of streams that there may be two different kinds of streams;

(*) However, the situation here is not so simple as in the case of streams not sweeping the Earth. In particular, the meaning and the numerical value of f is not very clear, since it is strongly connected with the degree of turbulence of the stream. More theoretical and experimental investigations are desirable.

those leading to large magnetic storms may correspond to larger $H_{\perp}$, since they originate presumably in the equatorial region. Here, instead of the weak general solar field, the sunspot fields will be frozen up. We call them « streams of the second kind » in distinction from the above « streams of the firts kind » with weaker fields, giving quiet diurnal variations. Let us follow the consequences of this supposition.

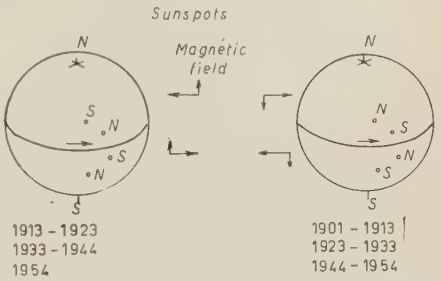

Fig. 3. – Sun spots and their magnetic fields for different 11-years semicycles of solar activity.

It is known, that sunspots occur in pairs, situated almost along solar parallels (Fig. 3) and move toward the equator during the cycle. Therefore in « streams of the second kind » $H_{\pm\odot}$ may be almost parallel to the ecliptic plane. Its vertical component is much smaller than H, determined from cosmic ray magnetic disturbances, thus being of the order of $(1/10)H \sim 10^{-5}$ Oe. If such a stream does not sweep the Earth [10], there are two cases.

1) If it passes to the left or to the right of the Earth, then only a small vertical component of H acts, and it gives exactly the same effect (with positive or negative sign for different 11-year periods), as the streams of the first kind, and we do not need to separate them. From the constancy of the sign of χ_{eff} (*) we conclude, that it is considerably smaller than $H_{\pm\odot}$ in the streams of the first kind.

2) If it passes above or under the Earth, its main, « horizontal », component acts. It must influence the quiet diurnal variations, but we know too little of streams to define this influence safely. However, we may hope that here we may find a solution of a very puzzling problem of diurnal variations—that of the 22-year cycle of displacement of χ_{eff} from $\sim 90°$ to $\sim 20 \div 30°$ (see, for instance, [1, 10]). This displacement may be understood to be a result of the splitting up of variations into two waves with changing relative intensities, as was discovered by SARABHAI [1, 11]. The period of change is 22 years. An example of a possible explanation (in no way a theory, but rather a possible working hypothesis) is as follows toward the Earth.

When we have a pair of streams, one above, another under the Earth,

(*) χ is an angle formed by the projection on the ecliptics of the direction to the source of diurnal variations and by the line Earth-Sun. It is positive when we look from the northern hemisphere to the Sun and the source is to the left of us.

coming from different hemispheres of the sun, both of them act in the same sense: either they both accelerate (in one 11-year period), or both decelerate (in another one) the particles, passing through them.

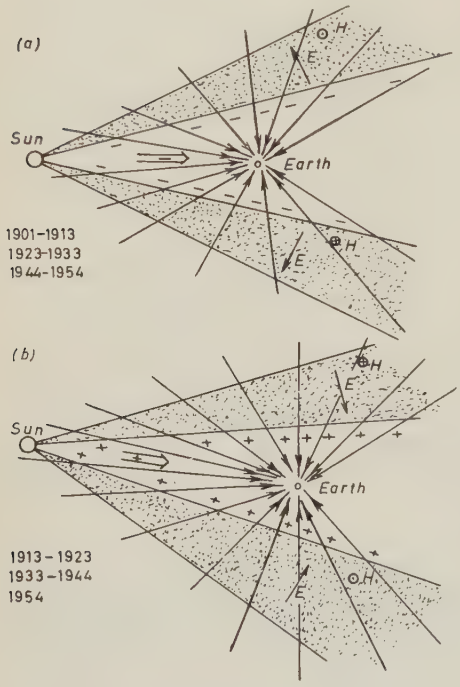

Fig. 4. – Effective sources on the Sun equivalent to the action of a pair of streams above and under the Earth for fast particles.

Consider first the fast particles which are not deflected by the magnetic field. Variations of energy of those particles which come from the half space where the sun is situated will be equivalent to the appearance of a source on the Sun. Those which come from the other half space give an « anti-source ». The net result is determined by a ratio of solid angles under which the corresponding parts of the stream, (Ω_1 and Ω_2) are seen from the Earth. It is easy to show, that

$$(8)\quad \begin{cases} \dfrac{\Omega_1}{\Omega_2} = \dfrac{1}{\cos\alpha}\,; \\ \Omega_1 - \Omega_2 = \dfrac{\delta(1-\cos\alpha)}{\sin\alpha} \approx \dfrac{\delta\cdot\alpha}{2}\,. \end{cases}$$

Therefore, in « *b* » periods (1933-1944, 1954-1965, etc.) this will be equivalent to a positive source on the Sun, in « *a* » periods (1944-1954, etc.) to a negative source. The intensity of this source is proportional to the number of streams and to α. Since α is maximal at the beginning of an 11-year cycle and later decreases [12], while the number of spots increases (almost linearly), the variation of their product after the minimum of the activity is passed should not be large. It depends on details, of which there is not enough knowledge.

Now let us consider slower particles. They will be considerably deflected by the magnetic field, and it is easy to see (Fig. 5), that this will act *always* as a positive source on the sun. These two actions tend to cancel each other in the « *a* » periods (1944-1954, etc.) and enhance each other in « *b* » periods (1933-1944, etc.).

This simple picture would give the necessary 22-year change of diurnal variations with the maximum intensity of the solar source in the first half

of every « b » period. Thus the exact position of the phase of this change is displaced from the necessary one by a few years. No doubt, the picture is too crude, such details as the overlapping of sun spot cycles (known to be of the order of two or three years); the actual rate of change of α and of a number of spots in the vicinity of minimum of activity; the fraction of time which the Earth spends so high above the solar equator, that both streams (from the southern and northern solar hemispheres) are on the same side, especially in the middle and in the end of the 11 year period, this giving a zero net effect, etc., can displace the phase of change considerably. Moreover, such unknown regularities as dependence on solar activity of the magnetic field H in streams, of the distance at which streams become turbulent, etc., are no less important. We wish only to show by an example that some first order effects may account for the necessary changes of the « solar » source of diurnal variations, if we connect terrestrial variations of cosmic rays not only with the streams of the 1st kind (which seem to be loosely connected with solar activity), but with the streams of the 2nd kind, strongly dependent upon the sun spot cycle, having 22 years periodicity, as well.

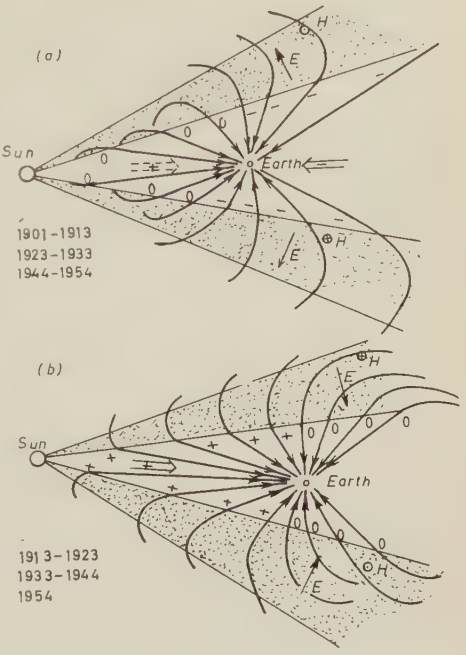

Fig. 5. – The same as Fig. 4 for slower particles, deflected considerably by the magnetic field.

Now, we mention some further consequences of the action of streams on cosmic rays.

1) *Change of diurnal variations during magnetic storms.* Eqs. (5) and (6) give the change of intensity during magnetic storms due to reflection of particles. Similarly a variation of the spectrum of particles passing through the stream is [1, 8]:

$$(9)\qquad \frac{\delta D}{D} = \pm \frac{r(1+\gamma)\Delta\varepsilon_{\odot}^{\pm}}{\varepsilon} \begin{cases} 1 & \text{if } \varepsilon > \frac{1}{2}\varepsilon_{\odot\,\min}^{\pm} \\ 1 - \frac{2}{\pi}\arcsin\left(\frac{\varepsilon_{\odot\,\min}^{\pm}}{2\varepsilon} - 1\right) & \text{if } \frac{\varepsilon_{\odot\,\min}^{\pm}}{4} < \varepsilon < \frac{\varepsilon_{\odot\,\min}^{\pm}}{2} \\ 0 & \text{if } \varepsilon < \frac{\varepsilon_{\odot\,\min}^{\pm}}{4}, \end{cases}$$

($r \sim 1$). Using coupling coefficients, the amplitude of diurnal variations may be calculated (see Table II), for various $H_\perp$, i.e., for various $\varepsilon^{\perp}_{\min} = 300 H_\perp l_\perp$. For very large storms and decreases of cosmic ray intensity of the type of that of 26 July 1946 and 24 January 1949 [13] we have found $\varepsilon^{\perp}_{\min} \simeq (120 \div 160)$ GeV (see above). Therefore, for $u = 2 \cdot 10^8$ we should expect for the sea level hard component at $\lambda = 50°$ an increase of 0.7%. The time of maximum, as may be shown, must be displaced towards earlier hours. This coincides with the experimentally observed changes, but the increase is 0.4%, instead of 0.7%. This difference can be hardly attributed to the wrong determination of $\varepsilon^{\perp}_{\min}$. Then it must be a result of smaller velocity of the stream, or of $r \neq 1$ ($r \lesssim 1$). It must be

$$u \approx \frac{2 \cdot 0.7\,\%}{0.4\,\%} \cdot 2 \cdot 10^3 \gtrsim 1.2 \cdot 10^1 \text{ cm/s} .$$

For 26 July 1946 storm u can be determined directly by using retardation of storm ($18^h\,46$, 26^m July) with respect the solar flare event ($16^h 20^m$ 25 July). This gives $u = 1.6 \cdot 10^8$ cm/s in excellent agreement with the cosmic ray determination.

It is interesting to note, that diurnal variations during such storms should be observable underground, at 45 m H_2O, with the amplitude $\approx 0.5\%$, although the decrease of intensity does not penetrate on such depth. Such an event, indeed, was observed by MACANUFF [14] (diurnal variations during the storm of the order of a few tenths of percent, while normal diurnal variations are considerably smaller in agreement with the theory). Therefore, this experimental result by MACANUFF need not be considered as due to an error or fluctuations.

TABLE II. – *Expected additional amplitudes* (%) *due to accelerati*

$\varepsilon_{\min}$ (GeV)	Corresponding magnetic field strength in the vicinity the Earth (gauss)	Ionizing component, upper boundary of atmosphere		Ionizing component 700 mb		Neutrons 700 mb	
		$\lambda=50°$	$\lambda=0°$	$\lambda=50°$	$\lambda=0°$	$\lambda=50°$	$\lambda=0°$
3	$0.5 \cdot 10^{-5}$	0.62	0.13	0.21	0.04	0.35	0.08
6	10^{-5}	1.24	0.26	0.42	0.08	0.70	0.16
18	$3 \cdot 10^{-5}$	0.53	0.77	0.64	0.22	0.80	0.48
30	$5 \cdot 10^{-5}$	0.34	1.22	0.56	0.36	0.56	0.76
60	10^{-4}	0.18	1.00	0.47	0.64	0.30	0.67
120	$2 \cdot 10^{-4}$	0.10	0.58	0.38	0.55	0.17	0.40
300	$5 \cdot 10^{-4}$	0.05	0.26	0.31	0.43	0.08	0.19
1500	$2.5 \cdot 10^{-3}$	0.01	0.11	0.18	0.18	0.02	0.08

2) *Direction of magnetic field within a particular stream, sweeping the Earth*, may be found best of all if during the storm we measure at the equator amplitudes of diurnal variations for particles coming from the south (A_S), and from north (A_N). If magnetic field is directed along the revolution of the Earth around the sun (i.e., from east to west), then the particles coming from the south will be accelerated, those from the north—decelerated and we shall have $A_S > A_N$ and vice versa. This field may be correlated with the direction of the field in pairs of sun spots. We may, instead, compare simply diurnal variations for any point in northern hemisphere with that in the corresponding point in the southern one, but here the necessity of eliminating the meteorological effects will arise. We may, moreover, remark that if the streams causing magnetic storms would have a vertical component comparable with the horizontal one, then before the storm and after it we would have a large change in the amplitude of diurnal variations (due to acceleration or retardation of particles, having H ten times greater than in the usual streams of the first kind, leading to normal diurnal variations. It seems that experiments disprove this possibility, thus favouring the horizontality of H in these streams.

3) *Correlation with magnetic activity* should be well pronounced in cosmic rays. In particular, an increase of magnetic activity must be accompanied by an increase of amplitude and by a displacement of maximum toward earlier hours. A definite ratio of effects in various components must be observable. This seems to be the case for weak seasonal variations, which remain after eliminating strong meteorological variations [15, 1].

On the other hand, not every magnetic storm must lead to a cosmic rays intensity decrease. The magnetic storm depends on the density of a stream and on its velocity. The magnetic field in it has no direct influence on distur-

treams, sweeping the Earth (for $u = 2 \cdot 10^8$ cm/s, $r = 1$).

Hard component sea level		Underground (depth in m H_2O)			
$\lambda = 50°$	$\lambda = 0°$	22	45	117	400
0.07	0.07	0.021	0.013	0.006	0.002
0.15	0.14	0.43	0.027	0.011	0.004
0.44	0.42	0.122	0.080	0.033	0.010
0.70	0.70	0.21	0.13	0.060	0.02
0.91	0.92	0.43	0.27	0.11	0.04
0.70	0.77	0.87	0.53	0.22	0.07
0.39	0.49	0.88	0.23	0.56	0.18
0.12	0.18	0.30	0.44	0.91	0.88

bances in the geomagnetic field, while for cosmic ray perturbations it plays the main role (together with velocity). If, for instance, a dense stream is highly turbulent, it will cause nevertheless a geomagnetic disturbance, but no cosmic ray perturbations. Such cases are in fact known. However, statistically, the larger the storms, the more likely that the magnetic field within the stream is large. This agrees with analysis of variations [15, 1].

4) The *27-day recurrence* is expected to have characteristic features. If it is caused by equal recurrence of streams, sweeping the Earth, then we may expect that with an increase of magnetic perturbations and a corresponding decrease of cosmic ray intensity both the 27-day variations and the 27-day recurrence of the diurnal variations should become more pronounced. In this 27-day recurrence period the amplitude of diurnal variations must increase and the time of maximum must be displaced to earlier hours. There seem to be experimental facts agreeing with this conclusion. In the period of maximum of solar activity the 27-day variations should be especially large (also in agreement with observations).

REFERENCES

[1] L. I. Dorman: *Variations of Cosmic Rays* (Moscow, 1957; in Russian).
[2] H. Alfvén: *Cosmical Electrodynamics* (Oxford 1950).
[3] E. Å. Brunberg: *Tellus*, **5**, 135 (1953).
[4] B. Trumpy: *Physica*, **19**, 645 (1953).
[5] H. Elliot and D. W. Dolbear: *Proc. Phys. Soc.*, **63**, 137 (1950); *Journ. Atm. Terr. Phys.*, **1**, 205 (1951).
[6] L. I. Dorman and E. L. Feinberg: *Proceedings of the Guanajuato Conference*, 1955 (in press).
[7] K. Nagashima: *Journ. Geomagn. and Geoelect.*, **7**, 51 (1955).
[8] L. I. Dorman: *Dissertation*, Moscow (1955).
[9] D. T. Martyn: *Nature*, **167**, 92 (1951).
[10] L. I. Dorman and L. E. Feinberg: in this issue, p. 358.
[11] V. Sarabhai, V. D. Dessai and D. Venkatesan: *Phys. Rev.*, **96**, 969 (1954).
[12] M. Waldmeier: *Ergebnisse und Probleme der Sonnenforschung* (Basel, 1941).
[13] H. Elliot: in *Progress of Cosmic Rays*, Vol. **1** (Amsterdam, 1952).
[14] I. W. MacAnuff: in George's review in *Progress in Cosmic Rays*, Vol. **1**, (Amsterdam, 1952).
[15] E. S. Glokova: *Proceedings of the Institute of Terrestrial Magnetism*, **8**, 59 (1952) (in Russian).

SUPPLEMENTO AL VOLUME VIII, SERIE X
DEL NUOVO CIMENTO

N. 2, 1958
2° Trimestre

The Generation and Propagation of Solar Cosmic Rays.

L. I. DORMAN

Scientific Institute for Terrestrial Magnetism, Ionosphere and Propagation of Radio Waves - Moscow

1. – Introduction.

Since many papers at this conference give the analysis of the outburst that took place on February 23, 1956, we shall not present our results which coincide with those of other investigators. We shall discuss mainly two points, which we think are of interest, that is: the mechanism of generation and the propagation of solar cosmic ray particles in the solar system.

Firstly, let us sum up the results of the references [2, 3] obtained when analysing the experimental data received by Soviet stations as well as those by ELLIOT and GOLD [4]. These results agree with the conclusions in ref. [7].

1) In the initial period of the outburst, there was a well expressed impact zone which showed the anisotropy of the additional cosmic ray flow from a source having angle dimensions of about $(15 \div 30)°$. This flow was coming from the sun, as is shown by calculations by the FIROR method [5]. However, in contrast with the result expected in [5], the background zone does not cover all the longitudes but only a limited region of the longitudes. The particles arrive in the impact zone and in the background zone almost simultaneously in the various points (with a few minutes interval), but evidently there is a tendency of an earlier arrival at the lower latitudes than at the higher ones (Tbilisi and Cape Shmidt, with a difference of approximately $2 \div 3$ minutes). On the rest of the earth's surface (we shall call it the scatter zone) the particles begin to arrive with a considerable delay of approximately 10 minutes. The American stations on the central latitudes and stations in the higher polar regions are included in this zone.

2) Maximum is reached very quickly in the impact zone and in the background zone (in a few minutes), but in the scatter zone the intensity increases rather slowly and maximum is reached much later (approximately in $20 \div 30$ minutes).

3) Intensity in the impact zone and in the background zone decreases at first very quickly (twice in a quarter of an hour), but in the scatter zone it decreases much slower. Therefore, in approximately an hour's time the intensities in both zones become equal. This shows that the additional flow by that time becomes isotropic.

4) In the period of isotropy the spectrum of the solar cosmic ray particles found with the aid of the coupling coefficients [1, 2] was:

$$\delta D_{sc}(\varepsilon) \sim \varepsilon^{-7}\,, \tag{1}$$

the spectrum did not change as time went on (see Fig. 5 from ref. [1]). Here and further on ε designates the particle's energy.

5) The flow of particles $\delta D_{\odot}(\varepsilon)$ coming directly from the sun was found by *subtracting the results found in the scatter zone from those in the impact zone*:

$$\delta D_{\odot}(\varepsilon) \approx 10^{10}\,\varepsilon^{-7} \exp\left[-t/T_{\odot}\right]\ \mathrm{cm^{-2}\,h^{-1}\,GeV^{-1}}\,. \tag{2}$$

Here t is measured in hours and $T_{\odot} = \frac{1}{4}$ hour.

2. - The propagation of solar cosmic rays and electro-magnetic conditions in interplanetary space.

1) It is known [7] that certain impact zones exist at the initial stage of the outburst, their location being in agreement with what is expected due to the influence of the earth's magnetic field on the trajectories of solar particles. This means that a regular, uniform magnetic field between the sun and the earth does not exist, or to be more exact, its field intensity

$$H \lesssim \frac{cp_{\min}}{300\,R_{\odot}^{-}}\,, \tag{3}$$

where $cp_{\min}$ is the minimum momentum of solar cosmic ray particles just arriving on earth. Even when $cp_{\min} \sim 10^{9}$ eV, this gives $H \lesssim 2 \cdot 10^{-7}$ Oe (actually, particles with even smaller energy come to earth).

This fact proves that the Galactic magnetic field with $H \sim 10^{-5}$ Oe must somehow be forced out of the solar system. One of the possible mechanisms of such a phenomenon was suggested by DAVIS [6].

2) Now we shall discuss the variation of the intensity during the outburst period. The investigation of this variation led other investigators [7] to the supposition that near the sun there is a cavity with a radius of about $R_{\odot}$, the external magnetic barrier ensuring a decrease in the intensity during the

period of isotropy according to the law $t^{-\frac{3}{2}}$. Here we shall show that such strictly formulated assumption is not obligatory. It is possible to understand the change of intensity of cosmic rays not only in the last stage, but also in the beginning of the outburst, if we assume that there are magnetic clouds in the solar system which are situated from each other roughly at a distance of about a radius of the earth's orbit and that they equally well scatter particles of both low and high energy (this is possible if the radius of the curvature of the particles' trajectories in the clouds is smaller than (or equal to) the size of the clouds). Let us examine such a model.

Let the distribution of clouds in space be at random and the mean square path of the particles between scatterings be λ. Then, for $t \gg \lambda/c$, which is only of interest to us ($R_{\odot}/c \approx 8$ min), the possibility of finding a particle on the orbit of the earth (in the volume element $\mathrm{d}\boldsymbol{R}$) is (this formula is also true for any value of t, if the lengths of separate paths between scatterings are distributed according to a gaussian law [8]):

$$W_t(R_{\odot}) = \frac{\exp\left[-3R_{\odot}^2/2tc\lambda\right]}{(2\pi tc\lambda/3)^{\frac{3}{2}}} . \tag{4}$$

If $n_{\odot}(\varepsilon, t_0)$ is the flux of cosmic particles from the sun, then the intensity on earth is:

$$I(\varepsilon, t) = \int_0^{t - R_{\odot}/c} n_{\odot}(\varepsilon, t_0) \cdot W_{t-t_0}(R_{\odot})\, \mathrm{d}t_0 . \tag{5}$$

Taking into account that according to (2), $n_{\odot}(\varepsilon, t_0) \sim \delta D_{\odot}(\varepsilon, t_0) \sim \exp\left[-4t_0\right]$, with the help of (5), we find $I(\varepsilon, t)$ under various suppositions concerning the value of λ. The results of the calculations for $\lambda = R_{\odot}/4$; $R_{\odot}/2$; $R_{\odot}$ and $2R_{\odot}$ are shown in Fig. 1 by solid lines. This chart also shows the experimental data received for Chicago and Godhaven (all data are normalized to $t = 5$ hours after the beginning of the outburst). From Fig. 1 it is seen that for moderate latitudes, the effective value for

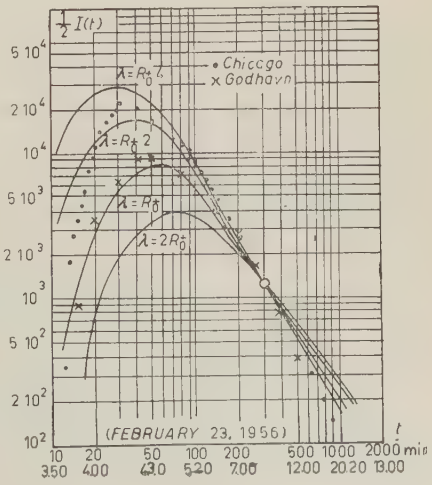

Fig. 1. – The expected variation of intensity of cosmic rays during the outburst for different values of λ and observed variations in Chicago and Godhaven.

λ is about $R_\odot/2$, while the particles that arrive in and around the polar region seem to have somerwhat higher λ, nearer to $R_\odot$. Therefore, we may come to the conclusion that as we go further from the ecliptics plane, the clouds become rarer. From the fact that in the period of isotropy observations reveal a rather quicker decrease of intensity than was expected theoretically, follows, firstly, that the reflecting border is not really necessary and, secondly, that the space within which the scattering clouds are found is limited (or rather the distance between the scattering clouds should substantially increase as we move farther away from the sun).

A rather quick decrease of intensity of solar cosmic ray particles which proves the impossibility of accumulation of particles in the solar system is an important argument against any theory of the solar origin of cosmic radiation (even of the low energy part of it).

3. – Generation of solar cosmic rays.

3·1. *Energy relations.* – The generation of the flux of solar cosmic rays took place in an enormous chromospheric outburst. The energy emitted in the optical region of the spectrum may be found by taking into consideration the luminosity of the outburst. In the maximum it was not less than a few per cent ($\gtrsim 5\%$) of the brightness of the rest of the sun's surface in the unperturbed spectrum. Therefore

$$E_\odot^{\mathrm{opt}} \gtrsim 0.05 \cdot 8 \cdot 10^7 \ \frac{\mathrm{erg}}{\mathrm{cm^2\ min}} \cdot \frac{S_{\mathrm{flare}}}{S_\odot} \cdot 2\pi R_\odot^2 \Delta t \approx 6 \cdot 10^{31}\ \mathrm{erg}\,, \tag{6}$$

where $\Delta t \sim 1$ hour is the approximate duration of the visible phase of the outburst.

The kinetic energy of the motion of the gas mass in the outburst is

$$E_\odot^{\mathrm{kin}} \approx \tfrac{1}{2} \varrho u^2 h S_{\mathrm{flare}}\,,$$

where $S_{\mathrm{f.re}}$ is the visible area of the outburst, $h \gtrsim 10^9$ cm the thickness of the chromosphere, $\varrho \approx 10^{-12}$ g/cm^3 is the average density and u the velocity of the moving substance. This gives $E_\odot^{\mathrm{kin}} \approx (10^{30} \div 10^{32})$ erg with $u = 10^7$ and 10^8 cm/s respectively.

The energy of solar cosmic rays is

$$E_\odot^{\mathrm{c.r.}} \approx \int_0^\infty \mathrm{d}t_0 \int_1^\infty (\varepsilon - 1) n_\odot(\varepsilon, t_0)\, \mathrm{d}\varepsilon\,, \tag{8}$$

where

$$n_\odot(\varepsilon, t_0) = \delta D_\odot(\varepsilon, t_0) \cdot 2\pi R_\odot^2 \approx \frac{10^{37}}{\varepsilon^6} \exp\left[-4t_0\right]\ \mathrm{GeV^{-1}\ hr^{-1}}\,,$$

This gives $E_\odot^{\mathrm{c.r.}} \approx 10^{32}$ erg.

Therefore, the energy emitted in the optical region, the kinetic energy of the motion of the gas mass in the outburst and the energy of the solar cosmic rays are of the same order of magnitude. This allows us to suppose that the generation process of particles of comparatively high energy is based on the transfer of kinetic and magnetic energy of the motion of the substance of the outburst to the charged particles by means of various electromagnetic processes which inevitably must take place during the outburst. It should be noted that the acceleration mechanism should be thus extraordinarily effective. For example, if we assume that acceleration took place only within the volume of the flare, which is $\sim 10^{28}$ cm^3, then the production of energy per 1 cm should be of the order of 10^4 erg.

5·2. *Kinetic equation for the function of distribution of relativistic particles in the outburst.* – In ref. [9] some acceleration mechanisms of solar particles were investigated and it was suggested that the statistical acceleration mechanism due to irregular motion of magnetized clouds is most preferable.

Further on we shall try to show that an important role in the generation of solar cosmic ray may play the acceleration of particles in « traps » between two colliding shock waves in a magnetized ionized medium [10], the acceleration in magneto-hydrodynamic waves [11], the acceleration of particles in cylindrical shock waves within the magnetized plasma formed by discharges similar to the ones artificially created in the laboratory [12].

The main characteristics of the acceleration process are:

1) the rate of increase of particle's energy $\alpha = (1/\varepsilon)\,\mathrm{d}\varepsilon/\mathrm{d}t$ (the value of α is determined by the combined action of all acceleration mechanisms: $\alpha = \sum \alpha_i$);

2) the rate of leakage of particles from the volume in which acceleration is taking place;

3) the energy losses due to ionization, to nuclear absorption, to the inverse Compton effect, to bremsstrahlung and to magnetic bremsstrahlung losses;

4) the rate of injection of particles with energy exceeding some critical value ε_{cr}.

We consider the total number of particles in the whole volume of the flare. Therefore it is unnecessary to study the spatial co-ordinates' dependence. We shall take into account diffusion by introducing the effective lifetime of the particles T_0 in the acceleration volume.

When treating the acceleration of heavy particles (protons and nuclei) up to a comparatively low energy, we may disregard the loss due to the inverse Compton effect, the bremsstrahlung and magnetic bremsstrahlung radiation.

If we are also to disregard the fluctuation of the energy lost by particles due to ionization and nuclear absorption (the validity of such a treatment will

be cleared below), then the kinetic equation for the distribution function of relativistic particles in the acceleration volume is

$$\frac{\partial N(\varepsilon, t)}{\partial t} = \varkappa(t)\,\delta(\varepsilon_0 - \varepsilon) + \frac{\partial}{\partial \varepsilon}\left[\alpha(t) c \varepsilon N(\varepsilon, t)\right] - \frac{N(\varepsilon, t)}{T_0}\,. \tag{9}$$

Here $N(\varepsilon, t)$ is a total number of particles having the energy ε in the acceleration volume at the moment t after the beginning of acceleration; $\varkappa(t)$ is the number of particles with energy ε_0 formed in the whole volume (ε_0 is the energy of injection for the given mechanism). The first term at the right hand side is the rate of injection of particles, the second the acceleration, the third the leakage from the space of acceleration.

The solution of the equation (9) is [13]:

$$N(s, x) = \varkappa(x) \exp\left[-\int_0^s \alpha(x + s)\,\mathrm{d}s - \frac{s}{T_0}\right], \tag{10}$$

where x and s are determined by the equation

$$\varepsilon = \varepsilon_0 \exp\left[\int_0^s \alpha(x + s)\,\mathrm{d}s\right]; \quad t = x + s\,, \quad \text{when} \quad \varepsilon \leqslant \varepsilon_0 \exp\left[\int_0^s \alpha(s)\,\mathrm{d}s\right]. \tag{11}$$

The meaning of x and s is obvious: s is the time which is necessary for the particles starting their acceleration in the moment x with the energy ε_0 to attain the energy ε.

It is seen from (10) that the spectrum of the high energy particles depends on the form of $\varkappa(t)$ and $\alpha(t)$.

Let us suppose [2] that the acceleration mechanism was put into operation at a certain moment $t = 0$ and was switched away at the moment $t = t_{\max} \gg T_0$, the functions $\alpha(t)$ and $\varkappa(t)$ throughout this period remaining constant, i.e.:

$$\begin{cases} \alpha(t) = \alpha\,; \quad \varkappa(t) = \varkappa & 0 < t < t_{\max}\,, \\ \alpha(t) = \varkappa(t) = 0 & t < 0;\ t > t_{\max}. \end{cases} \tag{12}$$

Then for $t < t_{\max}$

$$N(\varepsilon, t) = \begin{cases} \varkappa \left(\dfrac{\varepsilon}{\varepsilon_0}\right)^{1 + (1/\alpha T_0)} & \text{at} \quad \varepsilon \leqslant \varepsilon_0 \exp\left[\alpha t\right], \\ 0 & \text{at} \quad \varepsilon > \varepsilon_0 \exp\left[\alpha t\right], \end{cases} \tag{13}$$

and for $t > t_{\max}$

$$N(\varepsilon, t) = \begin{cases} \varkappa \left(\dfrac{\varepsilon}{\varepsilon_0}\right)^{1 + (1/\alpha T_0)} \exp\left[-\dfrac{t - t_{\max}}{T_0}\right] & \text{at} \quad \varepsilon \leqslant \varepsilon_0 \exp\left[\alpha t_{\max}\right] \\ 0 & \text{at} \quad \varepsilon > \varepsilon_0 \exp\left[\alpha t_{\max}\right]. \end{cases} \tag{14}$$

3·3. *Estimation of the main parameters determining acceleration.* – The value of α may be calculated if we know the acceleration time t_{max} and the maximum energy of the accelerated particles ε_{max}:

$$\alpha = \frac{1}{t_{max}} \cdot \ln \frac{\varepsilon_{max}}{\varepsilon_0} . \tag{15}$$

The duration of time of action of the acceleration mechanism may be connected with the delay of the beginning of the outburst of cosmic rays with respect to the solar flare ($t_{max} \approx 15$ min). ε_{max} should be $\gtrsim 20$ GeV. Then from eq. (15) we receive (assuming that $\varepsilon_0 \approx 1$ GeV):

$$\alpha \sim 2 \cdot 10^{-3} \text{ s}^{-1} . \tag{16}$$

In order to obtain the observed energy spectrum (2) for the solar particles flux it is necessary to put in (14):

$$1 + \frac{1}{\alpha T_0} = 7 , \qquad \alpha T_0 = \frac{1}{6} . \tag{17}$$

Keeping in mind (16) we see that we can satisfy the relation (17) if $T_0 \sim 10^2$ s. Characteristic dimension for the space of acceleration is $R_0 \sim 10^{10}$ cm. Therefore the average free path with respect to scattering for the particles in this volume is:

$$l_0 \approx \frac{R_0^2}{2 T_0 c} \gtrsim 2 \cdot 10^7 \text{ cm} , \tag{18}$$

which seems to be a plausible figure for the value of quasi-uniform parts of the field in the flare. (We could not find in the literature any definite data for this quantity.) If $T_0 \lesssim 10^2$ s, then the particle flux from the flare at $t > t_{max}$ will diminish according to (14), quite rapidly, more rapidly than the observed flux of solar particles at the earth (since $T_0 \ll T_\odot \approx \frac{1}{4}$ hour). This means that in the vicinity of the solar flare must take place processes of scattering and accumulation of accelerated particles, leaving the small volume of the flare. If we take the dimension of the accumulating volume to be of the order of the radius of the sun $R_\odot \sim 10^{11}$ cm, then it is necessary for the mean free path within this volume to be

$$l_\odot \sim \frac{R_\odot^2}{2 T_\odot c} \approx 2 \cdot 10^8 \text{ cm} .$$

In order to secure an effective scattering of particles at a distance $l_\odot$, it is necessary for the non-homogeneous fields of the solar atmosphere, first of all in the corona, to have a field strength $H \gtrsim 0.3$ Oe, which seems to be satisfied.

If, on the other hand, we start from the angular dimension of the source, which is equal to $15° \div 30°$, then $R \approx 5 \cdot 10^{12}$ cm, $l \approx 5 \cdot 10^{11}$ cm and the field in the source should be $H \gtrsim 10^{-4}$ Oe (for $\varepsilon = 2 \cdot 10^{10}$ eV).

3·4. *Ionization losses and nuclear absorption.* – Now, we may clarify the conditions for the possibility of neglecting the ionization losses and nuclear collisions. The ionization losses of non-relativistic protons (mass M) in completely ionized hydrogen are given by the equation (see [14])

$$(19) \qquad -\left(\frac{\mathrm{d}\varepsilon}{\mathrm{d}t}\right)_{\mathrm{ion}} = 7.62 \cdot 10^{-9} n \sqrt{\frac{2Mc^2}{\varepsilon_{\mathrm{kin}}}} \left\{42 - \frac{1}{2} \ln n + \ln \frac{\varepsilon_{\mathrm{kin}}}{Mc^2}\right\} \quad \mathrm{eV/s} \,,$$

where n is the concentration of electrons. From (19) it follows that for $n \lesssim 10^{12}$ (central chromosphere and higher levels) $\alpha\varepsilon \gtrsim (\mathrm{d}\varepsilon/\mathrm{d}t)_{\mathrm{ion}}$ when $\varepsilon_{\mathrm{kin}} \gtrsim$ $\gtrsim 0.02$ GeV. Therefore, if the acceleration takes place mainly in the region where the density of the particles $n \lesssim 10^{12}$ cm^{-3}, and if $\alpha \gtrsim 2 \cdot 10^{-3}$ s^{-1}, then we may neglect the ionization losses beginning with protons whose energy is about 20 MeV. Particles with such energy may appear due to acceleration in variable sun spot fields [15]. In the course of collisions of gas masses moving at a velocity of $\sim 10^8$ cm/s, particles with a kinetic energy of only $(10^4 \div 10^5)$ eV may appear. Therefore, in order to accelerate the particles with such energy, it is necessary to have $\alpha \sim (10^{-1} \div 10^{-2})$ s^{-1}, i.e., in the first stage of the acceleration process α should be considerably greater than in the following period. Furthermore, in the interval of densities of $n \gtrsim 10^{12}$ cm^{-3} we may neglect nuclear collisions as well, since during the acceleration time ($\lesssim 10^3$ s) a particle penetrates through a layer of substance whose thickness is $\lesssim 50$ g/cm^2. Nuclear collisions may play an important part for heavier nuclei even if they are generated in layers with $n \lesssim 10^{12}$ cm^{-3}. The knowledge of a nucleus energy spectrum for various Z would greatly help in determining the main characteristics of the accelerating mechanism of cosmic rays on the sun.

3·5. *Efficiency of various accelerating mechanisms.* – Now that we know the values of α, we may determine the conditions under which a particular accelerating mechanism of particles is efficient enough to secure the necessary value of α.

According to Fermi's statistical mechanism

$$(20) \qquad \alpha = \frac{vu^2}{c^2 l} \,,$$

where v is the velocity of inhomogeneities, l is the average scattering free path. According to (18) the size of the moving inhomogeneities should be $l \gtrsim 2 \cdot 10^7$ cm. Therefore, the statistical mechanism may be efficient only if

the velocity of the turbulent motion is (for $v \approx c$)

$$u = \sqrt{\alpha c l} \gtrsim 10^9 ; \quad 3 \cdot 10^8 ; \quad 4 \cdot 10^7 \text{ cm/s} , \tag{21}$$

for $\alpha = 1$, 10^{-1} and $2 \cdot 10^{-3}$ s^{-1} respectively.

However, according to the astrophysical data, it is hardly possible for the velocity to exceed $\sim 3 \cdot 10^7$ cm/s. Thus the statical mechanism cannot play any important role in the beginning of the acceleration. It can become important only at the following stages, when the particles receive enough energy (for example, due to the acceleration in the fields of spots [15]).

For the acceleration in « trap » [10]

$$\alpha = \frac{f u v^2}{l c^2} , \tag{22}$$

where u is the velocity of the shock waves approaching each other, l is the size of the trap, f is the probability for the particle to be caught in the trap. The same equation for α holds for the acceleration of the particles within high voltage discharge [12]. In this case, u is the velocity of the contracting cylinder, l being its diameter. In both cases the acceleration stops when the particle acquires enough energy to overcome the magnetic field holding it within the trap or within the plasma column. The acceleration in this case becomes noticeable if

$$\frac{f u v^2}{l c^2} \sim 2 \cdot 10^{-3} \text{ s}^{-1} . \tag{23}$$

For $l \approx 2 \cdot 10^7$ cm, $f \sim 1$, $v/c \sim 0.01$ and $u \sim 3 \cdot 10^7$ cm/s, the acceleration may be efficient and this mechanism, in principle, can provide the initial acceleration of particles even beginning with low energy.

Acceleration of the particles in magneto-hydrodynamic waves [11] gives:

$$\alpha = \frac{2}{9} \nu \left(\frac{\delta H}{H} \right)^2 = \frac{2}{9} \frac{u}{\lambda} \left(\frac{\delta H}{H} \right)^2 , \tag{26}$$

where ν frequency, λ wave length and u the phase velocity of the magneto-hydrodynamic wave; $\delta H/H$ the ratio of the wave amplitude to the average magnetic field. If $\delta H/H \gtrsim 1$, we shall find out that it is necessary for this mechanism to be efficient to have a frequency of the magneto-hydrodynamic wave $\nu \gtrsim 10^{-2}$ s. For $\lambda \gtrsim 10^7$ cm, this gives $u \gtrsim 10^5$ cm/s, which is quite possible in the solar atmosphere [16].

Therefore, none of the mechanisms of generation of high energy particles considered above is absurd under the conditions of the solar flare.

It is possible that all these mechanisms play a certain role in the acceleration of particles, and their relative efficiency varies considerably when the energy of the particles increases. It is possible that in the beginning of the acceleration process the latter two mechanisms are the most efficient and it is only when the particles attain high energy that the statistical mechanism comes into operation. It is clear that without a detailed knowledge of the process of development of the solar flare, it is difficult to solve these problem.

Moreover, the investigation of this process is of great interest not only for the understanding of the nature of the solar flare, but also for the solution of the origin of cosmic rays problem. There exists a great similarity between the solar flares and the outbursts of Super Novae. Both of them are accompanied by an emission of visible light and by radio emission. In both cases generation of cosmic rays takes place and in both cases we observe intensive turbulent flow of ionized gas masses.

From this point of view the problem of production of relativistic electrons during the solar flares is of great interest.

3·6. *Production of fast electrons during the solar flares.* – It is evident that if the electrons were accelerated in some way up to the energy of $\sim 10^9$ eV, then their further acceleration would take place, similarly to the acceleration of protons with $\alpha \gtrsim 2 \cdot 10^{-3}\ \mathrm{s}^{-1}$. But for electrons of such a high energy we have a bremsstrahlung radiation due to collisions with protons and the magnetic bremsstrahlung radiation while they are moving in magnetized clouds.

The corresponding energy losses are equal to [14]

$$\left\{ \begin{array}{l} -\left(\dfrac{\mathrm{d}\varepsilon}{\mathrm{d}t}\right)_{\mathrm{br.}} \approx 8 \cdot 10^{-15} n\varepsilon \quad \mathrm{eV \cdot s^{-1}}\,, \\ -\left(\dfrac{\mathrm{d}\varepsilon}{\mathrm{d}t}\right)_{\mathrm{magn.\text{-}br.}} \approx 10^{-3} H^2 \left(\dfrac{\varepsilon}{m_0 c^2}\right)^2 \quad \mathrm{eV \cdot s^{-1}}\,. \end{array} \right. \tag{27}$$

The acceleration of electrons is impossible if

$$\left(\frac{\mathrm{d}\varepsilon}{\mathrm{d}t}\right)_{\mathrm{accel.}} < -\left[\left(\frac{\mathrm{d}\varepsilon}{\mathrm{d}t}\right)_{\mathrm{br.}} + \left(\frac{\mathrm{d}\varepsilon}{\mathrm{d}t}\right)_{\mathrm{magn.\text{-}br.}}\right]. \tag{28}$$

For simplicity, let us take into consideration the magnetic bremsstrahlung losses alone (because for the layers with $n \lesssim 10^{12}\ \mathrm{cm}^{-3}$ they are most essential when the energy is $\varepsilon \gtrsim 10^9$ eV). We see that electrons may be accelerated only up to an energy of

$$\varepsilon \lesssim \frac{2(m_0 c^2)^2}{H^2} \sim \frac{5 \cdot 10^{11}}{H^2}\ \mathrm{eV}\,.$$

Therefore, if the field strength is $H \gtrsim 10$ Oe (e.g., near the sun spots), then the electrons may be accelerated up to $\varepsilon \sim 5 \cdot 10^9$ eV. Under these conditions their spectrum in this region should be steeper than that of the protons. The injection energy for electrons, if $\alpha \sim 2 \cdot 10^{-3}\,s^{-1}$ should be by an order of magnitude greater than for protons (which is equal to about $2 \cdot 10^8$ eV). That is why we can suppose that the flux of electrons in the outburst will probably be smaller than the proton flux. The magnetic bremsstrahlung radiation of electrons in the region of the flare and in the region of accumulation (i.e., mainly in the region of the corona) may lead to a powerful outburst of radioemission which indeed was observed experimentally.

In the region of accumulation, the electrons will stay during a time which is $\gtrsim 10^3$ s, and during this time the electrons with an energy of $\sim 5 \cdot 10^9$ eV will lose a greater part of their energy due to the magnetic bremsstrahlung radiation, already if $H \gtrsim 2 \cdot 10^{-2}$ Oe. Therefore, even if electrons were generated at the same rate as the protons (which is hardly probable) then their flow from the sun would be certainly much smaller than the flow of heavy particles (of protons and of nuclei).

REFERENCES

[1] L. I. Dorman and E. L. Feinberg: in this issue, p. 358.
[2] L. I. Dorman and G. I. Freidman: *Trudy YaFAN, Ser. Fiz.*, 2 (1957).
[3] L. I. Dorman: *Variations of Cosmic Rays* (Moscow, 1957; in Russian).
[4] T. Gold and H. Elliot: *The Solar Cosmic Ray Outburst*, 1956, February 23, Royal Greenwich Observatory, 1956.
[5] J. Firor: *Phys. Rev.*, **94**, 1017 (1954).
[6] L. J. Davis: *Phys. Rev.*, **100**, 1440 (1955).
[7] P. Meyer, E. N. Parker and J. A. Simpson: *Phys. Rev.*, **104**, 768 (1956).
[8] S. Chandrasekar: *Stochastic Problems in Physics and Astronomy.*
[9] L. I. Dorman: *Dissertation*, Moscow, *FIAN* (1955).,
[10] E. Fermi: *Astrophys. Journ.*, **119**, 1 (1954).
[11] W. B. Thompson: *Proc. Roy. Soc.*, **233** A, 402 (1955).
[12] I. V. Kurchatov: *Atomic Energy*, **3**, 65 (1956).
[13] S. A. Kaplan: *Žu. Èksper. Teor. Fiz.*, **29**, 406 (1955).
[14] V. L. Ginzburg: *UFN*, **51**, 343 (1953).
[15] P. F. Kolpakov: *Astr. Journ.*, Moscow, **34**, 222 (1957).
[16] H. Alfvén: *Cosmical Electrodynamics* (Oxford, 1950).

INTERVENTI E DISCUSSIONI

— L. Biermann:

I would like to make two remarks. The first of which refers to the correlation of the cosmic ray intensity with the indices of solar activity. There is the well known correlation with the intensity of the solar corpuscular radiation, which was mentioned by the speaker. Secondly there is the possible influence of the non-thermal electromagnetic radiation, particularly in the UV range, which is connected with solar activity. We looked into this question a number of years ago and this work, which is mainly due to v. Roka, has been described in the treatise *Kosmische Strahlung*, p. 40, written by members of our Institute and edited by W. Heisenberg (Berlin, Göttinge, Heidelberg, 1953). The result of these investigations was that there is not only the well known negative correlation of the cosmic ray intensity with the corpuscular activity of the sun, but that there is also an independent negative correlation with the intensity of the excess non-thermal electromagnetic radiation, for which Bartel's values, derived from the amplitude of the daily variation of the geomagnetic field in Huancayo, were used. My question is then, whether this correlation has been taken regard of in the work of our Russian colleagues. — Secondly I would like to comment on the value of the particle density in the solar corpuscular streams. These enter also in the theory of the comet's tails, which I developed since 1951. In this theory the acceleration of the ion tails (Bredichin type I) is regarded as being due to the interaction of the solar corpuscular radiation with the tail plasma. Furthermore it appears that the most effective mechanism, by which the cometary molecules are ionized, is the exchange of charge with the ions of the solar corpuscular streams. The observed rate of formation of ion structures in the tails can then be used to derive a value to a particle density in the solar corpuscular radiation. Values of the order 10^4 cm^{-3} are then found for intense streams (possibily up to 10^5 cm^{-3} in very big magnetic storms), and values of the order of several times 10^2 or 10^3 for normal conditions. Such values were first derived by Chapman and Unsöld (*Observatory*, **69**, 219 (1949)) on a different basis. They are higher by some powers of ten than the values mentioned by our Russian colleagues, in agreement with earlier estimates by geophysicists. Personally I would be inclined to regard the argument from the mechanism of ionization on the comets as the most reliable one among all those which have been mentioned in this connection.

The same line of arguments leads then to the conclusion that the solar corpuscular radiation is visible as part of the polarized component of the zodiacal light (this answers at the same time a subsequent remark by Professor Menzel) and that there is no stationary interplanetary gas; these aspects have been discussed more in detail in a recent letter to *Observatory*.

— L. I. Dorman:

Note added in proof. – Concerning the remarks by Professor L. Biermann we would like to notice, that:

1) According to Roka, UV solar radiation may lead to a negative temperature effect of cosmic rays due to heating of the ozone layer. It was shown in [3], pp. 135 and 272, that if this effect exists at all, it may tell only on 27-days and small solar flares cosmic ray variations.

2) Figures for corpuscular stream densities used by us seem to be again supported by the recent special symposium on streams, held in Moscow in 1955 (see « Physics of Solar Corpuscular streams », *Akad. Nauk SSSR*, (1957).

PART II.

Origin Problem.

The Origin of Cosmic Rays: Some Astrophysical Problems.

G. R. Burbidge

Mount Wilson and Palomar Observatories, Carnegie Institution of Washington, California Institute of Technology - Pasadena, Cal.

The following discussion of the origin and acceleration of cosmic-ray particles will be divided into four parts:

1) The possible sources of the particles and their primary acceleration before injection into the interstellar gas,
2) The acceleration mechanism inside galaxies,
3) The source of energy and the energy-transfer problem,
4) The acceleration mechanism outside galaxies.

The discussion will be confined mainly to aspects of these problems which are related to investigations that have been made by the author and his associates. No attempt at completeness will be made, but those parts of the problems which are likely to be discussed by others at the conference will be omitted.

1. – The possible sources of the particles and their primary acceleration before injection into the interstellar gas.

We shall exclude any discussion of the solar system as the only source of cosmic rays. Particles can either be ejected from stellar atmospheres, in stellar explosions, or from gaseous nebulae. Thus astronomical evidence for the primary sources can come from a number of directions:

a) Evidence for nuclear activity on the surfaces of stars,
b) Evidence for explosions of various types which might eject particles,
c) Other evidence for the presence of high-energy particles in our Galaxy.

a) *Evidence for nuclear activity on the surfaces of stars.* – The primary evidence for nuclear activity on stellar surfaces is obtained from the spectra

of the stars discovered by H. W. Babcock to have strong magnetic fields [1]. Analyses of some of these spectra [2, 3] show that a large number of elements are anomalously abundant relative to the abundances in normal stars having similar temperature and ionization conditions in their atmospheres. The types of effects which are seen are shown in Table I, where abundances estimated from curve-of-growth studies for two magnetic stars are given. In addition to this, it appears from measurements of the isotope-shift effect that in another magnetic star a large amount of ^{3}He may be present [4].

Some of the abundance effects can be explained if it is supposed that the nuclear activity produces a flux of free neutrons (following proton acceleration and (p, n) reaction on the light nuclei), some of which can eventually be captured by the comparatively abundant elements in the iron peak of the abundance curve which have large neutron-capture cross-sections at appropriate energies. Other abundance effects may be due to α-particle reactions. The conditions for acceleration and synthesis have been discussed elsewhere [5], and accelerations produced by other mechanisms, e.g. that discussed by Sweet [6] and others in flares, might be invoked. It should be emphasized that a major difficulty associated with this mechanism is that a large flux of particles needs to be accelerated at one time, so that so-called hot spots are produced on the surface of the star. Other difficulties have been discussed by Biermann [7]. Whatever type of energy spectrum is produced, it appears highly probable that its tail would extend out to energies $\gtrsim 10^8$ eV which are needed as injection energies in all of the variations of the Fermi mechanism so far proposed. It seems probable that far more stars than just the magnetic A- and F-type stars have magnetic activity going on in their surfaces. For in the A and F stars it appears that the peculiar conditions demanded so that the abundance anomalies are seen, namely that only a very thin surface layer be affected, are fulfilled. However, a number of stars in which the mixing zones are probably much deeper, and in which, therefore, we should not expect to see abundance anomalies, have been detected by Babcock to have magnetic fields in the kilogauss range. Furthermore, there is a very severe observational selection effect present, since Babcock can only hope to detect fields in stars whose spectra have intrinsically very sharp lines.

If we confine ourselves to the magnetic A- and F-type stars it appears that there may be about 10^7 currently present in our Galaxy with mean field strengths in excess of one kilogauss. The average life of such stars can be supposed to be $\sim 10^8$ years, which is sufficiently long, as compared with the average life of a cosmic-ray proton in the Galaxy, to permit us to assume that all of the cosmic rays present in the Galaxy have come from a single generation of magnetic stars (neglecting the spread in star births). Now the total cosmic-ray energy in the Galaxy may be $\sim 10^{56}$ ergs, and if the mean energy per particle is presently $\sim 10^{-2}$ ergs, about 10^{58} particles have been

TABLE I. – *Abundances of the elements in two « peculiar A » stars, relative to those in a normal star.*

Element	Magic number isotope (A, N) for anomalous elements	α^2CVn	HD 133029
Magnesium	—	0.4	1.4
Aluminium	—	1.1	2.2
Silicon	28, 14	10	25
Calcium	40, 20	0.02	0.05
Scandium	—	0.7	—
Titanium	—	2.6	2.3
Vanadium	—	1.3	3.2
Chromium	52, 28	5.2	10.3
Manganese	—	16	15
Iron	—	2.9	4.1
Nickel	—	3.0	2
Strontium	88, 50	14	11.5
Yttrium	89, 50	20	—
Zirconium	90, 50	30	40
Barium	138, 82	$\leqslant 0.9$	—
Lanthanum	139, 82	1020	200
Cerium	140, 82	400	190
Praseodymium	141, 82	1070	630
Neodymium	142, 82	250	200
Samarium	144, 82	410	260
Europium	—	1910	640
Gadolinium	—	810	340
Dysprosium	—	760	460
Lead	208, 126	1500	1500

produced. This would imply that each star has generated about 10^{51} particles with a mean energy ~ 500 MeV ($8 \cdot 10^{-4}$ ergs injection energy) and has therefore emitted about $8 \cdot 10^{47}$ ergs in the form of cosmic rays, i.e. $\sim 0.7\,\%$ of its total radiant energy emitted in its lifetime, or near $15\,\%$ of that emitted in a period $\sim 5 \cdot 10^6$ years. This is a large proportion, and it would suggest perhaps that a wider population of stars than these alone contribute to the primary flux. On the other hand, the possibility that in their early lives, perhaps during condensation, such stars were much more active than they are today, cannot be ruled out.

Another argument is obtained from the requirements of a theory of element synthesis in stars [8]. This theory is unable to explain the observed abundances of D, Li, Be, and B, unless it is supposed that they are produced in cool, low-density regions, since they are always rapidly destroyed in hydrogen-burning in stellar interiors. Thus the argument has been put forward that

they may have been produced in spallation reactions high in the atmospheres of stars. In this case the observed result that the (Li, Be, B) abundance is of the same order of magnitude as the (C, N, O) abundance in the primary cosmic-ray flux is explained by the fact that the spallation producing this has gone on in the stellar atmospheres as well as in the interstellar gas. It should be emphasized that the difference in density between the upper layers of an average stellar atmosphere and the interstellar medium means that the probability, per unit time, of experiencing a nuclear collision is about 10^{10} times greater in the atmosphere than in the interstellar gas. It is also found, in the theory of element synthesis, that to produce the so-called cosmic abundances of Li, Be, and B, it is necessary to suppose that a wider class of stars than the magnetic stars takes part, so that if this picture were accepted there would be more than 10^7 stars available as primary sources. Deuterium, which has a very high abundance on the earth, cannot be produced in sufficient quantities by this mechanism.

Another direct method of showing that nuclear activity is taking place in limited regions on the solar surface, is to detect the presence of some of the first isotopes which will be synthesized in such activity, i.e. D, ^{3}H, and ^{3}He. It is of some interest that at the University of Michigan attempts are under way to detect some of these isotopes by examining the spectral features in flares under very high dispersion [9], while in the USSR Severny [10] claims already to have detected deuterium in flare regions, and he estimates that the D/H ratio is $\sim 10^{-5}$.

b) Evidence for explosions of various types which might eject particles. – Stellar explosions are characterized by sudden large increases in luminosity, and in some cases by measurements on the Doppler shifts of spectral features which show that material is moving rapidly out from the seat of the explosion. Supernovae, novae, and flares all appear to be different types of stellar explosion. For novae and flares, little new information is available. Though it is certainly possible that enough material can be ejected to provide the primary source of cosmic radiation, it does not appear that we can make any new estimates until the mechanisms which trigger these outbursts are understood. Supernovae have long been proposed as primary sources of cosmic rays. We shall consider here the circumstances under which primary particles could be produced in the context of a theory of element synthesis in stars which has recently been proposed [8]. According to this theory supernovae are the source of production of the neutron-rich isotopes of the heavy elements and of uranium and thorium and the trans-uranium elements. They are synthesized when a base material, which is taken to be the elements in the iron peak of the abundance distribution, is subjected very rapidly to an extremely large neutron flux. Observational evidence in favor of the theory ist he fact

that after 50-100 days the light curves of supernovae of Type I decay with a half-line of 55 days, while the most recent values of the decay half-life against fission of ^{254}Cf are 56.2 ± 0.7 [11] and 61 days [12], so that it has been proposed that this is the isotope responsible for the observed decay curve. ^{254}Cf is the only β-stable neutron-rich nucleus which decays predominantly by spontaneous fission and which has a half-life between 10 days and 10^4 years. The optimum conditions under which isotopes with atomic weights up to ~ 260 will be synthesized are obtained when the envelope of the supernova is hydrogen-poor, so that the abundance of H, He, C, N, O, are all about equal (by number) while the abundance of Fe is about 1% of these light elements. The production of neutrons occurs when, following the initial implosion of the core and the inner envelope of the supernova, (p, γ) reactions on nuclei such as ^{20}Ne generate temperatures of the order of 10^9 degrees and also produce ^{21}Ne following the β-decay of ^{21}Na. Then (α, n) reactions of the type $^{21}\mathrm{Ne}(\alpha, n)^{24}\mathrm{Mg}$ taking place at these temperatures are sufficient to produce tremendous fluxes of neutrons amounting to $\sim 4 \cdot 10^{32}$ cm^{-2}s^{-1}, the net effect of this sequence of events being to transform a large proportion of the protons to neutrons. These neutrons are then captured by the Fe, and the material is driven up to about $A = 260$, at which point the fission rate becomes faster than the rate at which neutrons can be added. Thus the material will fission and if further neutrons are added it will begin to cycle and thus to build up the abundances in the region between $A = 110 \div 150$ (the two peaks in the fission fragment curve) and $A = 260$, while continuously depleting the iron.

Thus if any of this material eventually forms part of the primary cosmic-ray flux, and if it has not been modified by any further nuclear reactions, we might expect to find that:

i) the abundances of light elements such as C, N, O, Ne, relative to hydrogen, are very much greater than the values given in the abundance tables;

ii) the abundance of Fe relative to hydrogen is very much greater than normal;

iii) the abundances of isotopes with $A \gtrsim 110$ are very much greater than normal, and in the extreme case are comparable with or greater than the abundance of Fe.

Another process which is demanded in the theory of element synthesis in stars is that which builds the elements in the iron peak. It has been proposed that this process takes place under conditions in which statistical equilibrium is reached between nuclei, neutrons, protons, and radiation. Under such conditions the nuclei will tend to converge to the condition of maximum stability, i.e. to the bottom of the packing fraction curve, so that ^{56}Fe will appear in maximum

abundance, the abundances of nuclei with $A > 56$ falling away very rapidly. To reproduce the abundances of the isotopes in the range $50 \leqslant A \leqslant 62$ in the solar system it has been found that a freezing temperature $\sim 4\ 10^9$ degrees, and a ratio of free protons to free neutrons of about 300, is required. Under these conditions about 80% (by mass) of the core of the star will be transmuted to ^{56}Fe. Further contraction of the core and increase of temperature and density beyond this point may result in the conversion of the ^{56}Fe to ^{4}He together with the development of an instability which may trigger a supernova outburst. Thus it would appear that in some circumstances a supernova explosion would lead to the ejection of core material in which case we might expect to find in an unmodified cosmic ray flux that:

i) the abundance of ^{56}Fe would be extremely large,

ii) the abundance of ^{4}He might be very large.

Some evidence has already been put forward that the composition of the cosmic-ray flux is not normal. For example, Noon, Herz, and O'Brien [13] have found that together with the usual anomaly associated with Li, Be, and B, which they find to be greater than 100 times their normal abundances, the abundance of elements with $Z > 10$ is more than six times normal.

It should be emphasized that the temperature demanded to produce such synthesis is only $\sim 10^9$ degrees (100 keV) so that there is no possibility that the injection energy required for particles to be accelerated in the interstellar gas (~ 100 MeV) could be supposed to be provided by the high-energy Maxwellian tail of such an energy distribution. The acceleration mechanism which might be responsible for the gain to the injection energy in the interstellar gas will be discussed in the following sub-section.

c) Other evidence for the presence of high-energy particles in the Galaxy. – The most striking result obtained in recent years has been the explanation of the high degree of polarization of the light from the Crab nebula as being due to synchrotron radiation emitted by electrons (and positrons) accelerating in the magnetic field which must be present there. This explanation, first proposed by Šklovskij [14], shows that in the only supernova remnant which can be investigated in any detail there is a tremendous flux of high-energy particles and magnetic field. Calculation of the minimum amounts of energy in particles and field which are able to explain the power levels in both visible light and radio emission shows that there are at least $\sim 10^{48}$ ergs in each of the energy modes, kinetic energy of the filaments, magnetic energy, and high-energy particles. The mean energy of the electrons in the model of Oort and Walraven [15] is about 100 GeV. Both Šklovskij, and Oort and Walraven have proposed that systems such as the Crab are by themselves important sources of cosmic radiation. They have assumed that all of the high-energy

nucleons in the Crab will eventually escape, and if the rate of supernova outbursts in our own Galaxy is about 1 every 100 years, they conclude that a considerable proportion of the energy of cosmic radiation currently present is due to objects such as this. A number of qualifying statements concerning these ideas can be made.

Oort and Walraven have assumed that there is equipartition in energy between the electrons and the nucleons. Now if the particles gain their energy by a Fermi-type mechanism which is operating inside the nebula, it would not be expected that this approximate equipartition would be reached, but that far more energy would be gained by the nucleons, in the limit (M/m) times as much as the electrons. This would mean that the average nucleon energy at maximum would be near 10^{14} eV and this would destroy the equipartition between the different energy modes. If such a situation were reached, it would mean that the pressure exerted by the cosmic rays would be overbalancing the other pressures and the nebula would be expanding because of this pressure. While there is no direct observational reason for excluding this, it is difficult to see how such an extreme situation could have arisen. For if the particles have continuously gained their energy at the expense of the turbulence and magnetic energy, it seems that after approximate equipartition is reached, the rate of particle-energy gain will be very considerably slowed down as the pressure exerted by the already present particle flux tends to reduce the turbulence and give rise to some alignment in the magnetic field. Now some degree of alignment in the field has been observed [16]. This might suggest that some degree of inequality between the energy of the particles and the hydromagnetic energy of the gas has been reached, with the particle energy perhaps a few times greater than the total energy in the other modes, and the expansion is mainly governed by the cosmic-ray pressures, i.e. the equipartition condition has only been slightly overshot.

This argument leads us to propose that a more plausible idea concerning the origin of the electrons (and positrons) is as follows. The primary flux of particles is the nucleon flux which has been ejected first from the supernova outburst, and later has been reinforced by further ejection in the form of wisps of material (oberved by Baade [17]). Following some acceleration in the nebula these nucleons collide with the atoms in the « stationary » gas, and, after meson production and decay, they produce the flux of electrons and positrons. This problem will be discussed in more detail elsewhere [18], but it appears that the electrons and positrons are produced at fairly low energies ($\sim 10^8$ eV) and then a fraction is accelerated by the small-scale structure in the nebula to give the energies demanded so that they will emit radiation in the visible region, while the remainder is responsible for the radio-emission of the nebula.

Such a model suggests that supernova remnants of this kind do contribute

to the primary cosmic-ray flux, but there are some modifications when we consider the chemical composition of the particles. A considerable amount of nuclear activity takes place inside the nebula and it is this which may well affect the primary flux which we have earlier suggested may be ejected in the supernova outburst. Thus the results of Noon *et al.* might be explained by supposing that the material with anomalous composition was initially ejected in the outburst, that it was accelerated in the early life of the nebula (in the first few days) by a Fermi mechanism acting in the turbulent gas and magnetic field amplified by the initial shock front. Further acceleration spread over a time-scale of years increased the energies of nucleons above the thresholds for meson production in nucleon-nucleon collisions, so that the electron-positron flux began to build up. Acceleration over a time-scale $\sim 10^3$ years has resulted in a large proportion of the energy being transferred to the high-energy nucleon flux that is mainly responsible today for the expansion of the nebula. The smaller hydromagnetic eddies in the gas are still able to accelerate the secondary electrons and positrons.

Throughout this sequence of events the Li, Be, and B have been built up, while the Fe which was exceedingly over-abundant initially has been spallated to some extent, though its abundance has not been reduced to the normal value before escaping. A model of this sort for the Crab would contain more energy in the nucleons ($\sim 10^{50}$ ergs) than was proposed in the earlier models so that if sufficient of these could escape a large proportion of the primary flux could be supposed to originate in supernovae. The radio source Cassiopeia A may also be a supernova remnant. It is a more powerful source of radio emission than the Crab, though no synchrotron radiation in the visible part of the spectrum has been observed. Its distance is in some dispute, but if it is $\geqslant 3$ kiloparsecs, a distance which has been estimated by radio techniques, the total amount of energy in particles and field necessary to explain the radio power is also $\sim 10^{50}$ ergs.

A reasonable estimate of the rate of supernovae is perhaps 1 every 300 years, a value slightly smaller than that previously proposed. Since some type of Fermi mechanism for further acceleration of particles following escape from the primary sources does appear to exist in the Galaxy, there does not appear to be any virtue in attempting to prove that acceleration in supernova remnants can account for all of the cosmic ray energy in the Galaxy. In any attempt of this sort the explanation of the extremely high-energy particles must prove to be an overriding difficulty.

Apart from abnormal astronomical objects such as magnetic stars, gaseous nebulae which form supernova remnants, novae, and flare stars which may also accelerate particles at their surfaces, it is entirely possible that normal stars make a considerable contribution to the flux of primary particles. Unfortunately studies of particular events on the sun (such as the well-known

flare of February, 1956) do not allow us to extrapolate to obtain the total amount of activity produced by stars on the main sequence. Thus one possible way of deciding which of these types of source makes the most important contribution is to determine in detail the composition of the primary flux. Then, provided that we use detailed models of supernovae or atmosphere of magnetic stars, and also provided that more information on spallation products and cross-sections becomes available, we may be able to determine the probable places of origin. The amount of spallation which takes place in the interstellar gas is still not known. We have generally supposed that nuclear collisions were all-important in limiting the times for acceleration as was originally conceived by Fermi. However, the time may be limited instead by the leakage out of the accelerating volume. In this case the chemical composition of the primaries might more nearly reproduce the composition of the material ejected from the stellar or nebular sources.

2. – The acceleration mechanism inside galaxies.

Modified Fermi acceleration mechanisms which may be effective in the disk of our Galaxy have been discussed by L. Davis and C. Y. Fan at this conference. Therefore I shall not consider them here, but instead I shall give an outline of the arguments which suggest that a very powerful mechanism of acceleration must exist in the haloes surrounding galaxies.

In the last two or three years it has become clear that in the radio sources associated with galaxies the distribution of radio emission is very different from the distribution of starlight, in that, while in spiral systems the light is emitted predominantly from the disk of the galaxy, and in ellipticals from a central spheroidal region, the radio emission comes both from these central regions and also from roughly spherical volumes. These volumes are very large when compared with the volumes inside which the majority of the stars are concentrated, and they are roughly centered on the centers of the disks. Baldwin [19, 20] has shown that such a halo distribution exists in our Galaxy and in M 31 (the Andromeda nebula), while Mills [21] has described possible extended distributions of radio emission in a number of bright southern galaxies. Following earlier suggestions by Šklovsij and other Russian workers, the author [22] has considered the conditions which are demanded to explain haloes such as these.

The argument which leads to a direct relationship between the halo as a source of radio emission and as an accelerator of cosmic ray particles can be summarized as follows. On the well-founded assumption that the synchrotron mechanism is responsible for this radio emission, it follows that the halo contains both a flux of high-energy electrons and positrons and a magnetic field.

If a magnetic field is present, then associated with it there must be a low-density gas. Since the Galaxy has a high rotational velocity, this gas will remain in an extended volume only if sufficient turbulent or kinetic pressure is exerted to keep it there. Otherwise it would collapse towards the disk. This demands in our Galaxy turbulent velocities of the order of 100 km/s, or kinetic temperatures $\sim 10^6$ degrees [23]. Then, provided that the halo has a turbulent structure, particles must be accelerated in it by the original Fermi mechanism [24]. If the acceleration takes place in this way, the isotropic distribution of cosmic rays is more easily explicable, without the necessity of introducing various mechanisms which will scatter but not always accelerate particles in the disk.

The conditions in haloes, or in any radio sources, cannot be determined completely from the measurements of total radio power emitted from them and from the radio spectra. The parameters which enter into the calculation are the mean magnetic field strength, the total particle energy, the particle spectrum, and the ratio of the total magnetic energy to the total particle energy. Since we do not have independent measurements of the average magnetic field strengths in halo regions, or in any regions other than in the disk of our Galaxy, the method of calculating the energy in the different modes has been to assume various magnetic field strengths and then to calculate the total particle energy in each case. Then to make the problem determinate it is supposed that the total energy present is the *minimum* energy necessary to account for the radio power emitted. This is what has been done in the majority of the calculations, and at the energy minimum there is equipartition between the two modes.

The question arises, when we are calculating the total particle energy, as to what the ratio total energy (nucleus)/total energy (electrons) is taken to be. The author has concluded that unless the electrons and positrons are produced in a very remarkable way (cf. Sect. 3), it is the nucleons which are the *primary* particles while the electrons and positrons are *secondary* and are produced by high-energy nucleon-nucleon collisions which result in meson production and decay. The reasons for this are twofold. In the first place, as has been stated in Sect. 2, the accelerating mechanism will almost certainly give much more energy to the nucleons than to the electrons. Thus even if electrons were accelerated, protons would also be accelerated to such an extent that electrons and positrons could be produced as secondaries, and the multiplicities of the mesons produced in the intermediate step would be large enough so that the secondaries would outweigh the primary electrons.

Secondly, a cogent argument against the presence of primary electrons in galactic haloes can be based on the argument originally given by Fermi [24] for the non-appearance of electrons in the primary cosmic-ray flux down to the limits then given. This was simply that the energy losses by electrons

through collisional ionization or bremsstrahlung are so great at low energies ($\lesssim$ rest energy) that even in a gas as tenuous as the interstellar medium they will outweigh any energy gain by the Fermi mechanism. Now the density in the halo regions (perhaps $\sim 10^{-26}$ g/cm^3) is much lower than it is in the disk ($\sim 10^{-24}$ g/cm^3) and therefore, although we are concerned with emission in the halo, primary electrons would arise by one process or another in the disk only, and they would encounter this difficulty associated with their injection energy. GREENSTEIN [25] attempted to show that in some radio sources in the disk (e.g. the source in Cassiopeia) the difficulty associated with the injection energy might be overcome by supposing that the electrons were emitted in low-energy nuclear reactions so that injection energies $\gtrsim 1$ MeV might be achieved. Unfortunately it appears that the rate of reactions involving deuterons, for example, is far too low, due to the rarity of deuterium and the low density, to give rise to sufficient electrons.

This difficulty is overcome if it is assumed that the electrons and positrons are secondaries, since the average injection energy is then ~ 50 MeV which is entirely adequate for further Fermi acceleration processes. In our Galaxy a further argument in favor of this mechanism can be invoked. If we calculate the rate of production of the secondaries, using the currently accepted values of the cosmic-ray energy density and spectrum, measured nucleon-nucleon cross-sections in the GeV range, and the statistical theory to estimate the meson multiplicity, we find that the rate at which energy is transferred to secondaries is equal (to within an order of magnitude) to the rate of radio radiation by the whole Galaxy [26]. Thus it may be concluded that an equilibrium situation has been reached, and that all normal galaxies with the same energy content of cosmic rays and similar magnetic fields would radiate at approximately the same power level.

Something more can be said about the turbulence and the magnetic field in the haloes. Provided that we do not suppose that this is purely a high-temperature halo, the existence of the turbulence means that at most the magnetic field energy is in equipartition with turbulent energy. In this case we shall be dealing with a hydromagnetic turbulent gas and the eddy sizes and velocities can be determined only from a hydromagnetic theory. On the other hand, the magnetic energy might be small as compared with the turbulent energy and be in the process of being amplified by the turbulence. However, the simplest postulate that can be made is to suppose that equipartition is reached, so that the total energy in a halo is approximately three times the energy of each mode, the heat content being assumed small.

There is no reason to suppose that a halo is static. Thus it might well be expanding; the necessary pressure conditions for this to occur have been previously discussed [22]. It may be fed by gas which is continuously ejected from the disk and by stars which evolve and lose mass while passing through

the halo (some 20% of the total galactic mass may be contained in stars of the halo population).

To give some idea of the total energies that are contained in particles and magnetic field, we show in Table II the results of computations made along the lines described above for the radio sources in a number of galaxis [27-29]. The evidence for haloes around the radio sources in NGC 5128, NGC 1316, and NGC 4486 (M 87) has been described elsewhere [28, 30]. Among the extragalactic radio sources only M 87 contains a jet of synchrotron radiation in visual wavelengths which can be observed [31], and in this case it is tempting to relate the halo to the jet in some way. If the halo has originated from the jet, this might mean that an exceedingly powerful source of unknown origin is feeding into the jet which is then acting as a funnel channelling the particles into the halo.

Mention of such a source leads us to the discussion of the whole energy problem associated with the radio sources. The discovery of radio sources and the identification of their mechanism of radio, and in some cases non-thermal optical, emission has led to considerable advances in our understanding of the cosmic-ray problem. Thus we known that all of the radio sources will act as powerful emitters of cosmic rays, that whatever the mechanism of particle acceleration is, it is very efficient, and that most galaxies probably will contain a large flux of cosmic-ray particles. However, we still have a very considerable problem associated with the energy sources for all of this activity.

TABLE II. – *Estimates of total energies and magnetic field strengths in radio sources.*

	Total Energy (magnetic + particles)		Magnetic field $\overline{H}$	
	(I) (assuming that only electrons and positrons are present) (erg)	(II) (assuming that a primary proton flux produces electrons and positrons in nuclear collisions) (erg)	(I) (gauss)	(II) (gauss)
Galaxy (disk)	—	10^{55}	—	10^{-5}
(halo)	10^{55}	—	—	$1\text{-}2\cdot10^{-6}$
M 87 (NGC 4486) (optical jet)	$2\cdot10^{55}$	$4\cdot10^{56}$	10^{-3}	10^{-2}
(radio source)	$5\cdot10^{55}$	10^{57}	10^{-4}	10^{-3}
NGC 5128 (central region)	10^{55}	10^{57}	10^{-6}	10^{-5}
(halo)	10^{57}	10^{59}	10^{-5}	$2\cdot10^{-4}$
NGC 1316 (central region)	10^{55}	10^{57}	10^{-6}	10^{-5}
(halo)	10^{57}	10^{59}	10^{-5}	$2\cdot10^{-4}$
Cygnus A	10^{58}-10^{59}	10^{60}	$5\cdot10^{-5}$-$5\cdot10^{-6}$	$5\cdot10^{-4}$

3. The source of energy and the energy transfer problem.

On current theories of the origin of cosmic rays and of radio emission the energy required is taken in the first instance from galactic magnetic fields and from the kinetic energy of the interstellar gas and dust. In normal galaxies the sources of energy which are available to feed these modes are the energy of galactic rotation and the nuclear-energy sources in the stars. The rotational energy amounts to $\sim 10^{59}$ ergs, while the total amount of nuclear energy available (that given up if all of the hydrogen were converted to helium, making some allowance for that already transmuted) is $\sim 10^{63}$ ergs. However, although both sources appear entirely adequate to supply the energy of kinetic motions and magnetic flux, the method of energy transfer is not understood.

If galactic rotation were responsible, then a mechanism by which the energy is transferred by viscous forces and the differential rotation would seem to be required. A quantitative investigation of such a mechanism has not been made. However, the coupling afforded by the viscous forces is very weak. Also only 1 or 2 % of the galactic mass is concentrated in the gas and dust, so that the energy reservoir in the rotation is effectively reduced by a factor ~ 100, since the coupling between stars and gas is so weak as to be negligible. An observation which may have some bearing on this mechanism is that obtained from the 21 cm work which shows that the velocities of the clouds of neutral hydrogen towards the galactic center are far higher (~ 50 km/s) than they are in the spiral arms in the vicinity of the sun [32]. This might argue against the generation of motions from the galactic rotation, since from observations of extragalactic nebulae it appears that in these regions galaxies may tend to rotate as rigid bodies.

Nuclear energy sources present problems of a different nature. The transfer of nuclear energy must involve the same kind of mechanism as that suggested by Oort and Spitzer [33] to be important in star formation. They have pointed out that a newly formed very luminous star will heat the surrounding gas by ultraviolet radiation, the resultant increase in pressure leading to a high acceleration and generation of motions in the gas. No quantitative estimates of whether the rate of formation of hot stars is sufficient to generate all of the motions in the gas have yet been made. In any mechanism the dissipation which takes place in collisions between clouds is of importance. Magnetic fields can be amplified from very weak seed fields once the motions of the clouds have been generated. However, it has been recently pointed out that the dissipation of magnetic energy in the interstellar medium can no longer be considered negligible in the lifetime of the Galaxy [34], as was once thought to be the case. Thus a characteristic decay time for a neutral

hydrogen cloud is $\sim 5 \cdot 10^8$ years or less than one tenth of the age of the Galaxy.

Hence for our Galaxy we may conclude that neither of the mechanisms proposed for the generation of motions have been shown quantitatively to be adequate to account for the observed effects. (A third mechanism has been speculated upon [35], but will not be discussed here.) The further steps by which the magnetic field is amplified by these motions and the energy transferred to accelerating particles also need investigation.

Some of the extragalactic radio sources which have been identified with optical objects, and certainly all of the most powerful sources, are not « normal » galaxies which are easily fitted into a classification system. It has been widely suggested that these are colliding systems, the criteria used to determine this being rather arbitrary (i.e. decided opinions as to what a collision *looks* like), and in one case, that of NGC 1275, the suggestion being based on fairly detailed measurements of relative velocities in different parts of the system [36]. Measurements of large relative velocities cannot by themselves offer proof that collisions are taking place. For *any* mechanism which can provide large fluxes of high-energy particles must almost certainly also give rise to large-scale motions which could be measured spectroscopically. In some cases it is very hard to disentangle the two systems, if they really are two formerly separate galaxies, while there are also many apparently interacting systems which are not identified as radio sources.

The primary theoretical argument in favor of the hypothesis that the strong sources are colliding systems, is that the collision provides a large reservoir of energy which may be transformed into magnetic and particle energy. In the case of two large spirals with a relative velocity of 1000 km/s this energy supply would amount to about 10^{60} ergs. This is adequate to account for the energies of particles and field in all of the known sources, though in the case of the Cygnus source, the most powerful of the extragalactic sources, an efficiency of energy conversion of unity is required if the particle flux is primarily nucleons, while an efficiency of 1-10% is demanded if only electrons are present. Such an efficiency in a sequence of hydromagnetic processes of great complexity appears almost unbelievable. For example, it can be seen in a qualitative fashion how a magnetic field can be amplified by a factor ~ 100 in a collision, in a very limited volume.

The problem is one of the passage of very strong shock waves in a medium containing a very weak magnetic field. The amplification obtained is then given by the degree of compression which can be attained by the gas; using the classical theory this compression factor is given by $(\gamma+1)/(\gamma-1)$, so that if $\gamma = \frac{5}{3}$ the factor is 4. Thus multiple collisions in which two clouds collide, a third collides with the multiple system, and so on, will lead to the required amount of amplification. However, such a mechanism would only tend to increase the field in limited volumes, so that the total efficiency of a collision

in this respect would be low. Further energy transfer to particles is an even more indirect process.

A special puzzle, if galactic collisions are proposed as the origin of synchrotron emission, is that of M 87. Here we have an apparently normal E 0 galaxy, though it has a very high luminosity, in which there is no visible evidence for interaction with another system, and yet a very large energy supply is demanded. The only peculiar visible feature in M 87 is the jet which appears to come from the central regions. (It might be mentioned in passing that the discovery of the jet may be in itself somewhat of a fluke. Thus it can only just be resolved, and there may be very many systems in which such phenomena remain undetected, e.g. our own Galaxy.) The presence of haloes in abnormal systems is not as difficult to explain on a collision hypothesis if it is supposed that haloes are features of normal galaxies, though it might be expected that in any interaction they would be highly distorted. It was these energy difficulties which led the author, when discussing M 87, to speculate on the possible presence of antimatter in the system, and then HOYLE and the author [35] considered the consequences of the speculation that antimatter exists both in our Galaxy and in other radio sources, and is the primary cause of the radio emission. There are serious difficulties attached to this speculation which we shall not discuss here. However, it should be pointed out that if the idea were accepted, it would in turn destroy some of the arguments by which we have related the sources of radio emission and of cosmic rays. For the production of electrons and positrons from proton-antiproton annihilation would mean that no high-energy nucleon component would be associated with them.

We conclude this section by emphasizing that although recent developments in radio astronomy have gone a long way towards explaining some of the problems of the origin of cosmic rays, they have brought to the fore again, and in a more severe form, the important astrophysical problem of the source of energy for all of the activity.

4. – Extragalactic acceleration mechanisms.

Since primary particles having energies $\sim 10^{18}$ eV and in one case 10^{19} eV have been detected already in the primary flux [37], and since these particles can neither be contained nor accelerated in our Galaxy, an extragalactic origin must be presumed to account for them. The first source that comes to mind is the jet in M 87 where the magnetic field may be sufficiently large ($\sim 10^{-3}$ gauss) so that the spiralling radius of a 10^{19} eV proton will be only about 11 parses ($= 34$ light years) so that it could be contained there and possibly be accelerated by the largest hydromagnetic eddies that might be present. However,

although such a source may be important, it is worthwhile looking for more general conditions under which sufficient acceleration could take place.

Suitable conditions may be found in dense clusters of galaxies, and we shall conclude by outlining a theory of acceleration in such clusters which has recently been proposed [38]. There is considerable evidence available today which shows that most galaxies exist in clusters. Our own Galaxy is a member of what is known as the local group, a loose cluster comprising only about a dozen members lying inside a volume with a dimension $\sim 5 \cdot 10^5$ parsec. On the other hand there are very many clusters which have diameters in the range $2 \cdot (10^6 \div 10^7)$ parsec, containing $\sim 10^3$ or more members measured down to a certain limiting brightness. The diameters of such systems are very ill-defined, the populations in many cases becoming extremely dense towards the center. Of these dense clusters the Coma cluster and the Corona cluster are well known, and a recent survey by ABELL [39] has shown that within the distance of the Hydra cluster (which has a red-shift of 60 500 km/s so that using the red-shift constant of 180 km/s/10^6 parsec puts it at a distance of $3.4 \cdot 10^8$ parsec) there are hundreds or even thousands of such dense clusters There is considerable evidence from the work of ZWICKY that much material exists between galaxies. Also, the haloes which have previously been dis cussed, and the 21 cm observations of neutral hydrogen in the Coma cluster [40] and about the Cygnus radio source [41], all suggest that diffuse and tenuous gas and perhaps dust is present in the space between the mass and light concentrations which we describe as galaxies. It seems very reasonable to suppose that there is a weak intergalactic magnetic field associated with this material.

If this assumption is made, then we can consider the acceleration of particles which escape from galaxies, and which now are accelerated between galaxies in the same way that Fermi originally proposed for cosmic-ray particles among the interstellar clouds in our own Galaxy [24]. The parameters which are then of importance are the random velocities of the galaxies, their mean separations, and the total time which is available for acceleration. In very dense clusters the mean random velocities are ~ 2000 km/s, and in the central regions the separations of the galaxies are not much greater than their own diameters, so that they are continuously making collisions among themselves. The time available for acceleration appears to be limited, not by the destruction by nuclear collisions, since the particles spend most of their lives in regions of very low density, but rather by the age of the universe. If we assume that an evolutionary cosmological model is correct we find that the conditions in the Coma cluster lead to energies with an upper limit $\sim 5 \cdot 10^{20}$ eV. It is of interest that the nearest source of ultra-high-energy particles on this theory will be the Coma cluster which is about $3 \cdot 10^7$ psc away. Acceleration in the local group is negligible.

It is of interest that the upper energy limit may be determined from cosmological considerations. This gives *in principle* the possibility of a cosmological test. If no other mechanism of acceleration were available, and the rate of acceleration at an earlier epoch were understood, the detection of primary particles with energies $\gg 10^{21}$ eV might lead to the conclusion that the steady state cosmological model was indicated. However, in an earlier epoch, the acceleration mechanism might have been more efficient, and in an expanding universe the acceleration of particles among clusters of clusters of galaxies might also be important.

* * *

I am indebted to Dr. MARGARET BURBIDGE for discussions about this topic.

REFERENCES

[1] H. W. BABCOCK: *Astrophys. Journ. Suppl.* (in preparation).
[2] G. R. BURBIDGE and E. M. BURBIDGE: *Astrophys. Journ. Suppl.*, **1**, 431 (1955).
[3] E. M. BURBIDGE and G. E. BURBIDGE: *Astrophys. Journ.*, **122**, 396 (1955).
[4] E. M. BURBIDGE and G. R. BURBIDGE: *Astrophys. Journ.*, **124**, 655 (1956).
[5] W. A. FOWLER, G. R. BURBIDGE and E. M. BURBIDGE: *Astrophys. Journ. Suppl.*, **2**, 167 (1955); E. M. BURBIDGE, G. R. BURBIDGE and W. A. FOWLER: *Proc. Stockholm Conference on Electromagnetic Phenomena in Cosmical Physics*, 1956.
[6] P. A. SWEET: *Proc. Stockholm Conference on Electromagnetic Phenomena in Cosmical Physics*, 1956.
[7] L. BIERMANN: *Zeits. f. Astrophys.*, **41**, 46 (1956).
[8] E. M. BURBIDGE, G. R. BURBIDGE, W. A. FOWLER and F. HOYLE: *Rev. Mod. Phys.*, **29**, 547 (1957).
[9] L. GOLDBERG: private communication.
[10] A. B. SEVERNY: *Proc. Stockholm Conference on Electromagnetic Phenomena in Cosmical Physics*, 1956.
[11] J. R. HUIZENGA and J. DIAMOND: *Phys. Rev.*, **107**, 1087 (1957).
[12] S. G. THOMPSON: private communication.
[13] J. H. NOON, A. J. HERZ and B. J. O'BRIEN: *Nature*, **179**, 91 (1957).
[14] I. S. ŠKLOVSKIJ: *Dokl. Akad. Nauk USSR*, **90**, 983 (1953).
[15] J. H. OORT and T. WALRAVEN: *Bull. Astron. Soc. Netherlands*, **12**, 285 (1956).
[16] W. A. HILTNER: *Astrophys. Journ.*, **125**, 300 (1957).
[17] W. BAADE: *Bull. Astron. Soc. Netherlands*, **12**, 312 (1956).
[18] G. R. BURBIDGE: *Astrophys. Journ.*, **127**, January (1958).
[19] J. E. BALDWIN: *Nature*, **174**, 320 (1954).
[20] J. E. BALDWIN: *Month. Not. Roy. Astr. Soc.*, **115**, 690 (1955).
[21] B. Y. MILLS: *Austr. Journ. Sci. Research*, A **8**, 368 (1955).
[22] G. R. BURBIDGE: *Astrophys. Journ.*, **123**, 178 (1956); *Phys. Rev.*, **101**, 906 (1956).

[23] L. Spitzer: *Astrophys. Journ.*, **124**, 20 (1956).
[24] E. Fermi: *Phys. Rev.*, **75**, 1169 (1949).
[25] J. L. Greenstein: *Radio Astronomy, International Astronomical Union Symposium* No. 4, (Cambridge, 1957), p. 179.
[26] G. R. Burbidge: *Phys. Rev.*, **103**, 264 (1956).
[27] G. R. Burbidge: *Astrophys. Journ.*, **124**, 416 (1956).
[28] G. R. Burbidge and E. M. Burbidge: *Astrophys. Journ.*, **125**, 1 (1957).
[29] G. R. Burbidge: unpublished.
[30] J. E. Baldwin and F. G. Smith: *Observatory*, **76**, 141 (1956).
[31] W. Baade: *Astrophys. Journ.*, **123**, 550 (1956).
[32] K. K. Kwee, C. A. Muller and G. Westerhout: *Bull. Astron. Soc. Netherlands*, **12**, 211 (1956).
[33] J. H. Oort and L. Spitzer: *Astrophys. Journ.*, **121**, 6 (1955).
[34] T. G. Cowling: *Month. Not. Roy. Astr. Soc.*, **116**, 114 (1956).
[35] G. R. Burbidge and F. Hoyle: *Nuovo Cimento*, **4**, 558 (1956).
[36] R. Minkowski: *Radio Astronomy, International Astronomical Union Symposium* No. 4, (Cambridge, 1957), p. 107.
[37] B. Rossi: private communication.
[38] G. R. Burbidge: *Phys. Rev.*, **107**, **269** (1957).
[39] G. Abell: private communication.
[40] D. S. Heeschen: *Astrophys. Journ.*, **124**, 660 (1956).
[41] A. E. Lilley and E. F. McClain: *Astrophys. Journ.*, **123**, 172 (1956).

SUPPLEMENTO AL VOLUME VIII, SERIE X
DEL NUOVO CIMENTO

N. 2, 1958
2° Trimestre

Some Problems of Radioastronomical Theory of the Origin of Cosmic Rays.

I. S. Šklovskij

Sternberg State Astronomical Institute - Moscow

1. – Introduction.

In 1950 Alfvén and Herlfson [1] as well as Kiepenheuer [2] showed that non-thermal cosmic radiation may be explained by relativistic electrons moving in the interstellar magnetic fields. In the years that followed the « synchrotronic » theory of non-thermal cosmic radioemission was further developed in the U.S.S.R. owing the investigations made by V. L. Ginzburg and his collaborators (see references in the paper [3]). Since the non-thermal radioemission of the Galaxy is caused by relativistic electrons that move in the interstellar magnetic fields, it becomes possible to observe the electron component of the primary cosmic rays in the universe. Before this the primary cosmic rays could be observed only in the immediate proximity of the Earth. At the same time the problem of the origin of cosmic rays which in the essence is astrophysical could not be solved in principle.

From the analysis of the nature of non-thermal radioemission and of the physical conditions of discrete sources followed a conclusion that only relativistic electrons moving in the magnetic fields can be responsible for their radiation [6]. Proceeding from the observed flux of radioemission of the Crab nebula, one of the most powerful galactic discrete sources, in [4] we evaluated the quantity of relativistic electrons enclosed therein and their energy. Preliminarily the average intensity of magnetic field of this nebula was estimated on the basis of the data obtained from the observation in the optical region of the spectrum.

These calculations clearly showed that an explosion of a Supernova results in formation of a large number of relativistic particles ($\sim 10^{50}$). Although for a number of objects radioastronomical observations allow to reveal only the electron component of cosmic rays, it is natural to consider that also nuclei

of very high energies should be available in these sources because it is difficult to imagine any accelerating mechanism which would influence only electrons.

In [4] and [5] is was shown that taking into account the frequency of outbursts of Supernovae in our Galaxy and the « duration of life » of cosmic rays in the interstellar medium, the quantity of relativistic particles actually formed during these outbursts is quite enough to provide the observed concentration of the primary cosmic rays. Thereby it was shown that Supernovae explosions may be the injectors of primary cosmic rays in our stellar system. Thus, radioastronomy not only solved the question of the localization of cosmic rays in the Galaxy, but also pointed to the objects where they are generated. As was especially emphasized in [4] and [5] radioastronomy made the science of the origin of cosmic rays a branch of observation astronomy, while previously the origin of cosmic rays was the field of more or less witty speculations.

The further development of the radioastronomical theory of the origin of cosmic rays was given in the works published by V. L. Ginzburg [7] and by his collaborators (see, for example, a detailed paper [8] and also paper [9] and [10]). In [8] and [9] it was explained in particular why no relativistic electrons were hitherto found in the composition of the primary cosmic rays.

For a full recognition of the new theory of the origin of cosmic rays it was important to obtain an irrefutable proof of the fact that the nebulae resulting from Supernovae outbursts actually contain many relativistic electrons. Although radioastronomical data were very convincing, it was desirabel to give a proof based on more usual conceptions of optical astronomy in order to overcome certain conservatism and scepticism.

Such proof appeared to be the new interpretation of the optical radiation of the Crab nebula with continuous spectrum proposed by us in the same 1953 [11]. In [11] we revealed those insuperable difficulties which were then encountered by the usual in astrophysics interpretation of this radiation and showed that the superenergetic relativistic electrons (with the energy E of 10^{11} to 10^{12} eV) can explain the observed radiation of the Crab nebula. Thereby it was shown that both optical (with continuous spectrum) and radioemission of this nebula are explained by the same mechanism: radiation of relativistic electron in magnetic fields.

Proceeding from the new interpretation of Crab nebulas spectrum it was possible to predict that its optical radiation should by considerably polarized. The theoretically predicted polarization of Crab nebula's optical radiation was for the first time revealed by Dombrovskij in 1954 [12]. Prof. Oort, in co-operation with Valraven made an important investigation of the polarization of this nebula [13]. At the same time Baade, using the largest modern optical telescope, obtained splendid photographs of the Crab nebula with different orientation of the polaroids [13]. These photographs very convincingly prove that the light of separate details of the Crab nebula is almost

completely polarized. Such a high degree of polarization excludes the possibility of explaining this effect by any other causes different from the « synchrotronic mechanism ». As a result of these investigations, the new theory of Crab nebula's luminiscence was universally recognized also in the West.

Alongside with other reliably established facts (for example, the discovery of the theoretically predicted phenomenon of polarization of the optical radiation of the remarkable « jet » in the central part of the radiogalaxy M 87 [14]) the phenomenon of polarization of the Crab nebula's radiation serves as a firm foundation for the radioastronomical theory of the origin of cosmic rays.

In this paper we shall consider two problems which seems to us to be significant for the theory.

A short survey of the main statement of the radioastronomical theory of the origin of cosmic rays developed in the studies made by Soviet authors as well as the criticism of other theories are given in the paper by V. L. Ginzburg,

2. – Spatial distribution of cosmic rays in the Galaxy.

In 1952, analyzing the isophot curves of cosmic radioemission on different frequencies we arrives to a conclusion that the spatial distribution of radiation sources of the Galaxy is contious and that they form a gigantic spherical system, halo, which is comparatively little concentrated towards the galactic plane and towards the centre [15]. Soon S. B. Pikel'ner, analyzing the problem of cosmic ray retention in the Galaxy, came to a conclusion that the interstellar magnetic fields are connected not only with the interstellar gas clouds forming a « flat » system (as it was considered before) but are also localized outside clods [16]. Since the density of the gas in the space between the clouds is considerably less than the clouds themselves, it followed from the condition $\frac{1}{2}\varrho V^2 = (1/8\pi)H^2$, that the velocity of turbulent movements of this very rarefied medium should be very large: of the order of 50 to 100 km s^{-1}. Therefore the intercloud rarefied gas the concomitant magnetic fields should rise very high from the galactic plane ($\sim 10\,000$ parsec) thus forming a spherical system. This system proved to be identical with the system of continuously distributed sources of galactical radioemission [6].

Soon extensive halos were discovered in other Galaxies (for example, in M 31 whose properties are similar to those of our Galaxy). Thus, it was established that the distribution of relativistic electrons (and consequently, as is natural to suppose, of the relativistic particles) in our stellar system is unusual, quite different from the distribution of stars and nebulae.

If existence of a gigantic, almost spherical, « corona », in which relativistic particles of our Galaxy are localizes, now scarcely will be disputed by anyone,

the question of physical conditions in which the interstellar gas is found in this corona still remains debatable. Meanwhile this question is very important for investigating the « conditions of existence » of the primary cosmic rays in the Galaxy.

In 1956 SPITZER tried to ground the conception that the concentration of this gas is very small ($n \sim 5 \cdot 10^{-4}$ cm^{-3}); while the kinetic temperature is very high ($\sim 10^6$) [17].

Recently I and S. B. PIKEL'NER have come to another conclusion [18]. As a result of the analysis Usee the paper presented to the Conference on Cosmic Aeromechanics simultaneously held in Cambridge, U.S.A.) we succeeded in finding the main characteristics of the gaseous medium forming a halo. The intensity of magnetic field at the halo's periphery ($Z \geqslant 10\,000$ parsec) proved to be $H \sim 3 \cdot 10^{-6}$, while comparatively close to the galactic place ($Z \sim 1000$ parsec) it was $H \sim 6 \cdot 10^6$ G. The pressure of magnetic field and of cosmic rays in the halo's upper layers ($Z \sim 10\,000$ parsec) must be balanced by the weight of the layer lying above. Since the gravity potential of the Galaxy is known, the concentration of gas particles in the halo can be accounted. For the upper layers n $6 \cdot 10^{-3}$ cm^{-3}, and for the lower ones $\sim 10^{-2}$ cm^{-3}. Because of fast macroscopical motions (~ 100 km s^{-1}) the gaseous medium forming the halo is strongly heated, though remains in the main unionized.

These properties of the interstellar gas in the halo where cosmic rays are localized essentially influence their principal characteristics.

The small density of the gas in the halo provides considerable « duration of existence » of the cosmic particles and, first of all, of the protons. According to existing data, each collision of a cosmic proton with the nucleus of an interstellar atom (mainly of hydrogen) result in that the former looses 20% of its energy.

Assuming for the effective cross-section the « geometrical » value of $4 \cdot 10^{-26}$ cm^{-2}, we shall find that with $n = 6 \cdot 10^{-3}$ cm^{-3} and the rate of cosmic proton movement $V = c$, such collisions will take place approximately once per 7 or $8 \cdot 10^9$ years.

Hence it is possible to draw a conclusion that the main cosmic ray component relativistic protons, can remain in the Galaxy for a long time. We shall remind that, proceeding from the erroneous *a priori* conceptions on the properties of the interstellar medium in which cosmic rays travel, the initial version of the Fermi theory deduced very short « life priod » of relativistic protons: about 30 million years. Hence it followed that cosmic rays regenerate very soon.

Since our analysis shows that the life period of relativistic protons in the contemporary Galaxy is in any case comparable with and most probably exceeds the time of essential evolution of the Galaxy, the conception of « dynamical equilibrium » and « continuous regeneration » of cosmic rays looses a noticeable

part of its attract attraction. Thus, for example, one may not consider completely excluded that considerable part of cosmic protons is of « relict » origin.

The matter is quite different in the case of heavy nuclei found in the composition of the primary cosmic rays. For them the effective cross-section of nuclear collisions is much larger. Taking the effective cross-sections for the collisions in conformity with existing data, we shall find the life period of cosmic α-particles is approximately $1.6 \cdot 10^9$ years, of the oxygen group nuclei $6 \cdot 10^8$ years and of the heavy nuclei $3 \cdot 10^8$ years.

Only existence of nuclei in the composition of the primary cosmic rays makes it possible to maintain the conception on continuous « regeneration » of cosmic rays (*). Still it is necessary to emphasize that considerable, if not major, part of the energy of the cosmic rays localized in the Galaxy was « stored » when the Galaxy's characteristics essentially differed from the modern ones.

It should be noted that if the interstellar gas in the clouds forming a flat system is uniformly spread over the whole volume of the halo, the mean concentration of this gas will be approximately $5 \cdot 10^{-3}$ cm^{-3}.

Hence it is evident that existence of denser clouds practically will not affect the above calculations of the « life periods », especially if one takes into account that these clouds in the Galaxy plane occupy only $\sim 10\%$ of the volume.

The characteristics of the interstellar gas in the region where cosmic rays are localized make possible a rough extimation of the real significance of the parameter of the statistical mechanism of acceleration $\alpha = u^2 v / c^2 l$. Assuming $u \sim 10^7$ cm s^{-1}, $l \sim 3 \cdot 10^{20}$ cm, $v = c$, we shall find that $\alpha \sim 10^{-17}$ s^{-1}.

Taking into account that Galaxy's age hardly exceeds $t_1 = 6 \cdot 10^9$ years $= 2 \cdot 10^{18}$ s the statistical mechanism by no means can provide acceleration of protons even to energies higher than

$$Mc^2 \exp [\alpha t_1] \approx 10^{10} \text{ eV} .$$

In reality the problem is much more complicated. As was already emphasized above, the life period of relativistic protons in the « contemporary » Galaxy is larger than the period of its evolution. Therefore it is not excluded that several billion years ago conditions in the Galaxy were absolutely different and acceleration of protons by the statical mechanism could be effected.

It is necessary to bear in mind another possibility. At the earlier stage of Galaxy's evolution the outbursts of Supernovae could not take place at all, because the star is likely to pass a long evolutionary way in order to explode

(*) The significance of the nuclei for the problem in question wes pointed to us by B. L. Ginzburg.

as a Supernova. In this connection we shall point that elliptic galaxies as well as Sa type spirals produce very insignificant radioemission (in contradistination to Sb and Sc spirals). This fact be compared with the possible evolution of our Galaxy.

As far as the nuclei more heavy than protons are concerned, they are probably not influenced by statistical mechanism of acceleration in the interstellat medium at all (see [8, 10]).

3. – The origin of electrons in the composition of the primary cosmic rays.

The cosmic electrons observed by radioastroonmical methods in the interstellar space can be « injected » as a result of supernovae outbursts. On the other hand, relativistic electrons and positrons can be formed in the process of collisions between cosmic protons and other heavy particles and nuclei of the interstellar atoms. This was indicated by V. L. Ginzburg [9, 10]. It is undoubtful that both these mechanisms of interstellar medium « replenshment » with relativistic electrons and positrons are in operation. It is niiteresting to clear up which of these mechanisms is more essential.

Very important characteristics of the system of cosmic particles enclosed in our stellar system is the frequency integrated power of radioemission generated by the Galaxy:

$$L = \int L_\nu \, \mathrm{d}\nu$$

It is necessary to emphasize that at present we possess the necessary observation data to make possible rather accurate determination of this value. Taking into account the spectrum of galactic radioemission and the spatial distribution of its sources, it is possible to show that

$$L = 2.5 \cdot 10^{38} \text{ erg s}^{-1},$$

with a probable error of $\pm 50\%$.

On the other hand, knowing the absolute value of the density of cosmic ray energy in the sun's neighbourhood ($\sim 2 \cdot 10^{-12}$ erg cm^{-3}) and the spatial distribution of the primary cosmic rays and interstellar gas (on the basis on the analysis of radioastronomical data) it is possible to find the power of the energy losses of the primary heavy cosmic particles caused by the collisions with the nuclei of the interstellar atoms. The calculations show that the energy losses of the heavy component of cosmic rays constitute approximately 1.5 10^{39} erg s^{-1} in the clouds of the interstellar medium situated near the galactic plane, $0.3 \cdot 10^{39}$ erg s^{-1} in the region of the Galaxy's nucleus and

$1 \cdot 10^{39}$ erg s^{-1} in the halo's volume. Altogether the power of energy losses of the heavy component in the whole Galaxy is $2.8 \cdot 10^{39}$ erg s^{-1}, the probable error being several tens of percent.

On the basis of existing data it is possible to make a conclusion that about 10 to 15% of the energy lost by the primary heavy particles in nuclear collisions should transfer to the electrons and positrons; this constitutes 3 or $4 \cdot 10^{38}$ erg s^{-1}.

But this value, within the limits of calculation error (which cannot be very large) is in a very good agreement with the total power of the Galaxy's non-thermal radioemission which is equal to the power of the energy losses of cosmic electrons.

Thereby it was shown that collisions between heavy cosmic particles and nuclei of the interstellar gas are the main « injector » of cosmic electrons and therefore the direct cause of the major part of the Galaxy's non-thermal radiation.

It is undoubtful that certain part of relativistic electrons emitted into the interstellar space is given by the dissipating nebulae resulting from supernovae's outbursts. But this part should be small. This is evident from the following consideration. As was shown by GETMANCEV [19] if the differential energy spectrum of the injected electrons has the form

$$N_1(E) = \frac{K_1}{E^{\alpha}},$$

where $\alpha > 1$, it will assume the following form due to the energy losser for the « synchronic radiation » in the interstellar medium

$$N_2(E) = \frac{K_2}{E^{\alpha+1}}$$

Since the density of interstellar gas in the halo is small, the radiation and ionization losses of relativistic electrons will not affect their spectrum.

If the differential energy spectrum of relativistic electrons is represented in the form of $N(E) = K/E^{\gamma}$ the spectral distribution of the « synchrotronic » radiation will have the form (see, for example, [8]):

$$I(\nu) \alpha \nu (1 - \gamma)/2.$$

From the analysis of the data of radioastronomical observations (see [20]) it follows that for the relativistic electrons found in the interstellar space $\gamma = 2 \div 2.6$.

If the relativistic electrons were « injected » chiefly during supernovae's outbursts, then according to (1) in the nebulae remaining after such explosions γ would be equal to $1 \div 1.6$. This would mean that the spectrum of radioactive radiation of the nebulae formed after supernovae outbursts would be $I(\nu) \propto \nu^{0} \div \nu^{0.3}$,

i.e., very gentle. Meanwhile the spectra for the known galactic sources of non-thermal radioemission are considerably steeper. The whole body of the available information concerning the spectra of the discrete sources, remnants of supernovae outbursts, points to their great similarity with the spectrum of Galaxy's non-thermal radioemission (*).

Since this is so, these sources cannot be considered to be the main « injectors » of cosmic electrons. At the same time this shows that relativistic electrons in the sources, remainants of supernovae outbursts themselves are of the secondary origin.

The conditions under which relativistic electrons are formed in such secondary processes may be very different for different sources. These conditions are essentially determined by the density of matter in the envelope formed during the supernovae's outbursts, by the envelope mass, by the rate of expansion and the epoch when the heavy cosmic particles are to accelerated. For example, although the latest observations do not confirms existence of radiation sources at the place of novae's outbursts [21], it is not excluded that relativistic electrons because of small mass of their envelopes had no time to be formed in the secondary processes. At the same time in the case of such objects as the Crab nebula the conditions for forming relativistic electrons of very high energies (for example, those responsible for its optical radiation) were very favourable.

Since the differential energy spectrum of heavy cosmic particles in the region of comparatively small energies has the form of $N(E) \propto E^{-2}$, then, if the initial energy of the secondary electrons (and positrons) was strictly proportional to the energy of heavy particles, the initial electron spectrum would be the same. Further on it would be « treated » by the magnetic field and would become $N(E) \propto E^{-3}$. In reality the spectrum is noticeably more gentle. This can be explained by the insignificant deviation from the proportionality between the energies of the primary and secondary particles.

REFERENCES

[1] H. Alfvén and N. Herlofson: *Phys. Rev.*, **78**, 616 1950).
[2] K. Kiepenheuer: *Phys. Rev.*, **79**, 738 (1950).
[3] V. L. Ginzburg: *Suppl. Nuovo Cimento*, **3**, 38 (1956).

(*) The only exclusion is the spectrum of the Crab nebula at the meter range. Let us notice however that in the range $\lambda \sim 10$ m as well as at high frequencies, the spectrum of the Crab nebula as well as of the other sources is rather steep. In general it is necessary to note that the Crab nebula probably, is not a « typical » source.

[4] I. S. Šklovskij: *Dokl. Akad. Nauk SSSR*, **91**, 475 (1953).
[5] I. S. Šklovskij: *Astr. Žu. SSSR*, **30**, 577 (1953).
[6] I. S. Šklovskij: *Astr. Žu. SSSR*, **30**, 15 (1953).
[7] V. L. Ginzburg: *Dokl. Akad. Nauk SSSR*, **92**, 1133 (1953).
[8] V. L. Ginzburg: *Usp. Fiz. Nauk*, **51**. 343 (1953).
[9] V. L. Ginzburg: *Izv. Akad. Nauk SSSR, Ser. Fiz., Žu. SSSR*, **20**, 5 (1956).
[10] V. L. Ginzburg and M. I. Fradkin: *Astr. Žu. SSSR*, **33**, 579 (1956); *Dokl. Akad. Nauk SSSR*, **31**, 523 (1956).
[11] I. S. Šklovskij: *Dokl. Akad. Nauk SSSR*, **90**, 983 (1953).
[12] V. A. Dombrovskij: *Dokl. Akad. Nauk SSSR*, **94**, 21 (1954).
[13] J. Oort and T. Walraven: *Bull. Astr. Soc. Netherlands*, **12**, no. 462, 285 (1956).
[14] I. S. Šklovskij: *Astr. Žu. SSSR*, **32**, 207 (1955).
[15] I. S. Šklovskij: *Astr. Žu. SSR*, **29**, 418 (1952).
[16] S. V. Pikel'ner: *Dokl. Akad. Nauk SSSR*, **88**, 229 (1953).
[17] L. Spitzer: *Astrophys. Journ.*, **124**, 20 (1956).
[18] S. V. Pikel'ner and I. S. Šklovskij: *Astr. Žurn.*, **34**, 145 (1957).
[19] G. G. Getmancev: *Dokl. Akad. Nauk SSSR*, **83**, 557 (1952).
[20] I. S. Šklovskij: *Kosmičeskoe Radioizlučenie* (Moscow, 1956).
[21] B. Mills, A. Little and K. Sheridan: *Austr. Journ. of Phys.*, **9**, 84 (1956).

SUPPLEMENTO AL VOLUME VIII, SERIE X
DEL NUOVO CIMENTO

N. 2, 1958
2° Trimestre

On the Origin of Cosmic Rays.

V. L. GINZBURG

P. N. Lebedev Institute of Physics of the USSR Academy of Sciences - Moscow

The theory of the origin of cosmic rays based, in the first place, on radio astronomical data was developed already in 1953 by the author, I. S. ŠKLOVSKIJ and others. At that time this theory was stated in detail in the paper [1] and then was several times mentioned in the reports sent to the International Conferences (see, for example, [2, 3]). Recently the author has considered this problem in a rather complete review, taking into account new data; this review was written for the Vol. 4 of the series *Progress in Cosmic Ray Physics* (Amsterdam, 1957) (*). Therefore it seems not to be necessary to consider again this theory in the present report in detail. Below we shall give only a short resume in this respect, then well give a more detailed consideration of recent results, and finally dwell critically on the other theories on cosmic ray origin.

1. – If one interprets the non-thermal cosmic radio emission (and, in some cases, the optical emission with a continuous spectrum) as being the emission of relativistic electrons moving in weak magnetic fields, one can receive some information about the cosmic ray electronic component in the Galaxy and beyond it. At the same time it becomes clear that cosmic (relativistic) electrons and consequently, most probably, all other relativistic particles fill the quasi-spherical volume with radius $R \sim (3 \div 5) \cdot 10^{22}$ cm. An equatorial plane of this system includes the stellar Galaxy (the Milky Way) surrounded by a galactic « corona » (halo), and the average gas density in the total system is $n \sim (0.01 \div \div 0.1)$ cm^{-3} (see [5]). If one knows the spectrum and intensity of cosmic radio

(*) This paper was sent to prof. J. WILSON in January, 1957. Simultaneously it was published in Russian [4]. The review of the radio astronomical theory of the c.r. origin is given, also, in the book of ŠKLOVSKIJ [6], chap. V.

emission, one can determine the electron spectrum in the Galaxy; the result is

$$(1) \qquad N_e^{(a)}(E) \simeq \frac{5\cdot 10^5}{E^3}\ (\mathrm{eV})^{-1}\ \mathrm{cm}^{-3}; \qquad N_e^{(b)}(E) \simeq \frac{5\cdot 10^2}{E^{2.64}}\ (\mathrm{eV})^{-1}\ \mathrm{cm}^{-3}\ ,$$

were version «*b*» is in a closer agreement with the radio astronomical data [4, 6], but the previously used version «*a*» [1-3] also cannot yet be excluded.

It should be noted that in determination of the spectra (1) it is assumed that the galactic corona includes chaotic magnetic fields having strength $H \sim 10^{-5}$ Oe, as it follows also from a number of independent considerations.

It is evident from (1) that (for $E > E_0 = 10^9$ eV)

$$(2) \qquad \int_{E_0}^{\infty} N_e(E)\,\mathrm{d}E \simeq (2.5 \div 5.5)\cdot 10^{13}\ \mathrm{cm}^{-3}\ .$$

This value does not contradict with the information about the primary electronic component near the Earth (according to the available data $N_e(E_0 > 10^9\ \mathrm{eV}) \leqslant \leqslant 10^{-12}\ \mathrm{cm}^{-3}$). From (1) it follows further that the average energy density of cosmic electrons with $E_0 > 10^8$ eV is $w_e \sim 10^{-2}$ eV/cm^3 and the total corresponding energy in the Galaxy with the volume $V \sim (4\pi/3)R^3 \sim 10^{68}$ cm^3 is

$$(3) \qquad W_e \sim w_e V \sim 10^{54}\ \mathrm{erg}\ .$$

The total cosmic ray energy in the Galaxy is by two orders higher

$$(4) \qquad W_{cr} \sim w_{cr} V \sim 10^{56}\ \mathrm{erg}\ ,$$

since the total concentration of cosmic ray particles near the Earth is $N(E_K > 10^9\ \mathrm{eV}) \simeq 1.5\cdot 10^{-10}\ \mathrm{cm}^{-3}$ and the density of their energy is $w_{cr} \sim \sim 1$ eV/cm^3. The lifetime of protons T_p and electrons T_e in the Galaxy with average gas concentration $n \sim 0.01 \div 0.1$ is (*)

$$(5) \qquad T_p \sim T_e \sim (4\cdot 10^8 \div 4\cdot 10^9)\ \mathrm{years} \cong (1.2\cdot 10^{16} \div 1.2\cdot 10^{17})\ \mathrm{s}\ .$$

From (3)–(5) it is clear that in the time unit the following energy is to be transferred to relativistic electrons and protons in the Galaxy in a steady

(*) Grounds, more precise definitions and, also, an analysis of other possibilities in this case as well as in others, see in [4]. The possibility of using the nuclear life time for protons and nuclei (for the case $T_p \sim 4\cdot 10^8$ years) is also founded there by an estimate of the number of particles leaving the Galaxy.

If $n \sim 0.01$, the time T_p is close to the life time of the Galaxy. However, this fact as can be shown, does not contradict with our conclusions [4].

state (*):

$$(6) \qquad U_e \sim \frac{W_e}{T_e} \sim 10^{38} \text{ erg/s}, \qquad U_{cr} \sim \frac{W_{cr}}{T_p} \sim (10^{39} \div 10^{40}) \text{ erg/s}.$$

The power U_e, probably, may be transferred to the electronic component as a result of cosmic ray proton nuclear collisions. But the known accuracy of all the values does not permit to take this possibility for an undeniable fact.

Thus, it is permissable to assume that the secondary electrons and protons formed as a result of nuclear collisions and a subsequent $\pi \to \mu \to e$ decay carry away only $\sim 1/10$ of the total electronic component energy (for electrons with $E > (1 \div 3) \cdot 10^8$ eV). The residual energy is, in this case, to be supplied by the primary sources which seems, perhaps, to be more probable (**).

As for the main part of the power U_{cr}, transferring to cosmic rays, this power is to be supplied by the primary sources including (in the theory of Fermi-type) the moving interstellar gas cloud.

Consideration of the energy requirements given in (6) is absolutely necessary for any cosmic ray theory since it is not easy to satisfy them. Thus, the average power transferring to cosmic rays from the Sun is $10^{21} \div 10^{22}$ erg/s and therefore even 10^{11} the sun-like stars will give only $10^{32} \div 10^{33}$ erg/s what is by 6-8 orders less than it is necessary. In the theories of the interstellar cosmic ray acceleration the main part of the energy is taken from the kinetic energy of gas clouds, but also in this case injectors (stars) must give about 10^{-3} part of the total energy. Obviously, under such conditions the intensity of cosmic rays emitted by stars must be by $3 \div 5$ orders higher than from 10^{11} sun-like stars. However, this assumption is far going as the Galaxy consists only of $\sim 10^{11}$ stars and there is no reason to take most of them as being more active than the Sun. If some peculiar stars are cosmic ray sources their number should be less than the total number of stars, and thus, the said difficulty cannot decrease.

The energy difficulties are absent if one basing on the radio astronomical data assumes that cosmic rays are formed as a result of the outbursts of supernovae and, probably, novae stars [1-4, 6]. The estimates based on the infor-

(*) Above, T_e is the life time of electrons relative to radiative losses (γ-quantum emission under collisions). Radiative losses due to the acceleration in magnetic fields are, at $T_e \sim 4 \cdot 10^8$ years, of the same order of magnitude. That is why there is accepted the value $U_e \sim 10^{38}$ obtained also from the data on radio emission spectrum [4].

(**) In his report I. S. Šklovskij gives an additional argument for the statement that most of electrons have the secondary origin (the question is about the similarity between the spectra of discrete sources and the spectrum of the general galactic radio emission). This argument, however, is not free from objections, but here it seems to be impossible to dwell on them (see [4]).

mation about the spectrum and intensities of radio emission (*) show that the energy from 10^{37} to $3\ 10^{39}$ erg/s can be transferred to electrons as a result of the nova and supernova outbursts. The energy being even $M/m = 1\,836$ times larger can be transferred to protons and nuclei (see below) and therefore there is no problen to keep energy balance in such a scheme.

The main thing is however that relativistic particle generation in the envelopes of supernovae is a real fact, not only a hypothesis (+).

As we are basing on the observation data showing the acceleration efficiency as a result of the supernova outbursts the question of the mechanism and character of this acceleration, becomes an independent and, in some sense, less essential problem. Therefore we only point out that the statistical acceleration mechanism of Fermi-type can be especially effective in the envelopes of supernovae and novae stars, since the velocity of the gas mass movement is high in these regions and the effective free path length is there relatively short.

Under statistical acceleration the energy transferred to a particle is proportional to its rest mass and thus protons gain the energy $M/m = 1836$ times larger than electrons do. We have already hinted at this fact above; and it permits to assume that the Crab nebula contains now many protons with the energy $(10^{14} \div 10^{15})$ eV, since there are electrons with $E \sim (10^{11} \div 10^{12})$ eV in this nebula (this follows directly from the observation data [6]). From here and from other estimates [1-4, 7] it is easy to conclude that due to the supernova outbursts protons and, especially, nuclei can probably gain the highest energy $\sim (10^{18} \div 10^{19})$ eV otbained in cosmic rays.

At the same time there is no difficulty in assuming that the observed cosmic ray energy spectrum is an averaged one (averaging is made on millions of outbursts).

Thus, the state of affairs with the problem of the acceleration of particles in the envelopes of supernovae and novae seems to be favourable. Undoubtedly, however, a number of questions concerning the very star outbursts and the acceleration of particles on different stages of an envelope formation and separation remain obscure and need further investigation (see in this connection [7, 8]).

2. – Apart from the requirements concerning energy spectrum and total energy of cosmic rays it is necessary to dwell on their charge spectrum and simultaneously, isotropy in space. Within the theory mentioned in Sect. 1 this

(*) In the case of the Crab nebula (Supernova of 1054 A.D.) one can use also the spectrum of continuous optical radiation.

(+) At present, when the predicted (see, in particular, [1]) polarization of radiation is discovered and, simultaneously, the radio emission of a number of discrete sources is investigated more completely, the magnetic bremsstrahlung origin of this radiation results obvious beyond any doubt.

was done in [4, 9] on the basis of the equation system,

$$\frac{\partial N_i}{\partial t} = \nabla(D_i \nabla N_i) - \frac{N_i}{T_i} + \sum_j p_{ij} \frac{N_j}{T_j} + q_i \,. \tag{7}$$

Here N_i is the concentration of i-nuclei; D_i and T_i are diffusion coefficient and lifetime of these nuclei, respectively; p_{ij} is the probability of formation of i-nuclei under disintegration of j-fast nucleus as a result of a nuclear collision in the interstellar medium; and q_i is a quantity of i-nuclei, formed in sources (normalized to the units of volume and time).

Supernovae and novae are concentrated in the galactic plane and, consequently, only there $q_i \neq 0$. At the same time particle diffusion takes place through all the galactic corona and

$$D_i \simeq D = \frac{vl}{3} \lesssim 3 \cdot 10^{37} \text{ cm}^2/\text{years} \,,$$

since $v \sim 10^{10}$ cm/s and $l \lesssim 3 \cdot 10^{20}$ cm. One can assume also that $T_N = (2 \div 6) \cdot 10^7$ years and $T_L : T_M : T_N = 3 : 2 : 1$, where T_L, T_M and T_N are the life times of L (Li, Be, B), M (C, N, O, F) and H ($Z \geqslant 10$) nuclei respectively. Using all these values and the coefficients p_{ij} accepted in literature the solution of the system (7) leads to the following conclusion. The composition of the primary cosmic rays near the Earth is the same as in reality, if contents of M and H nuclei in sources is only by several times higher than on the average in the Universe (it is so if one accepts that the acceleration efficiency for protons and nuclei is approximately the same). Simultaneously the quantity of Li, Be and B near the Earth when they are absent in sources, cannot be substantially less than 0.1 as compared to the quantity of M nuclei. This conclusion is compatible even with the results of the paper [10], according to which the ratio of concentrations of L and M nuclei is $N_L/N_M \leqslant 0.1$. If we take into consideration the new data [11] according to which $N_L/N_M \sim 0.3 \div 1$, the explanation of the observed cosmic ray composition becomes possible even using the value $D \lesssim 10^{37}$ cm^2/year and, in general without any difficulties. This is true in spite of using the life time $T_p \sim 4 \cdot 10^8$ years or even by 2-4 times higher value (this is an essential distinction our model from the model accepted in [12]).

For the cosmic rays anisotropy we have

$$\delta = \frac{\Delta F}{F} = \frac{4D}{c} \frac{|\mathrm{d}N/\mathrm{d}r|}{N} \,, \tag{8}$$

where $F = \frac{1}{4} rN \simeq \frac{1}{4} cN$ is a cosmic ray flux in some direction, ΔF is a difference of fluxes in opposite directions, and for simplicity, the fast particle

concentration N is considered to be dependent only on the radius r (the origin of the co-ordinates is placed in the centre of the Galaxy). Evaluating δ on the basis of solution of the equation (7) and neglecting the reflection of particles from the galactic boundary, in the simpliest case we have

$$\delta = \frac{4D}{c}\left(\frac{1}{r} + \frac{1}{\sqrt{DT}}\right), \qquad N = \frac{Q}{4\pi Dr}\exp\left[-r/\sqrt{DT}\right]. \tag{9}$$

Hence, when $D \sim 10^{30}$ cm^2/s $= 3 \cdot 10^{37}$ cm^2/year, $r = 2.5 \cdot 10^{22}$ cm (the solar system's distance from the galactic centre) and $T = T_p \sim 4 \cdot 10^8$ years, i.e., for protons, $\delta_p \sim 6 \cdot 10^{-3}$. For H nuclei when $T = T_N = 2 \cdot 10^7$, $\delta_N \sim 10^{-2}$.

Under the pratically total reflection of particles from the galactic boundaries, which is probable, the value δ decreases and for protons $\delta_p \sim 6 \cdot 10^{-4}$. The possibility of lowering the used value of D by several itmes and some other arguments show that there is no difficulty to get the values [13, 14] $\delta < 10^{-3}$ for the energy $E \lesssim 10^{15}$ eV and $\delta < 10^{-2}$ for $E \lesssim 10^{18}$ eV accepted in literature.

Summarizing we can say that the theory of cosmic ray origin discussed here is able to explain all the known facts and, as far as it is known, does not meet at present with any difficulties.

This conclusion, however, cannot be a rigorous proof of the theory, since there are alternative possibilities, and, on the other hand, the accuracy of a number of estimates is relatively low and some points need more precise estimates and verification. The latter point and, especially, the aims of experiment are discussed in the end of the paper [4]. Since in the first place, the question is about the obvious necessity of having more precise data on the cosmic ray composition and energy spectrum through all the energy interval, we shall mention here only the great importance of finding electrons and positrons in the primary component near the Earth.

As the same time it seems to be necessary to dwell here on the theories of the cosmic ray origin different from the theory accepted by us in order to compare them (for more details see [4]).

3. – In favour of the solar cosmic ray origin theories two arguments are advanced. The first of them, the energetical argument (a small quantity of the cosmic ray energy), does not seem to be serious. Suffice it to say that the cosmic ray energy density $W_{cr} \sim 1$ eV/cm^3 is of the same order as the interstellar gas energy density and magnetic field energy density: therefore it cannot be considered as an anomalously large one. Therefore the only argument in favour of the solar cosmic ray origin is essentially the fact of particle generation with the energy $E \lesssim (10^9 \div 10^{10})$ eV, during the solar outbursts.

At the same time a number of strong arguments speak against this theories. The radio astronomical data undoubtedly show that the whole Galaxy contains cosmic rays, not only the solar system region with radius $r \sim (10^{16} \div 10^{18})$ cm.

Further the permissible field in this region $H \sim 10^{-4} \div 10^{-5}$ cannot hold particles with the energy $E > (3 \cdot 10^{14} \div 3 \cdot 10^{15})$ eV. At the same time in order to keep in balance the number of cosmic ray particles generated on the sun, decreasing as a result of collisions and leaving the system, it is necessary to provide practically absolute particle « insulation » in the above-mentioned region. If such an insulation is altogether possible what has not been proved (*) it needs at any rate some absolutely specific conditions; and there is no independent reason to assume that these conditions take place. Finally, since it is impossible to keep the particles of a very high energy near the solar system, and may be the Sun does not produce such particles at all, it becomes necessary to consider the high energy particles ($E > E_K$) to be of non-solar origin, but, for example, of galactic one. Such a scheme is complicated by itself. Besides in such model it is strange that there is no « knee » in the cosmic ray spectrum at $E \sim E_K$ (for E_K one may select various values from 10^{10} to, e.g., 10^{14} eV).

All above-stated proves that at present the assumption about the solar origin of the main part of cosmic rays is, in our opinion, out of criticism.

The hypothesis of the cosmic ray metagalactic origin also encounters serious objections. The energy arguments, radio astronomical data (the concentration of cosmic electrons rapidly decreases beyond the galactic boundaries) and consideration of particle entrance and outcome conditions in the presence of galactic magnetic fields speak against this hypothesis. At this time there is no convincing reason also for the assumption [13] concerning the metagalactic origin of only a part of cosmic rays with a relatively higher energy $E > 10^{10}$ eV. The arguments in favour of such a theory, given in ref. [13] are connected with isotropy and cosmic ray composition; but if we take into consideration the discussion of Sect. 2, these arguments become absolutely unfounded. Absence of « knee » in the cosmic ray spectrum and non-efficiency of the intergalactic acceleration already mentioned in ref. [13], is also against such a hypothesis (**).

As for the galactic theories of cosmic ray origin, they differ both in respect of accepted cosmic ray space distribution, and in respect of sources and mechanism of cosmic ray acceleration. It seems to be unnecessary to dwell on the first difference, since the quasi-spherical cosmic ray distribution fol-

(*) The question is that generally speaking the particles must leave the region even with closed lines of a magnetic field (it is connected with the drift due to the magnetic field inhomogenity).

(**) The exit of the particles with energy $E \gtrsim 10^{16}$ eV from the Galaxy can be essential due to existence of the drift in the inhomogeneous magnetic fields (see [4]). In this connection it may be necessary to admit that cosmic rays with $E \gtrsim 10^{16}$ eV still have metagalactical origin and, for example, are generated in peculiar radiogalaxies of Virgo and Cygnus type.

lowing from the radioastronomical and astrophysical data [1-6] became, apparently, generally accepted.

As for the cosmic ray sources, the assumption about the purely stellar acceleration is connected with great difficulties (see Sect. **1**). Moreover, this assumption is highly arbitrary and vague because of absence of any elaborate theory of stellar accelerators taking into account the high conductivity and mobility of stellar atmospheres.

Energy difficulties are reduced in the combined model where stars are used only as injectors, and the main acceleration takes place in the interstellar medium [12, 15-18].

However, as it has been indicated in Sect. **1**, in this case injectors also must supply a very high energy. Further, to produce similar proton and nucleus energy spectra it is necessary to assume that the life time of particles in the accelerating region depends on the particle leakage from this region. This life time T must therefore be less than the nuclear life time for heavy nuclei: hence $T < 10^7$ years and, according to [12], $T = 4 \cdot 10^6$ years. For producing the necessary spectrum, α should be $\sim 10^{-14}\,\mathrm{s}^{-1}$, where α is a coefficient in the law of energy change $\mathrm{d}E/\mathrm{d}t = \alpha E$. But from the astrophysical data it follows that in the Galaxy as a whole $\alpha \sim 10^{-17} \div 10^{-18}$. The same low value of α one can obtain using the results of the radio astronomical observations, since, under high values of α electrons must be accelerated and cannot have spectrum (1). Moreover, for the quasi-spherical Galaxy, a high value of α is incompatible with a short leakage time $T \sim 4 \cdot 10^6$ years (see [4, 19]). Therefore, in the theory of interstellar acceleration it is necessary to assume that the acceleration takes place only near the galactic plane in the arms of the galactic spiral or in its separate regions, with especially « favourable » conditions. In such a version (see, for example, [16-18]) the difficulties, connected with a high energy output of hypothetical injectors, only increase (in connection with the decrease of star number). Moreover, analogous new difficulties take place due to the necessity to renew completely the kinetic energy of gas masses in the arms for $(10^6 \div 10^7)$ years. To provide such a high energy supply is very difficult (see [17]). Finally, the whole theory is, strictly speaking, purely hypothetical: the theory does not point at the injectors and mechanism of their operation, at the concrete regions of the interstellar acceleration and the reasons for high efficiency of this acceleration. A very important question of energy balance is also actually neglected.

For all these reasons, as it seems to us, the discussed models of interstellar acceleration cannot be compared with the theory discussed in Sect. **1** and **2**. At the same time the similarity of this last theory with the model of interstellar acceleration in the galactic spiral and, especially, in some of its regions is evident. In both cases the distribution of sources is the same and the particle energy and charge spectra are determined by sources or by relatively

small interstellar regions, where acceleration takes place. Probably, the acceleration mechanism is also in both cases the same.

However, the radical difference is that we consider the cosmic ray sources to be quite concrete objects (supernovae and novae envelopes) and base this conclusion on the radio astronomical observations. At the same time in the interstellar acceleration scheme it is not only necessary to use some similar views but also to make additional substantial and yet groundless assumptions.

In this connection a continuous and rather great transformation of the interstellar acceleration theories seems to be not accidental. At the same time it is easy to see that the theory of the cosmic ray origin presented in Sect. 1, 2 has not changed substantially from the very beginning of its development in 1953 (see, for example, [1]).

We should like to note in conclusion that a certain combined model is possible where supernovae and novae are injectors, but acceleration takes also place in the interstellar space. In such a model all the difficulties connected with injection vanish. But the problem of the energy supply to the interstellar media is unsolved as before. However, the main objection is that in such a scheme the assumption about the high interstellar acceleration efficiency is unfounded and, essentially, purely hypothetical and problematical. Therefore, it seems to us that at present there is no reason for such a model with two-staged acceleration. It is especially true since assumption of cosmic ray acceleration due only to supernovae and novae outbursts is, as it has been mentioned above, permissible and sufficient for the explanation of all the known facts.

REFERENCES

[1] V. L. Ginzburg: *Usp. Fiz. Nauk*, **51**, 343 (1953); *Fortschritte d. Physik*, **1**, 659 (1954).

[2] V. L. Ginzburg: *Colloque Intern. d'Astrophys.* (Liege, 1954). Summary is published in *Memoires Soc. R. Sc.*, **15**, 682 (Liege, 1955).

[3] V. L. Ginzburg: *Intern. Conf. on Cosmic Rays* (Guanajuato, 1955). This report is published in *Suppl. Nuovo Cimento*, **3**, 38 (1956).

[4] V. L. Ginzburg: *Usp. Fiz. Nauk*, **62**, 37 (1957). Sent for publication in vol. **4** of series *Progress of Cosmic Ray Physics* (Amsterdam, 1952).

[5] S. B. Pikel'ner: *Dokl. Akad. Nauk SSSR*, **88**, 229 (1953); S. B. Pikel'ner and I. S. Šklovskij: *Astron. Žu. SSSR*, **34**, no. 2 (1957). See also I. S. Šklovskij: *Astron. Žu. SSSR*, **29**, 418 (1952).

[6] I. S. Šklovskij: *Cosmic Radio Emission* (Moscow, 1956).

[7] V. L. Ginzburg: *Dokl. Akad. Nauk SSSR*, **92**, 727 (1952); V. L. Ginzburg, S. B. Pikel'ner and I. S. Šklovskij: *Astron. Žu. SSSR*, **32**, 503 (1955); **33**, 447 (1956).
[8] I. M. Gordon: *Dokl. Akad. Nauk SSSR*, **94**, 413 (1954); S. B. Pikel'ner: *Astron. Zu. SSSR*, **33**, 785 (1956).
[9] V. L. Ginzburg and M. I. Fradkin: *Astron. Žu. SSSR*, **33**, 579 (1956); *Žu. Eksp. Teor. Fiz.*, **31**, 523 (1956); *Sov. Phys., J.E.T.F.*, **4**, 462 (1957).
[10] B. Peters: *Proc. Ind. Acad. Sc.*, **40**, 231 (1954).
[11] W. R. Weber: *Nuovo Cimento*, **4**, 1285 (1956); J. M. Noon, A. J. Herz and B. J. O'Brien: *Nature*, **179**, 91 (1957). P. H. Fowler, R. R. Hillier and C. J. Waddington: *Phil. Mag.*, **2**, 293 (1957).
[12] B. Rossi: *Suppl. Nuovo Cimento*, **2**, 275 (1955); P. Morrison, S. Olbert and B. Rossi: *Phys. Rev.*, **94**, 440 (1954).
[13] G. Cocconi: *Nuovo Cimento*, **3**, 1433 (1956).
[14] *Oxford Conference on Extensive Air Showers* (1955).
[15] E. Fermi: *Phys. Rev.*, **75**, 1169 (1949); *Astrophys. Journ.*, **119**, 1 (1954).
[16] L. Davis: *Phys. Rev.*, **101**, 351 (1956).
[17] E. N. Parker: *Phys. Rev.*, **99**, 241 (1955).
[18] C. Y. Fan: *Phys. Rev.*, **101**, 314 (1956).
[19] V. L. Ginzburg: *Dokl. Akad. Nauk SSSR*, **99**, 703 (1954); *Izv. Akad. Nauk SSSR, Ser. Fiz.*, **20**, 5 (1956).

SUPPLEMENTO AL VOLUME VIII, SERIE X
DEL NUOVO CIMENTO

N. 2, 1958
2° Trimestre

Variation of the Intensity of Cosmic Radiation During Earth's Geological History and Their Possible Influence on Life's Evolution.

V. I. Krassovskij and I. S. Šklovskij

Institute of the Physics of Atmosphere
Sternberg State Astronomical Institute - Moscow

At present it appears to be proved that both Crab nebula's radio and optical emission (the latter with continuous spectrum) are caused by relativistic electrons that move in magnetic fields [1, 2]. Since it is so, we have to recognize with the fact that this nebula, a remnant of Supernova's outburst in 1954, contains a great number of relativistic particles, i.e. primary cosmic rays. Indeed, both remnants of Supernova's explosions in 1572 and 1604 are the sources of radioemission [3, 4]. Recently it was found that the network nebulae in Cygnus, undoubtful remnant of Supernova's explosion which took place several thousand years ago [5] are also the sources of radioemissions. According to [6], average concentration of relativistic electrons in the Crab nebula with the energy $E > 10^9$ eV is equal to $3 \cdot 10^{-7}$ cm $^{-3}$. The concentration of relativistic protons may be expected to be of the same order. When, owing to the Crab nebula expansion, its radius will be ~ 5 parsec, the concentration of relativistic particles will be $\sim 3 \cdot 10^{-9}$ cm^{-3}, i.e. still approximately 30 times larger than the concentration of the primary cosmic rays in the Earth's neighbourhood.

Such a comparatively « old » nebula which resulted from a Supernova's outburst is the I C 443, whose linear dimensions are 7 to 10 parsec and the concentration of the relativistic particles 50 to 100 times larger than in the Earth's neighbourhood.

A question arises whether the Sun with all its surrounding planets, moving in the Galaxy could get into such regions of the interstellar space where the density of the primary cosmic rays is tens or even hundreds times larger than

now. We may answer this question affirmatively. This took place when the Supernovae exploded in the immediate proximity of the Sun.

Till recent time the frequency of outbursts of the Supernovae in the Galaxy was determined from the average data on other Galaxies. In [6] it was shown that it is not so and that the frequency of these outbursts is at least one order higher. In this respect our Galaxy is similar to those of NGC 3184, 6946 and 4321 in which the frequency of Supernovae outbursts is abnormally large. Indeed during the last millennium at least 5 explosions of Supernovae (1006, 1054, 1572, 1604 and 1843) took place in our Galaxy, the last Nova being the Carina (see [7]). They all were very bright; consequently the distance to them did not exceed 2 to 2.5 thousand parsec, especially if one takes into account the interstellar light absorption. Hence a conclusion may be drawn that approximately each 1000 years a Supernova explodes at a distance not more than 1000 parsec. Assuming that the Supernovae form in the Galaxy a very flat system ~ 100 parsec thick, we shall find that for example each 200 million years a Supernova explodes at a distance less than 8 parsec. This means that during the period of the Earth's existence the stars in the Sun's neighbourhood outburst several times (~ 10) as Supernovae.

What phenomena could take place in such an extraordinary event? The brightness of the flashed star hardly exceeded -20^m, i.e. the flux of radiation from the star was several thousand times less than from the Sun. It is not excluded however that the flux of hard, say, X-ray radiation from the star and from the nebula at the earliest stages of its development could essentially exceed the flux of hard radiation from the Sun. This could involve serious consequences (see below). Expanding at a rate of $\sim 10^8$ cm s^{-1} the gaseous envelope resulting from the Supernova's outburst will pass through the Solar System. Taking into account, however, insignificant gas density of this envelope ($\sim 10^{-22}$ g cm^{-3}), this will scarcely involve any consequences.

It is very essential that in such epochs during several thousand years the flux of cosmic radiation at the Earth will exceed several tens of times the mean level. It is also necessary to take into account that the distribution of relativistic particles of the expanding nebula, a remnant of Supernova's outburst, will be strongly non uniform. Thus, there may exist periods of many hundred years when the flux of primary cosmic rays on the Earth will be hundred times larger than now. This question is very important, therefore we shall consider it more thoroughly.

Let the volume in which outbursts of Supernovae in the Galaxy take place be V. Taking into account that Supernovae form a very flat system, V will be $\sim 10^{66}$ cm^3. Let us designate through v the volume of a nebula resulting from a supernova outburst in which the density of cosmic ray energy is u times larger than ε_0, mean density of cosmic ray energy in the proximity of the galactic plane. Then the average period of time between the Sun's runs through

these regions, in which the density of cosmic ray energy is n times higher than the average one, will be

$$t = \frac{1}{\nu} \frac{V}{v} = \frac{1}{\nu \cdot L} \cdot V \cdot n \cdot \varepsilon_0 ,$$

where ν is the frequency of Supernova outbursts in our Galaxy, L the average energy of cosmic rays formed during the explosion of one Supernova. But the product $\nu \cdot L$ is nothing more but the power of cosmic ray injectors. This value is obtained from the analysis of the conditions of cosmic ray existence in the Galaxy and is independent of the taken values of ν and L.

According to existing data (see the paper by one of the co-authors), $\nu \cdot L \sim 3 \cdot 10^{39}$ erg s^{-1}.

Assuming $\varepsilon_0 = 1$ eV cm^{-3} $= 1.6 \cdot 10^{-12}$ erg cm^{-3} we shall find that

$$t = 4.5 \cdot 10^{14} \cdot n \text{ s} .$$

If, for example, $n = 20$, $t = 3 \cdot 10^8$ years.

It is not excluded that a considerable increase in cosmic ray intensity may involve serious biological and first of all genetical consequences. Till recent time it was considered that evolution of living beings on the Earth is determined by influence of natural selection and of various physical conditions of the environments. But at the same time account was never taken of such important factor as the total level of hard radiation. By virtue of the stated above we must recognize that the latter factor at certain stages of evolution could have important if not decisive significance.

According to existing data (see, for example, [8]), radioactivity in the lower layers of the Earth's atmosphere caused by cosmic rays is now 0.04 r per year, i.e., about one third of the total level of natural radiation. The genetical significance of hard radiation is known to be now the subject of intensive investigation. Although much in this important problem is for the time being not clear enough, the principal conclusions may be summarized as follows.

Even a twofold increase in frequency of mutations as compared with the natural level can involve serious genetical consequences for certain species.

In a number of cases doubling of mutation frequency in the species with a short cycle of propagation will require a hundreds and thousands times increases in intensity of cosmic radiation. But doubling of mutation frequency in long-living species requires only a 3 to 10 times increase in intensity of cosmic radiation.

Hence it follows that a long increase in intensity of cosmic rays lasting for millennia can involve catastrophic consequences for many long-living specialized animal species with comparatively small population. It is pos-

sible, for example, to suggest a hypothesis that the so called « great dieing out » of reptiles at the end of the Cretaceous period was caused by this factor.

On the other hand, for other animal and plant species a considerable increase in intensity of cosmic rays may prove to be the factor that favours their further evolution. It is not excluded, for example, that the magnificent prosperity of vegetation in the Carbonic period was to a considerable extent due to the increase in the level of hard radiation.

Paying attention to the biological and genetical consequences of the considerable increase in intensity of cosmic radiation in certain periods of the Earth's hystory, we should note that this factor could once stimulate the formation from simple organic compounds of complicated complexes out of which life could develop on the Earth.

REFERENCES

[1] I. S. Šklovskij: *Dokl. Akad. Nauk SSSR*, **90**, 983 (1953).
[2] J. Oort and T. Walraven: *Bull. Astron. Neederland*, **12**, no. 462, 285 (1956).
[3] R. Hanbury Brown and C. Hazard: *Nature*, **170**, 364 (1952).
[4] J. Shakeshaft, M. Ryle, J. Baldwin, B. Elsmore and J. Thomson: *Mem. of Roy. Astron. Soc.*, **67**, no. 3, 106 (1955).
[5] D. Walsh and R. Hanbury Brown: *Nature*, **175**, 808 (1955).
[6] I. S. Šklovskij: *Kosmičeskoe Radioizlučenie* (Moscow, 1956).
[7] A. D. Thakerey: *Observatory*, **76**, 103 (1956).
[8] N. C. Dubinin: *Vestnik Akad. Nauk. SSSR*, No 8, 22 (1956).

SUPPLEMENTO AL VOLUME VIII, SERIE X
DEL NUOVO CIMENTO

N. 2, 1958
2° Trimestre

An Examination of the Fermi Mechanism.

L. DAVIS, JR.

California Institute of Technology - Pasadena, Cal.

By now Fermi's mechanism [1-3] for the acceleration of cosmic rays by the random motions of magnetic fields embedded in gas clouds is so well known that there is no need to outline here its general principles. Many different modifications have been proposed and it does seem worth while to examine some of them. When this is done as quantitatively as possible, in each case serious difficulties are found. Nevertheless it still seems likely that when the origin of cosmic rays is finally understood, it will turn out that some variant of the Fermi mechanism is involved.

The region in which the mechanism operates may be the atmosphere of a star, it may be a supernova, it may be the spiral arm of our galaxy as Fermi assumed in his second detailed discussion [2], it may be the H II regions where the motions of the gas clouds originate, it may be the halo of our galaxy, or it may be a cluster of galaxies. I shall consider mainly the spiral arm case and leave the other cases to other speakers on the progran. Of course many features of the discussion will apply in any case if one makes a suitable change of scale. It is customary to isolate a number of features of the Fermi mechanism for separate discussion under such sub-titles as injection, storage, removal processes, isotropy, and acceleration mechanisms. I shall devote most of my attention to the acceleration mechanisms, but shall start with brief comments on the other topics.

The part of the acceleration that carries ions from thermal energies to the order of 10^7 or 10^8 eV per nucleon must occur quite rapidly and is called injection. (If the same process continuous to 10^{13} eV or beyond, it is called primary acceleration.) It is believed that the sun emits particles of somewhat lower energy than 10^8eV quite copiously and at least occasionally it is observed to emit particles with energies of the order of 10^{10} eV. Accordingly it is plausible to suggest that injection is due to processes, quite possibly small

scale Fermi processes of the type suggested by GINZBURG [4] and TELLER [5], in turbulent magnetic regions in the upper atmospheres of stars. However, the observed relative excess of heavy ions in cosmic rays poses a difficulty. If the injection process turns out to favor heavy ions, perhaps for reasons similar to those suggested by BIERMANN [6], CRAWFORD [7], and many others, all is explained. Otherwise it will be necessary to suppose that injection takes place from supernovae or from those stars where element building has produced a relative excess of heavy elements.

The discrepancy between the low rate at which any accelerating mechanism seems able to feed energy into cosmic rays and the large observed energy density forces us to assume that cosmic rays are stored by magnetic fields. It is now rather generally accepted that the spiral arms of the galaxy are occupied by fields of the order of 10^{-5} G and it is plausible that the spherical halo of radius about 50 000 light years that surrounds the disk is occupied by a field of perhaps 10^{-6} G. Since a $3 \cdot 10^{15}$ eV proton has a radius of curvature of 1 light year in a 10^{-5} G field, there is no difficulty with storage except at energies above about 10^{17} eV. FERMI originally [1] assumed that the magnetic field in the galactic disk was chaotic, but it now seems more likely that in the spiral arms the field runs along the arm [8]. Superposed on this approximately uniform field are hydromagnetic waves of moderate amplitude. It is possible that the sun lies just outside a spiral arm or in some kind of a rift where it is immersed in the chaotic magnetic field of the halo, but it seems better to assume that the sun lies in a spiral arm where the field is roughly uniform.

Either model of the field explains the observed fact that cosmic rays are much more isotropic than is starlight. But the observed very high degree of isotropy often tends to strain any detailed theory that one may work out. It is now clear that below $10^{12} \div 10^{13}$ eV there is no problem. The material ejected from the sun disturbs the magnetic field in the solar system and in any of a number of models [9-12] the resulting non-uniform field should render the low energy cosmic rays isotropic at the top of the atmosphere. The high energy primaries detected by extensive air showers are a different matter and should give information about magnetic fields in an extensive region of the galaxy. It should be a profitable test of any proposed structure of the galactic magnetic field or any theory of the origin of cosmic rays to investigate the predicted degree of isotropy of extensive air showers.

A very important and much quoted paper of MORRISON, OLBERT and ROSSI [13] analyzes the degree of isotropy expected with a rather peculiar model of the magnetic field. They assume that the field occurs in isolated knots separated by nearly field-free space where the cosmic rays travel in nearly straigth lines. Thus the theory of isotropic diffusion by a simple random walk is easily applied. But there seems no reason to expect the magnetic

field to be confined to the hot ionized regions; even the so-called unionized regions have enough conductivity to maintain large scale magnetic fields for many times the age of the universe. If the energy density in turbulent gas motion exceeds that in the magnetic field, a very chaotic field will result of the kind considered by FERMI in his first model [1]. This field fills the galactic disk. Cosmic rays of ordinary energy, whose trajectories have radii of curvature of the order of 10^{-5} light year, may be expected to spiral around a single line of force, running back and forth along it wherever it goes. Thus the basic question is whether on a large scale the magnetic field lines describe a random walk. They may appear to do so on a small but not on a large scale if, for example, the lines of force never leave the galactic disk. This would correspond to perfect reflection at the boundaries. Any tendency toward a large scale structure of the magnetic field as demanded by the observed polarization of starlight will drastically affect the conclusions of MORRISON *et al.* Nevertheless, if suitably modified, their analysis may be applied to the case in which the field is roughly uniform along the spiral arm. The motion normal to the magnetic field is compounded of a drift of the helical trajectory normal to the gradient of the magnetic field and of a random wlak due to abrupt scatterings. The drift velocity does not carry a particle out of the spiral arm. The scattering displaces the helix by only a small fraction of the radius of curvature in a random direction. Thus, except at the very highest energies, the escape time normal to the field is easily shown to be large compared to the time for a nuclear collision. Thus the only diffusion to be considered is that along the spiral arm, and one has essentially a one-dimensional problem. MORRISON, OLBERT and ROSSI treat this problem when they consider diffusion in a disk of thickness $2h$ and radius R_0. It is only necessary to let R_0 go to infinity and to take $2h$ to be the *length* of the spiral arm. Since the scatterings now seem more likely to be through small than through large angles, one must include a high degree of « persistence of velocity » in the statistical analysis. Finally, the interactions that change the energy and those that change the direction are not identical; this makes the diffusion in position nearly independent of that in energy.

The basic mechanism by which isotropy is maintained in an approximately uniform galactic field is by encounters with inhomogeneities in the magnetic field. These may be hydromagnetic shock waves as suggested by FERMI, short ordinary hydromagnetic waves, or the disturbed regions around stars as suggested by FAN. The connection between the anisotropy and the experimentally observable siderial time variation of cosmic rays was discussed in a paper of mine [8] about three years ago. The general mathematical treatment still seems valid, but the detailed numerical values have mostly either been superseded or, in the case of the Pic du Midi results, were copied incorrectly due to my confusing the symbols for percent and per mill. Also the conjecture

that the betatron acceleration process will lead to an excess flux normal to the field has proved to be incorrect; and hence all conclusions reached in that paper must be reconsidered. This cannot be done properly until convincing experimental data on the anisotropy are obtained.

In order to explain the energy spectrum of cosmic rays, FERMI supposed that cosmic ray particles were removed from the population we observe with a probability that is independent of their energy once their velocity approaches that of light. He first assumed that this result is accomplished by nuclear collisions, but this was made dubious by the abundance of heavy nuclei in cosmic rays. Several authors [2, 13] have suggested that diffusion out of the storage field would meet this difficulty, and there may be other possibilities.

We now come to the principal problem with the Fermi mechanism, the processes that increase the energy of the cosmic rays. As FERMI pointed out, the fact that the magnetic field may be regarded as imbedded in moving gas clouds means that in effect the cosmic rays collide with these clouds and tend to gain energy. The basic result is that α, the exponent in the integral energy spectrum, is given by

$$\alpha = \frac{t_1}{\tau \langle \Delta w/w \rangle_{\mathrm{Av}}}, \tag{1}$$

where w is the total energy, including rest energy, of the particle, Δw is the increase in energy per collision, $\langle \Delta w/w \rangle_{\mathrm{Av}}$ is the mean fractional increase, averaging over both losses and gains, t_1 is the mean time between interactions, and τ is the mean time for removal from the population we observe. For a simple model with a chaotic magnetic field and a turbulent gas

$$\langle \Delta w/w \rangle_{\mathrm{Av}} \approx (v_g/c)^2 , \tag{2}$$

where v_g is the relative velocity of neighboring gas clouds. It was soon realized [14, 13] that astronomically plausible values of v_g, τ, and t_1 led to a value of α that was incorrect by about two orders of magnitude. Accordingly, many efforts have been made to find a modification of the Fermi mechanism that would be more efficient. The simplest modification is to look for regions where (v_g/c) is larger than $3 \cdot 10^{-5}$, the value that corresponds to the $v_g \approx 10$ km/s characteristic of our region of the galaxy. Many authors have tried to find terms in $\langle \Delta w/w \rangle_{\mathrm{Av}}$ that are of first order in (v_g/c). Obviously, if any process does this, it does not have to occur frequently to explain the observed α. Before considering such processes a digression is necessary.

Even if interactions in which the cosmic ray loses energy are as likely as those in which it gains, so that $\langle \Delta w/w \rangle_{\mathrm{Av}} = 0$, some cosmic rays by chance will experience more than their share of collisions of one type and the observed

energy spectrum will result. One has a diffusion or random walk in energy that has been discussed by DAVIS [15, 16], by KAPLAN [17], and by CRAWFORD [7]. The resulting value of α is of order

$$\alpha = \left(\frac{2t_1}{\tau \langle (\Delta w/w)^2 \rangle_{\text{Av}}} \right)^{\frac{1}{2}}. \tag{3}$$

Since with the interactions considered by FERMI

$$\langle (\Delta w/w)^2 \rangle_{\text{Av}} \approx (v_g/c)^2 \tag{4}$$

and since α is of order unity, (3) and (4) seem to lead to essentially the same result as (1) and (2). Nonetheless, a real increase in efficiency has been uncovered because one can consider a variety of additional processes. One such process that is so appealing that is has been independently discovered by almost everyone is the « betatron » acceleration and deceleration that takes place as the particle in its spiraling along the field comes to a region where the field strength is increasing or decreasing with time. With this mechanism it seems possible to devise simple models [15, 16] for the acceleration of cosmic rays from the injection energy up to somewhere above 10^{16} eV by means of hydormagnetic waves running along the spiral arm of the galaxy. The models are not in as obvious disagreement with astronomical and cosmic ray evidence as Fermi's first model turned out to be; but there is enough difficulty so that some will undoubtedly reject them, and everyone would be glad if a model could be found for which a correspondingly detailed treatment revealed fewer difficulties.

One major difficulty with very high energy particles is apparent. The time, t_1, required for an interaction with the field cannot be less than the time required for the field to deflect the particle through, say a radian. This is 3.5 years for a 10^{16} eV proton in a 10^{-5} G field. Thus t_1 tends to increase and τ, the time to diffuse out of the field, to decrease with increasing energy and radius of curvature. It is difficult to see why $\Delta w/w$ should increase, and hence it is very hard indeed to see why α should remain constant above about 10^{15} eV. Up to about this point there should not be too much difficulty. In any model this difficulty appears when the radius of curvature becomes comparable with the scale of the inhomogeneities in the magnetic field.

The betatron acceleration has one feature, first called to my attention by Dr. SCHLÜTER, that is not always fully appreciated. In a region where the magnetic field is uniform in space but is increasing in time, a charged particle describes a helix that gets continuously flatter as the energy is increased. The longitudinal Fermi collisions, it will be recalled, make the helices get steeper when the energy is increased. It seems plausible then that the combination

of the Fermi longitudinal collisions and the betatron accelerations would tend to preserve an isotropic distribution and would keep the particles in flat helices where the longitudinal collisions could continue to add energy. Nothing could be farther from the truth. For consider the adiabatic invariant of the motion [18, 19]

$$(w^2 - m^2c^4) \sin^2 \theta / B_a = I \,, \tag{5}$$

where m is the rest mass and may be disregarded for our high energy particles, θ is the pitch of the helix, and B_a is the axial component of the magnetic field. The adiabatic invariant I will be a constant as long as the field changes slowly in time compared to the Larmor period and slowly in space compared to the radius of curvature. Now (5) holds both for the Fermi longitudinal collisions and for the betatron process. Hence if we measure the helix angle after the process is over and the particle has come to a standard region where the magnetic field has a standard value, the change in helix angle depends only on the change in energy and not on which process produced the change.

Let us now apply this result to some of the processes that may seem to lead to energy increases that are of first order in v_g/c. One such example is Fermi's [2] system of traps, which has been elaborated by Fan [20]. If hydromagnetic waves that change the field strength run along an approximately uniform field, cosmic rays in flat helices will be trapped between adjacent maxima in the field strength. If these maxima move together particles will make only head-on collisions with the gas clouds from which they are reflected and they will gain energy; if the maxima are moving apart, the trapped particles will lose energy. Fermi and later Fan argued that the former situation predominated. But a particle enters or leaves such a trap only when θ is essentially 90° at a maximum in B. For if θ is less the particle will just continue on through both jaws of the trap; while if θ becomes 90° before reaching the maximum, the particle is not near a state where it can enter or leave. If we assume that B has the same value at all maxima, the maximum energy of each particle is proportional to the square root of its value of I. As long as I remains constant, the energy will fluctuate a bit in the traps but there will be no net change. If it starts to increase, the particle will escape from the trap and the only possible further energy change will be a decrease in an expanding trap. There are two ways to avoid this result. Fermi pointed out that the scattering from small scale inhomogeneities would flatten the spiral of an accelerated particle. But in order to get an acceleration it is necessary to find a systematic effect that would lead to a consistent increase in I. If the scatterings change θ at random, they lead to a random walk in I and hence in energy. Fan has suggested on the basis of a complicated treatment of the motion of a charged particle in a magnetic field that there is a tendency

for particles to prefer to stay in traps whose jaws are coming together rather than in traps whose jaws are separating. But one sees immediately from (5) that this is possible only if the field maxima are larger at the edges of traps whose jaws come together. There seems to be no reason to expect this, especially since the maximum that are important form part of two traps, an accelerating trap on one side and a decelerating trap on the other.

Another way of getting a first order effect with hydromagnetic waves running along a uniform galactic field has been proposed by THOMPSON [21]. He supposes that one starts with an isotropic distribution of cosmic rays and then allows a wave to change the field strength by a substantial fraction of its original value. This is done adiabatically with no small scale scatterings; hence I remains constant for each particle and the distribution becomes quite anisotropic. Next, while the energy remains constant, small scale scatterings restore the isotropy. Then the field returns to its original value adiabatically, and finally scattering again restores the isotropy. I get, correcting an error in Thompson's analysis, a net change in average energy due to this process of

$$\langle \Delta w/w \rangle_{\text{Av}} = (4/45)(\Delta B/B)^2 - (4/45)(\Delta B/B)^3 + \dots , \tag{6}$$

where ΔB is the change in the field strength. The difficulty with this procedure is that if there is no scattering to restore isotropy half way through the process, there is no energy change. If scattering maintains isotropy during the field change, again there is not net energy change. Unless the field changes come in isolated sharp steps separated by long intervals during which isotropy slowly returns, it is hard to see how this mechanism could avoid being much less efficient than the maximum value given by (6).

If one is looking for first order effects, my own preference is to try to devise some mechanism using damped hydromagnetic waves, an idea suggested to me but I think later discarded by PARKER [22]. It is well known [23, 24] that the shorter waves are strongly damped. They must, then, originate at discrete centers and propagate outward for a few wavelengths before they die out. Cosmic rays either will go clear through the source if traveling in a steep helix or will be reflected by a wave they meet head-on if traveling in a flat helix. Thus all energy changes are increases with $(\Delta w/w) \approx 10^{-4}$ since the wave velocity should be of order 30 km/s or 10^{-4} c. The problem with this mechanism is to find enough sources of hydromagnetic waves. If τ in (1) is $4 \cdot 10^6$ years, then t_1 must be about 600 years. It now seems very probable that the sun disturbs the galactic magnetic field in its vicinity [9-11] and it is reasonable to suppose that all stars produce similar effects. But what is required is one star per 30 cubic light years generating waves that extend out of the order of $\frac{1}{2}$ light year with enough amplitude to reflect a substantial fraction of the cosmic rays; and this seems improbable. Stars such as Bab-

cock's magnetic stars or the hot O and B stars that are thought to stir up most of the non-rotational motion of the galactic gas would send out hydromagnetic waves to much greater distances, but all such stars are entirely too rare.

Finally, I shall summarize the thesis research of Dr. T. W. Layton [19] at the California Institute. By means of a diffusion equation, he treats the distribution in energy, position, and direction of motion of an ensemble of cosmic rays moving in an approximately uniform galactic magnetic field perturbed by a random spectrum of hydromagnetic waves. It is a considerable improvement over the earlier treatment of the subject [16].

First, he considers the motion of a charged particle in a slowly changing magnetic field. He obtains Eq. (5) above, which may be regarded as stating that the angular momentum of the particle about the axis of its helix is an adiabatic invariant. As independent variables he uses

$$\varepsilon = \ln w\,, \qquad \mu = \cos\theta \tag{7}$$

in place of w, the total energy, and θ, the angle between velocity and the magnetic field. Under the circumstances in which (5) applies,

$$\frac{\mathrm{d}\varepsilon}{\mathrm{d}t} = \frac{1}{2}(1-\mu^2)\frac{\partial(\ln B_a)}{\partial t}\,, \tag{8}$$

$$\frac{\mathrm{d}\mu^2}{\mathrm{d}t} = (1-\mu^2)^2\frac{\partial(\ln B_a)}{\partial t} - (1-\mu^2)\frac{\mathrm{d}(\ln B_a)}{\mathrm{d}t}\,, \tag{9}$$

where B_a is the axial magnetic field, $\mathrm{d}/\mathrm{d}t$ denotes a rate of change following the motion of the particle, and $\partial/\partial t$ denotes a rate of change at a fixed point in the inertial frame of reference. These relations are doubtless not essentially new, but his form is convenient.

Next, Dr. Layton defines $W(\mu, \varepsilon, z, t)\,\mathrm{d}\mu\,\mathrm{d}\varepsilon\,\mathrm{d}z$ to be the number of particles at the time t in the indicated interval of μ, ε and z, which is distance along the magnetic field. In the usual way he deduces the diffusion equation for cosmic rays in this space,

$$\begin{aligned}\frac{\partial W}{\partial t} = &-\frac{\partial}{\partial z}[c(\mu + D_\mu)W] - \frac{\partial}{\partial \mu}[D_\mu W] + \frac{\partial}{\partial \varepsilon}[D_\varepsilon W] + \\ &+ \frac{1}{2}\frac{\partial^2}{\partial \mu^2}[D_{\mu\mu}W] + \frac{1}{2}\frac{\partial^2}{\partial \varepsilon^2}[D_{\varepsilon\varepsilon}W] + \frac{\partial^2}{\partial \varepsilon\,\partial \mu}[D_{\varepsilon\mu}W] + \\ &+ \frac{n_2\sigma_\theta^2}{4}\left[(1-\mu^2)\frac{\partial^2 W}{\partial \mu^2} - 2\mu\frac{\partial W}{\partial \mu}\right] - \frac{W}{\tau} + Q(\mu, \varepsilon, z; t).\end{aligned} \tag{10}$$

The term in Q at the extreme right-hand side of this equation represents the injection of cosmic ray particles; it is later taken to be zero except at low energies. The term $-W/\tau$ represents the losses due to nuclear interactions. The block of terms multiplied by $n_2\sigma_\theta^2$ give the effect of inhomogeneities that are small compared to the helix radius. They are assumed to deflect the trajectory through a small angle whose root-mean-square value is σ_θ and whose plane is random, there being n_2 deflections per unit time. It is this interaction that tends to restore isotropy. The remaining terms on the right give the effect of a statistical distribution of hydromagnetic waves whose scale is very large compared to the radius of curvature of the trajectories. Only a single cell size normal to the field is assumed, but this should not greatly affect the result. The various diffusion coefficients are calculated with the aid of (8) and (9), and in the highly relativistic case are

$$
\left\{
\begin{aligned}
D_\mu &= -\frac{K(1-\mu^2)^3(1+\mu^2)}{\mu^3|\mu|}, \\
D_\varepsilon &= -\frac{K(1-\mu^2)^2(1+\mu^2)}{2\mu^2|\mu|}, \\
D_{\mu\mu} &= \frac{K(1-\mu^2)^4}{\mu^2|\mu|}, \\
D_{\iota\varepsilon} &= \frac{K(1-\mu^2)^2}{|\mu|}, \\
D_{\varepsilon\mu} &= \frac{K(1-\mu^2)^3}{\mu|\mu|},
\end{aligned}
\right. \tag{11}
$$

where K characterizes the distribution of hydromagnetic waves and is proportional to the square of the gas velocity. For example, for a particular spectrum in which all waves have a wavelenght of a light years perpendicular to the magnetic field and have a distribution of wavelengths parallel to the field such that b is the mean wavelength and $2b\delta$ the width of the wavelength spectrum at half maximum

$$
K = 2\pi\langle(v_a/c)^2\rangle_{\text{Av}}\, b\delta/a^2 . \tag{12}
$$

Terms representing ionization losses have been omitted from (10) since the main interets is at very high energies, but they could be included easily if desired.

All the information of interest is obtainable by solving (10) in various cases. Dr. LAYZER has considered certain steady state solutions. First he investigated the circumstances in which the diffusion along z could be treated

approximately in terms of a mean time τ_D to diffuse to the end of the spiral amd and the assumption that well within the arm the density is essentially independent of z. The nuclear interactions can be disregarded and τ in (10) replaced by τ_D, the terms in $\partial/\partial z$ being set equal to 0. For this case he obtained the distribution in energy and in angle by a combination of analytical and high-speed digital computer manipulations. The result is that the density in energy, w, and angle as given by μ is

$$n(w, \mu)\,\mathrm{d}w\,\mathrm{d}\mu = A f(\mu) w^{-(\alpha+1)}\,\mathrm{d}w\,\mathrm{d}\mu\,, \tag{13}$$

where A is a constant and $f(\mu)$ is a function that depends on the parameter λ defined below as shown by Fig. 1 [19]. This form holds for energies much greater than the injection energy and at positions several diffusion lengths from the end of the spiral arm. An isotropic distribution would be one in

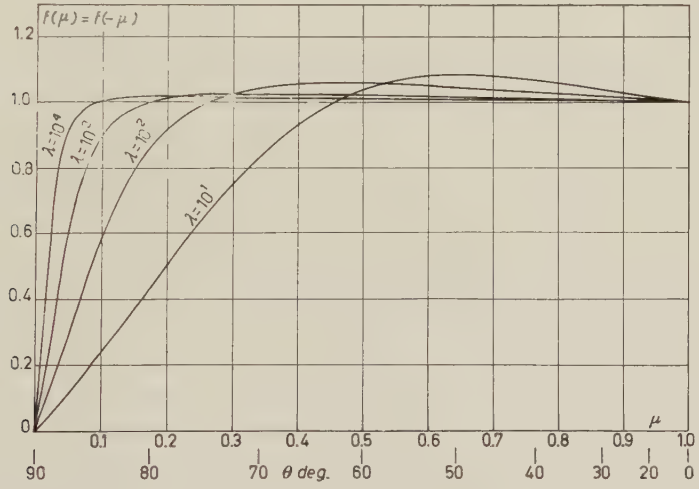

Fig. 1. – The angular distribution function $f(\mu)$ for $\alpha = 1.7$ and four values of λ.

which $f(\mu)$ was a constant. We see that the distributions tend to be nearly isotropic except near $\mu = 0$ (velocity perpendicular to the magnetic field) and that it is always predicted that there is a marked deficit of particles in very flat helices. This is the result of the efficient betatron acceleration of these particles to higher energy and steeper helices. The parameter of importance is

$$\lambda = n_2 \sigma_0^2 / 4K\,. \tag{14}$$

It measures the ratio of the scattering by very short waves to the acceleration by very long waves. To get the observed isotropy it appears that λ must

probably be about 10^4. The parameters cannot all be chosen independently; each solution provides a possible set. Dr. LAYTON has tabulated a number of these sets; one that seems as satisfactory as any is

$$\alpha = 1.7, \text{ exponent in energy spectrum,}$$

$$\lambda = 10^4, \text{ ratio of scattering to accelertaion,}$$

$$\tau_D = 4 \cdot 10^6 \text{ years, time to diffuse out of spiral arm,}$$

$$n_2 \sigma_\theta^2 = 24 \text{ milliradians}^2 \text{ yr}^{-1} = 0.08 \text{ deg}^2 \text{ yr}^{-1}, \text{ scattering parameter,}$$

$$L_a = 1.5 \cdot 10^6 \text{ light years, length of spiral arm,}$$

$$K = 6 \cdot 10^{-10} \text{ years, acceleration parameter.}$$

By Eq. (12) this value of K is consistent with wavelengths of 2 light years in each direction, a half-width factor $\delta = 0.5$, and a root-mean-squares gas velocity of 6 km/s. Thus a set of parameters can be chosen that gives the required exponent in the energy spectrum, leads to relatively little anisotropy, and does not require excessive velocities in the gas. The value of τ_D chosen is perhaps slightly less than that required to explain the most commonly reported values of the abundances of Li, Be, and B, but even so, it is long enough that α for the heavier elements will be perhaps 20% larger than for protons.

Further exploration of this model will be necessary to see whether or not this modification of the Fermi mechanism will account for the cosmic rays of energy up to 10^{18}eV and perhaps considerably higher. Probably the most important subject for further work is the nature of the hydromagnetic waves in the spiral arm of the galaxy. This mechanism requires enough very short waves to produce isotropy and enough waves whose length is of the order of a few light years to produce the acceleration; and it appears that careful theoretical work will be required to establish whether or not such waves with the required amplitudes are possible. This model would lead one to expect that the exponent in the energy spectrum would increase at and above energies where the helix radius becomes comparable with the wavelength of the accelerating waves. One would also expect first a noticeable anisotropy and then a high energy cut-off to set in as the helix radius becomes comparable with that of the spiral arm. It is to be hoped that observations will soon provide definitive information on these points although the possible large contribution at high energies of low rigidity heavy ions complicates the problem considerably.

The total power required for injection at, say, 10^5 eV is uncomfortably large and further investigation is needed to learn just what is required and to see if suitable mechanisms can be found. On the other hand, the energy

balance of the acceleration of cosmic rays from the injection energy to much higher energy is one of the most satisfactory features of the above model. The power that must be supplied to the cosmic rays, of order 10^{-26} erg cm^{-3} s^{-1}, is of the same order as that which must be supplied to maintain the irregular gas motions against viscous losses, and both are of the order of the expected power supply to irregular gas motion by the very hot O and B stars [25-27]. This power supply must be present to maintain the observed irregular gas motion against viscosity and hence must be available to supply the irregular motions with the energy needed to accelerate cosmic rays. This also enables one to explain the at-first-sight surprising result that α is about 1.5 to 2 whereas on the basis of equation (1) or (3) there seems to be no reason why the value of the various parameters such as t_1 and τ would lead to this result within one or two orders of magnitude. But a smaller value of α is clearly impossible because then the power that would have to be supplied to cosmic rays becomes much too large. With a larger value of α, corresponding to relatively little acceleration, the power supply to cosmic rays becomes very small and cosmic rays do not damp the irregular gas motions. These motions would then grow until held in check by the energy drain to cosmic rays. This condition might be expected to be reached when α has about the observed value and when the energy density in cosmic rays is comparable to the kinetic energy density of the irregular gas motions. Regardless of other considerations, the fact that the energy density in cosmic rays is comparable to the kinetic energy density of the gas seems to argue that the acceleration of cosmic rays must play an important part in the energy balance of galactic motion.

REFERENCES

[1] E. Fermi: *Phys. Rev.*, **75**, 1169 (1949).
[2] E. Fermi: *Astrophys. Journ.*, **119**, 1 (1954).
[3] S. Chandrasekhar: *Proceedings of the V International Cosmic Radiation Conference* (Guanajuato, Mexico, 1955).
[4] V. L. Ginzburg: *Dokl. Akad. Nauk SSSR*, **92**, 727 (1953).
[5] E. Teller: *Rep. on Progr. in Phys.*, **17**, 154 (1954).
[6] L. Biermann: *Ann. Rev. Nuc. Sci.*, **2**, 335 (1952).
[7] J. A. Crawford: *Thesis* (University of California, 1956); *Astron. Journ.*, **62**, 11 (1957).
[8] L. Davis: *Phys. Rev.*, **96**, 743 (1954).
[9] L. Davis: *Phys. Rev.*, **100**, 1440 (1955).
[10] P. Morrison: *Phys. Rev.*, **101**, 1397 (1956).

[11] P. Meyer, E. N. Parker and J. A. Simpson: *Phys. Rev.*, **104**, 768 (1956).
[12] E. N. Parker: *Phys. Rev.*, **103**, 1518 (1956).
[13] P. Morrison, S. Olbert and B. Rossi: *Phys. Rev.*, **94**, 440 (1954).
[14] A. Unsöld: *Phys. Rev.*, **82**, 857 (1951).
[15] L. Davis: *Phys. Rev.*, **93**, 947 (A) (1954).
[16] L. Davis: *Phys. Rev.*, **101**, 351 (1956).
[17] S. A. Kaplan: *Žu. Èksper. Teor. Fiz.*, **29**, 406 (1955); *Soviet Phys. JETP*, **2**, 203 (1956).
[18] G. Hellwig: *Zeits. f. Naturfor.*, **10***a*, 508 (1956).
[19] T. W. Layton: *Thesis* (California Institute of Technology, 1957).
[20] C. Y. Fan: *Phys. Rev.*, **101**, 314 (1956).
[21] W. B. Thompson: *Proc. Roy. Soc.*, A **233**, 402 (1955).
[22] E. N. Parker: private communication (August 1956).
[23] E. N. Parker: *Phys. Rev.*, **99**, 241 (1955).
[24] J. H. Piddington: *Mon. Not. Roy. Astron. Soc.*, **116**, 314 (1956).
[25] A. Schlüter: *Gas Dynamics of Cosmic Clouds* (Amsterdam, 1955), p. 144; *Proc. of Symposium at Cambridge* (England, July, 1953).
[26] J. H. Oort: *Bull. Astron. Soc. Netherlands*, **12**, 177 (1954).
[27] E. N. Parker: preprint of paper presented at the Symposium on the Interstellar Medium, Harvard University (June, 1957).

SUPPLEMENTO AL VOLUME VIII, SERIE X
DEL NUOVO CIMENTO

N. 2, 1958
2° Trimestre

Galactic Origin of Cosmic Radiations.

C. Y. Fan

Yerkes Observatory - Williams Bay, Wisconsin
University of Chicago - Chicago, Ill.

1. – If cosmic radiations are not the energetic particles « left over » from the creation of the universe itself, and if they are not produced by a violent process such as the explosion of super-novae, then the problem of the origin can be subdivided into three parts: *a*) the acceleration of charged particles from thermal energy to, say, 10^{10} eV; *b*) the subsequent acceleration from 10^{10} eV to an energy, say, 10^{17} eV, at which the Larmor radii of the particles in the galactic magnetic field become comparable to the size of the galaxy; *c*) and the acceleration of cosmic ray particles of higher energies.

The first acceleration can take place in the neighbourhood of stars, though the actual mechanism is still quite unknown. One of the outstanding evidences is the solar flare of February 23, 1956, when the cosmic ray intensity was increased by a factor of one hundred fifty and particles of energy up to $3 \cdot 10^{10}$ eV were detected. The acceleration of particles of energy higher than 10^{17} eV has to take place in the inter-galactic space or in some other galaxies [1], since these particles can no longer be confined in our own system. The acceleration of cosmic radiation of energies from 10^{10} to 10^{17} eV (the main component) is the subject of discussion of this paper.

2. – It seems to be clear now that the main component is not a local production of the solar system. The strongest evidence against the idea of solar origin is perhaps the effect found by Forbush [2] who observed the increase of cosmic ray intensity during the last period of minimum solar activity. It is just the opposite as expected if it were accelerated locally. An intergalactic origin implies that the cosmic radiations are the preponderant energy of the universe. The serious problem is then the lack of a mechanism which can turn a good fraction of the dynamic energy in the inter-galactic space into cosmic-ray energy. A galactic generation, which permits a greater range in assumed variables and more reasonable assumptions, is thus more hopeful.

3. – The fundamental work on the galactic origin of cosmic radiations was done by FERMI in 1949 [3]. The basis of his theory can be expressed in the following assumptions. 1) The cosmic-ray particles are accelerated in the galaxy. 2) A cosmic-ray particle, regardless of its charge, gains its energy at the rate

$$\frac{\mathrm{d}w}{\mathrm{d}t} = \frac{w}{A_0} \tag{1}$$

where w is the energy of the particle, including the rest mass, and A_0 is the time scale of the acceleration. 3) The cosmic-ray particles are eliminated at a rate governed by the statistical law,

$$p(t)\,\mathrm{d}t = \frac{\mathrm{d}t}{B_0}\ \exp\left(-\frac{t}{B_0}\right). \tag{2}$$

On these assumptions, the power law,

$$\frac{\mathrm{d}n}{\mathrm{d}w} \sim \frac{1}{w^{1+S_0}}, \tag{3}$$

where

$$S_0 = \frac{A_0}{B_0}, \tag{4}$$

readily follows.

The details of his first version were later modified by FERMI himsefl [4] and by others [5-8]. In these modified theories, much importance was attached to the similarity of the energy spectra of the heavy nuclear component and the proton component. Indeed, if the mass spectrum of the primary cosmic radiations remains unchanged up to energies of 10^{14} eV/nucleon, then the time scale of the acceleration must not be longer than the mean life of a heavy cosmic-ray nucleus as determined by nuclear collisions with interstellar particles. This is of the order of a few million years. The purpose of the modifications was to make Fermi's mechanism meet the demand of the efficiency implied by the short time scale.

4. – While the mechanism of acceleration is still a topic of discussion, the close connection of the origin of cosmic radiation and the non-thermal radio emission of the galaxy was soon realized [9, 10]. It can be shown that a mechanism which is efficient enough to accelerate cosmic ray particles within a few million years will also be efficient enough to accelerate electrons to a

sufficient energy to produce the non-thermal radio emission when they are spiraling along the galactic magnetic fields. Furthermore, as we will see, the spectra of the radio emission of radio sources can be explained within the framework of Fermi's theory of cosmic radiations [9]. This fact may be considered as lending support to the galactic origin of cosmic radiations.

5. – The general equation describing the rate of energy gain of a cosmic-ray electron differs in several respects from Eq. (1), because energy losses, which can be neglected in considering the energy spectra of cosmic-ray ions, must now be taken into account; namely, the energy loss by synchrotron radiation, the energy loss due to bremsstrahlung, and the energy loss due to inelastic collisions with interstellar particles. Let $-k^2w^2$, $-2\alpha_1 w$, and $-k_0^2$ be respectively these energy losses. Then the rate of energy gain of a cosmic electron will be in the following form:

$$\frac{\mathrm{d}w}{\mathrm{d}t} = 2\alpha_0 w - 2\alpha_1 w - k^2 w^2 - k_0^2 = 2\alpha w - k^2 w^2 - k_0^2 \tag{5}$$

where $2\alpha_0 = 1/A_0$, $\alpha = (\alpha_0 - \alpha_1)$, and k, α_1, and k_0 are regarded as constants.

Let

$$b = (\alpha^2 - k^2 k_0^2)^{\frac{1}{2}} \tag{6}$$

and

$$w_i = (\alpha - b)/k^2, \qquad \text{and} \qquad w_m = (\alpha + b)/k^2 \tag{7}$$

be the two roots of the quadratic expression in w on the right-hand side of Eq. (5). A simple integration of Eq. (5) yields

$$\frac{w - w_i}{w_m - w} = \frac{w_0 - w_i}{w_m - w_0} \exp[2bt], \tag{8}$$

w_i is thus the injection energy and w_m the high energy cut-off.

Now let us assume that the cosmic electrons are eilminated from the region where they are accelerated according to the statistical law given by Eq. (2). Then the energy spectrum of cosmic ray electrons with w_0 as a parameter is readily found to be

$$\frac{\mathrm{d}n}{\mathrm{d}w} \sim \frac{s(w_0 - w_i)^s (w_m - w_i)}{(w_m - w_0)^{s-1}} \cdot \frac{(w_m - w)^{s-1}}{(w - w_i)^{s+1}}, \tag{9}$$

where

$$s = \frac{1}{2b\bar{B}}.$$

The complete energy spectrum cannot be determined without a knowledge of the spectrum of initial energies. However, if we assume that the initial energy spectrum has a negligible amount of electrons of energy higher than $w_c(> w_i)$, then the energy spectrum for $w > w_c$ will be quite accurately given given by

$$\frac{\mathrm{d}n}{\mathrm{d}w} = J_0 \frac{(w_m - w)^{s-1}}{(w - w_i)^{s+1}}, \tag{10}$$

where J_0 is a constant.

In evaluating the values of w_i, w_m, and s, we make the following assumptions. The time scale of acceleration, $1/2\alpha_0$, equals to the life time of a heavy cosmic-ray nucleus as determined by nuclear collisions with interstellar particles (mean free path $\sim 10g$), and $1/2\alpha_0 B$ equals to 1.4, the same as in the spectrum of cosmic-ray protons. Then, in a medium of density of one proton per cm^3 and a magnetic field of 10^{-5} G, we have $2\alpha_0 = 5 \cdot 10^{-15}$/s, $2\alpha_1 = 7 \cdot 10^{-16}$/s, $k_0^2 = 4 \cdot 10^{-19}$ erg/s, and $k^2 = 2.4 \cdot 10^{-13}$ (erg s)$^{-1}$. Consequently,

$$\begin{cases} w_i = 0.94 \cdot 10^{-4} \text{ erg} = 0.06 \text{ GeV}, \\ w_m = 1.8 \cdot 10^{-2} \text{ erg} = 11 \text{ GeV}, \\ \text{and} \\ s = 1.6 . \end{cases} \tag{11}$$

With Eq. (10) as the energy spectrum of the cosmic-ray electrons and the given set of constants, the power of the radio emission in a frequency band $\Delta\nu$ at a frequency ν can be shown as

$$P(\nu) \sim \nu^{-1} \Delta\nu , \tag{12}$$

for ν in $20 \div 1000$ Mc/s. The observed spectrum of the general radio emission of the galaxy is ν^{-x} with x between 0.5 to 0.8.

6. – In discussing the acceleration of cosmic ray particles within the frame work of Fermi's theory, one is confronted with three major problems besides an efficient mechanism of acceleration, namely an injection mechanism, a process of producing isotropic distribution of the cosmic-ray particles, and a process of eliminating the particles.

Consider a cosmic-ray particle of momentum p, mass m, and charge e, spiraling around the lines of force of the galactic magnetic field H. The radius of the spiral orbit the particle describes is

$$r = pc \sin\theta / eH \tag{13}$$

and the time required for describing one complete loop is

$$T = 2\pi mc/eH \,. \tag{14}$$

If

$$|r\cdot\nabla H| \ll H \tag{15}$$

and

$$\left| T\frac{\partial H}{\partial t} \right| \ll H \,, \tag{16}$$

then the motion of the particle can be described by the approximate constancy of its angular momentum about the magnetic field H [11]:

$$M = E^2 \sin^2\theta/Hec \,. \tag{17}$$

where E stands for pc.

Eq. (17) implies that any ultimate increase of the energy of the particle will result in the decrease, of $\sin\theta$, making the flux of cosmic-ray particles anisotropic. This contradicts one of the fundamental properties of cosmic radiations. Therefore, a scattering mechanism which can change the angle of pitch to an isotropic distribution is a necessary requirement for any theory of galactic origin of cosmic radiations [7].

An injection mechanism is required for feeding into interstellar space a sufficient number of electrons and ions of energy high enough for subsequent acceleration. A process which is equally effective in eliminating ions as well as electrons insures a similar power-low spectra.

Recent advances made in solar physics and solar component of cosmic radiations seem to indicate two things: 1) a normal star such as the sun can eject particles of energies up to a few billion electron volts, and 2), the disturbance in the planetary medium produced by the solar corpuscular radiation can efficiently scatter cosmic-ray particles. These facts lead one to suggest that cosmic-ray particles are originally ejected from stars or particular types of stars, and the isotropy is a result of the scattering by the disturbance in the interstellar magnetic field primarily produced by stellar corpuscular radiations.

To the process of eliminating cosmic-ray particles, Morrison *et al.* [5] and Fermi [4] independently suggested that cosmic-ray particles are diffusing out of the galaxy and thus B would be the same for all components of cosmic radiations. This assumption can be slightly generalized by saying that the cosmic-ray particles are eliminated by leakage from the region or regions where acceleration is operating. The advantate of the modified assumption is that

there may be in the galaxy only a few regions where the physical condition is suitable for the acceleration of cosmic radiations.

7. – In Fermi's original theory or its modified versions, it is always assumed that cosmic-ray particles gain their energy through the interactions with interstellar magnetic clouds. In a non-uniform magnetic field, a cosmic ray particle, when spiraling around the lines of force, can have the longitudinal component of its momentum vector reversed when it encounters a magnetic cloud. Fermi showed that the energy change in each reversal is

$$(\Delta w)_F = (2B\cos\theta_0 + 2B^2)w/(1 - B^2)\,, \tag{18}$$

where θ_0 is the angle of pitch of the particle before collision, and B, the velocity of the cloud in units of the velocity of light. After Eq. (18) is averaged over both of the positive and negative values of B, one has thus only the second order term in B left. If τ is the frequency of collisions per unit time, the average rate of energy gain is then of the order of $4B^2\tau w$. It was then found that the rate can hardly meet the required efficiency when a plausible set of values of B and τ are inserted in the expression [12]. Therefore a mechanism of acceleration of higher efficiency is in demand.

It was first suggested by DAVIS that cosmic radiations can also be accelerated in the galaxy by the inductive action of varying magnetic field [13]. We shall show that, under a suitable condition, the interplay of Fermi's mechanism of acceleration and the inductive action can accelerate cosmic-ray particles at an efficiency to the first order of B [14]. It is thus suggested that cosmic radiations are primarily accelerated by such a mechanism in some favorable regions in our galaxy. The distribution of the regions are indicated by the non-thermal radio emission.

8. - Let us assume that there is a region in the interstellar space occupied by matter at extremely low density and constantly stirred by moving clouds of higher densities. The size of the clouds is of the order of $10 \div 100$ psc. The magnetic field in the medium is expected to be higher in the clouds than that in the low density regions. Let us further assume that when two clouds move towards each other, the magnetic field in the clouds is amplified at the rate of

$$\frac{\partial H}{\partial t} = qHcB/L\,, \tag{19}$$

where q is a constant and L is the linear separation between the two clouds. Eq. (19) also implies that when the two clouds are moving away from each other, $(B < 0)$, the magnetic field will decrease accordingly.

Under the foregoing assumptions, a cosmic-ray particle, spiraling around the general magnetic field H_0, will be trapped between the clouds if the angle of pitch θ_0 is greater than $\chi = \sin^{-1}(H_0/H_m)^{\frac{1}{2}}$ where H_m is the maximum intensity of the magnetic field in the clouds. The particle will be accelerated or deaccelerated by both Fermi's mechanism and the inductive action according to $B > 0$ or < 0.

For a positive value of B, the energy gain by Fermi's mechanism, is

$$(\Delta w)_F = 2B \cos\theta_0 w \,, \tag{20}$$

to the first order of B. In this mechanism, the time variation of the magnetic field is neglected. Thus, the quantity $E^2 \sin^2\theta_0$ is constant according to Eq. (17), and so an energy gain results in a decrease of θ_0:

$$-(\Delta\theta_0)_F = w(\Delta w)_F \operatorname{tg}\theta_0/E^2 \,. \tag{21}$$

On the other hand, in a varying magnetic field given by Eq. (19), the particle will also gain energy by induction of the following amount:

$$(\Delta E)_I = \frac{E}{2}\int_0^{T_0} \frac{1}{H}\frac{\partial H}{\partial t}\sin^2\theta \,\mathrm{d}t \,, \tag{22}$$

in one whole course of encounter with one of the clouds. In contrast to Fermis' mechanism of acceleration, the energy gain by induction results in an increase of θ_0:

$$(\Delta\theta_0)_I = (\Delta E)_I \cot\theta_0/E \,. \tag{23}$$

Thus the net variation of the angle of pitch θ_0 in one whole course of encounter can be positive or negative depending upon whether $|(\Delta\theta_0)_I|$ is greater or smaller than $|(\Delta\theta_0)_F|$.

After $(1/H)\partial H/\partial t$ being replaced by qcB/L, and $\mathrm{d}t$, by $\mathrm{d}x/c\cos\theta$, the net variation of the angle of pitch θ_0, $\Delta\theta_0 = (\Delta\theta_0)_I + (\Delta\theta_0)_F$, becomes:

$$\Delta\theta_0 = 2B\left(\frac{w}{E}\right)^2 \sin\theta_0 \left[\frac{q}{L4}\left(\frac{E}{w}\right)^2 \int \frac{\cos\theta_0}{\sin^2\theta_0}\cdot\frac{\sin^2\theta}{\cos\theta}\,\mathrm{d}x - 1\right], \tag{24}$$

where the integration is effected over the total distance traverse by the particle in the whole course of encounter.

The function $G(\theta_0)$, where

$$G(\theta_0) = \frac{q}{4L}\left(\frac{E}{w}\right)^2 \int \frac{\cos\theta_0}{\sin^2\theta_0} \cdot \frac{\sin^2\theta}{\cos\theta}\,\mathrm{d}x\,, \tag{25}$$

has the following properties:

$$\begin{cases} G\left(\dfrac{\pi}{2}\right) = 0\,, \\ \dfrac{\partial G}{\mathrm{d}(-\theta_0)} > 0\,, \\ G(\chi) > qE^2/4w^2\,, \end{cases} \tag{26}$$

since we have assumed that $\partial H/\partial x > 0$ when x is measured along H from a point, say, the middle point between the two clouds and that $\int \mathrm{d}x = L$ when $\theta_0 = \chi = \sin^{-1}(H_0/H_m)^{\frac{1}{2}}$. Therefore, if $q > 4$, there alway exists an angle θ_c in $(\chi, \pi/2)$ so that

$$G(\theta_0) >, =, \quad \text{or} \quad < 1 \text{ according to } \theta_0 \text{ is } <,\ =, \text{ or } > \theta_c \tag{27}$$

respectively.

For smaller values of q, the existence of the angle θ_c will depend more on the characteristics of $\partial H/\partial x$.

The physical significance of the existence of θ_c can be easily seen from Eqs. (24) and (27). When a cosmic-ray particle is trapped in a closing « jaw », $(B > 0)$, an energy gain results in a decrease or an increase of θ_0 according to whether θ_0 is in $(\theta_c, \pi/2)$ or (χ, θ_c). Therefore, all the particles with their pitch angles greater than χ will stay in the trap for the acceleration. On the other hand, when a cosmic-ray particles is trapped in a receding « jaw », $(B < 0)$, an energy loss results in an increase or a decrease of θ_0 according to whether θ_0 is in $(\theta_c, \pi/2)$ or (χ, θ_c). Therefore, all the particles with their pitch angles less than θ_c will be able to escape from the trap of de-acceleration. The stable range in θ_0 in a closing trap is thus over that in a receding trap by (χ, θ_c). The following is the consequence.

At the equilibrium angle θ_c, a relativistic particle gains energy of the amount

$$\frac{\mathrm{d}w}{\mathrm{d}N} = 2Bw \sec\theta_c\,, \tag{28}$$

per encounter. Let aL be the initial distance between the two clouds when the particles are trapped. It can be shown that the energy of the particle when the distance is $a'L$ will be approximately a/a' times of its initial energy. Accordingly, a particle gains energy at a higher rate than it loses energy. The rate of the energy gain will reach its peak when two clouds begin to collide.

Two colliding clouds can never pass each other because the collisional cross-section of an atom at thermal energy is $10^{-16}\,\mathrm{cm}^2$ at the least. Thus sharp spatial variations in magnetic fields are likely to be produced by the collision, so that the cosmic-ray particle will leave the trap to start another cycle of acceleration or de-acceleration with its angle of pitch at a random orientation. But since a closing trap is more stable than a receding one, an ultimate acceleration is more likely expected.

REFERENCES

[1] For discussions of some related subjects, see G. Cocconi: *Nuovo Cimento*, **3** 1433 (1956).
[2] S. E. Forbush: *Journ. Geophys. Research*, **59**, 525 (1954).
[3] E. Fermi: *Phys. Rev.*, **75**, 1169 (1949).
[4] E. Fermi: *Astrophys. Journ.*, **119**, 1 (1954).
[5] P. Morrison, S. Olbert and B. Rossi: *Phys. Rev.*, **94**, 440 (1954).
[6] C. Y. Fan: *Phys. Rev.*, **101**, 314 (1956).
[7] L. Davis: *Phys. Rev.*, **101**, 351 (1956).
[8] L. Davis: in this issue, p. 444.
[9] C. Y. Fan: *Astrophys. Journ.*, **123**, 491 (1956).
[10] V. L. Ginzburg: *Suppl. Nuovo Cimento*, **3**, 38 (1956).
[11] H. Alfvén: *Cosmical Electrodynamics* (Oxford, 1950), p. 19-23.
[12] A. Unsöld: *Phys. Rev.*, **82**, 857 (1951).
[13] L. Davis: *Phys. Rev.*, **96**, 743 (1954).
[14] The discussion is a modified version of the mechanism presented in ref. [6].

SUPPLEMENTO AL VOLUME VIII, SERIE X
DEI NUOVO CIMENTO

N. 2, 1958
2° Trimestre

Cosmic Rays in Intergalactic Space.

F. J. M. FARLEY

Centre Européen de Recherches Nucléaires - Geneva

Observations of large extensive air showers, according to present interpretation, indicate the existence of primary cosmic rays of energy approaching 10^{19} eV [1, 2]. It is difficult to see how particles of this energy can be confined to the Galaxy long enough to be accelerated. Accordingly it is of interest to examine the alternative hypothesis that cosmic rays escape rather easily from the Galaxy, and diffuse from galaxy to galaxy throughout the universe. The cosmic rays which have escaped from our galaxy will then contribute to the particle flux in distant regions, and conversely the loss of particles from our own galaxy may be partially or completely balanced by an incoming flux of particles which have escaped from other galaxies. A calculation presented below shows that the returning flux is considerable. The existence of cosmic rays in other galaxies with fluxes comparable to our own is inferred from observations of galactic radio emission [3-6].

On this picture a particle can travel from galaxy to galaxy undergoing some acceleration in each, and eventually reach a very high energy which is not limited by considerations of storage time in a particular galaxy.

While an acceleration process in intergalactic space is not excluded, we assume here that the particles are accelerated only while they are in galaxies, as proposed, for example, in the model of Morrison, Olbert and Rossi [7]. On this picture there is a constant probability for a particle to escape from the galaxy, independent of particle energy, implying that the energy spectrum of the escaping particles is the same as the energy spectrum of particles within the galaxy.

1. – Ratio of incoming to emitted flux.

We now calculate the ratio between the flux of particles escaping from our galaxy and the flux of incoming particles which reach us from other galaxies. We assume for simplicity that all galaxies are identical, and all contain

and emit cosmic rays with the same intensity and the same integral power law spectrum, $E^{-\gamma}$. To find the incoming flux one then integrates over the whole of space, making proper allowance for the Doppler shift of the spectrum from distant galaxies due to the expansion of the universe. In order to do this one must adopt some theory of cosmology, but the results do not depend sensitively on our choice. The calculations have been made using the steady state theory [8], which implies an exponentially expanding space, $r = r_0 \exp[t/\tau]$, with $\tau = 5.4 \cdot 10^9$ years to fit the astronomical data [9].

The effect of the Doppler shift is to reduce the intensity of the particle flux from a receding galaxy, but the spectrum is still a power law with the same value of the exponent γ. The integration over all space then gives (incoming flux)/(emitted flux) $= nAc\tau/(\gamma + 4) = 0.7$, where $n =$ number of galaxies per unit volume $= 10^{-19}$ (l.y.)$^{-3}$, $A =$ projected area of a galaxy $= \pi r^2 = \pi(5 \cdot 10^4)^2$ (l.y.)^2, and $c =$ velocity of light. The galaxies are assumed spherical with radius $5 \cdot 10^4$ l.y.

The result shows that there are enough galaxies per unit volume to provide a returning flux comparable to the escaping flux. As far as cosmic rays are concerned therefore, the universe looks like an almost totally reflecting enclosure. In view of the uncertainties in the astronomical data, particularly as to conditions at great distances which strongly influence the calculation, it is possible that the enclosure is more perfect than indicated by our result, and possibly the returning flux exactly balances the escaping flux. We now examine the consequences of such a hypothesis.

2. – The power-law spectrum.

In cosmic ray acceleration theories derived from that of Fermi [10], there is an exponential gain of energy with time, time-constant t_1, and this is balanced by an exponential loss of particles with time, time-constant t_2, to give the power law spectrum with $\gamma = t_1/t_2$. The loss mechanism postulated by Morrison, Olbert and Rossi is escape from the galaxy by a diffusion process. We postulate here that this loss is completely balanced, but now the exponential expansion of the universe itself provides a loss mechanism of exactly the right mathematical form with characteristic loss time $t_2 = \tau/3$.

The acceleration required to balance this loss must have $t_1 = \gamma\tau/3$ to give the correct spectrum. But by itself the expansion would naturally produce a deceleration with characteristic time τ. Allowing for this the acceleration mechanism itself must be more rapid and we require $t_1 = \gamma\tau/(3 + \gamma) = 2 \cdot 10^9$ years.

This is the acceleration time averaged over the history of a typical particle. If the acceleration process is confined to galaxies it must be more rapid by

the ratio of the time spent in galaxies to the total time. To estimate this we assume that the particles travel at random after leaving a galaxy, and that there is no special mechanism tending to trap them in a galaxy. The ratio required is then (volume of galaxies)/(volume of space) $= 5 \cdot 10^{-5}$. Therefore the characteristic time of the acceleration process in the galaxies $= 5 \cdot 10^{-5} \times$ $\times 2 \cdot 10^{9} = 100\,000$ years.

This figure represents a more rapid acceleration than at present envisaged in Fermi acceleration mechanisms, but it can hardly be excluded as impossible, particularly in the turbulent regions of the galactic corona. The figure is, of course, that for the acceleration time in an average galaxy, and it is possible that our galaxy is below average as far as gas turbulence is concerned.

Anything that increases the ratio of time spent in galaxies to total time will imply a slower acceleration mechanism. This ratio will not be affected significant by a short mean free path for scattering in the galaxy [11], or by a magnetic trapping mechanism, (which would be as effective in keeping some particles out as in trapping the favoured few), but it will be increased if particles are guided from galaxy to galaxy along lines of magnetic field or by bridges of intergalactic gas. This would be equivalent to an increase in the number of galaxies per unit volume of the universe accessible to cosmic rays, and would therefore also increase the ratio of incoming to emitted flux and improve the totally reflecting box effect suggested above.

But for a guidance mechanism from galaxy to galaxy to be effective, the leakage time for escape to « non-accessible » regions of the universe between galaxies would have to be long compard with $2 \cdot 10^{9}$ years. This would appear improbable, and it seems therefore that the simple volume ratio used above will give a correct estimate of the fraction of time spent in galaxies.

3. – Further remarks.

To obtain a roughly constant value of the exponent γ in the power law spectrum it is attractive to suppose that the expansion of the universe controls the loss of particles throughout the whole energy range. This would imply a characteristic time less than 100 000 years for diffusion of particles out of the galaxy. It will remain true, as in the theory of Morrison, Olbert and Rossi, that the lower energy cosmic rays come on the average from neighbouring regions of the galaxy, while higher energy particles come from farther and farther away, the origin of the highest energy rays being on the whole extra-galactic.

A consequence of our concepts is that the cosmic rays behave as though the Galaxy was embedded in an infinite sea of galactic plasma. The result is that the boundaries of the galaxies lose their significance, and the cosmic

rays diffuse in effect throughout the whole plasma. In this picture, in which the galaxies are imagined as touching, we must introduce a fictitious loss which is equivalent to the loss due to expansion in the real extended universe.

This model therefore implies isotropy of the cosmic ray flux at all energies, apart from local effects near the earth or solar system.

4. – Energy densities in the universe.

In conclusion it is appropriate to re-examine the argument that the cosmic rays must be confined to the Galaxy because of considerations as to the total energy respectively in the form of matter, light and cosmic rays [12, 13]. The average energy density of matter in the universe is about 10^{-6} erg cm^{-3}, (10^{-27} g cm^{-3}), while those of light and cosmic rays (if the flux near the earth extends throughout space), are both about 10^{-12} erg cm^{-3}. It has recently become clear [14], that the light flux in intergalactic space is not very different from the flux inside the Galaxy. Although the intensity from nearby galaxies is reduced by an inverse square law effect, there is a large contribution from the many distant galaxies exactly as in the case of cosmic rays presented above. The ratio of cosmic ray to electromagnetic energy suggested here for the universe as a whole is therefore the same as the ratio inside the Galaxy; an approximate equality which has often been regarded as acceptable.

5. – Conclusion.

Although the present discussion has been based on the model of Morrison Olbert and Rossi, the results are of more general application, and will apply whenever escape of cosmic rays from the Galaxy is envisaged. We have shown that, with present figures for the size and numbers of galaxies, the escape need not be a serious difficulty in any theory of acceleration, and it need not impose a high energy cut-off. Our relation between the strength or energy output of the accelerating mechanism and the expansion of the universe will be relevant whenever an extra-galactic origin is postulated for a part or the whole of the cosmic ray flux. If the source strength is sufficient to accelerate particles in galaxies with an equivalent characteristic time of order 100 000 years, then it is reasonable to postulate cosmic rays throughout all space. If, on the other hand, the acceleration mechanism is insufficient for this, then we must suppose that the particles are confined to the galaxy.

* * *

Note added in proof. - Similar calculations using a different cosmology have recently come to out attention [15].

Appendix (*)

In the presentation given above the ratio of incoming to emitted flux and the loss due to the expansion of the universe are calculated as separate problems, but clearly they are related. A unified treatment is given below.

Let the flux in the surface layers of galaxies of particles with energy greater than (one mean free path from the edge) E be $f_g = j_g E^{-\gamma}$, and let the corresponding flux in space outside galaxies be $f_s = j_s E^{-\gamma}$ with the same value of the exponent γ. If the acceleration time and loss time for the galaxies are t_1 and t_2, the equilibrium condition for the particles in galaxies is

$$-\frac{\mathrm{d}f_g}{\mathrm{d}E}\cdot\frac{E}{t_1}=\frac{f_g}{t_2},$$

where the left-hand side represents the rate of increase in the number of particles of energy greater than E due to acceleration of slower particles, and the second term represents the rate of loss. This leads to the usual power law spectrum with $\gamma = t_1/t_2$.

Applying the same concepts to intergalactic space we have: number of particles injected by galaxies per unit volume per unit time $= nA'(f_g - f_s)$, where A' is the surface area of a galaxy and n the number per unit volume; loss due to expansion of universe $= 3f_s/c\tau$, and loss due to deceleration time constant τ, $= -(\mathrm{d}f_s/\mathrm{d}E)\cdot(E/c\tau)$.

(The velocity of light, c, enters as the conversion factor from flux to particle density.) The equilibrium condition is therefore

$$nA'(f_g - f_s)=\frac{3f_s}{c\tau}-\frac{\mathrm{d}f_s}{\mathrm{d}E}\cdot\frac{E}{c\tau},$$

and remembering that

$$\frac{\mathrm{d}f_s}{\mathrm{d}E}=-\gamma\cdot\frac{f_s}{E}$$

we obtain

$$\frac{f_s}{f_g - f_s}=\frac{nA'c\tau}{\gamma+3}.$$

This expression is very similar to that obtained previously for the ratio of incoming to emitted flux, but now involves the total surface area $4\pi r^2$ of a galaxy instead of the projected area πr^2.

Using the figures given earlier we now find

$$\frac{f_g}{f_s - f_g}=1+\frac{nA'c\tau}{\gamma+3}=4.4$$

(*) Further developments not presented at the Conference.

and

$$\frac{f_s}{f_g} = 0.77$$

These figures imply that the particle distribution in the galaxies is considerably modified as a result of the incoming flux.

To estimate this effect we first relate t_2, the loss time for diffusion of particles out of a galaxy, to ε the ratio of the flux in the surface layers of the galaxy to the mean flux throughout the galaxy. (According to MORRISON, OLBERT and ROSSI there is an approximately sinusoidal distribution of particles in the galaxy so that ε is small if the scattering mean free path λ is small). Suppose that particles are lost only from a layer of thickness λ on the surface of a spherical galaxy of radius r. The mean loss time for these particles is $3\lambda/c$, and they represent a fraction $\varepsilon \times 4\pi r^2\lambda \div 4\pi r^3/3$ of the total particles in the galaxy. Hence the loss time averaged over all the particles in the galaxy is $t_2 = r/\varepsilon c$. To justify this rigorously one may solve the diffusion equation for a spherical galaxy and obtain $\varepsilon = \pi^2\lambda/3r$ and $t_2 = 3r^2/\pi^2\lambda c$ whence the result follows.

In the presence of an external flux f_s the loss of particles from the surface of a galaxy is reduced in the ratio $(f_g - f_s)/f_g$. Therefore the required acceleration time

$$t_1 = \gamma t_2 = \frac{\gamma r}{\varepsilon c} \cdot \frac{f_g}{f_g - f_s} = \frac{400\,000}{\varepsilon} \text{ years.}$$

This relates the acceleration time required to give the correct power law spectrum to the flux in intergalactic space, because $f_s = 0.77 \times f_g = 0.77 \times \varepsilon \times$ mean flux in galaxy: acceleration time, t_1 =(mean flux in galaxy)/(flux in intergalactic space) $\times$ 300 000 years.

It now appears that a rather slower acceleration mechanism than envisaged in the body of the paper is compatible with a considerable intergalactic flux.

REFERENCES

[1] G. CLARK, J. EARL, W. KRAUSHAAR, J. LINSLEY, B. ROSSI and F. SCHERB: in this issue, p. 623.

[2] T. E. CRANSHAW, W. GALBRAITH, N. A. PORTER, J. DE BEER and M. HILLAS: in this issue, p. 567.

[3] F. HOYLE: *Nature*, **173**, 483 (1954).

[4] R. Q. TWISS: *Phil. Mag.*, **45**, 249 (1954).

[5] B. Y. MILLS: *Aust. Journ. Phys.*, **8**, 368 (1955).

[6] G. R. BURBIDGE: *Phys. Rev.*, **103**, 264 (1956).

[7] P. MORRISON, S. OLBERT and B. ROSSI: *Phys. Rev.*, **94**, 440 (1954).

[8] H. BONDI and T. GOLD: *Month. Not. Roy. Astr. Soc.*, **108**, 252 (1948).

[9] M. L. HUMASON, N. U. MAYALL and A. R. SANDAGE: *Astron. Journ.* ,**61**, 97 (1956).

[10] E. FERMI: *Phys. Rev.*, **75**, 1169 (1949).

[11] F. J. M. FARLEY: *Oxford Conference on Extensive Air Showers* (1956).

[12] R. D. RICHTMEYER and E. TELLER: *Phys. Rev.*, **75**, 1729 (1949).

[13] P. MORRISON: *Rev. Mod. Phys.*, **29**, 235 (1957).

[14] H. BONDI: *Cosmology* (Cambridge, 1952).

[15] K. SITTE: *Bull. Res. Council Israel* **6A**, 61 (1956).

SUPPLEMENTO AL VOLUME VIII, SERIE X
DEL NUOVO CIMENTO

N. 2, 1958
2° Trimestre

The Exterior Ballistics of the Cosmic Radiation.

G. Cocconi

Laboratory of Nuclear Studies, Cornell University - Ithaca, N. Y.

The problem of the origin of cosmic rays has been deeply affected in the last years by two facts.

The first is the necessity of admitting that at least the most energetic part of the cosmic rays observed on the Earth arrives from outside the Galaxy [1].

The second is the proof that both in the Galaxy and outside there exist peculiar regions where particles are accelerated to relativistic energies with efficiencies as high as nobody suspected before [2]. I am referring to the sources of radio waves like, in our Galaxy, the Crab Nebula, which is the remnant of the Supernova of A.D. 1053 and, outside the Galaxy, the Jet Nebula M87. Both these regions emit polarized light, which indicates the presence of relativistic particles moving inside strong magnetic fields. The particles that generate polarized light are most likely electrons with energies of the order of 10^{11} eV. This is because electrons radiate $\sim 10^{13}$ times more than protons of the same total energy. However there is no reason why, if electrons are so efficiently accelerated, ions could not also be. So, these peculiar radio wave sources are quite certainly sources of cosmic rays also.

Estimates of the energy output of these sources show that, e.g., the Supernovae and the Novae in our Galaxy flare with sufficient frequency to supply all the energy we observe in cosmic rays, if the cosmic rays density is everywhere equal to that observed in the neighborhood of the Earth.

The same is probably true for the supply of cosmic rays in the intergalactic spaces from extraordinary objects like the Jet Nebula and the Colliding Galaxies.

These observations compel us, I think, to change the principal hypothesis on which most of the models of the origin of cosmic rays were based, after

the famous paper by FERMI. I am referring to the hypothesis that cosmic rays are accelerated in interstellar spaces as a result of collisions with magnetic clouds. I do not mean here that the Fermi or a Fermi-like accelerating mechanism does not operate in the galactic spaces; quite certainly it does. I mean instead that it has becomes apparent that the Fermi mechanism is of secondary importance, since the energy it transfers to cosmic rays is negligible as compared to the energy that cosmic rays have already acquired in the peculiar regions of the Universe where they originated.

I am convinced of this conclusion not only because of the existence of the strange objects mentioned, but also because the astronomical evidence is against the large velocities in the turbulent ionized gas required to make the Fermi mechanism important.

This conclusion, in a sense, brings us back many years: the Fermi mechanism had the beauty of governing at the same time the acceleration and the movement of the particles, i.e., of treating simultaneously both the interior and the exterior ballistics of the cosmic radiation. Now, instead, we must admit that magnetic fields wandering in the Galaxy and between Galaxies influence only the exterior ballistics of cosmic rays.

The interior ballistics, the process by which charged particles are accelerated to the highest energies in peculiar regions of the Universe, is going to constitute a separate problem, a problem that does not interest only cosmic ray people and astronomers, since from its solution practical applications of fundamental importance will presumably follow.

In the present discussion I will consider only one part of the story, namely the exterior ballistics.

The distribution of cosmic rays in space is essentially dictated by two parameters: the distribution of the sources and the transport mean free path, λ, of the cosmic rays in the medium.

The classification of the sources according to the maximum energy that they can generate probably does not allow discrete groupings, however here, for simplicity sake, we shall schematically subdivide them in three classes.

To *Class I* belong the most powerful sources, those capable of producing cosmic rays up to energies $U_{\max} > (10^{17} \div 10^{18})$ eV. No Galactic object belongs to this class, but only extragalactic sources, such as the colliding Galaxies or the Jet Nebula. Such sources are not frequent, only a few being presently very active within some 10^8 light years from us.

To *Class II* belong the sources with $U_{\max} \approx 10^{15}$ eV. Supernovae and perhaps Novae give rise to sources of this kind. They are distributed, in our Galaxy, mostly in the galactic disk. Few of them are active now in the Galaxy, none very near the solar system.

To *Class III* belong the sources with $U_{max} \approx 10^{12}$ eV. All stars are presumably capable of producing at least occasionally these particles, as witnessed by the Sun: however some types, e.g., the Red Giants and the T-Tauri, could be more efficient than others.

As far as the transport mean free path, λ, is concerned, we can say in general that it is a function of U, the energy of the particle, its value becoming larger, in the same medium, as U increases. The actual value of λ depends on the shape and intensity of the magnetic fields present in the medium, properties that are very far from being well known even for the space around the solar system.

A lower limit for λ is given by the radius of curvature of the (singly charged) particles in the average field:

$$\lambda \geqslant R = \frac{U}{300\, H} \text{ cm} .$$

(U in eV and H in gauss), provided R is smaller than the region where the field is present.

Let us now consider first the cosmic rays emitted by Class I sources, the distant colliding galaxies. These produce cosmic rays of all energies up to the largest, but to us there arrive only those that can diffuse here before the expansion of the Universe brings us too far from the source. We describe here the Universe as in a steady state condition and of course assume that magnetic fields are present in the intergalactic spaces. In this Universe, the particles presently emitted, e.g., by two colliding galaxies, will reach us only some billion of years from now, when the two galaxies will not constitute any more a peculiar object. However, at a comparable distance, other colliding galaxies existed billions of years ago, which supplied us with the cosmic rays we observe now. The maximum distance r_{max} from which the bulk of particles having a m.f.p. λ can reach us is then that for which the diffusion velocity equals the recession velocity.

The first is ($\langle r^2 \rangle = \lambda v t$)

$$\frac{dr}{dt} = \frac{\lambda v}{2r} \qquad (v = c = 3 \cdot 10^{10} \text{ cm s}^{-1}).$$

The second is

$$\frac{dr}{dt} = \frac{r}{T} \qquad T \approx 10^{10} \text{ years}.$$

It follows that

$$r_{max} \approx (\lambda v T)^{\frac{1}{2}} = \lambda^{\frac{1}{2}} \cdot 10^{14} \text{ cm} .$$

For instance, only particles with $\lambda \sim 10^{25}$ cm $= 10^7$ l.y. can reach us from the region where are now situated the two colliding galaxies of Cygnus A, $1 \cdot 10^8$ l.y. away, and these particles are presumably only the most energetic, since λ decreases as U decreases. The less energetic particles can come only from sources at smaller distances from us, and these are very few (*).

The galaxy is practically transparent to particles of more than 10^{17} eV, hence the density of these particles inside and outside the galaxy must be about the same.

We can thus summarize the situation by saying that the contribution of Class I sources is mainly felt at the extreme energies, while at the lower energies the contribution of the more abundant local sources is predominant.

Let's come now to Class I sources, Supernovae and Novae. The disk-like distribution of most of the gas in the Galaxy makes it unlikely that the particles emitted by these sources, that are more abundant in the vicinity of the galactic plane, reach us by diffusing along the disk. Most of these particles will diffuse from the disk into the galactic halo (and eventually into the intergalactic spaces) where they will be present with a density in first approximation inversely proportional, *coeteris paribus*, to their transport m.f.p. So the particles from this class observed on the Earth come preponderatly from diffusion from the halo back into the spiral arm, where we are located.

The situation is different, finally, for the particles of Class III, which being produced all around us, reach us mostly from our neighborhood.

The spatial distribution of Class I and II particles as seen from the Earth is essentially isotropic, since the diffusing media are all quite uniformly distributed around us. If any anisotropy can be foreseen, it is more likely to be expected in Class II particles ($\leqslant 10^{15}$ eV) that can feel the asymmetry of the galaxy, than in Class I ($> 10^{17}$ eV) particles that are produced by several sources probably uniformly distributed in the Universe.

Class III particles, of course, show the anisotropies of the local fields and of the nearest sources, the Earth's magnetic field and the Sun.

As far as the external ballistic is concerned, the total thickness of matter crossed by cosmic rays before reaching the Earth is always small, of the order

(*) Also the storage factor of the sources is presumably larger for the less energetic particles and reduces their probability of escape.

of few g cm^{-2}. In fact the low energy particles stay in our neighborhood for times of the order of

$$T = \frac{r^2}{\lambda v}$$

where $r \approx 10^{21}$ cm = thickness of the spiral arm, and $\lambda \approx 10^{18}$ cm $= 1$ l.y., as suggested by the dimensions of the local turbulences. Assuming a mean density in the arm of 10^{-24} g cm^{-3} this gives an average thickness of matter traversed of ≈ 1 g cm^{-2}.

The diffusion in the halo, where the density of matter is some orders of magnitude smaller, gives a similar result. Similarly the extragalactic particles are not expected to cross much more matter, even if they stay around billions of years.

The model thus satisfies the two conditions that we believe to be fundamental for any description of the origin of cosmic rays: the possibility up to the highest energies of a mass spectrum relatively rich in heavy ions, and the quasi-isotropy.

What remains out of the picture is that most remarkable fact that the integral energy spectrum seems to obey the same law, the U^{-2} law, from 10^{10} to $(10^{19} \div 10^{20})$ eV. Though it is appealing to think that such a law is a consequence of some fundamental property of the spaces or of the sources, as it was suggested by the Fermi model, here we are led to conclude that it may rather be the product of accident.

The word accident does not convey the real meaning of the situation. The uniformity of the integral energy spectrum reflects the uniformity of the universe, i.e., the uniform distribution of the sources. Besides, it must be remembered that the differential energy spectrum could have several bumps, but that the present methods of observation are not able to detect them. What we observe is the superposition of several energy spectra from many sources, all perhaps following power laws within limited ranges; in our location they sum up in such a manner as to give a power spectrum with nearly constant exponent over ten orders of magnitude. But one cannot help thinking that if we were living in the neighborhood of the Crab Nebula, the cosmic rays would be much richer in low energy particles (as, after all, occasionally happens here too, when the Sun is particularly active) giving a steeper energy spectrum, or that in a star near the rim of the galaxy the less energetic particles would be much less abundant than here.

Finally, a few words for the future. The neat separation between exterior and interior ballistics of cosmic rays somewhat decreases the importance of the problems connected with the first and increases those connected with the second.

Cosmic rays are particles carrying small information, being subject as they

are to the influence of all the wandering magnetic fields that they meet on their way: cosmic rays particles hardly give us any clue on where and when they are produced. They represent, so to speak, the product of an average over large parts of the universe and tell us only that somewhere and somehow they are accelerated to their fantastic energies.

For the study of the interior ballistic I feel that, at least for the time being, more information can be obtained from the analysis of the phenomena occurring on the Sun, where particles up to 10^{12} eV are occasionally created in well defined points and at well defined times, than from the analysis of the incoherent particles that form the bulk of the cosmic radiation.

REFERENCES

[1] G. Cocconi: *Nuovo Cimento*, **3**, 1433 (1956).
[2] V. L. Ginzburg: *Suppl. Nuovo Cimento*, **3**, 38 (1956); P. Morrison: *Rev. Mod. Phys.*, **29**, 235 (1957).

SUPPLEMENTO AL VOLUME VIII, SERIE X
DEL NUOVO CIMENTO

N. 2, 1958
2° Trimestre

Extragalactic Cosmic Radiation.

K. SITTE

Department of Physics, Technion, Israel Institute of Technology - Haifa.

It is one of the advantages of meetings like the present that they offer the opportunity to hold up even one's speculations and suppositions against the criticism of one's colleagues. For this reason and to this purpose only, some ideas on extragalactic cosmic radiation will be presented here, in spite of the fact that many details have not yet been formulated in a quantitatively satisfactory way.

Basically, there are two lines of thought which lead to an investigation of the problems of extragalactic cosmic radiation. On the one hand, the cosmological effects of the diffusion into intergalactic space of a radiation produced or stored in the galaxies should be studied; on the other, the possibilities and consequences of extragalactic production could be re-examined. We shall deal here very briefly with both aspects of the problem.

1) As to the first, it is by now probably generally accepted that there is a considerable leakage of cosmic radiation through the boundaries of the galaxy [1, 2]; only its extent may be somewhat in doubt, depending as it does on the model of the galactic fields, or one may say on the reflectivity of the boundary layer. In the extreme case of a pure random walk theory of production [3], the accumulated extragalactic density of cosmic radiation may well have risen to a sizeable fraction of its value inside the galaxies (which, for simplicity and for lack of better knowledge, we shall assume to be all equally efficacious in the production and storage of cosmic rays); but it is probably more realistic to assume a value smaller by a few orders of magnitude. However, even this constitutes a stream directed from the regions of higher curvature, the galaxies, into that of lower curvature, and it fills the latter space with energetic radiation: effects which tend to counter-act expansion. It is, therefore, tempting to see to what extent cosmic radiation may be acting as a regulating factor in the expansion of the universe.

As a first thought, one might compare the flux entering the intergalactic space from all galaxies, distributed over the entire volume of that space, with the rate of continuous production of matter in a steady-state universe [4, 5]. If, for instance, the assumption is made that a fraction of the order of 10^{-3} of the galactic flux is allowed to pass through the boundaries, the rate of increase of energy density in intergalactic space would be of the order of 10^{-33} erg/cm^3 s: or by many orders of magnitude less than that demanded by the steady-state theories.

However, this is not a fair comparison since it does not properly take into account the different way in which the production of matter at rest, and the increase of the level of high-energy radiation, would affect the metric of intergalactic space. Unfortunately, the calculations including the pressure effects due to the radiation leakage are rather complicated, and have so far proven too much for a mere experimental physicist. All that can safely be reported at this time is that, according to a crude model approximation, they appear to raise the effect by several orders of magnitude; but whether it would be sufficient to bring about equilibrium conditions—essentially a « steady state without creation of matter »—and whether a more precise calculation will confirm the results obtained with this model, must still remain doubtful. Perhaps the most that can be said is that it looks as if it were worth the time of somebody who understands cosmology, to look into this problem.

2) Turning now to the second point, we note first that the empirical material known about the primary cosmic radiation certainly does not *exclude* an extragalactic, or a mixed, origin. If so, we might follow two possible assumptions: first, that extremely energetic radiation may have been created at some early phase, either in a « catastrophical » beginning, or in a universe which only started to expand and in which collisions between the forming galaxies were still quite frequent. Second, that such radiation is continuously being created in a process replacing the matter creation of a steady-state world. That this second process would be more « economical » than that of the usual theories [4, 5], is qualitatively evident, and has been proven quantitatively by HEIDMANN (*) in a paper the general ideas of which run very much parallel to those presented here. In this picture, cosmic radiation passes through three phases: the extragalactic creation and propagation, collision in a galaxy with a nucleus of galactic matter giving rise to a number of still energetic secondaries, and acceleration by magneto-hydrodynamic processes of low-energy particles resulting from these collisions, as well as of others ejected from stars.

(*) I am much indebted to Dr. J. HEIDMANN for discussing his results and presenting me with his manuscript before its publication.

In estimating the energy spectrum of this radiation, the degradation of the energy resulting from Fermi-type collisions with the magnetic fields of the galaxies must be taken into account. Since the probability for a collision with galactic matter of a particle entering a galaxy is small even if we permit a certain amount of storage by the galactic field, the primary cosmic radiation will spend most of its time outside of galaxies, and as a rule undergo repeated « collisions » with them before being captured: and on the average, these collisions will be of the « overtaking » kind because of the general expansion.

A rather simple estimate of the energy spectrum has therefore been made on the basis of the following three assumptions:

i) that the primary radiation, produced with uniform energy, undergoes overtaking collisions with receding galaxies, thereby losing some of its energy;

ii) that the removing mechanism for these particles—and the initial state for the second-phase radiation—is given by the collisions with galactic matter;

iii) that from each such collision, n nucleons of equal energies emerge, and that their energy is proportional to that of the incident particle.

Under these assumptions, a straightforward calculation shows that the resulting energy distribution will be closely represented by a power spectrum with an exponent of the order 2 to 4. Its exact value depends on a number of parameters about which our knowledge is insufficient, like the « storage » of the primary radiation in the galaxies, the number n of second-phase cosmic ray particles, and the average age of the cosmic-ray primaries. Evidently, there is not much sense in attempting to establish agreement of this exponent, by a suitable choice of the parameters, with the empirical value of the power spectrum of cosmic radiation observed at the earth. At present it is quite sufficient to arrive at order-of-magnitude consistency.

This is, of course, not the only model of extragalactic production of cosmic radiation that could be considered. Perhaps more realistically, colliding galaxies have been mentioned as possible sources of high-energy particles, and undoubtedly still other mechanisms can be devised. Without discussing them in detail, we emphasize only that in each case, the essential features of the assumptions (i) to (iii) would still be operative.

One final point may be mentioned. Against any model which places the origin of cosmic radiation at an early phase of our expanding universe, or even permits them an extragalactic lifetime comparable with the age of the universe, the objection may be raised that at this early time, the absorption in the galaxies must have been much larger because of their higher density. It can easily be shown that this is not so: that there was a phase when col-

lisions between galaxies were frequent enough to ensure a sufficiently high rate of production, and yet the chance of the cosmic ray particles to escape absorption was already quite reasonable. This can be viewed as a consequence of the fact that the frequency of collisions between galaxies increases with the square of their density, while that of particle-galaxy collisions is proportional to the first power of the density of the galaxies.

Let it be stressed again, the views presented here are offered as speculations, not as a theory. But whether or not they will stand up, in their present form, to future tests when the formalism will be improved and the parameters better known, they might be worth discussion now: if only to remind us to investigate even the unlikely, and to take nothing for granted.

REFERENCES

[1] G. Cocconi: *Nuovo Cimento*, **3**, 1433 (1956).
[2] K. Sitte: *Bull. Isr. Res. Council*, A **6**, 61 (1956).
[3] P. Morrison, S. Olbert and B. Rossi: *Phys. Rev.*, **94**, 440 (1954).
[4] F. Hoyle: *Month. Not. Roy. Astr. Soc.*, **106**, 343 (1946); **108**, 372 (1948).
[5] H. Bondi and T. Gold: *Month. Not. Roy. Astr. Soc.*, **108**, 252 (1948).

SUPPLEMENTO AL VOLUME VIII, SERIE X
DEL NUOVO CIMENTO

N. 2, 1958
2° Trimestre

A Point Source of Cosmic Rays and Its Time Variation.

Y. Sekido, S. Yoshida, Y. Kamiya, H. Ueno and K. Nagashima

Physical Institute, Nagoya University - Nagoya

At Mexico Meeting in 1955, three of the authors [1,2] reported the existence of a point source of cosmic rays at declination $\delta = 0°$, right ascension $\alpha = 5^h\ 30^{min}$, before entering into the geomagnetic field, observed with two alt-azimuth G.-M. counter telescopes until August 1955. The observation was continued with the two telescopes, and the point source was observed every year at the same position.

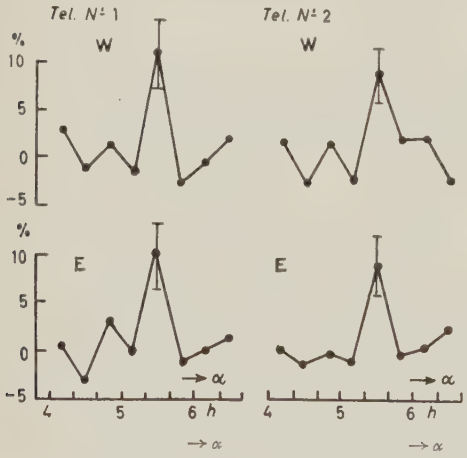

Fig. 1.

Since April 1954, observations were done at the zenith distance $Z = 80°$, twice a day at two azimuths $A = 85°$ and $A = 255°$, respectively. As shown in Fig. 1, every one of these four independent observations indicates the existence of the same point source. That is to say, the point source was observed four times, with two telescopes and at two azimuths, respectively.

The integrated curve of the total observations, from April 1954 to December 1956, in shown in Fig. 2. The error bar attached to every point corresponds to $\pm\sqrt{N}$, where N is the count at the position. For example, the count $N = 5\,039$ at the point source. Except the position of the point source, which was expected by the scanning in 1952 and 1953, the standard deviation of the intensities over the remaining 21 positions is 1.8%, while $1/\sqrt{N}$ is about 1.5%. The intensity difference between the point source and the remaining positions is more than 4 times as large as the standard deviation.

The position of the point source not corrected for the geomagnetic deflection may be called as the eastern image or the western image, according to the azimuth of the observation. The two telescopes gave the same position for the eastern image, and also the same position for the western image. As shown in Fig. 3, the two images were found identical to each other after the correction for the geomagnetic deflection. Through this identification, the charge and the average momentum of the effective primary particles and also the position before entering into the geomagnetic field can be determined. In the previous report, the charge was positive and the momentum was about 2 størmers. A little more exact values are as follows.

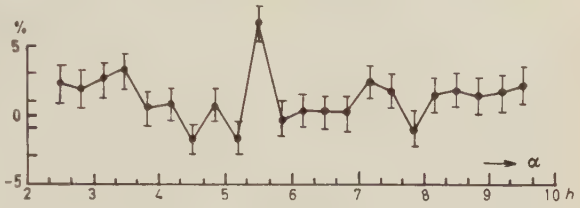

Fig. 2.

The most probable average momentum is 2.2 størmers or 280 GeV/c for protons. The most probable position is: declination $\delta = 0°30'$ N and right ascension $\alpha = 5^h 15^{min}$. The discrepancy of the identification is shown by the small circle in Fig. 3, which indicates that the error of momentum is about ± 40 GeV/c for protons and the error of position is about 1°. Another source of the error of position comes from the lack of our knowledge about the geomagnetic field, which was suggested by SIMPSON. This error was estimated to be less than 2.5°.

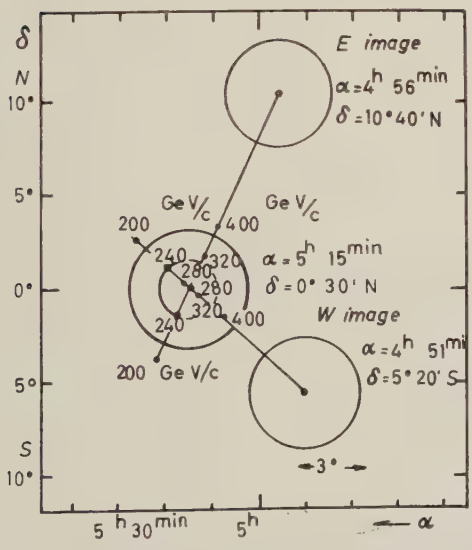

Fig. 3.

The radius of the image is 3° as shown in Fig. 3 by larger circles, which were determined from the duration of the appearance of the point source crossing through the field of the telescope. This radius $r = 3°$ is nearly equal to that expected from the geometry of the counter arrangement of the telescope. Consequently, the deviation of primary particles from a parallel beam and also the deviation due to the scattering in the atmosphere are considered to be less than about 2°. According to Murayama's estimate,

Coulomb scattering of μ-mesons is about 0.7°, the scattering due to π-μ decay is about $0.2^\circ \div 0.3^\circ$, and the dispersion due to the angular distribution of the π-meson production is about 2° if the distribution is assumed as $\cos^2\theta$ in the centre of mass system. This assumption is plausible in this region of primary energies. And the average momentum of the effective primarys rays, 280 GeV/c for protons described above, is also plausible as the result of atmospheric cut-off of the low energy part, without assuming any special spectrum of primary particles different from ordinary cosmic rays.

The intensity difference between the position and its vicinity ($4^h00^{min} < \alpha < 6^h40^{min}$) is $(8.9 \pm 1.5)\%$, which was measured with the solid angle $5^\circ \times 5^\circ$ during the period from 1954 to 1956. The number of cosmic rays from the point source is about $6 \cdot 10^{-8}$ particles per sec per cm^2 under the atmosphere at the zenith distance 80°. This intensity difference is not constant, but makes the time variations as follows.

There is no secular variation of the position of the point source, while there seems to be a secular variation of the intensity. As the significance level is about 0.5%, the existence of the secular variation is not conclusive. However if an exponential decay is assumed, the half period is about one year.

About the yearly variation of the intensity, both of the annual and semi-annual harmonics are well significant. Combination of these two harmonics indicates that the point source appears two times a year, and disappears two times a year. The 1-st maximum is about 3 times as high as the 2-nd maximum, and the 1-st maximum happens in May when the earth is on the side opposite to the point source with respect to the sun.

From a statistical examination of the day-to-day variation of the intensity difference, a periodic variation was found. In Fig. 4, amplitudes calculated for various values of assumed periods are shown. The most significant period is about 18 days the significance level being 0.27%, and the amplitudes corresponding to slightly different periods may be interpreted as an appearent effect due to the existence of the 18 day variation. The amplitude of the 18 day variation is about the same as the average intensity over a long time. That is to say, the point source appears and disappears once in every 18 days period.

The time variations described above may be summarized with the following empirical formula approximately:

$$I(t) = I_0 \exp\left[-\frac{t}{T_s}\right]\left(1 + \cos 2\pi \frac{t - t_a}{1 \text{ year}} + \cos \pi \frac{t - t_a}{1 \text{ year}}\right)\left(1 + \cos 2\pi \frac{t - t_{18}}{T_{18}}\right)$$

$$I_0 \approx 6 \cdot 10^{-8} \text{ s}^{-1} \text{ cm}^{-2}, \qquad T_a \approx 1.6 \text{ year}, \qquad t_a \approx \text{May},$$

$$T_{18} \approx 18 \text{ days}, \qquad t_{18} \approx \text{June 3, 1956}$$

which contains 5 empirical constants.

It is suggested, but not yet confirmed, that the 18 day amplitude observed with a wider solid angle seems to be constant, and the annual and semi-annual modulation may be caused by the deflection of cosmic rays from the point source due to some effect from the sun.

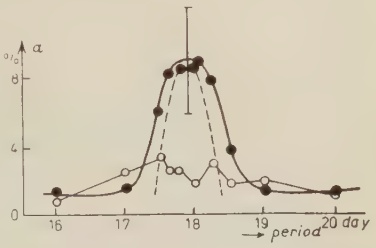

Fig. 4.

It has been considered to be difficult to observe any point source of cosmic rays through the galactic magnetic field. NAGASHIMA suggested a collimating effect of the galactic magnetic field. According to his idea, assume a localized origin of cosmic rays in a place where the galactic magnetic field is strong, and assume that the solar system is located at a place where the field is weak and which is not so much distant from the origin and connected with it by the magnetic lines of force. Under this special condition, he showed that the cosmic rays from the origin may come to the solar system, where the rays are nearly parallel to the lines of force (Fig. 5) and the intensity is much higher than that given by the inverse square law. At present, we have no proof whether this assumption is right or not. However, it will be difficult to say that the observation of a point source contradicts with the present knowledge.

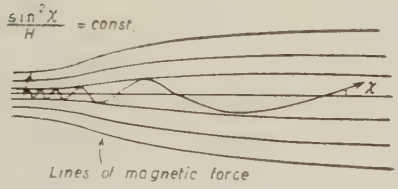

Fig. 5.

In conclusion, the authors emphasize that the existence of a point source of cosmic rays was confirmed again and its time variations were observed.

REFERENCES

[1] Y. SEKIDO, S. YOSHIDA and Y. KAMIYA: *Comm. to Meeting IUPAP Mexico from Working Ass. Primary Cos. Ray Res. Japan*, **45** (1955).

[2] Y. SEKIDO, S. YOSHIDA and Y. KAMIYA: *Nature*, **177**, 35, Jan. 7 (1956).

SUPPLEMENTO AL VOLUME VIII, SERIE X
DEL NUOVO CIMENTO

N. 2, 1958
2° Trimestre

Continuous Creation of Cosmic Rays.

J. HEIDMANN

Laboratoire de Physique, École Polytechnique - Paris

Recent experiments on large air showers indicate that cosmic rays exist with such a high energy that, as they cannot be confined in the Galaxy, they cannot get accelerated in the Galaxy by hydromagnetic processes. Furthermore the time scale for acceleration in extragalactic space cannot reasonably be made smaller than the expansion time constant of the Universe.

So we would like to consider a different approach to the problem of the origin of high energy cosmic rays, which is inspired by Bondi and Gold's theory of continuous creation. A rough picture would be the following: in a steady state infinite Universe there would be continuous creation, throughout all space, of nucleons of energy larger than the highest energy observed. They might appear either singly, without balancing momentum, either two or more at a time; as nucleons or as antinucleons; and neutral on the mean. These super-cosmic rays, as we shall call them, will travel in straight line through the Universe, crossing from time to time a galaxy. In a galaxy they will have some probability to suffer a nuclear collision with interstellar hydrogen. When doing so they will create a number of lower energy nucleons, which, when charged, will have some probability to get trapped in the galactic magnetic fields and degrade more and more into lower energy nucleons; then, in the galaxy, we shall get as secondary of super-cosmic rays, a spectrum of nucleons of intermediate energy, which we shall call meso-cosmic rays. They will have a low energy « cut-off » related to Hubble's constant, because the expansion of the Universe makes improbable a long degradation time by nuclear collisions.

Then lower energy cosmic protons *and heavy nuclei* would be ascribed to hydromagnetic processes in the Galaxy, such as are those occuring in solar flares, the Crab nebula and may be other loci like magnetic variable stars, interstellar turbulence.

The situation might then be schematized by the integral spectra of Fig. 1.

We assume implicitly that there is no appreciable degradation of super-cosmic rays in extragalactic space, i.e. that extragalactic space is empty enough. Later on we shall come back on this assumption.

Of course this scheme trespasses the law of conservation of energy, and perhaps momentum, but provided it does so within experimental certainty, as the theory of continuous origin of matter does, this is unrelevant. In this preliminary sketch we shall try to work out a few consequences in order that this scheme be not purely speculative.

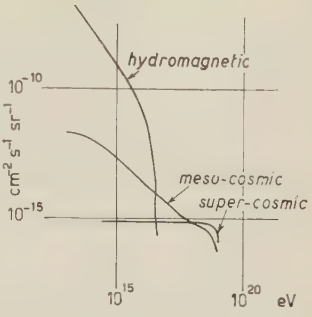

Fig. 1.

1) First, we simply note that in the high energy band there should be no heavy nuclei.

2) Second, a fine structure in the shape of the energy spectrum is likely to exist, as it results of the superposition of two different mechanisms. But one should not expect these two mechanisms to be completely unrelated, as it is schematized in Fig. 2.

3) Then, one would expect the meso-cosmic rays to contain antinucleons: even if all super-cosmic rays are nucleons, in the first encounter with interstellar hydrogen, they will create a large number of nucleons and anti-nucleons of which half will be anti-nucleons. When these degrade to lower energy they might tend to annihilate with interstellar hydrogen, thus reducing their relative abundance.

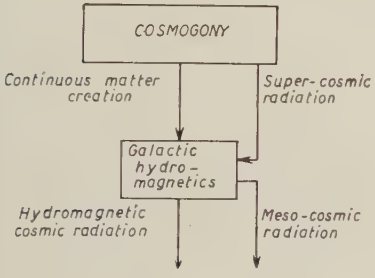

Fig. 2.

4) Also, pions should be created, appearing mainly like an inelasticity factor in the nucleonic chain. The charged one will readily decay into electrons which will loose their energy through synchrotron radiation and contribute to the galactic radio radiation.

5) The neutral pions will decay into γ-rays. These, being not trapped by galactic magnetic fields, will wander through all the Universe and fill it at a fixed density level.

6) The scheme leads to a power law meso-spectrum. Let us consider an oversimplifying case: assume that when a nucleon of energy E collides with an interstellar Hydrogen, we get, after the collision, a nucleons of energy αE each. The inelasticity is $k = a\alpha$. Let τ_a be the degradation time in the Galaxy by nuclear collisions with interstellar hydrogen and τ_e the escape time from the Galaxy of nucleons; n_s and E_s the number density and energy of

super-cosmic rays; τ_d and τ_e being much smaller than the Hubble constant T, we get the differential number density spectrum:

$$\frac{\mathrm{d}N}{\mathrm{d}E} = \frac{n_s}{E_s \log(a/k)} \left(\frac{E}{E_s}\right)^{\gamma} \tag{1}$$

with:

$$\gamma = -1 - \frac{\log a}{\log(a/k)} + \frac{\tau_d}{\tau_e \log(a/k)} \tag{2}$$

If k is not an extremely small number we have:

$$\gamma \sim -2 + \frac{\tau_d}{\tau_e \log a},$$

τ_d is about 50 My and $\log a$ around 5 to 10; then, if the escape time from the galaxy is larger than 10 My, we get $\gamma \sim -2$, and for τ_e smaller, γ is positive. From M.I.T. measurements γ should be about -3.

The discrepancy is not overwhelming, as the influence of many other factors should be investigated:

i) The number of nucleons a is a function of energy. From Fermi's thermodynamic theory of high energy nuclear events it is: $a \sim (E/m_0c^2)^{\frac{1}{4}}$.

ii) All nucleons are not emitted with the same energy αE in a collision. A more realistic model would be to assume $a/2$ nucleons with αE and $a/2$ with βE, with β/α taken from Fermi's theory.

iii) The cross-section for nucleon-nucleon interaction might be energy dependent, although there is no special evidence for it; in this case τ_d would be a function of energy.

iv) The escape time τ_e is a function of energy, which one could derive from Ecole Normale and M.I.T. anisotropy measurements.

v) Boundary condition effects should be considered; the sun being on the edge of a spiral arm of the Galaxy, an energy dependent edge effect should appear.

vi) Effects due to other galaxies should occur; for instance a fraction of meso-cosmic rays escaping from galaxies should reach our Galaxy and add to the meso-spectrum. This will be especially important in case the super-cosmic ray energy is so large that meso-cosmic rays of the first generations are not affected by galactic magnetic fields.

vii) Super-cosmic rays might not have a unique energy E_s. Shapes of suitable spectra should be investigated; and their relationship with the theory of continuous creation of matter would be important from a cosmological point of view.

7) Coming back to equations (1) and (2), one can estimate the total energy density ε_M contained in the meso-spectrum in galactic space. We simplify by introducing a galactic limit energy E_g such that under E_g we have $\gamma \sim -2$ and, above E_g, $\gamma \sim \tau_d \tau_{em} \log a$, where we set τ_{em} equal to its minimum value, i.e. the time for crossing the Galaxy in straight line. The galactic limit energy is such that the escape time is around 10 My from equation (2). D being the diameter of the Galaxy and λ the mean free path of cosmic rays in galactic magnetic fields, we have $\tau_e \sim D^2/\lambda c$. If one identified λ with the radius of curvature of the cosmic ray in the galactic field one gets: $E_g \sim 10^{18}$ eV.

In the low energy part of the meso-psectrum, a term of the order τ_d/T should be added to the exponent γ, where T is Hubble's constant, to take into account the expansion of the Universe. Then:

$$\varepsilon_M \sim n_s E_s \tau_{em}/\tau_d + n_s E_g T/\tau_d \,. \tag{3}$$

Now one has $n_s = 4\pi I_s/c$ where I_s is the directional intensity. Tentatively one can put $I_s E_s \sim 10^{-16}$ cm^{-2} s^{-1} sr$^{-1} \cdot 10^{19}$ eV from M.I.T. measurements. Then:

$$n_s \sim 10^{-26} \text{ particle/cm}^3\,, \qquad n_s E_s \sim 10^{-7} \text{ eV/cm}^3\,, \qquad \varepsilon_M \sim 10^{-6} \text{ eV/cm}^3\,.$$

8) We can now estimate the rate of continuous creation of super-cosmic radiation. It has to compensate for the expansion and for the absorption by galaxies:

$$\nu_s = n_s \left(\frac{3}{T} + \frac{g}{\tau_d} \right) \tag{4}$$

where g is the fraction of space occupied by galaxies; its values is 10^{-6} to 10^{-3}, so that we have:

$$\nu_s \sim 3 n_s/T \sim 10^{-43} \text{ particles/cm}^3 \text{ s}\,.$$

This represents an energy input of about 10^{-24} eV/cm^3 s. This value and those of 7) should be trusted only within a few orders of magnitude. They are just intended to show that, as a comparison, the energy input in the theory of continuous origin of matter is much larger. In the form of rest mass, it is about 10^{-11} eV/cm^3 s, if one takes 10^{-27} g/cm^3 as the density of the Universe.

Though the absorption of super-cosmic radiation by galaxies is negligible compared to the dilution due to expansion, its very existence implies a regulating mechanism for ν_s.

We have to come back on an assumption we made at the beginning and to

suppose now that intergalactic space is dense enough to degrade super-cosmic radiation by nuclear collisions. The average age of a super-cosmic ray in the Universe is determined, irrespective of degradation in intergalactic space, by the expansion time $T/3$ and the galactic absorption time τ_d/g. We have $\tau_d/g \gg T/3$; then, in order that super-cosmic rays should degrade in intergalactic space we must have $\tau_{di} < T/3$, where τ_{di} is the degradation time in intergalactic space. This requires the intergalactic density to be:

$$\varrho_i > 10^{-26} \text{ g/cm}^3 .$$

If this is so, galaxies would be immersed in a meso-spectrum of extragalactic origin which would pervade them, because the penetrating time, equal to τ_e, is small compared to the age of galaxies. The only important difference between this universal case and the above galactic case will be that the energy density of cosmic radiation in intergalactic space will be the same as in galactic space.

Gold objected that cosmic rays cannot be spontaneously created with their observed spectrum, because if one extrapolates this spectrum to the zero energy value of continuous creation of matter, one would get either an odd shape for the creation spectrum, or a divergency in the rate of continuous creation. But this objection does not hold here, because we do not assume cosmic rays to be created with their observed spectrum; this spectrum is obtained through degredation by nuclear collision with galactic or intergalactic matter.

SUPPLEMENTO AL VOLUME VIII, SERIE X
DEL NUOVO CIMENTO

N. 2, 1958
2° Trimestre

General Observations on the Origin Problem.

H. ALFVÉN

The Royal Institute of Technology - Stockholm

The following comments seem to be pertinent in considering the Sun as the primary source of cosmic rays:

1) The only direct evidence we have for particles of cosmic-ray energies coming from the Sun is during certain rare occasions when violent eruptions on the Sun occur. So far 5 such solar flares have resulted in particles reaching sea level on the Earth. It is reasonable to assume that if high energy particles in general come from the Sun the conditions would be most favorable when the Sun is most active. Actually cosmic rays are found to be at a minimum during an active period of the Sur

2) It has been suggested that there may be accelerating mechanisms in the extended corona of the Sun and that since the corona seems to be most extensive during a solar minimum this may be the most propitious time for particles, especially those of low energy, to arrive at the Earth, thus giving the phase found experimentally. In answer to this, one may remark that the chemical composition of the primaries suggests about equal numbers of lithium, beryllium, and boron nuclei compared with carbon, nitrogen, and oxygen existing in the primaries and that the Sun seems to be very deficient in the Li, Be, and B group of elements. To account for a sufficient number of these elements, the heavy nuclei of solar origin must have passed through several g cm^{-2} of matter before reaching the Earth and this is very difficult, since the amount of matter between the Sun and the Earth is probably not greater than 0.01 g cm^{-2}.

3) The third point against a solar origin has to do with the energy distribution of the primaries. No one has dared to suggest that the highest energy particles are of solar origin. If not, then it is difficult to understand how the energy distribution of particles of solar origin connects on so smoothly with those of cosmic origin. We, of course, do not have very precise information on the energy range from say, 10^{11} to 10^{15}, but it is hard to understand how any large difference could have escaped detection.

PART III

Composition of the Primary Radiation.

The Primary Alpha Particle Spectrum Over North America and Geomagnetic Cut-Off Energies.

P. Fowler, P. S. Freier and E. P. Ney

School of Physics, Institute of Technology, University of Minnesota - Minneapolis, Minn.

1. – Introduction.

The α-particles in primary cosmic rays represent a component of the radiation which is susceptible of detailed study. They are the second most abundant element in cosmic rays and are readily identified as primary cosmic rays over the entire energy range of interest. They can be easily distinguished from the proton component of cosmic rays and from other multiply-charged primaries in photographic emulsion. The contribution of the albedo to the measurement of primary α-particles can be shown to be negligible in contrast to the situation with primary protons. Because α-particles can be readily identified as primary cosmic rays and also represent a large fraction of the flux, they have become the best measured component of cosmic rays. It has previously been shown [1] that at very high geomagnetic latitudes and during a sunspot minimum, the primary α-particle differential spectrum shows a maximum at approximately 300 MeV/nucleon. At higher and lower energies the differential flux falls rapidly, and unless the distribution is assumed to be bimodal, the flux of α-particles of energy less than 150 MeV/nucleon must constitute less than 5% of the total α-particle flux. In the energy range from 150 MeV/nucleon to approximately 600 MeV/nucleon, the energy spectrum of the incident α-particles can be measured directly in emulsion without recourse to geomagnetic theory. It is possible, therefore, to determine the effect of the earth's magnetic field in producing cut-off energies in a vertical direction for incoming α-particles at various latitudes. This measurement has been carried out by Waddington [2] in England, where it has been shown that the cut-off energies are higher than would be anticipated from geomagnetic theory. The present series of measurements represents a corresponding ex-

periment carried out over northern North America, in order to determine the energy spectrum of cosmic ray α-particles independent of the earth's magnetic field and to find the cut-off energies operative at various latitudes in the United States.

2. – Description of the experiment.

The determination of differential energy spectra in emulsion requires balloon flights performed at constant level and at different geographic latitudes. It is desirable to have a means of determining whether the α-particles studied were produced at high altitude, where the residual pressure is precisely measured. In the series of flights reported here, the flights were either long enough so that the number of α-particles entering the plates during ascent was negligible, or the plates were turned from a horizontal to a vertical position after the balloon had reached ceiling altitude. The latter method is preferable, since long tracks of the type studied in this experiment are virtually nonexistent in horizontally exposed plates. The size of stack required to get a statistically significant measurement of the α-particle flux consists of a 4 in. × 4 in. stack of twelve 600 μ-thick pellicles. These plates are line-scanned for particles of greater than three times minimum ionization and of length greater than or equal to 8 mm, and having a zenith angle within $\pm 45°$ of the zenith. On each of the tracks found in this way, measurements are made of the ionization and the multiple Coulomb scattering. We have found that in the ionization range encountered in this experiment a photoelectric measurement of the ionization is a reliable and easy way of determining this parameter. Fig. 1 shows a plot of ionization vs. scattering, for the α-particles obtained in one of the exposures reported in this paper. It can be seen from this plot that the protons are completely resolved from the α-particle component and that both the ionization and the scattering indicate the variation in energy of the α-particles. A previous experiment [1] has shown that the ionization measurement gives a more precise determination of the energy, and the determination of the energy spectrum is therefore based upon the ionization distribution of the particles which are shown to be α-particles by such a plot as Fig. 1.

The conversion between measured ionization in the plates and α-particle energy is obtained from the densitometer reading. In the flights in which α-particles of energy less than 300 MeV/nucleon occurred, this calibration could be carried out directly with the α-particles themselves. In the Missouri flights, however, where these particles are missing, it was necessary to determine the energy calibration of the densitometer measurement by using slow protons

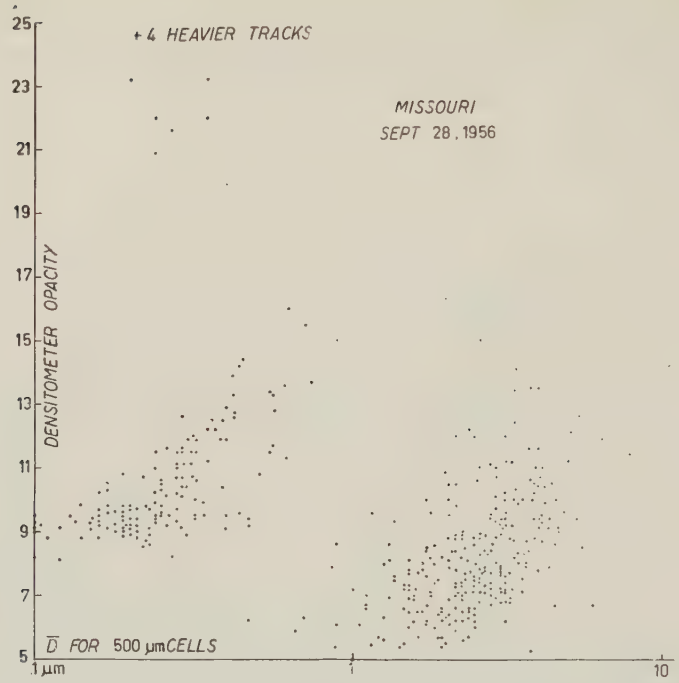

Fig. 1. – Ionization (Densitometer Opacity) as a function of multiple Coulomb scattering ($\overline{D}$ per 500 μm cells) for the particles obtained in the line scan of the Missouri plates.

for calibration. Fig. 2 shows such calibration. It has been demonstrated that if the ionization measurement is plotted as a function of Z^2/β^2, the measurements made on protons at known residual range will fall in a smooth curve with the corresponding measurements made on α-particles. It is therefore possible, by measuring slow protons in emulsion, to calibrate in the energy range of interest of the primary α-particles.

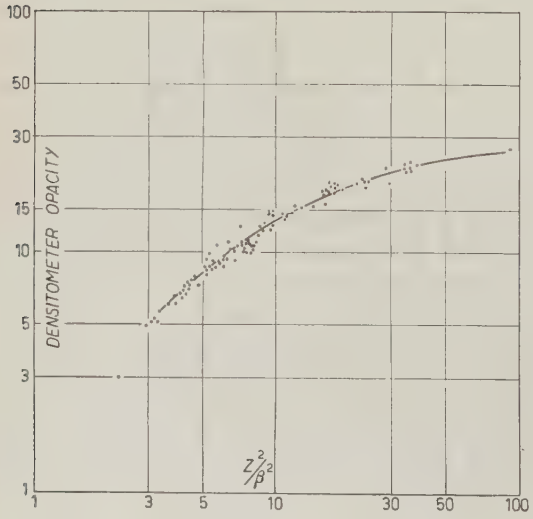

Fig. 2. – Densitometer calibration for the Missouri exposure. The densitometer opacity is given as a function of Z^2/β^2 for ending protons and α-particles. This calibration can be used for $.1 < \beta < .8$.

The ionization distributions of the particles measured in the four experiments carried out over the United States are shown in Fig. 3. Table I gives the pertinent characteristics of the flights in which these α-patricles where measured. The resolution of the densitometer measurement is indicated by the Texas distribution where the particles are all relativistic. It can be seen in Fig. 3 that the ionization distribution of α-particles in northern Iowa is very much the same as the ionization distribution in Saskatoon, Canada.

Fig. 4 shows the differential energy spectrum in Saskatoon corrected for absorption in the atmosphere and for production of α-particles by fragmentation. Within statistics the spectrum in northern Iowa is identical with the spectrum in Saskatoon. Table II gives the relative flux of α-particles at Saskatoon or northern Iowa, in various energy ranges. It can be seen that less than 5 % of the α-particles have energies less than 150 MeV/nucleon, approximately 18 % have energies between 150 and 300 MeV/nucleon, and 82 % have energies in excess of 300 MeV/nucleon, in this spectrum. Further examination of Fig. 2 shows that the spectrum obtained in northern Missouri is lacking in low energy particles and, in fact, indicates that a cut-off has become operative. This cut-off for the vertical direction corresponds to an energy of 300 MeV/nucleon. If it is assumed that the cut-off is produced by the earth's

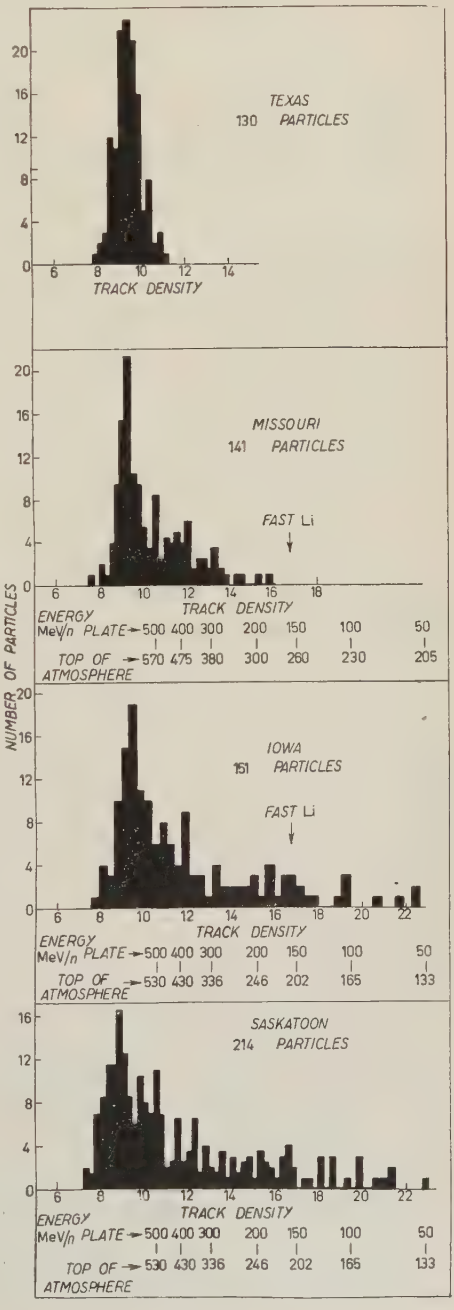

Fig. 3. – Ionization distributions for the α-particles of this experiment, The energy per nucleon at the plates and at the top of the atmosphere is indicated on the abscissa for each exposure.

TABLE I.

Site	Date of flight	Geographic longitude	Geographic latitude	Nominal geomagnetic latitude	Measured cut-off energy MeV/N	Cut-off appropriate to nominal geomagnetic latitude MeV/N	Integral flux corrected to top of atmosphere particles m^2 s sr.
Saskatoon Canada	June 18, 1954	107° W	52° 10′ N	61°	$\leqslant 150$	90	290 ± 20
Waukon Iowa	May 17, 1956	91° 30′ W	43° 50′ N	54°	$\leqslant 150$	350	255 ± 20
Kirksville Missouri	Sept. 28, 1956	90° W	40° 40′ N	50° 30′	300 ± 20	560	249 ± 20
San Angelo Texas	Feb. 6, 1956	101° W	31° N	41°	> 500	1 600	97 ± 8

magnetic field, the value of 300 MeV/nucleon measured must be compared with the vertical cut-off of 560 MeV/nucleon which would be calculated on the basis of conventional geomagnetic co-ordinates. If one believes that the vertical cut-off momenta are given by an expression of the type

$$p = 7.4 \cos^4 \lambda \quad \text{(GeV/c)/nucleon},$$

then the cosmic ray latitude in North America must be assumed to be 4° higher than the conventional geomagnetic co-ordinates determined by surface earth field measurements which lead to the conventional eccentric dipole approximation of the earth's field. This is in contrast to the situation in England where the measured cut-off energies indicate cosmic ray co-ordinates 4° lower than the conventional geomagnetic co-ordinates. WEBBER [3] has recalculated cosmic ray cut-off energies on the basis of an eccentric dipole determined by the most recent magnetic measurement. His calculations show somewhat better agreement with the measurements in England, but show a strong dis-

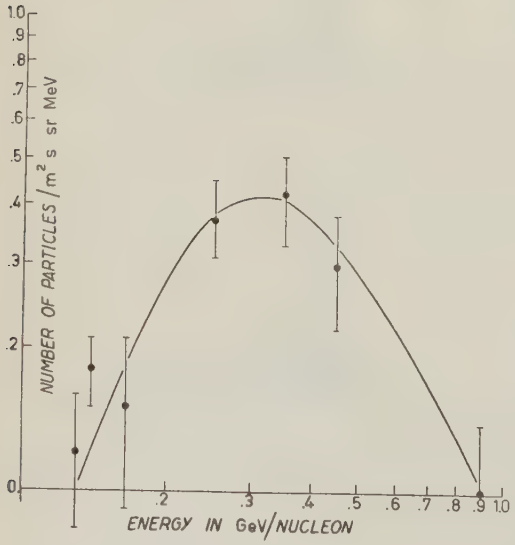

Fig. 4. – Differential energy spectrum of α-particles at high latitude corrected to the top of the atmosphere.

TABLE II. – *Relative flux of α-particles as a function of energy at high geomagnetic latitude, and corrected to the top of the atmosphere.*

Energy interval (MeV/nucleon)	% of α flux in the indicated energy interval	Absolute flux α-particles/m² s sr
$E < 150$	$< 5\%$	< 15
$150 < E < 300$	$18 \pm 3.5\%$	52 ± 10
$300 < E < 500$	24 ± 7 %	70 ± 20
$E < 500$	42 ± 7 %	120 ± 20
$500 < E$	58 ± 7 %	170 ± 20
$150 < E < \infty$	$> 95\%$	290 ± 20

agreement with the measured cut-off energies over the United States. Recent determinations of the geomagnetic equator also appear to be in disagreement with the position as deduced on the basis of an eccentric dipole model, even using the most recent magnetic data.

It has been suggested by ROTHWELL [4] that the cosmic ray co-ordinates seem to be in much better agreement with the dip magnetic co-ordinates of the earth than with the co-ordinates as deduced from the eccentric dipole. Our measurements, together with the English measurements, are in agreement with Rothwell's suggestion. The line of 71° dip in the northern hemisphere passes through Missouri, where our measured cut-off energy is 300 MeV/nucleon. The same line of dip crosses the British Isles at approximately 58° N geographic latitude. Although the cut-off energy has not been measured in northern England WADDINGTON [2] has observed a cut-off energy of 600 MeV/nucleon at a geographic latitude of approximately 52° N. If we assume that a line of constant magnetic dip represents a line of constant cut-off energy, we would therefore predict that over northern England at a geographic latitude of 58° the cut-off energy should correspond to northern Missouri, that is, 300 MeV/nucleon. If the change of cut-off energy with latitude corresponds to the Störmer equation, then the cut-off energy over England at 52° N geographic latitude would be 700 MeV/nucleon, in good agreement with the 600 MeV/nucleon measured by WADDINGTON. Another way to state this result is to give the difference in geographic latitude between longitude 0 (England) and longitude 90° W (mid United States) which will produce the same magnetic dip, geomagnetic co-ordinate or cosmic ray cut-off energy. This difference, (English latitude less American latitude) is $+16° \pm 1°$ for equal magnetic dip, $+14° \pm 1°$ for equal cosmic ray cut-off energy, and $+6° \pm 1°$ for equal geomagnetic co-

ordinates. It thus appears that the α-particle measurements made so far over England and the United States are consistent with the hypothesis that cosmic ray co-ordinates are more nearly determined by the dip co-ordinates of the earth's magnetic field than by the eccentric dipole geomagnetic co-ordinates.

Because of the possible effect of solar activity on cosmic ray particles, Fig. 5 shows the times during the solar cycle at which the experiments reported here were made. Because the experiment conducted at high latitude (Saska-

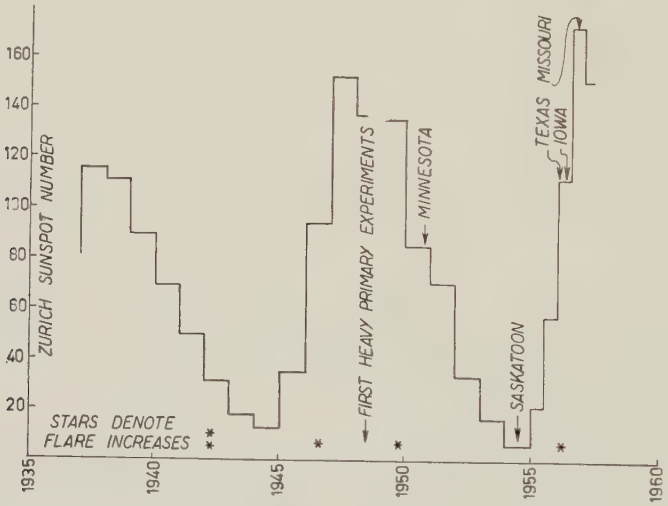

Fig. 5. – Plot of Zurich sunspot numbers to indicate solar activity at the times when the experiments reported here were carried out.

toon) was made during the sunspot minimum, it is quite clear that this does represent the pre-existing cosmic ray flux unaffected by the earth's magnetic field or by solar activity. Reference to Table I shows that the flux measured at Iowa during a period of high solar activity had the same absolute value as that at Saskatoon. The spectrum was identical in terms of energy spectrum as well as total flux, and it appears therefore that these measurements indicate no correlation or anti-correlation with the sunspot cycle within our statistics of $\pm 10\%$. Since the measurement at Missouri was made during an active solar period, it might be argued that the cut-off energy measured in this experiment was imposed by solar activity rather than by the earth's field. The previous arguments concerning cosmic ray latitudes, however, would be altered, then, in the following way: If the cut-off produced in Missouri were produced by solar activity rather than the earth's field, the earth field cut-off would be at least as low an energy as that found, namely 300 MeV/nucleon. If the cut-off were not earth field imposed, the discrepancy with geomagnetic co-ordinates would be even more severe than we have indicated.

3 – Conclusions.

The series of flights made in North America have shown that cosmic ray cut-off energies cannot be computed with conventional geomagnetic co-ordinates. The measured cut-off indicates that the effective cosmic ray latitudes in the United States are 4° higher than would be obtained from conventional geomagnetic co-ordinates. This effect is opposite to the effect observed in England where WADDINGTON found that cosmic ray cut-off energies indicated effective cosmic ray co-ordinates 4° lower than those given by geomagnetic co-ordinates. The measurements reported here, taken together with the English measurements, appear to be consistent with the suggestion of ROTHWELL that cosmic ray co-ordinates more nearly resemble the magnetic dip co-ordinates of the earth than they do the geomagnetic co-ordinates of the earth. Over the period of the sunspot cycle which these measurements cover, there appears to be no evidence within the statistics of our experiments (i.e. $\pm$ 10% for individual absolute flux measurements) of a correlation between the α-particle fluxes and the solar activity.

REFERENCES

[1] P. FOWLER, C. J. WADDINGTON, P. S. FREIER, J. NAUGLE and E. P. NEY: *Phil. Mag.*, **2**, 157 (1957).
[2] C. J. WADDINGTON: *Nuovo Cimento*, **3**, 930 (1956).
[3] W. WEBBER: in this issue, pag. 532.
[4] P. ROTHWELL and J. QUENBY: in this issue, pag. 249.

SUPPLEMENTO AL VOLUME VIII, SERIE X
DEL NUOVO CIMENTO

N. 2, 1958
2° Semestre

Study of Primary Cosmic Ray Alpha and Proton Energy Spectra, Geomagnetic Cut-Off Energies and Temporal Variations.

F. B. McDonald

Department of Physics, State University of Iowa - Iowa City, Iowa

1. – Introduction.

A new detector employing both a Čerenkov counter and a scintillation counter has been developed for measuring the cosmic ray charge and energy spectrum. A diagram of the telescope is shown in Fig. 1. A coincidence occurs when a particle traverses the NaI crystal and the lower tray of Geiger counters, and for each such event the pulse heights from the scintillation counter and from the Čerenkov counter are recorded on moving film. The expected variation of Čerenkov pulse height *vs.* the most probable [1] energy loss in the scintillation crystal as β, the particle velocity, is varied from 1 to $1/n$ (n is the index of refraction of the Lucite radiator), is shown in Fig. 2. For $\beta < 1/n$ (kinetic energy < 320 MeV/nucleon) the theoretical Čerenkov pulse height is zero. In actual practice there is

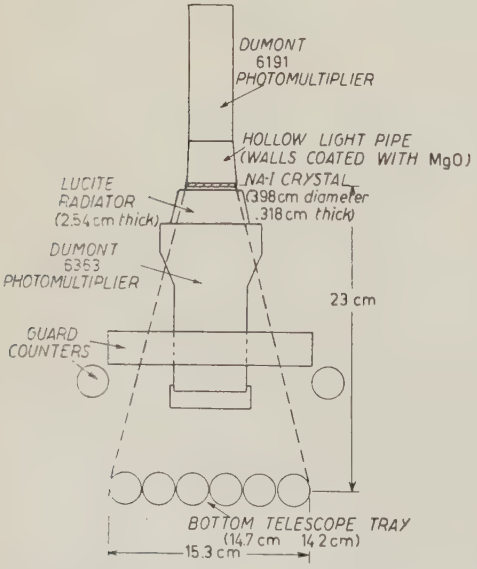

Fig. 1. – Schematic drawing of telescope.

Showers and multiple particle detection is achieved by noting whether one of the ring of guard counters or more than one counter in the bottom tray is triggered by a given event.

a very small amount of fluorescence in the Čerenkov counter for large values of energy loss and well defined particle distributions are obtained down to 100 MeV/nucleon for alphas and protons. The low energy proton and α distributions will not overlap due to the short range of protons in this interval.

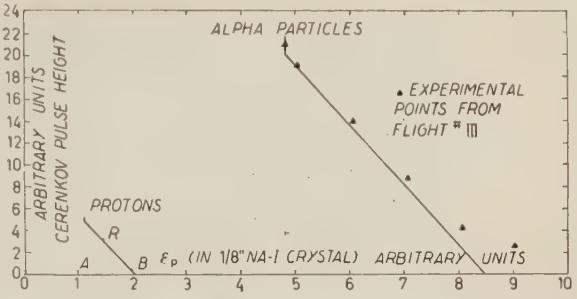

Fig. 2. – Plot of Čerenkov pulse height in 1″ lucite radiator *vs.* most probable energy loss for protons and α in 1/8 in NaI crystal. Fast upward moving particles will be located along line A-B due to the directional properties of the Čerenkov radiation.

Since both detectors are velocity sensitive, it is possible to measure directly the energy spectrum of α and protons in the range 150 to 900 MeV/nucleon. By studying the energy spectrum as a function of latitude, it is possible to determine effective geomagnetic cut-off energies. In addition the variations of the energy spectrum with time can be observed.

This report will deal with the α and proton energy spectra, α cut-off energies and temporal variations that have been obtained with a series of six skyhook balloon flights. All except one of the 6 skyhook flights reached an altitude greater than 114 000 feet (6 g/cm^2). The attainment of these very high altitudes greatly reduced the magnitudes of the corrections for energy loss in the atmosphere, fragmentation and loss of particles due to nuclear interactions.

2. – Alpha energy spectrum.

The α integral and differential energy spectrum data are collected in Table I and plotted in Fig. 3 and Fig. 4. The two flights which have been excluded from these data occurred during periods when there were large fluctuations in the neutron intensity. The α differential spectrum has a maximum in the vicinity of 325 MeV/nucleon and decreases at lower energies. It is found empirically that general agreement is obtained with a differential spectrum of the form

$$\frac{\mathrm{d}J_0^{\alpha}}{\mathrm{d}E} = -\frac{(415)(1.5)\{1-\exp[80E^3]\}}{(1+E)^{2.5}} \text{ particles/m}^2 \text{ s sr MeV}$$

where $J_{0\alpha}$ ($\geqslant E$) is the vertical flux of primary α-particles with kinetic energy $\geqslant E$ (measured in GeV). The integral of this function is in good agreement whit the integral flux data over the range .150 to 7.3 GeV/nucleon.

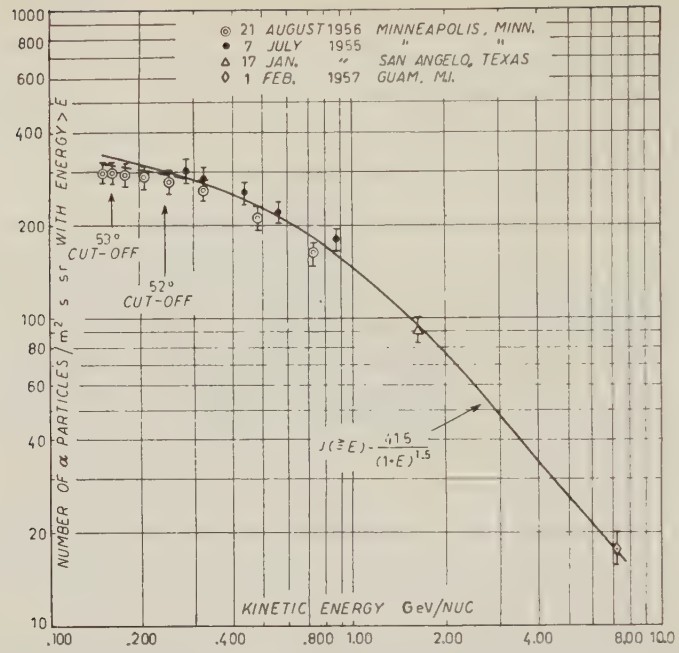

Fig. 3. – α integral energy spectrum data collected from 4 flights. The dotted line represents

$$J_0\,(\geqslant E) = -\,1.5\int_E^{\infty} \frac{(415)\,(1-\exp\,[-\,80E'^{3}])}{(1+E')^{2.5}}\,dE' \text{ particles/m}^2\text{ s sr}\,.$$

At energies greater than 350 MeV/nucleon this is identical with the power spectrum shown as a solid line.

In the range .350 to 7.3 GeV/nucleon the integral spectrum is accurately represented by:

$$J_{0\alpha}(\geqslant E) = \frac{415}{(1+E)^{1.5}} \text{ particles/m}^2\text{ s sr at 0 g/cm}^2.$$

The low energy differential spectrum is in excellent agreement with the measurements of FOWLER *et al.* [2] made at 62° and 55°.

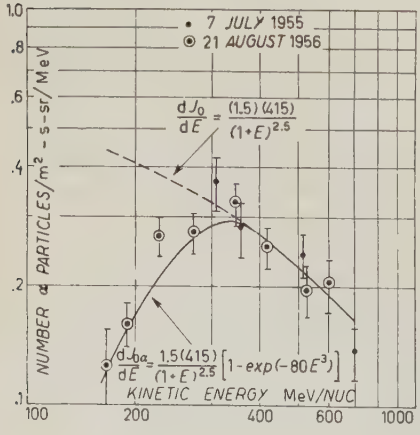

Fig. 4. – α differential energy spectrum. Amplifier saturation prevented the extension of the flight III data to low energies.

TABLE I. – *Summary of α data obtained with Čerenkov-scintillation counter.*

Flight III Energy E (GeV/nucleon)	7 July 1955 $\lambda = 55°$ No. of α-particles/m² s sr with kinetic energy $\geqslant E$
0.280	306 ± 25
0.320	294 ± 25
0.436	261 ± 20
0.563	225 ± 20
0.883	182 ± 18
Flight VIII **Energy E (GeV/nucleon)**	**21 August 1956 $\lambda = 55°$** **No. of α-particles/m² s sr with kinetic energy $\geqslant E$**
0.153	298 ± 25
0.167	297 ± 25
0.204	290 ± 25
0.249	278 ± 2
0.316	260 ± 21
0.350	250 ± 20
0.487	217 ± 16
0.730	167 ± 14
Flight I	17 January 1955 $\lambda = 41°$ N
	$J_{0\alpha}$ ($E = 1.65$ GeV) = 90 ± 9 particles/m² s sr
Flight XI	30 January 1957 $\lambda = 3°$ N
	$J_{0\alpha}$ ($E = 7.3$ GeV) = 18.0 ± 2 particles/m² s sr

3. – Proton flux and energy spectrum data.

The properties of the Čerenkov-scintillation detector are such that fast downward moving particles are readily distinguishable from splash albedo and slow secondaries. At $\lambda = 0$ it was observed that a plot of log counting rate vs. pressure had a constant positive slope in the region $6 \div 34$ g/cm² and a -18% correction was necessary to extrapolate the counting rate at 6 g/cm² to 0 g/cm². An upper limit to the proton flux is obtained by assuming no returning albedo and a lower limit by assuming all the vertical splash albedo

appear as returning albedo. The following flux values are measured:

At $\lambda = 0°$

Upper limit	$J_{0p}(E \geqslant 15.3 \text{ GeV})$	$= 115 \pm 12$	particles/m² s sr 0 g/cm² atm. depth
Lower limit	$J_{0p}(E \geqslant 15.3 \text{ GeV})$	$= 90 \pm 12$	particles/m² s sr 0 g/cm² atm. depth
	$J_{\text{splash albedo}}(E \geqslant .8 M_0 c^2)$	$= 19 \pm 3$	particles/m² s sr
	$J_{\text{splash albedo}}(.3 \leqslant E \leqslant .8 M_0 c^2)$	$= 12 \pm 3$	particles/m² s sr
	$J_{\text{slow protons}}(100 \text{ MeV} \leqslant E \leqslant 300 \text{ MeV})$	$= 12.5 \pm 3$	particles/m² s sr

At $\lambda = 41°$

(assuming .5 splash albedo appears as returning albedo)

$J_{0_p}(E \geqslant 4 \text{ GeV}) = 550 \pm 70$ particles/m² s sr.

In the region $\lambda = 0° \div 41°$ the proton energy spectrum can be represented by

$$J_{0p}(\geq E) = \frac{6\,600}{(1 + E)^{1.5}} \quad \text{particles/m}^2 \text{ s sr .}$$

The α and protons have the same energy spectrum in the region $\lambda = 0° \div 41°$. This conclusion will not be altered by moderate changes in geomagnetic cut-off energies. The proton spectrum presented here is not valid for energies less than 1.5 GeV. It is possible that a modification to this spectrum similar to that suggested for α might be appropriate in the low energy region.

4. – Alpha geomagnetic cut-off energies in the region $\lambda = 51° \div 54°$

A measurement at $\lambda = 55°$ revealed that α of all energies down to 150 MeV/nucleon (the atmospheric and apparatus cut-off) were present (Fig. 4). The calculated cut-off energy at 55° is 330 MeV/nucleon. This is in agreement with the data of FOWLER *et al.* [2] at 55°. In one flight on March 20, 1956, the balloon followed a trajectory extending from southern Iowa into central Michigan (Fig. 5). By dividing the scintillation data into two intervals of time it was possible by subtracting the distributions to obtain the flux and energy distribution of new particles arriving between two mean latitudes. In a similar manner, the scintillation counter data in the α region can be compared with

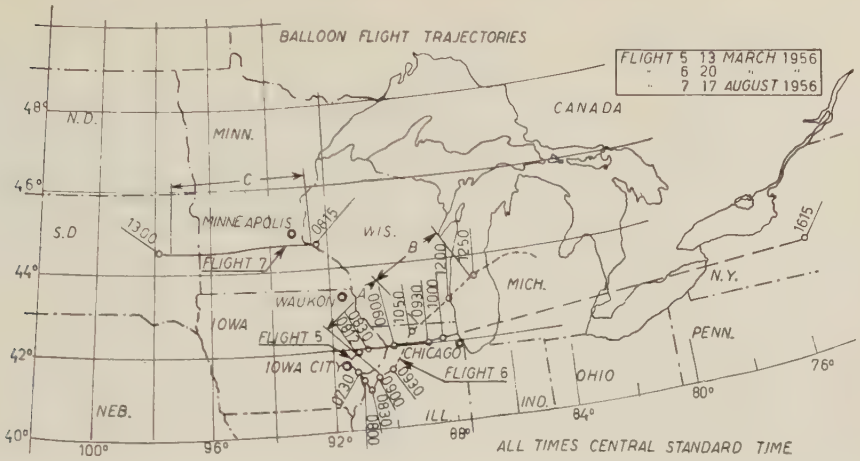

Fig. 5. – Trajectory of 3 skyhook flights. Periods A, B and C are indicated along the trajectory (see Fig. 6).

that obtained with a flight at a higher latitude. These three distributions are plotted in Fig. 6 along with the distributions that result when a subtraction technique is used. A summary of the pertinent cut-off data is presented in Table II. In general a 4° shift of latitude co-ordinates would bring the mesaured cut-off energies into agreement with the calculated value. This shift is much greater than the experimental errors involved in measuring the cut-off. Clearly standard geomagnetic theory is not applicable to cosmic rays in the latitude interval considered here.

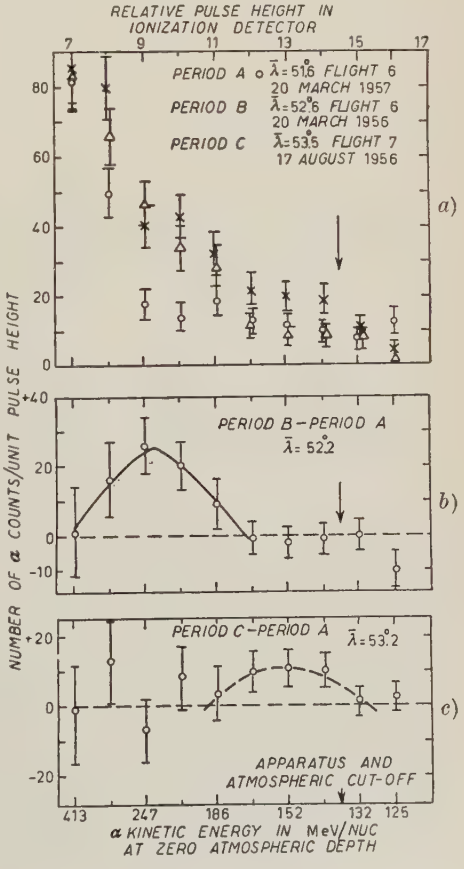
RELATIVE PULSE HEIGHT IN IONIZATION DETECTOR
PERIOD A ○ λ̄=51.6 FLIGHT 6 20 MARCH 1957
PERIOD B λ̄=52.6 FLIGHT 6 20 MARCH 1956
PERIOD C λ̄=53.5 FLIGHT 7 17 AUGUST 1956
a)
PERIOD B−PERIOD A λ̄=52.2
b)
PERIOD C−PERIOD A λ̄=53.2
c)
APPARATUS AND ATMOSPHERIC CUT-OFF
NUMBER OF α COUNTS/UNIT PULSE HEIGHT
α KINETIC ENERGY IN MeV/NUC AT ZERO ATMOSPHERIC DEPTH

Fig. 6. – Part *a*) gives the total number of counts per unit ionization interval in the low energy α region. There exists a small but appreciable fraction (25%) of background counts in the intervals which are removed when the intervals are subtracted. This is done in parts *b*) and *c*) and gives the number and energy distribution of new particles coming in between the mean latitudes.

TABLE II. – *Summary of measurements of geomagnetic cut-off energies.*

Flight. No. and data	Period	Geographic coordinates of endpoints of selected periods (*a*)	Geomagnetic latitude defined by periods	Mean geomagnetic latitude definited between two selected periods	Measured cut-off energy between selected periods in MeV/nucleon	calculated mean cut-off energy between selected periods in MeV/nucleon	Shift in coordinates necessary to bring mesured cut-off energies into agreement with calculated energies
VI 20-3-56	A	41°30′ N,90°43′ W 42°36′ N,88°09′ W	51° N 52°16′ N	*B-A* 52°16′ N	225±25	455 MeV	4° 15′
	B	42°36′ N,88°09′ W 43°43′ N,87°00′ W	52°16′ N 53°30′ N	*C-B* 53°10′ N	160±15	400 MeV	5°
VII 17-8-56	C	44°34′ N,92°40′ W 44°30′ N,97°43′ W	54° N 53° N				
V 13-3-56	D	42°12′ N,87° W 42°40′ N,65°30′ W	51°40′ N 53°05′ N	*D* 52°23′ N	220±30	445	4°

(*a*) see Fig. 5.

5. – Time variations.

A flight was launched on 13 March 1956 during a large Forbush decrease. The neutron counting rate at Mount Washington, N. H. and Sacramento Peak, N. M., was 10.5 and 13% below the counting rate during flight III on 7 July 1955. The latter flight occurred during what may be regarded as a quiet cosmic ray period. The α differential and integral energy-spectrum data for these two days are plotted in Fig. 7. These data indicate that during the decrease occurring around 13 March 1956 the low energy particles are not affected more strongly than the high energy particles (E>800 MeV/nucleon).

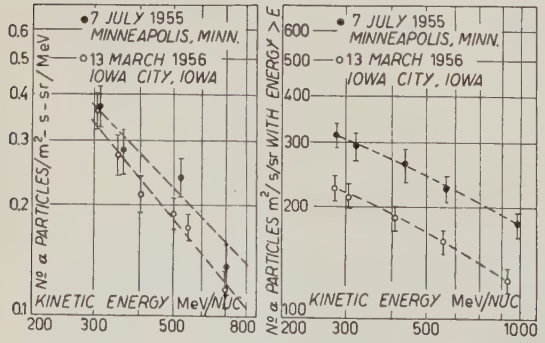

Fig. 7. – Differential and integral α energy spectrum for flight V (13 March 1956) and flight III (7 July 1955). In both cases the absence of data below 270 MeV/nucleon is due to amplifier subtraction.

Indeed the data suggest there was a large diminution of α-particles with energies > 800 MeV/nucleon and that particles in the energy region (300 ÷ 600) MeV/nucleon were not as strongly affected.

REFERENCES

[1] F. B. McDonald: *Phys. Rev.*, **104**, 1723 (1956).
[2] P. H. Fowler, C. J. Waddington, P. S. Freier, J. Naugle and E. P. Ney: *Phil. Mag.*, **2**, 157 (1957).

SUPPLEMENTO AL VOLUME VIII, SERIE X
DEL NUOVO CIMENTO

N. 2, 1958
2° Trimestre

The Charge Spectrum of the Cosmic Radiation at 41° N.

M. KOSHIBA, G. SCHULTZ and M. SCHEIN

Department of Physics and Enrico Fermi Institute for Nuclear Studies
University of Chicago - Chicago, Ill.

Summary (*). — From a large stack of GK5 emulsions flown at Texas, 41° N geomagnetic latitude, the charge spectrum of the cosmic radiation at 10400 feet was obtained. Special emphasis is given to the observation of the detailed shape of the spectrum in the region Z 9. The gap-counting is extensively used even at these hig Z values after very careful calibration with break-up events and δ-ray countings. The charge spectrum thus obtained was extrapolated to the top of the atmosphere by making use of the fragmentation probabilities in air which were obtained from the analysis of a total of 209 interactions in the same stack. This extrapolation gives for the ratio of the light nuclei, L, ($Z=3$, 4 and 5) and the heavy nuclei, H, ($Z \geqslant 9$), to the medium ones, M, ($Z=6$, 7 and 8) the values 0.32 ± 0.07 and 0.48 ± 0.10, respectively, at the top of the atmosphere. The fragmentation probabilities in hydrogen, the main constituent of interstellar matter, were also obtained from the careful study of the interactions in the stack and allowed to make a further extrapolation of the charge spectrum from the top of the atmosphere to the one at the source region of the cosmic radiation. The ratio of the heavy nuclei to the medium ones was found to be 0.66 ± 1.6 at the source. This charge spectrum at the source region is compared with the average chemical abundances of the elements in the universe as well as with those in certain types of stars. The results seem to indicate a close similarity of the chemical abundance curve of the cosmic radiation with that of certain types of young stars.

(*) The complete paper has been published in *Nuovo Cimento*, **9**, 1 (1958).

SUPPLEMENTO AL VOLUME VIII, SERIE X
DEL NUOVO CIMENTO

N. 2, 1958
2° Trimestre

Flux of Primary Helium Near the Geomagnetic Equator.

M. M. SHAPIRO, B. STILLER and F. W. O'DELL
U. S. Naval Research Laboratory - Washington, D. C.

The abundance of the elements in the primary cosmic radiation and the nature of their energy spectra is of great cosmological interest. In particular this information can help us distinguish between various theories of cosmic ray origin and acceleration. The intensity of the helium component, which is next in abundance only to hydrogen, is fairly well known from investigations north of 40° geomagnetic latitude. Until recently, however, the flux of primary helium near the geomagnetic equator, where the energy cut-off is ~ 6 GeV per nucleon, was not well known.

The most extensive work on primary He has been done by means of balloon flights in Minnesota and in the vicinity of White Sands, New Mexico. The magnetic latitudes in these two locations are respectively, 55° and 41° N. Of the published values at the latitude of Minnesota, probably the most definitive are those of DAVIS, CAULK and JOHNSON of the Naval Research Laboratory, and of WADDINGTON at Bristol. Their values of the He flux at the top of the atmosphere, obtained by quite different methods, and uncorrected for secondary α-particles due to the break-up of heavier primary nuclei, agree exactly, i.e., 320 particles/m^2 s sr with respective standard errors of 42 and 36 in these units, which we shall call « peters ».

The He flux over White Sands, New Mexico ($\lambda = 41°$ N) is probably the best determined primary cosmic ray intensity, as shown in the summary of WEBBER. The mean flux at this latitude is 90 ± 3 peters.

By contrast, there has been a paucity of He data at very low magnetic latitudes. Thus, in 1950, SINGER found an upper limit of (14 ± 20) peters. In 1950 POMERANTZ published a value of (49 ± 13) peters for this intensity, and MCCLURE reported an upper limit of 38 peters.

The equatorial flux is not only of *intrinsic* interest, but is also required to establish with confidence the energy spectrum of the helium component.

Therefore, we undertook to measure the flux of helium in a stack of stripped emulsion exposed in the stratosphere near the geomagnetic equator off the Galapagos Islands. The balloon flight took place in September, 1953. Our emulsion stack remained at a rather uniform height above 90 000 feet for a little over six hours.

Near the geomagnetic equator the elimination of low energy nuclei by the earth's magnetic field results in low intensities, so a good deal of scanning is required to find enough tracks. On the other hand, the flux measurements are simplified by the fact that all the primaries are relativistic. The ionization loss along the path of such a fast nucleus is close to the minimum value for a given charge. For helium, the ionization is very close to 4 times the absolute minimum. Thus, if this rate of ionization loss is maintained for a certain path length, one can rule out a singly charged particle, and be confident that the track is due to a helium nucleus.

In our preliminary search, we wished to pick up every track whose length exceeds 5 mm per emulsion and which might be due to helium or heavier nuclei. The price which must be paid in order to reduce to a minimum the danger of missing He tracks is the admission to one's initial track collection of a large number of tracks which, upon further scrutiny, turn out to be due to *singly* charged particles. Thus, our first recognition of a track as being *possibly* due to relativistic helium was based upon its grain density being anywhere near four times the minimum for singly charged particles. To be safe, we adopted a grain density two-and-a-half times the minimum as our lower limit for recording a track.

Out of some 15 000 tracks which were encountered and examined, $\sim$ 1600 met our dip criterion and also had at least a fair chance of being due to relativistic helium nuclei. These were grain counted, and then those which were still eligible were followed through the stack until they came to rest by ionization, or ended in a star, or left the stack.

The great majority—nearly 1200 tracks—either came to rest by ionization or else changed their grain density so markedly with range that they could be confidently ascribed to singly charged particles. 328 had to be attributed to relativistic He nuclei on the basis of their ionization vs. range; and 136, which left the stack, did not change their grain density sufficiently over the available path length to reveal their charge with certainty. These remaining 136 tracks were subjected to multiple Coulomb scattering measurements. Now, such measurements are by no means free from error. However, for our purposes, the error would have to be at least as large as a few hundred percent in order to cause a confusion of a fast helium track with that of a singly charged particle.

Table I compares the deflections of singly charged particles with those of α-particles having the same ionization loss.

TABLE I. – *Mean deflection per of particle/ Mean deflection of « fast » α.*

	$\bar{\alpha}(Z=1)/\bar{\alpha}(Z=2)$		
I/I_{min}	3	4	5
p	64	94	126
d	32	47	63
t	21	31	42
α		1	

Ideally, one would expect that at 4 times the minimum ionization, α-particle scattering would exceed the scattering of protons or deuterons or tritons by the factors shown in the Table. Even if a gross error in ionization measurement could give an estimate of 4 × minimum when the particle was really ionizing at 3 × minimum, a deuteron would still differ by a factor of 30 from an α-particle. In practice, the α-particles in our collection have a mean deflection barely distinguishable from the so-called noise, ($\bar{D} \sim 0.12$ μm) whereas the singly charged nuclei produce deflections well above the noise.

Of the 136 tracks for which we had to measure Coulomb scattering, 81 turned out to be due to helium; 49, to singly charged particles, and 6 remained uncertain (mainly because they occurred near the corner of an emulsion). Altogether, 412 helium tracks were identified. For zenith angles between 0° and 60° we found 340 helium tracks.

We corrected the observed intensity at altitude for the following effects.

Attenuation of helium nuclei above the stack, using a mean free path in air of (45 ± 5) g/cm².

Our *detection efficiency* was determined by having another scanner independently search the same volume for 56% of our total volume. All the scanners but one missed less than 4%. One observer missed at a rate of 18%, so her volume was completely re-scanned by one of the efficient observers.

We corrected for the contribution of *secondary* He *nuclei* produced by fragmentation of heavier primary nuclei above the stack. We estimated and

TABLE II. – *Uncertainty in* He *flux* (%).

Statistics	± 5.4
Error in the attenuation factor	5.8
Error in scanning efficiency	1.0
Geometry	1.0
Heavy primary nuclei contribution	1.8
Emulsion thickness	3.5
Rise and fall	1.0
Identification efficiency	1.0
Standard error in flux	± 9.1%

corrected for the number of helium nuclei incident during the *rise and fall* of the balloon.

Our value of the primary He flux at the top of the atmosphere, averaged between 0° and 60° of zenith angle, is (22.3 ± 2.0) peters.

Table II shows how we arrived at an estimate of the uncertainty. These numbers, except for the first, are *errors in* the correction, factors, and *not* the magnitudes of the corrections themselves.

If we combine our measured intensity with those at 41° and 55° to fit the numbers to a power spectrum, we obtain (see Table III):

$$N_{>W} = (350 \pm 50)\, W^{(-1.45 \pm 0.15)} \text{ peters},$$

where W is the total energy in GeV.

This may be compared with the power formula arrived at by FOWLER and WADDINGTON (F.W.), who based their result on two integral fluxes at two low cut-off energies.

TABLE III. – *Spectrum of primary* He (*).

λ	$W_{\min}$	I
10°	6.98	23.7 ± 2.2
41°	2.53	90 ± 3
55°	1.23	320 ± 23

$$N_{>W} = \begin{cases} (350 \pm 50) W^{-1.45 \pm 0.15} & \text{(N.R.L.)} \\ (370 \pm 90) W^{-1.50 \pm 0.18} & \text{(F.W.)} \end{cases}$$

(*) *Un*corrected for *secondary* helium, to permit comparison with results of others workers.

Because of the uncertainty in the absolute primary fluxes of hydrogen at various latitudes, it does not appear feasible at present to give a definitive figure for the relative abundance of helium and hydrogen in the cosmic radiation. We can, however give a reasonable lower limit by combining our results with those of MCCLURE which were obtained at the some location and time. MCCLURE gives an upper limit of 145 peters for the hydrogen flux at this latitude. Thus, the ratio of He to H probably exceeds 1 to 6.5.

SUPPLEMENTO AL VOLUME VIII, SERIE X
DEL NUOVO CIMENTO

N. 2, 1958
2° Trimestre

The Light and Medium Nuclei in the Cosmic Radiation.

C. J. WADDINGTON

H. H. Wills Physical Laboratory - Bristol

As part of an extensive investigation into the complete charge spectrum of cosmic ray nuclei the relative abundances of the L ($3 \leqslant Z \leqslant 5$) and M ($6 \leqslant Z \leqslant 9$) nuclei have been determined. This investigation used a nuclear emulsion detector. The results obtained using a densitometer on the H-nuclei ($Z \geqslant 10$) will be reported by R. R. HILLIER (*).

The stack of stripped nuclear emulsions used was exposed for 5.75 hours at a height of 106 000 feet over Northern Italy, and the cut-off energy for multiply charged particles has been determined to be (1.55 ± 0.06) GeV per nucleon [1]. It consisted of 80 600 μm G-5 emulsions measuring 15 cm $\times$ 20 cm and was normally developed.

Each emulsion had a line scan made across it, 1 cm below the top edge, for tracks with a grain density more than seven times minimum and a length greater than 3 mm per plate. These tracks produced by heavy primaries were identified from a visual estimate of the multiple scattering and by tracing them through the emulsions. Only tracks longer than 6 mm per plate and with zenith angles of less than 60° were considered in this part of the investigation.

The ionization, and thus the charges, of the L and M-nuclei, were measured by two statistically independent methods, δ-ray counting and blob-gap counting [2] on the cores of the tracks.

Blob-gap counts were originally made on all the tracks of particles whose charges had been estimated from a preliminary δ-count to be seven or less. Similar measurements were then made on all the remaining tracks in one half of the stack, characterized by its small grain size, whose producing par-

(*) In this issue, p. 520.

ticles were shown by the densitometer measurements to have charges of less than ten. The distribution of the blob-gap density g, is shown in Fig. 1, where those particles of charge seven and greater have been increased by a factor

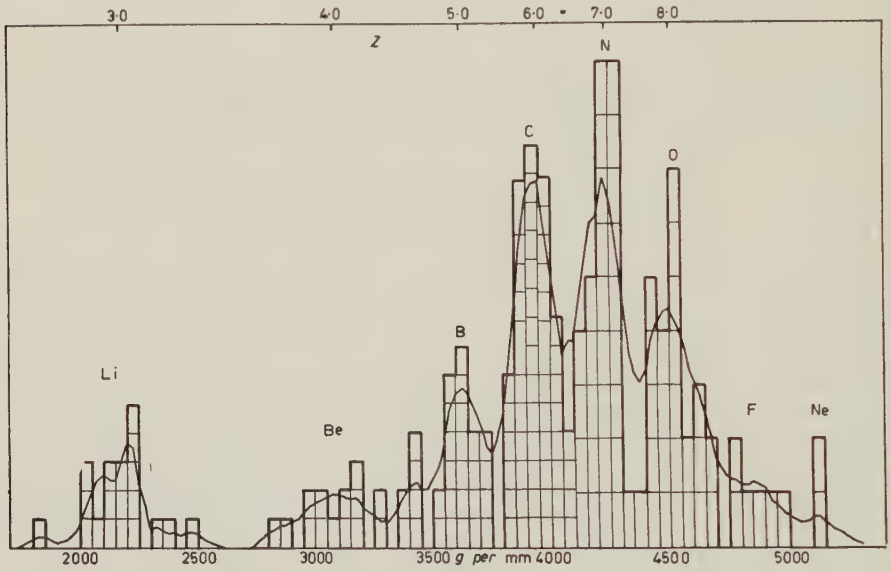

Fig. 1.

of 1.87 to allow for the unmeasured particles. The curve shown in this figure was obtained by representing each determination as a triangle of constant area and base width equal to twice the standard deviation. The charge scale was calibrated from measurements made on protons and α-particles, and from the observation of charge indicating interactions, Fig. 2.

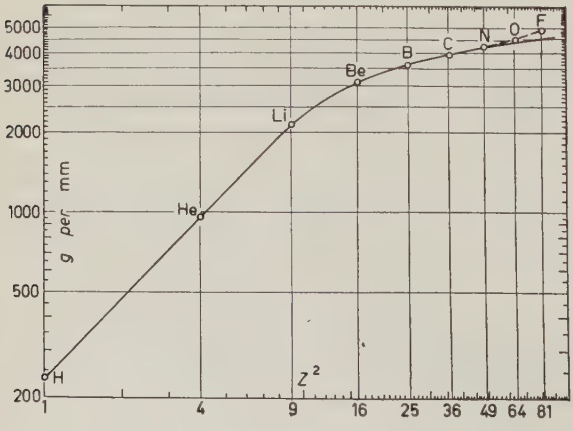

Fig. 2.

δ-ray counts were made on all the tracks of those particles which, from the blob-gap measurements, had $5 \leqslant Z \leqslant 10$, but care was taken to ensure that the precise charge derived from these measurements was not known while the δ-ray den-

sity was being determined. The results of these counts are shown Fig. 3. The charge calibration was based on measurements made on particles producing charge indicating interactions.

A comparison of the measurements is shown in Fig. 4, which gives a plot of the square root of the δ-ray density, $\sqrt{N_\delta}$, against the blob-gap density. In this figure lines of half integral charge are shown, so that points lying inside completed squares bounded by these lines represent tracks on which the same integral charge was measured by both methods. The overall agreement between these measurements is an important check on the correctness of the derived spectra.

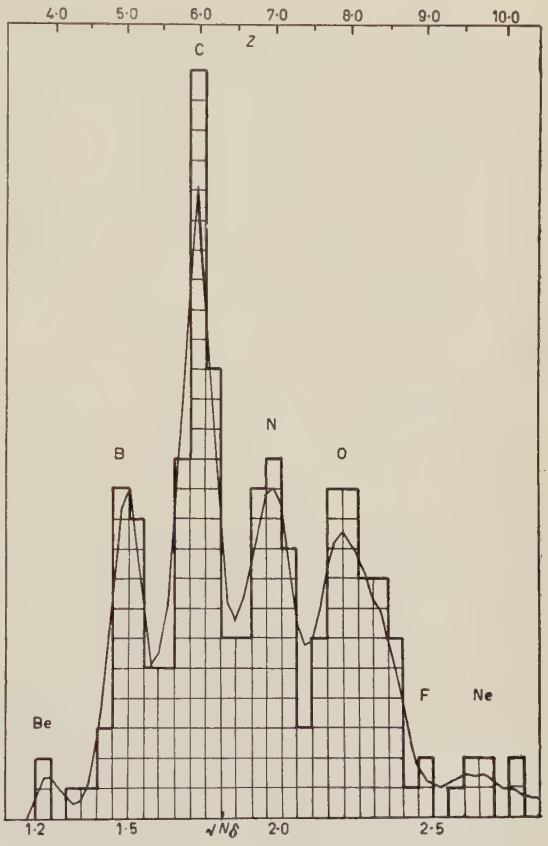

Fig. 3.

The numbers of particles of each charge found by these measurements are shown in Table I. In this table the numbers of particles on which the blob-gap measurements were made are given in brackets. Also shown are the mean numbers $\overline{N}$, of particles of each charge. To these mean numbers a correction for scanning loss, determined by rescanning, has to be added of 40% for Lithium and about 5% for the other nuclei. After a

TABLE I. – *Numbers of particles found from δ-ray counts N_δ, and blob-gap counts N_g.*

	Li	Be	B	C	N	O	F	$Z \geqslant 10$ (*)
N_δ	20	18	30	64	41	48	9	45
N_g	20	15	29	56 (53)	54 (28)	46 (24)	10 (6)	45
$\overline{N}$	20	16.5	29.5	60	47.5	47	9.5	45

(*) Determined from densitometer measurements.

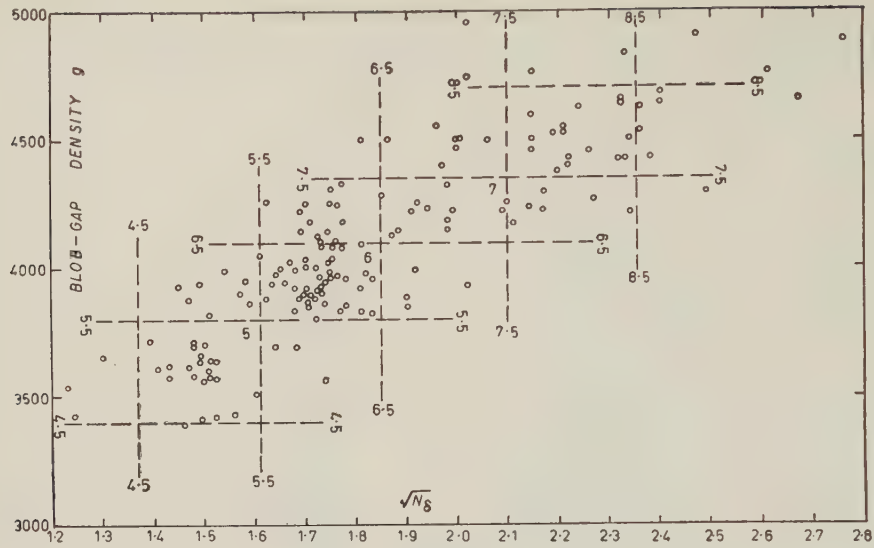

Fig. 4.

further correction for those particles that entered during the ascent of the stack to ceiling altitude, the observed fluxes of the L, M and H-nuclei were:

$$J_{L^x} = (2.02 \pm 0.24) \text{ particles/m}^2 \text{ sr s},$$

$$J_{M^x} = (4.29 \pm 0.33) \text{ particles/m}^2 \text{ sr s},$$

$$J_{H^x} = (1.35 \pm 0.16) \text{ particles/m}^2 \text{ sr s}.$$

These values have been corrected to the top of the atmosphere through 4.8 g/cm² of emulsion and 12 g/cm² of air, using the Bristol fragmentation probabilities [3], and gave values of:

$$J_{L^0} = (2.3 \pm 0.4) \text{ particles/m}^2 \text{ sr s},$$

$$J_{M^0} = (6.1 \pm 0.6) \text{ particles/m}^2 \text{ sr s},$$

$$J_{H^0} = (2.5 \pm 0.3) \text{ particles/m}^2 \text{ sr s},$$

so that $J_{L^0}/J_{M^0} = 0.37 \pm 0.07$ and $J_{H^0}/J_{M^0} = 0.41 \pm 0.06$.

The value obtained for J_{L^0}, and thus for J_{L^0}/J_{M^0}, is very dependent on the values used for these fragmentation probabilities. If, for example, those obtained by Noon and Kaplon [4] had been used instead, then J_{L^0} would be near zero. However, the values given for the Bristol figures are believed to be upper limits, and therefore the true value of J_{L^0} is unlikely to be much less than the quoted value.

REFERENCES

[1] P. H. Fowler and C. J. Waddington: *Phil. Mag.*, **1**, 637 (1956).
[2] P. H. Fowler and D. H. Perkins: *Phil. Mag.*, **46**, 587 (1955).
[3] P. H. Fowler, R. R. Hillier and C. J. Waddington: *Phil. Mag.*, **2**, 293 (1957).
[4] J. H. Noon and M. F. Kaplon: *Phys. Rev.*, **97**, 769 (1955).

SUPPLEMENTO AL VOLUME VIII, SERIE X
DEL NUOVO CIMENTO

N. 2, 1958
2° Trimestre

The Flux of Medium and Heavy Nuclei in the Cosmic Radiation Near the Equator.

C. J. WADDINGTON

H. H. Wills Physical Laboratory - Bristol

A determination has been made of the fluxes of the M ($6 \leqslant Z \leqslant 9$) and H ($Z \geqslant 10$) nuclei in the primary cosmic radiation, using a stack of nuclear emulsions exposed over Guam ($\lambda = 4°$ N), at an altitude of 101 000 feet for 7 hours.

The emulsions of this stack were scanned for the tracks of heavy nuclei with a length of more than 4 mm per emulsion, and a determination of the charge made by δ-counting. The quality of these δ-counts was such that a clear resolution was achieved between particles of the various charge groups.

The fluxes of the M and H nuclei in the emulsions, and extrapolated through 17 g/cm² of air to the top of the atmosphere were:

$$J_{M^x} = (0.66 \pm 0.08) \text{ particles/m}^2 \text{ sr s}$$
$$J_{H^x} = (0.18 \pm 0.04) \text{ particles/m}^2 \text{ sr s}$$

$$J_{M^0} = (0.95 \pm 0.11) \text{ particles/m}^2 \text{ sr s}$$
$$J_{H^0} = (0.35 \pm 0.08) \text{ particles/m}^2 \text{ sr s}$$

and

$$J_{H^0}/J_{M^0} = 0.37 \pm 0.09 .$$

It can be seen that the ratio of J_{H^0}/J_{M^0} is the same as that found at lower cut-off energies (see previous paper), indicating that the energy spectra of the two charge groups are the same over most of the latitude sensitive region, in disagreement with the prediction of SINGER [1].

Using the figures given by JORY [2] the vertical cut-off energy over Guam for multiply charged particles would appear to be about 7.2 GeV per nucleon, but is somewhat uncertain due to the controversy regarding the applicability

of geomagnetic theory. Assuming this value of the cut-off energy, these flux values together with those obtained over Northern Italy (see previous paper) at a cut-off energy of 1.55 GeV per nucleon [3], give the energy spectrum of the M and H nuclei. This integral spectrum is commonly expressed in the form $N(>E) = C/(m_0c^2+E)^n$, where C and n are constants, $N(>E)$ is the number of particles with an energy greater than E, and E is the kinetic energy in Gev per nucleon. For the M nuclei $C = 25.4^{+3.6}_{-4.2}$ and $n = 1.57 \pm 0.12$, while for the H nuclei $C = 11.3^{+2.8}_{-4.7}$ and $n = 1.66 \pm 0.21$.

WEBBER [4] has made a more recent calculation of the cut-off energies, and suggests a value of 7.6 GeV per nucleon. In this case n for the M and H nuclei is 1.50 ± 0.12 and 1.59 ± 0.20 respectively.

It may be noted that these values are in good agreement with that derived for the α-particles [3].

REFERENCES

[1] S. F. SINGER: *Progress in Elementary Particle and Cosmic Ray Physics*, Vol. **4** (Amsterdam, 1958).
[2] F. S. JORY: *Phys. Rev.*, **102**, 1167 (1956).
[3] P. H. FOWLER and C. J. WADDINGTON: *Phil. Mag.*, **1**, 637 (1956).
[4] W. WEBBER: in this issue, p. 532.

SUPPLEMENTO AL VOLUME VIII, SERIE X
DEL NUOVO CIMENTO

N. 2, 1958
2° Trimestre

The Heavy Nuclei in the Cosmic Radiation.

R. R. Hillier and V. Y. Rajopadhye

H. H. Wills Physical Laboratory - Bristol

The charges of relativistic nuclei in nuclear emulsions can be estimated by measuring the δ-ray densities along their tracks. In view of the difficulty experienced in visually counting δ-rays on the tracks of nuclei with $z > 10$, an attempt has been made to measure these δ-ray densities using a photometric densitometer.

The densitometer is illustrated in Fig. 1. The track under observation is scanned by the rapidly rotating cuboid and the voltage from the photomultiplier tube is applied to the horizontal plates of the cathode ray oscilloscope. A typical trace on the oscilloscope is shown in Fig. 2.

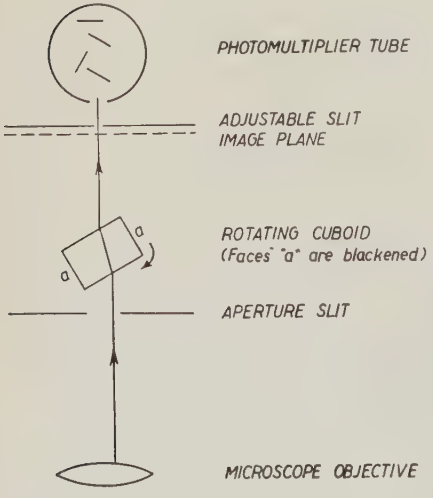

Fig. 1. – Diagram of the photometric densitometer.

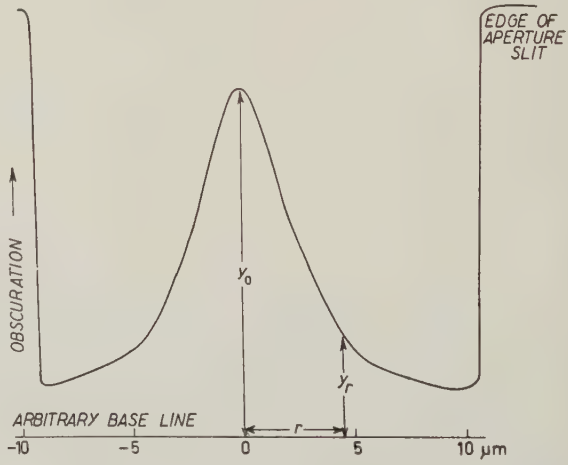

Fig. 2. – An illustration of a typical trace on the oscilloscope.

The basic principle of the method is to measure the ratio of the obscuration produced by the δ-rays to that produced by the core of the track. In Fig. 2, one measure of this ratio R is $(y_r - y_\infty)/(y_0 - y_\infty)$; y_∞ is not shown, but it is the value of y at large distances of r. The cores of the tracks in this region of the spectrum are saturated with silver grains, and their blackness does not vary with the charge. Thus the ratio, R, is a measure of the δ-ray density and, from it, a quantity has been calculated which is proportional to the charge of the nucleus.

This experiment was carried out in the same stack used by WADDINGTON, and is described in the previous paper. The results of measurements on 160 tracks are shown in Fig. 3*a*. The δ-ray density was averaged over three millimetres of each track. A statistical analysis of the readings showed that the standard deviation on a measurement was $\pm\frac{1}{2}$ charge throughout the spectrum.

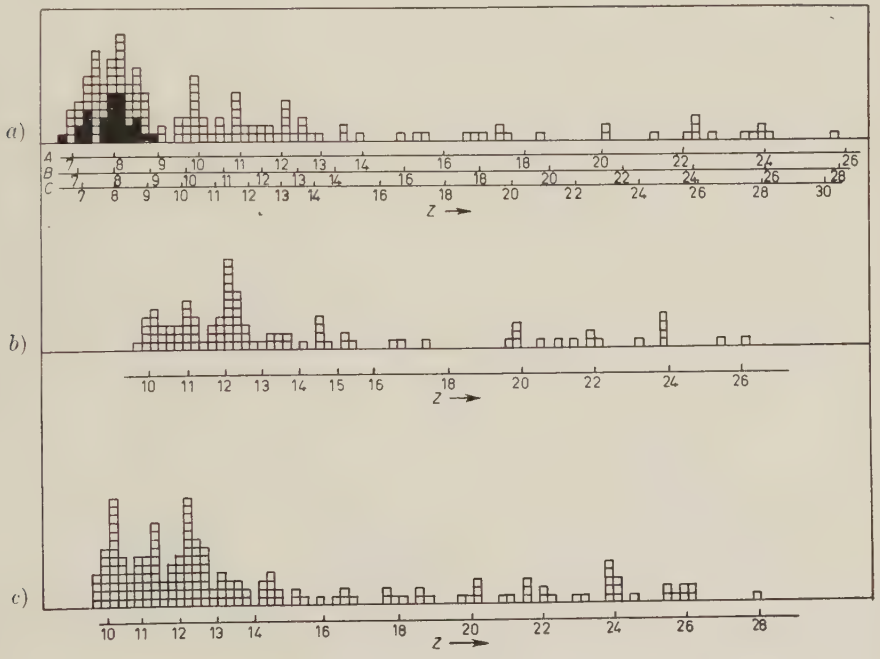

Fig. 3. – Histogram of the results. The charge scales are explained in the text.

The greatest difficulty in the experiment lies in assigning an accurate charge scale. The tracks which are shown as shaded squares have been measured by WADDINGTON and are believed to be due to oxygen nuclei. If the group of tracks at the upper end of the spectrum could be identified, a charge scale could be interpolated. There is no way of definitely identifying these tracks,

but the three charge scales which are drawn, show the results of the most plausible assumption as to their nature. In this spectrum the flux, in peters, of any group of nuclei can be obtained by multiplying the number in the group by the factor, 0.014.

Fig. 3*b* shows the results of an identical experiment carried out in a larger stack of emulsions which had been exposed under similar conditions over Northern Italy a year later. These results are not yet complete but they are shown in order to improve the poor statistics. Only one of the possible charge scales has been drawn. The combined results from the two stacks are shown in Fig. 3*c*.

Despite the lack of a reliable charge scale, some conclusions can be drawn from the results. It is clear that there are periodic fluctuations at the high end of the spectrum; these are most likely to be an « odd-even » effect. The variations in the abundances of the different elements are very much smaller than those in cosmic abundances. In this respect the spectrum shows more resemblance to the fragmentation spectrum from a heavy element such as iron. It may be pointed out that, at exposure, there were 15 g/cm^2 of matter between the top of the atmosphere and the regions of the emulsions where the spectrum was measured. It is not yet possible to estimate the detailed effects of fragmentation, but approximately six of the heavy nuclei in Fig. 3*c* could have come from the fragmentation of iron nuclei in this overlying matter.

SUPPLEMENTO AL VOLUME VIII, SERIE X
DEL NUOVO CIMENTO

N. 2, 1958
2° Trimestre

On the Charge and Energy Spectrum of Heavy Primaries.

R. Cester, A. Debenedetti, C. M. Garelli, B. Quassiati
L. Tallone and M. Vigone

Istituto di Fisica dell'Università - Torino
Istituto Nazionale di Fisica Nucleare - Sezione di Torino

Summary (*). — The relative abundance and energy spectrum of heavy primaries in the cosmic radiation were derived using 529 tracks found in two stacks flown at high altitude at a mean geomagnetic latitude of 46° North. The amount of atmosphere and of packing material above the scanned sections of both stacks was 17 g/cm². A good resolution was obtained in the range $3 \leqslant Z \leqslant 10$, while in the range $Z > 10$ the uncertainty was $\Delta Z = \pm 1$. In order to check the resolution between boron and carbon, gap-length measurements were made on 65 boron and carbon tracks. The results of the two methods are in good agreement. All tracks were traced through the stack and a total of 331 nuclear interactions found, in order to derive the interaction mean free path and the fragmentation probabilities. The results on the relative abundance of the three charge groups (light $3 \leqslant Z \leqslant 5$ (L), medium $6 \leqslant Z \leqslant 9$ (M), heavy $Z \geqslant 10$ (H)) on a total of 242 tracks whose angle of incidence to the vertical was less than 30° are the following:

	Flight altitude	Top of the atmosphere
N_L/N_M	0.46 ± 0.07	0.30 ± 0.09
N_H/N_M	0.40 ± 0.04	0.51 ± 0.11

To obtain the energy spectrum three types of measurements on 275 tracks were made: *a*) relative track to track scattering on the α-particles ejected in the interactions. *b*) mean opening angle of fragmentation products. *c*) multiple scattering on a few very flat primary tracks. The integral spectrum in the range 1.5 GeV ÷ 100 GeV agrees fairly well with a power law of the type: $N(E) = C/(m_0c^2+E)^n$, with $n = 1.54^{+0.16}_{-0.13}$.

(*) The complete paper has been published in *Nuovo Cimento*, **7**, 371 (1958).

SUPPLEMENTO AL VOLUME VIII, SERIE X
DEL NUOVO CIMENTO

N. 2, 1958
2° Trimestre

The Charge Spectrum of Light Elements at 41° N Geomagnetic Latitude.

B. J. O'Brien, A. J. Herz and J. H. Noon

The F.B.S. Falkiner Nuclear Research and Adolph Basser Computing Laboratories, School of Physics (*), *The University of Sydney - Sydney, Australia*

1. – Introduction.

Following our recent work on the cosmic-ray flux of light elements (already published [1, 2]) we decided, because of the great importance of obtaining an accurate light-element charge spectrum, to repeat and extend our measurements, and to use a number of different and independent methods of identification. The results are reported in this paper.

Details of the balloon flight, the stack and the method of scanning have already been given in our previous publication [1]; we therefore give only a summary here.

The stack, consisting of 15 sheets of 600-μm Ilford G-5 emulsion without support, 9 in. × 10 in., was flown for six hours at an altitude of 110 000 feet (8.6 g/cm²). The average thickness of packing material was 2 g/cm², and the total effective amount of material above the stack was less than 11 g/cm². The flight took place at San Angelo, Texas, geomagnetic latitude 41° N, on 6th February 1957. The emulsion sheets were vertical during the flight.

2. – Scanning and selection criteria.

One of the outer plates was scanned for tracks satisfying the following criteria: projected zenith angle $\leqslant 45°$, projected length per plate $\geqslant 2$ mm, grain density $\geqslant 10$ times plateau value (200 grains counted). Tracks were

(*) Also supported by the Nuclear Research Foundation within the University of Sydney.

accepted for analysis only if their projected zenith angle was less than 30°, and their length per plate more than 3 mm. These criteria led to the acceptance of all relativistic particles of charge 4 or greater, but tracks of relativistic Li nuclei were rejected. An additional scan in which all tracks with a grain density of more than seven times the plateau value were accepted was made on part of the same plate in order to find the tracks of Li nuclei.

The tracks of slow particles were eliminated by following all tracks satisfying the scanning criteria over a range of more than 4.5 cm. All non-relativistic particles having a grain density $g \geq 10 g_{pl}$ in the scanning plate either stop or show a significant increase in grain density over this range.

Further details of our scanning and selection methods were given in our previous paper [1].

A total of 144 tracks of relativistic nuclei in the range $4 \leqslant Z < 10$ were found in this way; all of these were included in the charge distribution obtained by δ-ray counting, the distributions obtained by other methods are based on an (unbiassed) sample of 86 tracks.

The average numbers of relativistic tracks found satisfying our acceptance criteria were 0.41 per cm² (30°, 3 mm) and 0.67 per cm² (45°, 2 mm).

3. – Delta-ray counting.

Fig. 1 shows the results of the δ-ray counts on all the 144 tracks. Each track is plotted as a triangle of unit area with base width of two standard deviations: thus the area under the curve, not the height of the peak, is a measure of the abundance of each charge. In almost all cases the number of

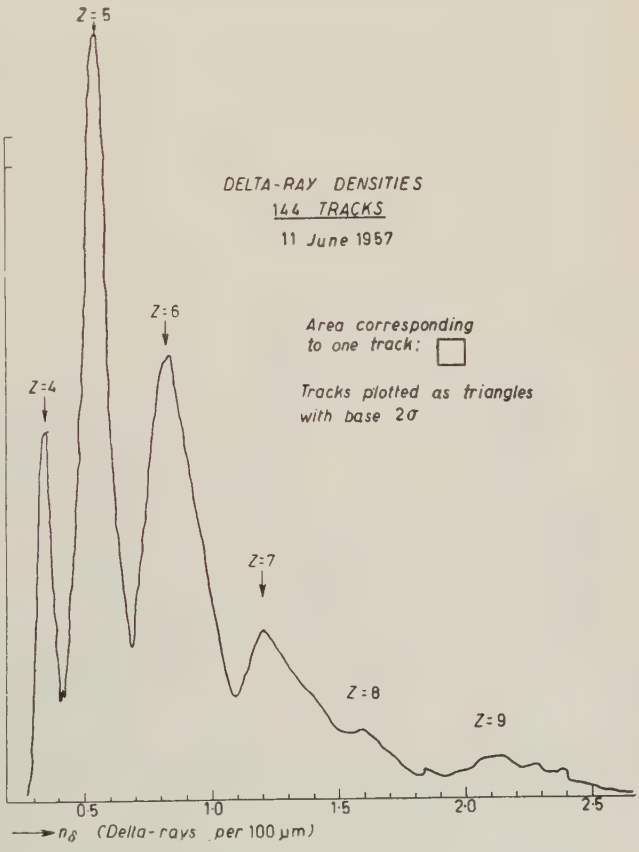

Fig. 1. – Distribution of δ-ray densities.

δ rays counted was 50, so that the δ-ray density obtained for each track had a relative standard deviation of 14%.

As is clear from the appearance of Fig. 1, the resolution obtained in the critical region around charges 5 and 6 is very good. The method of assigning the charges as given in Fig. 1 will be discussed in Sect. 4 below, but it can already be pointed out at this stage that in view of the resolution obtained by means of δ-ray counting the centre of each resolved peak in Fig. 1 must correspond to an integral value of Z.

4. – Charge calibration.

A basic problem in nuclear-emulsion work on heavy nuclei is to find a reliable method of assigning charges to the peaks found in the distributions of δ-ray densities and other track characteristics. The most satisfactory way is to make use of the fact that in some collisions of fast heavy nuclei with single nucleons in the emulsion the incident nucleus breaks up completely into singly and doubly-charged particles so that it is possible, in principle, to find the charge of the incident nucleus by adding up the charges of the fragments. However, if one or more of the fragments are singly-charged it is possible that they came from the struck nucleus or that they are mesons produced in the collision; in a reliable calibration event, therefore, all the fragments should be α-particles or heavier nuclei.

We have found only one such event: a break-up of the type Be $\rightarrow 2\,\alpha$. The event was very carefully examined by five different observers all of whom agreed that the secondaries were two α particles, and that there were no other secondaries. The primary must therefore be a Be nucleus, and this leads to the assignment shown in Fig. 1.

Our second method of charge calibration is based on measuring the total gap length and the Fowler-Perkins parameter on slow identified protons at residual ranges at which these quantities have values corresponding to 16 $\times$, 25 $\times$, and 36 $\times$ minimum ionization. We also measured these characteristics on 86 of the 144 tracks used in the analysis (see Sect. 5 and 6 below) and we were thus able to assign values of charge to the peaks in the δ-ray distribution.

In calculating the residual ranges at which the tracks of slow protons have the same characteristics as relativistic heavy nuclei of various charges, it is important to use the « restricted » rates of energy loss, that is rates of energy loss in AgBr to electrons which lose most of their energy in the grain in which they were produced. This requirement means that only those elementary acts are considered in which electrons with energies below a certain limit are produced.

Values of the restricted rates of energy loss have been given by BARKAS and YOUNG [3], who used an upper limit to the energy transfer of 5 keV and

an average ionization potential for AgBr of 376 eV. Recent work by ALEXANDER and JOHNSTON [4] suggests, however, that energy transfers up to 30 keV should be admitted and that the average ionization potential should be 537 eV.

In our calculations we have used both sets of values and, in addition, the combination of a maximum energy transfer of 30 keV and an ionization potential of 376 eV. The resulting restricted rates of energy loss are shown in Fig. 2. Also shown in Fig. 2 are the calculated minimum restricted rates of energy loss for various charges and the residual ranges at which proton tracks should have the corresponding characteristics (the fourth value of the proton ranges was obtained by combining the 30 keV/537 eV minimum value with the 5 keV/376 eV curve « *a* », to allow for the possibility that the parameters may be different at high and low primary-particle velocities.

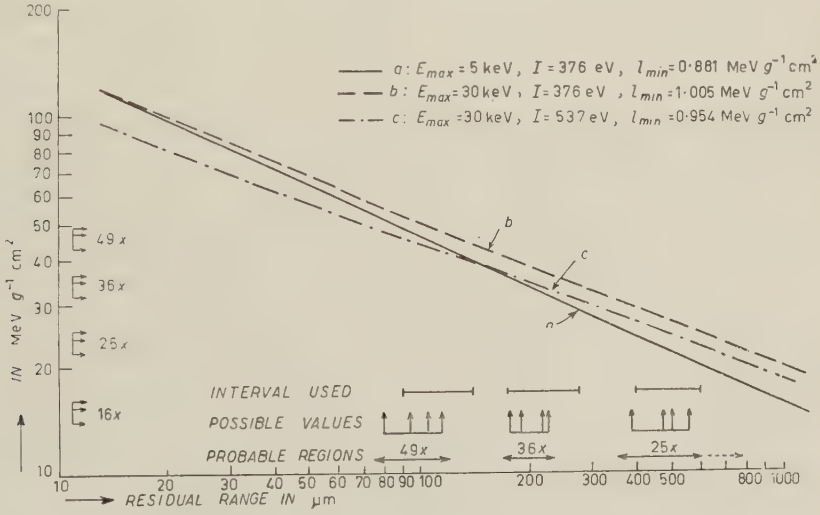
a: E_{max} = 5 keV, I = 376 eV, l_{min} = 0·881 MeV g^{-1} cm^2
b: E_{max} = 30 keV, I = 376 eV, l_{min} = 1·005 MeV g^{-1} cm^2
c: E_{max} = 30 keV, I = 537 eV, l_{min} = 0·954 MeV g^{-1} cm^2
IN MeV g^{-1} cm^2
49x
36x
25x
16x
INTERVAL USED
POSSIBLE VALUES
PROBABLE REGIONS
RESIDUAL RANGE IN μm

Fig. 2. – Restricted rates of energy loss for protons.

Fig. 2 shows that whatever parameters are used, the residual proton ranges corresponding to charges 5, 6 and 7 are well-separated and that the range corresponding to charge 6 is defined particularly well.

The range intervals actually used in the proton calibration were based on the tables of BARKAS and YOUNG [3] (curve « *a* » in Fig. 2).

5. – Measurement of Fowler-Perkins coefficient.

A triangle plot of the results of measurements of the Fowler-Perkins coefficient [5] is given in Fig. 3 which also shows the values for 16, 25, 36 and 49 times minimum ionization as deduced from the calibration protons.

In Fig. 4 are shown the values of the δ-ray densities plotted against the corresponding values of the Fowler-Perkins coefficient. The proton charge

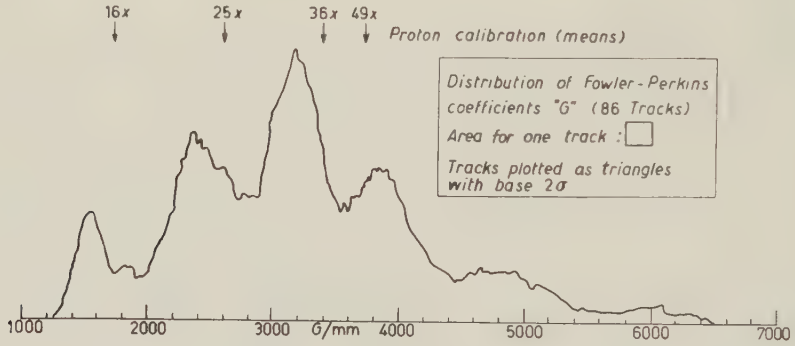

Fig. 3. – Distribution of Fowler-Perkins coefficients.

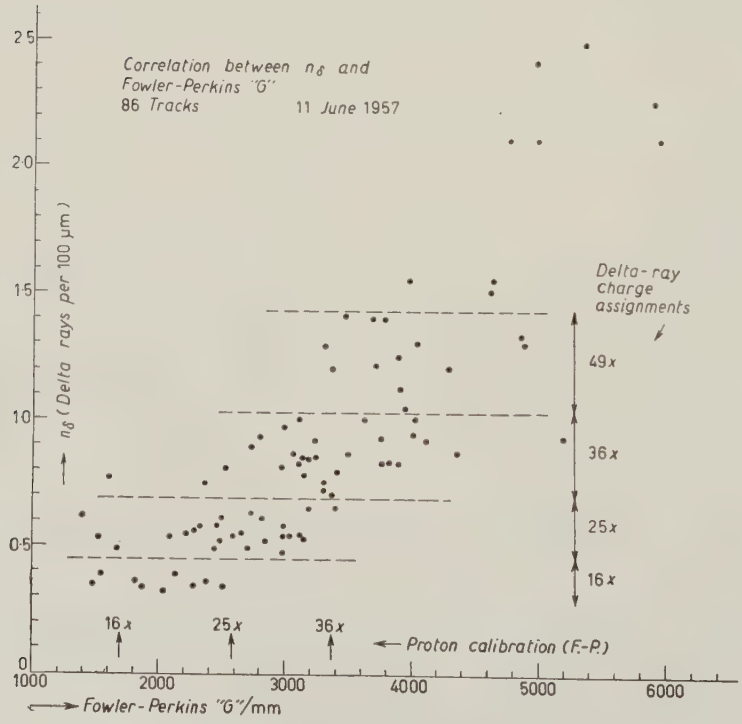

Fig. 4. – Correlation between δ-ray density and Fowler-Perkins coefficient.

calibration and the charge assignment as given in Fig. 1 are included for comparison.

6. – Integral-gap-length measurements.

Measurements of the integral gap length were made by means of a « gap counter » developed in our laboratory and similar to those in use elsewhere. The results of these measurements are given, again as a triangle plot, in Fig. 5.

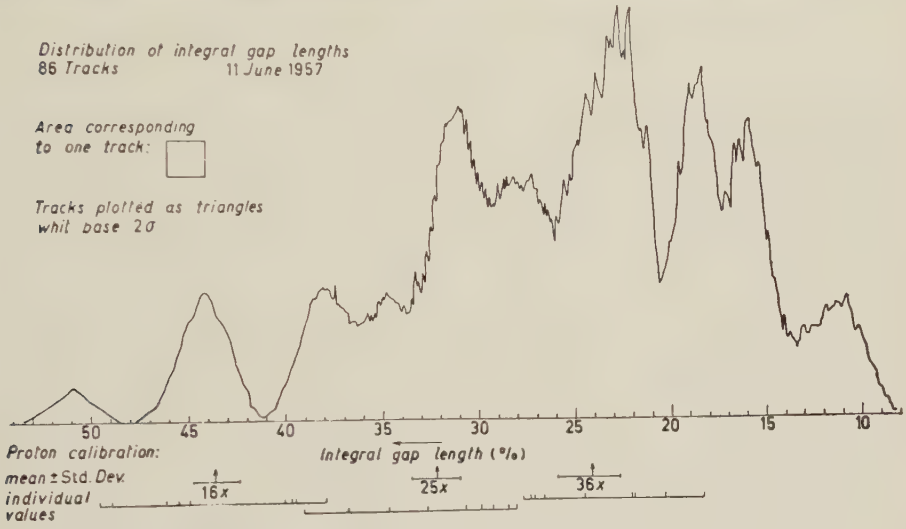

Fig. 5. – Distribution of integral gap lengths.

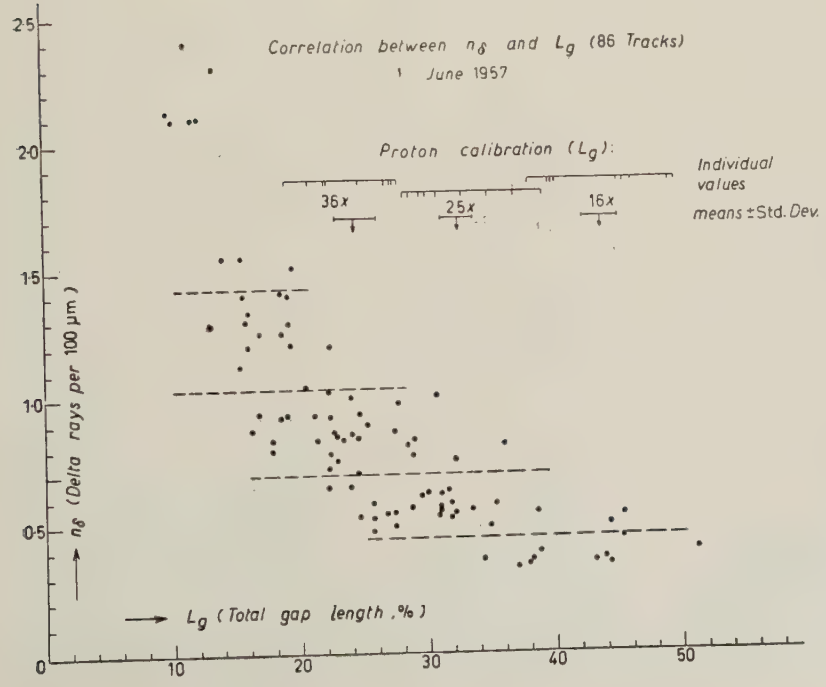

Fig. 6. Correlation between δ-ray density and integral gap length.

Also shown in Fig. 5 are the mean values for changes 4, 5 and 6 obtained from our nine calibration protons, and the individual values given by these protons.

In Fig. 6 the correlation between the δ-ray counts and the integral-gap-length measurements is shown, again confirming the charge assignment as given in Fig. 1.

7. – Abundance of the very heavy nuclei.

In addition to the 144 tracks of nuclei with $Z < 10$, we also found the tracks of thirty nuclei with $Z \geq 10$ in the area scanned. At the altitude of observation the abundance ratio of the heavy to the medium nuclei as found by us is therefore 35%.

8. – Conclusions.

The charge distribution for charges in the range $4 \leqslant Z \leqslant 9$ obtained by the three methods is summarized in histogram form in Fig. 7. The δ-ray distribution is given twice: once for all the 144 tracks and once for the 86 tracks on which the other distributions are based.

The good agreement between the results obtained by widely different methods shows that there cannot have been any serious systematic error affecting one of them.

In order to find the abundance ratio of the light (Li, Be, B) to the medium (C, N, O, F) nuclei at the altitude of observation, a correction must be made for Li nuclei in the way described in our previous paper [1]. When this is done, the ratios N_L/N_M as given in Fig. 7 are obtained. We conclude that the ratio of light to medium nuclei at the altitude of observation is of the order of 0.7.

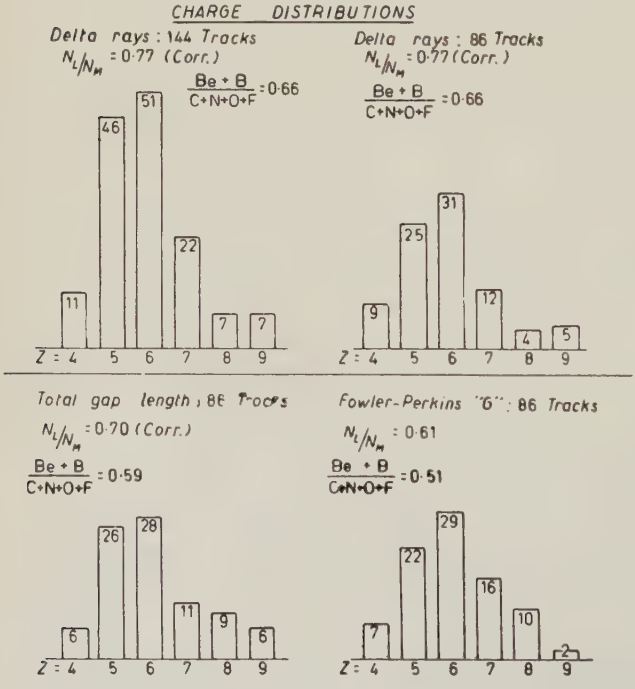

Fig. 7. – Histograms of charge distributions.

This value is far too high to allow one to admit the possibility that all the light elements are of secondary origin. The abundance of boron nuclei observed by us is large, nearly as great as that of carbon, and this is a point on which we still disagree with some other workers in this field. The reason for this disagreement remains obscure, especially as charge resolution in the region of $Z = 5$ and 6 is excellent.

* * *

We would like to acknowledge the help given to us by our team of scanners. Our thanks are due to the U.S. Office of Naval Research who arranged the ballon exposure, and to Professor H. MESSEL and the Nuclear Research Foundation within the University of Sydney for the excellent facilities put at our disposal. One of us (B. J. O'B.) is indebted to the Research Committee of the University of Sydney for a Research Studentship.

We are particularly grateful to Dr. N. SOLNTSEFF for a large number of helpful discussions.

REFERENCES

[1] J. H. NOON, A. J. HERZ and B. J. O'BRIEN: *Nuovo Cimento*, **5**, 854 (1957).
[2] B. J. O'BRIEN and J. H. NOON: *Nuovo Cimento*, **5**, 1463 (1957).
[3] W. H. BARKAS and D. M. YOUNG: *Heavy Particle Functions*, UCRL-2579 Rev., University of California, Radiation Laboratory (1954).
[4] G. ALEXANDER and R. H. W. JOHNSTON: *Nuovo Cimento*, **5**, 363 (1957).
[5] P. H. FOWLER and D. H. PERKINS: *Phil. Mag.* **46**, 587 (1955).

SUPPLEMENTO AL VOLUME VIII, SERIE X
DEL NUOVO CIMENTO

N. 2, 1958
2° Trimestre

The Charge Composition and Energy Spectra of Primary Cosmic Rays and the Energy Balance Problem (*).

W. R. Webber

Imperial College - London,

1. – Introduction.

The purpose of this paper is to summarize the results on the intensities and energy and charge spectra of the primary cosmic radiation obtained in a series of balloon flights at nominal geomagnetic latitudes of 41.5° and 4° using a Čerenkov detector [1, 2]. These results will be compared with those obtained by other observers. Finally the implications of these results will be discussed.

In order to facilitate presentation of the results and comparison with those of other observers it was found advisable to recalculate the expected geomagnetic cut-off energies for any point on the earth. These cut-off energies were determined from the eccentric dipole model of the earths geomagnetic field, the position and tilt of the dipole being determined from the data of the 1955 British Admiralty magnetic survey.

The energy spectra for the various charge components of the primary radiation as deduced in this paper have been used in a new attempt to explain the discrepancy, first noticed by Rossi [3], between the amount of energy carried into the atmosphere by the primary cosmic radiation and that dissipated in the atmosphere and underground by the primaries and various secondary components.

2. – Experimental apparatus.

The experimental flight apparatus used in these experiments is identical to that previously described [1, 2]. Briefly the detector consists of a two element Geiger counter telescope. Between these two elements is located a

(*) Work at University of Iowa assisted by joint program of Office of Naval Research and Atomic Energy Commission.

lucite Čerenkov counter. For each particle that traverses the telescope the output from the Čerenkov counter is recorded. A notation is also made when a telescope event is accompanied by the triggering of more than one counter in each telescope element or by one or more of a ring of guard counters. The outputs from the Čerenkov counter are displayed on the face of a cathode ray tube which is photographed by a continuously moving camera. The entire apparatus is enclosed in an airtight aluminium cylinder.

3. – Summary of experimental data.

The pertinent experimental data for the 3 balloon flights; 2 at $\lambda = 41°.5$ and 1 at $\lambda = 4°$ is shown in Table I and Fig. 1 and 2. The methods used

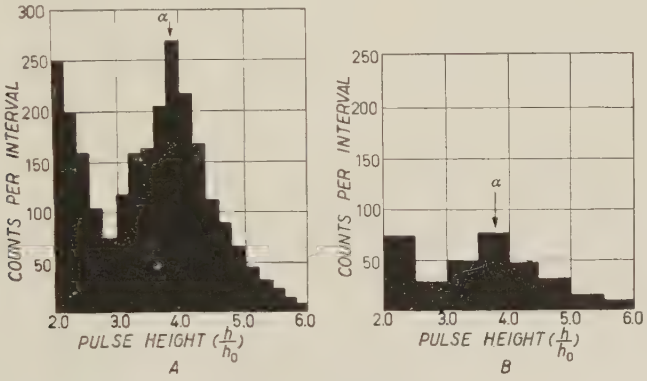

Fig. 1, *A-B*. – Pulse height distributions for α-particles at $\lambda = 41°.5$ and $\lambda = 4°$ (single particle events only).

in the reduction of this data and the discussion of errors involved are given in references [1] and [2].

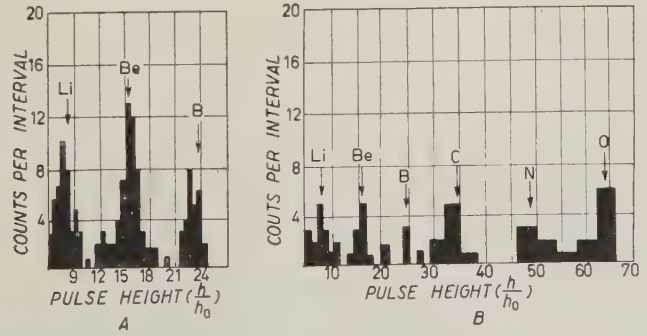

Fig. 2, *A-B*. – Pulse height distributions for light and medium nuclei at $\lambda = 41°.5$ and $\lambda = 4°$ (single particle events only).

TABLE I. – *Summary of experimental results obtained at* $\lambda = 41.5°$ *and* $\lambda = 4°$.

Date: Jan. 12 and 19, 1955 Location: San Angelo, Texas Avg. alt.: 16.0 g/cm² for 600 min (total) Avg. position at alt: 31°.9 N, 98°.5 W				Date: Feb. 20, 1957 Location: Guam, Marianas Is. Avg. alt.: 11.0 g/cm² for 190 min Avg. position at alt: 14°.5 N, 145°.8 E			
Component	Counts	Intensity at avg. alt.	Intensity at top	Component	Counts	Intensity at avg. alt.	intensity at top
protons ($Z = 1$)	21 700	615±20	480±50	protons ($Z = 1$)			
alphas	1890	57±3.5	78±5 (74)	alphas	340	10.7±1.2	13.5±1.7 (13.0)
Li	33			Li	4		
light Be	46	3.11±0.33	3.25±0.55 (2.28)	light Be	7	0.47±0.18	0.44±0.19 (0.34)
B	24			B	4		
				C	8		
medium	170	5.12±0.60	9.2±1.2	medium N	5	0.69±0.18	1.02±0.26
				O	9		
heavy ($Z \geqslant 9$)				heavy ($Z \geqslant 9$)	9	0.28±0.09	0.52±0.17

4. – Determination of the eccentric dipole (cut-off energies) for 1955.

In order to facilitate the presentation of the results obtained in this paper on the energy spectra of the various components and the energy balance of the total radiation and compare these results with those of other observers it was felt necessary to derive a set of up to date geomagnetic co-ordinates and cut-off energies for all points on the earth. During the magnetic survey of 1955 made by the British Navy, Colonial and Foreign governments and by the Carnegie Institution of Washington, measurements of the earths magnetic field were made at a large number of positions all over the world. For the analysis of these measurements it is customary to introduce a magnetic potential function. This function is the expanded in spherical harmonics, the coefficients of the expansion being called Gauss coefficients. These coefficients are adjusted so that the gradient of the magnetic potential renders a best fit to the experimentally measured field [4].

In the study of geomagnetic effects upon cosmic ray intensity, two different dipole approximations to the earths real magnetic field have been used. We shall consider here the second and higher approximation which is an

offcenter dipole located at the earths magnetic center. A line along the axis of the centered dipole determines the magnetic axis of the eccentric dipole.

The equations for the magnetic center involve the first eight Gauss coefficients and are given by SCHMIDT [5]. These Gauss coefficients have been calculated by FINCH and LEATON [6] for the year 1955. Using these Gauss coefficients and following the method of Schmidt the magnetic center and the tilt of the dipole have been calculated for 1955. These as well as other parameters relating to the earths magnetic field are shown in Table II for the years 1945 [7, 8] and 1955.

TABLE II. – *Parameters relating to the earths magnetic field in 1945 and 1955.*

Year	Geographic coordinates of magnetic center	Distance from geographic center	Geographic coordinates		
			Center pole	Off center pole	Off center dip pole
1945	14° N, 154° E	400 km	78°.6 N 70°.2 W	80°.1 N 82°.7 W	81°.0 N 120°.6 W
1955	15°.3 N, 151°.1 E	433 km	78°.2 N 69°.0 W	80°.9 N 83°.3 W	82°.2 N 142°.0 W

Note that the magnetic center continues to move away from the geographic center thus increasing the eccentricity of the dipole.

VALLARTA has shown [9] that, as a result of the off center dipole, the vertical cut-off energy now depends on geographic longitude, thus qualitatively explaining the cosmic ray longitude effect. This effect on the cut-off energies introduced by the off-center dipole can be expressed as a percentage correction on the vertical cut-off energies expected from the centered dipole [8].

The percentage correction on the vertical cut-off rigidities introduced by the eccentricity of the dipole is, following the form of JORY [8]:

$$\frac{R' - R}{R} = \frac{1}{r'^2} \frac{\cos^4 \lambda'}{\cos^4 \lambda} - (1 + 0.034 \sin (\omega - 320°) \cos^3 \lambda) ,$$

where R' is the vertical cut-off rigidity for the eccentric dipole, R is the vertical cut-off rigidity for the centered dipole, r' is the off center radius vector in units of earth radii, λ' is the off center latitude and λ and ω are the centered dipole latitude and longitude respectively. (Geomagnetic longitude is measured westward from the zero meridian passing through the centered dipole pole at 69° west geographic longitude.)

In the above expression the term $1/r'^2$ allows for the change in radius vector due to the eccentricity of the dipole and is most important at low latitudes. The term $\cos^4 \lambda'/\cos^4 \lambda$ allows for the change in apparent geomagnetic latitudes. introduced by the eccentricity of the dipole and is more prominent at higher latitudes. The third term, $0.034 \sin(\omega - 320^\circ) \cos^3 \lambda$ which was apparently not included in the Jory analysis, takes into account the fact that geographical vertical (also centered dipole vertical) is now different than magnetic vertical (the line between the observer and the magnetic center). This expression is approximately useful only near the vertical and for $\lambda < 60^\circ$ [10]. The effect of the addition of this term is to move the longitude at which the minimum cut-off energy is observed a particular geomagnetic latitude approximately 20° to the west at low latitudes [11]. At higher latitudes the effect of this term becomes more complicated (see Fig. 3).

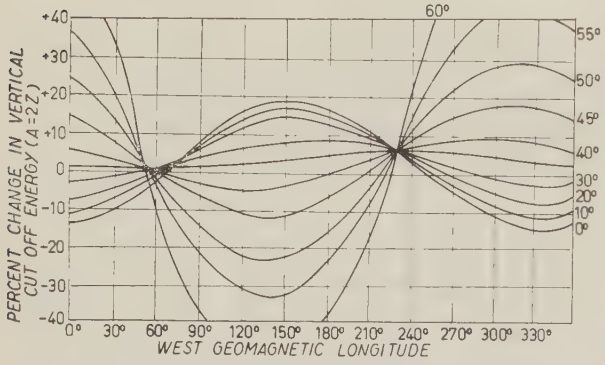

Fig. 3. – Percentage change in vertical cut-off energy per nucleon for particles with $A = 2Z$ due to the introduction of the eccentric dipole. (1955 data).

A graph of percentage change in vertical cut-off energy per nucleon for particles with $A = 2Z$ as introduced by the eccentricity of the dipole is shown in Fig. 3 for several geomagnetic latitudes in the northern hamisphere. The data are presented in this manner since actual measurements of cut-off energies can be made on these components at the present time [12-17]. Conversion to percentage change in cut-off energy for protons and cut-off rigidity can easily be made using the relativistic relation between momentum and energy.

Note that, in applying these corrections to the calculated centered dipole cut-off energies, the geomagnetic co-ordinates of points on the earths surface will have changed slightly since the determination of 1945 due to the change in the position of the centered dipole pole. To facilitate easy determination of the cut-off energies for $A = 2Z$ particles at any point in the northern hemisphere in 1955, Fig. 4 has been prepared.

It is not proposed to discuss in detail here the effect this new calculation of the expected geomagnetic cut-off energies will have on the conclusions reached by Simpson [18] and Rose [19] or more recently by the Bristol and Minnesota groups [13-15] as well as McDonald [17] that world wide discre-

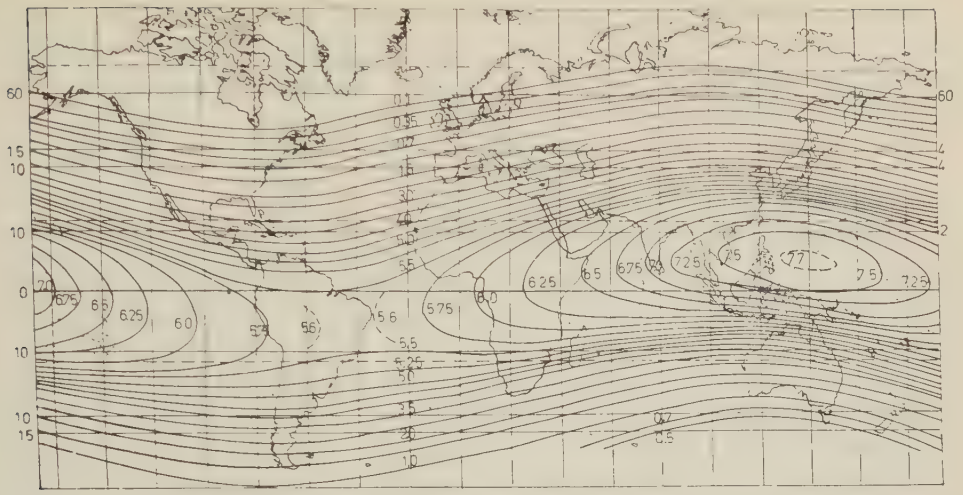

Fig. 4. – World wide cut-off energies in GeV per nucleon for particles with $A = 2Z$ based on the eccentric dipole model of the earth's 1955 magnetic field.

pancies exist between measured cosmic ray intensities and cut-off energies and those predicted by geomagnetic theory. It does appear, however, that the systematic changes in the earths magnetic field over the past 10 years can help to explain some of these difficulties.

5. – Energy spectra for the various charge components.

The intensities for α-particles, L, M and H nuclei summarized in an earlier section are plotted in Fig. 5 as a function of vertical geomagnetic cut-off

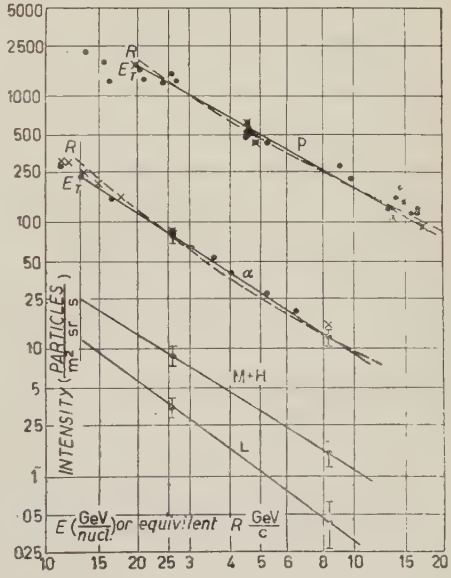

Fig. 5. – Integral intensity-energy and momentum spectra for the various charge components in the primary radiation in the latitude sensitive energy region as deduced from intensity measurements on p, α, L, M, and H nuclei at $\lambda = 41°.5$ and $\lambda = 4°$ using a Čerenkov detector and from a detailed analysis of total intensity measurements by other observers. $N_x(> E_T) = C_1/E_T^{\gamma_1}$ ---; $N_x(> R) = C_2/R^{\gamma_2}$ ---. Protons: most reliable determinations x, other determinations ●; α-particles: Waddington and Fowler [12-15] ●, McDonald [16-17] x, Shapiro [38] c.

energies. These cut-off energies were determined from the eccentric dipole analysis of the earths field discussed in the preceeding section. The experimental points are fitted with integral number spectra of the form:

$$N_x(>E_T) = \frac{C_1}{E_T^{\gamma_1}}, \qquad N_x(>R) = \frac{C_2}{R^{\gamma_2}}.$$

It is assumed in all cases that γ is a constant over the energy intervals. Likewise C_1, C_2 are constants. N_x refers to the numbers of particles/m² sr s of component x with rigidities (in GeV/c) greater than R - (pc/Ze), or total energies/nucleon greater than E_T (in GeV).

In order to determine the integral number spectrum of best fit for protons over the latitude sensitive region we have made a comprehensive analysis of the experimental measurements on the total intensity of the primary radiation at given latitudes. A standard set of corrections is then applied to these measurements in order to obtain the corresponding proton intensity. These proton intensities are then fitted with spectra of the form $N_x(>R) = C_2/R^{\gamma_2}$ and $N_x(>E_T) = C_1/E_T^{\gamma_1}$ as in the case of the heavier nuclei.

The intensity measurements analyzed fall into three broad categories. 1) Measurement of the total intensity above the atmosphere. 2) Measurement of the hard component near the top of the atmosphere. 3) Charge discriminating experiments which measure the proton component directly.

A complete list of measurements and corrections is given in Table III. The correction procedure is as follows.

1) The total intensities measured by the different observers at the highest altitudes attained are first recorded. More often than not these intensities are uncorrected for showers, interactions in the local material and other non-telescope events. In some cases trial flights have been made to determine the effect of these events [20, 21]. In other cases the frequency of these events has been measured in conjunction with the main experiment [17, 22-28]. In the remaining experiments no mention is made of these types of events [29, 30]. In any case it appears that the correction for these types of events has been made in very few of the experiments. For telescopes having similar geometrical configurations the percentage of this correction is greatest near the equator, ($\sim 25\%$) becoming less at high latitudes ($\sim 10\%$) [17, 21]. In experiments where the correction for non-telescope events is not given it is estimated by taking into account the above latitude dependence and similarities in geometrical configuration between the experiments.

2) The corrected total intensity at altitude is then extrapolated to the top of the atmosphere using the actual depth-intensity curves obtained by the various observers.

3) The total intensity thus obtained at the top of the atmosphere is then corrected for the presence of $Z > 2$ nuclei according to the spectra shown in Table IV for these nuclei. At high latitudes proper account is taken of the fact that the ionization range of many of these particles is insufficient to penetrate some of the experimental arrangements.

4) A final correction is made for albedo, both splash and reentrant. A summary of our sparse knowledge on the intensity of splash albedo as a function of latitude is given in Fig. 6 [17, 31-33]. The albedo intensities are those measured at $(10 \div 15)$ g/cm² residual atmosphere. Using the intensities as given in Fig. 6 plus additional results obtained by ANDERSON [33] which indicate *a*) that the intensity of splash albedo is roughly constant in the range $(10 \div 50)$ g/cm² residual pressure and hence is not much different at the top of the atmosphere, and *b*) that this splash albedo is apparently « absorbed » with a mean free path ~ 40 g/cm² at 41°, we are able to determine within an error of $\pm 50\%$ the amount of splash albedo passing through telescopes of various thicknesses at various latitudes at the top of the atmosphere. The work of WINCKLER and ANDERSON at 41° [31] indicated that this splash albedo was essentially isotropic at high altitudes. This means that, to a rough approximation, the reentrant albedo intensity is equal to the splash albedo intensity. The spectra derived for the various charge components are listed in Table IV. Because of the method of plotting these spectra, $N_x(> E_T)$ will be shown as a straight line for a constant γ_1, in Fig. 5 while $N_x(> R)$ will be a curved line for constant γ_2.

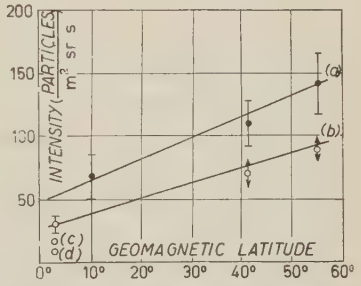

Fig. 6. Intensity of splash albedo as a function of geomagnetic latitude: *a*) upper limit for splash albedo able to penetrate 30 g/cm² of material at 15 g/cm² residual atmosphere (ANDERSON [32]); *b*) splash albedo with $E > 0.3 M_0c^2$ able to penetrate 10 g/cm² of material at 6 g/cm² residual atmosphere (MCDONALD [17]); *c*) as *b*) only $E \geqslant 0.8 M_0c^2$; *d*) as *b*) only $0.3 M_0c^2 \leqslant E \leqslant 0.8 M_0c^2$.

Several points are worthy of mention about these spectra. They are:

1) Within experimental error the integral number rigidity and number-total energy spectra for all components can be represented by the same values of γ_1 or γ_2. These values are best represented by the values $\gamma_1 = 1.45$ and $\gamma_2 = 1.38$ deduced for α-particles.

2) The energy spectrum obtained in this experiment for α-particles is in excellent agreement with the α-particle spectra of FOWLER and WADDINGTON [13] and MCDONALD [16].

TABLE III. – *Determination of primary proton intensities at various geomagnetic latitudes (all intensities in particles/m² sr s).*

Observer	E_T (GeV)	Total intensity measured at altitude	Correction for non-telescope particles	Net total intensity at altitude	Total intensity extrapolated to top of atmosphere	Correction for $Z \geqslant 2$ particles	Correction for albedo	Net proton intensity at top of atmosphere
McDONALD	17.2	—	—	140	115	—	20	95 ± 15*
RAO	16.4	272	30%	190	160	18	15	127 ± 35
POMERANTZ	16.4	265	25% (Est)	200	175	18	15	142 ± 30
WINCKLER	15.8	265	20% (Est)	210	175	20	30	125 ± 30
POMERANTZ	14.6	365	25% (Est)	275	230	21	20	189 ± 40
RAO	14.5	429	25%	320	250	21	20	209 ± 60
VAN ALLEN	13.6	280	—	280	280	22	70	188 ± 60
McCLURE	13.3	280	32%	185	160	22	20	118 ± 25*
WINCKLER	13.1	310	18% (Est)	255	205	23	35	147 ± 40
WINCKLER	9.4	460	15% (Est)	390	320	36	40	244 ± 50
VIDALE	9.0	570	25%	425	380	40	25	315 ± 60
WINCKLER	5.3	775	12%	685	635	75	50	490 ± 80
McDONALD	4.9	—	—	—	550	—	40	510 ± 60*
VIDALE	4.9	890	15% (Est)	760	670	90	30	540 ± 90
VAN ALLEN	4.6	730	—	730	730	100	130	500 ± 90
PERLOW	4.6	790	—	790	790	100	60	630 ± 70*
VAN ALLEN	2.7	1 800	—	1 800	1 800	220	160	1 420 ± 220
WINCKLER	2.6	1 980	5% (Est)	1 900	1 940	190	35	1 715 ± 220
POMERANTZ	2.4	1 680	5%	1 600	1 650	175	35	1 440 ± 150
VIDALE	2.1	1 900	10%	1 710	1 680	175	35	1 470 ± 180
DAVIS	1.9	2 060	—	2 060	1 900	—	60	1 840 ± 120*
WINCKLER	1.9	2 300	5% (Est)	2 180	2 080	205	100	1 775 ± 220
PULLAR	1.6	1 610	2%	1 580	1 630	175	35	1 420 ± 120
VAN ALLEN	1.3	2 900	—	2 900	2 900	280	180	2 440 ± 350
POMERANTZ	(1.0)	2 260	5% (Est)	2 150	2 300	175	40	2 085 ± 160

TABLE IV. – *Spectra derived for the various charge components in the primary radiation based on intensity measurements at* $\lambda = 41°.5$ *and* $\lambda = 4°$.

Component	E_T (Total energy)	R (Rigidity)
Protons	$4\,800/E_T^{1.40\pm0.10}$	$4\,200/R^{1.32\pm0.10}$
α-Particles	$300/E_T^{1.45\pm0.11}$	$250/R^{1.38\pm0.11}$
Li, Be, B	$15/E_T^{1.68\pm0.30}$	$12/R^{1.60\pm0.30}$
C, N, O and $Z \geqslant 10$	$40/E_T^{1.51\pm0.18}$	$30/R^{1.43\pm0.18}$

3) The energy spectra obtained in this experiment for the heavier component do not confirm the conclusions of DANIELSON [34] and SINGER [35] which indicate not only much larger values of γ, but also find these values energy, as well as charge, sensitive. The findings of the present experiment are closely confirmed, however, by the recent measurements of the Bristol Group using photographic emulsions [36].

4) The energy spectrum deduced for protons is steeper than has been determined in previous reviews [35, 37]. This is due principally to the lower equatorial intensities obtained when the different experiments are corrected for non-telescope and albedo events. This low intensity is corroborated by the work of MCDONALD [16] using a detector which for the first time effectively discriminates against albedo, heavy nuclei, and secondary events. Acceptance of such a steep spectrum for protons requires that a peak occur in the differential energy spectrum at about $E_T = 2.1$ GeV in order for high latitude data to give a consistant picture (see Fig. 5). This is at approximately the same rigidity ($R = 1.8$ GeV/c) as the peak in the differential energy spectrum for alpha [15, 16] (350 MeV/nucleon.

To investigate whether, perhaps, in view of the above facts, the number spectra for the various charge components follow rigidity spectra rather than total energy spectra, available data [12-17, 37] on the best known component, the α-particles, have been plotted in Fig. 6. In the first two experiments the energies could be measured independently of geomagnetic theory.

Unfortunately the present data in the latitude sensitive region are insufficient to decide between a total energy spectrum with γ_1 constant or a rigidity spectrum with γ_2 constant. If one desires γ to remain constant throughout the entire energy range to 10^{15} eV, however, the high energy data slightly favor the total energy spectra deduced over the latitude sensitive region because of their larger values of γ. (See next section).

6. – Energy balance of the primary radiation.

The integral number-total energy spectra derived in the previous Section have been used in a calculation of the total amount of energy brought in by the primary cosmic ray beam. As was first pointed out by ROSSI [3], the amount of energy brought in by the primary radiation appears to be a factor of two higher than that dissipated in the atmosphere by all known processes. Subsequent calculations, dealing mostly with the energy dissipated in the atmosphere [39-41] have succeeded only in reducing this discrepancy somewhat.

In order to simplify the calculation of the amount of energy brought in by the primary radiation we have assumed that all components have the same γ_1 in their total energy spectra and that the value of this exponent is constant over the entire energy range from « low » energies to 10^{15} eV. γ_1 has

then been taken equal to *a*) 1.5 and *b*) 1.4. The respective constants for p, α, L, M, H nuclei are, in case *a*): 5300, 330, 10, 30, 10 and in case *b*): 4800, 300, 9, 27, 9.

The remarkable agreement between the intensities above 10^{12} eV predicted by these spectra, which are close approximations to the data in the latitude sensitive energy region, and the actual observed intensities of the total radiation [42-46] and α-particles [13, 42] at these high energies is shown in Fig. 7. This strongly supports the argument that, for protons and α at least, γ_1 remains constant throughout this enlarged energy range.

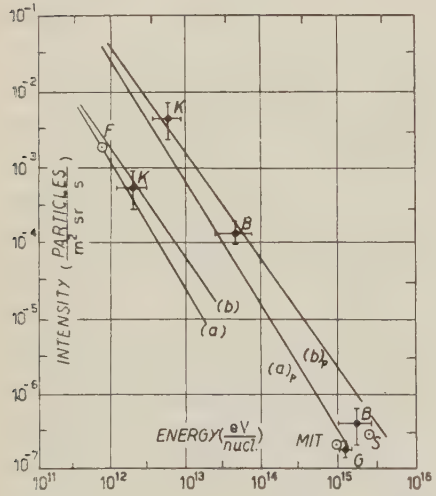

Fig. 7. – Predicted intensities of protons and α-particles in energy range $(10^{12} \div 10^{15})$ eV based on spectra derived from data in the latitude sensitive region. These intensities are compared with measured intensities of the total radiation and of α-particles in this energy region: *a*) spectra with $\gamma_1 = 1.5$; *b*) spectra with $\gamma_1 = 1.4$. Measured intensities are listed in the text under the appropriate letter.

The total energy brought in vertically by a given component above a given $(E_k)_{\min}$ in GeV/sr m^2 s is

$$\varepsilon_v = \int_{(E_k)_{\min}}^{\infty} E_k \, \mathrm{d}N(> E_T) \, \mathrm{d}E_k \,,$$

where $\mathrm{d}N(> E_T)$ is the differential number-total energy spectrum for that component and $(E_k)_{\min}$ is the vertical cut-off energy in GeV or GeV/nucleon for that particular component.

For the omnidirectional energy flux we have:

$$\varepsilon_0 = \frac{1}{\pi} \int_0^{2\pi} \mathrm{d}\varphi \int_0^{\pi/2} \sin\theta \cos\theta \int_{(E_k)_{\min}}^{\infty} E_k \, \mathrm{d}N(> E_T) \, \mathrm{d}E_k \,,$$

where φ is the azimuth angle, θ the zenith angle and $(E_k)_{\min}$ the minimum cut-off energy in GeV or GeV/nucleon at a given zenith and azimuth angle as given by ordinary geomagnetic theory [47]. (Corrected in part for eccentricity of the dipole).

The solid lines in Fig. 8 show the calculated incoming energy brought in directionally (vertically) by the primary radiation using spectra *a*) and *b*). The omnidirectional curves lie approximately 10% below the simple vertical calculation. This is due to the fact that at large zenith angles, due to shadow cone effects, the minimum cut-off energies in westerly directions are higher than would be expected in free space.

The incoming energy calculated on the directional (vertical) basis for either $\gamma_1 = 1.4$ or $\gamma_1 = 1.5$ is in good agreement with the values of energy dissipated in the atmosphere deduced by KOMURI [40] at $\lambda = 3°$ and 28°. However, Komuri's value at $\lambda = 55°$ and the values of PUPPI [39, 41] at $\lambda = 50°$ lie $10 \div 25\%$ below either of curves *a*) or *b*).

The same picture is obtained if we take the results of NEHER [48, 49] who has measured the total ionization in a vertical column of air using an omnidirectional ionization detector. Nehers ionization results have been corrected for non-ionizing energy losses as determined from the detailed balance results of KOMURI and PUPPI.

It appears then, that, using the energy spectra derived in this paper, reasonable agreement can be obtained between the energy brought in by the primary radiation and that dissipated by the primaries plus their secondaries in the atmosphere for $R > 5$ GeV/C ($\lambda < 40°$). At higher latitudes the ionization and detailed balance results give somewhat lower values. A possible explanation for this discrepancy is that the wall thickness of the detectors upon whose measurements the detailed balance calculations are based exclude an appreciable number of low energy particles [50].

It is quite probable that these particles contain a larger fraction of the incident primary energy at high latitudes than they do at low latitudes where meson production is more abundant, This would explain the smaller exponent ($\gamma_1 = 1.2$) required to fit the ionization and detailed balance results in the latitude sensitive region.

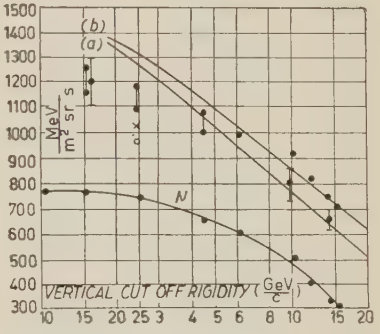

Fig. 8. – Comparison of the total energy brought in by the primary cosmic ray beam with that dissipated in the atmosphere by the primaries and secondaries in the latitude sensitive energy region. *a*) $\gamma_1 = 1.5$; *b*) $\gamma_1 = 1.4$. Detailed balance: KOMURI [40] ⊕, PUPPI and DALLAPORTA [39] x, PUPPI [41] ○; Ionization: NEHER ⁞, NEHER (corrected) ●.

* * *

The author is grateful to Professor J. A. VAN ALLEN for the hospitality of his laboratory and his helpful advice, and to various members of the Physics Departments at the University of Iowa and Imperial College, in particular to Dr. F. B. MCDONALD, Dr. H. ELLIOT and Miss P. ROTHWELL for helpful discussions. The flights provided by the Office of Naval Research and Winzen Research Inc. will be long remembered.

The author also wishes to thank Dr. FINCH and Dr. LEATON for providing the Gauss coefficients for 1955 prior to publication.

REFERENCES

[1] W. R. Webber: *Nuovo Cimento*, **4**, 1285 (1956).
[2] W. R. Webber: *Research Report* (University of Iowa, 1957).
[3] B. Rossi: *Rev. Mod. Phys.*, **20**, 537 (1948).
[4] S. Chapman and J. Bartels: *Geomagnetism* (New York, 1955).
[5] A. Schmidt: *Beitr. angew. Geophys.*, **41**, 346 (1934).
[6] H. F. Finch and B. R. Leaton: *Month. Not. Roy. Astron. Soc., Geophysical Suppl.*, **1** (1957).
[7] E. H. Vestine and J. Lange: Carnegie Inst. Wash., Publ. No. 578 and 580 (1947).
[8] F. S. Jory: *Phys. Rev.*, **102**, 1169 (1956).
[9] M. S. Vallarta: *Phys. Rev.*, **74**, 1837 (1949).
[10] F. B. Harris and J. Escobar: *Phys. Rev.*, **100**, 255 (1955).
[11] H. V. Neher: *Progress in Cosmic Ray Physics*, vol. **1** (Amsterdam, 1952).
[12] C. J. Waddington: *Phil. Mag.*, **45**, 1312 (1954).
[13] P. H. Fowler and C. J. Waddington: *Phil. Mag.*, **1**, 637 (1956).
[14] C. J. Waddington: *Nuovo Cimento*, **3**, 930 (1956).
[15] P. H. Fowler, C. J. Waddington, P. S. Freier, J. Naugle and E. P. Ney: *Phil. Mag.*, **2**, 157 (1957).
[16] F. B. McDonald: *Phys. Rev.*, **104**, 1723 (1956).
[17] F. B. McDonald: *Research Report* (University of Iowa, 1957).
[18] J. A. Simpson, K. B. Fenton, J. Katzman and D. C. Rose: *Phys. Rev.*, **102**, 1648 (1956).
[19] D. C. Rose, K. B. Fenton, J. Katzman and J. A. Simpson: *Can. Journ. of Phys.*, **34**, 968 (1956).
[20] J. R. Winckler, T. Stix, K. Dwight and R. Sabin: *Phys. Rev.*, **79**, 656 (1950).
[21] M. L. Vidale: *Phys. Rev.*, **88**, 266 (1952).
[22] A. S. Rao, V. K. Balasubrahmanyan, G. S. Gokhale and A. W. Pereira: *Phys. Rev.*, **91**, 764 (1953).
[23] J. A. Van Allen and S. F. Singer: *Phys. Rev.*, **78**, 819 (1950).
[24] G. W. McClure: *Phys. Rev.*, **96**, 1391 (1954).
[25] G. J. Perlow, L. R. Davis, C. W. Kissinger and D. J. Shipman jr.: *Phys. Rev.*, **88**, 321 (1952).
[26] M. A. Pomerantz and G. W. McClure: *Phys. Rev.*, **86**, 536 (1952).
[27] L. R. Davis, H. M. Caulk, C. Y. Johnson: *Phys. Rev.*, **101**, 801 (1956).
[28] J. D. Pullar and E. G. Dymond: *Phil. Mag.*, **44**, 565 (1953).
[29] M. A. Pomerantz: *Phys. Rev.*, **95**, 531 (1954).
[30] J. R. Winckler and W. G. Stroud: *Phys. Rev.*, **76**, 1012 (1948).
[31] J. R. Winckler and K. Anderson: work reported by E. P. Ney at International Congress on Cosmic Radiation, Guanajuato, Mexico (1955).
[32] K. Anderson: *Ph. D. Thesis* (University of Minnesota, 1954).
[33] K. Anderson: private communications (1956).
[34] R. E. Danielson, P. S. Freier, J. E. Naugle and E. P. Ney: *Phys. Rev.*, **103**, 1075 (1956).
[35] S. F. Singer: *Research Report* (University of Maryland, 1956).
[36] C. J. Waddington: in this issue, pp. 513, 518.
[37] B. Peters: *Progress in Cosmic Ray Physics*, vol. **1** (Amsterdam, 1952).
[38] M. M. Shapiro, B. Stiller and F. W. O'Dell: *Bull. Am. Phys. Soc.*, **1**, 319 (1956).

[39] G. Puppi: *Suppl. Nuovo Cimento*, **10**, 115 (1953).
[40] H. Komuri: *Progress in Theor. Phys.*, **13**, 205 (1955).
[41] G. Puppi: *Progress in Cosmic Ray Physics*, vol. 3 (Amsterdam, 1956).
[42] M. F. Kaplon, D. M. Ritson and E. P. Woodruff: *Phys. Rev.*, **85**, 933 (1952).
[43] P. H. Barrett, L. M. Bollinger, G. Cocconi, Y. Eisenberg and K. Greisen: *Rev. Mod. Phys.*, **24**, 133 (1952).
[44] K. Greisen: *Progress in Cosmic Ray Physics*, vol. **3** (Amsterdam, 1956).
[45] Results of the MIT Group: in this issue, p. 623.
[46] Results of the Sydney Group: in this issue, p. 653.
[47] See for example the useful graphs of R. A. Alpher: *Journ. of Geophys. Res.*, **55**, 437 (1950).
[48] H. V. Neher: *Progress in Cosmic Ray Physics*, vol. **1** (Amsterdam, 1952).
[49] H. V. Neher, V. Z. Peterson and E. A. Stern: *Phys. Rev.*, **90**, 655 (1953).
[50] L. Meridith: *M.S. Thesis*, University of Iowa (1952).

SUPPLEMENTO AL VOLUME VIII, SERIE X
DEL NUOVO CIMENTO

N. 2, 1958
2° Trimestre

Energy Spectra of Primary Cosmic Rays and the Interpretation of their Origin (*).

S. F. Singer

University of Maryland - College Park Maryland,

1. – Introduction.

This paper reports on a comprehensive analysis of experimental data on the primary cosmic radiation. Over the last 10 years more than 100 determinations have been obtained from ballons and rockets. In determining the energy, use is generally made of the geomagnetic field, *i.e.* the energy spectrum is derived from the latitude variation. But for heavy primaries (including α-particles) direct energy determinations can be made by means of photographic emulsions and various ionization detectors.

The last comprehensive review [1] shows the energy spectra of all components as having the same form, namely, an exponent of the integral energy spectrum of 1.2. This means that all components of the primary radiation have the same velocity spectrum, since

$$N(> E_t) = kE_t^{-1.2},$$

where k is a function of Z and where E is the total energy (including rest mass) per nucleon. The present analysis (2), on the other hand, gives energy spectra which are different for the protons and the α-particles, at least this holds true in the latitude sensitive range (which constitutes, however, a small fraction of the total range of energies).

(*) This work has been supported in part by the Air Force Office of Scientific Research under Contract AF 18(600)-1038.

2. – Results on energy spectra.

The energy spectra deduced from the analysis of high-altitude data are given in Table I. Note that Table I only refers to a restricted range of energy values. The detailed analysis of data on which these results are based is given in reference [2]. We shall now discuss some of the salient points of this analysis.

TABLE I. – *Collected energy spectra of primary components.*

Charge	Range of validity (E_t in GeV/nucleon)	Integral spectrum (particles/m² sr s)		Flux value	
		Best value	Extreme limits of exponent	$\lambda = 55°$	$\lambda = 0°$
H	2 ÷ 20	$4000\, E_t^{-1.15}$	1.05 to 1.25	1900	180
He	1.5 ÷ 8	$460\, E_t^{-1.6}$	1.5 to 1.7	300	20

2·1. *α-particles.* – The α-particles are least subject to any controversy. They are not subject to the albedo problems of the protons, nor to the problems of absorption and difficulty of identification which are peculiar to the heavier nuclei. Up until 1956, the form of the spectrum of α-particles was in controversy; since then the low flux value at the equator obtained from rocket-borne, low-efficiency telescopes has been confirmed by photographic plate determinations of the flux [3]. At other latitudes the differences between experimenters are minor (after proper corrections for geomagnetic co-ordinate shifts) so that we can consider the α-spectrum as well established.

2·2. *Protons.* – The flux value of primary protons has been obtained at $\lambda = 55°$ and 0°. The main problem is the elimination of upward-going and re-entrant albedo (*). Three methods have been employed to make corrections: they all give concordant results. i) Good geometry absorption measurements and measurements with Čerenkov counters. ii) Use of geomagnetic effects, such as east-west asymmetry. iii) Calculation of albedo based on empirical cosmic ray data. The situation is especially critical at the geomagnetic equator, since there albedo particles will loop around magnetic lines of force and, depending on their lifetime (or looping factor), their contribution

(*) All experiments, even those claiming to eliminate albedo, must be carefully analyzed to see: (i) if they generate any albedo of their own, (ii) if true primaries are not subtracted out in the analysis. A measurement with a « time of flight » scintillator telescope seems to be desirable.

could be large. In fact, it has been possible to analyze the albedo contribution there quite precisely, so that we have confidence in the high equatorial flux for primary protons, and therefore in the rather flat energy spectrum for primary protons. (For details of the analysis, see reference [2]).

3. – Discussions.

Until experimental evidence forces us to assume the contrary, we should accept the fact that the proton and α components of the primary radiation have different energy spectra. This statement applies only to the latitude sensitive, relativistic region; at higher energies the proton spectrum steepens.

We should therefore be prepared to accept the possibility that the spectrum changes slope. In fact, the spectrum exponent generally gets steeper as the energy increases.

If such a situation exists, it can be interpreted in the following way. We accept the premise that cosmic rays are accelerated in stellar envelopes, especially those of active stars and the shells of supernovae, but we depart on the following two points. The energy spectrum does not have an exponent of $1 \div 2$, but is in general much steeper. If we picture the acceleration as due to a statistical increase of energy of cosmic rays as the turbulent magnetic energy increases (similar to the way one can picture the mechanism to occur on the sun during a solar flare), then the exponent is determined by the ratio of the rate of acceleration to the rate of escape from the accelerating region. Large exponents, of the order of 10 to 100, should therefore be quite common. What we observe is the superposition of all these sources and the exponent of the primary cosmic ray spectrum then expresses the frequency distribution of exponents of the individual sources.

REFERENCES

[1] B. Peters: in *Progress in Cosmic Ray Physics*, vol. **1** (Amsterdam, 1952).
[2] S. F. Singer: in *Progress in Cosmic Ray Physics*, vol. **4** (Amsterdam, 1957).
[3] M. M. Shapiro, B. Stiller and F. W. O'Dell: *Bull. Am. Phys. Soc.*, **1**, 39 (1956).

SUPPLEMENTO AL VOLUME VIII, SERIE X
DEL NUOVO CIMENTO

N. 2, 1958
2° Trimestre

On the Origin of the Charge Spectrum of the Primary Cosmic Radiation (*).

S. F. SINGER

University of Maryland - College Park, Maryland

1. – Introduction.

A fundamental question to ask is the following. Is the charge spectrum of the primary cosmic radiation (i.e., at the top of the atmosphere) the same as the charge spectrum of the original cosmic radiation (i.e., at the point of origin), or have modifications taken place in the travel between the origin and the earth.

It is presently most widely held that no modifications, or at any rate very minor ones, have taken place and that the primary charge spectrum represents essentially the original charge spectrum and also resembles the general abundance of elements in the universe [1]. A consequence of this hypothesis is that the cosmic radiation during its existence cannot have made many collisions with interstellar hydrogen. This means that the lifetime of cosmic rays in the galaxy must have been very short, corresponding to a maximum path length of 2 g/cm² [2]. The lifetime must be less than 4 million years [3]. As a consequence of this hypothesis, therefore, the cosmic rays must escape rapidly from the galaxy, that is, the trapping field cannot be a very efficient one and, as a further consequence, the rate of acceleration of cosmic rays must be very rapid to replenish the cosmic rays which escape [2, 3].

Now this point of view hinges very crucially on the resemblance between the primary charge spectrum and the abundance of elements, but this resemblance, as we shall show, is quite superficial and can be achieved through nuclear fragmentations. In order to state the matter quantitatively, we sum-

(*) This work has been supported in part by the Air Force Office of Scientific Research under Contract AF 18(600)-1038.

marize in Table I the present data on cosmic abundances and on the charge spectrum of the primaries above the atmosphere.

TABLE I. – *Data on cosmic abundances, including the primary cosmic radiation (beyond $Z = 10$, only the most abundant species are listed).*

Z		a	b	c
1	H	$4 \cdot 10^{10}$	12.00	620
2	He	$3 \cdot 10^{9}$	11.06	90
3	Li	100	0.68	L-nuclei
4	Be	20	2.43	3
5	B	24	[5.0]	
6	C	$3.5 \cdot 10^{6}$	8.56	3 (4)
7	N	$6.6 \cdot 10^{6}$	7.98	2 (1)
8	O	$2.15 \cdot 10^{7}$	9.00	2 (1)
9	F	1600		
10	Ne	$8.6 \cdot 10^{6}$	8.81	
14	Si	$1 \cdot 10^{6}$	7.60	H-nuclei
18	A	$1.5 \cdot 10^{5}$	7.7	2.5
20	Ca	$4.9 \cdot 10^{4}$	6.38	
26	Fe	$6 \cdot 10^{5}$	6.76	

(*a*) H. E. SUESS and H. C. UREY: *Rev. Mod. Phys.*, **28**, 53 (1956). (These values are referred to silicon $= 1 \cdot 10^{6}$).

(*b*) log N for the sun, except that for He and Ne we give their ratios to H for stars (after ALLER).

(*c*) Vertical cosmic ray flux (in particles per m^2 sr s) at $\lambda = 41°$ [8].

A crucial point in this comparison is the question of the presence or absence of lithium, beryllium and boron (L-nuclei) in the primary radiation, because there the discrepancy is most severe. On the other hand, if the L-nuclei are absent, then the discrepancy will be less severe. In other words, if the L-nuclei are present, the hypothesis of fragmentation will be greatly enhanced, since it is not easy to conceive of a mechanism whereby Li, Be and B exist at the surface of stars or wherever cosmic rays are initially injected and accelerated.

Now the importance of Li, Be and B was first pointed out and discussed in great detail by BRADT and PETERS in their outstanding series of papers connected with the discovery of the heavy primaries. However, they interpreted the data to signify an *absence* of L-nuclei and therefore adopted the hypothesis of *no* fragmentations of cosmic rays [1]. The Bristol workers, on the other hand, who deduced evidence for the presence of Li, Be and B, adopted an opposite interpretation and were the first to suggest that even a substantial fraction of the protons and alphas could be produced by fragmentation [4]. This line was further developed on the basis of empirical data on production of various nuclear fragments in collisions between hydrogen and iron; these data were taken from the inverse process which occurs when iron meteorites

are bombarded by relativistic hydrogen nuclei. This work led to a calculation and a discussion of the significance of the production of tritium and ^{3}He in fragmentations of heavy primaries in interstellar space. An attempt was also made to calculate the charge spectrum which would result from an original cosmic radiation consisting only of iron [5] (*).

This charge spectrum is shown in Table II.

TABLE II. – *Charge spectrum of cosmic rays calculated as a function of pathlength.* An initial radiation is assumed composed only of Fe; fragmentation probabilities for « protons » (this includes neutrons and deuterons) and for « alphas » (including ^{3}H and ^{3}He) are obtained empirically from meteorite data; for Li, Be, B from data of NOON and KAPLON. The mean-free-path for primary iron nuclei in hydrogen is 1.9 g/cm^2. In this calculation we have neglected fragmentations of lighter nuclei since their mfp is considerably longer than 1.9 g/cm^2.

Path length	0	λ	2λ	3λ	4λ
« p »	0	1400	1900	2100	2160
« α »	0	276	378	415	430
Li, Be, B	0	63	86	95	98
Fe	100	37	13	5	2

The agreement with the actually observed charge spectrum is not too good, but, as was pointed out, it depends very much on what one takes for the fragmentation probabilities for the L-nuclei (Table III).

TABLE III. – *Comparison of observed and calculated charge distribution of primaries.*

	Observed primary charge distribution (normalized from Table I) at Lat. = 41°	Calculated charge distribution (normalized from Table II) for path length	
		2λ	3λ
H	1000	1000	1000
He	145	200	200
Li, Be, B	5	45	45
	10-15 (*a*)	22-15 (*a*)	22-15 (*a*)
$Z \geqslant 10$	4	6.8	2.4

(*a*) These values were calculated using the fragmentation probabilities of Ref. [9].

Since, then, a number of new proposals and data have come into the foreground.

(*) Another way of phrasing the question is: if all of the Li, Be and B is due to fragmentation of heavies, what fraction of the protons and α arise in the same fragmentations?

1) Prompted by the apparent success of the explanation of the synchrotron radiation from the Crab Nebula [6], HAYAKAWA [7] has again suggested a supernova origin for cosmic rays and pointed to the fact that the injected nuclei would be mostly heavies, since a supernova is thought to contain a high abundance of heavy nuclei (*).

2) Many more experiments have now been performed on the primary radiation in order to measure the energy spectrum and charge spectrum. This experimental evidence has been analyzed [8] and the flux values for Lat. $= 41^{c}$ are shown in Table III. These data indicate an appreciable abundance of primary L-nuclei.

3) Finally, the Bristol group has presented new data on fragmentation probabilities [9]. While these are based on relatively few stars and have not been critically discussed, we shall go ahead and use them, if only to illustrate the great dependence of our detailed conclusions on such experimental data. It is to be hoped that efforts will be made to check these results and make them more precise.

2. – Importance of fragmentation probability.

The results of the Bristol workers are given in Table IV and compared with results of fragmentation probabilities by other workers. The main immediate conclusion is that the fragmentation probabilities are less by a factor of two to three, as compared, for example, with NOON and KAPLON [10] (**). This result has two immediate consequences: 1) The number of L-nuclei produced in fragmentations in interstellars space will be reduced by a factor of two to three compared to α-particles, and 2) The primary flux of L-nuclei, which is derived normally from extrapolation of balloon data, can now be re-evaluated.

Using the smaller fragmentation probabilities, the primary flux will only be slightly less than the flux measured at balloon altitudes (which includes

(*) Another method for obtaining a preferential injection of heavy nuclei depends on the acceleration mechanism. If injection takes place from a stream moving with a velocity v, such as a beam of gas shot out from the sun, then those particles having a large enough radius of curvature to diffuse into the adjacent turbulent transition region may become accelerated there. Heavy primaries which are not yet fully ionized will have a larger radius of curvature than the main gas, which consists of protons.

(**) It is to be noted that the Bristol results do not refer as yet to collisions with hydrogen nuclei. However, there is little difference found in the fragmentation probabilities between emulsion nuclei in general, and the light nuclei in the emulsion or peripheral collisions; we will therefore assume that the fragmentation probability for hydrogen is similarly decreased by a factor of two to three.

a number of L-nuclei created in fragmentations of heavies in the atmosphere above the balloon). The result of this correction, as shown in Table III, is a rather good agreement between calculation of a primary spectrum on the basis of original iron plus fragmentation, and the observed primary spectrum.

TABLE IV. – *Data used in calculating primary charge spectrum.*

Fragmentation probabilities for L-Nuclei in light nuclei of emulsion (or in air)

	$P_{Fe,L}$	$P_{H,L}$	$P_{H,\alpha}:P_{H,L}$
(*a*)	0.33 ± 0.16	0.52 ± 0.08	
(*b*)	0.00	0.17 ± 0.07	
			(*a*) 4
			(*b*) 8
	$P_{Fe,\alpha}$	$P_{H,\alpha}$	
(*a*)	3.12 ± 0.72	2.00 ± 0.20	
(*b*)	2.08 ± 0.68	1.33 ± 0.26	

Fragmentation probabilities for singly and doubly charged nuclei with primary iron on hydrogen. Values are derived from nuclear evaporation theory (*c*) using a distribution of excitation energies in accord with empirical results from high altitude emulsion stars (checked by meteorite data) (*d*). Values shown are relative; in the calculation they are normalized to the $P_{Fe,\alpha}$, and $P_{H,\alpha}$ values.

^{0}H	^{1}H	^{2}H	^{3}H	^{3}He	^{4}He
15	6.2	1.1	.75	1.2	2.3

(*a*) Ref. [10].
(*b*) Ref. [9].
(*c*) K. J. LE COUTEUR: *Proc. Phys. Soc.*, A **63**, 259 (1950).
(*d*) Refs. [6] and [12].

The relative numbers of neutrons, protons, ^{2}H, ^{3}H, ^{3}He and ^{4}He produced in these fragmentations (*) were obtained by considering the inverse process, namely, the evaporation of a stationary iron nucleus which is struck by a cosmic ray proton. We have calculated the frequency of emission of these fragments, using evaporation theory and checking the applicability of the theory from experimental results on iron meteorites. It is not safe to use results from accelerators, as can be seen from the fact that the tritium cross-sections reported [11] are an order of magnitude smaller than those directly observed in meteorite samples which have been taken from recently fallen meteorites [12]. On the other hand, the fragmentation probabilities for light

(*) It should be noted that the first four species all become primary « protons » while ^{3}He and ^{4}He will be counted as primary « alphas ».

nuclei have been normalized to the proton and α values by using the experimentally determined ratio in photographic emulsions. In this way it is hoped that a consistent calculation is produced which is based entirely on empirical cosmic ray data. Our deuteron-proton ratio, for example, agrees very closely with that obtained from cosmic ray stars in emulsions [13], but the triton-deuteron ratio does not agree too well.

3. – Conclusion.

We find that we can account quite well for the observed primary charge distribution by assuming (quite artificially) a model in which the original radiation consists only of iron (*). After about three mean free paths (6 g/cm^2) a charge distribution is obtained which resembles very much the observed values. The good agreement is possible only if one uses results on « p » and « α » fragments obtained from meteorite measurements, and if one uses the smaller fragmentation probabilities obtained by the Bristol group for Li, Be and B.

It is seen that the charge distribution so calculated is much closer to the observed values than are the cosmic abundance values. In particular, we can reproduce very much better the large ratio of heavy to medium nuclei, which is of the order of $\frac{1}{2}$, as compared to the cosmic abundance value of 10^{-1}. The existence of an iron peak in the primary cosmic radiation can be explained more naturally as the remains of an initial large iron peak than in any other way. Certain features, such as the C:N:O ratio, are more in accord with fragmentation than with natural abundances, but here the evidence is not as conclusive.

Certain crucial tests of the fragmentation hypothesis are necessary and should be made. They consist principally in a measurement of the Li, Be and B flux *above* the atmosphere. The definitive *absence* of the L-nuclei would speak against the fragmentation hypothesis; the presence of the L-nuclei would be in accord with the fragmentation hypothesis, but would only be a necessary condition. More subtle measurements would help establish the fragmentation hypothesis: these consist of the measurement of the primary deuteron flux and primary ^{3}He and perhaps tritium fluxes. From the results of meteorite measurements some numerical values can be given for the fluxes to be expected, provided they originate from fragmentations (see Table V).

(*) On the other hand Ginzburg and Fradkin [14] consider that they can explain the primary charge spectrum without an original enhancement of the heavies; however they use $N_L:N_M \leqslant 0.1$ and large values for the relevant fragmentation probabilities. Therefore their conclusion is not surprising.

TABLE V. – *Primary flux values (at $\lambda = 41°$) for deuterons, tritons and helium-3. Calculated from the data of Table IV under the assumption that all of the « protons » and « alphas » come from fragmentation of original iron primaries.*

$$^2\mathrm{H}\ \text{flux} = \left(\frac{1.1}{15 + 6.2 + 1.1}\right)\cdot 650 = 32\ \text{peters}\,,$$

$$^3\mathrm{H}\ \text{flux} = 5\cdot 10^{-3}\varrho\ \text{peters}\ (*)\,,$$

$$^3\mathrm{He}\ \text{flux} = \left(\frac{0.75 + 1.2}{0.75 + 1.2 + 2.3}\right)\cdot 90 = 41\ \text{peters}\,.$$

(*) Ref. [5]; because of the short halflife of ^{3}H ($\sim$ 12 yrs when nonrelativistic) the flux depends on the gas density in which the cosmic rays have spent the preceding few decades. For an average interplanetary gas density of 200 protons/cm^3 the flux would be 1 peter.

REFERENCES

[1] B. PETERS in *Progress in Cosmic Ray Physics*, vol. **1** (Amsterdam, 1952).

[2] P. MORRISON, S. OLBERT and B. ROSSI: *Phys. Rev.*, **94**, 440 (1954).

[3] B. ROSSI: *Suppl. Nuovo Cimento*, **2**, 275 (1955).

[4] A. D. DAINTON, P. H. FOWLER and D. W. KENT: *Phil. Mag.*, **43**, 317 (1952).

[5] S. F. SINGER: *Proc. of Duke Univ. Cosmic Ray Conf.* (Nov. 1953), ed. by L. Nordheim (1954); S. F. SINGER: *Phys. Rev.*, **98**, 1163 (1955) (A).

[6] V. L. GINZBURG: *Usp. Phys. Nauk*, **51**, 343 (1953); V. L. GINZBURG, S. B. PIKEL'NER and I. S. ŠKLOVSKIJ: *Astron. Žu. SSSR*, **32**, 503 (1955).

SUPPLEMENTO AL VOLUME VIII, SERIE IX
DEL NUOVO CIMENTO

N. 2, 1958
2° Trimestre

General Observations on the Composition of the Primary Radiation.

B. PETERS

Tata Institute for Fundamental Research - Bombay

As a result of papers presented at this conference some of the information relating to the energy spectrum and composition of the primary radiation can be stated with greater precision than was possible heretofore.

1. – The Energy Spectrum.

In the non-relativistic region the work of the Minnesota and Iowa groups has confirmed earlier findings that α-particles (and presumably therefore other components) can arrive, at geomagnetic latitudes above 54°, with energies lower than those expected on the basis of existing information on the earth's field. They also find that there is at these latitudes no sharp energy cut-off and that the intensity of the low energy component can undergo appreciable variations. These phenomena reflect presumably not properties of the primary cosmic radiation but properties of the earth's field and of interplanetary space.

In the latitude sensitive region there appears to be general agreement that all heavy components follow approximately the same power law; if ε designates energy per nucleon (including rest mass) the integral spectra can be represented by $N_A = K_A/\varepsilon^{1.5}$. The proton component in the latitude sensitive part until now was believed to follow a flatter spectrum. However this conclusion was based on large and uncertain estimates about the contribution of albedo particles to the counting rate at the equator. The experiment of McDonald reported here, is to my knowledge, the only one in which simultaneously the charge, the velocity and the direction of motion of singly charged particles has been measured near the top of the atmosphere. It indicates a very much larger albedo than was believed so far, and if it is accepted the

proton spectrum has within errors of measurement the same slope as the heavy components.

In the high energy region we have the earlier measurements of the proton and α-particle flux at $1.6 \cdot 10^3$ GeV by LAL and of $4.5 \cdot 10^3$ GeV by KAPLON and RITSON. For these two components the power law exponent of 1.5 remains valid. At approximately the same energy measurements by PARKER and myself made in 1950 and measurements by FOWLER reported in 1956 indicate that also the ratio of heavy primaries to protons and α-particles is approximately the same as in the latitude sensitive region. This implies that the power spectrum with exponent 1.5 is valid at least in the region from 1 to 5000 GeV per nucleon and is accurately the same for all primary components.

2. – The charge spectrum.

From the point of view of astrophysics one is trying to answer three principal questions and they must be answered in the order in which they are stated:

(i) What happens to the primary particles after they have been accelerated? Do they escape from the galaxy or do they break up and finally dissipate their energy in collisions with interstellar hydrogen?

If their energy is dissipated in the interstellar gas an equilibrium distribution will be established between the injected nuclei and their break up products and one can show that under these conditions the ratio of N_L (the light nuclei Li, Be, B) to N_M (the medium nuclei C, N, O) must exceed unity. All results on the ratio $R = N_L/N_M$ which were reported here and most of the results published earlier agree that for particles of energy 1.6 GeV per nucleon, R is significantly smaller than unity and that therefore the ultimate fate of particles accelerated in our stellar system is escape from the volume which includes the earth as well as the region where cosmic-ray particles originate.

The second question is the following:

(ii) Does the relative flux of primary components incident on the earth represent approximately the composition of the beam at the time of acceleration or has the composition been modified substantially by fragmentation in the transition from the source to the earth? This depends of course on the average amount of matter traversed and determines the storage factor of radiation in the galaxy and the amount of energy which must be fed into cosmic radiation to keep it continuously at its present level.

The wide divergence in the values of R reported by various investigators does not yet permit a reliable answer to this question. Most investigators favor a value $R = 0.35$ for particles whose energies exceed 1.6 GeV/nucleon and this corresponds to the traversal of 4.5 g/cm^2 of hydrogen. The greatest

uncertainty in R comes from the correction for break up processes in the atmosphere above the point of observation. Higher flights make this correction smaller thereby reducing the uncertainty.

Our own work at Bombay was carried out with an exposure at 7 g/cm², a greater height than that obtained in earlier investigations. The investigation is not completed but indicates a value of R which may be substantially lower and could be less than 10%.

One should expect that the lower the energy and the radius of curvature of the primary particles, the larger the amount of matter traversed before they diffuse to the solar system. The corresponding decrease of R with energy is perhaps indicated in the results of McDonald who finds

R	Energy
0.32	>400 MeV/nucleon
0.18	>600 » »
0.17	$>$ 1.2 GeV/nucleon

Our own observations tend to agree with McDonald which corresponds to less than 2.25 g/cm² of hydrogen traversed by the average primary of energy above 1.5 GeV/nucleon. But the question can not be considered settled until different types of experiments and especially experiments carried out at greater altitudes get into agreement.

An average amount of 4.5 g/cm² of hydrogen corresponds to a lifetime of $t = (3 \cdot 10^6)/\varrho$ years where ϱ is the number of hydrogen atoms per cm³ along the trajectory.

The lower value favored by McDonald and by our group corresponds to half that time.

This leads to the third question:

(iii) Does the composition observed in cosmic radiation correspond to the chemical composition of any stellar object which can be considered as a possible source for cosmic radiation particles?

It seems almost impossible to answer this question if we accept an average amount of traversed matter of 4.5 g/cm² which corresponds to two collision mean free paths of iron in hydrogen. Even if the amount is half that much the finer features of the chemical composition particularly among the heavier elements should already be obliterated. The structural features which Schein found in the charge spectrum of the heavy component, the apparent alternation in the abundance of odd and even nuclei and the correspondence with certain features in the chemical composition of young stars leads one to suspect that the average amount of interstellar matter traversed and therefore the ratio R is still smaller than the value one obtains if one extrapolates the measurements made under 15 g/cm² of air to the top of the atmosphere.

In summary, it seems safe to conclude that all primary components have the same energy spectrum and that it can be expressed as a power law with exponent 1.5 ± 0.05. The proton spectrum below 10 GeV is perhaps somewhat flatter but this is not certain.

Cosmic ray particles produced in the galaxy escape after traversing on the average not more than 4.5 g/cm^2 of interstellar hydrogen. Certain experiments favor a considerably smaller value for the amount of matter traversed. Until this point is settled it is not clear whether detailed features of the composition of the primary radiation can be related to relative abundances in the chemical composition of various stellar objects.

INTERVENTI E DISCUSSIONI

— H. Messel:

I agree with Peters that the light to medium ratio is not compatible with an equilibrium ratio of one; however, it is my belief that one of the first things on which we must agree is that there is a substantial amount of Li, Be and B entering into the earth's atmosphere as primary cosmic radiation. As far as mechanisms of origin, storage and acceleration are concerned it is not necessary at the present stage to know whether the light to medium ratio is exactly $\frac{1}{2}$, $\frac{1}{3}$ or the like. After all we do not know ϱ, the density of matter in interstellar space to an accuracy of more than say a factor of five or ten.

— L. Biermann:

Do I understand correctly, that the opinion prevails, that the abundance of Li, Be, B is probably a fraction, but not a very small fraction of the abundance to be expected in fragmentation equilibrium in interstellar space; that hence the storage of cosmic radiation in the interstellar magnetic fields is somewhat less effective than one thought some years ago, such that for stationary conditions not 10^{-4} of the thermal radiation are required for the reproduction of cosmic radiation as in case of perfect storage (which would be indicated by fragmentation equilibrium) but that rather a fraction nearer to 10^{-3} of the thermal radiation (averaging over the galaxy and long periods of time) would maintain the present energy density of cosmical radiation in our galaxy.

PART IV.

Air Showers.

Section A: General Introduction.

Introductory Remarks about Air Showers.

G. Cocconi

Laboratory of Nuclear Studies, Cornell University - Ithaca, N. Y.

In this introductory talk I shall focus the attention on three topics that, at this time, seem to me most interesting.

The first topic is the lateral distribution of the ionizing particles. The experimental evidence accumulated in the last years allows us for the first time to draw definitive conclusions about the average behaviour of the showers in air.

On the second topic, the characteristics of the nucleon-nucleon interaction, is centered most of the attention of the high energy physicists. Though we are still far from a full understanding, the recent experimental evidence seems to show that the models thus far most commonly accepted, the statistical models, are incorrect.

The third topic, the primary energy spectrum, mostly of cosmological interest, cannot be omitted in any discussion about air showers.

1. – Lateral distribution of the ionizing particles.

The most extensive measurements on the lateral distribution of the ionizing particles around the core of the shower have been carried out, with G. M. counters, by the Russian workers. The measurements cover showers of different sizes and at different altitudes above sea level and distances from the core from 0.5 to 1000 m. Recently the MIT group has made similar experiments near sea level with scintillators (*).

(*) A priori, the densities measured with scintillators are not directly comparable with those obtained with G. M. counters. The amplitude of the pulse from a scintillator depends in fact not only on the number of ionizing particles falling on it, but also on their energy spectrum, and the energy spectrum is a function of the distance from the core of the shower. It seems however that the two measurements cannot differ, within the range of distances explored thus far, by more than a factor of two.

Some of the results are given in Fig. 1.

The distances from the core are expressed in displacement units,

$$r_2 = (73.5/(P - 0.07))(T/273) \text{ m},$$

where P is the pressure of the air in atmospheres, and T its average absolute temperature (*).

The curves drawn in Fig. 1 through the experimental points correspond all to the same distribution, that of Fig. 2, displaced vertically to fit the total number of particles in the showers.

It is remarkable that a single distribution can fit reasonably well all the experimental points, independent of the size of the shower ($10^3 < N < 10^9$), both at sea level and at mountain altitudes.

The distribution (heavy curve of Fig. 2), when compared to the curves calculated by NISHIMURA and KAMATA for the electrons in a pure electromagnetic shower, resembles that predicted for showers of age $s = 1.4$.

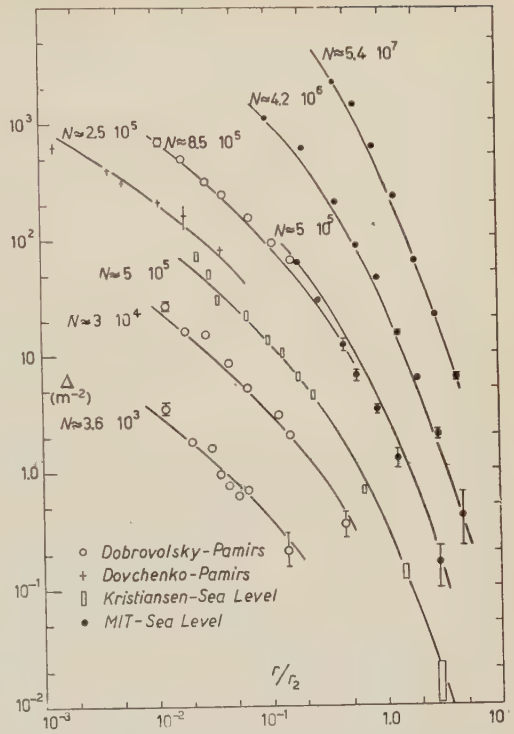

Fig. 1. – Lateral distribution of the density of all ionizing particles for showers of various sizes, measured with counters (Russian Authors) and with scintillators (MIT).

The agreement must be considered fortuitous, not only because at the largest distances most of the particles in the real showers are μ-mesons, and not electrons, but mostly because the electromagnetic theory would not predict a distribution independent of the size, N, of the showers.

A reasonably good fit to the experimental curve is given by the expression

$$f\left(\frac{r}{r_2}\right) = 0.25\left(\frac{r}{r_2}\right)^{-0.8}\left(\frac{r}{r_2} + 0.87\right)^{-2.64}.$$

(*) In this expression of the displacement unit the fact is taken into account that the distribution observed at the pressure P corresponds to the equilibrium distribution, for the electromagnetic component, reached about two radiation units (0.07 atm) above the place of observation.

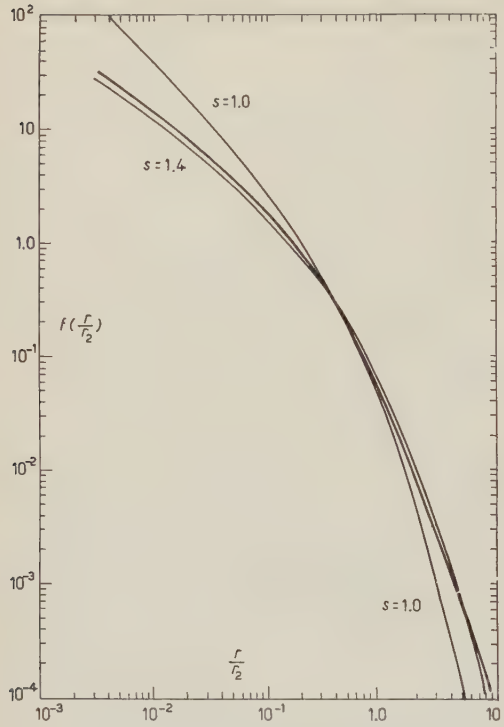

Fig. 2. – The heavy line represents the lateral distribution for all ionizing particles that fits reasonably well all the experimental points of Fig. 1. For comparison are also plotted the curves calculated by NISHIMURA and KAMATA for electromagnetic showers of age $s = 1$ and $s = 1.4$. The curves are normalized as follows: $\int_0^\infty 2\pi f(r/r_2)\, \mathrm{d}(r/r_2) = 1$.

The distribution function $f(r/r^2)$ and the density $\Delta(r)$ of the ionizing particles observed at a distance r from the core of a shower containing N particles are related by the equation:

$$\Delta(r) = N \frac{f(r/r_2)}{r_2^2} \ \mathrm{m}^{-2} .$$

Another remarkable point about Fig. 1 is that the density of the particles keeps increasing up to the smallest distances explored (≈ 0.5 m), even for the smallest showers. This lack of a plateau indicates that the most energetic particles feeding from the core the less energetic ones in the shower outskirts are concentrated in a very small region.

2. – Characteristics of the nucleon-nucleon interactions.

From the analysis of the properties of Extensive Showers at different altitudes given by ZACEPIN and by GREISEN, as well as from the results discussed in the preceding section, it appears that, in the lower atmosphere, the behavior of air showers is dictated by the nucleonic component still present in the core of the showers, and not by the electromagnetic cascade started in the upper atmosphere.

Since the primary particles initiating the showers are nucleons, the fact that after some 10 interaction mean free paths of atmosphere the nucleons in the core are still energetic enough to carry about 20% of the initial energy reveals some important characteristics of the nucleon-nucleon interaction at energies in the 10^{15} eV region.

The situation can be summarized by saying that, on the average, the primary nucleon loses in each interaction only a fraction, say $\sim \frac{1}{3}$ of its energy (elasticity parameter ~ 0.7) and after the interaction maintains its indivi-

duality as a particle. These conclusions indicate that the statistical models for high energy interactions, like those of FERMI and LANDAU, are fundamentally inadequate.

In fact, according to these models, all the energy available in the collision is shared among some secondaries; whenever one of these secondaries is a π^0-meson, its energy is lost as far as the propagation of the nucleonic cascade is concerned, and these models predict too high a probability for π^0 production.

In other words, the concentration of a large fraction of the available energy in π^0-mesons must be less probable than expected on the basis of pure statistical models.

Also, the angles predicted for the secondaries by the Fermi and the Landau models are too large to explain the absence of a plateau in the lateral distribution of air shower particles.

Models that can avoid these contradictions are those in which the secondaries produced in the interaction of a nucleon are the « virtual » particles shaken off in the collision while the primary nucleon maintains its individuality and, on the average, a large fraction of its energy.

We shall call these models « bremsstrahlung » models.

LEWIS-OPPENHEIMER-WOUTHUYSEN, BHABHA, KRAUSHAAR-MARKS, and others have proposed models that belong in this category, and a careful examination of their possibilities is certainly demanded by the present experimental evidence.

At machine energies it is already clear that only « bremsstrahlung » models can justify the experimental results, however thus far, probably because of their analytical beauty, most of the theoretical work has been polarized along the lines of the statistical models.

Another piece of evidence in favor of the models favored here is the discovery by the Japanese group of HIGASHI *et al.*, at 30 m w.e. underground, of showers of nearly parallel μ-mesons (from 4 to 30 particles) falling on a 0.3 m^2 cloud chamber with frequencies of $\sim 1/50\ h^{-1}$. These showers can hardly be explained as the remnants $\pi^{\pm}$ mesons decaying in the air. Instead, they can be easily interpreted as the remains of $\pi^{\pm}$ meson showers created in the earth above the cloud chamber by the high energy nucleons left in the core of air showers of $\sim 10^{15}$ eV.

3. – Number spectrum and energy spectrum.

The uniqueness of the lateral distribution function $f(r/r_2)$ discussed in the first section permits the unambiguous derivation from the shower density spectrum of the average number spectrum, $F(N)$, i.e., of the frequency of the showers as a function of the total number of ionizing particles in them. The number spectrum has also been deduced recently by the MIT group from

their measurements of the density at various distances from the core, by means of scintillators. Both results are plotted, for sea level, in Fig. 3.

In the lower part of the figure are given the differential spectra. The agreement between the two estimates, where they overlap, is very good.

The integral spectrum at the top of the figure, deduced from the average of the differential spectra, can be expressed by the equation:

$$F(N) = 0.59 N^{-(0.815 + 0.060 \log N)} \text{ m}^{-2} \text{ s}^{-1} \text{ sr}^{-1}$$

and can be considered experimentally determined for $10^3 < N < 10^9$.

It must be emphasized, that the spectra we dealt with thus far, as well as the energy spectrum we are going to discuss next, must be considered only as average spectra. No fine structure could be put in evidence in the number spectrum deduced from the density spectrum and even the more direct measurements (MIT) of $F(N)$ still have poor resolution. The situation is even more hopeless when, from the number spectrum, the energy spectrum is inferred; in this case, in fact, the relation between N and U, the total energy of the primary particle, is not unique, since the showers are initiated at various altitudes in the atmosphere.

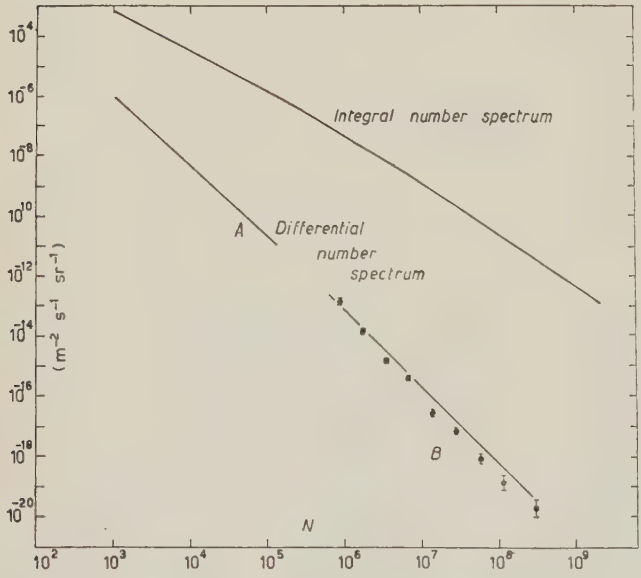

Fig. 3. – The differential number spectra A and B are deduced from the density spectra (sea level). The points are from MIT. The integral number spectrum is deduced from a continuous curve going through the differential spectra.

The *integral energy spectrum* $F(U)$ of the primary cosmic radiation is given in Fig. 4, where U is the total energy of the primary particle.

Up to energies $\sim 10^{16}$ eV its determination is quite direct.

The points around $(10^{12} \div 10^{13})$ eV are given by measurements on emulsions flown at the top of the atmosphere. Point A has been obtained, following the method outlined by GREISEN, by integrating the energy lost by air showers

of fixed total energy over all the atmosphere; it is known with an uncertainty of $\sim 20\,\%$ and its characteristics are the following: $N = 3.5 \cdot 10^5$; $U = 4.2 \cdot 10^{15}$ eV; $F = 2.5 \cdot 10^{-7}$ m^{-2} s^{-1} sr^{-1}.

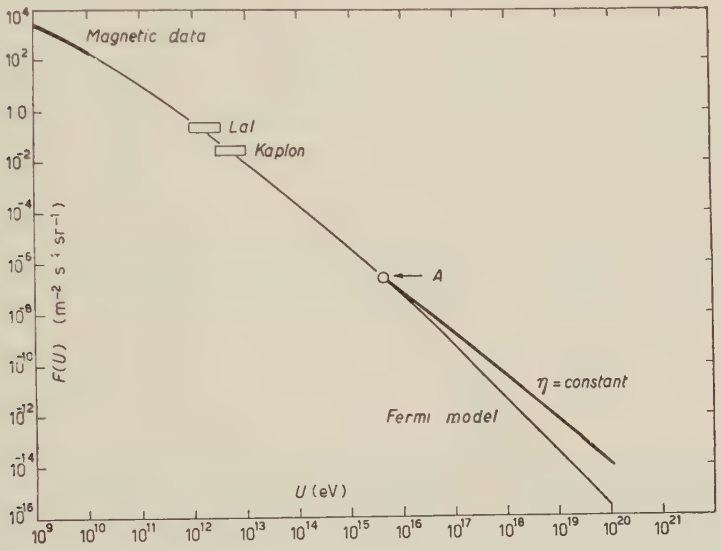

Fig. 4. – The integral energy spectrum of the primary cosmic radiation. Point A is discussed in the text. The two curves beyond point A represent reasonable upper and lower limits for the real spectrum.

Beyond point A the energy spectrum can be deduced, at least for the time being, only through the number spectrum, i.e., by estimating the energy of the primary that generates at sea level a shower containing N ionizing particles. The ignorance of a good model for the nucleon-nucleon and meson-nucleon interactions, as well as the uncertainties about the composition of the primary radiation allow only the determination of limiting values within which the real energy spectrum probably lies. The upper limit, represented in Fig. 4 by the curve $\eta = \text{constant}$, is deduced by assuming the ratio

$$\eta = \frac{\text{Total energy of primary cosmic rays}}{\text{Number of particles in shower at sea level}} =$$

$$= \text{constant} = 1.2 \cdot 10^{10} \text{ eV},$$

which is the value found for point A.

More likely η decreases when N increases, since all showers detected thus far are, at sea level, beyond their maximum development.

A lower limit is given by assuming that the primary particles are all protons and that all the interactions are describable with the Fermi model; in this case the energy of the primary is certainly degenerated too soon. The calculations utilized in plotting the branch labeled « Fermi model » are those by Oda.

The real spectrum probably lies between the two curves, somewhat closer to the lower one. An expression that represents a spectrum that satisfies the fixed points and then stays $\sim \frac{1}{3}$ of the way between the two limiting curves, closer to the lowest, is the following:

$$F(U) = 10^{13}\, U^{-(0.67\,+\,0.037 \mathrm{Log}\, U)} \ \mathrm{m^{-2}\ s^{-1}\ sr^{-1}}\,,$$

where $10^{10} < U < 10^{19}$ is the total energy of the primary, in eV. The logarithmic derivative is

$$\gamma = -\frac{\mathrm{d\ Log}\ F}{\mathrm{d\ Log}\ U} = 0.67 + 0.074\ \mathrm{Log}\ U\,.$$

PART IV.

SECTION B: **Harwell Air Shower Experiments.**

Harwell Air Shower Experiment.

T. E. CRANSHAW, W. GALBRAITH, N. A. PORTER, J. DE BEER and M. HILLAS

Atomic Energy Research Establishment - Harwell

The apparatus consists of 91 G.M. units on a triangular lattice covering an area of .5 km². A detailed description is published elsewhere [1]. Showers are recorded by the coincidences caused among the G.M. units, and sizes are estimated by the number of units triggered.

1. – Time variations of air showers.

An analysis of showers containing about $5 \cdot 10^6$, 10^7 and $2 \cdot 10^7$ particles has been made covering two years observations. In sidereal time, the distributions are isotropic to about 1% for the smaller showers and 3% for the larger showers. We do not propose to discuss the implications of this result here.

In solar time, the results are by no means clear cut. On two previous occasions we have reported that there appear to be both diurnal and semi-diurnal components in the rate of the large showers. Discussion has usually centred on the reality of the variations, and the significance of the statistical results. There have been two reasons for doubting the reality of the variations, even when the probability of such large amplitudes arising by chance is as small as say .1%. These are firstly the difficulty of finding a mechanism which could introduce the large variations, so that one has to balance the improbability of the statistics against the implausibility of the mechanism, and secondly, the fact that the statistics, even when significant, do not behave in the expected way. In our experiment, and in others, it has been found that the amplitude is large and of an encouraging significance early in the experiment, but that the am-

plitude and perhaps the significance, falls with time. If the variation were real, and constant, then the significance should increase exponentially with time.

Fig. 1.

Fig. 1 shows the measured amplitude of the solar diurnal and semi-diurnal waves in the rate of showers containing about $2 \cdot 10^7$ particles, from the beginning of the experiment to the present time. It will be seen that both amplitudes are large at the beginning, but that the semidiurnal wave falls to a constant value of about 11%, and that the diurnal wave is still decreasing at the present time. The line marked « expected » gives the amplitude which would be expected to be exceeded 50% of the time.

Fig. 2 shows the probability that amplitudes as large as the observed values should arise as a result of chance fluctuations. If the variation were real and constant, on a log plot this probability should decrease linearly with time, as seems to be the case at the present time for the semidiurnal wave. The diurnal wave, however behaves more erratically.

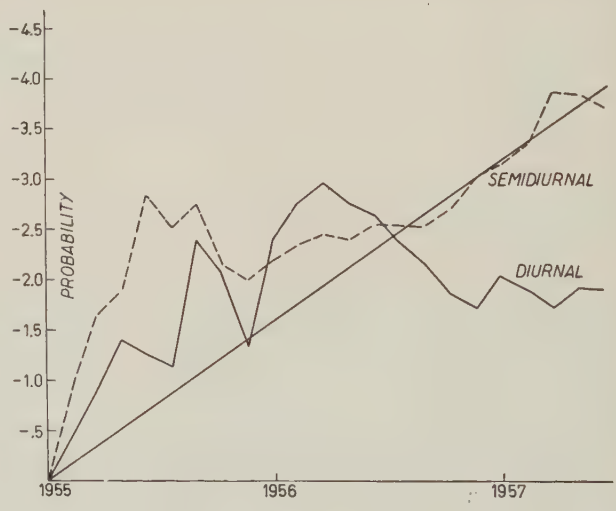

Fig. 2.

The observed behavior may be brought about in three ways.

i) The amplitude is a vector, and when a measurement of a vector is subject to an error vector of comparable length, the resultant vector is more likely to be larger than smaller than the true vector. This would lead to an overestimate of the amplitude at the beginning of the experiment, no matter when the experiment started. If the true vector is R, and the error vector is r, then the expectation of ϱ^2 the square of the observed vector, is the expectation of $R^2 + r^2 - 2rR\cos\theta$, where θ is the angle of the error vector with the true vector. The expectation of $2rR\cos\theta$ is zero, and the expec-

tation of r^2 can be calculated. This suggests estimating $R = \sqrt{\varrho^2 - r^2}$, and this is shown in Fig. 3. In this case it seems plausible to consider the semi-diurnal wave as nearly constant, though the diurnal term is still decreasing with time.

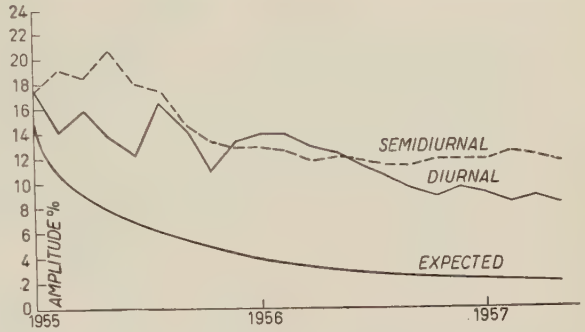

Fig. 3.

ii) A variation of the phase. This also gives an amplitude which is large at the beginning of the experiment, but the amplitude falls to the final value in such a way that the difference from the final value is inversely proportional to the square root of the observation time. If the phase changes in a time of the order of a month, it may require a very long time to reach the final value. Fig. 4 shows two specimen amplitudes which have been derived by accumulating individual amplitudes whose phase was allowed to vary in a roughly normal way. The asymptotic value is shown dotted. It can be seen that even after 30 steps, the amplitude is still quite far from the final value.

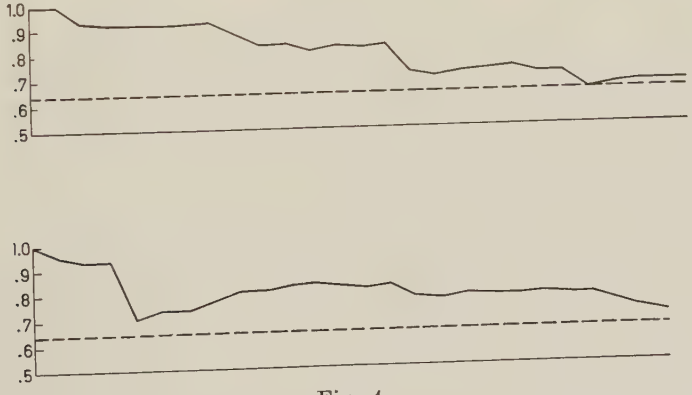

Fig. 4.

iii) A variation of amplitude, combined with a fortunate time of starting the experiment.

In our experiment i) is certainly operating. When allowance for i) is made, we find that the results for the semi-diurnal component are possibly consistent with a steady variation of amplitude 11 %. The diurnal term however, is still

falling at the present time. This suggests that ii) may be operating as was suggested by harmonic analysis about a year ago [2]. Fig. 5 is reprinted from this paper, and shows the diurnal and semi-diurnal vectors on a harmonic dial.

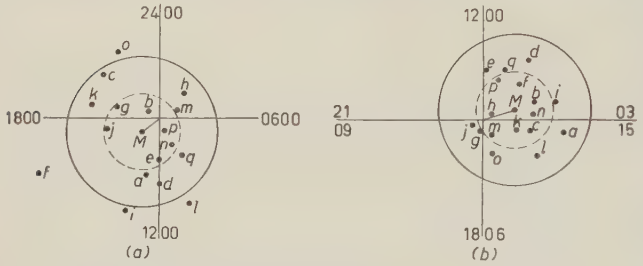

Fig. 5.

However examination of these results month by month shows that iii) is almost certainly operating as well. The phase of the variations during periods which show large amplitudes are quite similar.

The results of our analysis may be summarized as follows.

i) The variation appears to be confined to particular small groups of shower sizes.

ii) With limited statistical accuracy, no difference could be found in the structure of the showers at the maxima and minima of the variations.

iii) For most of the period, the mean rate of recording showers is independent of the amplitude of the variation.

iv) Exceptional periods occur when the variation extends to relatively small showers. During these periods, the amplitude may be large ($\sim 30\,\%$) and significant results can be obtained in a month or even 10 days. Such months have been August 1956, January, February and March 1957. The observations for these months are shown in Fig. 6. The probability of such amplitudes arising by chance is in all cases less than 2 %.

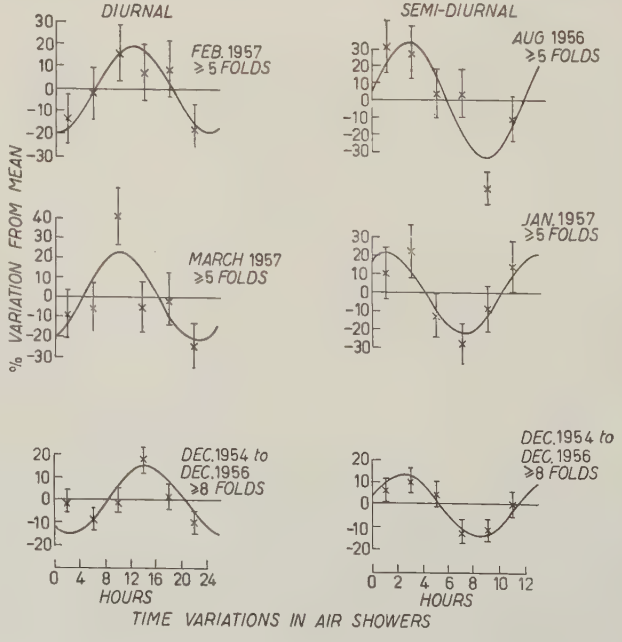

Fig. 6.

2. – The absorption of air shower particles.

The barometric pressure measures the mass of air above the apparatus, and therefore changes in the barometric pressure can be used to measure the apparent absorption of the particles. However, a change in pressure causes a change in density of the air and hence a change in the radiation length measured in metres, and this may cause a change in rate apart from effects due to absorption. The magnitude of this effect can be estimated from ths temperature coefficient, and the use of the gas laws,

$$\frac{\delta\varrho}{\varrho} = -\frac{\delta T}{T}\bigg|_t - \frac{\delta t}{t}\bigg|_x ,$$

where ϱ is the density, T the temperature and t the atmospheric depth.

Thus

$$\beta' = \frac{\delta R}{R}\frac{1}{\delta t} = -\frac{\delta R}{R}\frac{1}{\delta T}\cdot\frac{T}{t} ,$$

where β' is the contribution to the barometric coefficient due to the density effect. If T is measured in °K and t in cm Hg,

$$\frac{T}{t} \sim 4 \quad \text{and} \quad \beta' = -4\theta ,$$

where θ is the temperature coefficient.

The temperature coefficient has been measured in some cases, and can also be calculated. The Table I shows values of the barometer coefficient and

TABLE I.

N	$7\cdot10^3$	$3\cdot10^4$	$9\cdot10^4$	$4\cdot10^5$	$5\cdot10^6$	10^7	$2\cdot10^7$
B	$-9.9\pm.7$	$-10.4\pm.8$	-14.1 ± 1.7	-13.6 ± 3.7	$-14.3\pm.8$	-16.0 ± 1.5	-18.1 ± 4
θ	$-.89\pm.24$	$-.37\pm.26$	$-.37\pm.60$	-2.14 ± 1.25	$0.08\pm.07$	$+.21\pm.15$	$+.6\pm.7$
$-(B+4\theta)$	12 ± 1.5	12 ± 1.4	15.6 ± 2	14.6 ± 4	14.0 ± 1	15.2 ± 2	17 ± 4
Λ g/cm²	113	113	87	93	98	90	80
λ	195 ± 24	195 ± 24	140 ± 16	160 ± 50	165 ± 12	180 ± 25	160 ± 40

temperature coefficient for two shower experiments, the first four values being given by F. J. M. FARLEY (private communication). In the fourth row, a correction has been made using a judicious combination of the theoretical and measured values for the temperature coefficient. In the fifth row, we have calculated the apparent absorption. This seems to show a progressive softening of the radiation with increasing energy, as is also indicated by the

M.I.T. communication. However the absorption length of the particles in the shower is given by $\lambda = \gamma\Lambda$. It is difficult to see how an absorption length could decrease with increasing energy, and it is here suggested that over the range of shower sizes in the table, γ increases from about 1.5 to 1.9 or 2.0, so that the particle absorption is nearly constant at about 180 g/cm².

The present data on the absorption of the μ-component of extensive air showers are rather puzzling. Both GREISEN [3] and DOBROTIN *et al.* [4] agree that the μ's are about twice as abundant in showers at sea level as at mountain altitudes. This leads to an absorption length of about 350 g/cm² which seems unexpectedly short. We have accordingly tried to measure the dependence of the number of μ-mesons in our showers on barometric pressure.

A preliminary analysis shows that the number of μ-mesons increases by $1.5 \pm 4\%$ per cm Hg, which leads to $1/\lambda_{\text{abs}} = .004 \pm .003$ or $\lambda_{\text{abs}} = 250^{+700}_{-100}$. This result does not exclude the possibility of a long absorption length. We hope to increase the accuracy of this measurement.

3. – The spectrum of air showers.

We have used the data from the experiment to calculate the size spectrum of showers in the region $3 \cdot 10^6$ particles to $3 \cdot 10^8$.

The method of calculation is as follows:

We first calculate the probabilities $P(N, f)$ that f units will be triggered by a shower containing N particles. This is carried out by a Monte Carlo method. We then assume a spectrum of the form

$$J(N)\,\mathrm{d}N = kN^{-\gamma-1}\mathrm{d}N\,.$$

Then the rate of observing showers triggering f units is

$$R(f) = A\int_0^\infty J(N)\,\mathrm{d}N P(N, f)$$

where A is the sensitive area of the apparatus or

$$R(f) = Ak\int_{-\infty}^{\infty} \exp\left[w\gamma\right]P(w, f)\,\mathrm{d}w\,,$$

where $w = \ln N$.

If we assume a value γ_0, known nearly to satisfy the data, we may write

$$R(f) = Ak\left\{\int_{-\infty}^{\infty} \exp\left[w\gamma_0\right]P(w, f)\,\mathrm{d}w + \delta\gamma\int_{-\infty}^{\infty} w\exp\left[w\gamma\right]P(w, f)\,\mathrm{d}w\right\},$$

where $\delta\gamma$ is a correction to the value γ_0.

Both these integrals can be evaluated and the experimental rates for different values of f give a series of simultaneous equations which can be solved by a least squares method for k and $\delta\gamma$.

Finally an independent check can be applied in the following way. The mean number of particles in showers triggering more than f units is

$$\overline{N} = \frac{\int_0^\infty N^{-\gamma} P(N, \geqslant f)\, \mathrm{d}N}{\int_0^\infty N^{-\gamma-1} P(N, \geqslant f)\, \mathrm{d}N}$$

and using γ from above, this quantity can be calculated.

But N is also given by

$$\overline{N} = \int_0^\infty 2\pi r \varrho \, \mathrm{d}r \,,$$

where ϱ is the density at r.

This can be expanded as follows

$$a\overline{N} = \int_0^\infty (1 - \exp[-\varrho a]) 2\pi r \, \mathrm{d}r +$$

$$+ \frac{1}{2} \int_0^\infty (1 - \exp[-\varrho a])^2 2\pi r \, \mathrm{d}r +$$

$$+ \frac{1}{3} \int_0^\infty (1 - \exp[-\varrho a])^3 2\pi r \, \mathrm{d}r + \ldots .$$

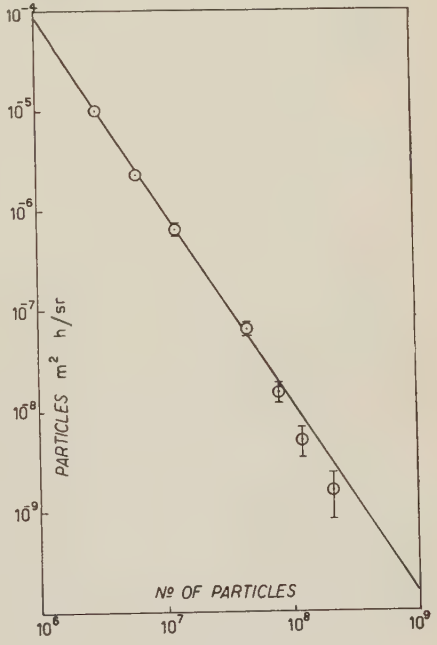

Fig. 7.

These terms give the mean probability averaged over many showers that one, two, three etc., counters of area a should be triggered in coincidence with the shower. We have used six counters of area 17 cm² to determine $\overline{N}$ for the showers which trigger $\geqslant 3$, $\geqslant 5$, $\geqslant$,8 units on the main array and have compared the results with the figures given by the calculation from the spectrum. The figures agree to within about 15%.

The results of the analysis are shown in Fig. 7.

We find for the spectrum,

$$J(> N) = 2.4 \cdot 10^{-12} \left(\frac{N}{10^{-6}}\right)^{-1.88} \mathrm{cm}^{-2}\ \mathrm{s}^{-1}\ \mathrm{sr}^{-1}.$$

4. – The lateral structure of soft and penetrating components in extensive air showers.

4·1. *All charged particles.* – The lateral distribution of all charged particles has been measured using the basic units, with one unshielded tray of 1200 cm² area. Information from the small « *b* » counters was used for small distances from the core, from both the « *b* » counters and the pairs of « *a* » counters for intermediate distances, and from the unshielded tray at large distances.

The centroid of units struck in a shower was determined either by visual estimation or by means of an analogue device, and its position taken as the position of the core. Concentric annuli were drawn about it, and the number of units struck in each annulus determined as a fraction of the total possible number. Densities were determined by repeated use of the expression $p = p(1 - \exp[-\varrho A])$.

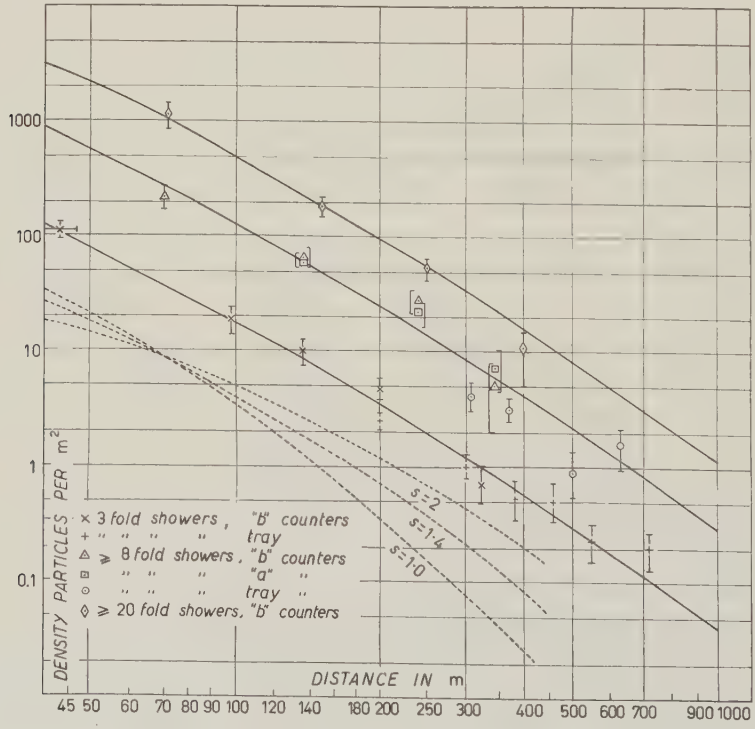
1000
100
10
1
0.1
DENSITY PARTICLES PER m²
× 3 fold showers, "b" counters
+ " " " " tray
△ ⩾ 8 fold showers, "b" counters
□ " " " "a" "
○ " " " tray "
◇ ⩾ 20 fold showers, "b" counters
s=2
s=1·4
s=1·0
DISTANCE IN m
45 50 60 70 80 90 100 120 140 180 200 250 300 400 500 600 700 900 1000

Fig. 8.

Lateral distribution for 3 fold, ⩾ 8 fold, and ⩾ 20 fold showers, have been determined for distance 45 ÷ 700 m from the core, and are shown in Fig. 8.

The distribution are all similar in form and compatible with the Nishimura-

Kamata curve for $S = 1.4$. Total numbers of particles derived by integrating the normalized theoretical curves are in good agreement with direct determinations (Sect. 3), implying that the Nishimura-Kamata curves are probably a good approximation also in the region $(0 \div 45)$ m. No correction has been applied for incident zenith angle. This will not alter the form of the distribution appreciably, but will give rise to a correction of about 5% in density values.

4·2. *μ-mesons.* – The μ-meson distribution has been measured from 50 to 1000 m from the core and is shown in Fig. 9. Four detectors were used, shielded with 20 cm of lead, and selecting particles of > 450 MeV. The counters in each detector were connected in two banks, and a rough separation between μ-mesons and interacting particles could be made by subtracting the number of double bank coincidences expected on the hypothesis that only μ-mesons occur, from the number observed in any part of the shower. The contribution from interacting particles was negligible at distances > 100 m from the core. Methods of analysis were similar to those employed for all charged particles. The μ-meson distribution is flatter than that for electrons, behaving as $r^{-0.87}$ at 50 m, $r^{-1.5}$ at 500 m and $r^{-1.3}$ at 1000 m.

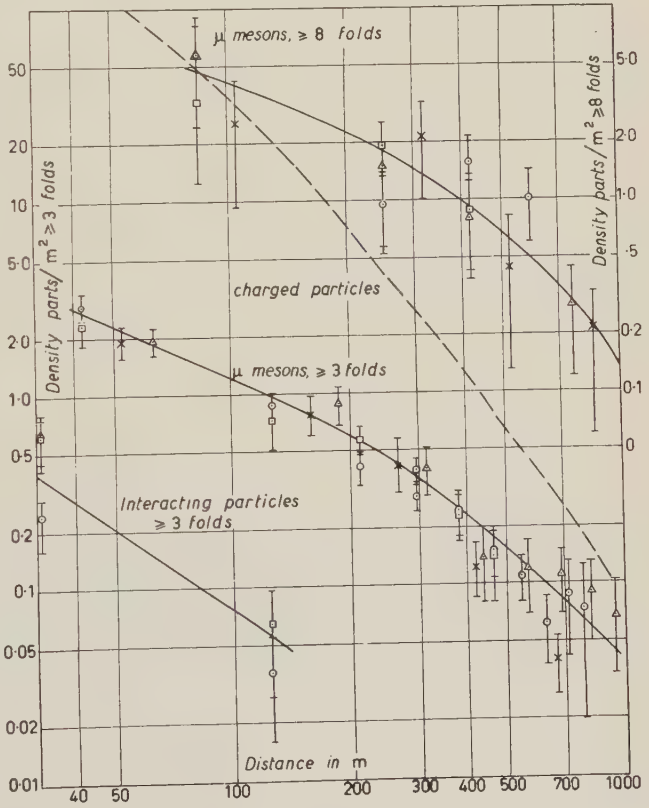

Fig. 9.

The proportion of μ-mesons is 1.5% at 50 m, and about 30% at 700 m. The proportion over the whole shower is uncertain, because of contributions from distances greater than 1000 m, but appears to be about 8%, if the observed distribution is extrapolated. This proportion and the form of the distribution are independent of shower size over the range studied.

4·3. *Interacting particles.* – The distribution is too steep to determine, because of the coarse lattice spacing of the array, and consequent uncertainty in the position of the core. Density determinations are consistent with results from smaller showers. The total numbers of interacting particles in the showers have been determined using shielded detectors in the centre of the array, and integrating over the whole structure as described in Sect. 3. The proportion of interacting particles in 3-fold showers is about 0.3%. It is not yet possible to determine whether this proportion changes with shower size.

4·4. *Energy distribution.* – The lateral distribution of energy in the electron photon component has been determined by total absorption in a water-filled Čerenkov counter. The distribution is very similar to that for all charged particles, and within the statistical errors the energy associated with each electron remains constant at about 270 MeV from $50 \div 500$ m from the core. Therefore, if the photon component is assumed to carry the same energy as the electron component, the mean electron energy is close to the critical value for air, 120 MeV, throughout this region. The mean energy per electron appears to increase somewhat for $r < 50$ m. The total energy appearing in the electron-photon component at sea level, in 3-fold showers, which contain $3.2 \cdot 10^6$ particles, is at least 10^{15} eV.

REFERENCES

[1] T. E. Cranshaw and W. Galbraith: *Phil. Mag.*, **2**, 797 (1957).
[2] T. E. Cranshaw and W. Galbraith: *Phil. Mag.*, **45**, 1109 (1954).
[3] K. Greisen: *Progress in Cosmic Ray Physics*, vol. **3**, (Amsterdam, 1956).
[4] N. A. Dobrotin, G. T. Zacepin, S. I. Nikol'skij and G. B. Hristiansen: *Suppl. Nuovo Cimento*, **4**, 635 (1956).

INTERVENTI E DISCUSSIONI

— H. Messel:

I would like to make a comment which not only applies to what Cocconi and the Harwell group have stated, but likewise will apply to a great deal of what we shall be hearing to-day on the structure of extensive air showers. I now refer to the Nishimura-Kamata expression for the lateral structure of extensive air showers. It has become evident that most people are not aware how this expression was derived and

therefore what its true significance is. Among the many approximations made which make the calculation inapplicable to true extensive air showers there is one very serious one: It stems from the fact that their expression for the lateral distribution function is essentially constructed from the second moment of the distribution function only and how this can lead to a result which gives agreement with experiment over distances varying from one to 300 m, is beyond me. In fact, there can be no explanation other than accident for the excellent agreement between experimental results and the Nishimura-Kamata expression. A realistic theoretical expression for the lateral distribution still waits to be worked out.

SUPPLEMENTO AL VOLUME VIII, SERIE X
DEL NUOVO CIMENTO

N. 2, 1958
2° Trimestre

Čerenkov Radiation in the Atmosphere and Its Application to the Study of Extensive Air Showers.

J. V. JELLEY

Atomic Energy Research Establishment - Harwell

1. – Introduction.

After BLACKETT's initial prediction [1] that a fraction $\sim 10^{-4}$ of the total intensity of the light of the night sky should be produced by the Čerenkov radiation from the passage of cosmic-ray particles through the atmosphere, GALBRAITH and JELLEY [2] discovered that intense pulses of light associated with air showers of primary energy $\geqslant 10^{14}$ eV could be detected with very simple apparatus. This initial discovery was then followed by a series of exploratory experiments [3, 4, 5] which revealed that the light pulses were in fact due to Čerenkov radiation; additional confirmation came from laboratory experiments on single particles in air in the absence of background light [6-9].

Except for a preliminary measurement of the lateral distribution of the light on the ground [10], and two theoretical studies of the phenomenon [11] and [12], work in the field has been very sporadic. This present paper is concerned with some of the general features of the technique and its practical applications to the direct study of the air showers themselves.

2. – Properties of light receivers and their applications.

As a detector of air showers, a light receiver has the following properties:

i) Showers may be detected by a *single* instrument.

ii) The effective collecting area of the receiver is large compared with its physical dimensions.

iii) The instrument is highly directional, its field of view being controlled by the optics of the system and the Coulomb scattering of the particles.

iv) Since, in a clear atmosphere, the light behaves as a penetrating component of the showers, it is possible to obtain information from showers that have died out at higher levels in the atmosphere; this is particularly noticeable when observing oblique showers at large zenith angles.

The applications of the technique to studies of air showers are very limited, and it is unlikely that any useful information would be obtained by using light receivers on their own. Used, however, in conjunction with air shower arrays which can measure simultaneously the location of a shower core, and the particle density, there is no doubt that one or more light receivers would gain much supplementary information on individual showers.

Since a light receiver measures, in effect, the integrated light from many particles, it is evident that the type of information obtained from such light detectors is of a very different type from that obtained by most other arrangements of apparatus for studying showers. Moreover, in view of the variation of the Čerenkov light yield and emission-angle with particle energy, and the many and varied effects produced by Coulomb scattering, and the angular and lateral distributions of the particles in the shower, the information gathered by light receivers is of a very indirect type.

With these considerations in mind the possible applications of the technique may be grouped under the following headings.

i) The direct determination of the vertical distribution of electrons in the atmosphere, for showers of different size; an experiment of this type which entails measuring the lateral distribution of the light from the shower core, has been performed by ČUDAKOV and is described elsewhere in this volume.

ii) The search for, or confirmation of « point sources » of high energy cosmic rays, if indeed such sources exist.

iii) The study, with the aid of ultra-fast electronics, of the duration of the light pulses; this would give information on the spread in the longitudinal development of showers, a result which would be complimentary to the findings of BASSI *et al.* [13] from their experiments on delayed particles.

iv) The determination of the zenith-angle dependence of the direction of arrival of showers of different type. For this, three or more spaced light receivers of large acceptance angle would be operated in coincidence, and connected to circuits for measuring time delays.

The light receivers themselves are exceptionally simple to construct and are also very cheap, particularly for work at the higher energies when single

photo-multipliers can be used without any additional optical system. The essential features of the equipment used by the Harwell group are shown in Fig. 1.

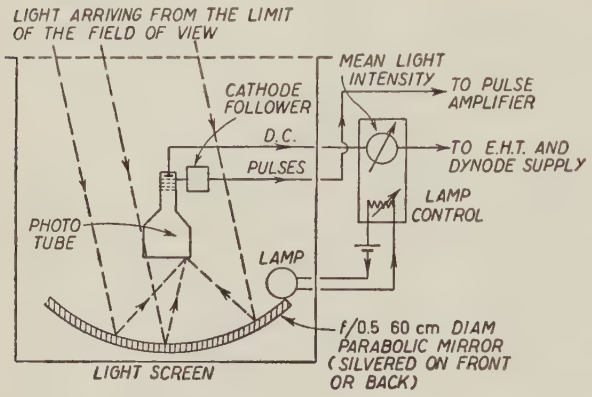

Fig. 1.

By far the most serious limitations to the technique are climate, that the work is severely restricted to dark clear moonless nights, and that it is almost essential to operate in a locality well removed from the lights and haze from nearby towns. It is expected that ideal conditions would be found at low latitudes for which the duration of twilight is short, and on a mountain plateau, to provide space for the associated air-shower array and to be above the haze normally found at sea-level.

3. – Sensitivities and counting rates.

The threshold sensitivity of a light receiver is determined by « noise ». This noise, which arises from the high intensity of the background light of the night sky, is due to the statistical fluctuations in the rate of emission of photoelectrons from the cathode of the phototube. It is a function of the collecting area A, and the field of view Ω, of the light receiver, and depends on the cut-off frequency f_c of the amplifier and the light flux φ_B of the background light of the night sky. The mean current flowing from the photocathode, is given by

$$i \sim \varphi_B A \Omega \eta \quad \text{photoelectrons per second}, \tag{1}$$

where η is the cathode conversion efficiency. The average number of photoelectrons emitted per unit resolving time $\Delta\tau$ of the system (where $\Delta\tau = 1/f_c$) is thus $\Delta i \sim \varphi_B A \Omega \eta \Delta\tau$ so that the noise-level N, due to the fluctuations on this number, is given by:

$$N = \sqrt{(\varphi_B A \Omega \eta / f_c)}\,. \tag{2}$$

For example, for a typical light receiver $A = 500$ cm², $\Omega = 0.15$ sr, $\eta = 10\,\%$ and $f_c = 5$ Mc/s. If we take a mean value for φ_B of $2.6 \cdot 10^4$ erg, or

$6.4 \cdot 10^7$ photons cm^{-2} s ^{1} sr^{-1}, from the works of ČUVEEV [14] and of BABCOCK and JOHNSON [15], we find from (2) that $N \sim 10$ photoelectrons. The light flashes detectable with such a receiver at a bias of say five times noise will then contain $\sim (50/\eta)$ photons, and the corresponding signal flux φ_s will be $(50/A\eta)$, in this case ~ 1 photon cm^{-2} $flash^{-1}$.

So much for the absolute sensitivity of a light receiver. We frequently wish however, to know the relative sensitivities of light receivers of different type, so that we can choose the parameters A, Ω and f_c, to determine in advance the threshold shower energy E_{min} and hence the counting rate R. To obtain the required relationships, the following assumptions will be made:

1) The bandwidth is never large enough to resolve the separate photoelectron pulses from the background light, i.e. complete « pile-up » of noise pulses is assumed.

2) The pulse-height distribution for the light pulses is of the form $N(>h) \sim h^{-1.5}$ (see reference [2]).

3) For showers falling always at the same distance from a light receiver, the pulse height h is proportional to E, the primary energy of the shower, so that $N(>E) \sim E^{-1.5}$.

4) The angular distribution of the axes of the showers is isotropic within the field of view of the receiver.

5) Scattering and absorption of the light is neglected, as also are diffraction, dispersion and refraction.

Let the diameter of the light-collector be $D (ie A = \pi D^2/4)$ and the half-angle of the field of view be $\circ (ie \Omega = \pi \varkappa^2)$, then, if S and N are the signal and noise amplitude (in terms of the number of photoelectrons liberated at the cathode of the phototube), we obtain the following relations.

a) $R(D)$; α *and* f_c *const.*

For a light pulse $S \propto A \propto D^2$

Background illumination $B \propto A \propto D^2$

But $N \propto \sqrt{B} \propto D$, $\therefore (S/N) \propto D$ and $B \propto D^{1.5}$

b) $R(\varkappa)$; D *and* f_c *const.*

The rate of reception of light pulses from showers of given E_0 is $\propto \Omega \propto \theta^2$, but their signal size $S = \text{const.}$

$(S/N) \propto 1/\theta$ and thus $R \propto (1/\theta)^{1.5} \cdot \theta^2 \propto \theta^{3.5}$

c) $R(f_c)$; *D and* θ *const,*
$N \propto \sqrt{(B/f_c)}$. Provided the duration of the flash is $\ll (1/f_c)$, S is independent of f_c. $\therefore (S/N) \propto \sqrt{f_c}$ and $R \propto (\sqrt{f_c})^{1.5} \propto f_c^{0.75}$.

The lowest detectable light intensity depends directly on the noise level, and the corresponding threshold light *flux* φ_s will depend on A, so that $E_{min} \propto (N/A)$.

d) $E_{min}(D)$; θ *and* f_c *const.*
From *a*), $N \propto D$ $\therefore E_{min} \propto (1/D)$.

e) $E_{min}(\theta)$; *D and* f_c *const.*
From *b*), $N \propto \theta$ $\therefore E_{min} \propto \theta$.

f) $E_{min}(f_c)$; *D and* θ *const.*
From *c*), $N \propto 1/\sqrt{f_c}$ $\therefore E_{min} \propto 1/\sqrt{f_c}$.

Although these relationships have not been individually tested, it is evident they are at least qualitatively correct, by comparing the observed counting rates obtained from time to time from various light receivers with those calculated from the above relations, see the following table.

D (cm)	A (cm²)	α (degrees)	Ω (sr)	Calc. R (min^{-1})	Exp. R (min^{-1})	φ_s photons (cm^{-2})	E_{min} eV	Remarks
25	490	12	0.15	1.5	1.5	3	10^{14}	First receiver
61	2900	5.8	0.032	3.9	~ 5	0.57	$2 \cdot 10^{13}$	Pic du Midi
61	2900	14	0.20	6.0	7	1.4	$5 \cdot 10^{13}$	»
150	17700	4.9	0.022	14	11	0.2	$7 \cdot 10^{12}$	Searchlight
12.7	126	30	0.85	0.84	1.0	14	$5 \cdot 10^{14}$	5in. phototube; no mirror.

The values of R_{calc}, φ_s and E_{min} have been normalized to the observed figures obtained with the first receiver. For showers falling at a given distance from a receiver, it is clear that the larger instruments will detect lower energy showers; the same instrument of course will also detect the larger showers falling further away. The experiment for which the light receiver is used, will determine the choice of instrument and its operating conditions.

4. – Future developments.

It is now evident, particularly from MILLAR's work reported elsewhere in this volume, that the angular distribution of the light from a shower is governed

primarily by the Coulomb scattering of the shower particles, the angles for which are in general greater than the Čerenkov angle. It is therefore very desirable to obtain the distribution of light across the image at the focus of the mirror. It is to be hoped that this may be achieved by the development of some form of pulsed image converter, pulsed in order to minimize the build-up of the considerable background light. If an Iconoscope or Orthicon storage camera could be constructed whose noise-level is limited by primary photoelectron emission, this would serve equally well, since the background noise could be wiped off at a high repetition rate.

The practical limits on the optical side have already been reached with parabolic mirrors of large diameter and a focal ratio of f/0.5. It is preferable, particularly with large fields of view, to use spherical optics instead; for this it would seem quite feasible to develop large telescopes of the Schmidt type, the optics for which of course need only be crude for this application.

Another attractive possibility is to detect Čerenkov radio-pulses in the millimetre region of the spectrum where there is no background radiation and the receiver could be run day and night. Since the yield of Čerenkov radiation is proportional to $\omega\,\mathrm{d}\omega$, where ω is the mid-band frequency and $\mathrm{d}\omega$ the bandwidth, it is essential to operate at the highest possible frequency. A second requirement is that the wavelength should be small compared with the average spacing of the electrons and positrons in the core of the shower, to avoid decoherence of the radiation from neighbouring particles. The upper limit to frequency is set by the O_2 and H_2O atmospheric absorption bands at wavelengths of $\lambda = 0.5$ and $\lambda = 1.3$ cm respectively, and by the noise factors of existing receivers. $\mathrm{d}\omega$ is limited to ~ 100 Mc/s by the duration of the pulses.

If we take the *measured* intensity of Čerenkov radiation in the *visible* region for a 10^{14} eV shower ($\omega_v \sim 7 \cdot 10^{14}$ c.p.s., $\mathrm{d}\omega_v \sim 1.5 \cdot 10^{14}$ c.p.s.), it is found that a pulse power of $\sim 2 \cdot 10^{-12}$ W should be obtainable from a shower of primary energy 10^{17} eV, with a parabolic mirror of diameter 300 cm, with $\omega_R \sim 4 \cdot 10^{10}$ c.p.s. ($\lambda \sim 0.8$ cm) and $\mathrm{d}\omega_R \sim 10^8$ c.p.s. The noise-level in a perfect receiver at this wavelength, for which the extra-terrestrial noise is negligible, is given by $kT_{273}\,\mathrm{d}\omega_R$, which in this example will be $\sim 4 \cdot 10^{-13}$ W. The signal to noise would then be $\sim 5/1$. The field of view of such a receiver would be severely restricted by the diffraction width of the aerial beam which is $\sim (\lambda/D)$ or, in this case, $\sim 0°.2$. Such an instrument might however find applications if evidence is ever found for « point » sources at the highest energies.

REFERENCES

[1] P. M. S. Blackett: *Emission Spectra of Night Sky and Aurorae*, in *Rep. Conf. Gassiot Comm. Roy. Soc.* (1947), (London, 1948), p. 34.
[2] W. Galbraith and J. V. Jelley: *Nature*, **171**, 349 (1953).
[3] W. Galbraith and J. V. Jelley: *Journ. Atmos. Terrestial Phys.*, **6**, 250 (1955).
[4] J. V. Jelley and W. Galbraith: *Journ. Atmos. Terrestial Phys.*, **6**, 304 (1955).
[5] N. M. Nesterova and A. Čudakov: *Žu. Èksper. Teor. Fiz.*, **28**, 384 (1955),
[6] A. Ascoli Balzanelli and R. Ascoli: *Nuovo Cimento*, **10**, 1345 (1953).
[7] A. Ascoli Balzanelli and R. Ascoli: *Nuovo Cimento*, **11**, 562 (1954).
[8] F. R. Barclay and J. V. Jelley: *Nuovo Cimento*, **2**, 27 (1955).
[9] R. J. Hanson and D. C. Moore: *Nuovo Cimento*, **4**, 1558 (1956).
[10] F. R. Barclay and J. V. Jelley: *Oxford Conference on Extensive Air Showers* (1956), p. 74, Atomic Energy Research Establishment - Harwell.
[11] A. Polikarov: *Compt. Rend. de l'Academie Bulgare des Sciences*, Tome 7, No. 2, 29 (1954).
[12] V. Gol'danskij and G. Ždanov: *Žu. Èksper. Teor. Fiz.*, **26**, [4], 405 (1954).
[13] P. Bassi, G. Clark and B. Rossi: *Phys. Rev.*, **92**, 44 (1953).
[14] K. Čuveev: *Dokl. Akad. Nauk SSSR*, **87**, 551 (1952).
[15] H. W. Babcock and J. J. Johnson: *Astrophys. Journ.*, **94**, 271 (1941).

PART IV.

SECTION C: **Soviet Union Air Shower Experiments.**

Brief Survey of Some Work on Extensive Air Showers Conducted in the Soviet Union.

G. T. ZACEPIN

P. N. Lebedev Physical Institute of the USSR Academy of Science - Moscow

The main direction in the study of extensive air showers which began in the USSR on the initiative and under the supervision of D. V. SKOBEL'CYN twelve years ago is an investigation of the mechanism of their development in order to get information about characteristics of nuclear interactions at superhigh energies.

At present research is being done by the Moscow and Georgian groups. The group of the Georgian Academy of Sciences was organized by Professor ANDRONIKAŠVILI a few years ago. The work begun by this group is devoted to an investigation of the lateral distribution of the penetrating components of showers observed in mines of different depth. These studies already enable to give an evaluation of transverse momentum of π-mesons generated in nuclear collisions.

The Moscow group connected with the Lebedev Physical Institute of the Academy of Sciences of the USSR and the Moscow University is conducting research according to co-ordinated plans at mountain altitude in the Pamirs and close to sea level in Moscow. The installations of our Moscow group, both in the Pamirs and at sea level, are of a combined type, making it possible to obtain various information concerning showers. Using huge hodoscope arrangements that include thousands of counters, the axis of each registered shower is located with an error of the order of one metre, and the number of particles in the shower is determined with an accuracy up to 10% (the method of correlated hodoscopes).

By means of additional counter devices and systems of ionization chambers connected in the set up, registrations are made not only of the electron component but also of the nuclear-active and μ-meson component of showers, and the lateral distribution and energy charateristiscs of different components at various distances from the shower axis are determined. Apparently, further progress in the study of showers will, to a considerable extent, be connected with arrangements that give still more deatiled information concerning each

individual registered shower. For this reason, we intend in future to continue developing our installations in this direction.

Recently, a number of studies of our group were directed towards elucidating the dependence of different shower characteristics on the total number of particles in them, that is, in the final analysis, on the energy of the primary particle.

A new element in the methods of our investigations is the study of the energy characteristics of showers, especially of the energy of nuclear-active particles in the region of the core of the shower. When a nuclear-active particle falls on a solid substance, a shower develops in the substance due to the nuclear-cascade process and practically all the energy of the incident particle is dissipated in ionization in a limited layer of the material, since μ-mesons and neutrinos in dense materials are not produced. Thus, by means of ionization chambers placed at different depths in matter, it is possible to measure the energy of the incident particles calorimetrically, so to say. This method is a direct generalization of the similar procedure which has been used by VERNOV for measurements of the energy of the electron component in the stratosphere. The first results obtained in the simplest version of this method, are presented in the papers of NIKOL'SKIJ and HRISTIANSEN and coworkers.

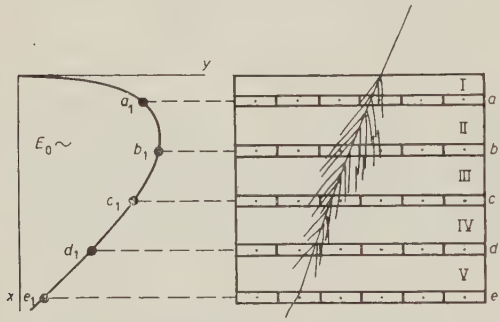

Fig. 1. – I, II, III, IV, V - layers of dense material; *a*, *b*, *c*, *d*, *e* ionization chambers; a_1, b_1, c_1, d_1, e_1 - sizes of ionization-bursts y in the respective layer of ion. chambers. Schematical representation of energy measurements of high energy nuclear-interacting particles.

Of great importance in determining the characteristics of the elementary act of nuclear interactions from data on extensive showers is the problem of fluctuations in showers. One of the experimental approaches to its study is the use (in conjunction with hodoscope arrangements) of systems of big ionization chambers placed under the layers of appropriate absorbers.

Another experimental method by means of which fluctuations in showers may be studied is the investigation of Čerenkov radiation of extensive showers in the atmosphere begun by JELLEY and GALBRAITH. In the Soviet Union, this trend is headed by A. E. ČUDAKOV.

We believe that further work in this direction will make it possible in the next few years to approach considerably to the understanding of elementary acts of nuclear interaction at super-high energies.

SUPPLEMENTO AL VOLUME VIII, SERIE X
DEL NUOVO CIMENTO

N. 2, 1958
2° Trimestre

The High-Energy Nuclear Active Component of Extensive Air Showers.

V. A. Dmitriev, G. B. Hristiansen and G. V. Kulikov

Moscow State University - Moscow

1. – Introduction.

In a number of recent investigations [1] an indication was obtained that in extensive air showers near sea level there should exist cascades of nuclear-active particles of high energy ($(10^{11} \div 10^{12})$ eV). A direct study of nuclear cascades without turning to the study of the secondary components accompanying it is of great interest in determining the characteristics of the nuclear cascade process.

In this connection we made an attempt to study statistically nuclear cascades in extensive air showers at sea level.

2. – Experimental arrangement.

Pulse ionization chambers placed under a combined absorber were used to register nuclear-active particles and to determine their energy. The streams of charged particles of extensive air showers were registred by 720 Geiger-Müller counters of different area (330 cm², 100 cm², 18 cm²) placed in groups of 12 and 24 counters uniformly around the room. Each counter was connected to a cell of the GK-7 hodoscope which used non-heater-type thyratrons [2]. The arrangement is shown schematically in Fig. 1, which also gives a cross-section of the detector of nuclear-active particles. The double circles designate the master counters.

The ionization chambers are cylinders of stainless steel with 2 mm thick walls. The diameter of the cylinder, which serves as external electrode, is

250 mm, the diameter of the internal electrode is 4 mm. The length of the operating part of the chambers is 1000 mm. After a thorough preparation, the chambers were filled with highly-pure argon to a pressure of 5 atm. The voltage was applied to the central electrode through a high resistance; the external cylinder was grounded. The chambers were calibrated electronically [3], and also using the pulses from single relativistic mesons. Curves were constructed of the number of bursts with amplitude above the given amplitude as a function of the voltage on the chamber. Transition to the plateau, at burst magnitudes corresponding to more than 100 and 40 relativistic particles, takes place with a potential less than 400 V. A voltage of 1200 V was estabilished for the operation of the chambers. The duration of the electronic pulse from the chamber was 30 μs.

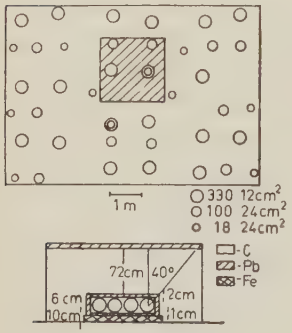

Fig. 1. – Experimental arrangement.

A block diagram of the chamber and counter circuits is given in Fig. 2. All counters are connected to the hodoscope arrangement (H); the hodoscope readings are recorded photographically by a register (R). Pulses from each chamber pass through a preamplifier (PA) to the additional device and amplifier (A). Moreover, two chambers have individual amplifiers.

The pulse amplitudes are measured by a multichannel amplitude analyzer (AA). The analyzer readings are also photographed.

The amplifier of the general channel is of the linear four-cascade type. Each cascade has a deep feedback and a separate output, due to which the dynamic range of linearly registered pulses exceeds 10^4.

The amplifiers of the separate chambers are non linear type; their dynamic range is 10^3. Only pulses that coincide with the master pulses enter the input of the analysers and the register. The resolving time is 100 μs.

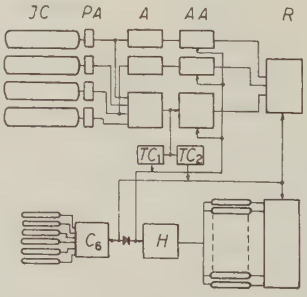

Fig. 2. – Block diagram of circuit: IC, ionisation chambers; PA, preamplifier; A, amplifier; AA, amplitude analyser; R, register; H, hodoscope; C_6, sixfold coincidences; TC_1 and TC_2, threshold circuit.

Control of the chambers and hodoscopes was effected by two systems. The first system is put into operation by sixfold coincidences of pulses from groups of counters connected in the circuit channels (C_6). The resolving time of the circuit is 2 μs. The area of each group was $(4 \cdot 330)$ cm² — 0.132 m². The arrangement of counter boxes of the control group

is shown in Fig. 1. The sixfold system of coincidences was effective to select extensive air showers with the number of particles $N \geqslant 1 \cdot 10^4$.

The second master system is operated from chambers with the pulse amplitude above the given amplitude. The duration of the pulse front from the chamber was 30 μs. Therefore, for pulses close to the threshold in amplitude, the delay in switching of the threshold circuit that selected the pulses by amplitude, is not less than 30 μs with respect to the instant of passage of particles through the chambers and counters. Still, the resolving time of the hodoscope apparatus was $(12 \div 10)$ μs. For this reason, work of hodoscope is controlled by two threshold circuits (TC_1 and TC_2) with thresholds that differ 10 times.

Pulse increase in a cylindrical chamber in the case of non local ionization is close to linear [4], therefore delay time for the first circuit is considerably less than it would be without this system.

The pulse from the first circuit controls the hodoscope and opens the input device of the analysers, but registration takes place only in case the second circuit is triggered. This ensures coordination of the chambers and hodoscope.

The threshold value of the pulse from the chamber that triggered the second system corresponded to the passage of 800 relativistic particles through the chamber. Nuclear-active particles that produce in the filter a shower containing about a thousand and more particles were therefore registered in the case of any density of the accompaning air showers.

As may be seen from Fig. 1 the absorber of the nuclear-active particle detector contains (in addition to the layer of lead adjacent to the chambers) about $1.8 \cdot R_{cmfp}$ grams of substance (R_{cmfp} is the collision mean free path). The detector is therefore highly effective for nuclear interactions. With a total probability of interaction of 0.8, the probability of interaction in carbon is 0.7 (*).

Given an interaction in any point of the graphite block, the development of an electron-photon cascade that has entered the chambers will not differ greatly, because the entire graphite corresponds to $2.5\, t_0$ units, whereas the layer of lead over the chambers contains $4\, t$ units. The average path of development of the cascade equals to $(6 \div 5)\, t$ units. In the case of such an effective

(*) The presence of a sufficiently large upper layer of lead leads to a strong softening of the energy spectrum of the soft component of the extensive air shower before hitting the graphite.

Therefore, the transition effect Pb-C in substances with critical energy differing by 14 times, leads practically to a screening of the chambers from the soft component of extensive air showers.

The effect from the soft component and other effects leading to the generation of large bursts will be examined in more details below.

layer, the electron-photon cascades produced by primary photons of energy from 10^8 to 10^{11} eV, are not far from cascade maximum.

For this reason, the number of particles in the cascade turns out to be proportional to the initial energy, irrespective of the number of primary particles carrying this energy, if the energy of the particles vary within these limits [7].

The picture is of course complicated by the presence of a nuclear cascade. It should be noted that the layer of lead under the chambers also justifies the use of cascade curves since the chambers are placed in « slits » in a homogeneous substance.

The transition effect in the walls of the chamber is not significant. One of the present authors (V.A.D.) calculated the transition effect from Pb into Fe similary to that carried out in paper [5] for the case Pb-Al.

The assumption that the spectrum of electrons and photons emerging from the lead is close to the spectrum at the cascade maximum is natural for our case.

It may be seen from the Fig. 1 that the screening used is pratically equivalent to an infinite filter.

For this reason, the boundary effects are not essential.

On the other hand, the big size of the graphite block does not lead to a perceptible increase in the effective area of registration: the emergence angle of π^0-mesons in the elementary act is small and scattering in graphite for electrons and photons is also insignificant.

The whole apparatus was housed in a special building with a roof of duralumin and foam plastics. The overall total of material over the unit did not exceed 2.0 g/cm^2.

3. – Results.

The unit operated with control by both systems for about 500 h in January and February 1957. Two hundred and eighty three bursts were registered in the chamber corresponding to a thousand and more relativistic particles. The burst spectrum is shown in Fig. 3. The spectrum is in a good agreement with a power law with the exponent for the integral spectrum $\gamma = -1.7 \pm 0.1$.

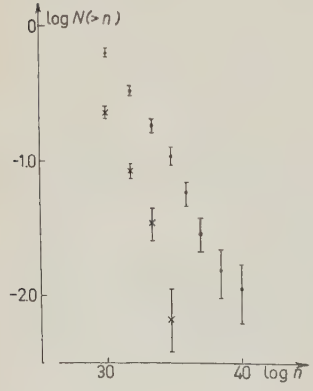

Fig. 3. – Spectrum of bursts. $\dot{\pm}$, upper points-total number of bursts. These points can be approximated by a straight line corresponding $N(>n) \sim n^{-1.7}$. $\dot{\pm}$, lower points-not accompanied by air showers. These points can be approximated by a curve $N(>n) \sim \exp[-n/560]$; N in h^{-1} m^{-2}.

The same figure shows a spectrum of bursts which were not accompanieds by air showers. They are obviously produced by strongly ionizing stars. The spectrum is quite well described by the law $N(>n) \sim \exp[-\alpha n]$, ($n$ is the burst size in ionization units with respect to a single relativistic particle that traverses the chamber with an average path, $(1/\alpha = 560)$). This agrees with data obtained in papers [6] for burst produced by stars. Bursts from stars thus determined amount to (0.36 ± 0.04) for all bursts when $n > 1000$. The total number of bursts with $n \geqslant 1000$ is equal to (0.62 ± 0.04) m^{-2} h^{-1}.

The spectrum of extensive air showers, selected by the unit is of a type that is usual for such units with a maximum at $N = 2.5 \cdot 10^4$.

The spatial distribution of axes proved practically uniform in the circle $R = 2.5$ m.

To check the « screening » of chambers from the soft component of extensive air showers, a preliminary comparison was made of the spectra of bursts (in chambers) produced by extensive air showers in the case of different thickness of the upper layer of lead: 2 cm, 4 cm and 5 cm. Spectra under 2 cm and 4 cm differ in intensity by more than twofold even in the region of $n \geqslant 1000$ Spectra under 4 cm and 5 cm do not differ (with an accuracy up to 10%) in the case of any bursts $(1000 > n > 10)$.

It is important to know the value of K, the constant of proportionality between a burst expressed by the number of relativistic particles and the energy of the primary particle that produced the given burst. Its value depends on assumptions concerning the characteristics of the elementary act.

We made an estimate of K with the following assumptions.

a) The collision mean free path (cmfp) of high-energy particles in graphite in the region of interest does not depend on the energy of the particle and is equal to $R_{\text{cmfp}} = 70$ g/cm^2.

b) The fraction of energy imparted, in each act, to mesons does not depend on the primary energy E_0 and is equal to $0.3\ E_0$. Thus $0.1\ E_0$ is given up to π^0-mesons.

c) The cross section of interaction of secondary $\pi^\pm$-mesons likewise does not depend on the energy and corresponds to $R_{\text{cmfp}} = 70$ g/cm^2. In the interaction $\frac{1}{3}$ of the initial energy of the mesons passes into π^0-mesons.

d) The number of mesons produced in interactions is not large.

We found the average fraction of energy imparted to the electron-photon component in the first three generations of the nuclear cascade that developed in graphite.

The primary spectrum of the nuclear active particles was taken into account.

It must be noted that the most probable value of energy differs from the average value only by 10%.

The development of a cascade in lead was considered on the basis of paper [7]. Insofar as the spectra of secondary π^0-mesons are unknown, the mean values were taken of number of particles under the lead. These values were obtained under the assumption that the cascade was caused by one π^0-meson of energy E or by 10 π^0-mesons of energy 0.1 E. (The difference in resulting figures is about 30%). The value of the coefficient thus obtained for bursts with $n \geq 1000$ is $K = 8 \cdot 10^8$ eV.

Analysis of hodoscope data made possible to determine in each individual shower the total number of particles N and the position of the axis. The accuracy in determing the position of the axis was about 1 m. A knowledge of the position of the axis of an extensive air shower permits the investigation of the lateral distribution of nuclear active particles of a given energy in the showers. If we have $N(r)$ showers, the axes of which fall at a distance $r, r + \Delta r$ from the detector and in $m(r, n)$ cases the accompanying bursts containing n particles are registered then

$$\varrho(r, n) = \frac{m(r, n)}{N(r) \cdot \sigma},$$

where σ-is the area of the detector, $\varrho(r, n)$ is the density of particles of given energy. In this experiment $m(r, n) \ll N(r)$ and therefore these formula is right.

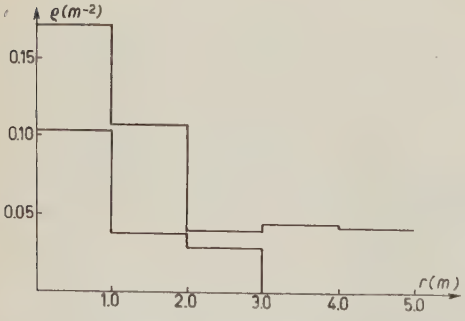

Fig. 4. – Lateral distribution of nuclear-active particles in showers. Upper histogram $100 < n < 1000$. Lower histogram $1000 < n < 10000$.

At first the functions $m(r, n)$ and $N(r)$ were determined and then the density of particles of given energy was found.

The results for particles which produce different bursts are given in Fig. 4. Data were obtained from 410 shovers with $N \geq 1 \cdot 10^4$. It must be pointed out that although the density of the nuclear-active particles producing bursts of $n \geq 1000$ quickly falls off to zero with growth of r, several cases were registered of the presence of such particles that were apparently sufficiently far from the axis in dense showers, i.e. in cases of considerable density of the soft component throughout the room in the absence of a clear gradient of density. Table I lists data on the quantity of particles of energy greater than the given energy in an average shower in a circle of radius 2.5 m, in the case of different total numbers of particles in

Table I.

N	N_{sh}	$n >$	50	100	200	400	800	1 000	1 500	2 000	3 000	4 000
$1\cdot10^4$ - $3\cdot10^4$	147	The average	2.0	1.6	1.3	0.8	0.4	0.3	0.3	0	0	0
$3\cdot10^4$ - $1\cdot10^5$	82	number of the	3.4	2.9	2.1	1.7	1.2	1.0	0.5	0	0	0
$1\cdot10^5$ - $3\cdot10^5$	35	particles in a	9.5	5.6	3.5	3.9	3.4	1.7	1.1	0	0	0
$3\cdot10^5$ - $2\cdot10^6$	9	shower $F(n)$	15	15	13	11	11	11	9	9	7	4
$1\cdot10^4$ - $3\cdot10^4$	147	The average	15	12	10	6	3	2	2	0	0	0
$3\cdot10^4$ - $1\cdot10^5$	82	number	14	12	9	8	5	4	2	0	0	0
$1\cdot10^5$ - $3\cdot10^5$	35	of the	17	10	7	7	6	3	2	0	0	0
$3\cdot10^5$ - $2\cdot10^6$	9	bursts $M(n)$	7	7	6	5	5	5	4	4	3	2

the showers: $1\cdot10^4 < N < 3\cdot10^4$; $3\cdot10^4 < N < 1\cdot10^5$; $1\cdot10^5 < N < 3\cdot10^5$ and $3\cdot10^5 < N < 2\cdot10^6$. A measurement is made of $M(n)$ number of bursts of given value with the shower axis inside the circle of radius 2.5 m and N_{sh} number of showers in the given interval of the number of particles with axes in the same circle. No matter what the form of the function of lateral distribution of particles of given energy in the shower and with a constant density of shower axes in the given circle, the number of particles of given energy in one shower in the selected circle $F(n)$ is determined by the following expression:

$$F(n) = \frac{M(n)\cdot S}{N_{sh}\cdot\sigma},$$

where S is the area of the circle and σ is the area of the detector. Indeed

$$F(n) = \int_0^R \varrho^{n.a}(r) 2nr\,dr,$$

$$M(n) = \int_0^R \sigma\cdot\varrho_{n.a}(r)\cdot 2\pi A\cdot r\,dr; \qquad N_{sh} = AS; \qquad S = nR^2,$$

whence the above expression follows.

Choice of $R = 2.5$ m followed from the requirement of constant density of shower axes within the circle.

The statistics are insufficient for building a spectrum in the region of bursts greater than $h = 1000$ for each of the shower groups.

The spectrum in this region of bursts for showers with $N > 10^4$ is a power spectrum, with the exponent $k = 1.1 \pm 0.4$ (see Fig. 5).

A knowledge of the position of the axis and the magnitude of the burst

produced by the shower makes it possible to determine the lateral distribution of the energy flux carried by the nuclear active component of the shower.

Fig. 6 shows the distribution of density of energy flux for two groups of showers: with $1 \cdot 10^4 < N < 3 \cdot 10^4$ and with $1 \cdot 10^5 < N < 2 \cdot 10^6$.

Table II lists the experimental values of energy (averaged over groups

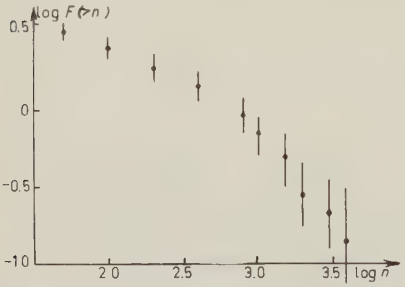

Fig. 5. – Energy spectra of nuclear active particles in showers (in number of particles per shower within a circle $R < 2.5$ m). $10^4 < N < 2 \cdot 10^6$.

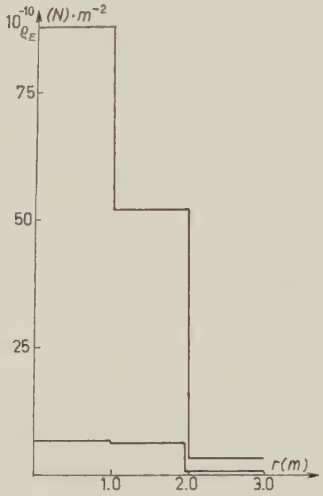

Fig. 6. – Lateral distribution of energy flux of nuclear-active particles in showers. Upper histogram $1 \cdot 10^5 < N < 2 \cdot 10^6$. Lower histogram $1 \cdot 10^4 < N < 3 \cdot 10^4$.

of showers) carried by the nuclear active component (n.a.c.) of the shower in a circle $R = 2.5$ m from the axis and also the assumed values of total energy carried by the electron, photon and nuclear cascades at the given level.

This total energy was found from the equation $E = N \cdot \beta \cdot R$ where β is the value of ionization losses per g/cm² of air; $1/R$ is the absorption coefficient of the number of particles in the shower ($R = 200$ g/cm²) and N is the total number of charged particles at the level of observation.

TABLE II.

N	$\bar{N}$	$E_{\text{n.a.c.}}$	E_{total}	$E_{\text{n.a.c.}}/E_{\text{total}}$
$1 \cdot 10^4 \div 2 \cdot 10^6$	$6.3 \cdot 10^4$	$2 \cdot 10^{12}$ eV	$2.5 \cdot 10^{13}$ eV	0.08

4. – Discussion of results.

Let us examine the data obtained. Let us first consider in more detail the nature of the observed big bursts which accompany extensive air showers.

The large bursts that are observed can in general be produced not only by nuclear active particles of high energy, but also:

1) is due to the penetration through the filter of electron-photon cascades from electrons and photons of high energy;

2) is due to the nuclear disintegrations in the walls of the chamber;

3) is due to the electromagnetic interactions of μ-mesons contained in the shower, with the formation of electron-photon cascades.

Let us evaluate the role of all these causes in an extensive air shower.

The role of electron-photon cascades in the creation of heavy ionized particles, as has already been stated due to the use of a complex filter of lead and graphite.

The electrons and photons that emerge from the last layer of lead are practically absorbed in the graphite.

If the thickness of the second layer of lead is such that electrons from electrons and photons ~ 10 MeV pass through it then absorption in the graphite filter will be complete that is an equivalent according to Rossi quantity of lead.

A calculation carried out by I. A. Patti has the form of the integral $\int_{E_0}^{\infty} \Phi(E,t)\,dE$, for example, for a primary electron or photon of energy $\sim 10^{15}$ eV we obtain that electrons below the complex filter, whereas for an equivalent according to Rossi filter of lead for number is [illegible] electrons.

If we assume that the energy spectrum of electrons may be extrapolated into the region of higher energies according to the law $E^{-\gamma}$ for $\gamma = 1.25$, which according to [illegible] is valid up to energies 10^{15} eV, then using the data of paper [8] we find that the number of electrons with $E > 10^{15}$ eV is not in disagreement with the number of particles I in (1). The question is an only how that the number of tracks with the number of registered particles > 100 observed in our showers.

From this point of view the result of the control experiments on the absorption of tracks in the case of changes in the upper layer of lead in the filter seems natural.

It should however be noted that if electrons and photons of energy $> 10^{15}$ eV are present in the extensive air showers, the role of the electron-photon cascades may grow considerably due to the Landau-Pomeranchuk-Migdal effect [9].

Nuclear disintegrations may be produced by nucleon-active particles of low energy. As is shown in [10], the products of nuclear disintegrations enter the volume of the chamber from the layer 1 g cm^{-2}.

However, in accordance with [11] even the portion of nucleon active particles of low energy does not exceed 1/10 of the number of electrons but the shower size we find that in the circle of radius 1.2 m these numbers should be small.

Assuming the range for interaction with the formation of nuclear disintegrations 100 g/cm², we obtain the number of nuclear disintegrations due to nuclear-active particles $3 \cdot 10^{-6} N$.

That is a value considerably below the observed value.

N is the number of shower particles.

The role of electron-photon cascade from radiation collisions of μ-mesons may be evaluated as follows. The radiation unit for a μ-meson $X_{0\mu} = (\mu/m)^2 X_{0e}$, where μ is the mass of the μ-meson, m is the mass of electron, and X_{0e} is the value of the radiation unit in g/cm² for the electron.

Thus, in lead the radiation unit for a μ-meson is $4.10^4 \cdot 5$ g/cm² $= 2 \cdot 10^5$ g/cm².

This is the reason why, as was shown by calculation the probability of generating a large burst due to μ-meson by using [12] is sufficiently small.

Thus, the big bursts that are observed are undoubtedly related to the presence in the shower of nuclear-active particles of high energy.

As may be seen from the type of energy spectrum of nuclear-active particles given in Fig. 5, there exists in shower a whole stream of high-energy particles, that is, a nuclear cascade. The high-energy nuclear-active particles are exceedingly concentrated near the shower axis.

We find that nuclear-active particles of energy $> 10^{12}$ eV are concentrated near the axis in a circle of radius $(1 \div 2)$ m.

Hence we obtain an estimate for the transversal momenta acquired by a nuclear-active particle in the case, of nuclear scattering or in the act of generation. Assuming the mean free path of a nuclear-active particle to be 500 m, we obtain $p_\perp \leqslant 10^9$ eV/c.

A striking feature is the sharp concentration near the shower axis of energy fluxes carried by the nuclear-active particles.

It may be considered that the basic energy carried by a nuclear cascade is concentrated in the circle of radius 2.5 m under consideration.

From the data given (Fig. 5 and Table I) concerning the energy spectrum of nuclear-active particles it is clear that we are unfortunately unable to determine the total energy carried by a nuclear cascade near the core, and are able to give only a minimum estimate*).

To attain equilibrium between the electron-photon cascade and the nuclear cascade it is necessary for the energy contained in the nuclear cascade to be approximately equal to the energy of the electron-photon cascade. Thus, experimental data on showers with a large number of particles do not contradict this picture.

Quite different is the case of showers of low energies ($10^4 < N < 3 \cdot 10^4$). Though we are likewise unable to determine the total energy near the shower

*) As a matter of fact, we determined the energy spectrum up to values of E where the decline is not faster than E^{-1}.

axis for an averaged shower with such a number of particles, the energy spectrum is continued to the region of such energies E as are met with in an averaged shower with a probability of less than unity.

Insofar as this energy may be of the order of energy carried by the electron-photon component of the shower with ($10^4 < N < 3 \cdot 10^4$), this circumstance indicates that in the development of low-energy showers there may be appreciable fluctuations, and in an individual shower equilibrium is not attained.

* * *

The authors wish to express their gratitude to Professor S. N. Vernov and Professor G. T. Zacepin for helpful discussions during the course of the experiments.

REFERENCES

[1] A. T. Abrosimov, A. A. Bedniakov, V. I. Zacepin, Ju. A. Nečin, V. I. Solob'eva, G. B. Hristiansen and P. S. Čikin: *Žu. Èksper. Teor. Fiz.*, **29**, 693 (1955); G. B. Hristiansen: *Oxford Conference on Extensive Air Showers* (1956).
[2] L. N. Korablev: *New Application of Lamps with Cold Cathode* (Moscow, 1957).
[3] H. S. Bridge, W. E. Hazen, B. Rossi and R. W. Williams: *Phys. Rev.*, **74**, 9 (1948).
[4] V. A. Dmitriev: *Žu. Techn. Fiz.*, **27**, 1 (1957).
[5] S. Z. Belen'kij: *Avalanche Processes in Cosmic Rays* (Moscow-Leningrad, 1948).
[6] W. W. Brown: *Phys. Rev.*, **93**, 528 (1954); H. Carmichael and J. F. Steljes: *Phys. Rev.*, **99**, 1542 (1955).
[7] I. P. Ivanenko: *Thesis* (Moscow State University, 1956).
[8] I. A. Ivanovskaja, G. V. Kulikov, I. V. Rakobolskaja and L. I. Sariceva: *Žu. Èksper. Teor. Fiz.*, **33**, 358 (1957).
[9] L. D. Landau and J. Ja. Pomerančuk: *Dokl. Akad. Nauk SSSR*, **92**, 535, 735 (1953).
[10] V. S. Murzin: *Thesis* (Moscow State University, 1954).
[11] G. Cocconi and V. Cocconi-Tongiorgi: *Phys. Rev.*, **79**, 730 (1956).
[12] E. L. Andronikašvili and M. F. Bibilašvili: *Žu. Èksper. Teor. Fiz.*, **32**, 403 (1957).

SUPPLEMENTO AL VOLUME VIII, SERIE X
DEL NUOVO CIMENTO

N. 2, 1958
2° Trimestre

On the Lateral Distribution of Electrons and μ-Mesons in Extensive Air Showers.

G. B. HRISTIANSEN

Moscow State University - Moscow

Many experiments [1-5] have been carried out recently with the aim of a detailed study of the lateral distribution of the densities of electrons, μ-mesons and nuclear-active particles in extensive ais showers of cosmic rays in the lower part of the atmosphere. The lateral distribution of electrons and μ-mesons was investigated up to distance of the order of several hundreds metres from the shower axis.

In connection with these experiments it is worthwhile considering the problem of the relative role of different factors that affect divergence of shower particles.

Shower particles may diverge from the direction of flight of the primary particle, that generates the whole shower, due to the following reasons:

1) Angular divergence of secondary particles:
   a) in elementary acts of the nuclear-cascade process and
   b) in acts of spontaneous decay.
2) Coulomb scattering (of charged particles) on atomic nuclei of the air.
3) The Lorentz force due to the magnetic field of the earth (acting on charged particles).

After the discovery of the so-called « anomalous » width of the shower [6] it was supposed [7] that the first of the above points is the main cause of the broad spatial divergence of shower particles.

However, a more detailed analysis of the second and third points shows that this conclusion must be reconsidered.

Let us first examine the lateral distribution of electrons. Electrons arise in an extensive air shower in electron-photon cascades generated by γ-quanta from the decaying π^0-mesons, which are produced in elementary acts of the nuclear-cascade process. As was shown in [7] the largest angles of emergence (that are possible from the point of view of the laws of the conservation of

energy and momentum) of π^0-mesons in these acts are sufficiently great for the cores of individual cascades to diverge at distances of the order of several hundreds of metres from the axis of the whole shower, creating at these distances such electron-flux densities as required for agreement with experimental data.

According to the calculations of MOLIÈRE (1943) and EYGES (1948), which up to recently were the only ones available, electrons in electron-photon cascades could not propagate on such large distances in sufficient quantity.

However, during recent years (1954, 1956) NISHIMURA and KAMATA and also GREISEN gave a more precise solution of the problem of the lateral distribution of electrons in electron-photon cascades, and their results lead to a quantitatively different conclusion.

Let us compare the experimental lateral distribution of electrons [1-5]) with the theoretical distributions according to NISHIMURA and KAMATA for various parameters S of the development of an electron-photon cascade. We note that despite the fact that the development of the electron-photon component in an actual cascade takes place differently on the whole than in an electron-photon csacades, such a comparison of lateral distributions is justified insofar as the latter is determined primarily by the energy spectrum of electrons and depends but very slightly on the « prehistory » of the electron-photon cascade.

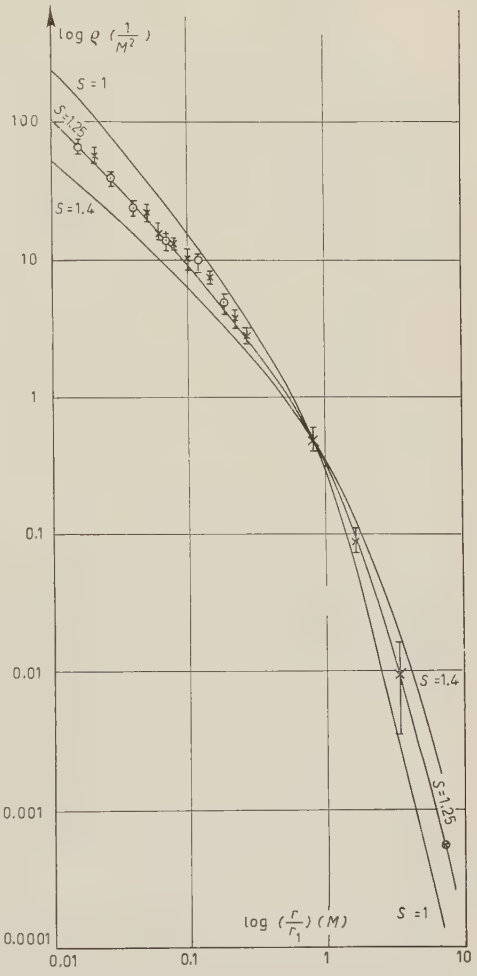

Fig. 1. – The comparison of experimental lateral distribution of electrons in extenair shower with theoretical distribution due to NISHIMURA and KAMATA (1954); at $r_1 \simeq 7$ (L. K. ÈJDUS *et al.* (1952)).

Fig. 1 shows the lateral distribution of electrons taken from the ref. [1-5]. The value $r_1 = (E_s/\beta)X_0$ ($E = 19$ MeV; $\beta = 72$ MeV and $X_0 = 270$ m above sea level) is taken as the unit of length. The theoretical curves are given for the

parameters $S = 1$; 1.25; 1.4. All curves are normalized with respect to the areas under them. The experimental points make a good fit on the theoretical curve $S = 1.25$ up to distances $r = 3$ [5], and do not contradict the slope of the curve with $S = 1.25$ for great distances up to $r = 7$ [4].

The coincidence of the experimental curve with the theoretical curve with one definite values of S in such a wide range of distances is not, of course, accidental, and it is natural to assume that this is due to the fact that the energy spectrum of the electron-photon cascade of age S, and the divergence of electrons is entirely determined by Coulomb scattering. Unfortunately, the energy spectrum of electrons has not as yet been measured; however, it should be pointed out that the absortpion coefficient of electrons obtained by studying the barometer effect and the altitude dependence of showers is in agreement with the value $S = 1.2$ [5, 8].

Thus, if the energy spectrum of the electrons in the shower coincides with the energy spectrum of electrons in the electron-photon cascade of age S, then the experimentally observed wide lateral distribution of electrons may be explained by taking into account only the Coulomb scattering of the electrons of individual electron-photon cascades. In this case there is no necessity of assuming that the cores of these cascades diverge considerably with the main core of the extensive air showers (*).

Let us now consider the lateral distribution of μ-mesons. μ-mesons arise from the decay of $\pi^{\pm}$ and $K^{\pm}$ mesons in the upper layers of the atmosphere. According to experimental data [9], the generation of μ-mesons ,in extensive air showers takes place in the altitude range from 5 to 20 km above sea level.

μ-mesons cóver a large distance from the point of generation to the level of observation without any interactions involving considerable losses of energy and lose their energy slowly on ionization of the air atoms. The lateral distribution of low-energy μ-mesons was investigated in some works [3-5]. According to experimental data, the meson density falls off much more slowly than the electron-flux density even at great distances of the order of hundreds of metres from the shower axis.

Since free path is large, an essential role is played in the lateral divergence of μ-mesons both by their Coulomb scattering on nuclei of air atoms and by deflection in the earth's magnetic field, even in the case of a relatively large value of energy.

The decrease of $\varrho_{\mu}(r)$ is not steeper than $1/r^2$. Therefore at the maximum distances from the axis, which where studied in the above-mentioned works, we shall not consider quantitatively the influence of Coulomb scattering and

(*) As was shown by Cocconi (1954) the earth's magnetic field does not affect appreciably the lateral distribution of electrons when observing showers in the lower-part of the atmosphere.

the deflections in the earth's magnetic field. We shall confine ourselves to an evaluation of the root mean square deflections of μ-mesons of energy E due to multiple scattering $\sqrt{\overline{r_s^2}}$ and their deflection in the magnetic field r_m.

Obviously

$$(1) \qquad \overline{r_s^2} = \int_0^H h^2 \frac{E_s^2}{(E + \beta t_0(1 - \exp[-\alpha h]))^2} t_0 \alpha \exp[-\alpha h]\, \mathrm{d}h \,.$$

Here H is the height of generation of μ-mesons above the observation level; t_0 is the depth of the observation level in cascade units; E_s is the parameter of the theory of multiple scattering; β is ionization losses calculated per radiation unit in air; $E_s = 21$ MeV; $\beta = 72$ MeV; α is the coefficient in the barometric formula $\alpha = (1/7000)\,\mathrm{m}^{-1}$.

For r_m we have the following expression:

$$(2) \qquad r_m = \int_0^H h \frac{\mathrm{d}h}{\varrho}, \qquad \varrho = \frac{E + \beta t_0(1 - \exp[-\alpha h])}{300\mathcal{H}},$$

where $\mathcal{H}$ is the component of the earth's magnetic field perpendicular to the axis of the extensive air shower.

Assuming the altitude of generation of μ-mesons $H = 10$ km above sea level and considering that the average energy of μ-mesons at great distances from the shower axis is close to the minimum energy still registered by the detector and equal to $3 \cdot 10^8$ eV in the experiments quoted above, we find $\sqrt{\overline{r_s^2}}$ and r_m given in Table I for sea level.

Table I.

$\sqrt{\overline{r_{exp}^2}}$	$\sqrt{\overline{r_s^2}}$	r_m
$\geqslant 400$ m	300 m	200 m

Table I also gives the experimental values of $\sqrt{\overline{r_s^2}}$ at sea level, for which an estimate may be made only of its minimum value.

Thus, the lateral distribution of low-energy μ-mesons, which are usually studied in experiments, is essentially determined by Coulomb scattering of μ-mesons and their deflection in the earth's magnetic field. The angular divergence of the «parents» of μ-mesons in elementary acts of the nuclear-cascade process is obviously also essential for the divergence of μ-mesons. However, the relative role of all these factors cannot at present be determined definitely without additional experimental data, and, above all, data on the lateral dis-

tribution of μ-mesons, their energy spectrum, and also their altitude of generation in the atmosphere (*).

Of special interest is an analysis of data concerning the lateral distribution of μ-mesons of high energy, since high-energy mesons arise in the nuclear-cascade process in elementary acts of still higher energies. Such data were obtained as early as 1952-53 in the works of George and Cocconi. However, they are of a qualitative nature, because the lateral distribution of μ-mesons was studied by the method of the correlation curve. Recently, E. L. Andronikašvili and M. F. Bibilašvili [10] using the method of correlated hodoscopes, obtained the lateral distribution of μ-mesons of energy $E \geqslant 1.5 \cdot 10^{10}$ eV in extensive showers at sea level.

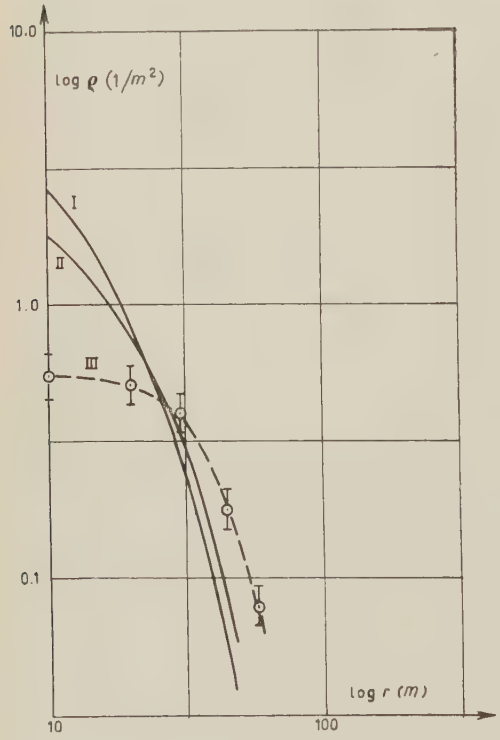

Fig. 2. – The lateral distribution of μ-mesons in extensive air showers. I) Theoretical curve $\varrho(r, > E_{\min})$; $\gamma = 0.7$; $H = 10^4$ m. II) Theoretical curve $\varrho(r, > E_{\min})$; $\gamma = 1.3$; $H = 10^4$ m. III) Experimental data [10].

The experimental data [10] are given in Fig. 2. As may be seen, the lateral distribution has been studied up to distances where there is a decline in the function $\varrho_\mu(r) \sim 1/r^3$. Hence, it follows that the experimental data permit of calculating the integral that corresponds to the total number of μ-mesons in the shower $\int \varrho_\mu(r) 2\pi r \, dr$, insofar as it does not diverge at the upper limit (+). Thus, it is worthwhile considering in detail the influence of Coulomb scattering and the earth's magnetic field on the divergence of μ-mesons (×) of high energy.

Let us find the function of lateral distribution $\varrho(r)$ for the case of divergence of μ-mesons due to Coulomb scattering and deflection in the

(*) The question should be considered of the sensitivity of $\sqrt{\overline{r_s^2}}$ and γ_m to altitude of generation of μ-mesons H. The value of r_m is highly sensitive to H. According to (2) and with account taken of ionization losses, $r_m \sim H^2$. The value of $\overline{r_s^2}$ is much less sensitive to H at $\alpha H > 1$: $\overline{r_s^2} \sim |2/\alpha^2 - H^2 \exp[-\alpha H]|$. But when $\alpha H < 1$, $r_s^2 \sim (\alpha H)^3$.

(+) It seems impossible to calculate $\overline{r^2}$ from experimental data, since its determination requires a study of $\varrho_\mu(r)$ up to distances that correspond to a decline of $1/r^5$.

(×) The installation of Andronikašvili and Bibilašvili was oriented in this direction.

magnetic field of the earth, ignoring the above point (1). The lateral distribution of μ-mesons of energy $E \geq \beta t_0(1 - \exp[-\alpha H])$ that suffer multiple scattering, has the form of the Gaussian curve $\varrho(r, E)\,dE = C(E)\exp[-r^2/r^2(E)]\,dE$ where $r^2(E)$ is determined by the above formula; C is determined from the condition

$$\int \varrho(r, E)dE\,2\pi r dr = F(E)\,dE$$

If $F(E)\,dE = AE^{-\gamma-1}dE$ then

$$C = \frac{A \cdot E^{-(\gamma+1)}}{\pi r^2(E)} = \frac{A \cdot E^{-(\gamma-1)}}{\pi B(H, t_0)}$$

since $r^2 = (1/E^2)\beta(H, t_0)$.

The action of the earth's magnetic field leads to a lateral separation of μ-mesons according to their energy and the sign of charge. If the shower axis is directed vertically, the positive μ-mesons will be deflected eastward, and the negative μ-mesons in the opposite direction. The deflection of all μ-mesons of energy E are the same and equal to $r_m(E) = (H^2/2E)\cdot 300\,\mathcal{H}$.

Thus, the combined action of Coulomb scattering and deflecting in the earth's magnetic field may be taken account of in the following expression for $\varrho(r)$, which gives the spatial distribution in the direction W-E (*).

$$\varrho(r, > E_{\min}) = \int_{E_{\min}}^{\infty} \frac{A}{\pi\beta(H, t_0)}\, E^{-(\gamma-1)} \exp\left[\frac{-(r - r_m)^2E^2}{\beta(H, t_0)}\right] dE_0 +$$

$$+ \int_{E_{\min}}^{\infty} \frac{A}{\pi\beta(H, t_0)}\, E^{-(\gamma-1)} \exp\left[\frac{-(r + r_m)^2E^2}{\beta(H, t_0)}\right] dE\,.$$

Fig. 2 shows the theoretical curves calculated in different assumptions with respect to γ [11], for $E_{\min} = 1.5\cdot 10^{10}$ eV, $H = 10$ km and for the altitude of Tbilisi. A comparison of tnese theoretical curves with experimental data shows that spatial divergence of high-energy μ-mesons can be due principally to the above points 2) and 3) (+).

(*) The transverse momentum acquired by a μ-meson due to point 1*b*) is according to the order of magnitude equal, for $\pi \to \mu + \nu$ decay, to $\mu_\pi c/2$ and, for $K \to \mu + \nu$ decay to $\mu_K c/2 = 2\mu_\pi c$.

(+) The discrepancy observed between the experimental and theoretical curves may be understood if we take into consideration the geometry of the apparatus (10). The detector of high-energy μ-mesons was at a depth of 27 m underground. The equipment that fixed the shower axis was situated on the earth's surface. Due to an inclination of the shower axis to the vertical there could arise a systematic error (an over estimation) in determining the distance from the shower axis to the detector of the order of one half the depth.

Using these data, it is possible to evaluate the size of the transversal momentum acquired by secondary particles, $\pi^{\pm}$ and $K^{\pm}$ mesons in elementary acts of the nuclear-cascade process. The transversal momentum of the secondary particle of energy E is $p_{\perp} = (E/c)\vartheta$, where ϑ is the angle of emergence of the secondary particle in the laboratory co-ordinates. If the energy spectrum of μ-mesons is of the form $F(E)\,dE = AE^{-(\gamma+1)}dE$, $E > E_{\min}$, then, disregarding ionization losses and the probability of decay of μ-mesons (this holds for $E \geqslant 10^{10}$ eV) we may obtain the differential spectrum of the decayed $\pi^{\pm}$ mesons or $K^{\pm}$ mesons:

$$f_{\pi \text{ or } K} = \frac{A}{[1-(m/M)^2]\gamma} \frac{1}{E} (E_{\min}^{-\gamma} - E^{-\gamma}), \qquad E_{\min} \leqslant E \leqslant \left(\frac{M}{m}\right)^2 E_{\min},$$

$$f_{\pi \text{ or } K} = \frac{A}{[1-(m/M)^2]\gamma} \left[\left(\frac{M}{m}\right)^{-2\gamma} - 1\right] E^{-(\gamma+1)}, \qquad E \geqslant \left(\frac{M}{m}\right)^2 E_{\min},$$

where M is the mass of $\pi^{\pm}$ or $K^{\pm}$ meson,

m is the mass of a μ-meson,

$E_{\min}$ is the minimum values of energy of the registered μ-mesons (equal in experiments of ref. [10] to $1.5 \cdot 10^{10}$ eV).

Let us determine here from the value of E^*, i.e. of such an energy that the $\pi^{\pm}$ (or $K^{\pm}$) mesons having the energy exceeding this E^* form one half of decaying mesons. For the case of $\pi^{\pm}$ mesons, $E^* = 2E_{\min} = 3 \cdot 10^{10}$ eV. For the case of $K^{\pm}$ mesons, $E^* = 7E_{\min} = 10^{11}$ eV.

$$p^* = \frac{E^*}{c}\vartheta \qquad \text{and since} \qquad \vartheta < \frac{50\,\text{m}}{10^4\,\text{m}} = 5 \cdot 10^{-3},$$

then

$$p_{\pi}^* < 1.5 \cdot 10^8 \text{ eV}, \qquad p_K^* < 5 \cdot 10^8 \text{ eV}.$$

In concluding it should be noted that Coulomb scattering should also be taken into account in analyzing data on the spatial distribution of charged nuclear-active particles in extensive air showers.

* * *

The author wishes to thank S. N. Vernov and F. T. Zacepin for a discussion of these problems.

REFERENCES

[1] I. N. Vavilov, S. N. Nikol'skij and E. I. Tukiš: *Dokl. Akad. Nauk, SSSR*, **93**, 233 (1953).

[2] A. T. Abrosimov, A. A. Bed'niakov, V. I. Zacepin, Ju. A. Nečin, V. I. Solob'eva: G. B. Hristiansen and P. S. Čikin: *Žu. Èksper. Teor. Fiz.*, **29**, 693 (1955).

[3] Ju. N. Antonov, Ju. N. Vavilov, G. T. Zacepin, A. A. Kutuzov, Ju. V. Skvorcov and G. B. Hristiansen: *Žu. Èksper. Teor. Fiz.*, **32**, 227 (1957).

[4] L. K. Èjdus *et al.*: *Žu. Èksper. Teor. Fiz.*, **22**, 440 (1952).

[5] A. T. Abrosimov, N. N. Gorjunov *Žu. Èksper. Teor. Fiz.*, in print 1957.

[6] G. T. Zacepin and V. V. Miller: *Žu. Èksper. Teor. Fiz.* **17**, 939 (1947).

[7] N. A. Dobrotin, G. T. Zacepin *Usp. Fiz. Nauk*, (Feb. 1953).

[8] A. Cranshaw: *Oxford Conference on Extensive Air showers* (1956).

[9] B. Rossi, G. Clark and P. Bassi: *Phys. Rev.*, **91**, 432 (A) (1953).

[10] F. L. Andronikašvili and M. F. Bibilašvili: *Žu. Èksper. Teor. Fiz.*, **32**, 403 (1957).

[11] M. Skvaralidze: *Thesis* (Tbilisi, 1956).

SUPPLEMENTO AL VOLUME VIII, SERIE X
DEL NUOVO CIMENTO

N. 2, 1958
2° Trimestre

Čerenkov Radiation of Extensive Air Showers.

A. E. Čudakov and N. M. Nesterova

P. N. Lebdev Physical Institute of the USSR Academy of Sciences - Moscow

Short light flashes superimposed on the background of the night-sky glow, correlated with the passage of cosmic rays in the atmosphere, were first detected in 1952 [1, 2]. It was soon established that at least some of these flashes are caused by Čerenkov radiation of extensive air showers ([3-5].

Further experiments in this direction were conducted by the authors in the autumn of 1955 in the Pamir Mountains (altitude 3860 m). The purpose of this work was to study the lateral distribution of the light flux relative to the core of the showers and also to investigate the relation between the intensity of the light flash and the size of the shower.

Fig. 1. – The arrangement of the hodoscope units. □, hodoscope unit. ⊗, light receiver.

The arrangement included an optical receiver that registered the light flashes, and a Geiger counter hodoscope. The latter consisted of 5 units, each containing 96 counters (each counter of area 330 cm²). The position of the units is shown in Fig. 1. The hodoscope was triggered at the instant of registration of the light flash. The hodoscope registers were photographed on film at all five units.

The point of incidence of the core and the total number of particles in the shower N was found for each shower of sufficient size, using the readings of all hodoscope units. This operation was carried out using the lateral distribution function of particle flux, which function was obtained in [6] and it was used only in those cases when not less than three counters in each unit were triggered in the central and at least in two periphery units. Given such a criterion that ensured sufficiently determined condition for the analysis of the hodoscope data, it was found possible to analyse showers with 10^5 or more particles, when

the distance from the centre of the system to the shower axis did not exceed 150 m (for $N < 10^6$) and 250 m (for $N > 10^6$).

The optical arrangement consisted of eight light receivers. Each receiver consisted of a parabolic mirror at the focus of which the cathode of a photomultiplier tube (type FEU.-19, diameter of photocathode 3.5 cm) was placed. The mirror of diameter 45 cm and focal length 19 cm had a front surface coated with an Al-reflecting layer. The coincident pulses from two receivers, whose axes were oriented parallel to each other, were used to present a master pulse.

This made it possible to increase the stability of the system, especially in the case of a relatively low triggering threshold.

The master pulse which ensured the passage of pulses through all eight channels for subsequent recording was produced at the output of the coincidence circuit. This same signal operated the hodoscope. The resolving time of the electronic apparatus for measuring pulse amplitudes from the photomultiplier tubes, was $2 \cdot 10^{-8}$ s, and for the hodoscope of the Geiger counters it was $5 \cdot 10^{-6}$ s.

Thus, the intensity of the light flash in all eight receivers and the flux density of particles at five hodoscope units, were simultaneously registered.

Two series of measurements were made with this apparatus. In both cases, the two master receivers were placed in the centre of the hodoscope system and oriented vertically, which determined the vertical direction of the showers registered (in a solid angle of 1/40 sr).

The sensitivity of the light receivers was adjusted so that about 100 pulses per hour were registered. It turned out that, on an average, each flash was accompanied by triggering of twenty hodoscope counters, while the number of cases when no counter was triggered, was 4%.

Thus, it was established that practically all light flashes of a given intensity were produced by extensive air showers.

The number of events, when it was possible to determine the point of passage of the shower core, amounted to 10 per hour.

In all these cases, a determination was made of the distance from the shower axis to the light receivers, and then the magnitude of the pulses from the photomultiplier tubes was correlated with the distance from the shower axis, and with the total number of particles in the shower.

In the first series of measurements, six receivers were situated in different places at a distance of about 40 m from the centre, and were oriented vertically (just as for the master receivers). This made it possible in principle to determine for each shower the light intensity at various distances from the core. However, in this experimental arrangement errors of light intensity measurements proved so great that the results could not be used. These errors were principally due to a dependence of sensitivity of the light receivers on

the angle of incidence of the shower. Since the cathodes of the photomultiplier tubes were not uniform, the angular characteristics of the telescopes (the dependence of sensitivity on the angle of incidence of the light) were likewise not identical, especially in the region of angles close to the limit of the field of view of the receiver.

To reduce errors due to registration of inclined showers, in the second series of measurements the receivers were disposed as follows. Two master receivers remained as before, in the centre of the hodoscope system, and were oriented vertically. The remaining six were placed around the circumference at a distance of 2 m from the master receivers and were inclined at an angle of 5° to the vertical towards the center of the circle.

Thus, all receivers registered the intensity of the light flash practically at the same place, namely in the centre of the system, but on the other hand it was possible to estimate the angle of inclination of the registered shower from the ratio of the pulse amplitudes from different receivers.

In order to avoid errors due to inclined showers, we selected only those cases for which the angle of inclination was sufficiently small (not more than $(3 \div 4)°$). The criterion for this was the requirement that the pulse amplitude in the vertical receivers should be at least not less than in any one of the inclined receivers.

To determine the intensity of the light flash use could be made both of the readings of the master and the inclined receivers. It was found that the most precise measure of the intensity of a flash is that corresponding to the sum of the pulse amplitudes in the six inclined receivers, which is apparently explained by a certain averaging of non-uniformities of the cathodes in this method of analysis.

During 80 hours of running, 230 showers were registered which satisfied the criterion of « verticality » and at the same time permitted hodoscope analysis. For each one of these, we know the total number of particles N and the intensity of the light flux q at a certain distance R from the axis, which distance varies at random from shower to shower.

Fig. 2 and 3 show the distribution of these showers according to N and to R. Because of the existence of hodoscope and optical « threshold », large distances ($R > 100$ m) are represented principally by greater size ($N > 3 \cdot 10^5$), and small distances ($R < 30$ m) are naturally represented principally by showers of size $N < 3 \cdot 10^5$.

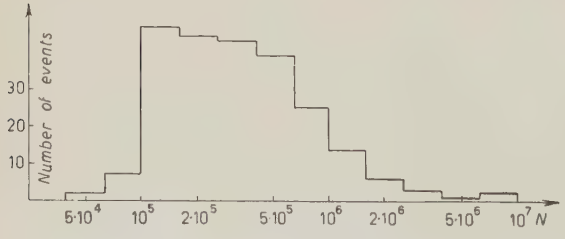

Fig. 2. – The shower size distribution of the events. N, the total number of particles in the shower.

Correspondingly, data concerning the intensity of the light flux at small distances from the axis were obtained for showers with $N < 3 \cdot 10^5$, and at great distances only for showers with $N > 3 \cdot 10^5$ in the interval $30\,\text{m} < R < 100\,\text{m}$. Showers from $N \approx 10^5$ to $N \approx 3 \cdot 10^6$ are represented.

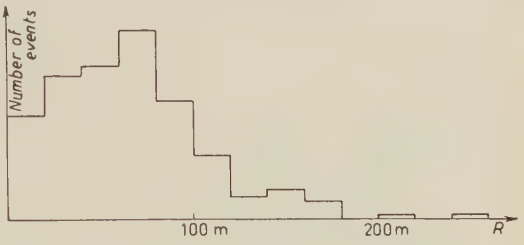

Fig. 3. – The distribution of the events with respect to R. R, the distance between the shower core and the light receiver.

If we assume that the form of the lateral distribution of the light does not depend on the shower size, and the light intensity is simply proportional to the number of particles in the shower, namely

$$\Phi(R, N) = N \cdot \varphi(R)\ [1]\,,$$

we may obtain the function $\varphi(R) = \Phi/N$ in the range of distances from 10 to 250 m, using for this purpose all registered cases, Fig. 4.

In this same figure, the solid line denotes one of the theoretical curves shown in Fig. 5 appropriately normalized. Normalization is necessary due to the fact that in these experiments only relative measurements of the light intensity were conducetd. By suitable normalization it is also possible to reconcile approximately the experimental results with curves A_2, B_1, B_2 and B_3.

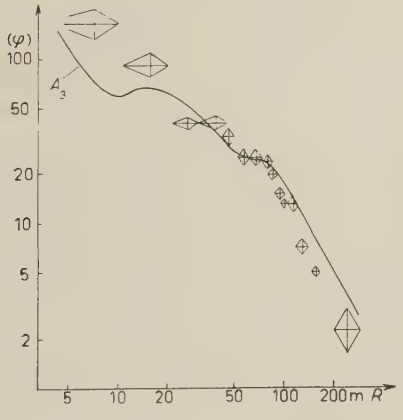

Fig. 4. – The lateral distribution of light intensity with respect to the shower core position. R, the distance from the core. $\langle\varphi\rangle$, the average light intensity in arbitrary units. The solid line is one of the theoretical curves (suitably normalized).

The errors of the experimental points in Fig. 4 are presented on the basis of the observed spread of $\varphi(R)$ for each interval R, taking into account the number of cases averaged. For all intervals of distances, the average deviation of the φ from the mean value at $R = \text{const.}$ is of the order of a factor $1.5 \div 2$ times.

These deviations (especially in the case of small R) may be explained to a certain extent by errors in the apparatus, but it is possible that they were mostly due to fluctuations in the development of the showers.

A trivial source of such fluctuations is a spread in altitude in the atmosphere, of the point of origin of the showers, which fact depends greatly on the cross-section of the interaction of the primary particle with the atomic nuclei of the air. It is possible that the subsequent development of the shower can also have fluctuations.

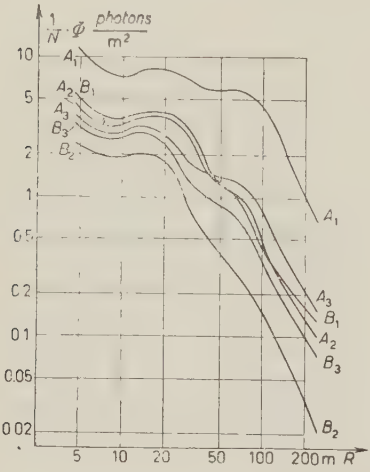

Fig. 5. – The theoretical lateral distributions of light for different models of shower development. Curves A_1 and A_2 correspond to the purely electromagnetic cascade with initial energy of electrons 10^{11} and 10^{13} eV. A_3 corresponds to a cascade curve of the type: $N(p) \sim p \exp[-p/p_0]$; $p_0 = 150$ g/cm². Curves B_1, B_2, B_3 correspond to the same models of development of showers, but with the point of origin on the depth 200 g/cm² in the atmosphere.

To get an idea of how variations in the form of the cascade curve, which describes the number of particles as a function of depth in the atmosphere, influence the intensity and lateral distribution of Čerenkov radiation, we calculated the function $\varphi(R)$ using several types of cascade curves. During the calculations it was found that the lateral distribution of light is to a large extent determined by the angular and lateral distributions of the electrons, and that, consequently, scattering cannot be neglected.

The effect of scattering is determined by the form of the energy spectrum of the electrons. To simplify calculations the spectrum was taken as constant (namely, equilibrium) throughout the depth of the atmosphere. This approximation corresponds to that made in paper [3]. Fig. 5 gives the results of calculations that refer to the level of observation at an altitude of 3 850 m.

Curves A_1, A_2 and A_3 correspond to the origin of the shower at the top of the atmosphere, while B_1, B_2 and B_3 correspond to a depth of 200 g/cm². The following cascade curves were taken.

1) The cascade curve for a purely electromagnetic development of a shower with initial energy of the electrons $E_0 = 10^{11}$ eV.

2) The same, but with $E_0 = 10^{13}$ eV.

3) $N \sim P \exp[-P/P_0]$, where P is pressure, $P_0 = 150$ g/cm².

As is seen from Fig. 5, the displacement of the point of origin of the shower by 200 g/cm² leads (in the distance range 50 to 200 m) to a change of φ of several times, and for curves A_1-B_1 even of 10 times.

Thus, the observed fluctuations of q (by 1.5 to 2 times) can be explained if fluctuations of the depth of origin are less than 200 g/cm².

It may be expected that it will be possible later to obtain in this manner valuable estimates for the cross-section of interaction of primary particles producing extensive air showers.

Another possible developemnt of such experiments consists in the verification of the assumption (1), which is naturally valid only if the form of the cascade curve does not depend on the initial energy. Such a verification requires an extremely large quantity of statistical material, since in this case it is necessary to average over the relatively narrow intervals N and R.

The results obtained up to the present time are insufficient for such an analysis.

REFERENCES

[1] W. Galbraith and J. V. Jelley: *Nature*, **171**, 349 (1953).
[2] J. V. Jelley and W. Galbraith: *Phil. Mag.*, **44**, 619 (1953).
[3] V. I. Gol'danskij and G. B. Ždanov: *Žu. Éksper. Teor. Fiz.*, **26**, 405 (1954).
[4] N. M. Nesterova and A. E. Čudakov: *Žu. Éksper. Teor. Fiz.*, **28**, 384 (1955).
[5] J. V. Jelley and W. Galbraith: *Journ. of Atmos. and Terr. Phys.*, **6**, 304, 250 (1955).
[6] S. I. Nikol'skij and V. M. Selesnev: *Žu. Éksper. Teor. Fiz.*, **32**, 1250 (1957).

SUPPLEMENTO AL VOLUME VIII, SERIE X
DEL NUOVO CIMENTO

N. 2, 1958
2° Trimestre

Combined Method of Investigation of the Extensive Air Showers.

N. Dobrotin, O. Dovženko, V. Zacepin, E. Murzina, S. I. Nikol'skij, I. Rakobolskaja and E. Tukiš

P. N. Lebedev Physical Institute of the USSR, Academy of Sciences - Moscow

In order to reconstruct the picture of an elementary act of nuclear interaction at extremely high energies basing on the data on extensive air showers, it is necessary to make a detailed and comprehensive study of all the characteristics of the showers. Therefore, in order to solve the problem, the investigation should be carried out with the use of a combined arrangement that will enable us to determine (for any given individual shower), as far as possible, not only the position of its axis and the total number of particles (i.e., not only to evaluate the energy of the primary particle), but also to obtain all the characteristics of the different components of the shower.

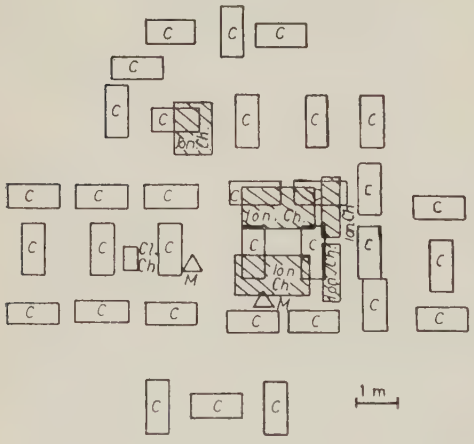

Fig. 1.

Below are given tentative data concerning partial results of measurements carried out with such an arrangement during the autumn of 1955 at an altitude of 3 860 m above sea level (the Pamir Mountains, Central Asia) by the workers of the laboratory of cosmic rays of the P. N. Lebedev Physics Institute of the Academy of Sciences of the USSR.

The scheme of the arrangement is shown in Fig. 1. The rectangles designated by *C* are 33 groups of hodoscope counters, each of which consisted of 24 counters, the area of each counter was 100 cm². In addition, there were three additional hodoscope sets arranged symmetrically at a distance of 18 m

from the centre of the arrangement (they are not indicated in Fig. 1). In each of them were 36 counters with an area of 330 cm^2 and 24 counters with an area of 22 cm^2. All hodoscope groups were placed in houses with thin roofs (~ 2 g/cm^2 of light substance).

In order to study the penetrating component of the shower, penetrating-particle detectors were installed directly under the central part of the installation in a specially dug shaft at a depth of 8 and 16 m of water equivalent, respectively. Each of them consisted of three trays, (one above the other) of counters with an area of 330 cm^2 each, separated by two layers of lead 6 cm thick each. At the depth of 8 m water equivalent, there were 36 counters in each of the three trays, and 48 counters at the depth of 16 m water equivalent. All these counters were also connected to corresponding hodoscope cells.

Thus, there was a total of 1224 hodoscope counters. The hodoscope system employed was that of L. N. Korablev, type GK-7. Systematic control showed that the whole arrangement operated satisfactorily.

There were 30 pulse ionization chambers of cylindrical form in the arrangement for studying the fluxes of energy carried by nuclear-active particles and by the electron-photon component of the shower as well as for studying the structure of the core of the shower. Eighteen of the chambers had an inside diameter of 22.5 cm and were 96 cm in length, twelve others had a diameter of 18.5 cm and 42 cm in length. The chambers were filled with chemically pure argon to a pressure of 5 atmospheres.

For measuring the amplitude of the electronic component of the ionization pulses, each chamber was connected to a special electronic device (developed by L. N. Korablev) of the type of an amplitude analyser with scaling circuit of neon lamps (*).

Calibration of the chambers was performed with the aid of bursts produced by μ-mesons passing along the chamber axis (in these calibration experiments the chamber was placed vertically) and the bursts from showers, the particle density of which at the given point was measured by a hodoscope. Both calibrating procedures gave practically coincident results, as long as account was taken of transition effects in the chamber walls and of the medium angle of inclination of paths of shower particles.

The electronic arrangement that was used allowed the measurement of bursts in one chamber within the ionization interval (from $6 \cdot 10^3$ to $1 \cdot 10^8$ ion pairs), which corresponded to the ionization caused by the passage through the chamber of 1 to $1.5 \cdot 10^4$ relativistic particles along its diameter and perpendicular to the axis.

(*) For control, each chamber was connected to two identical but independent arrangements. In the carried series of experiments their readings coincided.

The arrangement of 24 ionization chambers near the centre of the installation (cross-hatched rectangles « ion. ch. » in Fig. 1) is shown in Fig. 3 and 4. Numbers 1 to 12 denote the large chambers, and 13 to 24 the small ones. Common absorbers of different thickness that covered all the chambers were placed in turn over these chambers, their thicknesses being 1 cm, 2 cm, 3 cm, 5 cm, 10 cm Pb; 1.1 cm, 3.5 cm and 7.5 cm Fe, an absorber of Al and C with a total thickness that corresponded to 230 g/cm², and also an absorber that consisted of 3 cm Pb, placed directly above the chambers, 80 cm of graphite (with a density of 1.6) and 2 cm Pb that covered the graphite from above. The remaining six large ionization chambers were arranged at the point shown in Fig. 1 by a cross-hatched rectangle Ion. Ch. (upper left). Above this group of chambers there were alternatively arranged the common lead absorbers, having thicknesses of 20, 50 and 80 cm. A 2 cm thick layer of lead was placed under the ionization chambers in order to surround them by a homogeneous medium.

At the point indicated in Fig. 1 by a small rectangle Cl. Ch., a rectangular 100 litres cloud chamber containing seven lead plates with a total thickness equal to 100 g/cm² was situated. This chamber was used to study the spectrum of the electron-photon component at various distances from the axis in the central regions of the showers. The energy of electrons and photons was determined from the total number of ionizing particles in the cascade shower that arose during the passage of electrons and photons through the lead plates in the chamber.

The entire arrangement was mastered by fourfold coincidences of the counters, with an area of 500 cm² divided into two groups denoted in Fig. 1 by *M*. The distance between the two groups of master counters was 2 m.

The master group of counters produced 60 master pulses per hour (*); $4 \cdot 10^4$ showers were recorded.

In the case of about 20% of the showers, the axes of the latter passed within 6 m from the centre of the unit (i.e., from the middle of a line connecting the two groups of master counters). For such showers, a determination was made of the total number of particles in the shower starting from the particle density recorded by the hodoscopes and from the forms of the function of lateral distribution of particles at large distances from the axis. This function was established in our previous experiments [1]. The error in determining the

(*) Due to the long « dead time » of the cloud chamber (3 min), three parallel groups of threefold coincidences of counters connected in anticoincidence with the master one and situated at a distance of 19 m from the centre of the installation were connected with the chamber control. Thus, the cloud chamber was triggered by showers, the axes of which passed close by the centre of the arrangement and the total number of particles passing was restricted not only from below but also from above.

position of the showers axis was approximately 10%. Distribution in number of particles recorded by the arrangement is shown in fig. 2. About 300 showers were used to determine the shape of this curve. A relative number of showers is plotted on the ordinate and the total number of particles in them is plotted logarithmically on the abscissa. (This spectrum does not include several showers with a very large number of particles, the density of which could not be determined by means of the hodoscopes that were employed).

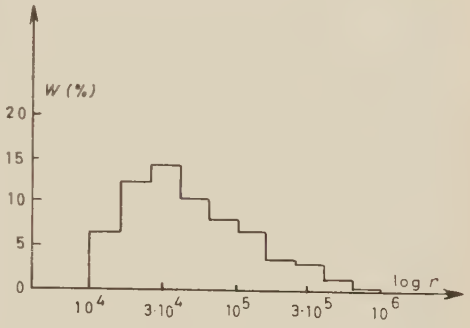

Fig. 2.

Using the scaling factor transferring the total number of particles of the shower into the energy of the primary particle, for our altitude of observation equal to $2.5 \cdot 10^9$, we find that the arrangement permitted the study of showers caused by primary particles with energies of $(3 \cdot 10^{13} \div 2 \cdot 10^{15})$ eV. From the spectrum shown in Fig. 2 it follows that if the energy spectrum of primary particles is represented in the form of $E^{-\gamma}$, then the value of γ in the interval $E_0 = (2 \cdot 10^{14} \div 2 \cdot 10^{15})$ eV is consistent with the value of 1.5.

As is well known [2], the method of correlated hodoscopes enables us to determine the position of the axis of an individual shower by proceeding from the concept of axial symmetry of the shower. In our arrangement, for the showers whose axes passed at a distance less than 5 m from the centre of the installation, the error in determining the position of the shower axis did not exceed 1 m.

The three trays of hodoscope counters separated by two layers of 6 cm Pb each in the detectors of penetrating particles housed underground made it possible to select those cases in which the core of the shower passed through the detector that was situated at a depth of eight meters water equivalent (*).

The criterion of such a passage of the core was the triggering of not less than 15 counters distributed in all three trays.

The obtained results are not sensitive to the number of triggered counters.

Proceeding from the number of cases of passage of shower axes through the central part of the installation on the surface of the earth, which was determined by means of the hodoscope, it was possible to calculate the expected

(*) Analogous cases were not registered in the detector at a depth of 16 m water equivalent due to the great thickness of the absorber. This is also an indication that the cores registered in the underground detectors are not due to μ-mesons from the extensive showers.

number of cases of passage of the core through the underground detector. It was established that for the showers with a total number of particles $< 10^5$ one should expect 14 traversals of the core. And these 14 cases were actually observed. But for the showers with the number of particles $> 10^5$, six cores were expected, whereas the number found was 15. Despite the fact that statistics is scarce, such a departure hardly can be explained by statistical fluctuations.

The nuclear-active particle which produces the secondary shower in the underground detector, should on the earth's surface possess an energy apparently not less than $5 \cdot 10^{11}$ eV. For this reason the data obtained show that in relatively small showers ($< 10^5$) there is, on average, one such particle, whereas in showers $> 10^5$ the number of nuclear-active particles with an energy above a certain effective threshold increases, and they are distributed in a region with a diameter of 1 to 2 m (which does not contradict available data on the lateral distribution of charged particles near the axis of extensive air showers).

It is possible that this is due to a change in the nature of the elementary act of nuclear interaction while passing over to superhigh energies, the hypothesis which we discussed earlier [3].

The results of the analysis of measurements conducted by means of ionization chambers are also in agreement with data obtained from the structure of the core of showers with the aid of an underground detector. Fig. 3 shows a typical picture of pulse distribution in ionization chambers when the axis of a shower with a total number of particles $2.8 \cdot 10^4$ passes through the area occupied by the ionization chamber. This case was recorded in an experiment with the absorber consisting of two layers of lead with graphite between the layers. The position of the shower axis found from the hodoscope data is designated on the layout diagram of the ionization chambers by a dashed circle. As may be seen from the figure, this case is characterized by a sharply defined single shower core that passed through ionization chamber N. 3.

Fig. 4 shows a characteristic case of the passage of the core of a shower with a total number of particles $1.5 \cdot 10^5$ through the area occupied by the ionization chambers. The position of the axis which was determined from hodoscope data is also denoted by a dashed circle. As may be seen from this figure, this case is characterized by complicated structure of the core.

In analyzing these data statistically, we put in the category of showers with complicated core structure the cases where in addition to the main burst in one of the ionization chambers, there were observed in two adjacent chambers or in one non-adjacent chamber, bursts, whose amplitude was not less than one half of the amplitude of the largest burst.

In experiments with a filter made of two layers of lead and one layer of graphite between them, and also in experiments with thick lead absorbers

$(20 \pm 10)\%$ of the showers of the first group (i.e., with a total number of particles $< 1 \cdot 10^5$) which have been analysed up to the present and the axes of which (according to hodoscope data) passed through the area occupied by ionization chambers, have a complex core structure; $(60 \pm 10)\%$ of the showers of the second group ($> 10^5$) have a complicated core structure.

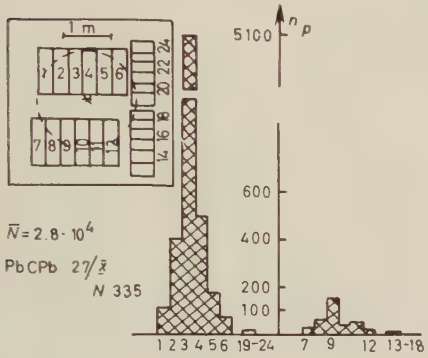

Fig. 3.

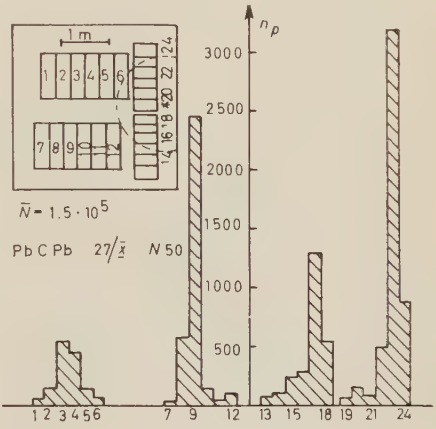

Fig. 4.

Figs. 3-4. – The number of relativistic particles is plotted on the ordinate and the ordinal number of the chambers is indicated on the abscissa.

A similar analysis of data obtained in the experiment with aluminium and graphite absorbers led to the following results:

Groups of showers classified according to the total number of particles in them	$(1\text{-}2) \cdot 10^4$	$(2\text{-}4) \cdot 10^4$	$(4\text{-}6) \cdot 10^4$	$(6\text{-}10) \cdot 10^4$	$(1\text{-}2) \cdot 10^5$	$(2\text{-}5) \cdot 10^5$	$(5\text{-}10) \cdot 10^5$
Number of cases with single core	5	7	6	4	3	1	0
Number of cases with complicated core	2	3	2	2	2	5	1
Fraction of cases with complicated core	$(29 \pm 10)\%$				$(67 \pm 25)\%$		

A series of experiments conducted with different absorbers over the ion chambers made it possible to draw certain conclusions concerning the energy pattern of the central regions of showers.

To determine the form of energy spectrum of nuclear-active particles near the axis of an extensive air shower, a measurement was made of the distribution of the magnitude of ionization bursts accompanied by air showers, the axis of which passed not less than eight metres from the ion chambers placed under an absorber.

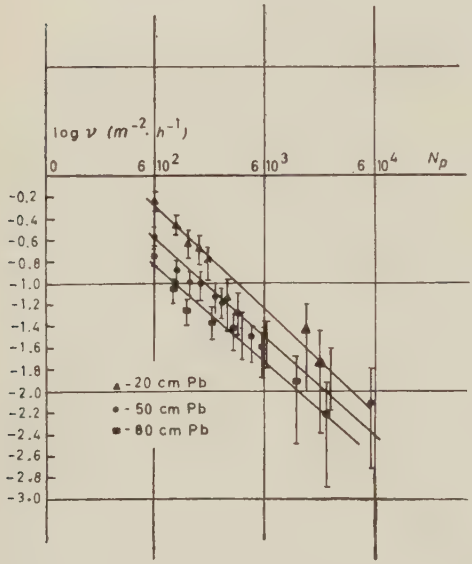

Fig. 5.

The spectrum of ionization bursts under filters of 20, 50 and 80 cm of lead for the interval of bursts from 600 to 60 000 relativistic particles per chamber, is shown in Fig. 5. It may be expressed as B/J^n, where $n = 0.9 \pm 0.2$ (*), and the coefficient B diminishes with increasing thickness of the substance in the proportion $\sim \exp[-x/500]$, where the thickness of lead x is expressed in g/c²m.

To evaluate the maximum energy of nuclear-active particles in the cores of extensive air showers with the number of particles from 10^4 to 10^5 ($\overline{N} = 3.5 \cdot 10^4$) let us consider cases of the passage of cores of extensive showers through ionization chambers placed under lead absorbers of various thickness. As a rule, for showers with a total number of particles within the interval under consideration, the burst in one of the ionization chambers exceeds several times the remaining bursts. The dependence of the average magnitude of the burst in the ionization chambers with the greatest burst on the thickness of lead over the chambers is shown in Fig. 6. The initial part of the curve

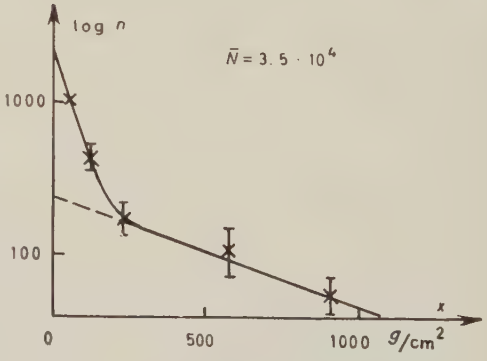

Fig. 6.

(*) Similar results were obtained by J. TANAKA, K. SUGA and S. MITANI using counter hodoscope arrangements covered with lead (a preliminary private communication). It should, however, be noted that data obtained by means of ionization chambers are more accurate and reliable.

with rapid absorption is explained, apparently, by the electron-photon component of the shower core that comes from the atmosphere; the subsequent slow absorption is due to diminution of the energy of particles of the nuclear-active component of the shower.

If we make use of the flux of charged particles J, under a thick absorber of lead and evaluate the quantity J_0, the value for the energy of those nuclear-active particles which produce the maximum bursts under big thicknesses of lead is

$$E_{\max} \simeq \int_0^\infty \beta_{\mathrm{Pb}} J_0 \exp\left[-\frac{x}{500}\right] \mathrm{d}x \simeq 7 \cdot 10^{11}\ \mathrm{eV}\ ,$$

where β_{Pb} is the energy loss due to ionization of the relativistic particle when passing through a Pb layer of 1 g/cm² ($\beta_{\mathrm{Pb}} = 1.22 \cdot 10^6$ eV/gcm^{-2}).

These data concerning the spectrum of nuclear-active particles in extensive air showers and the value of energy, above which the shower has not more than one particle, enable us even now (despite their tentative character) to estimate roughly the total energy carried by the nuclear-active component of the shower with an average number of particles $3.5 \cdot 10^4$ at an altitude of 3 860 m

$$\sum E_{\mathrm{n.a.}} \simeq \int_{10^9}^{E_{\max}} E \frac{E_{\max}^{0,9}}{E^{1,9}} \mathrm{d}E \simeq 6 \cdot 10^{12}\ \mathrm{eV}\ .$$

In this calculation, it is assumed that the obtained spectrum of bursts that reflects the energy spectrum of nuclear-active particles, continues into the region of low energies, down to energies of nuclear-active particles $\sim 10^9$ eV. In future, we shall measure in detail this region of bursts; at present, the measurements conducted by us earlier with counter detectors of nuclear-active particles (and also the above quoted data of Tanaka, Suga and Mitani) together with the fact that the exponent in the energy spectrum of μ-mesons in the showers which reflects the spectrum of π-mesons, is also close to unity [4], may serve as grounds for such an extrapolation. The value obtained for the total energy of nuclear-active particles in a shower only slightly depends on the value of the lower limit of integration and for this reason its precise determination for the above estimates is not essential.

From the same data for showers with $N = 3.5 \cdot 10^4$ particles, it is possible to estimate also the total number of nuclear-active particles of energy higher than the given energy:

$$N_{\mathrm{n.a.}} \simeq \int_{E_{\min}}^{E_{\max}} \frac{E_{\max}^{0,9}}{E^{1,9}} \mathrm{d}E\ .$$

Assuming $E_{\min} \sim 10^9$ eV, we obtain $N_{\mathrm{n.a.}} \sim 300$ particles. But in this case, the calculation result depends essentially on the selected value of $E_{\min}$ and for this reason it is only of a qualitative nature.

These estimates show that in the showers under consideration, at mountain heights, the flux of nuclear-active particles carries from $\frac{1}{3}$ to $\frac{1}{2}$ the energy of the shower (minus the energy carried by μ-mesons and neutrinos). This energy is distributed among a relatively large number (of the order of hundreds) nuclear-active particles. The particle that takes the maximum energy carries $\sim 10\%$ of the energy of the entire nuclear-active component.

The following example (Fig. 3) may be used to illustrate this conclusion. In the experiment with the combined absorber of 2 cm of Pb, 80 cm of C (about two nuclear free paths) and 3 cm Pb, a sharp peak of the ionization pulse in one of the chambers must be attributed, as a rule, to the formation of the electron-photon component, which is formed in graphite as a result of a nuclear interaction, then multiplies in the lower layer of the lead. Since 3 cm of lead correspond to approximately the maximum of the electron-photon cascade, it is possible, therefore, to determine directly and from the number of relativistic particles in the chamber, the energy transferred to the π^0-mesons in the layer of graphite (*). Assuming that $\sim 20\%$ of the energy carried by the nuclear-active particles (which appears to us to be the most probable figure) is transferred in the graphite to the electron-photon component, we find that for the case shown in Fig. 3 the energy of the nuclear-active particles, which determines the core of the given shower amounts to $\sim 10^{12}$ eV or $\sim 10\%$ of the total energy of the shower (with the exception of the μ-mesons and the neutrinos) at the given height.

For showers with a total number of particles $\gtrsim 10^5$ the picture obtained is less clear-cut . This is apparently due to the fact that for such showers the difference in the energy of a particle moving along the shower axis and of particles close to it is less pronounced, which is the reason that leads to the more complicated structure of the core pointed out above.

The investigation of the absorption of shower particles in the solid absorber gives us the method of comparing the characteristics of showers with different total number of particles.

The following very preliminary data were obtained by placing aluminium and graphite absorbers over the ionization chambers:

The ratio of the number of shower particles under the absorber to the number of particles in the air, determined from the hodoscope data	For showers with the total number of particles in the interval $10^4 \div 10^5$	For showers with the total number of particles in the interval from $1 \cdot 10^5$ to $8 \cdot 10^5$
A	0.4 ± 0.03	0.3 ± 0.03

(*) From the cascade curves it follows that 1000 particles at the peak of the cascade in lead correspond to an energy $\sim 1 \cdot 10^{11}$ eV.

Despite their insufficient statistical accuracy, these figures apparently show that showers with a total number of particles $1 \cdot 10^5 \div 8 \cdot 10^5$ are absorbed in the absorber a little more strongly than showers with a smaller number of particles (*).

The data obtained may also be correlated with absorption of showers in air. From the absorption of showers, characterized by the coefficient 200 g/cm², we find that for 230 g/cm² of air the ratio given in the table should be equal to 0.31, i.e. close to what is obtained for showers with a total number of particles $1 \cdot 10^5 \div 8 \cdot 10^5$. This also indicates stronger absorption of larger showers, since in the air a part of the energy of nuclear-active particles is used in the formation of μ-mesons; the latter carry a considerable energy to great depths below sea level. In a dense absorber the energy of $\pi^{\pm}$-mesons is imparted to the electron-photon component recorded by the ionization chambers.

The spectrum of the electron-photon component in the central regions of the showers was investigated with cloud chambers. As has already been pointed out, the energy of the electrons and photons was determined basingon the total number of particles in showers that developed in lead plates in a chamber. The obtained spectra of the electr on-photon component for the energy interval $2 \cdot 10^8 \div 10^{10}$ eV are shown in Fig. 7. The experimental points refer to different distances from the shower axis. The curves are calculated from cascade theory for $s = 1$ and $s = 1.5$.

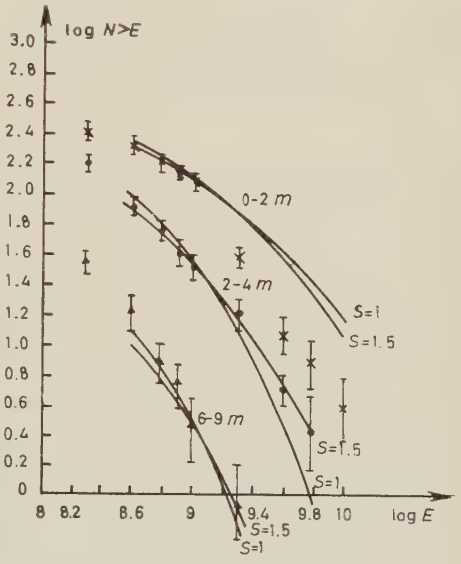

Fig. 7. – The energy spectrum of the component for three distances from the the axis: (0÷2) m, (2÷4) m and (6÷9) m.

As may be seen from these data, the spectrum at small distances from the axis, is very soft which, apparently, is an indication that in the generation of the electron-photon component an essential role is played by π^0-mesons with relatively small energies $\sim (10^9 \div 10^{10})$ eV. Independently similar experimental data were obtained earlier in [5].

An analysis of the remaining part of the experimental data obtained by our group will undoubtedly enable us to make the results and conclusions more reliable and definite.

(*) The total thickness of the absorber is 230 g/cm²; the ratio between the quantities of Al and C in the absorber was such (44% of Al) that it was roughly equivalent to air with respect to both the nuclear and radiation loss absorption.

REFERENCES

[1] S. P. Dobrovolskij, S. I. Nikol'skij, E. I. Tukiš and V. I. Jakovlev: *Žu. Èksper. Teor. Fiz.*, **31**, 939 (1956).
[2] I. N. Vavilov, S. I. Nikol'skij and E. I. Tukiš: *Dokl. Akad. Nauk SSSR*, **93**, 233 (1953).
[3] S. I. Nikol'skij, I. N. Vavilov and V. V. Batov: *Dokl. Akad. Nauk SSSR*, **111**, 71 (1956).
[4] O. I. Dovženko, B. A. Nelepo and S. I. Nikol'skij: *Žu. Èksper. Teor. Fiz.*, **32**, 463 (1957).
[5] W. E. Hazen, R. W. Williams and C. A. Randall: *Phys. Rev.*, **93**, 578 (1954).

PART IV.

SECTION D: M.I.T. Air Shower Program.

The M. I. T. Air Shower Program.

G. CLARK, J. EARL, W. KRAUSHAAR, J. LINSLEY, B. ROSSI and F. SCHERB

Massachusetts Institute of Technology - Cambridge, Mass.

1. - General description and preliminary results concerning the size spectrum and the zenith angle distribution (presented by B. ROSSI).

The M.I.T. air shower program includes three experiments.

1) A preliminary experiment, now completed, which was performed on the M.I.T. campus (latitude 42° N, sea level) by means of four detectors arranged at the vertices of a square 36 m on the side.

2) The « Agassiz experiment » which covers a circular area 460 m in diameter and has been in operation, intermittently since July 1955 and continuously since June 1956, on the grounds of the Agassiz Astronomical Station of Harvard University at Harvard, Massachusetts (latitude 42° N, 183 m above sea level).

3) The « Kodaikanal experiment » using four detectors at the vertices of a square 35 m on the side, which has been in operation since August 1956 at Kodaikanal, India (latitude 8° N, 2800 m above sea level). This experiment is being performed in collaboration with V. SARABHAI and E. CHITNIS of the Physical Research Laboratory in Ahmedabad.

I would like to describe briefly the Agassiz experiment and report on some of its results.

The detectors are disks of plastic scintillating material, 105 cm in diameter and 10 cm thick arranged as shown in Fig. 1. For most of the time we have used eleven detectors (*C*, *M* and *D* in Fig. 1) but during a short period we had four additional detectors placed near the center of the array (*E* in Fig. 1) in order to extend our measurements to showers of smaller size than those which could be recorded in the main experiment. The detectors are connected with cables to separate oscilloscopes which are placed in the control station and mounted on a rack so that they can be photographed by a single

camera. The sweeps of the oscilloscopes are triggered simultaneously whenever ten or more shower particles traverse each of at least three among a preselected group of detectors within a time interval of about 3 μs.

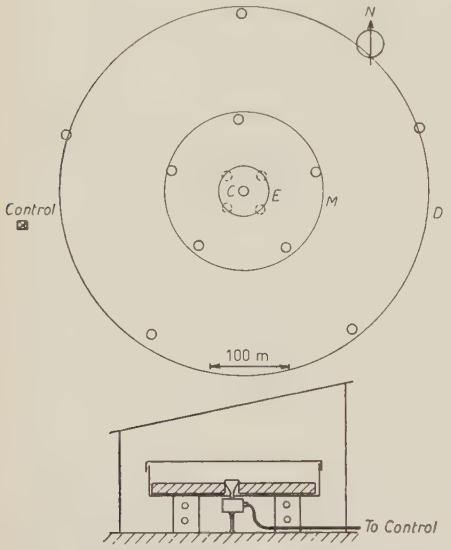

Fig. 1. – Detector array and schematic diagram of one of the scintillation counters.

On the film we measure:

a) the pulse height of each detector (from which we obtain the number of shower particles that have traversed the detector with an accuracy of about 10% in the range from 1 to 4000 particles);

b) the time intervals between the pulses from the various detectors (with an accuracy of about 0.1 μs).

The data pertaining to each individual shower are then analyzed to determine: 1) the direction of the shower axis, 2) the co-ordinates X and Y of the shower center, and 3) the total number of shower particles N.

For the determination of the direction of the shower axis we make use of the fact that the « shower front » is quite well defined and practically flat, i.e., that at any one instant of time most shower particles lie within a disk only a few feet thick perpendicular to the shower axis [1]. The actual method of computation is based on a least-square analysis of the observed differences between the times of arrival of the shower front at the various detectors. The uncertainty in the measurement of angles by this method turns out to be of the order of 5°. For the determination of N, X, Y, we assume that the density of particles at the distance r from the axis of the shower is given by:

$$f(r) = \frac{N}{2\pi} \frac{\exp[-r/r_0]}{r_0 r}, \tag{1}$$

where $r_0 = 74$ meters, and we compute the values of N, X and Y which minimize the mean square deviation of the observed from the computed densities. The general form of Eq. (1) was suggested by previous computations and experimental data. As will be explained later, our results show that the lateral density distributions of most showers are adequately represented by Eq. (1) for values of r less than 250 m.

All of the computations mentioned above are carried out by means of a fast electronic computer. Tests with « artificial » showers indicate that the uncertainty in the determination of N about 20%, and the uncertainty in the determination of the core location is about 10% of the distance from the center of the array.

I would like now to present our results concerning the size spectrum and the zenith angle distribution.

Let x_0 be the atmospheric depth of the station (in g cm^{-2}), θ the zenith angle of the shower axis and $x = x_0/\cos\theta$ the thickness of the atmosphere in the direction of this axis. From our data we wish to determine the « differential size spectrum » at x, i.e., the function $s(N, x)$ such that $s(N, x)A\,\mathrm{d}N\,\mathrm{d}\omega$ represents the number per unit time of showers with sizes between N and $N+\mathrm{d}N$ at the thickness x, whose axes lie within the solid angle $\mathrm{d}\omega$ and intersect perpendicularly the area A. To consider s a function of $x = x_0/\cos\theta$, but not explicitly a function of θ, implies the assumption that the development of a shower depends on the total mass of air traversed, but not on the distribution of the air density along its path. This assumption is well justified, although it is not rigorously correct because of the occurrence of unstable particles in the shower.

The first step of the analysis is a precise definition of an *acceptance area*, $A(N)$, for showers of given size N. This area is defined so that showers of N particles, striking within its boundaries are practically certain to trigger the recording system, irrespective of their directions of arrival.

Considering that the solid angle corresponding to a small interval Δx of atmospheric thickness is $2\pi(x_0/x^2)\Delta x$, we find that the expected number of accepted showers for which N lies in the interval ΔN and x in the interval Δx is $2\pi(x_0^2/x^3)A(N)Ts(N, x)\Delta N\,\Delta x$, where T is the duration of the experiment. We cannot use this result directly for the determination of $s(N, x)$ because, if we divide our data into groups corresponding to small intervals of both N and x, the number of events in each group is too small. We thus begin by investigating the x-dependence of showers belonging to comparatively wide size intervals. We note that the expected number of showers for which N lies between N_1 and N_2, and x lies between x and $x + \Delta x$ is:

$$\Phi(N_1, N_2, x)\Delta x = 2\pi(x_0^2/x^3)T\Delta x \int_{N_1}^{N_2} A(N)s(N, x)\,\mathrm{d}N\,.$$

In principle we can determine the quantity:

$$\int_{N_1}^{N_2} A(N)s(N, x)\,\mathrm{d}N\,,$$

by putting $\Phi(N_1, N_2, x)\,\Delta x$ equal to the observed number of showers in Δx for which $N_1 < N < N_2$. However, very large numbers of events are needed in order to obtain results with statistical errors small enough to reveal unambiguously the functional dependence of s on x. At the present time we have not recorded enough accepted showers to justify such a treatment. However, the zenith angle distributions of the very large numbers of showers recorded in the preliminary experiment at M.I.T. and in the Kodeikanal experiment, along with the zenith angle distribution of all showers recorded in the Agassiz experiment, indicate clearly that the dependence of s on x is approximately exponential. We are well justified, then, in assuming that s can be written as:

$$s(N, x) = s(N, x_0) \exp\left[-(x - x_0)/\Lambda\right]. \tag{2}$$

In order to determine whether or not Λ varies with the size of the showers, we divided the accepted showers from the Agassiz experiment into two size groups corresponding to $N_1 = 4 \cdot 10^5$, $N_2 = 3 \cdot 10^6$, and $N_1 = 3 \cdot 10^6$, $N_2 = 3 \cdot 10^7$ respectively. Assuming the exponential form of the dependence of s on x, we determined values of Λ according to the method of maximum likelihood and found $\Lambda = (90 \pm 16)$ g cm^{-2} and $\Lambda = (98 \pm 18)$ g cm^{-2} respectively. No significant difference is apparent between these values, and we have adopted the value $\Lambda = 95$ g cm^{-2} for use in the succeeding steps of the analysis. Note, however, that owing to a lack of sufficient data, no precise conclusion can be drawn regarding the dependence of s on x above $N = 3 \cdot 10^7$.

We can now make use of the known dependence of s on x below $N = 3\ 10^7$ to determine the dependence of s on N with reasonable statistical accuracy. In fact, t e expected number of showers coming from all directions between the vertical and a given zenith angle θ_1 and whose sizes lie within a narrow interval ΔN is given by:

$$R(N, \theta_1)\Delta N = 2\pi s(N, x_0) A(N) T \Delta N \int_{x_0}^{x_1} \exp\left[-(x - x_0)/\Lambda\right](x_0^2/x_3)\,\mathrm{d}x\,, \tag{3}$$

where $x_1 = x_0/\cos\theta_1$. This equation enables us to compute $s(N, x_0)$ starting from the experimental determination of $R(N, \theta)$. The actual procedure is as follows. For each shower in the interval ΔN we compute a *weight* which is the reciprocal of the quantity:

$$2\pi T A(N) \int_{x_0}^{x_1} \exp\left[-(x - x_0)/\Lambda\right](x_0^2/x^3)\,\mathrm{d}x\,.$$

We then add together the weights of all accepted events within the interval ΔN and call this sum the value of $s(N, x_0)\Delta N$ corresponding to the size $\overline{N}$,

where $\bar{N}$ is chosen so that $s(\bar{N}, x_0)$ is equal to t e average value of s over the interval ΔN.

In our analysis we took $\theta_1 = 30°$ (i.e., we included all showers up to a maximum zenith angle of 30) and obtained the results shown in Fig. 2 where the abscissa is the logarithm of N and the ordinate is the logarithm of s. We see that within the statistical fluctuations, the spectrum obeys a power law:

$$(4) \quad s(N, x_0) = K(10^6/N)^{\gamma+1},$$

with $\gamma = 1.84 \pm .15$ and $K = (6.9 \pm 2.3) \cdot 10^{-18}$ cm^{-2} s^{-1} sr^{-1}.

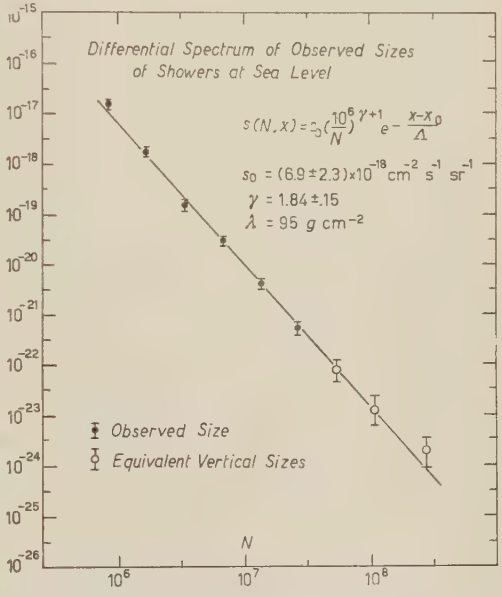
Differential Spectrum of Observed Sizes
of Showers at Sea Level
$s(N,x) = s_0 (\frac{10^6}{N})^{\gamma+1} e^{-\frac{x-x_0}{\Lambda}}$
$s_0 = (6.9 \pm 2.3) \times 10^{-18}$ cm^{-2} s^{-1} sr^{-1}
$\gamma = 1.84 \pm .15$
$\lambda = 95$ g cm^{-2}
Observed Size
Equivalent Vertical Sizes
N

Fig. 2. – Differential size spectrum of showers at sea level.

As we mentioned earlier, the range of sizes for which we have statistically significant experimental information about the zenith angle variation for showers, and therefore about the functional dependence of s on x, extends only to $N = 3 \cdot 10^7$. Notice that the dependence of s on x is determined both by the rate of atmospheric attenuation of individual showers (i.e., the rate of change of N with x) and by the shape of the primary spectrum. It is reasonable to assume that the rate of attenuation of showers does not change suddenly above $N = 3 \cdot 10^7$. However, we cannot rule out the possibility that the primary spectrum deviates considerably from a power law at energies above that required to produce showers of $3 \cdot 10^7$ particles at sea level. Indeed one of the main purposes of the experiment is to investigate the possible existence of a cut-off in the primary spectrum, such as is suggested by astrophysical considerations. If such a deviation occurs, then s ceases to be an exponential function of x, and a method of analysis based on the assumption of an exponential dependence of s on x ((Eq. 2)) with a constant value of Λ would blur the details of the actual spectrum. In order to avoid this source of error we have extended the size spectrum beyond $N = 3 \cdot 10^7$ by a method which is based *only* on the assumption that the rate of atmospheric attenuation of showers with N above $3 \cdot 10^7$ is approximately the same as for smaller showers.

For this analysis we first define a quantity N_v by the following equation:

$$(5) \quad s(N, x)\, \mathrm{d}N = s(N_v, x_0)\, \mathrm{d}N_v .$$

We may call N_v the « vertical equivalent size » of a shower of size N coming at a zenith angle θ such that $\cos\theta = x_0/x$. In fact (at least in the absence of fluctuations in the longitudinal development of showers) N_v represents the number of particles which would have been present in the given shower had it come from the vertical direction.

From Eqs. (2) and (5) we find:

$$N_v = N \exp\left[(x - x_0)/\lambda\right], \tag{6}$$

$$\lambda = \gamma \Lambda . \tag{7}$$

In the absence of fluctuations in the development of showers the quantity λ may be interpreted as the reciprocal logarithmic slope of the curve representing the number of particles in a given shower as a function of depth, and is therefore *independent of the primary spectrum*. We may be confident that this conclusion is still valid to a high degree of approximation even in the presence of fluctuations. We have seen, that for $N < 3 \cdot 10^7$, $\Lambda = 95$ g cm^{-2} and $\gamma = 1.84$; therefore we have $\lambda = 175$ g cm^{-2}. As pointed out above, we may assume that λ has the same value for $N > 3 \cdot 10^7$.

The expected number of showers with vertical equivalent sizes between N_v and $N_v + \Delta N_v$, coming from zenith angles less than θ_1, is:

$$F(N_v, \theta_1)\,\Delta N_v = T \int_{x_0}^{x} s(N, x)\,\Delta N\, 2\pi (x_0^2/x^3) A(N)\,\mathrm{d}x ,$$

where $\cos\theta_1 = x_0/x_1$, and N and N_v are related by Eq. (5).

The above equation, together with Eqs. (5) and (6), yields:

$$F(N_v, \theta_1)\,\Delta N_v = T s(N_v, x_0)\,\Delta N_v \int_{x_0}^{x_1} 2\pi (x_0^2/x^3) A\left(N_v \exp\left[-(x - x_0)/\lambda\right]\right) \mathrm{d}x . \tag{8}$$

Equation (8) offers a method for the determination of the size spectrum $s(N, x_0)$ which, as pointed out, can be safely used beyond the previous limit of $3 \cdot 10^7$. The procedure consists of converting each observed shower to vertical equivalent size by means of Eq. (6). For any given value of N_v, we then compute the integral:

$$\int_{x_0}^{x_1} 2\pi (x_0^2/x^3) A\left(N_v \exp\left[-(x - x_0)/\lambda\right]\right) \mathrm{d}x ,$$

(which represents an effective value for the product of the area and the solid angle of detection) and, as before, we assign to each observed shower a *weight*

equal to one over this integral multiplied by the time of observation T. The quantity $s(N_v, x_0)\Delta N_v$ is taken as equal to the sum of the weights of all observed showers for which $\theta < \theta_1$ and whose vertical equivalent sizes lie between N_v and $N_v+\Delta N_v$.

The results obtained by this method are identical with those based on the observed sizes up to $N = 6\cdot10^7$ and they extend the spectrum to $N > 10^8$. The additional points are indicated in Fig. 2 by open circles. We see that the power law, which by the previous method had been found to hold for $3\cdot10^5 < N < 3\cdot10^7$, remains valid up to about $N = 3\cdot10^8$, within the limits of our experimental accuracy.

The rigorous acceptance criteria which must be imposed on data used in constructing a statistically reliable size spectrum do not permit us to include several extraordinarily large showers which fell near or within the detector array. Perhaps the single most important qualitative result of the experiment has been the establishment by individual cases of the definite existence of showers with over 10^7 particles. The largest shower recorded so far had $1.4\cdot10^9$ particles and arrived at a zenith angle of 11°.

The next problem is to compute, from the observed size spectrum of showers, the energy spectrum of the primary radiation.

The solution of this problem requires a quantitative knowledge of the cascade processes initiated by primary particles of different energies.

S. Olbert of M.I.T. has developed a new method for the solution of the shower equations and has applied this method to the computation of the function $N(E_0, x)$ representing the average number of electrons at the depth x in the shower initiated by a proton of energy E_0. He has carried out the computation using both the Fermi and the Landau models of high-energy nuclear interactions, assuming in both cases complete inelasticity and a collision mean free path in the atmosphere of 100 cm^{-2}. The results are shown in Fig. 3 for three different energies, equal respectively to 10^6, 10^7 and 10^8 times the rest energy of protons. From these results we find that the relationhsip between the primary energy and the number of particles at sea level may be

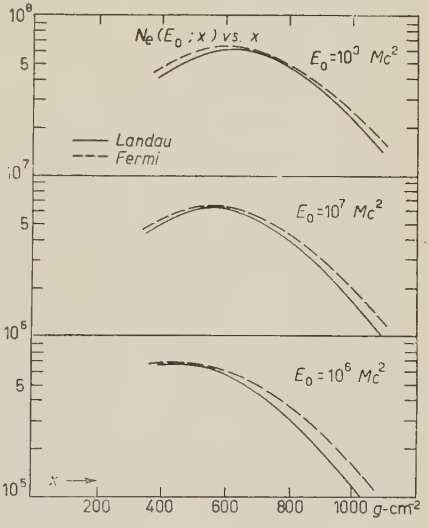

Fig. 3. – The average number of electrons $N(E_0, x)$ as a function of atmospheric depth for three primary energies, according to the calculations of Olbert.

approximated by the equations:

$$(9) \qquad \begin{cases} \text{Fermi model:} & N = 1.80 \cdot 10^5 (E_0/10^{15})^{1.10} , \\ \text{Landau model:} & N = 1.10 \cdot 10^5 (E_0/10^{15})^{1.16} . \end{cases}$$

If we neglect fluctuations in the longitudinal development of showers, i.e., if we assume a one-to-one relationship between the observed shower size N and the energy E_0 of the initiating proton, we can translate the size spectrum into an energy spectrum. Using, for example, Landau's model, we find the following expression for the *integral* energy spectrum, $J(E_0)$:

$$J(E_0) = 2.2 \cdot 10^{-10} (10^{15}/E_0)^{2.13} \text{ cm}^{-2} \text{ s}^{-1} \text{ sr}^{-1} .$$

With the same model, we obtain a value of $0.7 \cdot 10^{19}$ eV for the energy of the primary particle responsible for the largest shower observed so far ($N = 1.4 \cdot 10^9$). The radius of curvature of this particle in the average magnetic field of the galaxy (assumed to be $5 \cdot 10^{-6}$ G) is about 5000 light years.

The above results are based on the assumption that the primary particles are protons. At the present time, we cannot rule out the possibility that these particles are complex nuclei. In this case the energy corresponding to a given value of N at sea level is somewhat greater, but the corresponding magnetic rigidity of the particle is smaller than that computed for the case of protons. However, even if we grant the possibility that the primary particles responsible for the largest observed showers are complex nuclei, it appears unlikely that these particles may be effectively contained in the galactic disk. The existence of such particles is thus of great importance in connection with any speculation on the origin of cosmic rays. In particular, if we assume that cosmic-ray particles are accelerated through a mechanism of the type suggested by Fermi, we must conclude that the confining volume does not coincide with the galactic disk, but extends at least to the galactic halo.

Before closing, I would like to add a few words concerning the fluctuations, which we have neglected so far. These arise mainly from the random depth of the first interaction because, at the very high energies with which we are concerned, the mean number of secondary particles produced in this interaction is quite large.

W. KRAUSHAAR has made a quantitative estimate of the fluctuations, which will be described in Appendix II. From his analysis it follows that, if the primary spectrum obeys a power law, neglect of the fluctuations merely introduces an error in the absolute value of the intensity, and the corresponding correction factor amounts to 1.4.

It should be noticed, however, that the presence of fluctuations would smear out any sudden deviation from a simple power law that may occur in the primary spectrum.

2. The lateral distribution of electrons and μ-mesons (presented by W. KRAUSHAAR).

2·1. *Analysis for core location and shower size.* – As has been explained in Sect. 1, showers which have been recorded by the M.I.T. experiment are subjected to a rather complete analysis on a fast electronic digital computer. Some of the details of the analysis will be explained later in Appendix I. For the present, it is sufficient to note that in the first part of the analysis the shower direction is determined, and subsequent computations are carried out in a plane perpendicular to the shower axis. We have available, then, eleven measurements of shower density in the plane of the shower, and the purpose of further analysis is to determine the location of the shower core and total number of particles in the shower.

This further analysis proceeds as follows. We assume a lateral distribution function given by:

$$f(r) = \frac{N}{2\pi r_0} \frac{\exp\left[-r/r_0\right]}{r}, \tag{10}$$

where $f(r)$ is the number of particles per square meter at a distance r from the core of a shower having a total of N particles, and r_0 is a characteristic distance, taken to be 74 m. This distribution, as will be explained later, fits our data very well for $r < 250$ m, and as well approximates the Nishimura-Kamata distribution for $S = 1.4$ in this region. (The function is particularly useful because of its simple analytic form.) For each successive trial position X, Y of the shower core and trial shower size, N, we calculate the square of the difference between the measured and predicted densities at each detector, expressed in units of the standard deviation for the appropriate density measurement. This quantity, for the i-th detector, we call ψ_i^2, and the computer minimizes the quantity ψ^2, given by:

$$\psi^2 = \sum_{i=1}^{i=m} \frac{\psi_i^2}{m-3}, \tag{11}$$

where m is the total number of detectors in operation, for the variables X, Y and N. That is, a least squares fit to the data is made. We have estimated the uncertainties in detector calibrations and associated instrumental uncertainties to be about 14%. The standard deviations are therefore taken as 14% for densities greater than 50 particles per square meter, and the square

root of the «predicted» density (the detectors are about one square meter in area) for densities less than 50 particles per square meter. Printed out, with each analysis of a shower are N, ψ, the ψ_i's for each detector, the measured and «predicted» density for each detector, the distance each detector was from the shower core, the direction of arrival of the shower, and various other quantities of technical importance to the details of the computer program.

2.2. *Lateral distribution function of large showers.* – Of particular interest are the experimentally determined lateral distributions for two of the largest showers we have detected. Fig. 4 summarizes the results of a detailed analysis of the largest shower, No. 58042. The computer-selected core location for this shower was at «D», and the shower size was calculated to be $1.4 \cdot 10^9$ particles. In order to give visible evidence that the shower really did land at or very near D, we have plotted apparent lateral distribution functions for various other assumed core locations, and have computed for each of these locations the quantity ψ^2. It is evident from these plots and from the indicated values of ψ^2 that it would be highly artificial to assume that the shower core struck anywhere but near D. The smooth curve drawn in the D plot is the Nishimura-Kamata distribtuion for $S = 1.4$. Our empirical function, expression (10), fits the data well out to about 250 m, but is in definite disagreement with the data on the large shower at larger distances.

It is difficult to see how the shower could have been much smaller than $1.4 \cdot 10^9$ particles. Even if we assume that the density of particles did not increase at all inside of the position of our detector nearest the core (the nearest detector was 122 m from the core, and 4620 particles passed through it, dissipating about 50 GeV) the shower size would be $5 \cdot 10^8$ particles.

Another shower that is particularly interesting because of its large size and large zenith angle is No. 63906, shown in Fig. 5. Here it is more difficult to assign a core location with certainty, although it seems clear that it must have fallen near D. Once again, the data fit satisfactorily well the Nishimura-Kamata distribution for $S = 1.4$. For this particular shower, the thickness of atmosphere in the direction of the shower axis was 1500 g cm^{-2}. It is possible, of course, that the primary particle penetrated deeply into the atmosphere before interacting, and that the subsequent shower developed giving rise to a quite normal shower at sea level, reflecting not at all the large apparent atmospheric penetration.

2.3. *Lateral distribution function of smaller showers.* – Generally, showers having 10^8 or more particles, when they strike our array, result in densities in excess of 10 particles m^{-2} in most if not all of the eleven detectors. Such large showers usually fall between the M and D rings of detectors, and so we have, as a rule, eleven measurements of particle density in a wide range

of distances from the shower core, and each measurement has reasonable statistical accuracy. We therefore have, in effect, a measurement of the lateral distribution function out to distances of the order of 300 m or more for each of these large showers.

Smaller showers, on the other hand, having, say, 10^7 or fewer particles,

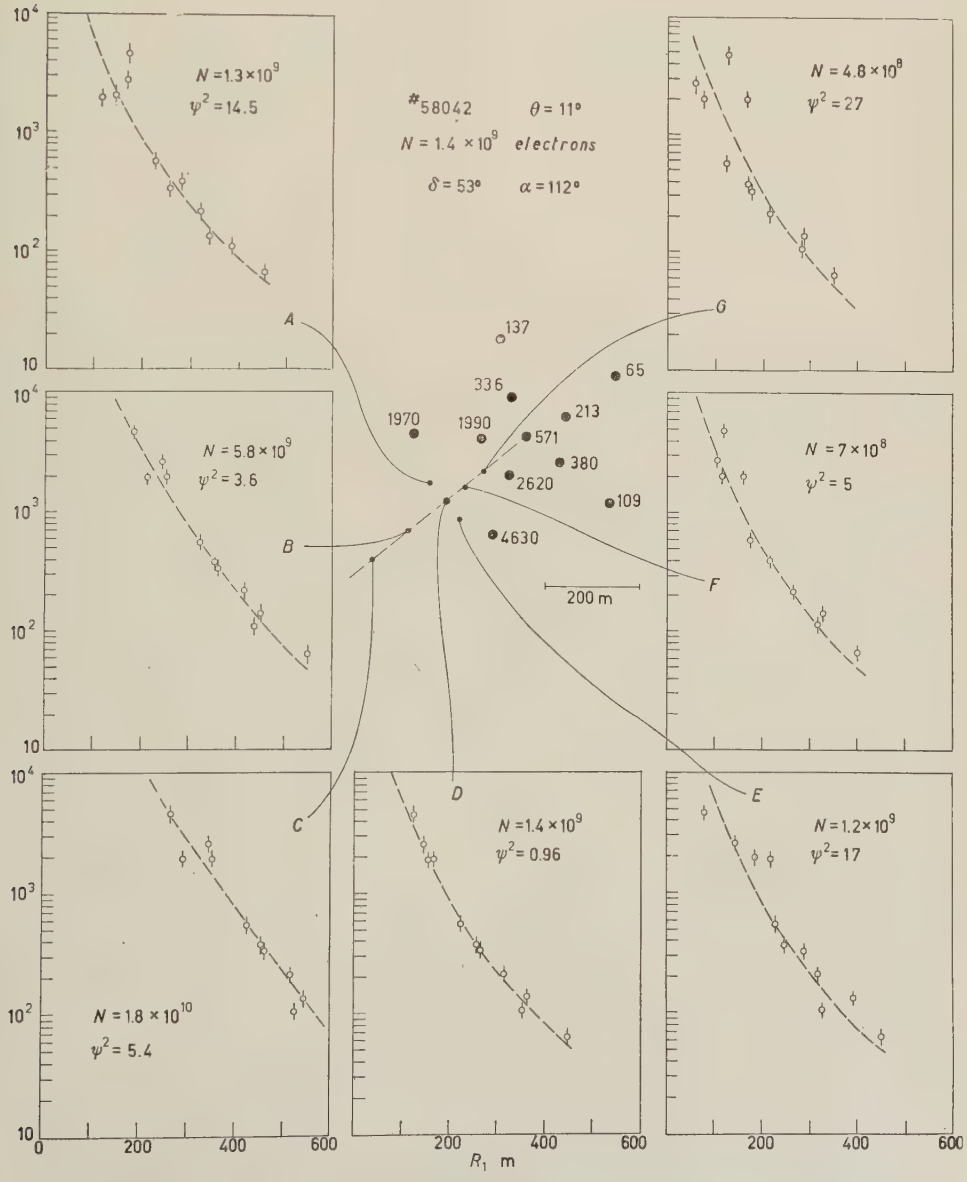

Fig. 4. – Detailed analysis of shower No. 58042, showing the apparent lateral distribution for various assumed positions of the shower core. The best core position is near *D*.

generally result in densities less than 10 particles m $^{-2}$ in several of the eleven detectors. For these showers, statistically accurate density measurements are available only within about 100 m of the shower core, and so the detailed structure of such showers at large distances from the core can only be studied by examining the average behavior of several showers. We have therefore

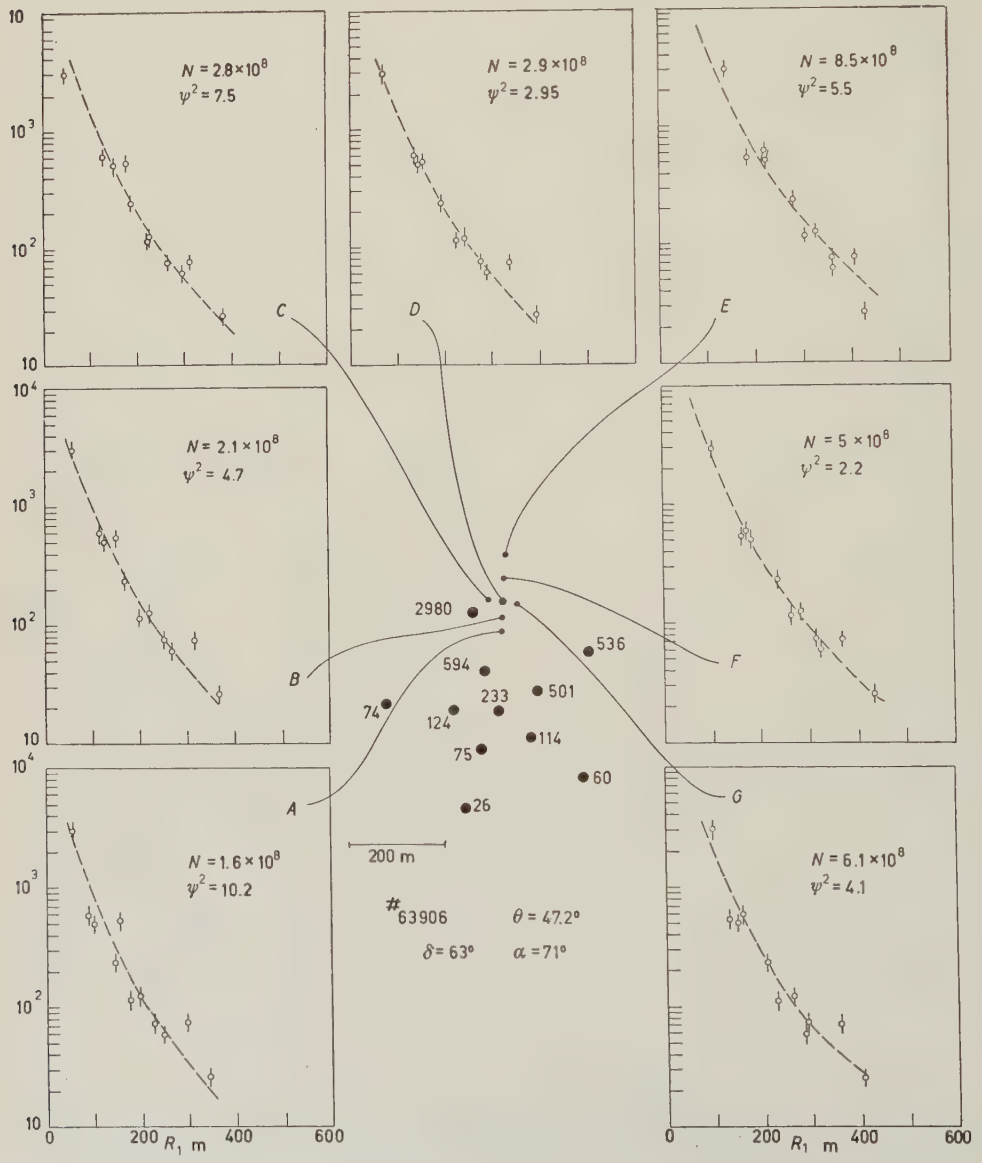

Fig. 5. – Detailed analysis of shower No. 63906. The best core position is not as well defined as in the case of No. 58042.

selected three groups of showers with N near $5.3 \cdot 10^5$, $4.2 \cdot 10^6$, and $5.4 \cdot 10^7$ particles, respectively, coming from approximately vertical directions, and one group of showers with N near $3.5 \cdot 10^6$ particles, coming from large zenith angles Each measured density was divided by N/r_s^2, where $r_s = 79$ m (*), the characteristic shower length, and N is the measured shower size. The resulting distributions are shown in Fig. 6. The curve in each case is the Nishimura-

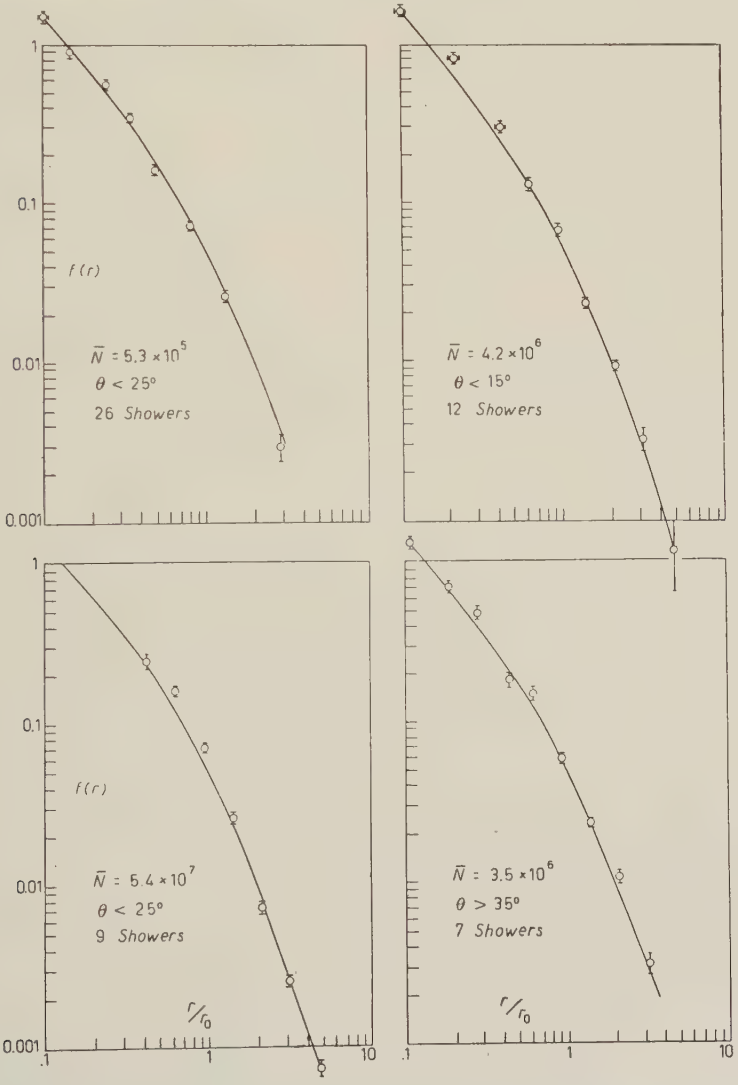

Fig. 6. – Composite lateral distributions for four groups of showers.

(*) There is no necessary connection between the r_0 that enters our empirical relationship, expression (10), and the characteristic length r_s that enters the Nishimura-Kamata distribution.

Kamata function for $S = 1.4$, and it is evident that all four of these distributions are consistent with the curves. There is, of course, no *a priori* reason that a single function should fit showers over such a wide range of size and atmospheric depth. The Nishimura-Kamata distribution, it will be recalled, refers to single electron or photon-initiated cascades, while the showers we are concerned with are certainly initiated by many photons produced in the nuclear cascade . It seems likely that the gross features of shower development are determined by the nuclear cascade and that the electronic component is more or less in equilibrium with the nucleonic component.

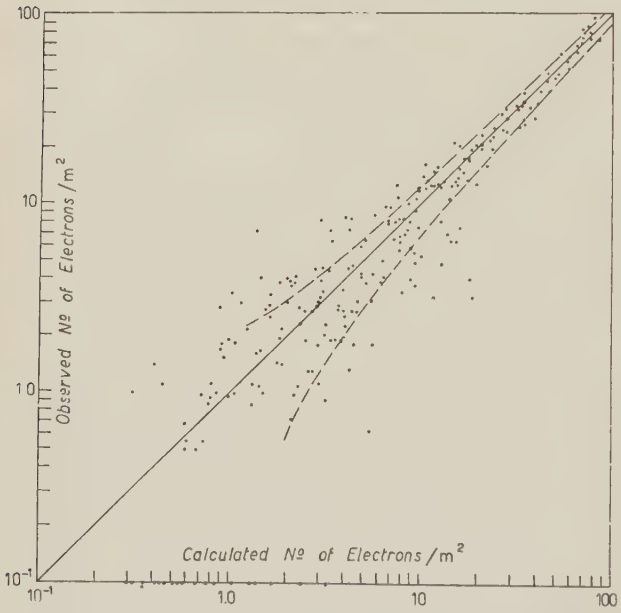

Fig. 7. – Observed versus calculated densities. The broken lines are appropriate to a Poisson distribution.

Fig. 7 shows a composite plot of observed versus calculated densities made from the results on about thirty showers picked at random. The abscissa is the observed density of particles at a detector, and the ordinate is the predicted density at that detector after the least squares analysis for the core position and shower size has been completed. The dashed lines indicate the magnitude of the standard statistical fluctuations corresponding to a Poisson distribution. Each of the detectors participated in the least-squares fit for the shower size and core location, so that, if the only source of density fluctuations were that inherent to the Poisson distribution, the scatter of the points in Fig. 7 should be somewhat less than for a Poisson distribution.

2·4. *Lateral distribution of μ-mesons.* – The apparatus is indicated schematically in Fig. 8. The large hodoscope was located first near the center of the air shower array, and later near the edge. Mesons traversing the hodoscope in coincidence with the arrival of an air shower can be examined for projected angle of arrival, since we have, from the main air shower experiment, the direction of the shower axis. This feature helps to insure that the observed particles

are really μ-mesons and not nucleons or other strongly interacting particles.

Mr. J. Earl has shown that if the lateral spread of μ-mesons is due entirely to their multiple scattering, the earth's magnetic field should produce an asymmetric lateral distribution, there being more particles at large distances from the shower core in the East-West direction than in the North-South direction. From the results shown in Fig. 9 this seems not to be the case, and one concludes that a significant portion of the lateral spread must be due to angular divergence of the μ-mesons at production.

In Fig. 10 there is plotted the lateral distribution of μ-mesons in showers of 1 to $3 \cdot 10^6$ particles for three different bands of shower arrival directions. The three distributions, appear to be the same out to 300 m from the shower core.

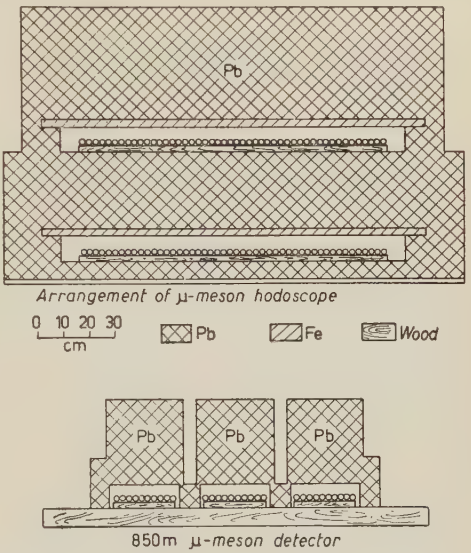

Fig. 8. – Detection apparatus for μ-mesons.

Fig. 11 shows the μ-meson lateral distribution for four different shower sizes. The observations within 600 m were all made with the large hodoscope. The data beyond 600 m were obtained with the « 850 m » μ-meson detector shown in Fig. 8. This detector was put into operation because the data from the hodoscope detector do not extend to distances sufficiently far from the shower cores to show any real departure from a $(1/r)$-like lateral distribution. A $1/r$ distribution cannot, of course, extend indefinitely far from the shower cores. An integration to obtain the total number of μ-mesons has been attempted, and one gets $N_\mu/N \sim 0.1$. That is, roughly 10% of the particles in a large shower are μ-mesons. It is very difficult to say how this total number varies with

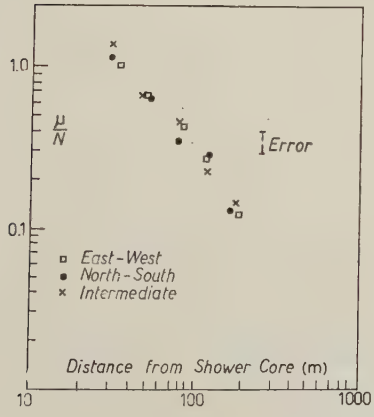

Fig. 9. – Lateral distribution of μ-mesons falling in various directions relative to the shower core. If multiple scattering were the only cause of the mesons' departure from the shower core, the E-W and N-S distribution should be different.

shower size, because such a large fraction of the total are at large distances from the shower core where the density of μ-mesons is very small and therefore inaccessible to accurate measurement.

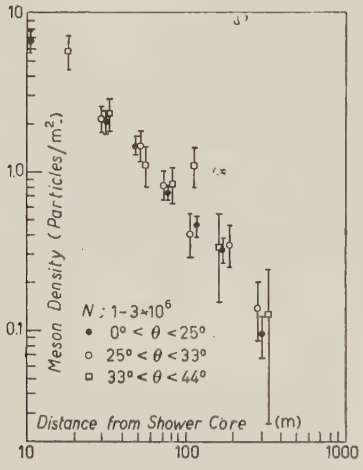

Fig. 10. – Lateral distribution of μ-mesons in showers of 1 to $3 \cdot 10^6$ particles arriving in three ranges of zenith angle.

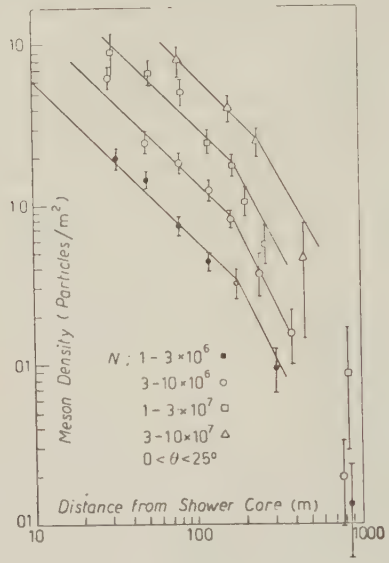

Fig. 11. – Lateral distribution of μ-mesons for four different shower sizes. The showers were selected to have directions within 25° of the zenith.

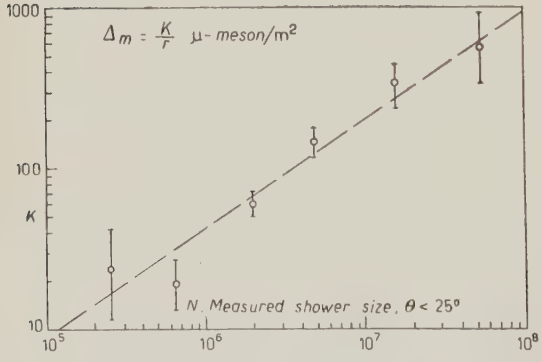

Fig. 12. – Variation of the number of mesons near the shower core with the shower size, N. The showers were selected to have zenith angles less than 25°.

Near the shower core, it is evident that the μ-meson density Δm varies roughly as $1/r$, and one can inquire as to how K, defined by

$$\Delta m = \frac{K}{r} \ \mu\text{-mesons m}^{-2},$$

varies with shower size and zenith angle. It is evident, for example, from Fig. 10 that showers of 1 to $3 \cdot 10^6$ particles have values of K that are roughly constant over a wide range of shower arrival directions. If one selects showers that arrive from near the zenith angle, K varies less than proportionally to the measured shower size, as shown in Fig. 12. That K should vary in this manner with shower size is understandable, since

high-energy showers are less efficient in producing μ-mesons than are low-energy showers. The higher average energy of the produced π-mesons makes their decay into μ-mesons less likely.

3. – Arrival directions of air showers (presented by G. Clark).

3·1. *Introduction.* – The results on the arrival directions of air showers cover a range of primary energies from 10^{14} eV to 10^{18} eV and a range of celestial declinations from $-30°$ to $+80°$. Below primary energies of about 10^{17} eV our data are consistent with the hypothesis that the primary flux is isotropic. Within the statistical accuracy this result is in agreement with results obtained in many other experiments. On the other hand, the distribution of the arrival directions of showers with $N > 3 \cdot 10^7$ recorded by the large experiment gives evidence of a lack of isotropy in the flux of primaries with energies greater than 10^{17} eV. We shall discuss the results obtained so far, beginning with the low energies and working up.

3·2. *Kodaikanal experiment. Small timing array.* – We are operating a simple fast timing apparatus at Kodaikanal, South India (altitude 2 800 m, latitude 8° N), in co-operation with V. Sarabhai and E. Chitnis of the Physical Research Laboratory of Ahmedabad. The apparatus consists of four scintillators 0.13 m² in area located at the corners of a square array 35 m on a side. Showers are recorded at the rate of 1 000 per day. The most likely size of the recorded showers has been computed and found to be $1.0 \cdot 10^5$ particles. Showers of this size at 2 800 m are produced by primary energies of about $2 \cdot 10^{14}$ eV.

So far we have recorded about 50 000 showers. The arrival directions of 15 000 showers have been calculated, and the celestial distribution of a sample of 7 800 showers has been analyzed. The 15 000 showers from which the sample was drawn were recorded during a period of only about 10 days, and because of the various unavoidable interruptions which occur in the data recording, the sidereal ON-TIME for the period varies considerably from hour to hour. In order to eliminate the possibility of apparent anisotropy arising from errors in the evaluation of ON-TIME and from variations of detection efficiency with sidereal time we have rejected events at random from various « overexposed » sidereal time intervals so as to equalize the numbers of events observed in each interval. This procedure amounts to using the intensity from all directions during a given sidereal time interval as a monitor of detection efficiency and permits one, in effect, to compare accurately the relative intensities of areas within the field of view of the timing apparatus. If the real celestial

distribution is random, the only possible effect which this procedure can have on the observed celestial distribution is to reduce the fluctuations so that the procedure is, in fact, a conservative one which will render any evidence of anisotropy more convincing.

The fluctuations which have been observed in the Kodaikanal data are shown in Fig. 13. We tabulated the numbers of events from each $10^\circ \cdot 10^\circ$ region of the sky, and computed the average number of events per $10^\circ \times 10^\circ$ region for each 10° band of declination. On the basis of these averages we computed the deviations and the values of χ^2 for each declination band. The results which are indicated in the figure are consistent with the assumption of an isotropic flux of primaries.

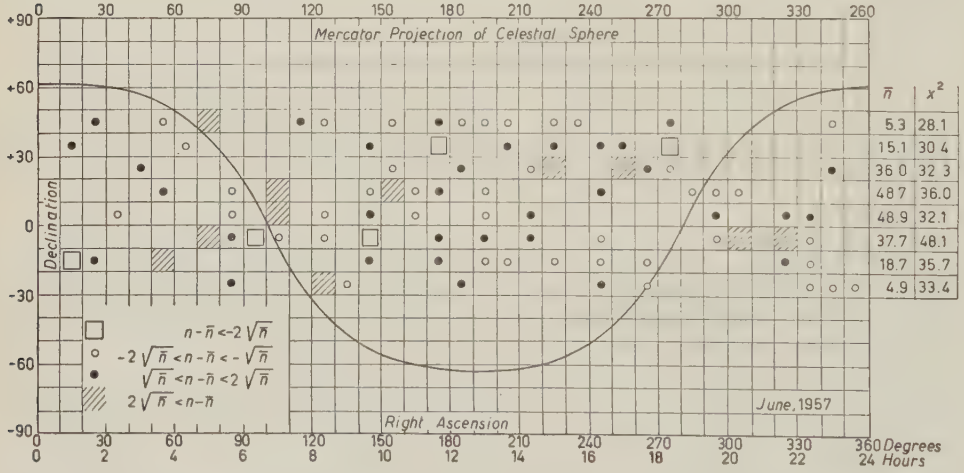

Fig. 13. – Fluctuations and χ^2 tests on the arrival directions of 7700 showers recorded at Kodaikanal. The most probable energy of the primaries is $\sim 2 \cdot 10^{14}$ eV.

Comparisons have also been made between the observed numbers of events from special regions and the numbers expected on the basis of the average intensities computed for each declination interval. The regions selected and the results obtained are shown in Table I, from which it can be seen that the observations are consistent with the assumption of isotropy.

3·3. *Cambridge experiment. Small timing array* [2]. – An experiment exactly similar to the one at Kodaikanal was performed on the M.I.T. campus as a part of the development program for the large experiment. Arrival directions of 2600 showers were determined. The most likely size of these showers is also 10^5 particles, but at sea level this corresponds to a primary energy of about 10^{15} eV. The same statistical tests were applied to these data as were

later used on the Kodaikanal, and none of them gave results inconsistent with isotropy. Table I shows the expected and observed numbers of events from three celestial regions which are within the range of observation at Cambridge. Again the results are consistent with isotropy of the primary radiation.

TABLE I. – *Comparison of observed numbers of events from special regions with the numbers expected for an isotropic primary flux.*

Region	Kodaikanal expected	($\sim 2 \cdot 10^{14}$ eV) observed	Cambridge-campus expected	($\sim 10^{15}$ eV) observed
20° band centered on galactic equator	786	747	996	972
20° band perpendicular to spiral arm	1 296	1 335	945	968
$40° \times 40°$ region around spiral out	420	389	325	297
$40° \times 40°$ region around spiral in	96	101	—	—
$20° \times 20°$ region around $\delta = 0$, $\alpha = 83°$	173	186	—	—

3·4. *Agassiz experiment.* – The Agassiz experiment gives accurate data on the sizes and the arrival directions of showers of over 10^6 particles. Consequently, we can analyze the arrival directions of groups of showers within well defined ranges of sizes.

Fig. 14 is a celestial map in which the arrival directions of all showers with $N > 2 \cdot 10^6$ are represented by points. No evidence of anisotropy is apparent in the distribution of points.

Fig. 15 is a plot of the arrival directions of especially large showers. There is, in these data, some evidence of anisotropy. Nine out of the ten showers

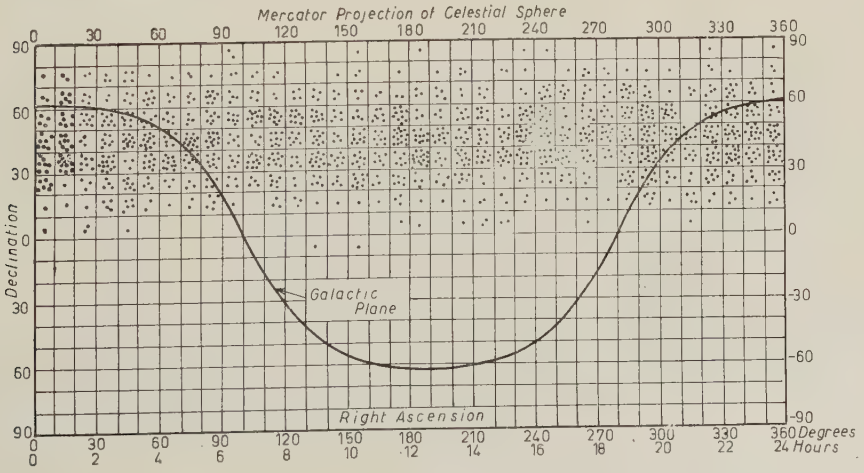

Fig. 14. – Arrival directions of 1 000 showers with $N > 2 \cdot 10^6$ recorded in the Agassiz experiment. The primary energies were greater than $\sim 10^{15}$ eV.

with equivalent vertical size $N_v > 10^8$ arrived from the hemisphere bounded by $300° < \alpha < 120°$. Fifty-six out of eighty-seven showers with $N_v > 3 \cdot 10^7$ came from the same hemisphere. The probability of fluctuations as large as these in an isotropic distribution is small. The isotropic distribution of the showers with $N > 2 \cdot 10^6$ is obvious evidence for the uniformity of the ON-TIME. Furthermore, of 8 showers recently added to this plot, 7 arrived from the more intense hemisphere bringing the present total to 63 out of 95. Also in the case of this latest data the distribution of arrival directions of the smaller showers was consistent with isotropy. Of course, we would have been equally surprised had a fluctuation as large as this occurred for any other choice of hemispheres so that the statistical significance of the observed fluctuation is less then if the choice of hemispheres were really made *a priori*.

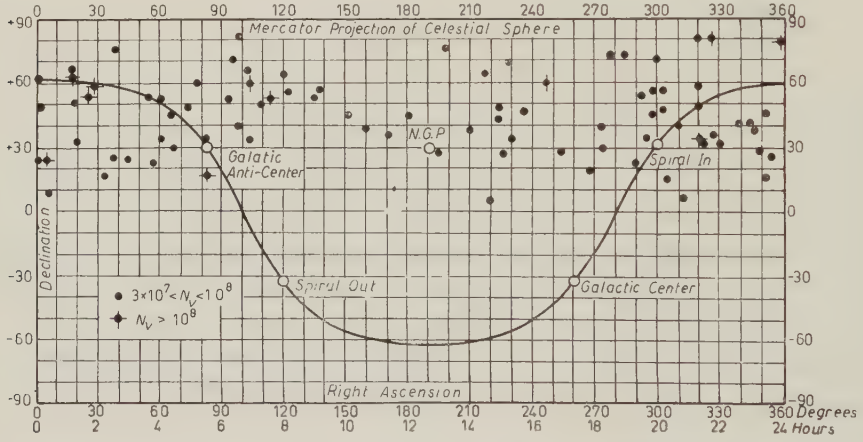

Fig. 15. - Arrival directions of 87 showers with equivalent vertical sizes greater than $3 \cdot 10^7$.

Since the data were obtained during only a fraction of one year (July, September, October, November, December, February; 1956-1957), it is not possible to distinguish between a solar and a sidereal effect. Table II summarizes the results of harmonic analyses of the data for all showers with $N > 3 \cdot 10^7$ in both solar time and in right ascension.

TABLE II. – *Harmonic analyses of arrival directions of showers with* $N > 3 \cdot 10^7$.

Correlation	Amplitude	Position of max. intensity	Probability of occurrence of observed variation in an isotropic flux
Right ascension	38%	0°	12%
Solar time	32%	0 h	22%

We therefore draw the tentative conclusions from the M.I.T. experiment that

1) There is no evidence of anisotropy for showers of size less than 10^7 particles.

2) There is evidence of anisotropy for showers with equivalent vertical sizes greater than $3 \cdot 10^7$ particles corresponding to primary energies greater than 10^{17} eV. The hemisphere of greatest intensity contains the plane of the Milky Way.

Appendix I

Methods of analysis (presented by G. Clark).

A) *Introduction.* – The methods used in the M.I.T. air shower experiments give detailed and relatively accurate information about each individual shower. The information, however, can be fully utilized only at the expense of somewhat complex procedures of data analysis which are made practical through the use of high speed automatic electronic computers and card sorting machines. In order to clarify the basis of the conclusions we have drawn concerning the atmospheric attenuation, the size spectrum, and the arrival directions of air showers, we shall describe the reduction of data and the statistical analysis in somewhat greater detail than in the previous discussions.

B) *Data Reduction.*

B.1) Determination of arrival directions. At a given instant most of the particles in an air shower lie within a thin flat disk perpendicular to the shower axis and moving in the direction of the axis with the velocity of light. Therefore the arrival times of the shower particles at each of a group of detectors spread laterally on the ground are related to one another in a way which depends on the orientation of the shower axis. One can therefore determine approximately the arrival direction of a shower by finding the orientation of a moving plane which intersects the various detectors at a set of times which best fits the observed arrival times of the shower particles.

For the analysis we adopt a set of coordinates whose z-axis is in the direction of the zenith, whose y-axis points north, and in which the ground is the plane $z = 0$. We call $\boldsymbol{k} = (l, m, n)$ a unit vector normal to a plane moving in the direction of $\boldsymbol{k}$ with the velocity of light c. This plane intersects a given point with coordinates, x, y, z at the time

$$t = t_0 - \frac{1}{c}(lx + my + nz),$$

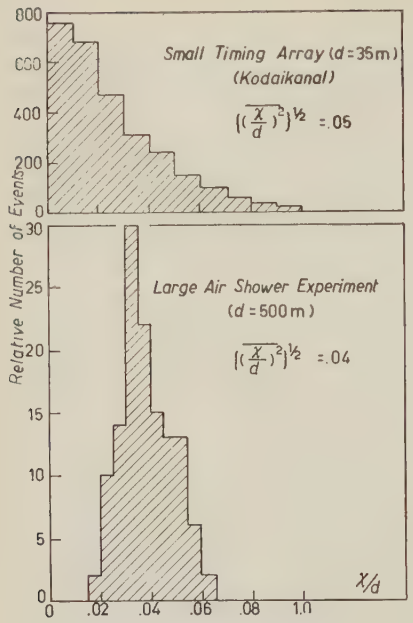

Fig. 16. – Distributions of χ/d for a small timing array (above) and for the Agassiz experiment.

where t_0 is some constant. We call x_i, y_i the coordinates of the ith detector ($i = 1, 2, \ldots, n$), and t_i the observed arrival time of the shower particles at the ith detector. Then the values of l, m, and t_0 which minimize the function

$$\chi^2 = \frac{1}{n-3} \sum_{i=1}^{n} (ct_i + lx_i + my_i - ct_0)^2 ,$$

specify the moving plane which gives the best fit to the timing data according to the method of least squares. The solution of the problem for data from any detector array is a simple algebraic problem. In order to demonstrate the good quality of the fits one obtains to timing data from both the small square array and from the large timing array we have plotted in Fig. 16 the distributions of the quantity χ/d where d is the maximum distance between detectors in a given array. The deviations of the measured values from those predicted according to the fitted planes are small compared to the dimensions of the arrays and this fact indicates that the arrival directions are well determined by this method. Values of χ^2 for individual showers indicate the precision of determinations and provide a basis for rejecting poorly determined events or for detecting blunders.

Once the direction cosines l and m are determined the zenith angle θ, the declination δ and the right ascension α are computed according to the following formulas:

$$\theta = \text{arc sin } \sqrt{l^2 + m^2} ,$$

$$\delta = \text{arc sin } (m \cos \delta_0 + \sqrt{1 - l^2 - m^2} \sin \delta_0) ,$$

$$\alpha = \gamma + \text{arc sin } (l/\cos \delta) ,$$

where δ_0 is the latitude of the station and γ is the sidereal time.

In the small experiments concerned primarily with the arrival directions, the timing analysis is carried out on an IBM 650 computer and the results are punched directly on IBM cards with which the statistical analysis is carried out. In the large experiment the timing analysis is done on Whirlwind, a fast electronic digital computer, and the results, in addition to being included in the final output, are used in the analysis of the particle density data. In all these experiments the distribution of χ^2 indicates that the typical uncertainty in the determination of an arrival direction is about $\pm 5°$.

B.2) Determination of the size and core location. Only in the large experiment with eleven detectors do we determine the core location and size of each shower. In this experiment we determine, in addition to the arrival times, the densities of shower particles at the detectors. We call g_i the measured density of particles at the i-th detector. The problem is to determine a core location with coordinates X and Y, and a shower size N which, according to some suitably chosen function $f(X, Y, N; l, m, x, y)$, will predict a set of particle densities that satisfactorily fit the measured values. We find that the function given by equation (1) of Sect. 1, where

$$r = \sqrt{(x - X)^2 + (y - Y)^2 - [l(x - X) + m(y - Y)]^2},$$

gives good fits for values of r less than 250 m when X, Y, and N are chosen so as to minimize the function

$$\psi^2 = \frac{1}{n - 3} \sum_{i=1}^{n} [f(r_i, N) - g_i]^2 w_i .$$

The weighting factor w_i is chosen so as to balance properly the relative importance of low density data in which the principal kind of error is statistical against high density data in which instrumental errors ($\simeq 14\%$) predominate.

Naturally, the computation by hand of the values of X, Y, and N which minimize the complicated function ψ^2 is impractical. Several analogue devices have been constructed and used. Although one of them was used in an essential way in designing the array, they suffer from a lack of speed and objectivity. All the results we have presented have been obtained by minimizations performed on Whirlwind according to a program which computes first an initial rough approximation to the desired values of X, Y, and N and which then adjusts these approximations in steps guided by the computed changes in ψ^2 and its derivatives. The program automatically stops the computation when the changes in ψ^2 and its derivatives meet a set of criteria which indicates that the function ψ^2 is near a minimum. A detailed justification of the program for all possible circumstances would be difficult. However, the results of computations which have been performed on a group of test showers indicate its reliability for the purposes of this work.

In order to test the overall performance of the data reduction program we analyzed twenty-five « artificial » showers. The core locations, sizes, and arrival directions of these showers were chosen to be equal to the corresponding computed parameters of the twenty-five largest showers which had been recorded during one month of operation and which had been analyzed in a routine fashion by the data reduction program. For each set of parameters we computed the expected numbers of particles at each of the detectors according to equation (1) of Sect. 1. The computed numbers were then modified by adding random fluctuations according to the Poisson distribution for numbers up to fifty particles per detector, and according to a normal Gaussian distribution with a standard deviation of 14% for numbers greater than fifty particles. (Fifty particles per square meter is approximately the density at which instrumental errors and statistical errors are equal). These artificial shower data were therefore essentially representative of what one would expect to find for data from a typical set of large real showers provided that the lateral distribution is

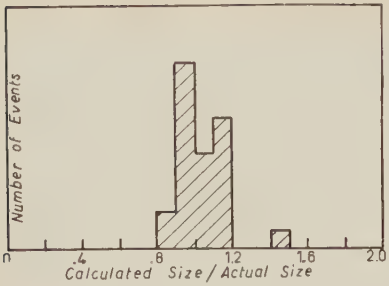

Fig. 17. – Distribution in the ratio of computed to actual sizes of « artificial » showers analyzed on the Whirlwind computer.

well represented by equation (1) of Sect. **1**, and the fluctuations are Poisson. Figs. 17 and 18 show comparisons between the values of the parameters of the showers on the basis of which the input data were computed and the final computed values of the parameters obtained by the data reduction program. No systematic change in the computed size was found and the standard deviation of the computed sizes from the true ones was 13%. The average displacement of the computed core locations from the true ones was about 10 m, and no systematic direction of motion was noticeable.

C) *Statistical Analysis of Reduced Data.*

C.1) Acceptance areas. In order to calculate the size spectrum and zenith angle dependence of showers from the computed parameters of a large population of shower events, we select samples of events from the population according to a set of criteria whose statistical effects can be accurately evaluated. We call $\varepsilon(N, \theta, \varphi, X, Y; C)$ the probability for the detection of a shower of size N, coming from the direction with zenith angle θ and azimuth angle φ, and whose core strikes the ground at a point whose coordinates are X and Y. ε depends, of course, on the electronic triggering requirement of the detection apparatus, and on any minimum requirements which may be placed on the observed pulse sizes in order that the event be accepted for data reduction. We represent these requirements by C. The quantity

Fig. 18. – Chart of displacements between the computed and actual core locations of « artificial » showers analyzed on the Whirlwind computer.

$$(1) \qquad R(N)T\,\mathrm{d}N = T \int_{\Omega_1} \int_{A_1} s(N, \theta, \varphi)\varepsilon(N, \theta, \varphi, X, Y; C) \cos\theta\,\mathrm{d}A\,\mathrm{d}\Omega\,\mathrm{d}N\,,$$

therefore represents the expected number of showers that will be detected in the time T with sizes in the interval $\mathrm{d}N$, arrival directions in the solid angle Ω_1 and core location within the area A_1.

The dependence of ε on N, θ, φ, X and Y for any given triggering requirement C is very complicated in areas where ε is appreciably less than 1. We therefore restrict our consideration to areas in which $\varepsilon \approx 1$. Since all the projected distances from any given shower axis to the various detectors decrease with increasing zenith angle θ, it is clear that ε must always increase

and approach the value 1 as θ increases. It follows that in areas where $\varepsilon \simeq 1$ for vertical showers ε is essentially only a function of the size N and the triggering requirement C for all angles θ and q. Consequently, the integration over A_1 in equation (1) yields just the area of A_1. Since we select the area A_1 so that $\varepsilon \simeq 1$ for vertical showers of size N, the integral over A_1 becomes a function $A(N; C)$ of the size and triggering requirement. We call $A(N; C)$ the *acceptance area* for showers of size N according to the triggering requirement C.

In order to illustrate the method for determining the acceptance areas we consider the triggering requirement that three or more detectors give pulses corresponding to a density of sixteen or more particles per detector. If a shower of size N strikes in such a position that the expected numbers of particles traversing three or more detectors exceeds 24, then $\varepsilon > .93$ for this event. This value is sufficiently close to 1 for our purposes. We therefore first compute an acceptance radius $r_0(N; C)$ which is the distance from the axis of a shower of size N at which the density equals 24 particles per detector area. We then draw a map of the regions containing all points within a distance

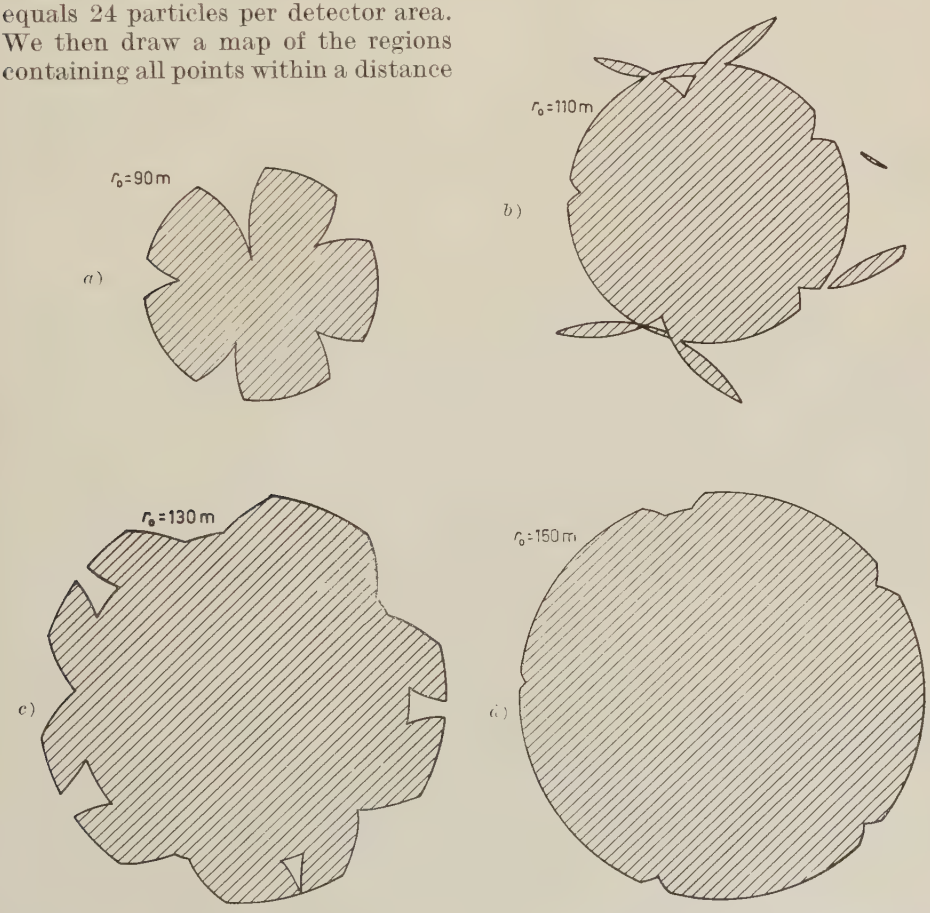

Fig. 19. – Diagrams of sensitive areas corresponding to the requirement that three or more detectors lie within a specified distance from the core.

r_0 of three detectors, and measure the area of these regions. We define this area to be the acceptance area for showers of size N. Acceptance areas for several sizes are measured and a graph of $A(N; C)$ *versus* N is prepared. An event of size N is now accepted or rejected according to whether or not a circle of radius $r_0(N; C)$ drawn around the computed core location contains three or more detectors.

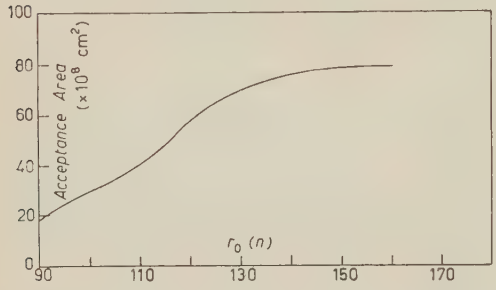

Fig. 20. – Plot of acceptance area versus acceptance radius for any three of M, D and CE.

In order to eliminate events whose size and core locations are not well determined, we superpose on the above acceptance area criterion the requirement that the core land within a distance of 160 m from the center. This additional criterion obviously sets a limit on the value of the acceptance area which is approached as N increases. The chief advantage of the method is that the intensity of showers can be measured over a considerable range of sizes for which the acceptance area does not include the entire circle of radius 160 m. Fig. 19 illustrates acceptance regions corresponding to several acceptance radii and a particular triggering requirement, and Fig. 20 is a plot of the corresponding acceptance area *versus* N.

C.2) Calculation of size spectra. Acceptance areas vary considerably over most size intervals which are broad enough to include reasonably large numbers of events. Consequently, one would have to use a weighted average of the acceptance area in order to compute an average intensity for an interval from the observed number of events. However, since the proper weighting function involves the size spectrum which is presumably unknown to begin with, this method is not satisfactory.

The method we have used can be illustrated by the problem of determining the distribution in size of fish in the ocean by taking samples with a net having a range of hole sizes. If we call $\varrho(x)\,\mathrm{d}x$ the density of fish with sizes in $\mathrm{d}x$, and $r(x)\,\mathrm{d}x$ the expected number of fish caught with sizes in $\mathrm{d}x$, then ϱ and r are related by the equation

$$r(x)\,\mathrm{d}x = W(x)\varrho(x)\,\mathrm{d}x\,,$$

where $W(x)$ is proportional to the area of the net through which fish of size x cannot pass. If we suppose that we have only a relatively meagre catch to work on, then a satisfactory procedure for determining an average value of $\varrho(x)$ over some interval between x_1 and x_2 in which there are n fish is to evaluate the average of $(r(x)/W(x))$ for the n values of x represented in the catch and within the interval x_1 to x_2. In other words, we take

$$\frac{1}{x_2 - x_1}\int_{x_1}^{x_2}\varrho(x)\,\mathrm{d}x = \varrho(\bar{x}) \sim \frac{1}{x_2 - x_1}\sum_{i=1}^{n}\frac{1}{W(x_i)}\,,$$

where the index i runs over the n fish in the interval x_1 to x_2. Once the functional form of $\varrho(x)$ has been determined $\bar{x}$ can be found and $\varrho(\bar{x})$ can be plotted as a function of $\bar{x}$.

In the determination of the spectrum of observed shower sizes, the effective « net area » for showers of size N is

$$W(N) = A(N) \int_{x_0}^{x_1} 2\pi \exp\left[-\frac{x - x_0}{\Lambda}\right] \frac{x_0^2}{x^3} \, \mathrm{d}x \,,$$

or, in other words, the product of the acceptance area and the effective solid angle out to $\theta_1 = \arccos(x_0/x_1)$. In the equivalent vertical size method, the effective « net area » is the integrated area-solid angle within which we record accepted showers of a given vertical equivalent size, namely

$$W(N_v) = \int_{x_0}^{x_1} 2\pi \frac{x_0^2}{x^3} A\left(N_v \exp\left[-\frac{x - x_0}{\Lambda}\right]\right) \mathrm{d}x \,.$$

In practice $W(N_v)$ is determined by numerical integration using the graphically determined values of $A(N)$.

Appendix II

Fluctuations in shower development (presented by W. Kraushaar).

While there can be little doubt that very large air showers are initiated by primary cosmic rays of very great energy, there is uncertainty in how one should assign an energy to the primary particle responsible for a shower of a given number of particles, and how one should relate a measured shower number-of-particle spectrum to a primary energy spectrum.

Recently S. Olbert has developed a theory of the cascade process which permits one to predict, given a model for the high energy nuclear interactions, the average number of particles, N, at atmospheric depth x that arise from a primary particle of energy E. Having observed a shower of N particles, then, one can infer the approximate primary particle energy. Such an inference, however, is subject to at least two important uncertainties. On the one hand, there is no model of high energy nuclear interactions that can be considered as established beyond its very gross predictions. On the other hand, all showers initiated by a primary particle of a given energy do not develop identically, and in principle the inference mentioned above requires a detailed treatment of the fluctuation problem and a knowledge of the primary particle energy spectrum. This latter uncertainty is of particular concern, since there would appear to be the possibility that showers having very large numbers of particles (hence apparently very high energy primaries) arise in fact from improbable fluctuations in the development of showers from the relatively very abundant lower energy primary particles.

The important sources of fluctuations are certainly in the very early stages of the shower's development, and in particular, as has been pointed out by

JÁNOSSY and MESSEL [3], the first interaction of the primary is most significant. Two aspects of this first interaction are important. There is, first, the place or depth at which the interaction takes place. Showers initiated at different depths will be in different stages of development, and so have different numbers of particles by the time they reach the observation equipment at say, sea level. Then there is the possibility of fluctuations in the multiplicity and energy distribution of the particles produced in this first interaction. These fluctuations we believe to be relatively unimportant, because electron shower sizes at sea level are so nearly proportional to the initiating energy. If, for example, a secondary particle of energy ε produces a shower with $k\varepsilon^{\beta}$ particles, a primary interaction of total energy E and multiplicity m will produce a shower of $N = mk(E/m)^{\beta}$ particles and N is nearly independent of m if β is near one. In what follows only fluctuations which arise from fluctuations in the atmospheric penetration of the primary particle will be considered.

We shall need the quantity $n(E, x)$ where n is the average number of electrons at thickness x below a nuclear interaction of energy E. Most often one is concerned not with $n(E, x)$ but with $N(E, x')$ where N is the average number of electrons at atmospheric depth x' that arise from a primary particle of energy E incident upon the top of the atmosphere. It is $N(E, x')$, for example, that has been calculated by OLBERT. These two quantities, $N(E, x')$ and $n(E, x)$, are related by the expression

$$N(E, x') = \int_0^{x'} \exp\left[-\frac{(x'-x)}{l}\right] n(E, x)\,\frac{\mathrm{d}x}{l}\,, \tag{1}$$

where $\exp[-y/l](\mathrm{d}y/l)$ is the probability that the first interaction occurs at atmospheric depth y in $\mathrm{d}y$, and where the primary particle mean free path is l. From expression (1) above it follows immediately that

$$n(E, x) = N(E, x) + l\,\frac{\partial}{\partial x}\,N(E, x)\,. \tag{2}$$

The quantity $N(E, x)$ as given by Olbert for the Fermi model of nuclear interactions and a primary particle energy of $10^8\ \mathrm{mc^2}$ is shown in Fig. 21. Also

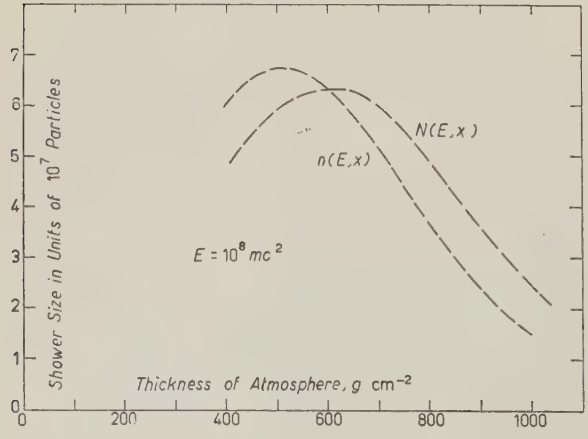

Fig. 21. – The average number of particles, $N(E, x)$ at atmospheric depth x that arise from a primary particle of energy $E = 10^8\ \mathrm{mc^2}$ incident on the atmosphere according to the calculations of S. Olbert, based upon the Fermi model of nuclear interactions. The function $n(E, x)$ is the average number of particles at a depth x below a nuclear interaction of energy $E = 10^8\ \mathrm{mc^2}$.

shown in Fig. 21 is the function $n(E, x)$ as obtained from expression (2).

The nuclear mean free path, l, has been taken as 100 g/cm^{-2}. From the $n(E, x)$ curve it is evident that the smallest possible number of particles is $1.5 \cdot 10^{7}$, and corresponds to zero penetration of the primary particle into the atmosphere. It is also evident that the largest possible shower size is $6.7 \cdot 10^{8}$ particles, and this corresponds to a primary particle penetration of about 500 g into the atmosphere. The average number of particles, from the $N(E, x)$ curve is $2.5 \cdot 10^{8}$ particles. The probability distribution in n can be obtained as follows.

The probability that the shower develops through a thickness x in dx is $\exp[-(x'-x)/l]\,\mathrm{d}x/l$, and so the probability that a primary particle of energy E gives rise to a shower at x' with a number of particles between n and $n+\mathrm{d}n$ is

$$P(E, x', n)\,\mathrm{d}n = \exp\left[-\frac{x'}{l}\right] \exp\left[\frac{x(E, n)}{l}\right] \frac{\mathrm{d}}{\mathrm{d}n}\left(\frac{x(E, n)}{l}\right) \mathrm{d}n\,. \tag{3}$$

Here $x(E, n)$ is the thickness of atmosphere through which a shower initiated by an interaction of energy E must develop in order to have n particles. That is, $x(E, n)$ is an inverse of the function $n(E, x)$. Fig. 22 shows the function $P(E, x', n)$ vs. n for $E = 10^{8}\,\mathrm{mc}^{2}$ and $x' = 1000$ g cm^{-2} (vertical showers at sea level). The most probable number of particles is the smallest possible number, and this corresponds to the situation in which the primary interacts at the very top of the atmosphere. Larger showers result when the primary penetrates into the atmosphere, and the largest possible shower results when the primary interaction occurs so as to place the shower maximum at sea level. The primary can, of course, penetrate even further into the atmosphere, and the shower at sea level has then not yet reached its maximum. This deeper penetration accounts for the fact that P is double-valued. To a very good approximation, $P(E, x', n)$ can be expressed as a power law function of n between the upper and lower bounds of n.

$$P(E, x', n)\,\mathrm{d}n \approx \frac{K\,\mathrm{d}n}{n^{\alpha}}\,. \tag{4}$$

The value of α for the case we have considered, $E = 10^{8}\,\mathrm{mc}^{2}$, $x' = 1000$ g cm^{-2}, is 2.7. If one starts with the assumption that the number of particles in a shower falls off exponentially with atmospheric depth, the power law expression for the probability

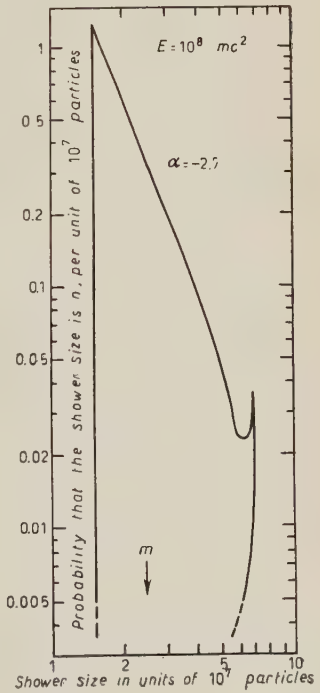

Fig. 22. – The probability $P(n, E, x)$ that a primary particle of energy $E = 10^{8}\,\mathrm{mc}^{2}$ gives rise to a shower of n particles at sea level, $x = 1000$ g cm^{-2}. Shower sizes are measured in units of 10^{7} particles, and the probability is per unit shower size.

distribution in n is exact, and one obtains

$$\alpha = \frac{\lambda}{l} + 1 , \tag{5}$$

where λ is the shower absorption length and l is the primary mean free path.

To proceed further and to evaluate the effect of fluctuations on primary particle intensity measurements, one must make explicit assumptions on how $n(E, x)$ varies with E. Over a limited range of shower sizes and primary energies it is sufficient to assume that n in the region of interest (shower maximum and below) is proportional to the primary energy, and that the ratio of maximum possible size to minimum possible size has a constant value, independent of E. In the particular case shown in Fig. 21, this ratio is $(6.7/1.5) = 4.45$.

The results of these considerations are best summarized as follows. Measurements of the intensity of showers of a given size can be converted to intensity of primary particles of a given energy in two ways. One can, and this is the method usually used, and the method used by the M.I.T. group, simply assume that showers of a given size arise from primary particles of a single energy. That is, shower sizes can be converted to primary energies through a relationship such as $N(E, x)$ in Fig. 21. Let us call the primary particle intensity obtained in this way I. Primary particle intensities can also be obtained if one makes the initial assumption that the primary energy spectrum is of the form $E^{-\gamma}\mathrm{d}E$ and then folds together the $P(n, E, x)$ distribution and the energy distribution. From an assumed primary intensity one then predicts a shower intensity and so from a measured shower intensity a primary particle intensity, I', may be deduced. For vertical showers, under the assumptions we have outlined in the previous discussion, the ratio I/I' is 1.4. That is, under our assumptions, one tends to overestimate primary particle intensities by a factor of 1.4 if fluctuations are neglected.

A further effect of this source of fluctuations is the tendency to smear out possible sudden changes in the form of the primary particle energy spectrum. It is interesting to notice that the only reason fluctuations do not have a more pronounced and perhaps disastrous effect on the detailed interpretation of shower measurements is that the number of particles at the shower maximum is not enormously greater than the number at the level of detection. For this reason it is dangerous to infer primary particle energies from measurements on showers that have arrived from large zenith angles.

Showers of moderate sizes from large zenith angles may have arisen from very high energy primary particles that interacted early in their flight through the atmosphere, or they may have arisen from *much* lower energy primary particles that happened to penetrate deep into the atmosphere before interacting. On the other hand, fluctuation effects can be made very small if shower measurements are made at mountain altitudes where large showers are near their maximum stage of development.

REFERENCES

[1] P. Bassi, G. Clark and B. Rossi: *Phys. Rev.*, **92**, 441 (1953).
[2] G. Clark: in publication.
[3] L. Jánossy and H. Messel: *Proc. Phys. Soc.*, A **63**, 1101 (1950).

PART IV

SECTION E: **Sydney Air Shower Experiments.**

The Sydney Air Shower Experiment.

M. H. BRENNAN, J. A. LEHANE, J. MALOS, D. D. MILLAR,
C. S. WALLACE and M. M. WINN

The F.B.S. Falkiner Nuclear Research and Adolph Basser Computing Laboratories, School of Physics (*), *The University of Sydney - Sydney, N.S.W.*

1. – Introduction.

Since the beginning of February, 1957, observations have been in progress in Sydney on the extensive air showers of cosmic rays of size 10^5 to 10^7 particles. The following measurements are currently being made:

a) determination of shower size and core location,

b) directions of incidence of showers,

c) comparison between particle densities as measured by a scintillation counter and a tray of Geiger counters,

d) the lateral spread of μ-mesons and of high energy and low energy nucleons,

e) Čerenkov light pulses associated with showers.

Results of the measurements *a*), *b*) and *c*) are reported in Sect. 5. Statistics from the measurements *d*) are limited and will not be reported, while the measurements *e*) are reported separately in this issue, pag. 662. The next sections contain a brief description of the experimental arrangement, and of the method of recording and analyzing the data obtained from it.

(*) Also supported by the Nuclear Research Foundation within the University of Sydney.

2. – Experimental arrangement.

Scintillation counters. The detecting array is shown in Fig. 1 and consists of nine xylene scintillation counters, each of area 0.25 m², and of liquid depth 10 cm. These are distributed over an area of 30 m by 70 m with approximately 30 m spacing between counters. Three of these scintillators in coincidence provide the master pulse which triggers the apparatus. The same three scintillators are used for the determination of shower directions. Pulse heights are recorded from all nine scintillators in binary notation on punched paper tape, with an accuracy of ± 1 in the range 0 to 20 particles and ± 2 in the range 20 to 60 particles. The average pulse height given by a single, vertical, penetrating μ-meson was determined in a separate experiment, and this has been taken as the pulse height corresponding to a single air shower particle in subsequent work.

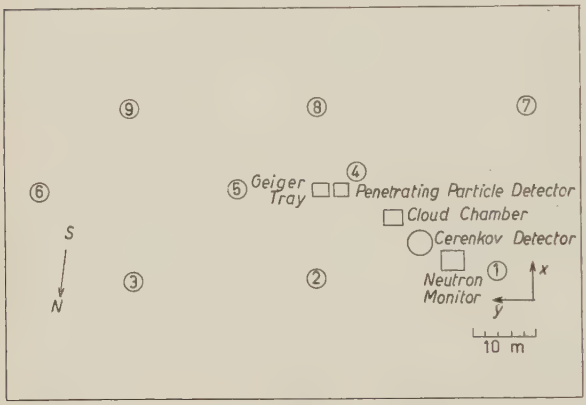

Fig. 1. – The Sydney Array. The sizes of individual pieces of equipment are not drawn to scale. Showers are detected by a three-fold coincidence between scintillators 2, 3 and 8.

Fast timing facility. Pulses from the three scintillators which, as mentioned above, provide the triggering pulse are displayed on a fast oscilloscope with artificially introduced separation between pulses of 140 mμs. Time delays can be measured with an accuracy of the order of 5 mμs, and shower directions obtained with an accuracy of the order of 2° in zenith angle and 4° in azimuth.

Cloud chamber. A cylindrical expansion chamber of diameter 60 cm and illuminated depth 30 cm is included in the array. It is expanded when an incident shower sets off three or more Geiger counters under a thin (~ 1 cm) lead shield placed below the chamber in addition to the three coincident scintillators. Directions of incidence of shower particles traversing the cloud chamber are measured and these directions are compared with the directions of incidence of the shower front as measured by the fast timing facility.

Tray of Geiger counters. A tray of 45 Geiger counters of total area 0.384 m² are also in the array. Each counter is hodoscoped and the hodoscope data are recorded as a pattern of holes punched on paper tape. The number of Geiger counters discharged at each event is therefore known. The information obtained makes it possible to compare the densities of shower particles as measured by the Geiger counters with those measured by the scintillators.

Penetrating particle detector. Three trays of 46 individually hodoscoped Geiger counters and each of area 0.4 m² are placed one above the other in lead shielding. There is 15 cm lead above the topmost tray and 5 cm lead between trays. μ-mesons may be distinguished from high energy interacting nucleons from examination of the hodoscope records.

Neutron detector. A neutron monitor whose prime function is to look at the intensity variations of the low energy nucleon flux is situated within the array. It is intended to record the number of pulses from the neutron counters in coincidence with air showers.

3. – Recording of data.

Data from the cloud chamber and from the fast timing apparatus are recorded photographically. Cloud chamber photographs are reprojected stereoscopically and spatial angles of tracks determined. Photographs of the screen of the fast oscilloscope are projected on to a screen and the distances between the points of initial rise of the three pulses are measured. Every tenth photograph is that of an artificial test pulse which serves as a check on the constancy of the performance of the electronics.

All other data are recorded on punched paper tape in a form which is suitable for processing and analysis by the School of Physics' electronic computer « SILLIAC ». Since the punching of paper tape is a slow process, means of storing the information from the various detectors is required. Photomultiplier pulse heights, from the scintillation counters and from the Čerenkov detector, are stored by means of stretching circuits which charge up polystyrene dielectric condensers to a voltage proportional to the height of the input pulse. The stretching circuits include a gate of resolution time 5 μs opened by the three-fold coincidence master pulse. Information from the Geiger counters is stored on screen grid thyratrons; the gating pulse is applied to the screen grid and the Geiger pulse to the control grid. The output is taken from the plate. The thyratron is fired by the arrival of a master pulse alone; it is not fired if there is a coincident Geiger pulse on the control grid.

The D.C. voltage levels on each of the stretching circuit outputs are taken to the pins of a stepping switch. The voltage level, in the range 0 to 60 V, is compared with a voltage produced by a free-running stepping switch sweeping over a dividing chain of resistors. When the two voltage levels become equal, a binary number in the range 0 to 42, determined by the position of the second stepping-switch, is placed in a temporary store of 6 relays. The contents of this temporary store are fed into the tape punch machine and punched out. The D.C. levels on the plates of the hodoscope thyratrons are also taken to the pins of a stepping switch and are compared with a fixed D.C. level of 50 V. If the thyratron output is below 50 V, one of the 6 temporary store relays is closed and a hole is punched on the tape.

Other information recorded on the tape includes the time of the event to the nearest minute, the serial number of the event and the high tension on the Čerenkov photomultipliers.

The total time taken to record the data from each shower on tape is of the order of $3\frac{1}{2}$ minutes.

The punched tape obtained in the above way is decoded by « SILLIAC » which transforms the raw data as recorded into a form, on a second paper tape, suitable for computation. It also prints out in decimal notation the serial number of the shower, the time of the event, various D.C. voltage levels of interest, and the pulse heights from the photomultipliers. Data from the hodoscoped Geiger counters are at present read visually from the raw data tape. The time taken for decoding is approximately 3 s of machine time per shower.

4. – Computation of shower size and core location.

In this computation, carried out by « SILLIAC », it is assumed that all showers are vertical and that all showers conform to the same structure function as determined by the M.I.T. group:

$$\varrho(r) = \frac{N}{2\pi} \frac{\exp[-r/r_0]}{(r+1)r_0},$$

where $\varrho(r)$ is the density of particles m^{-2} at a distance r metres from the core of the shower, N is the total number of particles in the shower and $r_0 = 75$ m. At each point on a grid of size 150 m by 150 m centred on the scintillator array and with a grid spacing of 15 m the following error function is minimized to give the best value of N:

$$E(X, Y, N) = \sum_{i=1}^{9} \frac{(n_i - \overline{n_i})^2}{n_i + 1} + \gamma \ln N,$$

where n_i is the observed number of particles through the i-th scintillator, $\bar{n}_i$ is the predicted number for the assumed X, Y and N using the shower structure function above and where (X, Y) is the assumed position of the core. The term $\gamma \ln N$ introduces the a priori probability that large showers are less likely to occur than are small ones. γ is here taken as equal to 2.5. Having found the point on the grid where E is a minimum, the computer hunts around this point in 4 m steps to find the lowest minimum in the vicinity. The point where this occurs is taken as the position of the shower core, and the corresponding value of N as the shower size. In order to obtain some idea of the goodness of fit, the value of the error function, E, is printed out as well as X, Y and N at the end of the computation. Furthermore the limits $\pm \mathrm{d}X$, $\pm \mathrm{d}Y$ on the position of the shower core are also printed out. The four points so designated correspond to limits on the possible positions of the core where the probability of fit has decreased to one-eighth of its value at the point (X, Y). Of the four corresponding values of N which have been computed, that one which differs most from the value at (X, Y) is also printed out. This computation takes 1 to 1½ minutes of machine time per shower.

A systematic bias in N, arising from the maximization of the joint likelihood for X, Y and N was suspected and evidence for it has indeed been found. This bias has been determined for various classes of showers, according to shower size and position of the shower core, whether inside or outside the area enclosed by the array of scintillators, by, in effect maximizing the independent likelihood for N. The computer searches over a grid measuring 168 m by 168 m and centred on the previously determined best position of the core, in 14 m steps. At each point on this grid the minimum value of E and the corresponding best value of N is computed, as in the earlier calculation. If

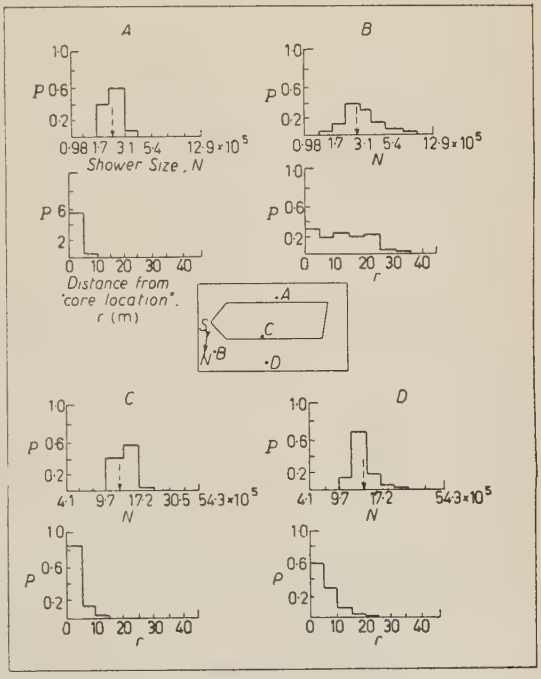

Fig. 2. – The probability distributions in N and in r for 4 showers whose cores were located at the points indicated in the central figure. The dashed arrows indicate the shower sizes as computed in the normal analysis.

the value of E corresponds to a probability of fit to the experimental data greater than 10^{-6} of that at the previously determined « best » position for the core, then a further search is made around this point on a grid of area 6 m by 6 m and with 3 m steps. At each point on this grid the probability of fit is determined and if it is greater than 1/3 600 of that at the supposed core, this probability is added into the appropriate probability distributions in N and in r, where r is the distance from the supposed core to the point under consideration.

This last computation is a lengthy one, taking several minutes of machine time, and consequently is done for a representative sample of showers only. It is found from this more detailed computation that values of N are determined with an accuracy better than 30% with 90% certainty, but that the simple calculation gives values of N which are some 10% lower than the medial value of the probability distribution in N. The distributions in r have half their area within the range 0 to 5 m from the previously determined position of the core. These figures apply to showers whose cores fall within, or close to, the scintillator array. At larger distances from the array the distributions tend to become wider (Fig. 2).

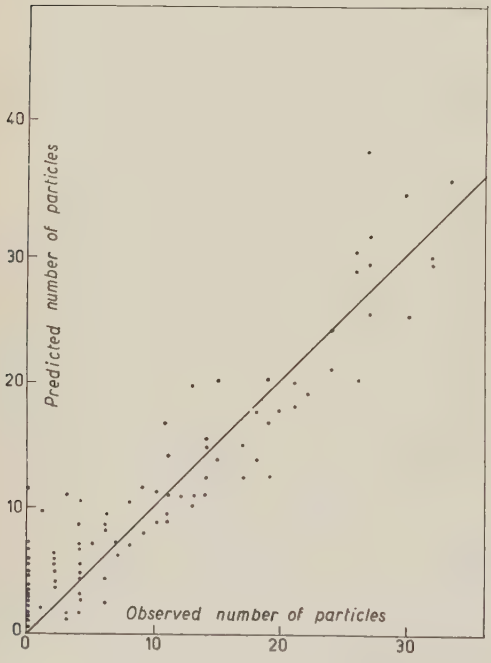

Fig. 3. – Comparison between the number of particles predicted to traverse a scintillator and the observed number.

5. – Results.

Comparison between scintillation and Geiger counters. – One of the calculations carried out by «SILLIAC» consists in computing the density of shower particles at various specified points in the array for each shower. Fig. 3 shows the results of such computation for a random sample of showers analyzed for shower size and core location taking into consideration the responses from only eight of the nine scintillators in the array. The densities of shower particles at the position of the ninth scintillator were then predicted by « SILLIAC » and compared with the observed response of the scintillator. It will be observed that there is good agreement between prediction and observation.

The computer was also asked to predict the densities of « scintillator particles », that is the densities of particles as would be measured by one of our scintillators, at the position of the unshielded tray of Geiger counters described in Sect. 2. In Fig. 4 are plotted points for 415 showers with the predicted density of scintillator particles as ordinate and the number of Geiger counters discharged in each event as abscissa.

If the density of scintillator particles is denoted by ϱ and if it is assumed that the density of particles to which the Geiger counters respond is $\beta\varrho$, where β is assumed constant, then for a given density of scintillator particles on the Geiger counter tray the relative frequencies with which different numbers of Geiger counters, k, are discharged out of the total number of 45 in the tray are given by the following Poisson probability expression:

$$P(k, \varrho) = \frac{45!}{k!\,45!}\,(1-\exp[-\beta\varrho A])^k \cdot \exp[-\beta\varrho A(45-k)],$$

where A is the area of a single counter. The observed events have been grouped into 30 density intervals and the observed frequencies, $n(k, \bar{\varrho})$, form a 30×45 matrix, where $\bar{\varrho}$ is the mean density for each of the 30 density intervals. This observed frequency distribution matrix has been compared with a computed matrix using the above Poisson expression, and, using a maximum likelihood method, the best value of β has been obtained. It is found that $\beta = 0.89 \pm 0.03$ where the error limits correspond to the 30% probability level. It is apparent that the density of particles as measured by our scintillators is not very different from that measured by a tray of Geiger counters.

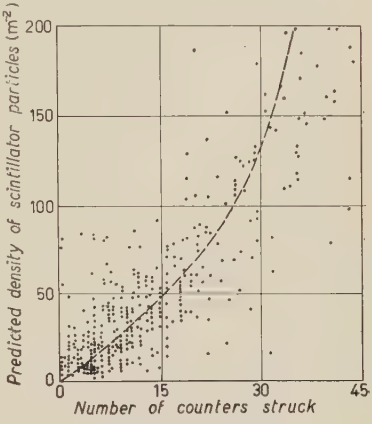

Fig. 4. – Comparison between the density, ϱ, of particles predicted at the tray of Geiger counters and the number of counters discharged. The dashed line passes through the most probable number of Geiger counters discharged for a density $0.9\cdot\varrho$ particles on the Geiger tray.

Shower structure function. In Fig. 5 the particle densities as measured by our scintillators is plotted as a function of distance from the computed position of the shower core for a number of showers. All densities have been normalized to a shower size of $3\cdot10^5$ particles. It will be seen that agreement with the shower structure function used in the analysis is good.

Shower directions. As mentioned in Sect. 2, shower directions can be determined using the M.I.T. method (Bassi, Clark and Rossi, 1953) measuring, with fast timing techniques, the time delays between scintillator pulses, also

by measuring the directions of shower tracks in the large Wilson cloud chamber. Comparison of the results of the two methods is currently being made.

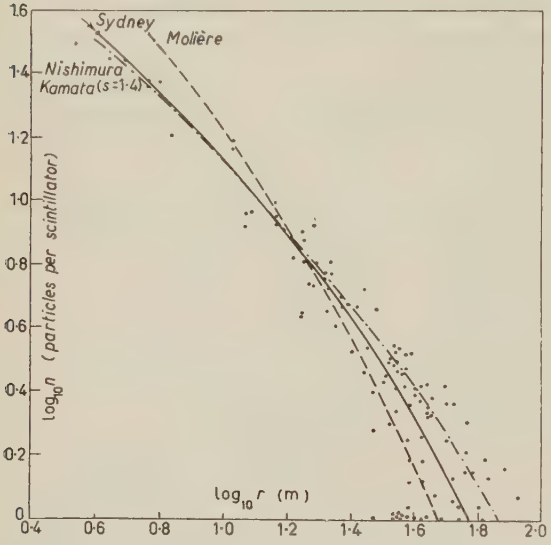

Fig. 5. – The shower structure function. Particle densities as measured by the scintillators, plotted as a function of distance from the shower core. Data for 14 showers have been used. Shower sizes are normalized to a size $3 \cdot 10^5$ particles.

So far 49 showers have been recorded for which a direction of incidence has been measured by the fast timing method and which also gave a direction in the cloud chamber. The selection criterion for the cloud chamber photographs was that there should be at least 5 tracks all parallel to within 10° in the cloud chamber. A mean direction for the tracks was determined and an error at the 5% level of significance has been assigned to this direction from the distribution of the individual track directions about this mean and on the assumption that this distribution is normal. Of the 49 showers, 18 gave a mean cloud chamber direction with errors at this level ranging up to 20° in zenith angle and up to 90° in azimuth. The directions as given by the time-delay method fell within these limits. The remaining 31 showers had better determined directions, the errors being less than 8° in zenith, and 20° in azimuth angle. For 24 of these showers the time-delay directions fell within the error

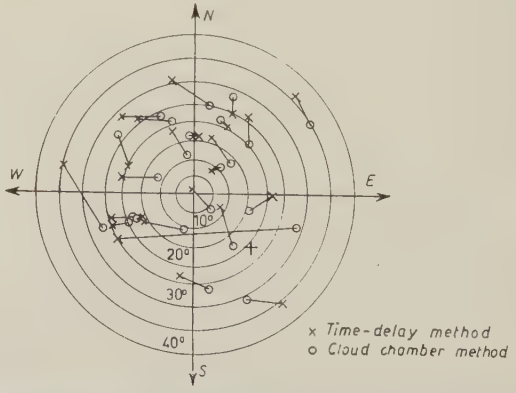

Fig. 6. – Directions of 25 showers as determined by the time-delay method and from the mean direction of cloud chamber tracks. The two results for each shower are linked. Zenith angles are measured radially, azimuth angles are measured from North. In the single case where the difference in azimuth angles is greater than 90°, the time-delay determination is suspect (see text).

limits, 6 fell just outside them and one was well outside them. For two events out of the 6, also for the last event, the time-delay determination is suspect since at least one of the scintillator pulse heights was small. Statistics at present are insufficient to tell whether the imperfect agreement between the two methods is caused by the non validity of the assumption of a normal distribution of the track directions about the mean value, or whether the differences between the directions as measured by the two method are correlated with distance from the shower core to the cloud chamber.

In Fig. 6 are plotted the mean direction of the cloud chamber tracks and the direction of the shower front as measured by the time delay method for 25 showers.

Shower size spectrum. Only showers of size $> 3.5 \cdot 10^5$ particles (corrected by $10\,\%$ to convert from « scintillator particles » to « Geiger particles ») whose cores fall within an area 20 m by 28 m around the three triggering scintillators are here considered. The probability for such a shower to be recorded is $> 95\,\%$. 49 showers were recorded in 115 hours sensitive time conforming to an integral shower size spectrum

$$K(> N) = 4.5 \cdot 10^{-8} (N/10^6)^{-1.6 \pm 0.1} \text{ m}^{-2} \text{ s}^{-1} .$$

REFERENCE

[1] P. Bassi, G. Clark, and B. Rossi: *Phys. Rev;* **92**, 441. (1953).

SUPPLEMENTO AL VOLUME VIII, SERIE X
DEL NUOVO CIMENTO

N. 2, 1958
2° Trimestre

Čerenkov Light from Air Showers.

M. H. BRENNAN, J. MALOS, D. D. MILLAR and C. S. WALLACE

The F.B.S. Falkiner Nuclear Research and Adolph Basser Computing Laboratories, School of Physics (*), *The University of Sydney - Sydney, N.S.W.*

1. – Introduction.

A general description of the Sydney air shower experiment has already been given in the preceding report [1]. Included in the experimental array is a Čerenkov detector in the position indicated in Fig. 1, page 654 of this issue. This detector consists of a search-light mirror of diameter 110 cm and aperture f/0.5 which looks vertically upward into the night sky. At the focus of the mirror are placed 7 photomultipliers, one on the optic axis and the other six surrounding this central one. Each photomultiplier accepts light from a cone of half angle 3°. The axes of the offcentre photomultiplier cones are at an angle of 7° to the vertical. At present only three of these photomultipliers, the central one and a diametrically opposite pair, are in use. Pulse heights from them in coincidence with air showers detected by the scintillator array, are punched on paper tape in the manner already described for the scintillator pulse heights. The high

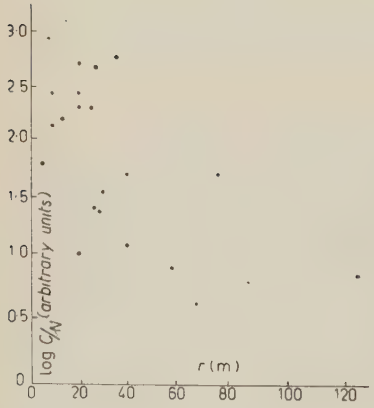

Fig. 1. – The dependence of C/N, the Čerenkov pulse height divided by the shower size, upon r, the distance from the core of the shower to the Čerenkov detector.

(*) Also supported by the Nuclear Research Foundation within the University of Sydney.

tension supply to the photomultipliers is controlled so that the anode current remain constant at 100 μA in order to ensure stability of operation. The value of this high tension is recorded on the punched paper tape at each event, and from the dependence of photomultiplier gain on high tension, which has been measured using scintillation pulses, the observed light pulses may be corrected to their equivalent size at 1000 V high tension. Only light pulses are considered if their equivalent height at 1000 V is greater than 50 mV at the photomultiplier anode, corresponding to some 10000 photons incident on the photocathode. Such a high threshold is dictated by the back-ground noise level. With improved electronics this threshold will be reduced.

It may be noted that one point of difference between this experiment and those of JELLEY and of ČUDAKOV is that we are triggering our apparatus on incident air showers rather than on incident light pulses. Furthermore no attempt has been made, on the basis of Čerenkov pulse heights alone, to select only vertical showers, as has been done by ČUDAKOV [2].

2. – Results.

During the time of observation while the background night sky illumination has been acceptably low, i.e., when the photomultiplier high tension has been greater than 980 V, 226 showers have been recorded which could be analysed for shower size and for the position of the shower core. These were showers of size greater than approximately 10^5 particles. Of these 226 showers, 28 were accompanied by Čerenkov light pulses greater than the minimum acceptable size. In addition several showers, too small to give sufficient data from the scintillation counters for an accurate determination of size and core location, were also accompanied by Čerenkov pulses.

For these 28 out of 226 events no direct correlation between shower size and Čerenkov pulses was established. Similarly no direct correlation between pulses and distance of the Čerenkov detector from the core was discerned: for showers whose cores fell within a distance of 20 m from the detector 12% (6 events) gave a Čerenkov pulse, from 20 m to 40 m the ratio was 15% (15 events) and at distances greater than 40 m it was 9% (7 events). On the other hand when one plots the ratio of Čerenkov pulse height to shower size, C/N, as a function of distance from the detector the Fig. 1 is obtained. In this figure each point refers to an individual shower and although there is a trend for C/N to decrease with increasing distance from the core the scatter of the points is so large as to make any simple functional relation proposed between these quantities of doubtful value.

One likely source of these fluctuations lies in the fact that the showers detected are not incident in the vertical direction. Out of the 226 showers

recorded by the scintillator array during the time of Čerenkov observations 46 were considered to have a sufficient number of particles traversing the three triggering scintillators for the directions of incidence of these showers to be determined unambiguously by the fast-timing technique already described. The number of Čerenkov events accompanying these 46 showers was 7. The number is too small for any classification to be made according to shower directions, however the events have been divided into two categories according to whether the skew distance from the optic axis of the Čerenkov detector to the trajectory of the shower core is greater than, or less than, 10 m. It is found that out of 14 showers having skew distances less than 10 m, 5 were accompanied by a Čerenkov pulse, whereas out of 32 having skew distances greater than 10 m only 2 were accompanied by a Čerenkov pulse. It appears therefore that a shower whose core traverses the acceptance cone of our Čerenkov detector is more likely to give a detected pulse than is a shower which does not do so. Furthermore the direction of incidence of the shower need not be closely parallel to the optic axis of the detector; indeed two of the 5 events with skew distance less than 10 m were showers whose direction of incidence was greater than 30° to the optic axis.

Again when the three collinear photomultipliers at the focus of the mirror were in use, several events were observed with detectable pulses from all three, indicating that the angular spread of the light from these showers was at least 9°.

It is apparent therefore the angular distribution of shower particles produced by Coulomb scattering in the air can not be neglected in the interpretation of Čerenkov light pulses from extensive air showers and, furthermore, that a single Čerenkov detector has a poor angular resolution if used as a means of selecting showers with directions of incidence coinciding with the direction of the optic axis of the detector.

REFERENCES

[1] M. H. Brennan, J. A. Lehane, J. Malos, D. D. Millar, C. S. Wallace and M. M. Winn: in this issue, pag. 653.

[2] A. E. Čudakov and N. M. Nesterova: in this issue, pag. 606.

PART IV

SECTION F: **Tokio Air Shower Research.**

Underground Studies of μ-Meson Component in Extensive Air Showers.

M. ODA

Institute for Nuclear Study, University of Tokyo - Tokyo

The importance of studying high energy μ-mesons in the extensive air showers is obvious. μ-mesons, once produced, do not make strong interaction with the material and come directly to the point of observation from the point of production. If detailed information on this component is obtained, the development of the nucleon cascade in the atmosphere will be fairly well understood. When the air shower hits the ground, there remain μ-mesons which are not absorbed and penetrate into the ground to a considerable depth as the skeleton of the air shower. Observations at various underground depths give us the knowledge of the μ-mesons of various energies corresponding to the various depths.

Results of experiments by the Cornell University group, the London group and the Osaka City University group (*) (referred by Cornell, London and Yaizu respectively) are briefly summarized in the following:
d, depth; E, the lowest energy at sea level of the μ-meson which reaches the depth; S, effective area of the equipment; R, radius of lateral spread of μ-mesons; f_i, rate of i μ-mesons entering the equipment; F_i, rate of i-fold coincidences of equipment of area S.

[1]: *a*) Cornell $d \sim 1600$ m w.e., $E \sim 600$ GeV $S \sim 0.8$ m^2
$f_2 \sim 1/100$ h $R \sim 13$ m
exponent of density spectrum (diff.) is estimated as 3.4 ± 0.1

(*)S. HIGASHI, H. MITANI, T. OSHIO, H. SHIBATA, K. WATANABE and Y. WATASE. Osaka City University, Osaka. The station is at Yaizu, Shizuoka.

[2]: *b*) London $d \sim 60$ m w.e., $E \sim 20$ GeV $S \sim 0.3$ m^2
$F_2 \sim 10$ day^{-1} $R \sim 60$ m
$F_4/F_3 \sim 0.2 \div 0.45$ $F_3/F_2 \sim (1.7 \div 2.8)\ 10^{-2}$
$F_2/F_1 \sim (4.5 \div 6.0) \cdot 10^{-5}$

[3]: *c*) Yaizu I

1) $d \sim 32$ m w.e., $E \sim 10$ GeV $S \sim 0.16$ m^2
$f_2 \sim 2/100$ h
corresponding electron density above ground is on the average $10 \sim 50$ m^{-2}

2) $d \sim 200$ m w.e. $E \sim 60$ GeV
f_2 is about one tenth of the above.

[4]: *d*) Yaizu II

1) $d \sim 40$ m w.e. $E \sim 10$ GeV $S \sim 0.3$ m^2

No. of μ-mesons in S	4	5	6	7	9	13	14	30
Cases in 1080 h	2	3	3	4	1	1	1	1

2) $d \sim 210$ m w.e.
One case of 8 mesons in 750 h so far.

The density spectrum of μ-meson showers at a few tens of GeV is determined from the ratios of London experiment. The rates of London and Yaizu I of 32 m w.e. are consistently derived from this spectrum: $(0.05 \div 0.2) \cdot \Delta^{-2.2 \div 2.4}$ h^{-1} for the density Δ from 10^{-4} m^{-2} to at least a few m^{-2}. If the exponent of this spectrum is insensitive to E, we may expect the density spectrum for $E \geqslant 60$ GeV as $(0.005 \div 0.02) \cdot \Delta^{-2.2 \div 2.4}$ h^{-1}.

For $E \geqslant 600$ GeV, $\sim 10^{-3} \cdot \Delta^{-2.1 \pm 0.1}$ h^{-1} is expected.

From the above density spectra for three different energies the energy spectrum of μ-mesons in the air shower is derived; that is roughly inversely proportional to the energy.

Spectra of the total number of μ-mesons in the shower, M, are derived as well if a flat lateral distribution of the μ-mesons is assumed. Combining those with the size spectrum of the air showers worked out by the M.I.T. group, relations among the size of the shower, N, M and the density Δ of μ-mesons for various energies are presented as follows:

N	$E \gtrsim 10$ GeV		$\gtrsim 60$ GeV		$\gtrsim 600$ GeV	
	M	Δ (m^{-2})	M	Δ (m^{-2})	M	Δ (m^{-2})
10^5	$4 \div 8 \cdot 10^2$	$3 \div 6 \cdot 10^{-2}$	$64 \div 110$	$2 \div 4 \cdot 10^{-2}$	~ 13	$\sim 3 \cdot 10^{-2}$
10^6	$3 \div 6 \cdot 10^3$	$0.1 \div 0.4$	$500 \div 900$	$0.2 \div 0.3$	90	~ 0.2
10^7	$2.5 \div 5 \cdot 10^4$	$2 \div 4$	$4 \div 7 \cdot 10^3$	$1 \div 2.5$	580	$\sim 1\frac{1}{2}$

These figures are to be compared with theoretical calculations of the air shower. It is worth to be noticed that the densities of high energy μ-mesons in an air shower seem to be more or less constant regardless of the energy of the μ-mesons. This fact being combined with the $1/r$ distribution of low energy μ-mesons, say $\gtrsim 1$ GeV, is at least qualitatively understood with a reasonable model of the air shower.

If the above density spectrum of $E \gtrsim 10$ GeV derived for the densities from 10^{-4} m^{-2} to a few/m^2 is to be extrapolated up to higher densities of μ-mesons, say to the order of 10 or more per m^2, the results of Yaizu II [4] seem to contradict this spectrum. The rate of μ-meson showers of high density observed in Yaizu II is more than ten times higher than expected by the extrapolated spectrum, whereas the rate for lower densities in Yaizu II seems to be consistent with the earlier studies. Thus, those μ-meson showers of high densities, called m.p.p., seem to request other explanations than those by a conventional picture of the μ-meson component in the air shower.

REFERENCES

[1] P. H. Barrett, M. C. Bollinger, G. Cocconi, Y. Eisenberg and K. Greisen: *Rev. Mod. Phys.*, **24**, 133 (1952).

[2] E. P. George, J. W. MacAnuff and J. W. Sturgess: *Proc. Phys. Soc.*, A **66**, 346 (1952).

[3] S. Higashi, I. Higashino, M. Oda, T. Oshio, H. Shibata, K. Watanabe and Y. Watase: *Journ. Phys. Soc. Japan*, **11**, 1021 (1956).

[4] S. Higashi, T. Oshio, H. Shibata, K. Watanabe and Y. Watase: *Nuovo Cimento*, **5**, 597 (1957).

SUPPLEMENTO AL VOLUME VIII, SERIE X
DEL NUOVO CIMENTO

N. 2, 1958
2° Trimestre

A Measurement of Energy Flow in the Extensive Air Showers.

T. Matano, I. Miura, M. Oda, K. Suga, G. Tanahashi and Y. Tanaka

Institute for Nuclear Study, University of Tokyo - Tokyo

Electronic components of the extensive air shower develop cascade showers and dissipate energies in the material. The total amount of Čerenkov radiations emitted in the material is proportional to the sum of path lengths for these cascade showers which is again proportional to the energy carried by the electronic components. Thus, the collection of Čerenkov light emitted in a thick material, which is so thick as to essentially dissipate the whole energy of the electronic components as cascade showers, provides a means of measuring the energy flow in extensive air showers. It is attempted in the present air shower project to measure the energy flow of the electronic component and Čerenkov detectors based on the above principle are prepared (called e-detectors). Essential feature of two kinds of e-detectors are given as follows:

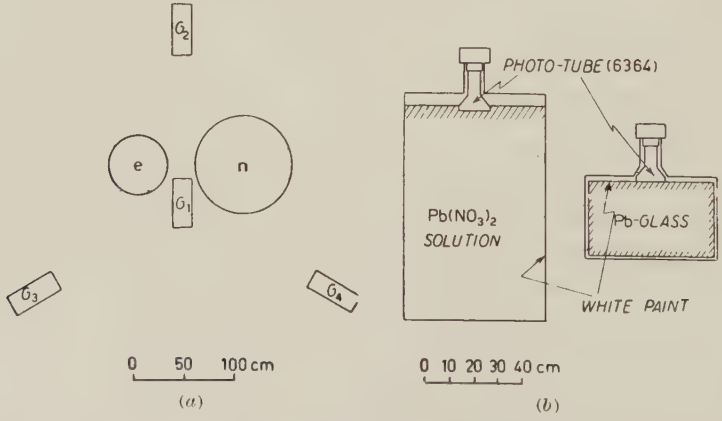

Fig. 1. – (*a*) Experime ntal arrangement. *G* represent the G.M. counter trays of 640 cm². e represents the e-dete ctor; n represents the n-detector which measures the density of the shower and is sim ilar to the scintillation detector of M.I.T. (*b*) The structure of the e-detector.

a) $Pb(NO_3)_2$-solution (30-35%)
Total thickness = 80 cm = 6 ÷ 7 radiation lenghts
Sensitivity: Several photo-electrons/relativistic particles of 80 cm track length.

b) Pb-glass block (made by Nippon Kogaku K.K.)
Area: 2000 cm²
Thickness = 30 cm = 12 radiation lenghts
Both with DuMont 5 in. photo-tube.

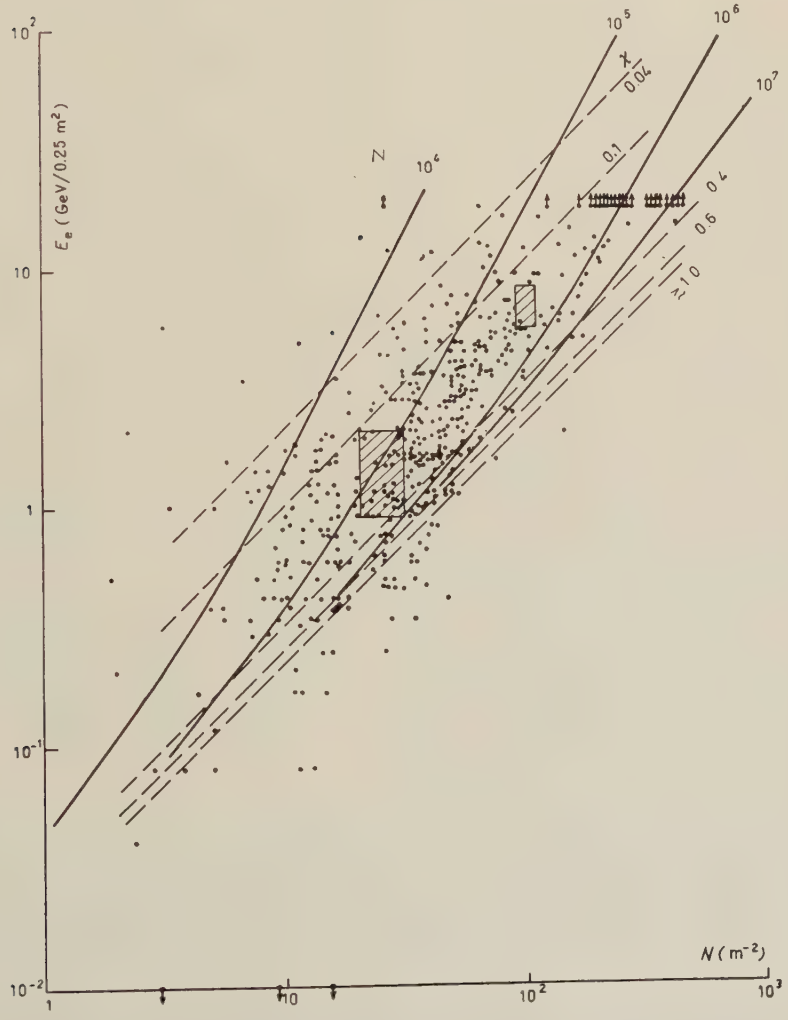

Fig. 2. - Relations of the energy flow E_e and the particle density N of the extensive air showers.

For the preliminary test, an e-detector of type *a*) was set one meter apart from another detector which is a scintillation detector similar to that of M.I.T. (called n-detector). Simultaneous records of both were obtained whenever they were triggered by coincidences of four G.M. counter trays (Fig. 1). Detectors are calibrated by a single relativistic particle. Records are plotted in Fig. 2. Each point in the figure represents a shower which discharges G.M. trays where E_e is the amount of energy carried by electronic components through a certain area (0.25 m²) and N is the number of particles in 1 m² at essentially the same point. Thus, the relation of the energy flow and the particle density of the extensive air shower is presented.

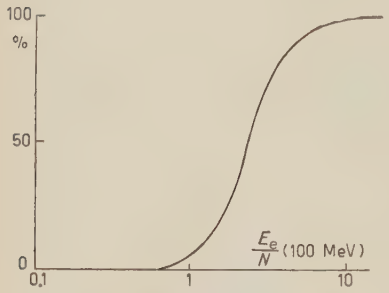

Fig. 3.–The rate of the showers whose E_e/N is smaller than the value on the abscissa. The scale of the ordinate is expressed as the percentage of the total number of the showers.

The lateral distribution of the electron density has been almost established. On the other hand the distribution of the energy flow has so far not been well investigated(*). Present results may give us a crude idea of the lateral distribution of the energy flow as described in the following.

The probability of discharging four counter trays by an air shower is calculated as a function of the distance, x, expressed in Molière units, of this point from the core of the shower. Let us, meanwhile, assume that E_e/N, i.e. the energy flow divided by the number of electrons, is a unique function of x and make up a distribution of E_e/N from the above results. Appropiately relating the probability as a function of x with this distribution one may derive a relation of E_e/N and r. This has been done as is seen in Fig. 3, 4 and 5. Fig. 3 represents the distribution of showers whose E_e/N are smaller than the corre-

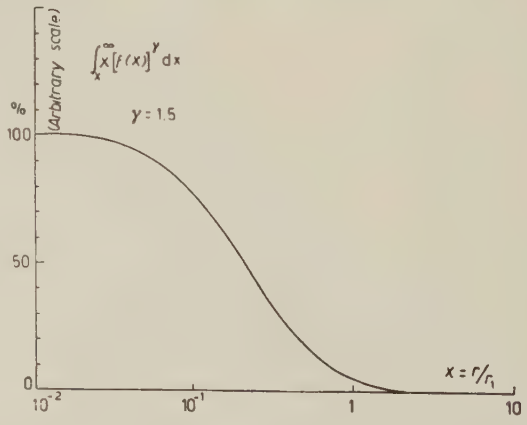

Fig. 4. – The discharging probability of four G.M. counter trays as a function of x.

(*) S. Miyake *et al.* also attempted to derive a part of the lateral structure of the energy flow by an analysis of experimental results obtained with a core-selector and G.M. counter trays in their air shower experiments.

sponding values on the abscissa. Fig. 4 represents the discharging probability of four counter trays for those showers, the distance from the axis of which is larger than x, with an arbitrary scale. Relating these two curves, we tentatively obtain the relation of E_e/N and x which is presented in Fig. 5.

J. NISHIMURA has worked out a theoretical calculation of the cascade shower concerning the lateral distribution of the energy flow (**). The result of the calculation is also presented in Fig. 5. The agreement between the conclusion of the analysis of the experimental results and the theoretical conclusion is fairly good. However, one should consider various simplifications involved in the above analysis of experimental data and detailed arguments have to be reserved until further investigation will be made using rather detailed information for each shower with the aid of, for instance, the array of detectors.

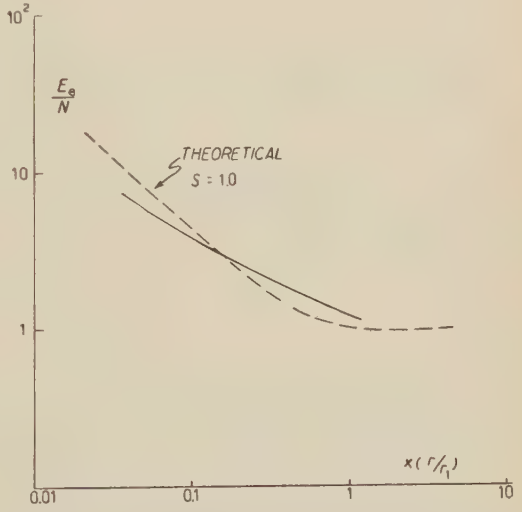

Fig. 5. - The relation of E_e/N and x derived from Figs. 3 and 4.

Once the lateral distribution of energy flow will be known to us, we may combine this with the conventional lateral distribution of electron density and, provided both are not very similar, obtain contour-lines for the size of the shower and x on the E_e/N-diagram. The lines tentatively calculated with Nishimura's theory of energy flow and Nishimura-Kamata's theory of the electron density are shown in Fig. 2 as an example. N is the size of the shower. The squares show espected statistical errors. Looking at this diagram one may, in principle, hope to determine the size of the shower and x by measuring E_e and N at a point simultaneously.

* * *

Authors are greatly indebted to Prof. J. NISHIMURA for making available to them his unpublished results of calculations as well as for his continuous discussions on the whole project. They wish also to express their gratitude to Prof. M. CROUCH for his most effective collaboration to the air shower project of this Institute.

(**) To be published. The theory tells us that $E_e \cdot x/N$ is a slowly varying function of x.

SUPPLEMENTO AL VOLUME VIII, SERIE X
DEL NUOVO CIMENTO

N. 2, 1958
2° Trimestre

Lateral Distribution of Energy Flow of Cascade Showers.

J. NISHIMURA

Institute for Nuclear Study, University of Tokyo - Tokyo

Lateral distribution of electrons in extensive air showers have hitherto been studied by many authors. In 1956 Prof. ODA in this institute has pointed out the possibility to observe the lateral distribution of the energy flow of shower particles using large Čerenkov detectors.

Independently from this plan, a similar experiment has been carried out by the Harwell group as reported at the Oxford Conference.

Thus it seems desirable to evaluate the lateral distribution of energy flow of shower particles, which can be derived using the solutions of lateral distribution functions reported in our previous papers (*Prog. Theor. Phys.*, **5**, 899 (1950); **7**, 185 (1952)).

Let $N_e(E_0, E, r, t)\,\mathrm{d}E\,2\pi r\,\mathrm{d}r$ and $N_\gamma(E_0, E, r, t)\,\mathrm{d}E\,2\pi r\,\mathrm{d}r$ be the number of electrons and γ-rays at depth t in the energy interval E, $E+\mathrm{d}E$ the annular area lying between radius r and $r+\mathrm{d}r$, with an incident electron energy E_0.

Then

$$(1)\qquad N_e = -\frac{1}{8\pi i}\int\int\int \mathrm{d}s\,\mathrm{d}p\,\mathrm{d}q \left(\frac{E_0}{E}\right)^s \frac{1}{E}\left(\frac{E}{K}\right)^2 \left(\frac{\varepsilon}{E}\right)^q \left(\frac{E^2 r^2}{K^2}\right)^{-p-1} \cdot \Gamma(p+1)\Gamma(-q)\mathcal{M}(p, q\cdot s\cdot t)\,,$$

where $\mathcal{M}$ is given by the equation

$$(2)\qquad L(s+2p+q)M(p\cdot q\cdot s) = \left(\frac{\partial}{\partial t}+\sigma\right)\{p(\xi-t)^2 M(p-1, q) + (s+2p+q)qM(p\cdot q-1\}\,,$$

with

$$\mathcal{M} = \lim_{(\xi - t) \to 0} M \tag{3}$$

and

$$M(0, 0, s, t) = H_1(S) \exp[\lambda_1(s)t] + H_2(S) \exp[\lambda_2(S)t] . \tag{4}$$

For γ-rays, we get

$$N_\gamma = -\frac{1}{8\pi i} \int_{-\infty}^{+\infty} \int_{-\infty}^{+\infty} \int_{-\infty}^{+\infty} ds\, dp\, dq C(s + 2p + q) \left(\frac{E_0}{E}\right)^s \left(\frac{1}{E}\right) \left(\frac{E}{K}\right)^2 \left(\frac{\varepsilon}{E}\right)^q \left(\frac{E^2 r^2}{K^2}\right)^{-p-1} \cdot \Gamma(p + 1)\Gamma(-q)\mathcal{M}'(p, q, s, t) , \tag{5}$$

with

$$\mathcal{M}' = \lim_{(\xi - t) \to 0} \exp[-\sigma t] \int_0^t \exp[\sigma t] M\, dt , \tag{6}$$

where M is given by the eq. (2).

Multiplying E on the both sides of the formulae (1) and (5) with respct to E and integrating from 0 to ∞, we get following formulae for the lateral distribution of energy flow of electrons (W_e) and γ-rays (W_γ)

$$W_e = -\frac{\varepsilon}{4\pi^3} \int_{-\infty}^{+\infty} \int_{-\infty}^{+\infty} ds\, dp \left(\frac{E_0}{\varepsilon}\right)^s \left(\frac{\varepsilon}{K}\right)^2 \left(\frac{\varepsilon^2 r^2}{K^2}\right)^{-p-1} \cdot \Gamma(p + 1)p(s - 1 + 2p)\mathcal{M}(p_1 - 2p - s + 1) , \tag{7}$$

$$W_\gamma = -\frac{\varepsilon}{4\pi^3} \int_{-\infty}^{+\infty} \int_{-\infty}^{+\infty} ds\, dp C(1) \left(\frac{E_0}{\varepsilon}\right)^s \left(\frac{\varepsilon}{K}\right)^2 \left(\frac{\varepsilon^2 r^2}{K^2}\right)^{-p-1} \cdot \Gamma(p + 1)\Gamma(s - 1 + 2p)\mathcal{M}(p_1 - 2p - s + 1) . \tag{8}$$

For $\varepsilon r/K \ll 1$, W_e and W_γ are represented by the formula $\varepsilon(r/r_1)^{3-s}$, which is r_1/r times more steep than the usual lateral structure functions. The consequence is that the higher energy particles are less scattered from the shower axis.

Numerical evaluations of (7) and (8) are carried out for $s = 1$ (*). The results are shown in Table I.

(*) The numerical evaluations of (7) and (8) are much more tedious than that of usual lateral structure functions.

TABLE I (**).

r/r_1	0.	0.01	0.1	0.4	1.0	2.0	4.0
$\pi\cdot\{(W_e+W_\gamma)/\varepsilon\}(r/r_1)$	0.36	0.40	0.46	0.57	0.97	2.00	4.00

As shown in Table I, the relation $(r_1/r)\cdot\pi\sim W_e+W_\gamma$ is held only for $0<r/r_1<1$.

Structure function of energy flow for $r/r_1>1$, which is mainly contributed by W_γ), does not decrease so much as r_1/r compared with π. The results may be so interpreted that the range of low energy γ-rays $(1/\sigma)$ is much longer than that of low energy electrons, E/ε, and γ rays are more accumulated compared with electrons for $r/r_1\gg 1$.

Thus the results obtained by the Harwell group can not be interpreted from these calculations.

(**) The precision of numerical evaluation is expected to be 10% or 20%.

PART IV

Section G: Other Air Shower Experiments.

Time Variations of Extensive Air Showers.

A. Citron (*) and G. Stiller

Physikalisches Institut der Universität - Freiburg im Breisgau

On the Schauinsland near Freiburg i.Br. (48° N, 8° E, 1230 m) extensive showers have been recorded from November 1953 to October 1956. The apparatus [1] (Fig. 1) consists of 10 trays of G-M counters with an effective area of 1700 cm² each. Five of these trays (1 through 5) are located on a straight line at equal separations, the two extreme ones (1 and 5) having a distance of 11 m. Threefold coincidences (I_3) of the two outer and the centre tray (1, 3, 5) and fivefold ones (I_5) of all five trays are recorded. The remaining five trays (6 through 10) are situated immediately adjacent to 1 through 5 and constitute a duplication of the apparatus, giving coincidences II_3 and II_5. The two parts I and II of the apparatus are electrically independent and permit a constant check on its functioning. Their results can be added up (K_3, K_5) to improve statistics. A correction for common events is applied. We also record tenfold coincidences of all trays (K_{10}) and three- and fivefold coincidences with each pair of adjacent trays (e.g. 1 and 6) connected in parallel (M_3 and M_5). $K_{3\,5} \equiv K_3 - K_5$ etc., represent low density showers.

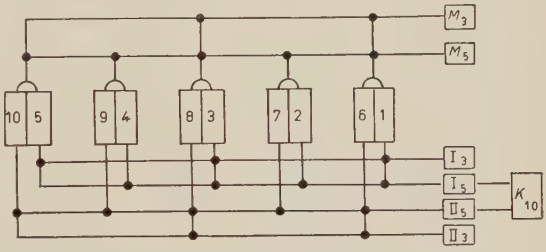

Fig. 1. – Block diagram of the apparatus.

Table I gives mean densities, counting rates, estimated particle numbers and energies for the various events recorded. The counting rates were also

(*) Now at CERN, Geneva.

TABLE I.

(a)	(b) (m^{-2})	(c) (h^{-1})	(d) (h^{-1})	(e)	(f) (eV)	(g) (10^6 counts)
$M_{3\text{-}5}$	2.35	150.2	152	$3.2 \cdot 10^4$	$2.2 \cdot 10^{14}$	2.84
$K_{3\text{-}5}$	4.7	58.3	59	5.8	4.0	
M_3	8.7	316.5	322	6.3	4.3	6.02
K_3	17.4	120.4	124	$1.12 \cdot 10^3$	7.6	
M_5	14.5	166.3	171	1.15	7.8	3.18
K_5	29	62.1	65	2.1	$1.4 \cdot 10^{15}$	1.79
K_{10}	45	32.6	36	3.4	2.4	0.38

(a) Counter arrangement.
(b) Mean particle density for $\gamma = 1.435$.
(c) Counting rate (measured).
(d) Counting rate calculated for a lateral distribution according to NISHIMURA and KAMATA with $s = 1.28$, $r_1 = 92$ m and Greisen's number spectrum, interpolated to the altitude of the Schauinsland.
(e) Mean number of particles under the same assumptions.
(f) Estimated energy for 6.8 GeV per observed particle.
(g) Total number of counts used for diurnal variations.

calculated using the number spectrum of GREISEN [2], including his normalization factor. We find excellent agreement with the measured rates at low energies. Greisen's exponent γ' varies between 1.37 for $M_{3\text{-}5}$ and 1.46 for K_{10}. A stronger variation of γ' in this range would improve the agreement at the higher energies.

1. – Diurnal variations.

Table I also gives the total number of events included in the analysis with respect to diurnal variations. The results of this analysis are reproduced in the histograms of Fig. 2 and 3. The data are corrected for barometric pressure.

A χ^2-test on the hourly intensity figures yields P-values less than 1% for the *solar* variations of M_3, M_5 and K_5. The variations in all recorded events are similar in aspect (broad maximum between 0 and 4 h, second maximum between 12 and 14 h), even for pairs of counter arrangements which record no common events (e.g. $M_{3\,5}$ and M_5). They repeat reasonably well from one year to another (Fig. 3). We conclude that a solar diurnal variation exists. It can be explained qualitatively as being due to a variation in air density (see below). From the regression coefficient obtained from day-to-day variations in temperature (about 0.3% °C^{-1}) and the known day-to-night temperature variations in the free air (~ 0.5 °C) a somewhat smaller amplitude would be

expected. Lack of precise information about the diurnal temperature variation in the free air makes a more detailed comparison impossible.

No significant *sidereal* variations were found in the data which group the

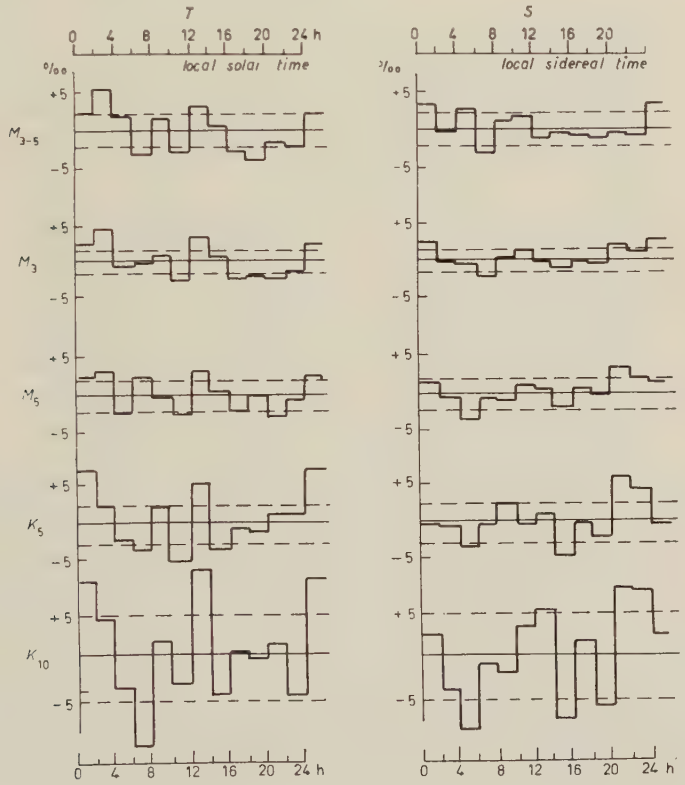

Fig. 2. – Solar and sideral diurnal variations (three years). Relative deviations of two-hourly means from the daily mean value are plotted against solar (T) and sideral (S) local time for the various counting arrangements. The broken line indicates the standard error on the two-hourly means.

three years together. In the data of 1954 (Fig. 3*a* S) a variation with a significance level of 2% (χ^2-test) was found for the K_5 events [3]. The maximum between 20 and 24 h local sidereal time agrees well with that found by DAUDIN [4] in the years 1951 to 1953 and, taking into account the difference in latitude, also with the one found by FARLEY [5] in New Zealand in 1952.

But the fact that the effect does not reproduce itself in the two subsequent years indicates that it is not a true sidereal variation.

Using the « antisidereal » correction [5] we were able to show that it is improbable that the apparent sidereal effect in 1953 was due to atmospheric

influences, or that the absence of an effect in 1955 and 1956 could be explained as a compensation of a true sidereal effect by an atmospheric one. In this analysis we included several harmonics of the daily variation and also allowed for some yearly phase modulation of the solar diurnal variation [6].

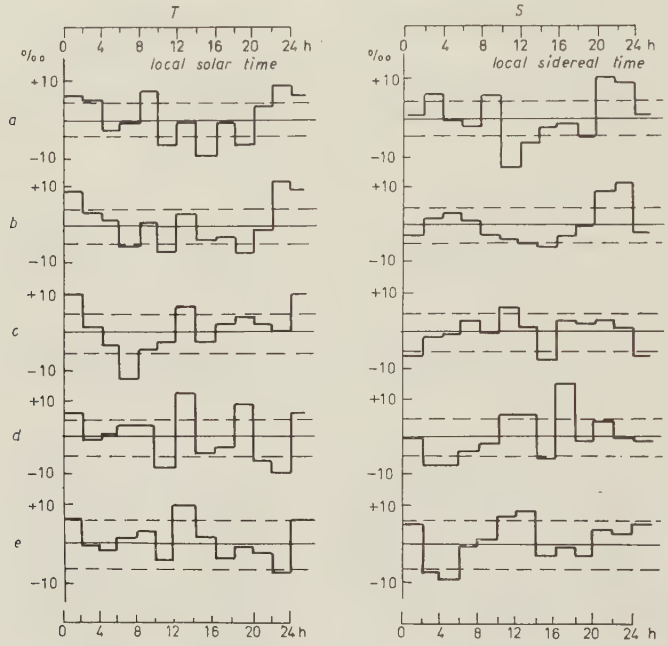

Fig. 3. – Solar and sidereal variations of events K_5 for different one-year periods. *a*) Nov. '53 - Oct. '54; *b*) May '54 - April '55; *c*) Nov. '54 - Oct. '55; *d*) May '55 - April '56; *e*) Nov. '55 - Oct. '56.

2. – Atmospheric effects.

A multiple correlation analysis between daily shower rates, local pressure and free air temperature has been carried out. The temperatures used were those measured twice daily (2 and 14 h GMT) above Payerne [7] (150 km SSW of Freiburg) at the standard pressure levels 850, 700, 500, 400, 300 and 200 mb.

Temperatures taken at a fixed pressure level are a direct measure for the air density. The *partial* regression coefficient with respect to density, eliminating pressure, gives the temperature effect. The *partial* regression coefficient with respect to pressure gives the influence of pressure after elimination of density effects, thus the absorption effect.

It was found that partial correlation coefficients with respect to temperature vary little with the level at which the temperature is taken, provided one of the levels between 850 and 300 mb is chosen. 200 mb temperatures give a poorer correlation. The best correlation is obtained for the temperature averaged over all levels from 850 to 300 mb.

The results of the analysis are given in Table II. The small values found for the residual variations show that there were no significant fluctuations apart from those caused by pressure and temperature variations.

Table II.

(*a*)	(*b*) %(cm Hg)$^{-1}$	(*c*) (‰°C^{-1})	(*d*)	(*e*)	(*f*) (‰°C^{-1})	(*g*) (g cm^{-2})
$M_{3\text{-}5}$	-10.6 ± 0.4	-1.2 ± 0.3	1.6	1.35	-2.0	173 ± 6
M_5	-11.9 ± 0.3	-2.8 ± 0.2	1.1	1.45	-2.8	166 ± 4
K_5	-12.1 ± 0.4	-3.4 ± 0.3	1.2	1.50	-3.2	168 ± 6
K_{10}	-12.9 ± 0.6	-3.7 ± 0.4	1.2	1.55	-3.6	163 ± 8

(*a*) Counter arrangement.
(*b*) Absorption effect.
(*c*) Temperature effect for the average air temperature at the levels 850, 700, 500, 400 and 300 mb over Payerne.
(*d*) Residual variance of the daily values in units of their standard deviation.
(*e*) Exponent of the number spectrum.
(*f*) Temperature effect (theoretical).
(*g*) Absorption length of particles in the shower, derived from (*b*) and (*c*).

The temperature effect is seen to increase strongly with energy. If it is a purely geometrical effect the shower rate is expected [8] to vary as a function of temperature T as $T^{2\gamma-2-\beta}$, which yields a temperature effect of $(2(\gamma-1)-\beta)/T_0$. Here γ is the exponent of the number spectrum, β that of the decoherence curve and T_0 the mean temperature. We assume $\beta=0.2$ [9, 10] and $T_0=250$ °K. For γ we take the values listed in Table II, which are deduced from the measured shower rates. They show a steeper variation than those of Greisen's spectrum. We then find the theoretical temperature coefficients given in the table. They are in reasonable agreement with the measured values. We conclude that the density effect can be understood as a purely geometrical one. The same result is obtained by Jánossy [10].

The absorption effect also increases with increasing energy, as found earlier [11]. The corresponding absorption length Λ for showers with a fixed number of particles is related to the absorption length λ describing the altitude variation of the number of particles within a shower by $\lambda = \gamma\Lambda$. With the values of γ used above we find the λ's listed in the table. The figures are compatible with a constant absorption length, as also suggested by Cranshaw [12].

REFERENCES

[1] A. LANGENBACHER: *Diplomarbeit Freiburg i. Br.*, (1954), unpublished.
[2] K. GREISEN: *Progress in Cosmic Ray Physics*, **3**, (Amsterdam, 1956), p. 68.
[3] A. CITRON and P. KEIHLER: *Zeits. f. Naturfor.*, **10***a*, 499 (1955).
[4] J. DAUDIN, P. AUGER, A. CACHON and A. DAUDIN: *Nuovo Cimento*, **3**, 1017 (1956).
[5] F. J. M. FARLEY and J. R. STOREY: *Proc. Phys. Soc.*, A **67**, 996 (1955).
[6] G. STILLER: *Diplomarbeit Freiburg i. Br.* (1956), unpublished.
[7] P. ACKERMANN: *Ann. d. Schweizerischen Meteorologischen Zentralanstalt* (1954-5): No. 6 Aerologische Station Payerne. Data for 1956 were kindly made available to us before publication.
[8] A. DAUDIN and J. DAUDIN: *Journ. Phys. Rad.*, **10**, 394 (1949).
[9] A. DAUDIN and J. DAUDIN: *Journ. Atm. Terr. Phys.*, **3**, 245 (1953).
[10] L. JÁNOSSY, T. SÁNDOR and A. SOMOGYI: in this issue, p. 701.
[11] A. CITRON: *Zeits. f. Naturfor.*, **7***a*, 712 (1952).
[12] T. E. CRANSHAW, W. GALBRAITH, N. A. PORTER, J. DE BEER and M. HILLAS: in this issue, p. 567.

SUPPLEMENTO AL VOLUME VIII, SERIE X
DEL NUOVO CIMENTO

N. 2, 1958
2° Trimestre

Further Measurements on Extensive Air Showers.

K. GREISEN

Laboratory of Nuclear Studies, Cornell University - Ithaca, N. Y.

At Cornell University, near sea level in Ithaca, New York, we began a year or so ago to set up a large experiment on extensive air showers, similar in many respect to that at M.I.T.

Unlike the other experiments which are discussed in greater detail at this conference, ours has not yet had a significant period of operation and systematic analysis. Therefore we cannot yet add appreciably to the fine results being reported from M.I.T., Culham, Tokyo, Moscow and Sydney. The only reason for speaking at all is to satisfy the interest, shared by all workers in this field, in knowing the nature and current status of each of the experiments.

As shower detectors we use 15 plastic scintillators, each 0.85 m^2 in area like those of M.I.T., which we made with the kind help of Dr. ROSSI's group. Five of the detectors are near the center of the array at spacings of 3 to 80 m. Five others are spaced about the center on a circle of 150 m radius, and the remaining five are on a circle of 500 m radius. For comparison, the radius of the M.I.T. array has been 230 m.

The other main component of the apparatus is a magnetic meson spectrometer, located near the central counters. The mesons are deflected by a magnet weighing 25 tons, dissipating 150 kW, and giving a field of 13 kG over a region of length 1.2 m, width 0.5 m and depth 0.2 m. The detectors are heavily shielded against electrons. A coarse measurement of deflection is provided by Geiger counters 16 mm in diameter, and a fine measurement by banks of Conversi-type neon discharge tubes 3 mm in diameter. The position error is expected to be about $\frac{1}{2}$ mm and the maximum measurable momentum about 300 GeV. The aperture is 25 cm^2 sr.

The scintillators are connected by cables to a central station where a variety of discriminators, mixers, and coincidence circuits operate on the pulses.

When a large shower occurs, a photograph is taken of a bank of 15 oscillograph tubes upon which all the scintillator pulses are registered. The times and the heights of the pulses determine the direction and location of the shower axis and the size of the shower as in the M.I.T. experiment. If a meson has been recorded simultaneously, this fact and the approximate meson energy are registered on the same film by means of neon bulbs.

If a meson is recorded, we do not require the shower to be very large in order to trigger the recording system. But if a meson is not recorded, the trigger demands a very large shower.

In addition to the above events which are subjected to a detailed analysis, other showers are recorded in a simpler way. Namely, simple 3-fold and 4-fold coincidences among scintillators at different spacings define showers of various mean sizes. These events are recorded by marks on moving tapes, for the purpose of studying time variations and the barometric and temperature effects. The smallest of these showers correspond to primary energies around 10^{13} eV and are recorded about 10000 per day; the largest refer to energies around 10^{17} eV and have a rate of 50 per day. With the oscilloscope method we examine about 200 showers per day, of which several are found to contain more than 10^8 electrons.

Furthermore, the scintillators exhibit a fairly good plateau in their background counting rate, which represents mainly mesons and soft component in approximate equilibrium with the mesons. This plateau permits us to monitor the integrated background rates on 3 Esterline Angus recorders, not only to check the correct functioning of the apparatus, but also to observe solar flares and other cosmic ray variations of short period. The total detector area is 13 m^2 and the background rate is 2250 s^{-1}. Therefore we can follow even small changes in rate with a short resolving time.

It is obvious from the above description that the purposes of the apparatus are multiple, and include observations of solar flares, time variations of extensive showers of various sizes, the directional and size distribution of very large showers ($10^7 : 10^9$ particles), the absorption rate of showers as a function of size, and the distribution in space and energy of the mesons in the showers.

Thus far, we have accumulated only incidental observations. For instance, I believe we are the first to make accurate timing measurements on showers over such a broad base, and consequently we find the curvature of the shower front quite noticeable. The radius seems to be on the order of 1500 m (agreeing with the earlier measurement by Bassi, Clark and Rossi made on a much smaller base). The existence of this curvature means that in applying the timing method to determine the direction of the shower axis, neglect of the

curvature would lead to large errors whenever the shower is not centrally located relative to the counters.

It has also been verified that in spite of the small aperture of any magnet spectrometer such as ours, significant numbers of real coincidences between mesons and air showers can be recorded. It is already apparent that the energy distribution of the mesons is rather flat, and the size distribution of the showers in which mesons are recorded is also not as steep as that of the unassociated showers.

SUPPLEMENTO AL VOLUME VIII, SERIE X
DEL NUOVO CIMENTO

N. 2, 1958
2° Trimestre

Air Shower Observation between 5200m and 3260m Altitude (*).

K. SITTE

Departments of Physics, Syracuse University - Syracuse, N. Y.
University of São Paulo - São Paulo, (+)

I. L. KOFSKY

Department of Physics, Smith College - Northampton, Mass.

D. L. STIERWALT

Department of Physics, Syracuse University - Syracuse, N. Y.

S. LEHRER (×), K. TAUSK and A. WATAGHIN (†)

Department of Physics, University of São Paulo - São Paulo.

1. – Introduction.

Extensive air showers, the manifestation of the collisions of ultra-energetic cosmic ray primaries in the atmosphere, are studied for two main reasons: first to determine the frequency and the energy distribution of those primaries, and second, to obtain evidence on details concerning the nature of their nuclear interactions. Of the two, the former—connected with the astrophysical aspect of cosmic ray research—can be carried out, in principle, with relatively simple detection apparatus (although of course the scarcity of primaries compels the experimenter to complicate his setup by multiplying the number of detectors

(*) Supported in part by the U. S. Atomic Energy Commission.

(+) Now at the Department of Physics, Technion - Israel Institute of Technology, Haifa, Israel.

(×) Now at the Physical Laboratories, The University, Manchester.

(†) Now at the H. H. Wills Physics Laboratory, University of Bristol.

used). The second, however, faces the inherent difficulty that the observer is dealing with the phenomenon only after many generations of complex cascade processes, and that simple apparatus, accordingly, can produce at the best ambiguous results. In order to permit the detailed and critical description required for an analysis, each observation should register a multitude of facts, such as number and energy spectrum, lateral and angular distribution of the shower electrons, number, energy, and distribution of penetrating particles. In addition, the variation with altitude of all these features should be known.

In recent years, several ambitious air shower experiments have been carried out [1, 2], or have been started [3, 4], which could be described as attempts to force advances in this formidable task by attacking it on a broad front, both in scale and in techniques. Yet, while considerable progress has been achieved especially in our knowledge of the lateral distribution of all shower components, a good deal more remains still to be disentangled. In particular, very little attention was paid, even in these large-scale experiments, to the longitudinal development—the « ageing »—of the showers. All events recorded at the level of observation were thrown together, without regard to the spread in their points of origin It appeared, therefore, worth while to supplement these investigations with another study of extensive showers in which more age-sensitive equipment is used.

The series of experiments reported here is an outgrowth and a continuation of earlier work of the Syracuse group (KASNITZ and SITTE [5], and SITTE, STIERWALT and KOFKSY [6], in the following quoted as KS and SSK respectively). It was carried out between 1952 and 1954 at three mountain stations: Echo Lake, Colorado, 3 260 m; Mt. Evans, Colorado, 4 300 m; and Chacaltaya, Bolivia, 5 200 m; and though more modest in scope than the investigations mentioned above, it aims at supplying some of the missing data on the development of air showers in the atmosphere. An attempt was made to classify the showers, at each altitude, according to their « age », and thus by comparing the lateral distributions of showers of different age to obtain evidence on the longitudinal structure of the cascade. Simultaneously, by comparing the rates of the showers of equal size *and* age at the various altitudes, information about the interaction length of the shower primaries and on the attenuation length of the cascade electrons can be collected.

As it will be explained in more detail later on, the unanticipated results of part of the experiment—as well as a number of similar observations of other authors published after this work had been started—cast, unfortunately, some doubt on the degree of reliability of the assumption on which the age classification was based. But although the quantitative precision of our age determination is lower than expected, the main conclusions remain valid even if our grouping is only in a very crude, almost qualitative, way representative of the shower age, and arguments will be presented to substantiate the claim

for at least that much confidence in the method used. We believe, therefore, that in the following report a survey of the effect of the « ageing » of showers of various size on their lateral distribution, of the attenuation of showers classified according to age and size, and of the production rate of showers as a function of the atmospheric depth, can be given.

2. – The experimental arrangement.

2·1. *General description. The triggering system.* – Since it was intended to include in the present analysis of shower observations the data of the 1952-experiment reported in SSK, the apparatus used at the other stations differed only slightly from that already described [6], and only its essential features will be summarized here. Basically it consists of three parts: unshielded counter trays, all of them hodoscoped, to determine the density of the shower electrons; a multiple-plate cloud chamber to give evidence of the penetrating particles in the shower; and an array of shielded counter trays and scintillators to observe the spectrum of the shower electrons. However, the cloud chamber was not operating all the time, and consequently only the data obtained with the counter-scintillator part of the arrangement will be discussed.

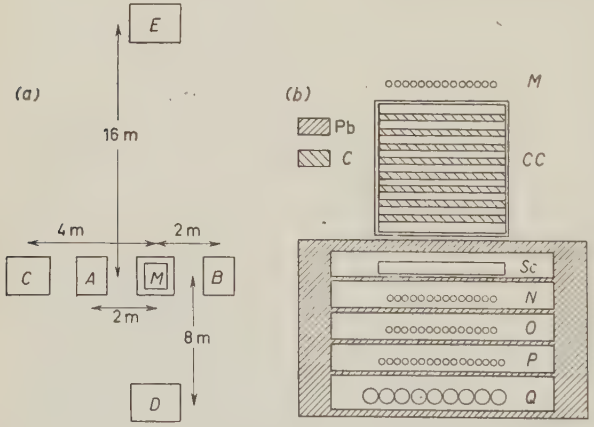

Fig. 1. – Schematic diagram of the experimental arrangement. (*a*) Relative position of the density-recording hodoscope trays *M*, *A*, *B*, *C*, *D*, and *E*. (*b*) The central part consisting of tray *A*, the cloud chamber *CC*, the scintillator *Sc*, and hodoscope trays *N*, *O*, *P* and *Q*.

A schematic diagram of the arrangement is shown in Fig. 1. The central tray *M* of fourteen 1 in. ×16 in. counters, and the extension trays *A*, *B* (both of ten 2 in. ×24 in. counters), *C* (fourteen counters 2 in. ×24 in.), and *D* (sixteen counters 2 in. ×24 in.), placed at 2 m, 4 m, and 8 m respectively, were also used in the SSK experiment. A new tray *E* of sixteen 2 in. ×24 in. counters placed at 16 m distance from *M* was added, and as a further improvement over the 1952-run, the *M*-counters were also fed into the hodoscope circuit. The relative position of *C* with respect to *A* and *B* was likewise changed;

C was now in line with those trays, and the two more distant trays D and E were at right angle to them.

The arrangement was triggered when at least two of the M-counters were struck in coincidence with at least one counter each in A and B. In demanding a considerably higher electron density at M than at the nearest extension trays, the apparatus was biased in favour of events with axes close to M: a simple, though not very efficient, core selector. Its performance will be discussed below; the condition imposed in the analysis of the SSK-experiment that the density everywhere else must not exceed that at the center, was no longer enforced.

2·2. *The transition analyser.* – The arrangement designed to analyse the transition effect in lead consisted of a group of four liquid scintillators, each 8 in. $\times$ 8 in. $\times$ 2 in., of the usual Terphenyl solution in Toluene with 80 mg Diphenylhexatriene added for higher sensitivity, and the four counter trays N, O, P and Q. N and O held each fourteen 1 in. $\times$16 in. counters, P sixteen equal counters, and Q ten counters of 2 in. $\times$24 in. size. A 1 in. lead plate was placed above the scintillator, and $\frac{1}{2}$ in. plates above each of the counter trays. Together with tray M, this system permitted thus to follow the transition of the shower electrons through 3 in. of lead.

The pulses of the four scintillators were displayed separately, with suitable delays, on the screen of a cathode ray oscilloscope (CRO). Since only the average density of the electrons is of interest, a single scintillator would have sufficed in principle; the use of four separate ones permitted, however, a larger range of measurable densities. The calibration of the scintillator system was carried out, as in an earlier experiment [7], by placing the unshielded scintillator in the center of a triangular arrangement of larger Geiger counters, and triggering the oscilloscope sweep by triple coincidences of these counters. Since the density spectrum of air showers is well known, and the small bias owing to the different triggering probabilities for showers of various densities can be precisely evaluated, the pulse height distribution recorded allows a direct co-ordination between the number of particles traversing the scintillator, and the sum of the pulse heights on the CRO. This method also permits a number of useful cross-checks on the reliability of the apparatus.

After rigorous screening of the hodoscope records for counters and circuit failures, a total of 4371 events registered at Echo Lake, 3054 at Mt. Evans, and 4236 at Chacaltaya were accepted for analysis.

3. – Discussion of the performance.

3·1. *Analysis of the triggering probabilities.* – With only 80 counters in the extension trays, the method of attempting precise location of each shower axis used in the large-scale experiments [1-4] was deemed inappropriate; it

will be shown later that on the average, the position of the shower core could be determined with an accuracy of about 4 m. Instead, the statistical approach described in KS was preferred.

Assuming for the moment that the lateral distribution $f(r)$ of the showers is known, and that the differential size distribution of the showers can be written as

$$s(N)\,\mathrm{d}N = K\cdot N^{-(\gamma+1)}\,\mathrm{d}N\,, \tag{3.1}$$

with a constant $\gamma \approx 1.5$ over the entire range of efficient selection, the rate R of showers recorded by the arrangement is

$$R = K\int_0^\infty N^{-(\gamma+1)}\,\mathrm{d}N\int_0^\infty 2\pi r\,\mathrm{d}r\int_0^{\pi/2}[p_M(r_M,\,NS)]^2\cdot p_A(r_A,\,ANS)\cdot p_B(r_B,\,BNS)\cdot\mathrm{d}\theta\,. \tag{3.2}$$

Here $p_M(r_M, NS)$ has been written for the probability that tray M, of area S and at a distance r_M from the axis, is struck; and similarly the expressions p_A, p_B for the trays A and B with areas AS and BS (in the present case $AS = BS$). In the following, it will be assumed that the detection efficiencies of the trays are unity, and that the other corrections affecting p, like the finite resolving time, are likewise negligible. It is easily seen that any errors introduced by these simplifications are quite small as long as the method is not applied for a computation of *absolute* counting rates. With these assumptions, p_M for instance is given by

$$p_M(r_M, NS) = 1 - \exp\left[-NS/f(r_M)\right] \tag{3.3}$$

and similar expressions are obtained for p_A, p_B.

It is now useful to consider the auxiliary quantity $I(r, NS)$, defined as the triggering probability, due to all showers striking at a distance r from the central tray M, as a function of the number N of electrons in the shower:

$$I(r, NS) = r\int_0^{\pi/2}[p_M(r_M, NS)]^2\cdot p_A(r_A, ANS)\cdot p_B(r_B, BNB)\cdot\mathrm{d}\theta. \tag{3.4}$$

From it, one computes two important functions:

a) By integrating over N, the contribution $P(r)$ to the recorded events from showers of all sizes as a function of the distance r of their axis from the center of the arrangement is obtained:

$$P(r) = K\int_0^\infty N^{-(\gamma+1)}I(r, NS)\,\mathrm{d}N\,. \tag{3.5}$$

b) By integrating over r, the contributions $F(N)$ from showers of various particle numbers striking at all distances r is found:

$$F(N) = 2\pi K N^{-(\gamma+1)} \int_0^\infty I(r, NS)\, \mathrm{d}r \,. \tag{3.6}$$

For the Chacaltaya run, the results of calculations carried out with the use of the Bethe distribution [8] $f(r)$ as structure function:

$$f(r) = \frac{c}{r}(1 + 4r)\cdot \exp\left[-4r^{\frac{1}{2}}\right], \tag{3.7}$$

are shown in the curves of Fig. 2 and Fig. 3. From the latter it is seen that at this altitude, the average particle number $\langle N \rangle$ is about $7.5 \cdot 10^4$, corresponding to a primary energy of the order 10^{15} eV. The efficiency of the « core selection » is demonstrated by $P(r)$ in Fig. 2: about 50 % of all showers strike inside a radius $r \gtrsim 0.05 r_0$ (r_0 is the Molière shower radius, about 150 m at Chacaltaya).

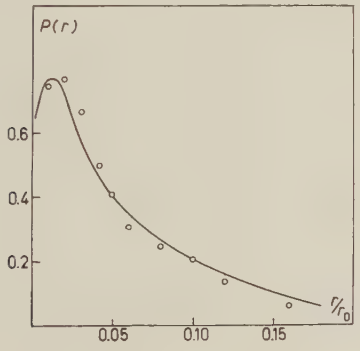

Fig. 2. – The relative contribution $P(r)$ of showers of all particle numbers with axes incident at a distance r from the center of the arrangement. The smooth curve is calculated with the Bethe distribution (3.7) as structure function, the crosses are the experimental points (Chacaltaya run, all shower ages).

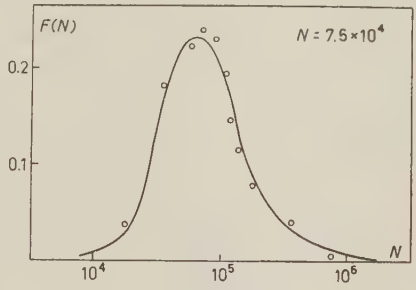

Fig. 3. – The relative contribution $F(N)$ of showers containing N electrons striking at all distances from the center. The smooth curve is calculated with the use of the Bethe distribution (3.7) as structure function, the crosses are the experimental data (Chacaltaya run, all shower ages).

Returning now to the task of locating the individual shower cores, it is easy to see that in about one-half of all cases it could be solved with good accuracy, while in the other half the position was much less precisely known. On the average, an uncertainty of about 4 m must be accepted, and this was considered too much for satisfactory analysis of the individual showers. Only

after the structure function was determined from a statistical analysis described in the next section, the « experimental » distributions shown as circles in Fig. 2 and 3 could be obtained. The agreement, however, is quite reasonable and thus confirms the reliability of the basic assumptions made.

3·2. *Discussion of the transition analysis.* – As in SSK, the central arrangement was used for the classification of the recorded events with regard to their average age. Cascade theory predicts for the differential energy spectrum of shower electrons an inverse power law with an exponent $(1+s)$, where s is the age parameter of the shower. Since comparatively small changes in s will effect in a quite considerable measure the number of very energetic electrons in the shower, the transition effect in lead can be used to distinguish « old » from « young » showers. They will differ both in the position of the cascade maximum, and in the height of the maximum. As it has been pointed out in SSK, the method can scarcely be expected to become useful for an absolute determination of the age parameter s, in particular since the uncertainties of the low-energy end of the spectrum—the region between the critical energy in lead and that in air—alone would prevent an exact evaluation of the transition effect for a given s. Moreover, the observed effect will depend on the distance of the shower axis from the analysing set, and this distance may, on the average, not be precisely the same for « old » and for « young » showers, However, although these arguments prove that this method may not lead to an absolute determination of the shower age, its validity as a guide for classification of the events in groups characterized by equal *average* age can certainly be claimed, and this is all that is required for our present purpose. It will be shown later on that this claim is borne out by the consistency of the results of this experiment.

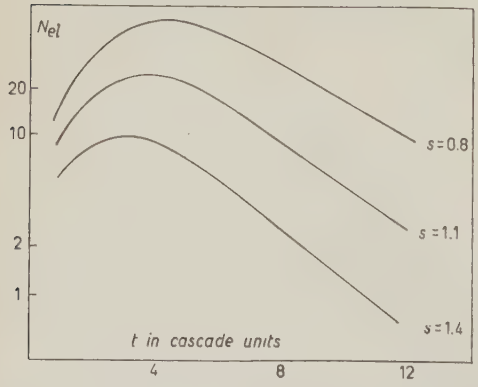

Fig. 4. – Calculated transition effect in lead for an incident power spectrum of the form $s(E)\,dE = dE/(E+E_c)^{1+s}$, for three values of the age parameter s: 0.9, 1.1 and 1.4.

For the present analysis, new calculations have been used, based mainly on the data of IVANENKO [9]. It was decided, after inspection of the experimental data, to restrict the classification to three groups: « old » showers with an apparent age parameter, as deduced from the spectrum, of $s \geqslant 1.3$; « medium » showers with $0.9 \leqslant s < 1.3$; and « young » showers with $s < 0.9$. The theoretical transition curves for the three age groups are shown in Fig. 4.

An age parameter was now assigned to each individual shower, by fitting to the corresponding transition thicknesses t of Fig. 4, the observed densities at four depths: at tray M, in the scintillator, the average densities at trays N and O, and the average densities at P and Q (restricting the analysis to four thicknesses in order to improve the statistics). This procedure was of course not entirely free of arbitrariness and quite large fluctuations were encountered in a few cases, but in general there was not much ambiguity in the choice. No attempt was made to correct for the zenith angle effect in each individual case, and only the average thicknesses were computed according to a $\cos^n \theta$ law for the distribution, and choosing $n = 6$, 5.5, and 5 respectively at the three stations.

A complete survey of the number of showers recorded in each age group, and for the three largest size groups (two, three, and four or more, M-counters struck) is given in Table I.

TABLE I. – *Number of events recorded at the three stations, grouped according to their average age, and according to the densities of the center tray M.*

Stations	No. of M-counters struck	« young » showers	« medium » showers	« old » showers	All showers
Echo Lake	2	687	995	669	2351
	3	432	514	331	1277
	$\geqslant 4$	242	303	198	743
	Total	1361	1812	1198	4371
Mt. Evans	2	515	674	429	1618
	3	270	358	263	891
	$\geqslant 4$	191	225	129	545
	Total	976	1257	821	3054
Chacaltaya	2	746	919	684	2349
	3	431	455	304	1190
	$\geqslant 4$	235	293	169	697
	Total	1412	1667	1157	4236

4. – Results.

4·1. *The lateral distribution.* – To determine the lateral distribution of the showers, the method used in KS was adapted to the new experiment. As a first step, the differential density distribution $h(\Delta)$ expected at each of the hodoscope trays M, A, B, C, Ω and E can be computed with the help of the triggering probabilities $I(r, NS)$ defined in (3.4):

$$h(\Delta) = \Delta^{-\gamma} \int_0^\infty \int_0^{2\pi} \{f(r')\}^\gamma I(r, \Delta/f(r))\, \mathrm{d}r\, \mathrm{d}\theta\,, \tag{4.1}$$

where r' stands for the distance between the shower axis and the hodoscope tray. Choosing again for $f(r)$ the Bethe distribution (3.7), one obtains, for instance, for the Echo Lake run the curves shown in Fig. 5. The actual density distributions observed in the experiment are marked as crosses and circles in the graph: evidently a poor fit for all but the most distant trays.

A correction was, therefore, applied to the lateral distribution (since it is well known that $h(\Delta)$ is much more sensitive to variations of this function, than to those of the number distribution). Denoting the true lateral structure function by $\varphi(r)$, we assume

$$\varphi(r) = A \cdot r^\varepsilon \cdot f(r)\,, \tag{4.2}$$

with a *small* ε, so that the corrected distribution $h'(\Delta)$ becomes

$$h'(\Delta) = A\Delta^{-\gamma} \int_0^\infty \int_0^{2\pi} r'^{\varepsilon\gamma} \{f(r')\}^\gamma I(r, \Delta/f(r))\, \mathrm{d}r\, \mathrm{d}\theta\,, \tag{4.3}$$

since the effect of the correction on I is small and can be neglected. The quantity $\varepsilon\gamma$ can then be chosen so as to give the optimum fit of the calculated $h'(\Delta)$ to the experimental points.

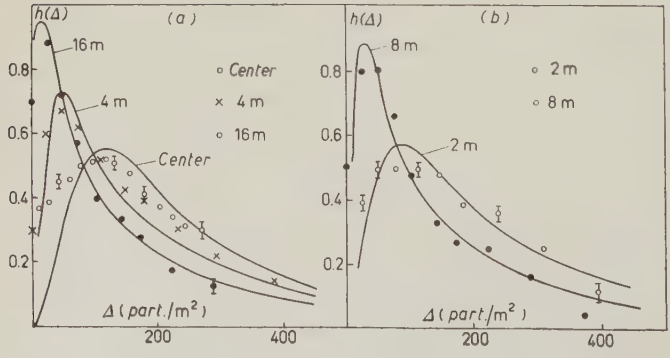

Fig. 5. – The differential density distribution $h(\Delta)$ at the hodoscope trays. (*a*): trays M, C, and E (0.4 and 16 m distance from the center); (*b*): trays $A+B$, and D (2 m and 8 m distance). The smooth curves show the distributions calculated with the Bethe distribution (3.7), the circles and crosses the experimental data (Echo Lake run).

However, in the present experiment it cannot be expected that a single ε would serve to describe sufficiently the entire range of distances r: the lateral distribution, it is known, is flatter in the core region than outside. Now we learn from the graphs of Fig. 2 that only few of the showers strike at large distances; thus, in particular, the distributions found at trays D and E are essentially representative of the structure function outside the core region (of perhaps 2 to 3 m radius)—with the possible exception of the points for the highest particle densities. On the other hand, the distributions at trays M, A and B are essentially determined by the *core* structure function, except for the region of the very lowest densities. It is, therefore, possible first to determine the large-distance correction ε_R from the results found at trays D and E, and then to construct a combined structure function with a different small-distance correction ε_r, with a smooth transition to the outside distribution. In carrying out this computation, a remarkable feature was found: First attempts to represent the data at all stations by a structure function with a correction extending to equal distances *expressed in shower units* r_0 were not successful; a much better agreement could be achieved when the corrections were applied to equal distances *expressed in meters*. As an example, the experimental data observed at the 2 m-trays at Chacaltaya are reproduced in Fig. 6, together with the distributions calculated with the Bethe function, and with corrections up to $r/r_0 \lesssim 0.03$, and $r \lesssim 3$ m.

In summarizing the results, classified according to the shower age, we make use of the fact that at least over the range of distances involved, the Bethe distribution can be approximated by a $1/r$-law. Writing, therefore, the true lateral structure function $\varphi(r)$ in the form

$$\varphi(r) = B \cdot r^n , \tag{4.4}$$

we give in Table II the values of n computed from the observed frequencies $h'(\Delta)$.

The data suggest two conclusions: Firstly, that there is a slight but systematic difference between the distributions of old and of young showers—each of those groups giving consistent results at all altitudes,—and this both for the core region and for larger distances from the axis. Secondly, the differences in the exponents are in both regions considerably smaller than what one might expect from the variation in age as determined from the spectrum.

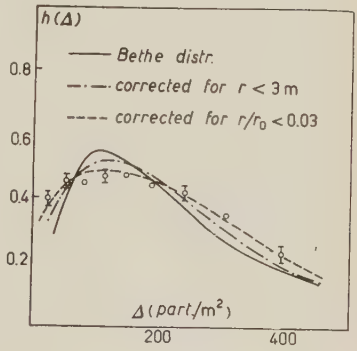

Fig. 6. – The differential density distribution for the 2 m-trays at Chacaltaya. The full line shows the results calculated with the Bethe distribution (3.7), the broken lines are computed with the corrected core distribution up to 3 m, or up to $r/r_0 \lesssim 0.03$.

TABLE II. – *Exponents n of the lateral distribution function* $\varphi = B \cdot r^n$, *near the core and at larger distances, for the three age groups and at the three stations.*

Station	« young » showers		« medium » showers		« old » showers		Average	
	$r \lesssim 3$ m	$r \gtrsim 5$ m	$r \lesssim 3$ m	$r > 5$ m	$r \lesssim 3$ m	$r \gtrsim 5$ m	$r \lesssim 3$ m	$r \gtrsim 5$ m
Echo Lake	$0.92 \pm .04$	$1.04 \pm .03$	$0.86 \pm .02$	$0.96 \pm .02$	$0.86 \pm .03$	$0.95 \pm .03$	$0.87 \pm .03$	$0.97 \pm .02$
Mt. Evans	$0.94 \pm .04$	$1.10 \pm .04$	$0.84 \pm .04$	$1.01 \pm .03$	$0.84 \pm .04$	$0.98 \pm .04$	$0.86 \pm .03$	$1.02 \pm .03$
Chacaltaya	$0.93 \pm .04$	$1.02 \pm .04$	$0.87 \pm .04$	$1.04 \pm .03$	$0.85 \pm .04$	$0.94 \pm .04$	$0.88 \pm .03$	$1.02 \pm .03$
Average	$0.93 \pm .03$	$1.05 \pm .03$	$0.86 \pm .02$	$1.00 \pm .02$	$.085 \pm .03$	$0.96 \pm .03$		

4·2. *Interaction and attenuation mean free paths.* – The radial distributions thus obtained can first be used to compute, for each individual event, the most likely total number of particles contained in the shower. This result has been checked against the calculated frequency distributions $P(r)$ and $F(N)$ (Fig. 2 and 3). As it was stated above, in view of the fact that the computations had been done with the Bethe distribution (3.7) instead of the correct function (4.4), the agreement is quite satisfactory.

A further analysis of the frequency distribution permits conclusions concerning the attenuation process of the cascade, and about the interaction mean free path of the shower primaries. To introduce this analysis, the recorded rates in the various age and size groups will be summarized in Table III.

It is now possible to assign to each of these groups, the corresponding average number of shower electrons, and thus to derive a frequency-vs.-number distribution for showers of the three age groups at each of the stations. The results are shown in Fig. 6 *a*) to 6 *d*). These data can now be further analyzed in three ways.

(i) Postulating, as usual, for the distribution law the form

$$H(N) = k \cdot N^{-\gamma'} \tag{4.5}$$

one can determine the value of the exponents γ' for each group. The results, given in Table IV, are not particularly revealing because of the insufficient accuracy of the values—not surprising since the experiment was not designed for this purpose. They are quoted here only for the sake of completeness.

(ii) The attenuation process can be studied in two manners. First, writing as usual for the frequency $H(\Delta, t)$ of showers of a given *density* Δ (in

TABLE III. – *The recorded rates of showers for the three age categories, and for the three largest density groups, at the three stations.*

	No. of M-counters struck	« young » showers	« medium » showers	« old » showers	All showers
Echo Lake	2	0.213 ± .006	0.284 ± .006	0.188 ± .004	0.685 ± .009
	3	0.106 ± .004	0.128 ± .005	0.084 ± .003	0.318 ± .007
	⩾4	0.038 ± .02	0.048 ± .002	0.031 ± .002	0.117 ± .004
Mt. Evans	2	0.416 ± .014	0.536 ± .013	0.351 ± .010	1.303 ± .025
	3	0.197 ± .008	0.249 ± .009	0.167 ± .007	0.613 ± .020
	⩾4	0.082 ± .005	0.096 ± .005	0.055 ± .004	0.233 ± .015
Chacaltaya	2	0.736 ± .013	0.869 ± .015	0.602 ± .012	2.207 ± .025
	3	0.347 ± .009	0.390 ± .010	0.247 ± .009	0.984 ± .016
	⩾4	0.122 ± .005	0.153 ± .006	0.088 ± .005	0.363 ± .010

TABLE IV. – *Values of the exponents γ' of the number distribution, $H(N) = k \cdot N^{-\gamma'}$ of shower particles at the three stations, and in the three age groups.*

Station \ Age	« young »	« medium »	« old »	« Average »
Echo Lake	1.50 ± .05	1.45 ± .03	1.40 ± .04	1.45 ± .03
Mt. Evans	1.50 ± .06	1.50 ± .04	1.45 ± .05	1.48 ± .04
Chacaltaya	1.60 ± .05	1.50 ± .05	1.50 ± .06	1.52 ± .04

particles m^{-2}) at depth t an expression,

$$H(\Delta, t) = K(t) \cdot \Delta^{-\gamma} \tag{4.6}$$

and assuming an exponential altitude variation of $K(t)$, a direct comparison of the rates of events—recorded with equal geometry, and hence sensitive to the same densities Δ—permits the determination of the « density attenuation length » Λ_Δ defined as

$$1/\Lambda_\Delta = -\partial(\ln K)/\partial t\,. \tag{4.7}$$

TABLE V. *Attenuation mean free path* $\Lambda_A = -\partial[\ln H(N)]/\partial t$, *at fixed counter geometry, between Echo Lake and Chacaltaya.*

Altitude (g/cm²) \ Shower age	« young »	« medium »	« old »	Average
692 to 600	134 ± 8	139 ± 6	141 ± 8	138 ± 5
600 to 537	155 ± 12	143 ± 9	138 ± 11	145 ± 7

Table V shows the results, proving that the variation of the attenuation length is small in the lower half of the atmosphere, though perhaps indicating a somewhat larger mean free path for the younger showers—as it is expected. They are also, on the whole, in accordance with earlier observations as discussed by GREISEN [10]. If (4.6) is translated into an attenuation of the number N of shower particles,

$$H(N, t) = J(t) \cdot N^{-\gamma} , \tag{4.8}$$

then the « number attenuation length » Λ_N, defined similarly as in (4.7),

$$1/\Lambda_N = -\partial(\ln J)/\partial t , \tag{4.9}$$

which is related to Λ_A by $\Lambda_N = \gamma \Lambda_N$, has values close to 200 g/cm².

In a second procedure, however, one can ask for the attenuation of the particle numbers in showers of equal *frequency*, a definition similar to that used in describing the attenuation of particle fluxes. Since the slope γ of the logarithmical frequency-vs.-numbers curves of Fig. 7 is very nearly equal throughout, the attenuation mean free path thus defined under the assumption of an exponential altitude variation,

$$\Lambda_H = -\partial(\ln N)/\partial t , \tag{4.11}$$

gives a consistent value $\Lambda_H \approx 125$ g/cm². Its significance will be discussed below.

(iii) Finally, a comparison of the variation with altitude of the rate of showers of *equal size and age*, permits a determination of the interaction mean free path of the shower primaries. Evidently, showers of well-defined particle number, when observed at equal stages of cascade development, must have been initiated by primaries of the same energy, and must have descended through an identical amount of matter. Their rate will, therefore, vary with altitude as the rate of the primaries does with the depth in the upper layers of the atmosphere. Obviously, however, it is the *interaction* and not the *attenuation* mean free path of the shower primaries that will be measured by

this method, since the first collision initiates the shower, and all possible subsequent interactions of the primary will simply be part of the nucleonic cascade associated with it.

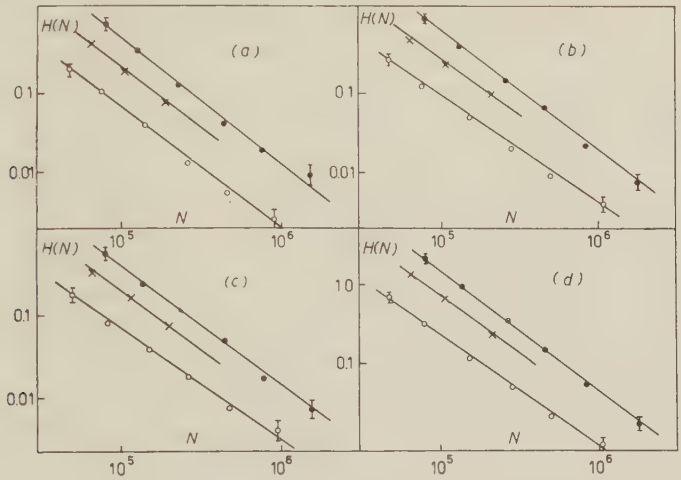

Fig. 7. – Frequency $H(N)$ of showers containing N or more particles, plotted against N. (*a*) « young » showers; (*b*) « medium » showers; (*c*) « old » showers; (*d*) all shower ages. Open circles: Echo lake data; crosses: Mt. Evans data; full circles; Chacaltaya data.

Again, it follows from the parallelity of the graphs in Fig. 7 that the interaction mean free path λ has a well-defined values. Taking an average over all age groups and at various particle numbers, one obtains as the most probable result,

$$\lambda = (87 \pm 7) \text{ g/cm}^2 .$$

It should perhaps be stressed that the uncertainty of this figure, resulting from the statistical errors of the counting rates and the uncertainty in the particle numbers, would not be affected by systematic errors in the *absolute* values of N. Only a distortion of the *differences* between the particle numbers evaluated at the three stations would lead to a serious fault in the determination of λ.

5. – Discussion of the results.

Most of the results reported, and of their interpretation, stand and fall with the reliability of the age classification used; it is, therefore, appropriate to look again at this procedure. Its possible weaknesses have already been emphasized; now we have assembled sufficient material to point out its positive

achievements, too. The very consistency of the data can be quoted as strong evidence in favour of its reliability. Wherever we could expect systematic trends of the observed quantities with the shower age, we find that our groups consistently yield the « right » results: in the lateral distribution near and far from the core, in the variation of γ, in the attenuation processes. Thus, we are led to the conclusion that although the numerical values of the age parameters assigned to the groups in accordance with their electron spectrum near the core, may not be precisely the correct data (as far as any definition of a single age parameter for an extensive air shower makes sense at all), nevertheless the age groups are properly defined, and represent at all stations a collection of events of equal average « history ».

Let us now briefly discuss the implications of the results reported above. Turning first to the lateral distribution, we note, in confirmation of earlier results [5, 6] and in agreement with some other more recent studies [1, 11], that the flattening in the core region as well as the variation of the outside structure function with the shower age—whether it is taken from the transition data or from the altitude variation—does not differ greatly for all the showers observed. It is certainly much less pronounced than the variation predicted in the calculations of NISHIMURA and KAMATA [12]. This fact, of course, is just a reflection of the interplay of the many generations of mixed cascades which continuously « rejuvenate » the shower.

In the same vein, the lack of spread of the core region with decreasing air density must be re-emphasized. It, too, is naturally explained as the result of the predominant influence of the *nuclear* component on the core structure: the spread of this component is not determined by scattering like that of the electrons, but by the angular distribution of the secondaries emerging from high-energy nuclear interactions, and hence not dependent on the density of the atmosphere. But the mere fact that even down into the lower half of of the atmosphere, the nucleons still retain this high concentration of energy in the core region, demonstrates two features: firstly, the comparatively low degree of inelasticity in high-energy interactions, and secondly, the comparatively strong forward « peaking » of the secondaries. But it would still be premature to expect accurate results from the quantitative discussion of these points; we shall, therefore, not carry this argument any further.

In the interpretation of the attenuation results, attention should be drawn to the value of the « number attenuation length » $\Lambda_N = 125$ g/cm^2. Its agreement with the attenuation mean free path for the nucleonic primaries of local penetrating showers (e.g. TINLOT [13]), the validity of which for interactions up to very much higher energies has recently been shown (e.g. KAPLON *et al.* [14], SITTE *et al.* [15]), is surely not fortuitous. Rather, it must be understood as yet another proof for the continued effect of the nucleonic cascade regenerating in its descent the electron cascade.

Finally, the importance of a determination of the interaction mean free path of the shower primaries is self-evident. The value quoted above, $\lambda' = (87 \pm 7)$ g/cm², is in quite satisfactory agreement with that expected for *proton* primaries, but sharply inconsistent with that of heavy nuclei. It might be pointed out that as a result of the difference by a factor of three to five between the interaction lengths of the two possible primary components (depending on the atomic number of the heavy nuclei), the attenuation between Chacaltaya and Echo Lake would differ quite radically: if in the energy region concerned heavy primaries would predominate, the comparable rates at Echo Lake should be smaller by a factor of the order 100 to 1 000 than those recorded. The discrepancy seems much too large to be explained away in any plausible manner, and the conclusion appears inescapable that protons are in fact the primaries initiating the air showers registered in this experiment. However, in view of the very great importance of this question, and since some doubt may still remain as to the reliability of the age classification, it would be highly desirable to repeat an experiment of this kind, perhaps with a better age selection based on another criterion.

* * *

The experiment was supported in part by funds granted by the U.S. Atomic Energy Commission, and by a grant from the Conselho Nacional de Pesquisas of Brazil to the University of São Paulo. During operation at Echo Lake and Mt. Evans, the facilities of the Inter-University High Altitude Laboratories were made available, and the authors wish to express their thanks to Prof. Byron E. Cohn and Mario Iona, Jr., of the University of Denver for their assistance. At Chacaltaya, Prof. Ismael Escobar V. and his staff, in particular Mr. J. Saavedra and Mr. R. Vidaurre, kindly offered their continuous help as well as Mr. T. Bowen of the University of Chicago and Ch. R. Thom of the Centro Nacional de Pesquisas Físicas. Thanks are also due to other collaborators: at Syracuse Dr. F. E. Froehlich, Dr. I. Nadelhaft, and Mr. E. J. Rizzo, and at São Paulo and Chacaltaya Dr. J. Meyer, Prof. U. Camerini, Dr. Estrella M. de Mathov and Miss A. Pirosky.

REFERENCES

[1] N. Dobrotin: *International Conference on Cosmic Rays* (Guanajuato, 1955); A. T. Abrosimov, A. A. Bedujakov, V. I. Zacepin, Y. A. Nečin, V. I. Soloveva, G. B. Hristiansen and P. S. Čikin: *Žu. Eksp. Teor. Fiz.*, **29**, 693 (1955); N. A. Dobrotin, O. Dovženko, V. I. Zacepin, E. Murzina, S. I. Nikol'skij, I. Rakobolskaja and E. Tukiš: in this issue, p. 612;

A. E. Čudakov, N. A. Dobrotin, N. L. Grigorov, G. N. Vernov and G. T. Zacepin: in this issue, p. 737.

[2] P. Bassi, G. Clark and B. Rossi: *Phys. Rev.*, **92**, 1441 (1953); G. Clark: *International Conference in Cosmic Rays* (Guanajuato, 1955); G. Clark, J. Earl, W. Kraushaar, J. Linsley, B. Rossi and F. Scherb: in this issue, p. 623.

[3] T. E. Cranshaw and W. Galbraith: *Oxford Conference on Extensive Air Showers* (1956); T. E. Cranshaw, W. Galbraith, N. A. Porter, J. de Beer and M. Hillas: in this issue, p. 567.

[4] K. Greisen: in this issue, p. 681.

[5] H. L. Kasnitz and K. Sitte: *Phys. Rev.*, **94**, 977 (1954).

[6] K. Sitte, D. L. Stierwalt and L. Kofsky: *Phys. Rev.*, **94**, 988 (1954).

[7] K. Sitte, F. E. Froehlich and I. Nadelhaft: *Phys. Rev.*, **97**, 166 (1955).

[8] H. A. Bethe: *Phys. Rev.*, **59**, 684 (1941).

[9] I. P. Ivanenko: *Dokl. Akad. Nauk SSSR*, **107**, 819 (1956).

[10] K. Greisen: *Extensive Air Showers*, in *Progress in Cosmic Ray Physics*, vol. **3** (Amsterdam, 1956).

[11] G. Fujioka: *Journ. Phys. Soc. Japan*, **10**, 245 (1955).

[12] J. Nishimura and K. Kamata: *Progr. Theor. Phys.*, **5**, 899 (1950); **6**, 628 (1951); **7**, 185 (1952).

[13] J. Tinlot: *Phys. Rev.*, **73**, 1746 (1948); **74**, 1197 (1948).

[14] M. F. Kaplon, J. Z. Klose, D. M. Ritson and W. D. Walker: *Phys. Rev.*, **91**, 1573 (1953).

15] K. Sitte, F. E. Froehlich and I. Nadelhaft: *Phys. Rev.*, **97**, 166 (1955).

SUPPLEMENTO AL VOLUME VIII, SERIE X
DEL NUOVO CIMENTO

N. 2, 1958
2° Trimestre

The Temperature Effect of Extensive Air Showers.

L. JÁNOSSY, T. SÁNDOR and A. SOMOGYI

Central Research Institute of Physics of the Hungarian Academy of Sciences, Department for Cosmic Rays - Budapest

1. – Introduction.

The investigation of the intensity variation of extensive cosmic ray air showers has lately gained interest from a new point of view. It is hoped that by its investigation some light may be thrown on the origin of cosmic ray particles of the highest energies. However, the intensity variations of extensive air showers are to a great extent due to causes other than the intensity variations of the primary radiation, i.e. to changes in the atmospheric conditions. The accurate knowledge of shower intensity variations arising from atmospheric causes is therefore an indispensable first step in any further investigation and inference from results obtained.

Among the atmospheric effects it is the barometer effect which has been known longest and which has been investigated most. Several authors using apparatuses of different sizes and base lengths have measured the effect and found for the barometer coefficient in rather good agreement values about $-10\,‰$ per mmHg [1]. EULER was the first who called attention to another atmospheric effect, namely the intensity variations caused by changes in the density (i.e. temperature, supposing the pressure to be constant) of the air [2]. The mechanism of this effect was discussed in detail by J. DAUDIN [3], and measurements of it were carried out by A. DAUDIN and J. DAUDIN [4] and HODSON [5]. The temperature coefficient according to the measurements of Daudin lies between -0.7 and -2.5 per °C, depending on the base length and also on the season. For a base length of 80 m DAUDIN even found a positive temperature coefficient. HODSON found for the temperature coefficient the value $(-3.8 \pm 1.1\,‰)$ per °C. Thus the temperature coefficient is not yet known with sufficient accuracy and further measurements were indicated so as to reduce the statistical error.

Higher accuracy is desirable also in order to check experimentally the formula for the temperature coefficient deduced theoretically by DAUDIN:

$$\Delta C/C = -(2\gamma - 2 - \beta)\Delta T/T . \tag{1}$$

Here $\Delta C/C$ means the relative variation of the shower rate caused by the relative change in the absolute temperature $\Delta T/T$, γ the exponent of the shower density spectrum and β the exponent of the decoherence function, i.e. of the function

$$C/C_0 = (l_0/l)^{\beta} ,$$

where l denotes the side length of the square in the corners of which are placed the measuring surfaces. In order to check (1) experimentally it is important to measure the values β, γ and the temperature coefficient with the same apparatus, since β strongly and to a lesser extent also γ depend on the geometry of the measuring apparatus.

Registrations of extensive air showers have been carried out in our laboratory since August 1953. Preliminary results concerning the temperature effect were already published ([6] and [7]). The entire material obtained throughout three years will be presented in this paper.

2. – Experimental arrangement. Control measurements.

2·1. – The measurements were carried out at 410 m a.s.l. in a wooden hut the roof of which was about 8 g cm^{-2} thick. The counters used by us were of the all-metal type, filled with the usual mixture of argon-alcohol (for a more detailed account of these counters see [8]). The efficiency of each counter was measured before use according to the method of JÁNOSSY and KISS [9], respectively by the improved method of FENYVES [10]. Only counters having an efficiency higher than 99.8% were used.

Four counter batteries were placed in the corners of a rectangle and connected in coincidence. Each battery consisted of ten identical counters, each of these having a sensitive area of 320 cm^2. In the first stage of the measurement all counters in a battery were connected directly in parallel, afterwards, in order to reduce the dead time only some of the anode wires were connected, the pulses from 1, 2, 2 and 5 connected counters being mied by diodes. This arrangement is shown in the block diagram of Fig. 1.

The pulses of the counters were uniformized by a shaping circuit consisting of a univibrator, a differentiating amplifier and a cathode follower [11].

The rectangular output pulse had a length of (2.5 ± 0.2) μs and this determined the resolving time of the Rossi coincidence circuit used. The base surface covered an area 9 m × 10 m and 10 m × 10 m, respectively in the later measurements. In order to determine the decoherence function observations were made also with base surfaces of 3.3 m × 3.3 m and 1.2 m × 1.2 m, respectively. During the last period (see remarks in Table I) the counter batteries were placed on a lead base 5 cm thick and surrounded by a lead wall 7.5 cm thick, while at other times neither lead base nor lead wall was being used. For the determination of the temperature effect only such measurements were taken into consideration which were carried out without absorber above the counters, apart from the 1.5 mm thick aluminium box containing them.

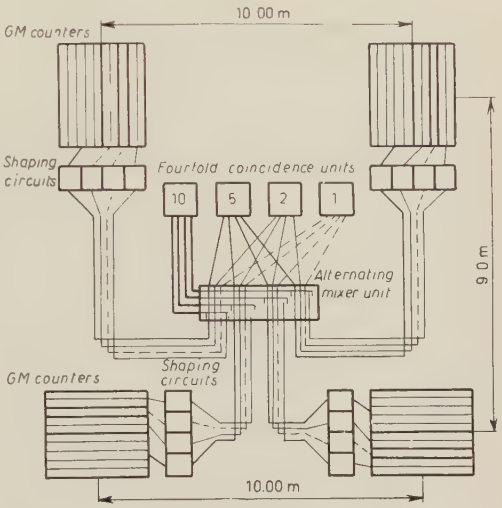

Fig. 1. – Experimental arrangement.

2·2. – Besides the systematic control of the apparatus by oscilloscope the following strict method was used in order to check the stability of the apparatus.

The counter batteries were placed above each other for an hour each second day, always in just the same geometrical position and the number of fourfold coincidences, i.e. the flux of the ionizing component of the total cosmic radiation in the solid angle subtended by the apparatus was measured during this time.

The rate of fourfold coincidences in this position was about 63 000 h^{-1}, therefore the standard error of a measurement lasting one hour equals 0.4 %. If the apparatus functions properly the differences in the daily registrations —after barometer—and temperature corrections—should not exceed the standard error to any significant extent.

The method is extremely sensitive to any failure of the apparatus. Continuous discharge or failure of even a single counter out of the forty making up the whole arrangement reduces the rate of the fourfold coincidences by $(8 \div 10)$ %, i.e. $(20 \div 25)$ times the standard error. Only those data were used in the course of the analysis of the shower registrations where the preceding as well as the subsequent registration of the total radiation showed normal results.

These control measurements enabled us to determine the absorption coefficient and the isobar-height coefficient of the total radiation. On the basis

of $17 \cdot 10^6$ observed coincidences we obtained for the absorption coefficient the value $(-1.76 \pm 0.07)‰$ per mmHg and for the isobar-height coefficient $(-7.3 \pm \pm 0.2)\%$ per km (the correlation was calculated for the height of the 500 mb level).

3. – Analysis of data. Results.

3·1. – The temperature data were taken from the balloon soundings of the National Institute of Meteorology, which were carried out twice daily at the observatory at Pestlörinc, lying to the south-east at a distance of 20 km from the place of the shower registrations. The mean temperature of the atmospheric level showing a barometric pressure by 100 mb less than that of the level of observation was calculated for each time interval of the registrations. The subtraction of the 100 mb $-$ 2.5 cascade units is based upon the consideration that the lateral spread of the showers is largely due to electrons and photons which are scattered away from the axis at a height of a few cascade units above the level of observation [12].

The solution of the equation of regression taking as independent variables the pressure p at the level of observation and the temperature T mentioned above, as well as other pertinent results are shown in Table I. Only such registrations were grouped into one and the same set of measurements in the course of which no modification of the apparatus was made. The calculations were carried out separately for each set of measurements, consequently separate barometer and temperature coefficients were computed from each set. The modifications of the apparatus, such as reduction of the dead time, variation of the base length from 1 m to 10 m or application of a lead base, do not appreciably influence either the barometer or the temperature coefficient. The coefficients calculated from the different sets agree within the limits of the threefold statistical error, this justifying computing the mean values of the corresponding coefficients calculated from different sets. The mean values were calculated using individual values weighted corresponding to their statistical errors and are shown in the last column of Table I.

3·2. – The method used for the calculation of the statistical errors was that outlined by JÁNOSSY and ROCHESTER [13] for simple correlation. This method takes into consideration that the changes in the atmospheric pressure and temperature are not of stochastical character, but represent real changes in the mass and density of an absorber. The measuring error of these quantities can be neglected in comparison with the stochastical fluctuation of the intensity values. If we have two independent variables in the equation of regression (e.g. in our case the barometric pressure p and the temperature T), the statistical errors of the regression and correlation coefficients and related quantities are as follows (for further details see [14]):

TABLE I.

Series of measurements	1	2	3	4	5	Sums resp. mean values
Date	Aug. 21, 1953- -May 5, 1954	May 5, 1954- -June 12, 1954	June 15, 1954- -Sept. 2, 1954	Sept. 12, 1954- -Jan. 17, 1955 and May 4-12, 1955	Jan. 4, 1956- -Aug. 11, 1956	Aug. 21, 1953- -Aug. 11, 1956
Base	9 m × 10 m	1.2 m × 1.2 m	3.3 m × 3.3 m	9 m × 10 m	10 m × 10 m on a lead base 5 cm thick	
	All 10 counters in each battery were connected in parallel			The pulses from 1, 2, 2, 5 counters were mixed by diodes in each battery		
Number of observed coincidences	123 271	62 538	43 670	38 291	140 923	408 693
Total time of measurement	1716 h	569 h	499 h	520 h	1834 h	5138 h
Barometer coefficent	$(-11.3 \pm 0.5)\%_{00}$ per mmHg	$(-9.4 \pm 1.5)\%_{00}$ per mmHg	$(-11.9 \pm 1.8)\%_{00}$ per mmHg	$(-10.0 \pm 1.2)\%_{00}$ per mmHg	$(-9.41 \pm 0.6)\%_{00}$ per mmHg	$(-10.47 \pm 0.35)\%_{00}$ per mmHg
Temperature coefficient	$(-2.7 \pm 0.5)\%_{00}$ per °C	$(-1.5 \pm 1.1)\%_{00}$ per °C	$(-1.2 \pm 1.4)\%_{00}$ per °C	$(-1.3 \pm 1.0)\%_{00}$ per °C	$(-2.4 \pm 0.3)\%_{00}$ per °C	$(-2.33 \pm 0.24)\%_{00}$ per °C
Partial correlation coefficient of the temperature	-0.43 ± 0.07	-0.20 ± 0.14	-0.19 ± 0.23	-0.20 ± 0.16	-0.61 ± 0.06	-0.47 ± 0.04
Specific dispersion (original)	6.9 ±0.6	2.6 ±0.5	3.1 ±0.7	6.4 ±0.7	4.5 ±0.5	
Specific dispersion (residual)	1.6 ±0.3	1.3 ±0.4	0.8 ±0.4	1.0 ±0.3	1.2 ±0.2	1.21 ±0.13
Amplitude of the residual systematic variation	(2.1 ±0.5)%	(1.3 ±0.8)%			(1.1 ±0.5)%	(1.2 ±0.4)%

a) Partial regression coefficient of the barometric pressure b_p. Denoting its statistical error by δb_p we get

$$\delta b_p = [\bar{n}/(1 - r_{pT}^2) \sum t_i (p_i - \bar{p})^2]^{\frac{1}{2}}, \tag{2a}$$

where $\bar{n} = \sum N_i / \sum t_i$, N_i being the observed number of events during the period t_i; p_i is the mean value of the barometric pressure during this period, $\bar{p} = \sum t_i p_i / \sum t_i$ and r_{pT} is the simple correlation coefficient between the observed pressure and temperature data.

An analogous formula holds for the partial regression coefficients of the temperature.

b) Partial correlation coefficient of the barometric pressure ($r_{Np.T}$). Its statistical error is

$$\delta r_{Np.T} = [\bar{n}(1 - r_{Np,T}^2)/(1 - r_{NT}^2) \sum t_i (n_i - \bar{n})^2]^{\frac{1}{2}}, \tag{2b}$$

where $n_i = N_i/t_i$ and r_{NT} is the simple correlation coefficient between the observed intensity and the temperature.

An analogous formula holds for the partial correlation coefficient of the temperature.

c) Total correlation coefficient ($r_{Np.T}$). Its statistical error is

$$\delta r_{Np.T} = [\bar{n}(1 - r_{Np,T}^2)/\sum t_i (n_i - \bar{n})^2]^{\frac{1}{2}}. \tag{2c}$$

d) Residual dispersion, that is $(1 - r_{Np,T}^2) \sum t_i (n_i - \bar{n})^2/(k-1) \equiv K_{\min}^2$, where k is the number of observations. The statistical error of $K_{\min}^2$ is

$$\delta K_{\min}^2 = 2[(1 - r_{Np,T}^2) \sum t_i (n_i - \bar{n})^2/(k-1)^2 \bar{n}]^{\frac{1}{2}}. \tag{2d}$$

e) Amplitude of the relative residual systematic variations in percents, that is

$$100 \left[\frac{k-1}{\sum N_i} \left(\frac{K_{\min}^2}{\bar{n}} - 1 \right) \right]^{\frac{1}{2}} = A. \tag{3}$$

Its statistical error (neglecting that of $\sum N_i$ and $\bar{n}$) is

$$\delta A = (1/A \sum N_i)[(k-1) K_{\min}^2/\bar{n}]^{\frac{1}{2}}. \tag{2e}$$

3·3. – In order to check the validity of the formula (1) we carried out measurements so as to determine γ and β.

γ was measured by the method of the variation of the surface [15]. On the basis of measurements carried out simultaneously with four different sur-

faces ranging from 320 cm² to 3200 cm² we obtain [7, 16]

$$\gamma = 1.421 \pm 0.009 . \tag{4}$$

So as to determine the value of β the distance between the counter batteries was varied. Measurements were carried out with base surfaces of area 1.2 m × 1.2 m, 3.3 m × 3.3 m and 9 m × 10 m, respectively, resulting in

$$\beta = 0.20 \pm 0.01 . \tag{5}$$

4. – Discussion.

4·1. – The temperature coefficient shown in Table I ($B_T = (-2.33 \pm 0.24)‰$ per °C) has a smaller statistical error than the values reported hitherto. It agrees within the limit of one and a half times the standard error with the data of HODSON ($B_T = (-3.8 \pm 1.1)‰$ per °C) and completely agrees with the value calculated on the basis of (1). Namely, introducing (4) and (5), i.e. the values of γ and β measured with one and the same apparatus as the temperature coefficient, into equation (1), we get $B_T = (-2.32 \pm 0.08)‰$ per °C. The temperature T figuring in (1), i.e. the temperature of the atmospheric level considered averaged over the total time of measurement was 275.8 °K).

4·2. – Thus our measurements confirm the statement that the observed rates of extensive air showers have to be corrected for the temperature variations of the atmosphere. Further systematic variations of the shower rate cannot be deduced from our measurements since the residual dispersion does not differ essentially from the dispersion according to the Poisson law. Nevertheless, attributing the residual dispersion in the cases in which this exceeds the Poisson value to systematic variation, the relative amplitude A of such a variation can be calculated by means of (3) (see [17]). The values of A shown in Table I were computed in this way, the mean value of A as well being computed by means of (3) from the mean value of the residual dispersions.

The agreement of the residual dispersion with the Poisson dispersion shows that the apparatus was satisfactorily stable throughout the whole time of observation. Moreover the registration of the intensity of the total radiation yields a better check on the stability of the apparatus than the statistical calculation based on the registrations of extensive air showers, because of the higher rates and smaller statistical fluctuations of these registrations. In these measurements also no instability of the apparatus showed itself. At any rate the systematic variations caused by the apparatus were smaller—even throughout several years—than a few per mille.

4·3. – For the sake of simplicity we have so far supposed that the total lateral spread of the showers stems from a thin atmospheric layer, namely from that of pressure $p = 100$ mb, p meaning the barometric pressure at the level of observation. In connection with this assumption the problem arises which is the isobaric layer which influences the shower intensity to the greatest extent, i.e. in which manner the strength of the correlation between shower intensity and temperature of the layer of pressure $p - p_0$ depends on p. The results of our calculations in this respect are shown in Table II. Similar calculations were made also by DAUDIN [18], his results (in particular the mean values of the data of Table I in [18]) weighted corresponding to the length of time of measurements, are also shown in Table II.

TABLE II. – *Partial correlation coefficients of temperature dependence.*

	Aug. 21, 1953- -Apr. 5, 1954	May 5, 1954- -June 12, 1954	June 15, 1954- -Sept. 2, 1954	Mean values	Data from Daudin measurements	
$p = 970$ mb p_0	1 479 h	569 h	499 h	2 547 h	$p = 720$ mb p_0	4 320 h
17 mb	-0.42 ± 0.07	0.12 ± 0.15	-0.22 ± 0.22	0.36 ± 0.06	0 mb	-0.19
50 mb	0.44 ± 0.07	0.17 ± 0.15	-0.22 ± 0.23	0.38 ± 0.06	20 mb	-0.19
100 mb	0.44 ± 0.07	0.24 ± 0.15	0.19 ± 0.23	0.39 ± 0.06	220 mb	0.28
250 mb	0.43 ± 0.07	-0.28 ± 0.15	-0.07 ± 0.32	0.39 ± 0.06	420 mb	0.41
500 mb	0.46 ± 0.07	-0.27 ± 0.15	0.34 ± 0.22	0.42 ± 0.06	520 mb	-0.11
					620 mb	-0.10

As can be seen from Table II, on the basis of our measurements no difference can be established in the role of the different isobaric layers. Unfortunately, DAUDIN does not give statistical errors, so that no definite conclusion can be drawn from his data.

It is very difficult to select the atmospheric layer which has the strongest influence upon the shower intensity, since there is a strong correlation between the temperature variations of the different atmospheric layers. The changes of the temperature of the different layers take place very often in the same direction, moreover they obey mostly a certain regularity. Obviously, on the basis of such temperature variations differences in the strength of correlation of the temperature of different atmospheric levels and the shower intensity cannot be established. However, if the measurements last long enough a suf-

ficient number of such events may occur, in which the temperature changes of some layers are of a nature different from the temperature changes of the remaining layers (e.g. by inrush of new air volumes in a thin layer), thus making possible to establish any difference in the role of the different layers.

It is clear that the exact procedure would consist in taking into consideration with adequate weights the temperature changes of all layers, that is the correlation between the shower intensity and the properly weighted mean temperature of the whole atmosphere ought to be calculated. Unfortunately, this method of calculation is of no practical value as the observed data are generally insufficient to establish any difference in the role of the different atmospheric levels.

REFERENCES

[1] J. Clay: *Proc. Ned. Ak. Wed.*, **52**, 450 (1949); C. Castagnoli, A. Gigli and S. Sciuti: *Nuovo Cimento*, **7**, 307 (1950); D. Millar: *Proc. Roy. Ir. Ac.*, A **54**, 115 (1951); A. L. Hodson: *Proc. Phys. Soc.*, A **66**, 49 (1953); A. Daudin and J. Daudin: *Journ. Phys. Rad.*, **14**, 169 (1953).

[2] H. Euler: *Zeits. Phys.*, **116**, 73 (1940).

[3] A. Daudin and J. Daudin: *Journ. Phys. Rad.*, **10**, 394 (1949).

[4] A. Daudin and J. Daudin: *Journ. Phys. Rad.*, **14**, 169 (1953); *Journ. Atm. Terr. Phys.*, **3**, 245 (1953).

[5] A. L. Hodson: *Proc. Phys. Soc.*, A **64**, 1061 (1951).

[6] T. Sándor and A. Somogyi: *Bulletin of the Central Research Institute for Physics*, Budapest, **2**, 466 (1954) (in Hungarian).

[7] L. Jánossy: *Suppl. Nuovo Cimento*, **1**, 247 (1955).

[8] A. Somogyi: *Bulletin of the Central Research Institute for Physics*, Budapest, **2**, 38 (1954).

[9] L. Jánossy and D. Kiss: *Acta Phys. Hung.*, **4**, 173 (1954).

[10] E. Fenyves: *Acta Phys. Hung.*, **4**, 363 (1955).

[11] K. Zsdánsky: *Bulletin of the Central Research Institute for Physics*, Budapest, **3**, 22 (1955).

[12] L. Jánossy: *Cosmic Rays*, (Oxford, 1950), p. 322.

[13] L. Jánossy and G. D. Rochester: *Proc. Roy. Soc.*, A **183**, 786 (1944).

[14] L. Jánossy, A. Somogyi and F. Telbisz: *Bulletin of the Central Research Institute for Physics*, Budapest, in the press.

[15] G. Cocconi, A. Loverdo and V. Tongiorgi: *Nuovo Cimento*, **1**, 314 (1943); *Phys. Rev.*, **70**, 841 (1946).

[16] J. Koch, T. Sándor, A. Somogyi and J. Szivek: *Bulletin of the Central Research Institute for Physics*, Budapest, **1**, 61 (1953) (in Hungarian).

[17] L. Jánossy: *Cosmic Rays*, (Oxford, 1950), p. 380.

[18] A. Daudin and J. Daudin: *Compt. Rend.*, **236**, 1352 (1953).

PART V.

Interactions of Cosmic Radiation.

Nucleon-Nucleon Interactions at Energies Greater than 10^{12} eV (*).

MARCEL SCHEIN and D. M. HASKIN

Enrico Fermi Institute for Nuclear Studies
Department of Physics of the University of Chicago - Chicago, Ill.

An emulsion stack consisting of 100 sheets of 600 μm Ilford G-5, 15 cm × 30 cm, and flown for 8 hr at 104 000 feet on a Skyhook balloon flight over Texas ($\lambda = 41°$ N.), has been scanned for high energy events. Two events seemed particularly suitable for analysis. Event 1, shown in Fig. 1, is pro-

Fig. 1. – Projection drawing of Event 1. The event has an inclination of 1°.2 to the plane of the emulsion and a secondary length of 16 cm.

duced by a primary proton. Twenty minimum ionizing particles emerge as secondaries. The collision can be interpreted as a nucleon-nucleon interaction in which a high energy proton collides with a hydrogen nucleus or a single proton on the periphery of a heavier nucleus. The angular distribution of the secondaries was measured and the momentum of each individual track deter-

(*) Supported by a joint program of the Office of Naval Research and the U. S. Atomic Energy Commission.

mined by the measurement of multiple Coulomb scattering. It was found that particles in the central core of the shower carried such a high energy that the momentum could be determined only by using track to track scattering. Utilizing this method, momenta up to about 100 GeV/c were measurable. Knowing the momenta and angular distribution of the secondaries it was possible to deduce a reliable estimate of the energy of the primary proton of $5 \cdot 10^{12}$ eV. This also makes it possible to carry out a relativistic transformation into the center of mass system (C.S.). The results show clearly the sharp collimation of particles of high energy in the C.S. around 0° and 180°. See Fig. 2. The half angle of the cones is approximately 10°, which is considerably smaller than predicted by the theory of Fermi (30° to 40°). In contrast, the low energy particles in the C.S. show a considerably wider angular distribution. The half angle is greater by at least a factor of 2.

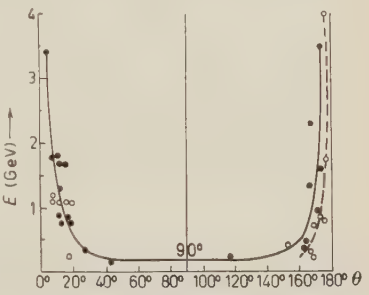

Fig. 2. – Angular and energy distribution of particles in the center of mass system for Event 1 and *S*-star.

It is of interest to point out that the average energy of the charged particles in the C.S. is only 1.4 GeV.

Each of the charged secondaries was followed through the stack in order to find secondary interactions. A number of secondary interactions were

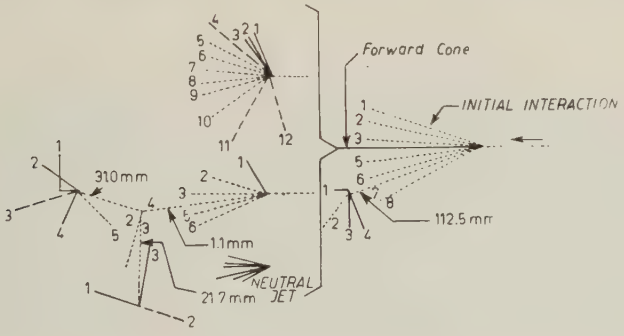

Fig. 3. – Interactions of secondary tracks from event 1.

located and some of the minimum tracks of these interactions were followed in order to find tertiary interactions. Fig. 3 above shows the interactions of secondary tracks. The mean free path was found to be about 28 cm.

Evidence that a large number of neutral particles were emitted in the primary interaction was found. This consisted mostly of electron pairs most probably

originating from the decay of neutral pions. These pairs are located in general in distances of a few mm from the primary star. At a distance of 5.7 cm from the primary star, a neutral interaction consisting of a high energy jet was found. The event consists of 20 minimum tracks only. The origin is within the center core of the primary event and the core of the neutral jet is closely parallel to the same direction. Because of the considerable distance from the origin, the event cannot be caused by a neutral pion. It is most probable that it is produced by a very high energy K^0-meson, a neutron, or anti-neutron. The neutral jet is shown in Fig. 4 and is designated as event 2. It was analyzed in the same manner as event 1.

Fig. 4. – Projection drawing of event 2.

The energy and angular distribution show similar characteristics as event 1. The energy of the neutral particle was found to be about $2 \cdot 10^{12}$ eV, which is

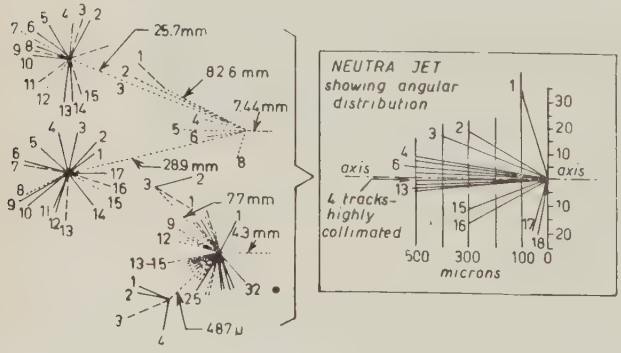

Fig. 5.
Interactions of secondary tracks from event 2.

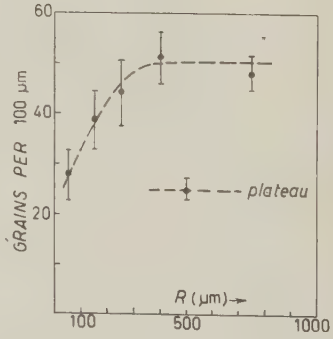

Fig. 6. – Ionization vs. range of high energy electron pair.

a considerable fraction of the primary energy of $5 \cdot 10^{12}$ eV. Tracing of the charged particles yielded a mean free path of secondary and higher order interactions of 24 cm. Fig. 5 shows the type of interactions found. Taking both

events together, there are six cases where the secondary and tertiary interactions followed each other within distances of only a few milimeters.

At a distance of 6.38 mm from the origin of event 1, an electron pair of unusually high energy was found. A visible separation of the electron-positron tracks could be seen only at a distance of more than 1 cm. The opening angle of 10^{-5} radians indicates a lower limit to the energy of about $5 \cdot 10^{11}$ eV. The ionization of the pair was determined over the first 2 mm and compared with two neighboring minimum ionization tracks from the primary interaction that were parallel and less than 10 μm away. The results are shown in Fig. 6. A considerable decrease in ionization is found in the first 500 μm, in agreement with the results of PERKINS. The theoretical estimate of the reduction in ionization by ČUDAKOV was found to be in reasonable agreement provided the energy of the pair was about $5 \cdot 10^{11}$ eV, as estimated from the opening angle.

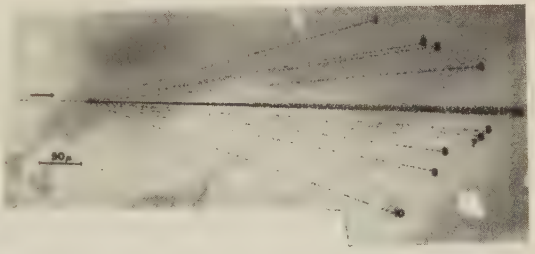

Fig. 7. – Projection drawing of event 3. The event is inclined at 11° to the emulsion surface and has a secondary length of 12 cm.

Two additional events shown in Fig. 7 and 8 are under analysis. One of them was found in the same stack and consists of the collision of a primary proton producing 22 minimum tracks with no evaporation prongs. The second was found in a large stack exposed for 7 h at 102 000 feet over Guam, Marianas Islands on a Skyhook balloon flight. It contains 52 minimum tracks and

Fig. 8. – Projection drawing of event 4. The event has an inclination of 5° and a secondary length of 25 cm.

3 evaporation prongs. This event seems particularly favorable for analysis since the number of secondary and higher order interactions may be has high as 50.

A more detailed publication will follow in the *Physical Review*.

SUPPLEMENTO AL VOLUME VIII, SERIE X
DEL NUOVO CIMENTO

N. 2, 1958
2° Trimestre

One Case of Nuclear Interaction in Photoemulsion at the Energy of $\sim 5 \cdot 10^{13}$ eV/Nucleon.

I. M. Gramenizkij, G. B. Ždanov, E. A. Zamčalova,
M. I. Tretjakova, M. N. Ščerbakova.

P. N. Lebedev Institute of Physics of the USSR Academy of Sciences - Moscow.

In the stack of stripped emulsions, which we have got owing to a kind assistence of professor C. F. Powell (the stack was exposed at 25.5 km in the autumn of 1955 in Italy), we found out and investigated one of the rare cases of nuclear interaction of a very high energy. The conditions of observation allowed to follow the shower development through a distance of 6 cm.

The principal characteristics of the phenomenon and their comparison with the hydrodynamical theory of multiple particle production are given below.

1. – The type of interaction: $1 + 0 + 37\alpha$.

A relatively low multiplicity of fast particle generation in the presence of only one slow particle permits to consider the process as a peripherical collision of an α-particle with a photoemulsion nucleus and to interpret all the quantitative characteristics of the phenomenon from the viewpoint of nucleon-nucleon interaction.

2. – Penetrating component, angular distribution.

The angular distribution averaged to the measurements of three observers is given in Fig. 1. The calculated curves for the case of isotropic distribution and for the distribution predicted by the theory of Landau [1] are also given there.

The method of χ^2-tests has shown that the probability of agreement between experiment and theory is about 90%, and the probability of agreement with isotropic distribution is about 0.1%. At the same time the only calculated parameter L has been determined from the relation

$$L = \lg 2\gamma_c \,, \tag{1}$$

$$\lg \gamma_c = -\overline{\lg \operatorname{tg} \theta} = 2.35 \,. \tag{1a}$$

Systematical and chance errors in the determination of γ_c will be discussed below.

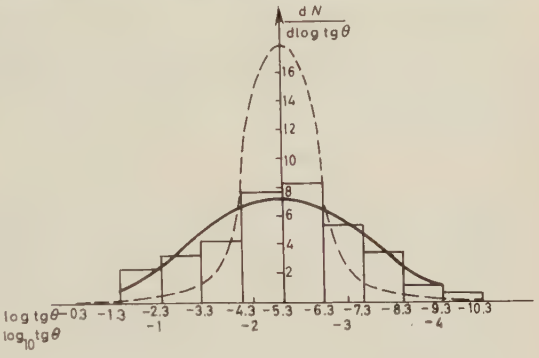

Fig. 1.

In the meanwhile at the comparison of the angular distribution with the theory the particle velocities are assumed to be sufficiently close to c. In this connection the angular distribution curve in the centre of mass system (C.S.) is obtained by a simple shift of the curve for the laboratory system (L.S.) by the value $\lg \gamma_c$.

3. – Penetrating component, secondary interactions.

Table I gives the principal characteristics of three secondary interactions observed within the narrow cone of penetrating particles.

TABLE I.

Type of star	The angle to shower axis	γ_c	Energy in L.S. (1) n-n collision	Energy in L.S. (2) n-column interaction	$p_\perp/\mu c$ (1)	$p_\perp/\mu c$ (2)
9+13p	$3 \cdot 10^{-3}$	5.5 ± 1.5	$6 \cdot 10^{10}$ eV	$1.8 \cdot 10^{11}$ eV	1.3 ± 0.6	4 ± 2
3+10p	$6 \cdot 10^{-4}$	13 ± 4	$4 \cdot 10^{11}$ eV	$8 \cdot 10^{11}$ eV	1.7 ± 1.0	3.5 ± 2
1+10p	?	~ 200	$\sim 10^{14}$ eV	$\sim 10^{14}$ eV	—	—

The following two points should be stated:

1) transverse momenta ($p_\perp$) of particles differ considerably less than their energies do;

2) the interaction of 1 + 10p type is caused by the particle with the energy close to the primary one, but at the same time the multiplicity of particle generation turns out to be by several times less.

4. - Soft component and transverse momenta of π^0 mesons.

Table II gives angular and energy characteristics of 10 electron pairs formed not further than 0.9 cascade units from the point of shower generation. This condition permits to exclude the pairs of bremsstrahlung origin in every individual case.

TABLE II.

Number of pair	α	s (mm)	$h\nu$ (GeV)	φ	$\frac{p_\perp}{\mu c} = \frac{2h\nu\varphi}{\mu c^2}$	Remarks
1	$1 \cdot 10^{-4}$	4.5	130	$1 \cdot 10^{-3}$	1.8	—
2	$1 \cdot 10^{-4}$	4.5	130	$1 \cdot 10^{-3}$	1.8	—
3	$3.5 \cdot 10^{-4}$	2.7	30	$2 \cdot 10^{-3}$	0.85	Photon (γ) and π^0-meson emergence angles coincide
4	$2.5 \cdot 10^{-4}$	2.1	40	$2 \cdot 10^{-3}$	1.2	—
5	$1 \cdot 10^{-4}$	4.6	130	$0.6 \cdot 10^{-3}$	1.2	γ and π^0 emergence angles coincide
7	$2 \cdot 10^{-4}$	2.25	90	$1.4 \cdot 10^{-3}$	1.8	—
12	$4 \cdot 10^{-4}$	1.25	25	$0.7 \cdot 10^{-3}$	0.25	—
15	$1.2 \cdot 10^{-4}$	6.0	110	$0.35 \cdot 10^{-3}$	0.6	—
16	$0.9 \cdot 10^{-4}$	6.0	160	$0.25 \cdot 10^{-3}$	0.5	—
20	$< 3 \cdot 10^{-5}$	10	> 1000	$0.4 \cdot 10^{-3}$	> 6	γ and π^0 emergence angles coincide

At the same time the energy of a given photon $h\nu$ was determined from the relation

$$\text{(2)} \qquad \begin{cases} X = \dfrac{4}{\alpha}\sqrt{(\log X)^2 + 5s}\,, \\ X = \dfrac{h\nu}{m_e c^2}\,, \end{cases}$$

where α is the divergence angle of pair components measured at the distance of s mm. The relation (2) is an approximate relation between the energy

and the mean value of the angle α derived from Stearns' formula [2] taking into account electron and positron scatterings in the assumption of uniform division of energy $h\nu$ between them.

The following ratio is also approximate

$$p_{\perp} = \frac{2h\nu \cdot \varphi}{\mu c} . \tag{3}$$

It connects transverse momenta of the photon and the corresponding π^0-meson. This approximation is justified (at the statistical analysis of results) by a relatively small value of the additional transverse mementum forming at the decay, if for the angle φ one takes the angle between the shower axis and the direction of photon motion.

As it was pointed out for the first time in the work of Rozental' and Miletin [3], the information about transverse momenta (including the data of Table I) obtained by us together with the data on the direct measurements of energies and emergence angles of penetrating particles in the shower observed by Italian authors [4] are a good confirmation of the unidimensional hydrodynamical theory in which transverse momenta are derived with account of the purely thermal motion of the generated particles at the temperature of divergence $\sim \mu c^2 (\mu = \pi$-meson mass).

Besides comparison with theory the determination of transverse momenta permits to solve also a purely methodical problem of the systematical error in the determination of the value γ_c by the given angular distribution of particles in the laboratory system of co-ordinates. Indeed, for the arbitrary particle velocity (β_0) in the c.m. system (with the velocity β_c) the transition to the laboratory system angles (θ_2 are angles in the L.S., θ_0 are angles in the C.S.) can be expressed by the formula

$$\operatorname{ctg} \theta_2 = \gamma_c \left(\operatorname{ctg} \theta_0 + \frac{\beta_c}{\beta_0} \frac{1}{\sin \theta_0} \right) . \tag{4a}$$

This formula can be approximated with a sufficient accuracy by the expression

$$- \log \operatorname{tg} \theta_2 - \log \gamma_c = \log \operatorname{ctg} \frac{\theta_0}{2} + \delta\lambda \tag{4b}$$

with the correction term

$$\delta\lambda \approx \frac{1}{2} \left[\frac{\sin^2 \theta_0}{(p_{\perp}/\mu c)^2} - \frac{1}{\gamma_c} \right] \frac{1}{1 + \cos \theta_0} . \tag{4c}$$

This correction term permits to calculate the error $\delta \lg \gamma_c$ obtained in the determination of the value γ_c from the relation (1*a*) with the certain function of particle angular distribution (*). In particular for the angular distribution, predicted by the theory of Landau, we have obtained $\delta \lg \gamma_c = 0.15 \div 0.20$, what corresponds to over estimating the true value of the primary energy ($E_0 = 2\gamma_c^2 \mu c^2$) by $2 \div 2.5$ times (depending on the value of the parameter $\mathcal{L}$ in angular distribution).

As for the chance error in the determination of γ_c from (1*a*), which depends as on angular distribution fluctuation, so on the errors of angle measurements it can be estimated from the spread of mean values $\lg \operatorname{tg} \theta$ for pair particles being symmetrical relative to the divergence angle of a half of shower particles. In the investigated case the mean spread of the value $\lg \operatorname{tg} \theta$ does not exceed 0.1. Thus, the most probable final value of the primary energy is $\lg \gamma_c = 2.2 \pm 0.1$ or $E_0 = (5^{+3}_{-2}) \cdot 10^{13}$ eV.

5. – Soft component, energy and space distribution.

When there is no possibility of sufficiently precise direct measurements of particle energies, one can derive the energy distribution of photons from the measurements of pair divergence angles (α). Besides the space distribution of pairs (in the directions being transverse and longitudinal relative to the shower axis) it is reasonable to investigate also the space distribution of single electrons: apart from checking the corresponding photon distributions it permits to estimate indipendently the total energy released with π^0-mesons, by the comparison of longitudinal particle multiplication with different cascade curves.

Space-energy distribution of photons is given in Table III, in which it is assumed that the quantity of the bremsstrahlung origin photons is small (**).

In this case the energy intervals are selected in accordance with the angular intervals for penetrating particles in Fig. 1 provided there are constant transverse momenta $p = 1.5\ \mu c$. It is easy to see that due to a small (at an average) value of p «spreading» of the photon emergence angles in the process of π^0-decay should be of the same order as the emergence angles between the corresponding π^0-mesons and the shower axis (†). On the contrary, on con-

(*) A rough estimate of the value $\delta \log \gamma_c$ can be obtained from (4*c*) by substitution of the mean angle $\overline{\theta_0} \approx 90°$.

(**) This assumption is probably justified so far as the photons with corresponding pairs formed just near the particle tracks of a previous pair or the photons of a sufficiently low energy ($h\nu < 20$ GeV) are not included.

(†) In Table III the angle θ means the angle relative to the shower axis, under which from the shower centre one can see the point of the corresponding pair formation.

Table III.

	$\alpha \cdot 10^4$	Photons 4.6-0.9	Photons 0.9-0.2	Sum	Penetrating particles
	$h\nu$ (GeV)	I 20-150	II 150-1 100		
I	$5 \cdot 10^{-3} > \theta > 7 \cdot 10^{-4}$	4	0	4	13
II	$7 \cdot 10^{-4} > \theta$	10 ($2T$.)	2-4	($\leqslant$) 10-12	5
	Sum	14 ($2T$.)	2-4	($\leqslant$) 14-16	18

dition that $p \quad \mu c$ the angles q formed by the directions of photons with the shower axis nearly coincide with the angles θ. The corresponding graph shows also (in brackets) the expected quantity of the bremsstrahlung origin pairs (for example, $2T$) in the given energy interval in order to be sure that such a selection based on the space distribution is reasonable (on condition that the particle energy of the second interval should not be lowered).

The possibility of lowering the photon energy in the 3-rd column of Table III and uncertainty of the estimate of such photons quantity are connected with the fact that the tracks of the pair components are overlapped by the tracks of new pairs of obvious bremsstrahlung origin (*) having a sufficiently high energy. These four photons are combined in pairs giving rise to two cores of angular distance between them of about $0.5 \cdot 10^{-3}$ in every core at a distance of the order of 1 cascade unit from the first photon and with an accuracy of the order of 5 m. On the prolongation of the corresponding pair tracks there takes place a conversion of the second photon connected, obviously, with the same π^0-meson. If we use ordinary cascade curves (which connect the number of secondary electrons with their minimum energy $E_{\min}$ and the primary electron energy) and also the ratio

$$\bar{\eta}_E \approx \frac{E_s}{E_{\min}}, \tag{5}$$

which connects the mean deviation of electrons from the shower axis with their energy ($E_s = 2.10^7$ eV), we should arrive at the conclusion that at least one of the observed narrow cores owes its origin to a π^0-meson with energy, at least, of the order of 10^{12} eV, though this estimate is certainly rather rough. For the second core (in which a closer coincidence of separate pair tracks is

(*) The investigation carried out in the work [5] has shown that already at energies of the order 10^{11} eV only a small part of similar cases can be the true tridents, i.e. the pairs directly produced by one of the electrons.

visible at a shorter distance) the energy of the initial π^0-meson should be estimated at $(2 \div 3)\cdot 10^{11}$ eV which, taking into account the mutual divergence given above, corresponds to a value p of the order of μc. It should be noted that the position of a higher energy core with the angular accuracy of the order of 10^{-4} corresponds to the direction of that secondary penetrating particle (see the third line of Table I) the energy of which is similar to the primary energy. According to the above stated considerations it can occur that the upper limit of the second interval photon energy is underestimated and due to it also a possible number of pairs of bremsstrahlung origin in the second interval is lowered.

If one takes into consideration that the probability of the photon conversion at the distance of 2 cascade units is about 0.8, the analysis of Table III can lead to the following conclusions.

1. The total number of π^0-mesons within the limits of statistical errors of the experiment does not differ from a half of the penetrating particle quantity.

2. Angular distribution of the photons of non-bremsstrahlung origin substantially differs from the penetrating particle distribution.

3. The total energy transferred to the shower soft component is about $(10 \div 15)\%$ from the primary particle energy (*) though it is not excluded that this estimate is somewhat underestimated (approximately by $2 \div 3$ times).

Table IV gives the longitudinal (along the shower axis) and transverse (at the distance of 2 cascade units) distribution of electrons measured within the limits of the narrow core of penetrating particles. The analysis shows that this data satisfactorily agree with the data concerning photons and confirms the above-mentioned conclusions about the angular distribution and total energy flux in the soft component. In particular, a special comparison of the

Table IV.

Longitudinal distance (cascade units)		Transverse deviation at $t = 2$ (cascade units)	
0.5	14	4	8
1.0	43	(4-8)	15
1.5	90	(8-12)	11
2.0	149	(12-25)	29
		(25-50)	32
		(50-100)	34

(*) If one assumes that not one but several nucleons of the primary α-particle take part in the generation of mesons, this estimate should be lowered correspondingly.

curve of transverse distribution of electrons and penetrating particles was done for the depth $t = 2$: the concentration of energy fluxes near the shower axis in both cases is practically the same and is expressed approximately by a function of $r^{-2.6}$ type (r is a distance from the shower axis). But just this coincidence shows that the initial (without taking into account Coulomb scattering) distribution of energy fluxes in the soft component has been more concentrated than in the penetrating one, since the divergence of π^0-mesons in the point of their formation is expressed on the average by a value being somewhat less than the total deviation connected with the following photon decay and Coulomb scattering of the electron cascade particles.

* * *

The authors thank scanners J. F. Šarapova, R. M. Gryzunova, and M. F. Soloveva for their help in the work and express their gratitude to professor N. A. Dobrotin, professor S. N. Vernov and I. L. Rozental′ for the fruitful discussion of the results.

REFERENCES

[1] L. D. Landau: *I v. Akad. Nauk SSSR, Ser. Fiz.*, **17**, 51 (1953); S. Z. Belen′kij and L. D. Landau: *Usp. Fiz. Nauk*, **56**, 309 (1955).
[2] M. Stearns: *Phys. Rev.*, **76**, 836 (1949).
[3] G. A. Milečin and I. L. Rozental′: in this issue, p. 770.
[4] A. Debenedetti, C. M. Garelli, L. Tallone and M. Vigone: *Nuovo Cimento*, **4**, 1142 (1956).
[5] A. Debenedetti, C. M. Garelli, L. Tallone and M. Vigone: *Nuovo Cimento*, **4**, 1151 (1956).

SUPPLEMENTO AL VOLUME VIII, SERIE X
DEL NUOVO CIMENTO

N. 2, 1958
2° Trimestre

Nuclear Interactions between 10^3 and 10^5 GeV.

B. Edwards, J. Losty, D. Perkins and J. Reynolds
H. H. Wills Physical Laboratory - Bristol

1. – Exposure.

Jets were detected by scanning for the resulting soft cascades, this method imposing a lower limit to the primary energy of about 10^3 GeV. 24 jets produced by protons, and 9 by α-particles were obtained in a total of 23 litres G5 emulsion flown for ~ 6 h at 100 000 ft. and 7 litres exposed for 0.5 years at 11 500 ft. The rate of events was 0.3 per litre hour at high altitude, ~ 0.5 per litre year at mountain altitude. In the same volume were observed 65 soft cascades, 52 originated by single photons, 13 by single electrons, entering the stacks from outside. No cascade of « multi-photon origin » was observed.

2. – Distribution of N_h and n_s.

Of the 33 jets observed, 18 were of $N_h \leqslant 2$, 13 of $N_h = 0$. The mean value of n_s for events of $N_h > 2$ was 3.2 ± 0.8 times that for $N_h \leqslant 2$. Clearly very few of the jets will correspond to pure nucleon-nucleon collisions, and secondary interactions must play an important role. In what follows, only proton-induced jets will be considered.

3. – Transverse momentum.

In general, complete analysis of individual events is impossible. We started therefore by measuring one parameter over a number of events. The parameter chosen was the transverse momentum p_t, of the secondary particles, since this is Lorentz invariant. p_t was determined for particles in the « inner

cone » by the angular distribution of secondary jets, in the outer cone by scattering measurements. Our results seem to show that

a) $(p_t)_{\text{av.}} \simeq 0.5$ GeV/c

b) 90% of the values of p_t lie within the interval $(0.1 \div 1.0)$ GeV/c;

c) p_t is almost independent of centre of mass system angle of emission θ, over the measured range $\bar{\theta} = 0.5° \div 179°$.

d) p_t is almost independent of primary energy E.

Result *a*) is in good agreement with the Japanese measurements of p_t on neutral pions. Although these measurements correspond to nucleon-nucleus collisions, one might expect the result for nucleon-nucleon collisions to be not very different, and it is therefore instructive to compare the results with theory:

Fermi: $p_t \propto E^{1/4}$, strong maximum at $\bar{\theta} = 90°$; $(p_t)_{\text{av}} \sim$ several GeV.

Landau: $p_t \propto E^{1/2}$, almost independent of $\bar{\theta}$; $(p_t)_{\text{av}} \sim 4$ GeV/c.

Heisenberg: as for Landau, but with $(p_t)_{\text{av}} \sim m_\pi c$.

The results therefore appear to exclude the Fermi theory; whereas only small numerical adjustments are required in the absolute value of p_t for the other theories.

4. – Inelasticity.

From a theoretical viewpoint, the distribution of the fraction k of energy radiated in a nucleon-nucleon collision is of great interest, since it depends directly on the radial distribution of field energy around the nucleons. FERMI and LANDAU both postulate that $k \sim 1$, HEISENBERG and BHABHA suggest much smaller values.

If p_t is really independent of $\bar{\theta}$, it becomes possible to say something about k, using the observed multiplicities and angular distributions. It will not be a true value, since we are dealing with the results of successive collisions in complex nuclei; but it should be right in order of magnitude, and we are more interested in how k varies from event to event, rather than the absolute value.

In very high energy events, nearly all the energy is carried away by a few forward particles, which make small angles to the primary direction (frequently $< 10^{-4}$ rad). The difficulty of measuring such small angles with precision suggests that we should go to the centre of mass system, where equal amounts will be radiated backwards and forwards. If we plot tg θ ($\theta =$ angle in the laboratory system) on a log scale, the centre of gravity of the distributions

corresponds to the geometrical mean value of $\mathrm{tg}\,\theta$, say $\mathrm{tg}\,\eta$. The energy of a nucleon in the centre of mass system is $\gamma_c = 1/(\mathrm{tg}\,\eta)$. On such a scale, the centre of mas system angular distribution is symmetrical about $\mathrm{tg}\,\eta$ ($\bar{\theta} = 90°$), since $\log(\mathrm{tg}\,\theta/\mathrm{tg}\,\eta) = + \log \mathrm{cotg}\,(\bar{\theta}/2)$. This transformation is valid provided $\theta < 90°$ and the secondaries are relativistic in the laboratory system which is nearly always the case. Assuming $p_t = 0.5$ GeV/c, one can therefore estimate the visible energy radiated. The fraction radiated backwards in the centre of mass system is almost independent of small errors in estimating γ_c, and this is the principal reason for making the transformation.

From the events analysed, we have found no certain case for which $k < 10\,\%$, the average being ~ 0.5. It will be seen that, at a fixed primary energy, small n_s corresponds to a strong forward-backward peaking in the centre of mass system; large n_s correspond to a more isotropic distribution. The striking feature of our results, is that at a given energy, the degree of anisotropy varies tremendously from event to event. If the distribution is put in the form $\cos^n \bar{\theta}\,\mathrm{d}\Omega$, then for 4 events between 30000 and 50000 GeV, n varies from 4 to 300. This variation is much greater than can be accounted for by angular momentum considerations alone, and suggests that the Heisenberg-Bhabha or Kraushaar-Marks models, in which the impact parameter plays an important role, are preferable to the Landau theory, where fluctuations are small.

5. – Fluctuations.

In some events of low multiplicity, the calculated values of k, when derived in the above manner, are less than 1%. We believe that these events represent extreme fluctuations, where most or all of the charged particles are emitted forwards in the centre of mass system. If symmetry in *total* number of particles is to be preserved with respect to backward and forward emission in the centre of mass system, the fluctuations in the ratio of neutral and charged particles have to be much greater than would be expected statistically. Such apparent lack of symmetry, in individual events, between the incident and struck nucleon, has indeed been suggested in the « excited nucleon » model of Kraushaar and Marks.

SUPPLEMENTO AL VOLUME VIII, SERIE X
DEL NUOVO CIMENTO

N. 2, 1958
2° Trimestre

A Cosmic Ray Jet in the 10^{12} Electron Volt Energy Range.

P. Fowler, P. S. Freier, C. Lattes, E. P. Ney

University of Minnesota - Minneapolis, Minn.

D. Perkins

University of Bristol - Bristol.

Summary. — A 22.4 litre stack of emulsions was exposed in Minnesota during September 1956 in a balloon flight at 116000 feet. The emulsion stack, which was flown in a cooperative experiment with University of Bristol, weighed 200 lbs and had dimensions of 16 in. × 12 in. × 7 in. The largest jet so far found by naked-eye scanning traversed the entire Minnesota half of the stack with a total lenght of 26 cm. The primary interaction is a $6+1\alpha$ star. In the nine radiation lengths of the Minnesota portion of the stack, the jet multiplied from nine particles, mainly in two cores, to 8000 particles. The electromagnetic cascade appeared to be initiated by several γ rays probably from the decay of two neutral mesons. The electromagnetic cascade was still increasing in numbers after nine radiation lengths. At approximately 23 cm from the primary interaction, the primary particle produced a meson jet in the core of the electromagnetic cascade. The meson star was classified as $4+80p$. The angle containing half of the 80 minimum ionization particles was $3 \cdot 10^{-4}$ rad. The energy of the primary π-particle is estimated to be $\sim 10^{15}$ eV. The energy in this event which appeared in electronic component is approximately 10^{14} eV.

SUPPLEMENTO AL VOLUME VIII SERIE X
DEL NUOVO CIMENTO

N. 2, 1958
2° Trimestre

Two Interesting Cases of Secondary High-Energy Interactions in Photographic Emulsion.

G. B. Ždanov, E. A. Zamčalova,
M. I. Tretjakova and M. N. Ščerbakova

P. N. Lebedev Physical Institute of the USSR Academie of Sciences - Moscow,

One of the most important questions that arise in the study of nuclear interactions by the photographic emulsion method is the determination of the energy of the incident particle. With a very few exceptions, this may be done only from the angular distribution of the secondary particles. In the case of nucleon-nucleon collisions, such a determination is based on a quite natural, but experimentally unproved assumption of the symmetrical divergence of secondary particles in the center-of-mass system. However, even the criteria for the selection of nucleon-nucleon collisions are not fully obvious. But in the cases of collisions of a nucleon with a nucleus or of a nucleus with a nucleus, the problem of determining the initial energy becomes still more difficult. It is possible that just the errors made in determining the initial energy result in too many cases from events found in emulsions, to which very high energies are ascribed.

In this connection, of special interest are those cases in which the secondary shower particles produced in the emulsion produce new interactions with energy comparable to the initial energy. For such cases, an attempt may be made to determine the energy of these secondary generating particles in the usual way by the angular divergence of the produced particles and to compare it with the energy of the primary particle.

Below, are described two interesting events with a number of secondary interactions found in emulsions exposed in the stratosphere in the autumn of 1955 during an expedition in the Po valley an obtained through the kindness of Professor C. F. Powell.

A microprojection of one of them is given in Fig. 1. The primary particle of $Z=3 \div 4$ (determined by grain counting along the track, by photometering it

and also by the δ-electrons) produced in the emulsion an interaction of a type $20 + 79Z$. From the angular distribution of secondary relativistic particles it was found ($\lg \gamma_c = -\lg \operatorname{tg} \theta$) that ${}_1\gamma_c = 15$. In order to coordinate this value ${}_1\gamma_c$ with the number of produced relativistic particles (according to the FERMI-LANDAU (*) theory) $n_s = 2A \cdot l \cdot \sqrt{\gamma_c}$ (A is the mass number of the incident nucleus and l is the ratio of the lengths of column of nuclear matter in the incident nucleus and in the target nucleus, with which the interaction took place), it is necessary to take $l=2$ for this case. Thus, we find that the primary particle had an energy $E_0 \approx (6 \div 8) \cdot 10^{11}$ eV/nucleon, (i.e. its total energy $\sim (4 \div 6) \cdot 10^{12}$ eV).

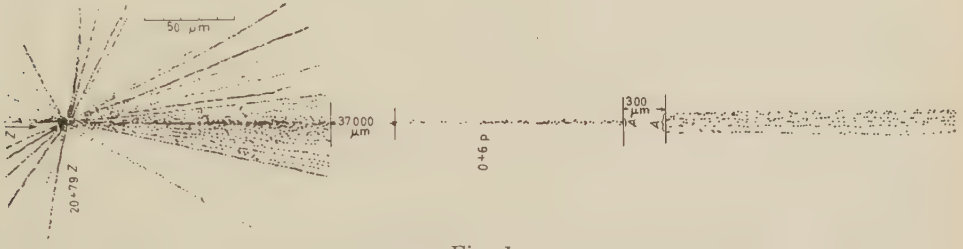

Fig. 1.

A shower of secondary particles pass in the emulsion a distance of 4.5 cm. Among the interactions produced by the secondary particles, of greatest interest is the type 0 + 6p interaction. This interaction is apparently of the nucleon-nucleon type, and for it from the angular distribution of the particles ${}_2\gamma_c \approx 100$ and hence the energy of the proton that produced it is found to be close to $2 \cdot 10^{13}$ eV, i.e. 30 times greater than the energy per nucleon in the primary particle.

Although in this case, the number of secondary particles is equal only to 6, it is difficult to believe that due to statistical fluctuation in the angular distribution of particles ${}_2\gamma_c$ was found to exceed by 5 to 6 times the true value. The probability of an accidental ejection of all 6 charged particles in such a narrow angle is considerably less than one per cent.

It is also difficult to suppose that the angular distribution of particles in the initial interaction gives a greatly reduced value of ${}_1\gamma_c$. This assumption contradicts the value of the energy transferred to the π^0-mesons in the interaction. Twenty-three V tracks were found within the limits of the angle that corresponds in the center-of-mass system to the forward cone of the particles of the given shower. If they are all regarded as electron-positron pairs, and and their energy is estimated from the divergence angles of the particles and if we calculate the total energy of the photons (taking into account the

(*) With respect to the number of particles produced, the conclusions of the Landau theory coincide with those of the Fermi theory.

probability of their conversion in the emulsion) it will be found that the total energy conveyed to the π^0-mesons does not exceed $2 \cdot 10^{11}$ eV. This value appears too small, if we assume that the sum of the energy of the nucleons of the primary is $2Z$ times the energy of the proton that caused the secondary interaction (i.e. $2 \cdot 10^{11}$ eV) and consequently it exceeds 10^{14} eV.

At present, there are indications that usually in the shower the component of the momentum of generated particles in a direction perpendicular to the track of the primary particle has a value, which has the magnitude $\sim 1.5\ \mu c$. From this fact it is possible to determine the total energy of the charged particles generated in the initial interaction. In this case, we find that $\sum E_{\pm} \sim 10^{12}$ eV, which is an entirely natural value if the total energy of the primary particle is $(4 \div 6) \cdot 10^{12}$ eV, but too small if its energy is 10^{14} eV.

Thus, we arrive at the conclusion that the energy of secondary interaction $0+6p$ as determined from angular distribution of particles is considerably overestimated, though it is, apparently, a nucleon-nucleon interaction. This conclusion is also supported by the small number of shower particles in this interaction.

The second case of nuclear interaction with secondary processes found in the emulsion stack P is caused by a heavy primary particle of $Z = 15 \div 20$ (Fig. 2).

Fig. 2.

In the initial interaction there were formed two relativistic alpha particles and 31 fast singly-charged particles. No slow secondary particles were observed. The beam of secondary particles penetrates ~ 4cm in the emulsion of the stack.

The secondary particles are rather sharply divided into two cones: a very narrow cone containing 10 singly-charged particles and two alpha particles emerging at angles $\lesssim 5 \cdot 10^{-3}$ rad and a broad cone with angle of emergence > 0.03 rad.

If we consider that the narrow and broad cones correspond to the forward and back cone in the center-of-mass system, then γ_c is about 200 and the energy of the primary particle about 10^{14} eV per nucleon. Such a high value of the energy seems to us to be rather improbable. The very great discrepancy between the narrow and broad cones is a factor against this assumption.

For this reason, we believe that the narrow cone is formed by nucleons and two alpha particles that arise from the nuclear desintegration of the primary particle, while the broad cone mainly consists from generated mesons. Using this model, the primary particle is found (from divergence angles of

the particles of the broad cone) to have a value $\gamma_c \approx 10$ and an energy equal to $\sim 2 \cdot 10^{11}$ eV per nucleon.

If this picture is valid, this means that the narrow cone is a beam of 10 protons with identical energy $\sim 2 \cdot 10^{11}$ eV and two alpha particles of the same energy per nucleon. Within the limits of this cone there should be approximately as many neutrons with the same energy.

A study of the emulsion within the limits of the narrow cone showed five secondary interactions for which determinations of the values γ_c were made (from the angular distribution, and the determination of the values of l and the energy of the particles that generated these secondary interactions from γ_c and the number of shower particles. These data are given in the following Table I.

TABLE I.

	Secondary interactions	γ_c	l	Energy (GeV/nucleon)
1	24+13p	5.5 ± 1.5	4 ± 1.5	250 ± 170
2	3+ 8n	23 ± 8	~ 1	$1000\ ^{+1000}_{-\ 500}$
3	3+11p	13 ± 3.5	2 ± 1	700 ± 500
4	3+35α	12.5 ± 2	1.5 ± 0.3	450 ± 170
5	6+11 (?)	2.5 ± 1	$\leqslant 7$	$\leqslant (85\ ^{+85}_{-55})$

The initial interaction: $E_0 = (200 \pm 90)$ GeV/nucleon.

The last interaction was formed near the initial interaction, where the particles of the narrow cone did not have time to diverge, and therefore it is impossible to determine in this case whether it is caused by a charged or a neutral particle. For it the value γ_c is possibly reduced by 10 to 20%. If we disregard this case, we see that the energies of the secondary generating particles determined from the angular distribution of secondary particles on the assumption of the interaction of nucleons with the «column» differ from each other within the limits of the experimental errors. However, in the last case, the value E_0 differs from the value averaged over all the remaining interactions (300 GeV/nucleon) by approximately a twofold probable error.

Thus, these data show, that the determinations of the energy of the primary particles on the assumption of the formation in a nuclear interaction of a single system with symmetrical divergence of secondary particles in the centre-of-mass system can quite easily lead to great errors in the evaluation of the energy of the primary nucleon.

The contradiction in the evaluation of the energy (of at least one order of magnitude) established in the first case, suggests that the usual conceptions concerning the mechanism of nuclear interactions at high energies are not sufficient for an explanation of such cases.

SUPPLEMENTO AL VOLUME VIII, SERIE X
DEL NUOVO CIMENTO

N. 2, 1958
2° Trimestre

Large Bursts Investigation and High Energy Particles (10^{12} eV ÷ 10^{13}) eV Interaction with Light Nuclei.

N. L. Grigorov, V. Y. Šestoperov,
V. A. Sobinjakov and A. V. Podgurskaja

Moscow State University - Mos ow

Bursts at an altitude 3200 m above sea level were studied.

The apparatus shown on Fig. 1 was used. It consisted of 44 ionization chambers made of brass. The chambers were filled with spectrally pure argon up to a pressure of 5 atm + 2% of nitrogen.

Each chamber was connected with its own amplifier. This enables to record the magnitude of bursts ranging from 100 to 50000 relativistic particles.

Below we shall deal only with bursts recorded simultaneously by two trays of chambers. According to our data, the integral spectrum of such bursts in the interval from 600 to 6000 particles may be represented by the formula $n(\geqslant N) = A/N^{\gamma}$ with the exponent $\gamma = 1.6 \pm 0.2$. Here N is the number of particles which have produced a given burst.

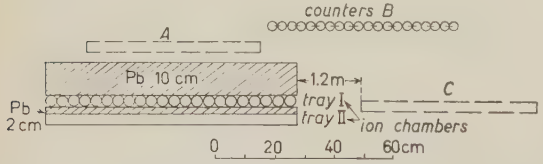

Fig. 1. – The apparatus used for the investigation of bursts.

Our data show that the probability for a burst to be accompanied by an air shower is (91 ± 5)%. In different series of experiments the counters were placed at various distances from the apparatus (positions A, B and C at Fig. 1), and thus could evaluate the average number of particles N_s in a shower, accompanying a given burst. Therefore we could find the distribution of the frequencies with which the bursts of a given size were accompanied by showers of a given density.

The results are shown on Fig. 2. The number of particles N_s in the air shower accompanying bursts with the number of particles from 1000 to 5000 is plotted on the abscissa. On the ordinate (curve 1) the number of particles with $E \geqslant 6.10^{11}$ eV accompanied by air showers with number of particles

greater than N_s is plotted. Curve 2 of this figure gives the absolute number of extensive air showers with the number of particles $> N_s$ traversing 1 cm² per second at the altitude observation.

The abscissa of the point of intersection of curves 1 and 2 gives the number of particles in the shower, in which there is one nuclear-active particle of energy $E \geqslant 6 \cdot 10^{11}$ eV at the level of observation.

As may be seen from Fig. 2, in showers with $N_s \geqslant 3\ 10^4$ particles there is only one particle with this energy.

Since we know the probability for the burst to be accompanied by air showers, we may estimate the collision mean free path — $R_{\text{c.m.f.p.}}$ for particles of energy of the order of 10^{12} eV.

In fact,

$$N_t(x) = kN_p(\geqslant E, 0) \exp\left[-(x/R_{\text{a.m.f.p.}})\right]$$

$$N_{\text{n.s.}}(x) > kN_p(\geqslant E, 0) \exp\left[-(x/R_{\text{c.m.f.p.}})\right],$$

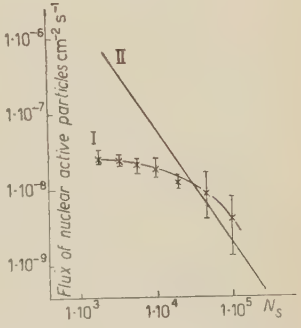

Fig. 2. – The flux of nuclear active particles (curve I) and the number of extensive air showers with number of particles exceeding N_s (curve II) versus N_s.

$N_{\text{n.s.}}(x)/N_t(x) > \exp\left[-x(1/R_{\text{c.m.f.p.}} - 1/R_{\text{a.m.f.p.}})\right]$ there N_t is the total number of all bursts. $N_{\text{n.s.}}$ is the number of bursts not accompained by air showers and $R_{\text{a.m.f.p.}}$ is the absorption mean free path.

This estimate gives $R_{\text{c.m.f.p.}} < 859$ cm^{-2}.

The use of ionization chambers having a diameter of 4 cm that cover a relatively large area enables to observe cases of bursts produced simultaneously in two and in even more chambers separated from each other by a considerable distance, with no ionization in chambers between them. We call such bursts « structural » bursts. A typical example of « structural » bursts is given on Fig. 3. Ionization pulses that produce the structure of the bursts usually differ from each other but slightly.

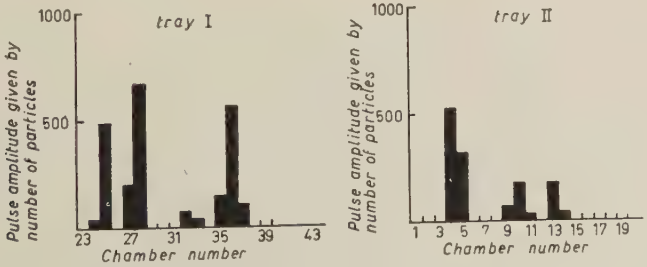

Fig. 3. – A typical example of a « structural » burst.

The total fraction of structure bursts amounts to $(19 \pm 4)\%$ of bursts with a number of particles $N \geq 1000$. Herefrom we conclude that roughly in 50% of recorded bursts several nuclear-active particles fall simultaneously on our apparatus.

This suggests that the interaction of particles of energy $(10^{12} \div 10^{13})$ eV with light nuclei may be schematically represented as being divided into two classes of interactions. One class corresponds to a relatively weak interaction, as a result of which the nuclear-active particle loses but a small part of its energy. The second class corresponds to a strong interaction in which the greater part of the « primary » particle energy is lost. The showers containing several high energy nuclear active particles that produce structural bursts are due to interactions of the second type.

We would like to make the following remark: if such a mechanism of interaction is extrapolated to the region of superhigh energies, responsible for the production of extensive air showers, then we can easy explain quantitatively such characteristics of showers as 1) the altitude dependence of showers; 2) the spectrum of shower densities; 3) the absolute number of extensive air showers.

A more detailed account is to be published in *Žu. Éksper. Teor. Fiz.*

SUPPLEMENTO AL V LUME VIII, SERIE X
DEL NUOVO CIMENTO

N. 2, 1958
2° Trimestre

Photographic Plates Investigation of the High-Energy Particles Interaction with Lead Nuclei.

S. I. Brikker, N. L. Grigorov, M. A. Kondrateva, A. V. Podgurskaja, A. I. Saveleva, V. A. Sobinjakov and V. Y. Šestoperov

Moscow State University, Moscow

The lateral distribution of shower particles in a plane perpendicular to the shower axis in the vicinity of the axis may be expected to reflect the angular distribution of streams of energy imparted to π^0-mesons in the process of their generation.

We studied the lateral distribution of electrons in showers generated in lead by nuclear-active particles of high energy, using electron-sensitive photographic plates with an emulsion layer of thickness 200 μm.

The photographic plates were placed into a special apparatus under a 10 cm thick lead absorber. Fig. 1 gives a schematic view of the apparatus which contained the photographic plates.

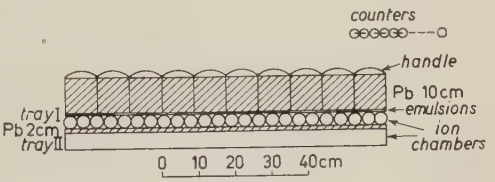

Fig. 1. – A schematic view of the apparatus

The apparatus consisted of two trays of ionization chambers having the length of 90 cm and the diameter 4 cm. The chambers of one tray were placed perpendicular to those of the other tray.

Each chamber was connected with its own amplifier.

When the chambers of both trays recorded a sufficiently big burst (equivalent to more than 100 relativistic particles) we removed the photogra-, phic plate corresponding to the intersection of the chambers giving coinciding bursts.

A new plate was inserted in place of the removed one, which was sent for development.

This procedure enables us to restrict ourself in the investigation only to those

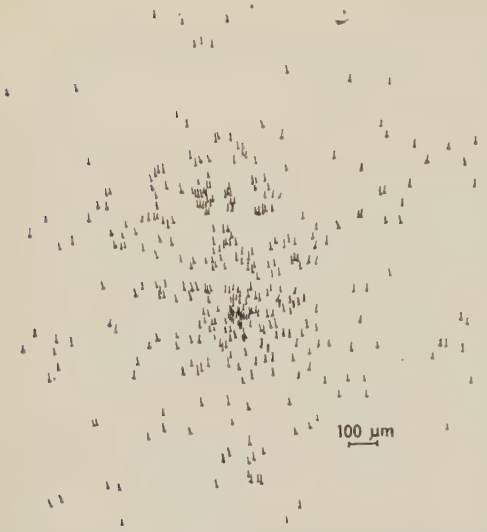

Fig. 2. – A view of a typical shower. Each dash is a single particle.

plates through which sufficiently large showers have passed. Besides, it gives the possibility of determining the place on the plate on which we should look for the shower. This shortens the time of examination of photographic plates.

The use of ionization chambers gives also certain supplementary data concerning the shower, the age of the given shower, and its correlation with air showers. (The apparatus had an additional tray with 10 counters connected with a hodoscope).

The experiment was performed at an altitude of 3200 m above sea level.

At the present time, only a small part of the showers that were found has been analysed.

Fig. 2 shows a typical shower. In this shower, 540 shower particles (after subtraction of background particles) were detected within a radius of about 1000 μm. The lateral distribution of particles of this shower and three other showers looks practically the same and is shown in Fig. 3 in double logaritmic scale (curve 1). The different points refer to four different showers normalized to the same total number of particles. The points on which errors are indicated show averaged lateral distribution. As

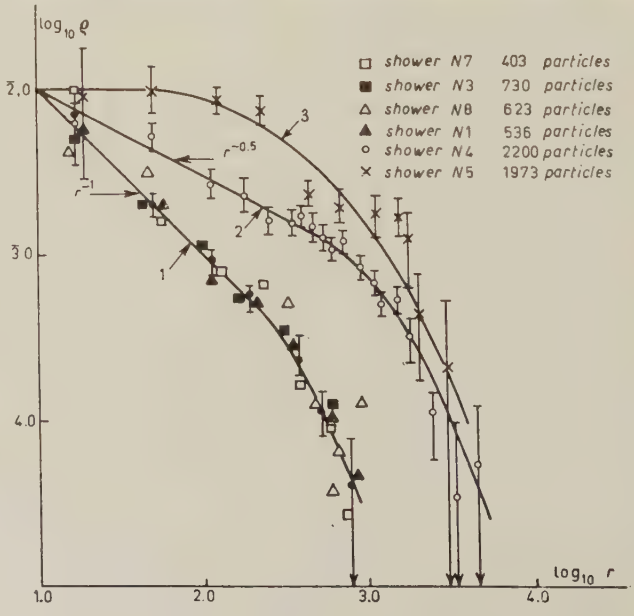

Fig. 3. – The logarithm of density ϱ of shower particles versus the logarithm of distance r from the shower axis. (ϱ is the number of particles per one micron square.)

may be seen from Fig. 3, the lateral distribution up to distances of 300 μm may be represented by the law $\varrho(r) = A/r$ (curve 1).

Among the six analyzed showers with the number of particles from 500 to 2000 there are observed large fluctuations in the lateral distribution of shower particles (within a radius of 100-300 μm. Curves 2 and 3).

Of special interest is the seventh shower. This shower is shown in Fig. 4. Clearly visible are three cores.

The continuations of the cores of all showers intersect at one point. This proves that all three showers

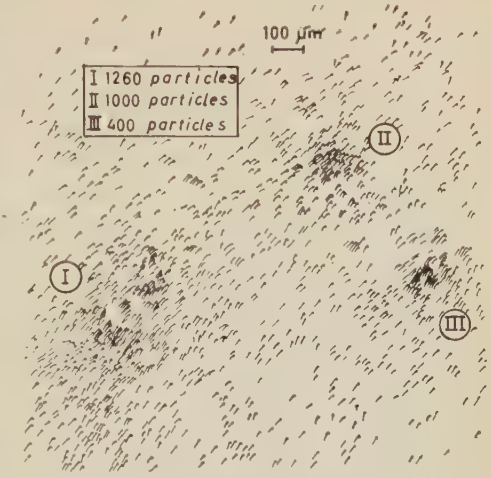

Fig. 4. – The shower consisting of three cores.

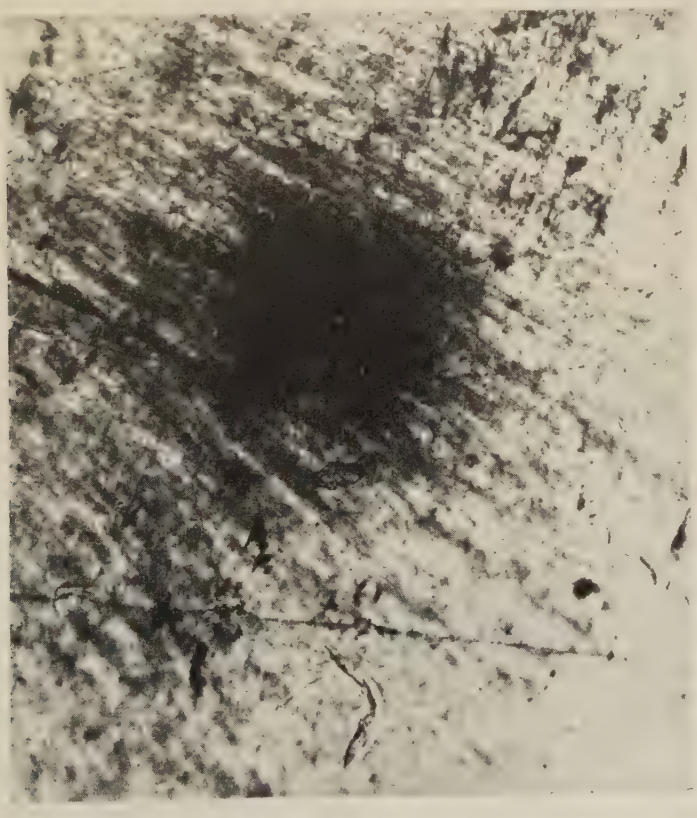

Fig. 5. – The central part of the shower consisting of about 200 000 particles.

were produced by three different π^0-mesons that were formed in the same nuclear interaction. It is possible to determine the minimum value of energy of theese π^0-mesons. Starting from the number of particles in each shower, it is possible also to determine transverse momenta of π^0-mesons from the angular divergence of the showers.

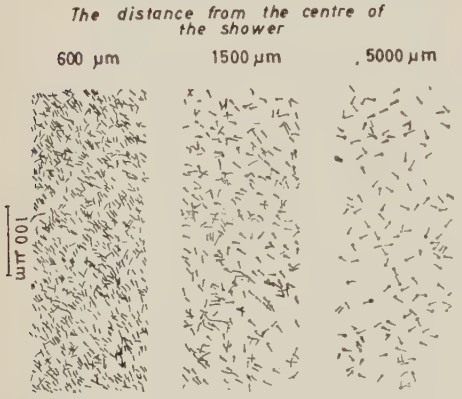

Fig. 6. – The density of the particles at the different distances from the shower axis consisting of about 200 000 particles.

Relatively to the shower axis I the transverse momenta of the π^0-mesons that produced showers II and III are $2.7 \cdot 10^9$ eV and $1.2 \cdot 10^9$ eV respectively.

The eighth shower has not yet been fully analyzed. Tentative data show that it contains about 200 000 particles. A photograph of the central part of this shower is shown in Fig. 5. An idea of the density of the shower may be obtained from Fig. 6 which shows the variation of particle density with distance from the centre of the shower.

The estimation of the energy gives the value, which exceeds $3 \cdot 10^{13}$ eV.

SUPPLEMENTO AL VOLUME VIII SERIE X
DEL NUOVO CIMENTO

N. 2. 1958
2° Trimestre

Investigation of Interaction at Extremely High-Energies Using the Analysis of Extensive Air Showers.

A. E. Čudakov, N. A. Dobrotin,
N. L. Grigorov, G. N. Vernov and G. T. Zacepin

P. N. Lebedev Physical Institute of the USSR Academy of Sciences
Moscow State University - Moscow

In the present paper we wish to summarize the conclusions, which, in our opinion, can be drawn on the basis of the data obtained in investigation of extensive air showers.

One can obtain the following characteristics of the processes at extremely high energies.

1) The interaction cross section, $\sigma = \text{const}/R_{\text{cmfp}}$ where R_{cmfp} is the collision mean free path.

2) The energy distribution of secondary particles:

$$\frac{\mathrm{d}N_{\text{n.a.}}}{\mathrm{d}E_{\text{n.a}}^{\text{sec}}} = f(E_{\text{n.a}}^{\text{sec}}) ,$$

where $\mathrm{d}N_{\text{n.a}}$ is the number of secondary nuclear active particles with energy between $E_{\text{n.a}}^{\text{sec}}$ and $E_{\text{n.a}}^{\text{sec}} + \mathrm{d}E_{\text{n.c}}^{\text{sec}}$.

The investigation of extensive air showers can also verify our hypothesis concerning the possibility of extrapolating to extremely high energies of our conclusion which was obtained when investigating cosmic rays in the stratosphere, namely the conclusion that the predominant part of primary particle energy is transferred to some one of the secondary nuclear particles, which most probably is a nucleon [1].

3) The angular distribution of the energy fluxes of secondary particles, which are generated in the interaction of a particle of extremely high energy

with the atomic nucleus of the atmosphere:

$$\frac{\sum_i^{sec} E(\theta)}{E_{prim}} = F(\theta).$$

4) The variation of characteristics, enumerated above, with the primary particle energy.

1. – Interaction cross section.

a) The collision mean free path of primary particles can be obtained by means of a study of fluctuations in Čerenkov radiation of extensive air showers in the atmosphere for the showers with a given total number of particles (for the further details see the paper by ČUDAKOV *et. al.* submitted to this conference).

b) The collision mean free path of high energy particles can also be obtained from the ratio of the number of cases when the nuclear active particle is not accompanied by the air shower to the total number of nuclear active particles in the same energy region (for further details see paper by GRIGOROV *et al.*, submitted to this conference).

Since the area covered by the ionization chamber was small and the duration of measurements was also small, we could obtain the data on the nuclear-active particles only for energy of 10^{12} eV. The collision mean free path was found to be < 85 g/cm^2. The simbol $<$ means that a part of showers generated in the upper atmosphere could not be recorded by our counters.

c) The absorption mean free path ($R_{c\,afp}$) can be determined for the region of very high energies. Since the interaction path is shorter than the absorption path, we can determine the upper limit for the first one.

From the data obtained by HRISTIANSEN and collaborators at sea-level and by NICOL'SKIJ and collaborators at 3860 m it follows that the flux of nuclear active particles with energy exceeding 10^{14} eV is equal to 0.01 h^{-1} m^{-2} and 0.1 h^{-1} m^{-2} at sea-level and at 3860 m respectively.

From the comparison of this data with the total number of primary cosmic ray particles having such energy (36 h^{-1} m^{-2}) it follows that the absorption mean free path is equal to 120g/cm^2.

d) Already in 1949 one of us (G.T.Z.) suggested to use the data on the altitude dependence of extensive air showers for the determination of the upper limit for the collision mean free path.

At present [2] it is known that the altitude dependence of extensive air sho-

wers in the energy interval of from 10^{14} eV to 10^{18} eV is characterised by a path $\Lambda = (90 \div 140)$ g/cm^2. It follows from this that the interaction mean free path of primary cosmic ray particles with the nuclei of nitrogen atoms is undoubtedly less than Λ.

Since the collision mean free path within the interval of $(10^{11} \div 10^{14})$ eV and the absorption mean free path in the interval of $(10^{11} \div 10^{15})$ eV are pratically constant, we suggest that for the purpose of further analysis it is reasonable to assume that the collision mean free path of protons with nitrogen nuclei is constant and equal to 70 g/cm^2 also in the region of extremely high energies.

2. – Energy distribution of secondary particles.

Let us assume that the fluctuations in energy losses in interactions are small. If the mean path between two interactions is equal to 70 g/cm^2 than the fact that the altitude dependence of the extensive air showers is characterized by the value 140 g/cm^2 can be explained by the assumption that the path of each individual cascade is practically equal 200 g/cm^2.

Thus the part of the energy which the nuclear active particle loses in one interaction is given by the ratio of the collision mean free path to the mean free path to the absorption of an individual cascade. This is $70/200 = 0.35$.

In order to obtain more detailed information about the character of the interaction acts, J. P. Ivanenko and E. V. Gorčakov have calculated the energy spectra of the nuclear-active particles using the method of successive generations [3].

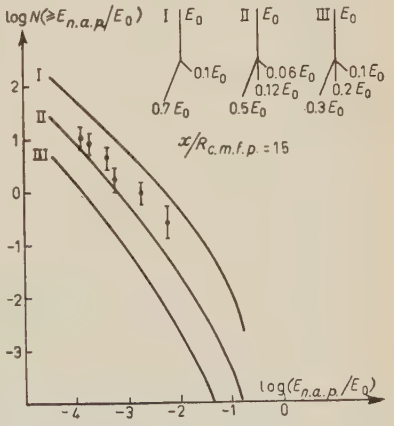

Fig. 1.

The Fig. 1 shows some results of these calculations, as well as some experimental data obtained by Hristiansen *et al.*

From the figure can be seen that the curve corresponding to the case when one of the secondary particles retains about 50% of the primary particle energy gives the best agreement.

However, if the fluctuations of the values of the energy losses in the interaction acts are large (as it is supposed in the paper by Grigorov *et al.*) then the energy losses will be greater.

3. – Angular distribution of secondary particle energy fluxes in the interaction act.

V. I. ZACEPIN carried out the calculations of the lateral distribution of particles basing on assumptions on angular dependence of the fluxes of energy of the secondary particle.

The idea of these calculations is that the shower caused by a primary particle with energy E is equal to the sums of showers produced by all the secondary particles generated in the first interaction act.

It is known from experiments on extensive air showers that the lateral distribution $\varrho(r)$ does not depend on the primary energy and that in the region $1m < r < 10m$ of the shower the particle density is inversely proportional to the distance from the axis: $\varrho(r) \sim 1/r$.

Therefore, in order to determine the lateral distribution of the particles of showers generated by the primary particle with energy E (according to the above assumptions) it is necessary to sum the extensive air showers generated by the secondaries.

The axis of these extensive air showers are distributed according to $F(\theta)$.

Calculations show that independent from the assumptions about the type of the function $F(\theta)$ for the agreement with the experimental data it is necessary to assume that the angle $\theta_{\frac{1}{2}}$ including a half of the energy fluxes of secondary particles is always approximately the same, i.e. 10^{-4} rad. for primary particles with energy 10^{14} eV.

If the lateral distribution for distances shorter than 1 m is also inversely proportional to the distance, than this angle should be less than 10^{-4} rad.

Besides, in the above analysis the deviation of the secondaries from the direction of the primaries has been taken into account only in the first act.

Therefore $\theta_{\frac{1}{2}}$ is apparently substantially less than 10^{-4} and, consequently, on the average $P_{\perp} \lesssim 10^{9}$ eV/c.

In principle similar estimates of the transverse momenta can be made by the comparison of the lateral distribution and of the absorption of the extensive air showers.

The absorption of an individual shower in a thin layer of air is determined by the energy spectrum of the soft components alone, because it is known that no small energy electrons are generated in nuclear collisions. Thus, the mean value of the exponent of the energy spectrum s can be obtained.

The lateral distribution of electrons is also determined by s alone, if the angular divergence of nuclear active particles is sufficiently small.

The experimental data ensure a satisfactory explanation of the mean absorption and of the mean lateral distribution by the single parameter s.

Therefore $p_{\perp}$ is sufficiently small to give no observable influence on the lateral distribution of the electrons.

4. – The variation of characteristics on primary particles.

The investigation of characteristics of the separate individual showers including the measurements of total number of particles in them enables us to study the dependence of their characteristics on the energy of primary particles.

Some preliminary results which were obtained both in our experiments and in experiments of other authors indicate the change of properties of showers with the change of the number of shower particles. It is quite possible that this means that our conclusion concerning the conservation of a greater part of primary energy on a single particle ceases to hold when we go over to extremely high energies.

REFERENCES

[1] S. N. Vernov and N. L. Grigorov: *Suppl. Nuovo Cimento*, **4**, 879 (1956).
[2] G. Clark, J. Earl, W. Kraushaar, J. Linsley, B. Rossi and F. Scherb: in this issue, p. 623; T. E. Cranshaw, W. Galbraith, N. A. Porter, J. de Beer and M. Hillas: in this issue, p. 567.
[3] G. T. Zacepin: *Oxford Conference on Extensive Air Showers* (1954).

INTERVENTI E DISCUSSIONI

— H. Messel:

Vernov's results are of considerable interest to me for nearly seven years ago we worked out a theory of nuclear development in which an absorption mean free path of 120 g/cm² and an interaction mean free path of about 65 g/cm² were used. This theory was based on ideas originally proposed by Jánossy and Heitler, however, with the difference that no specific model of meson production was assumed. The cross sections used were such that in the original nucleon-nucleon interaction about 70% of the energy was retained by the two nucleons; the remaining one third of the energy went into the production of one or more mesons. This theory though giving good agreement with many experimental results available at the time, was put into the background by the statistical theories of meson production. To-day the picture seems to have reversed again and it appears that extensive shower theory might be explained using an essentially multi-shot (bremsstrahlung type) model of cascade development such as that originally developed by us.

Our theory can be found in various publications but is partially summarized in *Progress of Cosmic Ray Physics*, **2** (Amsterdam 1953) and in *Nuovo Cimento*, **10**, 754 (1953).

SUPPLEMENTO AL VOLUME VIII, SERIE X
DEL NUOVO CIMENTO

N. 2, 1958
2° Trimestre

On the Number of Particles Spectrum of Extensive Air Showers.

G. B. Hristiansen and G. V. Kulikov

Moscow State University - Moscow

1. – Introduction.

A study of extensive air showers is of interest not only from the point of view of the investigation of the nuclear-cascade process, but also from the point of view of the investigation of the primary component of cosmic radiation that generates extensive air showers. In this connection, it is interesting to examine the number of particles spectrum of extensive air showers.

Up to the present time, mainly measurements of the spectrum of densities of extensive air showers were carried out, whereas the number of particles spectrum of showers was obtained by recalculation from the obtained density spectrum. However, this method of obtaining the number of particles spectrum of extensive air showers has serious disadvantages. Indeed, as is well known, the density spectrum is obtained from the number of particles spectrum by integration over an extremely broad range, in which the number of particles varies by $2 \div 3$ orders. Due to this fact, the density spectrum cannot reflect all the details in the behaviour of the particle-number spectrum. In this paper a direct study was made of the number of particles spectrum of showers. Measurements were performed at sea level during May 1954.

2. – Description of apparatus and of procedure.

The measurements were carried out on the apparatus used in paper [1] by means of the method of correlated hodoscopes [2], which in principle permits the individual study of each recorded shower.

The apparatus consisted of a large number (more than 1600) of Geiger-Müller counters connected with a GK-6 hodoscope [3]. These counters were

divided into groups, each of which consisted of 24 counters of the same area. Counters of three different areas: 24, 100, and 330 cm², were employed in the apparatus. Forty-seven of such groups of counters were uniformly distributed in the central part (Fig. 1) and nine groups were placed at distances of 15, 20 and 30 m from the centre of the installation. Fig. 1 shows the dimensions and relative position of the groups of hodoscope counters. Using this hodoscope installation it was possible to determine the position of the axis and the number of particles in showers with the total number of particles from $2 \cdot 10^4$ to $2 \cdot 10^6$.

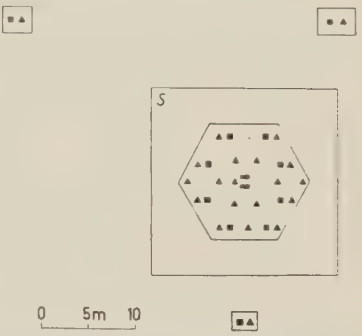

Fig. 1. – Plan of hodoscope arrangement for studying the number of particles spectrum of extensive air showers. □-1) A group of 24 hodoscope counters covering an area of 330 cm² each. △-2) A group of 48 hodoscope counters, of which 24 counters cover an area of 100 cm² each and 24 counters cover an area of 24 cm² each. ▭-3) A group of counters connected to the coincidence circuit.

The unit recorded only extensive air showers producing coincidences in six groups of counters covering an area of 0.132 m² each and positioned in the center of the installation. The hodoscope system enables one to determine the number of triggered counters in different groups of counters during the recording of each shower. Knowing the distribution of the counters that trigger in the plane of observation, it is possible, under certain assumptions, to find the number of particles N and the co-ordinates of the axis in the plane of observation X_0, Y_0. The probability that the recorded shower contains N particles and his axis has co-ordinates X_0, Y_0, when m_i counters out of n_i are triggered in the i-th point with co-ordinates X_i, Y_i is proportional to:

$$(1 - \exp[-\sigma_i \varrho_i])^{m_i} \cdot \exp[-\sigma_i \varrho_i (n_i - m_i)],$$

where σ_i is the area of each counter of the i-th group.

Let us assume [1]:

$$(1) \qquad \varrho_i = KN \cdot f(|\boldsymbol{r}_i - \boldsymbol{r}_0|), \qquad \text{with} \qquad K = 1.8 \cdot 10^{-3}\ \mathrm{m}^{-1},$$

$$f(|\boldsymbol{r}_i - \boldsymbol{r}_0|) = \frac{1}{|\boldsymbol{r}_i - \boldsymbol{r}_0|} \exp\left\{-\frac{|\boldsymbol{r}_i - \boldsymbol{r}_0|}{55}\right\},$$

$$|\boldsymbol{r}_i - \boldsymbol{r}_0| = \{(x_i - x_0)^2 + (y_i - y_0)^2\}^{\frac{1}{2}}.$$

Then the probability that the recorded shower has the inidvidual characteristics N, X_0, Y_0, when experimentally the combination (m_i, n_i) takes place

is proportional to:

$$W(X_0, Y_0, N) = \prod_{i=1}^{56} (1 - \exp[-\sigma_i \varrho_i])^{m_i} \cdot \exp[-\varrho_i \sigma_i (n_i - m_i)] . \tag{2}$$

Thus, the problem of determining the number of particles in the shower and the position of its axis reduces to the following extremum problem. Find the maximum of quantity (2) with respect to the variables N, X_0, Y_0 when the values of the other factors entering into this expression are given.

This problem was solved on the electronic computer at the computation center of the Moscow State University. The value N was found with an accuracy of 10%, while values X_0 and Y_0 were found with an accuracy of 0.5 m.

3. – Results and Discussion.

A total of approximately 3 700 showers were recorded during the 285 hours that the installation operated. In constructing the spectrum, those showers were selected whose axes were found in the region of an area of 400 m² designated in Fig. 1 by the superscript S. The dimensions of this area were prescribed by the necessity of studying the spectrum in the region of large values of N. For this reason, its dimensions were made as great as the hodoscope arrangement would permit. In this connection, the showers with axes in the region S were recorded by the master system with a probability of 100% if the number of particles N in them exceeded 10^5.

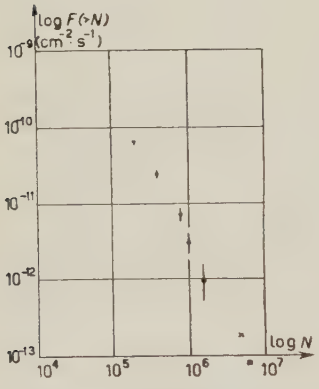

Fig. 2. – An integral number of particles spectrum of extensive air showers.
x- CRANSHAW [4];
⊡- KRAUSHAAR [5].

The number of showers with number of particles $N \geqslant 2 \cdot 10^5$ and with axes within the region S was 270.

The results of the construction of a number of particles spectrum of showers are given in Fig. 2. In the region of values of $N = (2 \div 8) \cdot 10^5$ the spectrum may be represented by a power function with the exponent $\varkappa = 1.5 \pm 0.1$. For values of $N > 8 \cdot 10^5$, the spectrum is more steep. Fig. 2 lists data concerning the absolute intensity of showers with number of particles $4.7 \cdot 10^6$ and $6 \cdot 10^6$ taken from papers [4] and [5].

Taking into consideration these experimental data we find that in the region of values of $N = (8 \cdot 10^5 \div 6 \cdot 10^6)$ the spectrum is approximated by a power law with the exponent $\varkappa = 2.2$ (*).

(*) The error in the exponent $\varkappa$ in this region of N depends on the accuracy of the CRANSHAW and KRAUSHAAR data, which is unknown to us.

Thus, one observes a variation of the exponent of the number of particles spectrum in a rather narrow range of variation of the number of particles. Whether the variation of the exponent of the number of particles shower spectrum which we observed is related to the corresponding variation in the form of the primary spectrum in the region of energies 10^{16} eV or whether it may be explained by peculiarities in the mechanism of the development of showers with the number of particles $\gtrsim 10^6$, may be established only after more experimentation. It is necessary to determine, for instance, the absorption coefficient of showers with the number of particles $\gtrsim 10^6$.

* * *

Note added in proof. – Using the results of the paper [6] one may find that the exponent of an integral number of particles spectrum is $\varkappa = 2.3 \pm 0.3$ in the region of values of $N = (1 \div 3.5) \cdot 10^6$.

REFERENCES

[1] A. T. Abrosimov, V. I. Zacepin, V. I. Soloveva, G. B. Hristiansen and P. S. Čikin: *Izv. Akad. Nauk SSSR, Ser. Fiz.*, **19**, 677 (1955).

[2] N. A. Dobrotin, G. T. Zacepin, S. I. Nikol'skij, L. I. Saryčeva and G. B. Hristiansen: *Izv. Akad. Nauk SSSR, Ser. Fiz.*, **19**, 666 (1955).

[3] L. N. Korablev: *Instr. and Techn. of Exper.*, **2**, (1956).

[4] T. E. Cranshaw: *The Cosmic Ray Conference*, (1955), Mexico.

[5] W. Kraushaar: *The Oxford Conference* (1956), p. 28.

[6] G. Clark, F. Earl, W. Kraushaar, F. Linsley, B. Rossi and F. Scherb: *Nature*, **180**, 406, (1957).

SUPPLEMENTO AL VOLUME VIII, SERIE X
DEL NUOVO CIMENTO

N. 2, 1958
2° Trimestre

On the Multiple Production of Particles in Weak Interaction of Nucleons by Means of their Excitation.

G. T. Zacepin

P. N. Lebedev Physical Institute of the USSR Academy of Sciences - Moscow.

It is ordinarily assumed that in the collision of nucleons there takes place a formation of a certain joined system into which enters the whole energy of the nucleons that collided (or a considerable part of this energy) while the break up of this system leads to the production of particles. An appreciable part of the experimental data obtained during the past ten years can indeed be described satisfactorily on the basis of this mechanism.

However, when the energy of the colliding nucleons is high, there is another possible mechanism of multiple production of particles to which the author pointed some seven years ago. (*)

This mechanism consists in the following. The interacting nucleons of high energy exchange a small portion of their momenta and energy. During this process one or both of the nucleons become excited, and then the excited state of the nucleons leads to the production of particles.

The process may be described through the values of the transferred momenta and energy as follows.

Prior to interaction the nucleon had a mass m, and energy $E_0 = \gamma_0 mc$, and a momentum $p_0 = \sqrt{\gamma_0^2 - 1}\, mc$. After interaction, the mass of the excited nucleon becomes $M = Km$, the energy $E_1 = \gamma_1 Mc^2$, and the momentum $p_1 = \sqrt{\gamma_1^2 - 1}\, Mc^2$. The change in energy $E_1 - E_0$ may be written as

$$E_1 - E_0 = mc^2(K\gamma_1 - \gamma_0) = \varepsilon mc^2 . \tag{1}$$

The change of momentum $p_1 - p_0$ is:

$$p_1 - p_0 = mc(K\sqrt{\gamma_1^2 - 1} - \sqrt{\gamma_0^2 - 1}) = qmc . \tag{2}$$

(*) Report at a seminar in P. N. Lebedev Physical Institute of the USSR Academy of Sciences, 1950.

From (1) and (2) we find:

$$K = \sqrt{\gamma_0}\cdot\sqrt{2\left(\varepsilon - q\sqrt{1-\frac{1}{\gamma_0^2}}\right) + \frac{1}{\gamma_0}(1 - q^2 + \varepsilon^2)}\,, \tag{3}$$

$$\gamma_1 = \frac{\sqrt{\gamma_0}(1 + \varepsilon/\gamma_0)\,.}{\sqrt{2(\varepsilon - q\sqrt{1-1/\gamma_0^2}) + 1/\gamma_0(1 - q^2 + \varepsilon^2)}} \tag{4}$$

If $\gamma_0 \gg 1$, the equations are simplified:

$$K \simeq \sqrt{2\gamma_0(\varepsilon - q)} \tag{5}$$

$$\gamma_1 \simeq \sqrt{\frac{\gamma_0}{2(\varepsilon - q)}}\,. \tag{6}$$

The solution shows that in the case of large γ_0 the nucleon can get strong excitation ($K \gg 1$), even if $(\varepsilon - q)$ is small. The break up of the excited system leads to the production of particles. The possible number of produced particles is determined by the number K, and the half angle of their emergence by the value $\theta_{\frac{1}{2}} = 1/\gamma_1$. A nucleon which was before the collision at rest in the laboratory system can undergo similar excitation and decay.

The problem of the possibility of a new mechanism of the multiple production of particles with a small transfer of momentum has again become of interest in view of the new experimental data. Studies of air showers conducted by our group during recent years give some indications to an increase in energy loss by nucleons in the range of energies $10^{14} \div 10^{15}$ eV. Apparently, cases have been found in photographic emulsions when one particle produces at first a shower with a very wide-open cone of shower particles, and then a shower with an unusually narrow cone of shower particles.

From the point of view of the above mentioned, both of these facts are easily explained. Disintegration of strongly excited nucleons leads to the production of numerous particles of relatively small energies. The decay of an excited nucleon which was at rest before the collision leads to the formation of a broad shower, while the excitation and subsequent decay of a nucleon that was in motion prior to collision leads to an anomalously narrow shower.

The formation of two independent excited systems in the interaction of nucleons may, generally speaking, take place in the case of peripheral collisions of nucleons when the virtual π-meson of one nucleon hits another nucleon.

However, this process is possible practically at any energy of the incident nucleon ($E_0 \geqslant 10^{10}$ eV). In addition, in this case the value $\varepsilon - q$ on the

average should not be too small ($\simeq \frac{1}{6}$) due to the relatively large mass of the π-meson, so that the difference in width of the cones of the generated showers should not be especially large (six times, on the average).

The above-mentioned experimental data permit to assume a special process that begins at very high energies ($E_0 \gtrsim 10^{11}$ eV) and that leads to a very great difference in the width of the generated showers.

If such a process actually exists, it may apparently be related to a « weak » interaction (β forces), the effective cross-section for which may increase rapidly along with energy.

In this case, interaction is accomplished by electron-neutrino pairs and the value of $\varepsilon - q$ for a moving nucleon interacting with one at rest should be of the order of the ratio of the mass of the electron to the mass of the nucleon, that is, $\simeq 10^{-3}$.

In the case of nucleon energy $(10^{14} \div 10^{15})$ eV ($\gamma_0 \simeq 10^5 \div 10^6$), the possible degree of excitation of the nucleon $K \simeq \sqrt{2\gamma_0 \cdot 10^{-3}} \sim 20 : 40$. The width of the shower cone in the case of decay of an excited nucleon which was at rest before the collision should amount to a magnitude of the order of $\theta_{\frac{1}{2}} \simeq \simeq \sqrt{2/(10^{-3} \cdot \gamma_0)} \simeq (1.5 \div 0.5) \cdot 10^{-1}$, while the width of the cone from the disintegration of a nucleon that was moving before the interaction is

$$\theta_{\frac{1}{2}} \simeq \sqrt{\frac{2 \cdot 10^{-3}}{\gamma_0}} \simeq (1.5 \div 0.5) \cdot 10^{-4}.$$

The interpretation of such showers from the point of view of generally accepted conceptions leads to energies (which are determined from the equation $E_0 = 2mc^2/\theta_{\frac{1}{2}}$) in the first case $E_0 \simeq (10^{11} \div 10^{12})$ eV, and in the second $(10^{17} \div 10^{18})$ eV, that is, with errors of 1000 times.

It is quite possible that there can also be observed stars produced simultaneously both by the ordinary interaction and by the interaction of the type under consideration, if in the ordinary interaction only the meson cloud participates and not the nucleon proper.

Due to a lack of sound experimental data on the existence of such a type of process, it is apparently too early to discuss the details of this possible mechanism. However, if the existence of such a mechanism were reliably established, this would be a serious indication of the existence of a new characteristic length of the nucleon which is much smaller than $r_0 \simeq 10^{-13}$ cm.

In this connection, it is necessary to take note of a variant of systematics of the elementary particles made by M. A. Markov, in which nucleons are characterized by dimensions of 10^{-19} cm.

SUPPLEMENTO AL VOLUME VIII, SERIE X
DEL NUOVO CIMENTO

N. 2, 1958
2° Trimestre

On the Three-Dimensional Development of an Electron-Photon Cascade Shower.

V. V. Gužavin, I. P. Ivanenko

Moscow - State University - Moscow

The problem of the one-dimensional development of an electron-photon cascade shower (*) may be considered as completely solved. The method of functional transformations [1] and the method of momenta [2] make it possible to find a sufficiently complete solution of the problem of the behaviour of a shower in light and heavy substances taking account of Rutherford scattering of charged particles and of the dependence of the total absorption coefficient of photons on energy.

The problem of the three-dimensional development of a cascade shower cannot be considered as completely solved. Because of the extraordinary complexity of the initial equations, the distribution function $f(E_0, E, t, \bar{r}, \theta)$ of particles for energy E, depth t, angles θ with the shower axis (+), and the distance $\bar{r}$ in a plane perpendicular to the shower axis, has not been found as yet. Such is also the case with an analytical expression for the function of spatial distribution (×). For the function of angular distribution there has been found an analytical expression, which, however, does not take account of ionization losses [1].

In a number of works (see for example [3]) numerical calculations were made of the function of angular and lateral distribution for various values of t at $E_0 = \infty$ and $E = 0$. However, these calculations are so involved that

(*) We consider the problem of the average behaviour of showers.

(+) We consider the shower axis to be the straight line that continues the direction of motion of the primary particle of energy E_0 that produced the shower.

(×) Throughout the paper, we shall call the function $f(E_0, E, t, \bar{r}, \theta)$ integrated over the angles as the function of spatial distribution; the function $f(E_0, E, t, \bar{r}, \theta)$ integrated over the plane perpendicular to the shower axis is the function of angular distribution.

up to the present time, even an approximate scheme of calculation has not been published.

In the works of [4] the functions of the angular and lateral distribution of particles in the shower were constructed from the moments by the method of graphical selection of an arbitrary function, the first several moments of which coincide with the precise ones. It seems to us that the method of moments is a very promising method for solving the problem of the angular and lateral distribution of particles in a cascade shower.

1. – Let us consider the function $\Phi(r, s)$ that depends on parameter s and a number of other parameters defined on the interval $r[0, \infty]$. Let us assume that when $r \to 0$

$$\Phi(r, s) = \varphi(r, s) r^{s-2} . \tag{1}$$

Here $\varphi(r, s)_{r\to 0} = \text{const} \neq 0$, the value s varies with in the limits $(0 \div 2)$. The moments with respect to r of the function $\Phi(r, s)$ determined by the equality

$$\overline{r^n_\Phi}(s) = \int_0^\infty \Phi(r, s) r^n r \, dr \Big/ \int_0^\infty \Phi(r, s) r \, dr , \tag{2}$$

we believe to be known. Then it will be easy to see that

$$\overline{r^n_\Phi}(s) = \overline{r^{n+s-1}_\varphi}(s) . \tag{3}$$

where the value

$$\overline{r^m_\varphi}(s) = \int_0^\infty \varphi(r, s) r^n \, dr \Big/ \int_0^\infty \varphi(r, s) \, dr ,$$

is the m^{th} moment of the function $\varphi(r, s)$.

We may note that a knowledge of all the moments of a certain function is equivalent to a knowledge of the function itself (the Stielties [5] problem of moments). However, in all cases of practical interest it has not been possible to obtain an explicit analytical expression for the n^{th} moment. It is usually possible to obtain a numerical value for only several of the first moments of the unknown function. For this reason, to calculate the unknown function from the moments it is advisable to approximate it by another function, the first several moments of which coincide with the moments of the unknown function. Let us approximate the function $\varphi(r, s)$ by means of a sum of poly-

nomials:

$$\varphi(r, s) = \exp[-\alpha r^{\beta}] \sum_{n=0}^{N} a_n(s) R_n(\alpha r, s) . \tag{4}$$

The polynomials $R_n(\alpha r, s)$ are orthogonal on the interval $[0, \infty]$ with the weight function $\exp[-\alpha r^{\beta}]$. We shall determine the coefficients of the expansion of $a_n(s)$ from the condition of orthogonality of the polynomials:

$$a_n(s) = \int_0^{\infty} \varphi(r, s) R_n^{+}(r, s)\, \mathrm{d}r \Big/ \int_0^{\infty} \exp[-\alpha r^{\beta}] R_n(\alpha r, s) R_n^{+}(r, s)\, \mathrm{d}r . \tag{5}$$

The coefficients $a_n(s)$ are expressed by means of the moments of the unknown function. It is natural to believe that the coefficient $a_n(s)$ is a linear combination of the first n moments different from zero, therefore the polynomials (taking account of equation (3)) are expressed by the formula

$$R_n^{+}(r, s) = \sum_{m=3}^{n} C_m(s) r^{m+s-1} .$$

It is now easy to write the equations for the determination of the polynomials:

$$\int_0^{\infty} r^{s+kn'-1} \exp[-\alpha r^{\beta}] R_n(\alpha r)\, \mathrm{d}r = \begin{cases} 0 \text{ for } n' < n, \\ \text{const} \neq 0 \text{ for } n' = n , \end{cases} \tag{6a}$$

$$\int_0^{\infty} \exp[-\alpha r^{\beta}] R_{n'}(\alpha r, s) R_n^{+}(r, s)\, \mathrm{d}r = \delta_{n n'} . \tag{6b}$$

Here $\delta_{n\,n}$ is the Kronecker symbol. We may note that (6a) determines the polynomials with an accuracy to the normalization constant. The coefficients α and β are determined from the asymptotical behaviour of the function $\varphi(r, s)$ at $r \to \infty$. If the behaviour of $\varphi(r, s)$ at $r \to \infty$ is not known, then α and β are determined from the condition of equality of the two highest moments (of those used in (4)) of the unknown function that correspond to the moments of the weight function, that is:

$$\int_0^{\infty} \exp[-\alpha r^{\beta}] r^{k}\, \mathrm{d}r \Big/ \int_0^{\infty} \exp[-\alpha r^{\beta}]\, \mathrm{d}r = \overline{r_{\varphi}^{k}} \tag{7}$$

Here k is a certain constant equal to a whole number. Condition (7) signifies that given a big k, the weight function should convey roughly the behaviour of the unknown function $\varphi(r, s)$.

It should be noted that when $\beta = 1$, $k = 1$, $s = 2$, the conditions (6) determine the polynomials that coincide with the polynomials of Laguerre. Putting α equal to the minimum value of the total absorption coefficient of photons $\sigma_{min}(E)$ we will find that the approximated equation (4) coincides with the equation used in works [2] in calculating the dependence of the number of electrons and photons on the energy and the depth in the cascade shower in light and heavy substances. We think that the suggested method of approximation of functions from their known moments may be applied in the solution of a broad circle of problems.

2. – Let us calculate the functions of the angular and lateral distribution of particles at the maximum of the cascade shower. At the maximum of the shower the value of the cascade parameter $s = 1$. It may be shown that at any value of the parameter s the functions of angular and lateral distribution depend on r, θ, and E only in combinations $x_\theta = E\theta/E_s$, $x_r = Er/E_s$ where $E_s = 21$ MeV. In paper [1] it is shown that the function of angular distribution of electrons $P(E_0, E, t, \theta) \to \text{const}$ when $\theta \to 0$, and that $P(E_0, E, t, \theta) \sim \sim \exp[-\alpha r]$when $r \to \infty$. Therefore, in approximating the function

$$P(x_\theta, s) = P(E_0, E, t, \theta)/P(E_0, E, t)\,,$$

by means of equation (4) we must put $\beta = 1$, $s = 2$. Here $P(E_0, E, t)$ is the differential function that describes the one-dimensional development of the shower [1]. Insofar as $N_p(x_\theta, s)$ is an even function, we assume $k = 2$. We determine the coefficient α from condition (7). Then we at last obtain

$$P(x_\theta, 1) = \exp[-\alpha x_\theta] \sum_{n=0}^{k/2} \alpha_n V_n(\alpha x_\theta)\,.$$

Here

$$(8)\quad \begin{cases} V_0(y) = \alpha; \quad V_1(y) = \dfrac{\alpha}{2}(-2 + y); \quad V_2(y) = \dfrac{\alpha}{8}(8 - 7y + y^2); \\ V_3(y) = \dfrac{\alpha}{48}(-48 + 57y - 15y^2 + y^3); \ \ldots \end{cases}$$

The polynomials orthogonal to $V_n(y)$ are determined by the equality (6*b*), their explicit expression is:

$$(8')\quad \begin{cases} V_0^+(y) = y; \quad V_1^+(y) = -y + \dfrac{y^3}{3!}; \quad V_2^+(y) = y - \dfrac{2}{3!}y^3 + \dfrac{y^5}{5!}; \\ V_3^+(y) = -y + \dfrac{3}{3!}y^3 - \dfrac{3}{5!}y^5 + \dfrac{y^7}{7!}; \ \ldots \end{cases}$$

The coefficients a_n are related very simply to the moments of the unknown function:

$$a_0 = 1; \qquad a_1 = -\frac{3!}{2}\left(1 - \frac{\alpha^2}{3!}\overline{\theta^2}\right); \qquad a_2 = \frac{5!}{\alpha^4}\left(1 - \frac{3}{3!}\alpha^2\overline{\theta^2} + \frac{\alpha^4}{5!}\overline{\theta^4}\right)$$

$$a_3 = -\frac{7!}{\alpha^6}\left(1 - \frac{3}{3!}\alpha^2\overline{\theta^2} + \frac{3\alpha^4}{5!}\overline{\theta^4} - \frac{\alpha^7}{7!}\overline{\theta}\right); \ldots$$

In similar fashion, it is possible to compute the integral function (by energy) of the angular distribution of electrons, and also the differential and integral function of distribution of photons.

It is known [6] that when $r \to 0$ the distribution functions $N_\gamma(E_0, E, t, r)\mathrm{d}r\mathrm{d}t$ of the number of electrons with energy greater than E at a depth $t, t + \mathrm{d}t$, which electrons are moving at a distance $r, r + \mathrm{d}r$ from the axis of the shower caused by a primary particle of energy E_0 is proportional to

$$N_\gamma(E_0, E, t, r) \sim 1/r^{2-s}\,. \tag{9}$$

Here s is the cascade parameter determined from condition [1]:

$$\ln E_0/E + \lambda_1'(s)t = 0\,.$$

Throughout this paper we assume that $\ln E_0/E \gg 1$, therefore we may ignore the dependence of s on r. Taking account of (9) we shall represent

$$N_\gamma(x_r, s) = N_\gamma(E_0, E, t, r)/N_\gamma(E_0, E, t)$$

in the form of:

$$N_\gamma(x_r, 1) = f(x, 1)/x\,. \tag{10}$$

Let us approximate $f(x, 1)$ by means of equation (4). Noting that $f(x, 1)$ is an even function, we must put $s = 1$ and $k = 2$. The coefficients α and β are determined by equation (7). For β we obtain a value very close to 0.5. Noting that in paper [7] it was shown that $N_\gamma(E_0, E, t, r) \sim \exp[-\alpha\sqrt{r_r}]$ at $r \to \infty$, we may put $\beta = 0.5$ and determine α from (7). In this case we obtain:

$$f(x_r, 1) = \exp[-x_r^{0.5}]\sum_{n=0}^{kl} a_n R_n(\gamma x_r) \tag{11}$$

Here

$$R_0 = \alpha^2/2; \qquad R_1 = \frac{\alpha^2}{8\,640}(-6 + \alpha^2 x); \qquad R_2 = \frac{\alpha^2}{1.8835\cdot 10^9}(1\,092 - 242\alpha^2 x + 3\alpha^4 x^2); \ldots$$

The polynomials that are orthogonal to $R_n(\alpha r_r)$ are determined by the equality (6*b*); their explicit expression is:

$$(11') \qquad R_0^+ = 1; \quad R_1^+ = -120 + \alpha^4 x^2; \quad R_2^+ = 6.854 \cdot 10^5 - 8.736 \cdot 10^3 \alpha^4 x^2 + \alpha^8 x^4; \ldots$$

Using equation (5) we shall find the following expressions for the coefficients:

$$a_0 = 1; \quad a_1 = -120 + \alpha^4 \overline{r^2}; \quad a_2 = 6.854 \cdot 10^5 - 8.736 \cdot 10^3 \alpha^4 \overline{r^2} + \alpha^8 \overline{r^4}; \ldots$$

Noting that when $r \to 0$, $\Gamma(E_0, E, t_{\max}, r) \sim 1/r$ and $N(_\Gamma E_0, E, t_{\max}, r) \sim 1/r$ it is possible to calculate similary the differential and integral function of the spatial distribution of photons at the maximum of the shower.

2. – Let us calculate the function of angular and lateral distribution of particles in a shower in the case of an arbitrary value of the parameter s. Noting [9], we calculate from equations (4, 5, and 6) the function of spatial distribution of electrons. For polynomials $R_n(\alpha x, s)$ and $R_n^-(x, s)$ we obtain the following expressions:

$$(12) \quad \begin{cases} R_0(\alpha x, s) = \dfrac{\beta}{\varphi_0(s)} \alpha^{s/\beta}; \qquad R_1(\alpha x, s) = \dfrac{\beta}{\varphi_1(s)} \alpha^{s+2/\beta}[-\Gamma_1 + \varphi_0(s)\alpha^{1/\beta - 1} \cdot \alpha x]; \\ R_2(\alpha x, s) = \dfrac{\beta}{\varphi_2(s)} \alpha^{(s+4)/\beta}[(\Gamma_1\Gamma_4 - \Gamma_2\Gamma_3) - (\Gamma_0\Gamma_4 - \Gamma_2\Gamma_2)\alpha^{1/\beta - 1} \cdot \alpha x + \varphi_1(s)\alpha^{2/\beta - 2}(\alpha x)^2]; \ldots \end{cases}$$

$$(13) \quad \begin{cases} R_0^+(x, s) = x^{s-1}; \qquad R_1^+(x, s) = -\dfrac{\Gamma_2}{\varphi_0(s)} \alpha^{-2/\beta} x^{s-1} + x^{s+1}; \\ R_2^+(x, s) = \dfrac{1}{\varphi_1(s)} (\Gamma_5\Gamma_2 - \Gamma_3\Gamma_4)\alpha^{-4/\beta} x^{s-1} + \dfrac{1}{\varphi_1(s)}(\Gamma_1\Gamma_4 - \\ \qquad - \Gamma_0\Gamma)\alpha^{-2/\beta} x^{s+1} + x^{s+3}; \ldots \end{cases}$$

Here

$$\varphi_0(s) = \Gamma_0; \ \varphi_1(s) = \Gamma_0\Gamma_3 - \Gamma_1\Gamma_2; \quad \varphi_2(s) = \Gamma_0(\Gamma_3\Gamma_6 - \Gamma_4\Gamma_5) - \Gamma_2(\Gamma_1\Gamma_6 - \Gamma_2\Gamma_5) + \Gamma_4(\Gamma_1\Gamma_4 - \Gamma_2\Gamma_3); \quad \Gamma_n = [\Gamma(s + n)/\beta]$$

the Euler γ-function. Using equations (5, 12, and 13), we obtain following expressions for the coefficients $a_n(s)$:

$$(14) \quad \begin{cases} a_0(s) = 1; \qquad a_1(s) = -\dfrac{\Gamma_2}{\varphi_0(s)} + \alpha^{2/\beta}\overline{r^2}; \\ a_2(s) = \dfrac{\Gamma\Gamma_2 - \Gamma_3\Gamma_4}{\varphi_1(s)} + \dfrac{\Gamma_1\Gamma_4 - \Gamma_0\Gamma_5}{\varphi_1(s)} \alpha^{2/\beta}\overline{r^2} + \alpha^{4/\beta}\overline{r^4}; \ldots \end{cases}$$

The coefficients α and β were found from equations (7); β was found to be $\simeq 0.5$. Taking account of the results of paper [7], we may put $\beta = 0.5$ and determine α from (7), which is what we, as a rule, took into account in numerical calculations. We assumed the value N in (4) to be equal to $K/2$, where K is the number of the highest moment used in the expression. We may note that from (12) and (13), given corresponding values for s, α and β it is possible to obtain expressions (8) and (11) as particular cases.

4. – In order to pass to numerical calculations of the unknown functions of distribution it is necessary to know several of their first moments. By a method analogous to the one used in papers [4], we obtained recurrent algebraic relations for calculation disregarding ionization losses of n angular and lateral moments of the distribution functions of particles in showers. Using these equations, a calculation was made of the numerical values of the first three even moments of the unknown functions in an interval of values of the cascade parameter s from 0.1 to 2.0. The results of the calculations of the electron moments are given in Table I, of photon moments, in Table II.

TABLE I. – $\overline{\theta^n}$ *and* $\overline{r^n}$ *values for electrons.*

s	$\overline{\theta^2}$	$\overline{\theta^4}$	$\overline{\theta^6}$	$\overline{r^2}$	$\overline{r^4}$	$\overline{r^6}$
0.1	$1.88 \cdot 10^{-1}$	$1.25 \cdot 10^{-1}$	$1.75 \cdot 10^{-1}$	$1.38 \cdot 10^{-2}$	$4.29 \cdot 10^{-3}$	$6.56 \cdot 10^{-3}$
0.2	$2.61 \cdot 10^{-1}$	$2.31 \cdot 10^{-1}$	$4.21 \cdot 10^{-1}$	$3.82 \cdot 10^{-2}$	$2.72 \cdot 10^{-2}$	$8.90 \cdot 10^{-2}$
0.3	$3.17 \cdot 10^{-1}$	$3.31 \cdot 10^{-1}$	$6.98 \cdot 10^{-1}$	$7.14 \cdot 10^{-2}$	$8.19 \cdot 10^{-2}$	$4.30 \cdot 10^{-1}$
0.4	$3.65 \cdot 10^{-1}$	$4.28 \cdot 10^{-1}$	1.01	$1.15 \cdot 10^{-1}$	$1.91 \cdot 10^{-1}$	1.48
0.5	$4.08 \cdot 10^{-1}$	$5.24 \cdot 10^{-1}$	1.34	$1.69 \cdot 10^{-1}$	$3.98 \cdot 10^{-1}$	4.36
0.6	$4.46 \cdot 10^{-1}$	$6.18 \cdot 10^{-1}$	1.68	$2.37 \cdot 10^{-1}$	$7.35 \cdot 10^{-1}$	$1.19 \cdot 10^{1}$
0.7	$4.81 \cdot 10^{-1}$	$7.08 \cdot 10^{-1}$	2.03	$3.21 \cdot 10^{-1}$	1.35	$3.10 \cdot 10^{1}$
0.8	$5.13 \cdot 10^{-1}$	$7.95 \cdot 10^{-1}$	2.39	$4.27 \cdot 10^{-1}$	2.35	$7.98 \cdot 10^{1}$
0.9	$5.41 \cdot 10^{-1}$	$8.77 \cdot 10^{-1}$	2.74	$5.55 \cdot 10^{-1}$	4.18	$1.96 \cdot 10^{2}$
1.0	$5.69 \cdot 10^{-1}$	$9.57 \cdot 10^{-1}$	3.10	$7.24 \cdot 10^{-1}$	7.23	$4.96 \cdot 10^{2}$
1.1	$5.94 \cdot 10^{-1}$	1.03	3.44	$9.37 \cdot 10^{-1}$	$1.29 \cdot 10^{1}$	$1.21 \cdot 10^{3}$
1.2	$6.16 \cdot 10^{-1}$	1.10	3.76	1.21	$2.22 \cdot 10^{1}$	$2.86 \cdot 10^{3}$
1.3	$6.32 \cdot 10^{-1}$	1.16	4.06	1.54	$3.80 \cdot 10^{1}$	$6.54 \cdot 10^{3}$
1.4	$6.54 \cdot 10^{-1}$	1.23	4.36	2.02	$6.70 \cdot 10^{1}$	$1.52 \cdot 10^{4}$
1.5	$6.70 \cdot 10^{-1}$	1.28	4.63	2.62	$1.16 \cdot 10^{2}$	$3.45 \cdot 10^{4}$
1.6	$6.85 \cdot 10^{-1}$	1.33	4.89	3.41	$2.01 \cdot 10^{2}$	$7.66 \cdot 10^{4}$
1.7	$6.99 \cdot 10^{-1}$	1.38	5.12	4.46	$3.45 \cdot 10^{2}$	$1.69 \cdot 10^{5}$
1.8	$7.11 \cdot 10^{-1}$	1.42	5.34	5.82	$5.89 \cdot 10^{2}$	$3.66 \cdot 10^{5}$
1.9	$7.22 \cdot 10^{-1}$	1.46	5.53	7.55	$9.78 \cdot 10^{2}$	$7.67 \cdot 10^{5}$
2.0	$7.32 \cdot 10^{-1}$	1.49	5.69	9.70	$1.59 \cdot 10^{3}$	$1.55 \cdot 10$

In paper [8], another procedure was used to calculate the values of θ^2, $\overline{\theta r}$ and $\overline{r^2}$ of electrons for s from 0.1 to 2.0. The values of these moments that we calculated for s from 1.1 to 1.9 differed by several per cent from those obtained

TABLE II. – $\overline{\theta^n}$ *and* $\overline{r^n}$ *values for photons.*

s	$\overline{\theta^2}$	$\overline{\theta^4}$	$\overline{\theta}$	$\overline{r^2}$	$\overline{r^4}$	$\overline{r^6}$
0.1	$6.63 \cdot 10^{-3}$	$2.22 \cdot 10^{-3}$	$2.11 \cdot 10^{-3}$	$1.69 \cdot 10^{-3}$	$5.75 \cdot 10^{-4}$	$1.22 \cdot 10^{-2}$
0.2	$1.84 \cdot 10^{-2}$	$8.34 \cdot 10^{-3}$	$9.15 \cdot 10^{-3}$	$9.88 \cdot 10^{-3}$	$9.36 \cdot 10^{-3}$	$5.13 \cdot 10^{-2}$
0.3	$3.32 \cdot 10^{-2}$	$1.84 \cdot 10^{-2}$	$2.67 \cdot 10^{-2}$	$2.27 \cdot 10^{-2}$	$5.16 \cdot 10^{-2}$	$5.49 \cdot 10^{-1}$
0.4	$5.05 \cdot 10^{-2}$	$3.21 \cdot 10^{-2}$	$5.23 \cdot 10^{-2}$	$6.42 \cdot 10^{-2}$	$1.89 \cdot 10^{-1}$	3.18
0.5	$6.91 \cdot 10^{-2}$	$4.95 \cdot 10^{-2}$	$8.79 \cdot 10^{-2}$	$1.22 \cdot 10^{-1}$	$6.06 \cdot 10^{-1}$	$1.40 \cdot 10^{1}$
0.6	$8.98 \cdot 10^{-2}$	$7.00 \cdot 10^{-2}$	$1.34 \cdot 10^{-1}$	$2.11 \cdot 10^{-1}$	1.38	$5.08 \cdot 10^{1}$
0.7	$1.11 \cdot 10^{-1}$	$9.36 \cdot 10^{-2}$	$1.90 \cdot 10^{-1}$	$3.41 \cdot 10^{-1}$	3.15	$1.62 \cdot 10^{2}$
0.8	$1.33 \cdot 10^{-1}$	$1.20 \cdot 10^{-1}$	$2.56 \cdot 10^{-1}$	$5.25 \cdot 10^{-1}$	6.72	$4.74 \cdot 10^{2}$
0.9	$1.54 \cdot 10^{-1}$	$1.48 \cdot 10^{-1}$	$3.30 \cdot 10^{-1}$	$7.81 \cdot 10^{-1}$	$1.40 \cdot 10^{1}$	$1.29 \cdot 10^{3}$
1.0	$1.76 \cdot 10^{-1}$	$1.78 \cdot 10^{-1}$	$4.14 \cdot 10^{-1}$	1.13	$2.64 \cdot 10^{1}$	$3.34 \cdot 10^{3}$
1.1	$1.98 \cdot 10^{-1}$	$2.09 \cdot 10^{-1}$	$5.04 \cdot 10^{-1}$	1.60	$4.96 \cdot 10^{1}$	$8.28 \cdot 10^{3}$
1.2	$2.18 \cdot 10^{-1}$	$2.41 \cdot 10^{-1}$	$5.98 \cdot 10^{-1}$	2.22	$9.10 \cdot 10^{1}$	$1.28 \cdot 10^{4}$
1.3	$2.37 \cdot 10^{-1}$	$2.71 \cdot 10^{-1}$	$6.89 \cdot 10^{-1}$	3.02	$1.61 \cdot 10^{2}$	$4.51 \cdot 10^{4}$
1.4	$2.58 \cdot 10^{-1}$	$3.06 \cdot 10^{-1}$	$8.00 \cdot 10^{-1}$	4.13	$2.31 \cdot 10^{2}$	$1.04 \cdot 10^{5}$
1.5	$2.77 \cdot 10^{-1}$	$3.38 \cdot 10^{-1}$	$9.03 \cdot 10^{-1}$	5.54	$4.96 \cdot 10^{2}$	$2.30 \cdot 10^{5}$
1.6	$2.95 \cdot 10^{-1}$	$3.71 \cdot 10^{-1}$	1.01	7.38	$8.51 \cdot 10^{2}$	$4.99 \cdot 10^{5}$
1.7	$3.13 \cdot 10^{-1}$	$4.03 \cdot 10^{-1}$	1.12	9.82	$1.44 \cdot 10^{3}$	$1.07 \cdot 10^{6}$
1.8	$3.30 \cdot 10^{-1}$	$4.34 \cdot 10^{-1}$	1.22	$1.29 \cdot 10^{1}$	$2.41 \cdot 10^{3}$	$2.25 \cdot 10^{6}$
1.9	$3.46 \cdot 10^{-1}$	$4.64 \cdot 10^{-1}$	1.32	$1.67 \cdot 10^{1}$	$3.92 \cdot 10^{3}$	$4.57 \cdot 10^{6}$
2.0	$3.60 \cdot 10^{-1}$	$4.92 \cdot 10^{-1}$	1.42	$2.15 \cdot 10^{1}$	$6.26 \cdot 10^{3}$	$8.99 \cdot 10^{6}$

in [8]. Fig. 1 gives the values θ^2, $\overline{\theta r}$, and $\overline{r^2}$ which we calculated from the data of (8). It should be noted that our calculations of $\overline{\theta^2}$, $\overline{\theta r}$ and r^2 using the equations of paper [8] coincide, to three decimal places, with the results of our earlier calculations and, consequently, for S from 1.1 to 1.9 differ by several per cent from the figures given by the authors [8]. The results of our calculations for $S = 1$ coincide with the values of the moments given in [4].

The results of calculations by means of equation [8] of the differential angular function using the first three even moments ($N - 3$) are given in Fig. 2 (curve 1). A series by moments (8) determines the function, only the first several moments of which coincide with the precise ones. The higher moments of this function will differ from the precise ones. However, noting that the asymptotic behaviour of [8] coincides with the

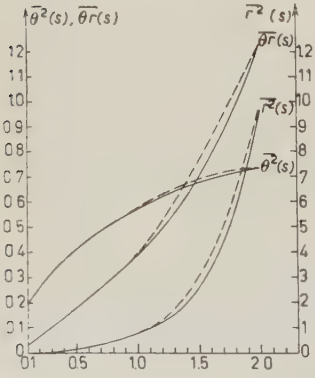

Fig. 1. – $\overline{\theta^2}$, $\overline{\theta r}$ and $\overline{r^2}$ electron values for various values of the age parameter s, calculated neglecting the ionization loss. Solid curves represent the results of our calculations. Dashed curves are constructed according to BORSELLINO's paper [8].

asymptotic behaviour of the precise function when $x \to \infty$, it may be expected that the higher moments of function (8) differ but slightly from the precise ones, and that function [8] differs from the precise one by not more than several per cent in a broad range of values of x. Using expression $P(x_\theta, 1)$ calculated from (8) at $N = 3$, we calculated $\overline{\theta^8}$ and $\overline{\theta^{10}}$. It turned out that the calculated values $\overline{\theta^8}$ and $\overline{\theta^{10}}$ coincide with the precise ones within 15%.

The value of the moment $\overline{\theta^n}$ is determined principally by a certain finite interval of values x_θ that depends on n. Therefore, by comparing the values of the function $P(x_\theta, 1)$ calculated, for example, from two (curve 2, Fig. 2) and from three (curve 1) even moments, it is possible to determine the limits of applicability with respect to x of approximation [8]. From Fig. 2 it is seen that even in using only the first two moments, the approximation [8] makes it possible to calculate $P(x_\theta, 1)$ in the interval x_θ from 0 to 3 with an error that does not exceed 10%. Curve 3 shows the results of calculations carried out in [4] by the method of graphical selection of an arbitrary function, the first three moments of which coincide with the precise ones. Curves 1 and 3 are in good coincidence with each other. Curves 4 and 5 are depicted on the same figure. These curves are constructed from the data of papers [1] and [9]. Table III lists the values of the first two

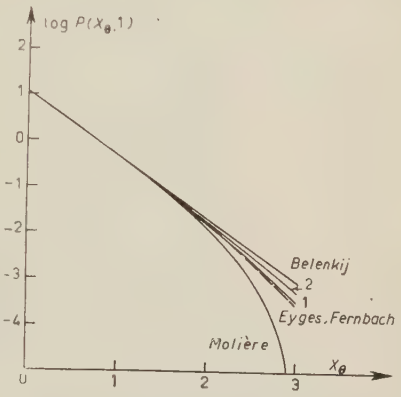

Fig. 2. – Differential functions of angular distribution reconstructed from their first two (1) and three (2) moments. The dashed curve is taken from [4]. The results of the calculations [1] and [2] are also represented there.

TABLE III. – $\overline{\theta^n}$ *values at the shower maximum according to different authors.*

$\overline{\theta^n}$	EYGES and FERNBACH	MOLIÈRE	BELEN'KIJ
$\overline{\theta^2}$	0.570	0.602	0.655
$\overline{\theta^4}$	0.959	1.72	1.43

moments that correspond to these curves. Curves 1 and 3, constructed from the same moments are in good coincidence with each other. The moments that correspond to curve 4 are greater than the precise ones, and those that correspond to curve 5 are less than the precise ones. For this reason, given big x, curve 4 is above 1 and 3, and curve 5 is below them.

The results of calculations, using equation (11), of the integral lateral func-

tion of electrons for the first three moments are given in Fig. 3. Using expression $f(x_r, 1)$ when $k/2 = 3$, we calculated $\overline{r^8}$ and $\overline{r^{10}}$. It was found that the

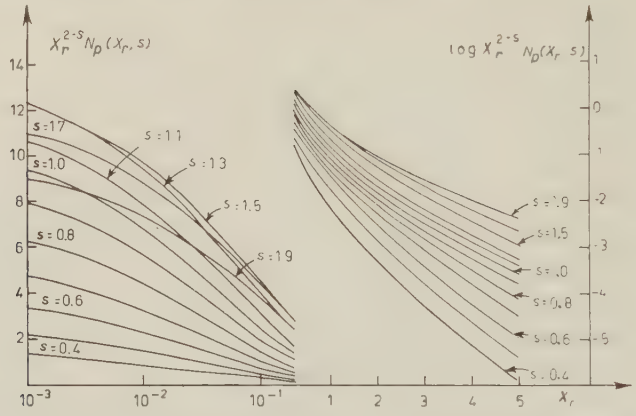

Fig. 3. – Integral functions of lateral distribution of electrons reconstructed from their first three moments for various values of the age parameter s.

calculated values of $\overline{r^8}$ and $\overline{r^{10}}$ coincide with the precise ones within 10%. Paper [10] developed a method of calculating the functions of the angular and lateral distribution over the moments, which method utilizes the Mellin transformation. The developed method enables one to calculate with satisfactory precision the distribution functions for large values of the argument. Thus, method [10], when using the first four moments, makes it possible to calculate the function of angulardistribution for $0.5 < x < 3$. A comparison shows that the function obtained within the limits of 10% coincides with the function constructed according to (8). It should be noted that for this purpose we required only three (or even two) moments. Fig. 4 shows a function of the lateral distribution constructed by the method of [10] according to four moments, curve 1 and curve 2 constructed according to (11) when $N = 3$. From $x \simeq 1$ to $x \simeq 15$, the curves are in good agreement with each other (*).

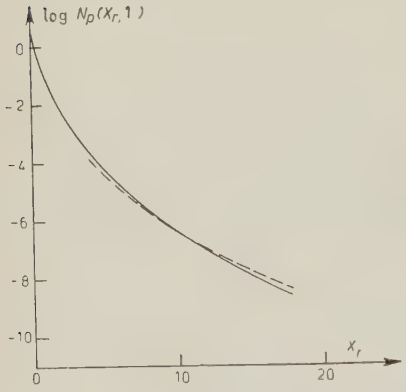

Fig. 4. – Integral function of lateral distribution of electrons at the shower maximum ($s = 1$). The dashed curve is constructed according to ref. [10].

(*) In order to evaluate the accuracy of the curve from $x \simeq 0$ to $x \simeq 1$, we compared the differential curve, which we had calculated, with the data of Molière [10]. It appeared that in this region, the curves diverge not more than 20% for $x \simeq 0$.

Fig. 3 shows the results of calculations of the integral lateral function of electrons calculated from the first three moments from equations (4, 12, and 14) for s from 0.4 to 1.1 through $\Delta s = 0.2$. In order to determine the borders of applicability with respect to x of the approximation that was used, calculations were made of the functions $N_p(x, s)$ with the use of the two and three first moments for $S = 0.5$, 1.0 and 1.9. The results of the calculation are shown in Fig. 5, from which it is seen that up to $x \sim 6$ the curves diverge

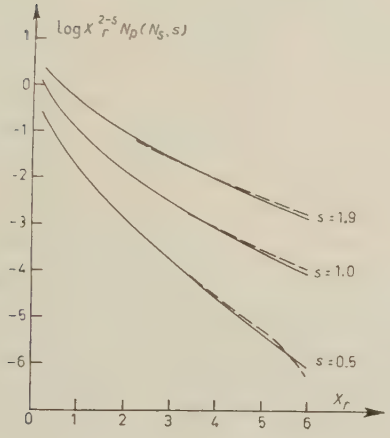

Fig. 5. – The solid curves represent the curves of Fig. 3 for three values of the parameter s. The dashed curves are reconstructed from the first two moments.

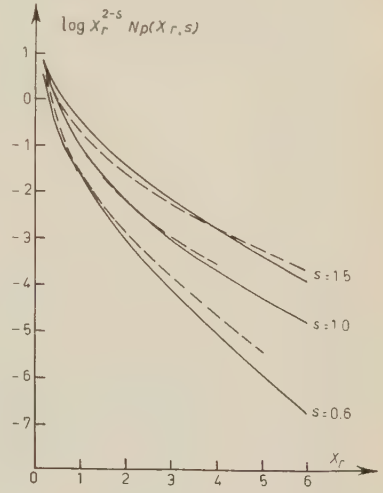

Fig. 6. – The solid curves are the same, as those in Fig. 3. The dashed ones are constructed according to ref. [4].

not more than 10%. In paper [4] the moments were used to construct functions for $s = 0.6$; 1.0; 1.5 by the method of graphical selections of an arbitrary function, the first three moments of which coincide with the precise ones (see Fig. 6). In costructing $N_p(x, 1)$ the authors made considerable use of the results of calculation [9] of the function of lateral distribution, which function is precise for small x. A comparison of $N_p(x, 1)$ from [4] with ours shows that within the limits of 10% the functions coincide. When constructing $N_p(x, s)$ for $s = 0.6$ and 1.5 the authors assumed that the nature of the behaviour of $N_p(x, s)$ for $x \to 0$ differs but slightly from the behaviour of $N_p(x, 1)$ and they considered that the nature of the peculiarity for $x \to 0$ for the given s does not affect the behaviour of the function for $x > 0.2 \div 0.4$.

A comparison of the functions $N_p(x, s)$ for $s = 0.6$ and 1.5 taken from [4] and calculated by (4), (12), and (14) shows that they differ essentially (about twofold) and the functions constructed from (4, 12, and 14) in the assumption

that $N_\gamma(x, s)_{x\to\infty} \sim 1/x$ when $s = 0.6$ and 1.5 coincides with the functions obtained in [4].

The results of the calculation of the differential and integral function of lateral distribution of photons for three moments from equation (11) are shown in Fig. 7. The same figure shows the corresponding functions taken from papers [4] and [9]. The comparison shows that with the exception of the region x near $x \simeq 1$, where the curves of [4] and [9] sharply change their inclination, the curves coincide satisfactorily.

Analogously, it is possible to calculate the function of the angular and lateral distribution of photons, given an arbitrary s. Thus, the proposed method enables one to calculate the functions of angular and lateral distribution of particles of a cascade shower in a broad range of values of the parameter s and arguments x with an error of the order of 10 % by using the first three moments of the unknown function.

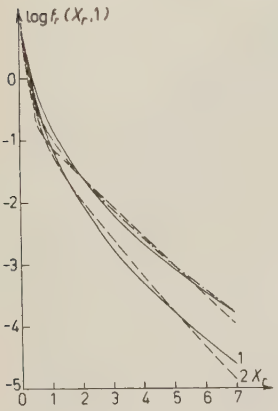

Fig. 7. – Functions of the lateral distribution of photons. 1) integral function constructed from the first three moments. 2) integral function constructed according to [9]. The solid curve is the differential function reconstructed from the first three moments; the dashed curve represents the differential function according to ref. [9], the dot dashed curve is the differential function according to ref. [4].

REFERENCES

[1] S. Z. Belen'kij: *Avalanche Processes in Cosmic Rays* (Moscow, 1948).
[2] I. P. Ivanenko: *Žu. Èksper. Teor. Fiz.*, **31**, 86 (1956); **32**, 334 (1957); *Dokl. Akad. Nauk SSSR*, **107**, 819 (1956).
[3] J. Nishimura and K. Kamata: *Progr. Theor. Phys.*, **5**, 899 (1950).
[4] L. Eyges and S. Fernbach: *Phys. Rev.*, **82**, 287 (1951); L. Eyges: *Phys. Rev.* **82**, 23 (1951); S. Fernbach: *Phys. Rev.*, **82**, 288 (1951).
[5] E. Titčmarš: *Introduction to the Theory of Fourier Integrals* (Moscow, 1948), p. 406.
[6] J. Ja. Pomerančuk: *Žu. Èksper. Teor. Fiz.*, **14**, 1252 (1944); A. B. Migdal: *Žu. Èksper. Teor. Fiz.*, **15**, 313 (1945).
[7] B. Chartress and H. Messel: *Proc. Phys. Soc.*, A **67**, 158 (1954).
[8] A. Borsellino: *Nuovo Cimento*, **7**, 323 (1950).
[9] G. Molière, *in Cosmic Radiation.* (New York, 1946).
[10] B. Chartress: *Phys. Rev.*, **105**, 707 (1957).

SUPPLEMENTO AL VOLUME VIII, SERIE X
DEL NUOVO CIMENTO

N. 2. 1958
2° Trimestre

Studies on Transverse Momenta of High-Energy Jets with Emulsion Cloud Chambers.

Co-operative Emulsion Group in Japan (*)

It has been suggested by one of us that transverse momenta of shower particles with respect to the shower axis are one of the most important quantities for the study of dynamical properties of high energy jet showers.

Some results of this analysis have already been presented by Z. Koba on the sixth Rochester Conference of last year, and the experimental data available at that time are shown in Table I.

Table I.

	Primary energy	Secondary energy	Transverse momenta
Emulsion			
Schein star	10^{13} eV	$10^{9} \div 10^{10}$ eV	100 MeV/c ÷ 200 MeV/c
Rochester	10^{13} eV	10^{12} eV	600 MeV/c
Air shower			
Cornell	$(10^{13} \div 10^{14})$ eV	$6 \cdot 10^{11}$ eV	several hundred MeV/c
George	$(10^{11} \div 10^{12})$ eV	10^{10} eV	100 MeV/c ÷ 200 MeV/c
Soft comp	$(10^{14} \div 10^{15})$ eV	$(10^{12} \div 10^{13})$ eV	a few hundred MeV/c ÷ a few GeV/c

(*) *Kobe University*: S. Hasegawa, O. Minakawa, M. Tsuzuki, Y. Nishimura and H. Yamanouchi.
Rikkuo University: H. Aizu and H. Hasegawa.
Saikyo University: Y. Ishii and S. Tokunaga.
Wakayama University: K. Nishikawa.
Yamanashi University: K. Imaeda, M. Kazuno and H. Mori.
Institute for Nuclear Study: Y. Fujimoto, J. Nishimura and K. Niu.

From this result it was plausibly concluded that the transverse momenta of secondaries are quite small even when the primary and the secondary energies are very high, and they seem to be insensitive to the energy of primary particles.

In order to get further experimental information on the transverse momenta of shower particles, the project so called « Emulsion Chamber Project» (E.C.P.) has been carried out in the last summer with a collaboration of several laboratories.

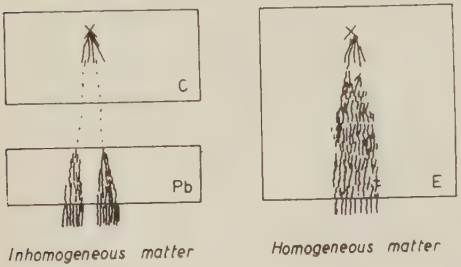

Fig. 1. – Principle of our E.C.P.

The energy of the shower particles in jet showers has to be measured for the determination of their transverse momenta. The energy of neutral π-mesons is measured much more accurately than that of charged π-mesons as shown later, if the cascade showers developed from neutral π-mesons are well followed. Information on neutral π-mesons may, perhaps, be generalized to those on charged π-mesons as shower particles of the jets. Thus, the Emulsion Chambers were designed so that neutral π-mesons are well detected and energies are accurately measured. Particular care was taken to observe separately each cascade shower developed from each γ-ray produced by neutral π-mesons (see Fig. 1).

Nuclear plates are piled up together with plates of materials. We put low Z material in the upper part of this chamber and the high Z material in the lower part.

γ-rays from the neutral π-mesons emitted by those jet showers produced

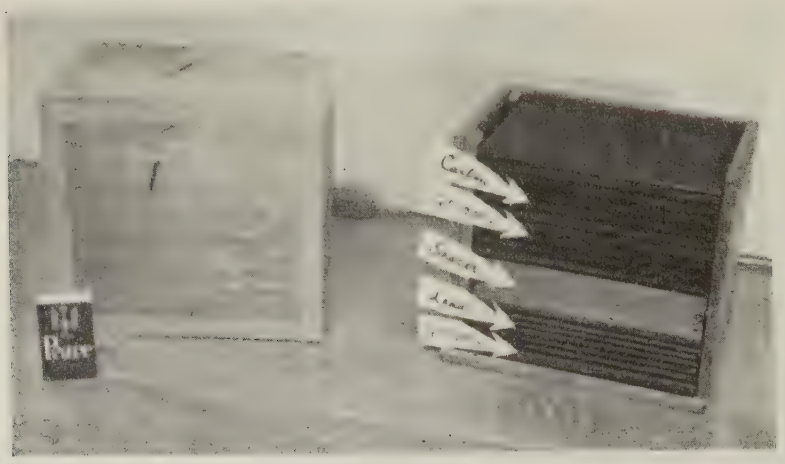

Fig. 2. – E.C.C.

in such low Z material layers penetrate through without any materialization until they reach high Z material layers. Thus, when the cascade showers corresponding to these γ-rays start to develop in high Z material, γ-rays have already passed some distance, and they have some spatial separation.

17 Emulsion Chambers have been flown by 8 plastic balloons (5600 m^3), and 13 of them were recovered after successful flight. Each chamber consisted of 17 G-5 6 in. $\times$ 8 in. $\times$ 200 μm nuclear plates, 10 carbon plates of 8 mm thickness each and 8 lead plates of 5 mm thickness.

Most of these chambers have been so far scanned. (2 $\div$ 4) jets of more than 3 cores with good separation are found in each chamber. Thus we have found about 30 such jet showers, and some of them are shown in Fig. 3, 4, 5 and 6.

The actual process of our analysis is as follows.

A) The development of a separated cascade shower is inspected. Comparing its transition curve with the theoretical one, one can estimate the energy of the primary γ-ray of each shower.

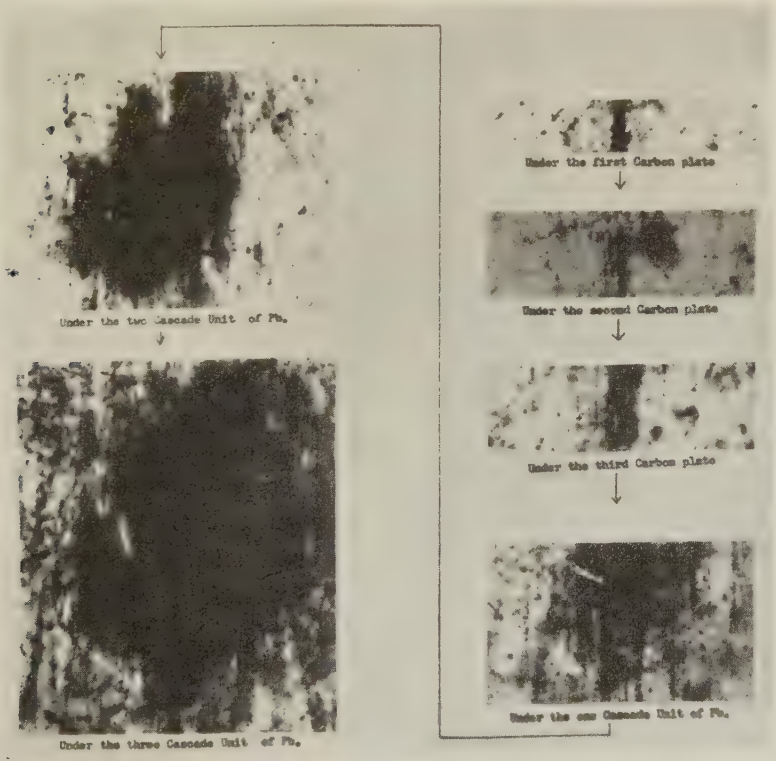
Under the first Carbon plate
Under the second Carbon plate
Under the third Carbon plate
Under the two Cascade Unit of Pb.
Under the three Cascade Unit of Pb.

Fig. 3. – Event S.H.1: the energy of the primary is expected to be $\sim 10^{14}$ eV.

A special three dimensional cascade theory without Landau's approximation is prepared (see Appendix A), and for the actual numerical evaluation corrections are also made for the thickness of the glass. Thus the errors of the theoretical curves are expected to be at most from 20 to 30%.

The actual analysis for the event T.H.4 is shown in Fig. 7. Here the relative errors for the energy determination quoted are $\sqrt{N}$, where N is the number of electrons at shower maximum.

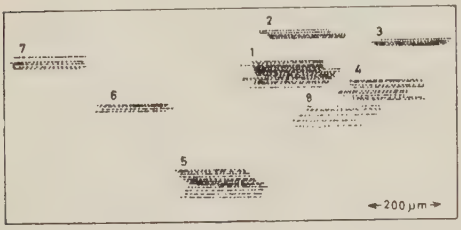

Fig. 4. – Separate electron showers of the event S.T.1.

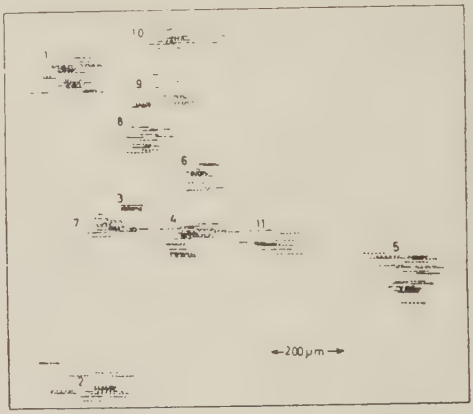

Fig. 5. – Separate electron showers of the event S.T.4.

B) Tracing back the direction for each of the separated cascade showers in several plates one may determine the point of production of the jet shower. Using the relation of the opening angle of 2 γ-rays belonging to the same π^0-meson, we examine the all possible combinations of separate electron showers.

The combination is usually uniquely determined for electron showers with less than 6 cores, using the energies of γ-rays determined in *A*). After the most probable combination is determined, energies of meson

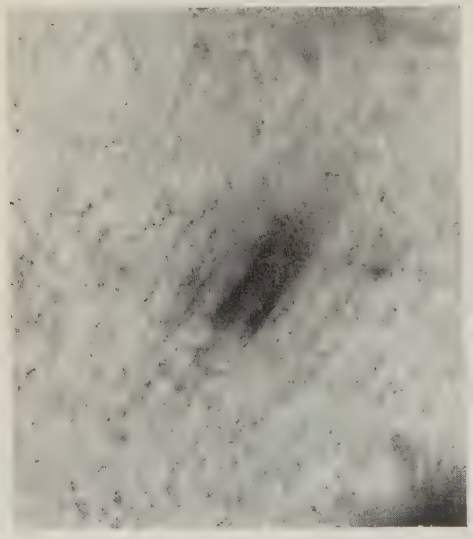

Fig 6. – One of the high energy electron showers of the event Yo.N.1: The energy of the γ primary of this electron shower is expected to be $5 \cdot 10^{12}$ eV.

are estimated using again the relation between the opening angles of 2 γ-rays and the energy of π^0-meson.

The accuracy of this energy estimate is quite good, and in general the errors introduced are less than 10%. The actual example for the event T.H.4 is shown in Fig. 8.

The most probable combination is the couple of (1, 2), (3, 4) and (5, 6), and the next probable one is that of (1, 3), (2, 4) and (5, 6). For the criterion for this determination, we take the ratio R of r (expected) to r (observed), where r observed is the distance between 2 γ-rays, and r (expected) is calculated using the energy determined in Fig. 7.

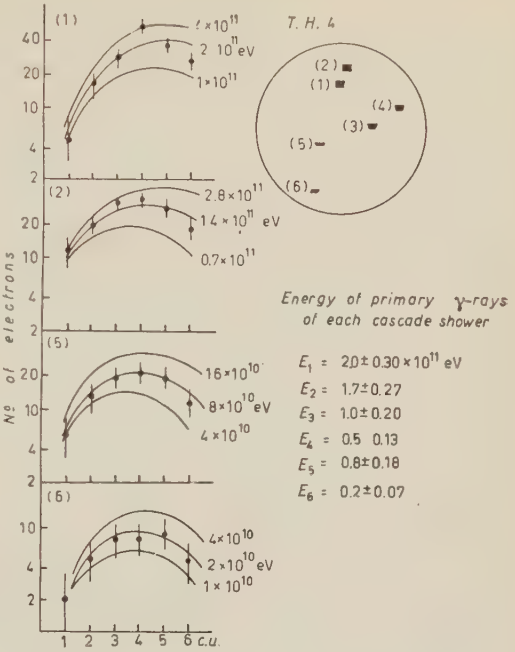

Fig. 7. – Analysis of the event T.H.4.

We take as the most probable one, that in which the values of those ratio is nearly one.

The ratios R for this event are as follows.

Most probable		Next probable	
couple	R	couple	R
(1, 2)	0.70 ± 0.11	(1, 3)	0.23 ± 0.03
(3, 4)	0.70 ± 0.13	(2, 4)	0.32 ± 0.06
(5, 6)	0.93 ± 0.22	(5, 6)	0.93 ± 0.22

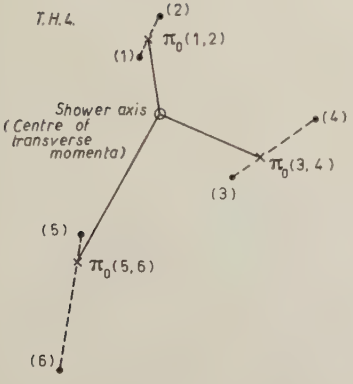

Using the most probable combination, and again the relation between the opening angle of 2 γ-rays and the energies of π^0-mesons, we get information of energies of π^0-mesons. Then the centre of transverse momenta is determined.

The energies of π^0-mesons thus determined and the transverse momenta are.

Fig. 8. – Combination of 2 γ-rays, determination of energies of π^0-mesons and the centre of transverse momenta of the event T.H.4.

	E (10^{11} eV)	P_t (MeV/c)
(1, 2)	2.14 ± 0.22	480 ± 39
(3, 4)	0.96 ± 0.09	308 ± 24
(5, 6)	0.85 ± 0.13	411 ± 52

C) We take the centre of transverse momenta as the shower axis. Then we get the transverse momenta of each π^0-meson. The example is also shown in Fig. 8.

TABLE II.

Event	No. of cores	Origin	E_0 (eV)	P_t (MeV/c)
H.A.1.	7	A	10^{13}	272 252 225 284
S.H.1.	14	C	10^{14}	*
T.H.1.	6	A	10^{13}	116 ± 23 361 ± 73 284 ± 57
T.H.2.	4	C	$4 \cdot 10^{12}$	286
T.H.3.	5	C	$2 \cdot 10^{12}$	289 ± 80 381 ± 108 661 ± 185
T.H.4.	6	C	$4 \cdot 10^{12}$	481 ± 38 308 ± 24 411 ± 52
K.I.1.	4	C	*	*
M.K.1.	4	C	*	*
E.M.1.	4	C	*	*
Ya.N.1.	4	C	10^{13}	192
Yo.N.1.	16	A	10^{14}	*

A: outside the chamber; C, chamber.
* Not yet analysed.

TABLE II (*continued*).

Event	No. of cores	Origin	E_0 (eV)	P_t (MeV/c)
Yo.N.2.	4	A	*	*
Yo.N.3.	4	C	$5 \cdot 10^{12}$	146
T.O.1.	4	*	*	*
T.O.2.	5	C	$7 \cdot 10^{12}$	285 186 143
T.O.3.	4	*	*	*
T.O.4.	4	*	*	*
T.O.5.	4	*	*	*
Y.T.1.	4	C	$8 \cdot 10^{12}$	600 ± 30
S.T.1.	8	A	$8 \cdot 10^{12}$	121 78 183** 248 230 173 31 42 53 348 300 234
S.T.2.	11	C	$2 \cdot 10^{13}$	470 450 577** 316 78 93 210 561 190 414 198 600 475 476 485
S.T.3.	4	C	*	280
S.T.4.	6	C	*	514 289 518
H.Y.1.	6	Pb	$5 \cdot 10^{12}$	196 146 62

A: outside the chamber; C, chamber.

* Not yet analysed.

** For these showers, we can not make a unique combination of γ-rays, so we here present the values of P_t for 3 different combinations.

The data now available are shown in Table II, and it results from these that the values of transverse momenta are ranging from 100 MeV/c to 500 MeV/c.

After the scanning and the analysis are completed, we make some correction for the uncertainty in the determination of the shower axis and get information on the distribution of transverse momenta of high energy jet showers.

Appendix A

Three dimensional cascade theory without Landau's approximations.

The theory here presented is a revised calculation of N.K. function (*Progress Theor. Phys.*, **7**, 185 (1952)), and is including rigorously the contribution of single and plural scattering. For the treatment of the effect of Coulomb scattering we follow Molière's scattering theory, (see Bethe: *Phys. Rev.*, **89**, 1256 (1953)). The course of our calculation is somewhat complicated, and we will give here the final results.

Let $\pi(r)2\pi r\,\mathrm{d}r$ be the total number of electrons lying the annual ring between r and $r+\mathrm{d}r$ at depth t of a photon-initiated shower with energy E. Then π is given by the following formulae, in the notation of Rossi and Greisen.

$$\pi = \pi^{(0)} + \frac{1}{G}\pi^{(1)}$$

where $G = 12.9$, and $K = 17.5$ MeV for lead,

$$\pi^{(0)} = -\frac{1}{4\pi^3}\int_{-i\infty}^{+i\infty}\int\left(\frac{E_0}{\varepsilon}\right)^s\left(\frac{\varepsilon}{K}\right)^2\left(\frac{\varepsilon^2r^2}{K^2}\right)^{-p-1}\Gamma(p+1)\Gamma(2p+s)\mathfrak{M}(p,0,-2p-s,s,t)\,\mathrm{d}s\,\mathrm{d}p$$

$$\pi^{(1)} = \frac{1}{4\pi^3}\int_{-i\infty}^{+i\infty}\int\left(\frac{E_0}{\varepsilon}\right)^s\left(\frac{\varepsilon}{K}\right)^2\left(\frac{\varepsilon^2r^2}{K^2}\right)^{-p-2}\Gamma(p+2)\Gamma(2p+2+s)(p+1)\cdot$$

$$\cdot\left\{\psi(p+1)+\psi(-p-2)-\ln\frac{\varepsilon^2r^2}{K^2}+2\psi(2p+s+1)-2\left.\frac{\mathfrak{M}'}{\mathfrak{M}}\right|_{q=-2p-2-s}\right\}\cdot$$

$$\cdot\mathfrak{M}(p,1,-2p-2)\,\mathrm{d}s\,\mathrm{d}p,$$

and $\mathfrak{M}$ is given by

$$\mathfrak{M} = \lim_{(\xi-t)\to 0} N,$$

$$\sum_{n=0}^{p}{}_pC_n\left(-\frac{1}{G}\right)^n L^{(n)}(s+2p+2u-q)N(p-n,n+u,q,s,t) =$$

$$= \left(\frac{\partial}{\partial t}+\sigma\right)\left[p\left\{(\xi-t)^2\left(1-\frac{1}{G}\ln(\xi-t)^2\right)\right\}N(p-1,u,q,s,t)+\right.$$

$$+u(\xi-t)^2N(p,u-1,q,s,t)+(s+2p+2u+q)q\cdot$$

$$\left.\cdot M(p,u,q,-1,s,t)-\frac{1}{G}pqN(p-1,u+1,q-1,s,t)\right],$$

with

$$N(0, 0, 0, s, t) = \frac{M(s)}{s^{\frac{1}{2}}} \left\{\exp\left[\lambda_1(s)t\right] - \exp\left[\lambda_2(s)t\right]\right\}.$$

For the analysis of the event in Emulsion-Chamber, numerical calculations are made for the shower in lead plates, where the corrections are made ofr the thickness of the nuclear plates between the lead plates.

In order to test the accuracy of this function, we have calculated the theoretical curves for the showers in emulsion and compared with Pinkau's results in Fig.9 (*Nuovo Cimento*, **3**, 1285 (1956)) and agreements between them are quite good.

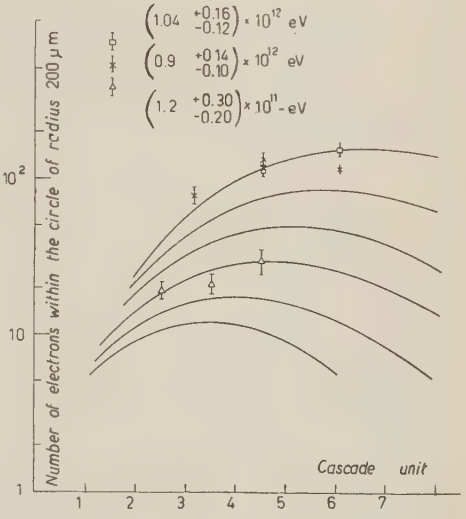

Fig. 9 – The energy of the data is determined experimentally by Pinkau, and the solid curves are those calculated by the theory in App. A.

SUPPLEMENTO AL VOLUME VIII, SERIE X
DEL NUOVO CIMENTO

N. 2, 1958
2° Trimestre

On Some Interaction Characteristics of Very High-Energy Particles and Their Interpretation from the View Point of the Hydrodymical Theory of Multiple Particles Production.

G. A. Milečin and I. L. Rozental'

P. N. Lebedev Institute of Physics of the USSR Academy of Sciences - Moscow

Landau [1] basing on the idea stated by Fermi [2] employed relativistic hydrodynamics for description of the very high energy particle collision. The first attempts [3] to compare the conclusions of hydrodynamical theory with experimental data on the multiplicity and angular and energy distributions of secondary particles already showed that the hydrodynamical theory satisfactorily described many multiple process characteristics. However, by comparison of the theory with the experimental data taken from the analysis of showers recorded in photographic emulsion and of extensive air showers, a number of essential additional assumptions was made. These assumptions, in spite of their natural character caused a certain obscurity of the conclusions. Thus, for example, it was assumed that the collision of nucleons with heavy nuclei took place in the co-ordinate system in which motion of substance was symmetrical. In order to describe these collisions one can use the model according to which a particle simultaneously interacts with the nuclear substance cylinder. The extensive shower analysis carried out on the assumption that the nuclear interaction cross-section is independent of energy, and neglecting fluctuations in the cascade development, etc. On the other hand, also the formal part of the hydrodynamical theory is not complete. Indeed, the mathematical aspect of the theory reduces to the solution of equations of the relativistic hydrodynamics at the initial conditions corresponding to the energy concentration of colliding particles in the relativistic compressed volume of a nucleon/energy equipartition within the limits of the disk with diameter $h/\mu c$, and length $h/\mu c\sqrt{M/E_0}$, where μ is the π-meson mass, M is the nucleon mass and E_0 is the colliding particles' energy

in the laboratory co-ordinate system). In his fundamental work LANDAU separates the solution of the above formulated complex problem into two stages. The first stage corresponds to the one-dimensional motion (i.e. lateral deflection is neglected) considered approximately. The second stage corresponds to the so-called conic motion, e.i. such process, when energy and entropy fluxes inside any cone with the axis coinciding with the direction of primary particle motion, are constant. However, the application limits of the conic motion are obscure. One can affirm only that the role of the conic motion increases with the colliding particle energy but, perhaps, it plays its role only at energies exceeding the experimental ones. In order to overcome this difficulty, another solution of the hydrodynamical equations was proposed. This solution was based on a method analogous to the successive approximations method [4].

Precise solution of the one-dimensional problem made by HALATNIKOV [5] was selected as the first approximation. The second approximation was formed from the first approximation solution sum and some addition considered small in comparison with the first term. The condition that this term be small in comparison with the first term is the condition of application of the whole approximation. It was found that for the final temperature value

$$T_f \geqslant \frac{1.5\mu c^2}{k}, \quad (k \text{ is Boltzman constant}),$$

and for primary energies being not very high ($(10^{13} \div 10^{14})$ eV) the one-dimensional approximation gave a good description of the problem of solution. At $T_f \sim \mu c^2/k$ the one-dimensional solution is of the correct order of magnitude (*). The one-dimensional variant of the theory permits to consider also an important part of the process—the leading edge, which has not been considered before.

Comparison of the one-dimensional variant conclusions and the theory including the conic motion shows that most of the characteristics predicted by the both variants are similar. However, one distribution, namely, the distribution of transverse components (+) p of shower particle momentum as we shall see further, is found to be different.

At the same time this characteristic plays a peculiar role at the theoretical and experimental data comparison. Indeed, in order to check directly the theory one must first of all to consider such collision characteristics which for their interpretation, are independent (or practically independent) of additional

---

(*) The estimates of the lateral motion influence showed that the one-dimensional solution at $T_f \sim \mu c^2/k$ had the accurace of $\sim 20\%$.

(+) *I.e.* momentum components being normal to shower axis.

assumptions, the correctness of which it is difficult to estimate. The distribution of transverse components $p_\perp$ is one of such characteristics. At the conic stage introduction the distribution of transverse components is determined by the hydrodynamical components, while their thermal components are assumed to be negligible in compare with the first ones. In this approximation the average transverse momentum $p_\perp \sim M$. While in the one-dimensional variant the distribution of values p is determined only by the thermal motion. Using the well-known expression for the particle density dN in the moment interval $dp_x dp_y dp_z$, we shall find in such approximation the transverse momentum distribution:

$$dN = \frac{g}{(2\pi\hbar c)^3} \frac{dp_x dp_y dp_z}{\exp[(\varepsilon - \mu)/kT_f] \pm 1}, \tag{1}$$

where g is a number of the particle internal degree of freedom, ε is the particle energy, and μ is the chemical potential which is assumed, according the hydrodynamical conception, to be equal to zero. The minus sign determines Fermi particles. After integration by p_x the distribution of transverse components will be

$$dN_\perp = \frac{g}{(2\pi\hbar c)^3} mc\, dp_y dp_z \int_{-\infty}^{\infty} \frac{dx}{\exp[z\sqrt{x^2 + \varrho^2 + 1}] \pm 1} \tag{2}$$

where

$$x = \frac{p_x}{mc}; \qquad z = \frac{mc^2}{kT_f}; \qquad \varrho^2 = \frac{p_y^2 + p_z^2}{(mc)^2}.$$

Using the ratio

$$\int_0^{\infty} \frac{dx}{\exp[z\sqrt{x^2 + \varrho^2 + 1}] \pm 1} = \sqrt{\varrho^2 + 1} \sum_{n=1}^{\infty} (\mp)^{n-1} K_1(nz\sqrt{\varrho^2 + 1}) \tag{3}$$

(K_1 Bessel function of imaginary argument) and integrating by the angle in the cylindrical co-ordinates we have finally:

$$dN_1 = \sqrt{\varrho^2 + 1}\, \frac{g}{2\pi^2} \left(\frac{mc}{\hbar}\right)^3 \sum_{n=1}^{\infty} (\mp)^{n-1} K_1\left(n \frac{mc^2}{kT_f} \sqrt{\left(\frac{p_\perp}{mc}\right)^2 + 1}\right) \frac{p_\perp dp_\perp}{(mc)^2} \tag{4}$$

The theoretical distributions of transverse components according to (4), calculated for Bose particles and different T_f, are plotted in the Fig. 1 (continuous lines).

Until recently the experimental data on the distribution of transverse components were very poor (only the estimates of the average value were available). However, the situation has improved due to the recording of the high energy unique shower (DE-BENEDETTI, GARELLI, TALLONE and VIGONE [6]). Owing to the unusually long particle path in a photographic emulsion the authors of the cited work were able to measure by scattering the momentum of the majority of secondary particles (35 out of 39). As their angular distribution was also known, it became possible to calculate simply the distribution of values $p_\perp$. This distribution is also plotted on the Fig. (dotted curve).

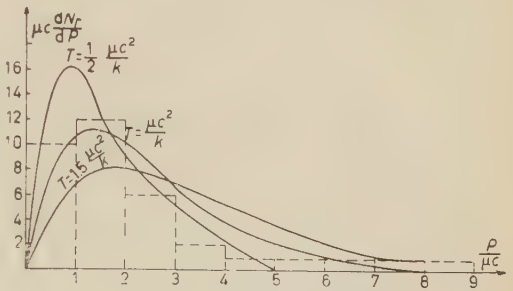

Fig. 1

A rather similar distribution of transverse components was also obtained on the grounds of measurement of the complete momentum of secondary π^0-mesons by the pairs connected with them [7]. In this case the distribution of transverse momenta had also the maximum in the region $(1 \div 2)\mu c$.

From the comparison of the experimental and theoretical curves transmitsone can draw some important conclusions.

1) The one-dimensional variant of the hydrodynamical theory transmits satisfactorily the character of the transverse component distribution.

2) The best agreement of both distributions is at

$$T_f = \frac{\mu c^2}{k} \quad (*)$$

It is already difficult to reconcile the values $T_f = \frac{1}{2}\mu c^2/k$ and $T_f = \frac{3}{2}\mu c^2/k$ with the experimental data, though it is impossible to exclude these values absolutely because of the scarcity of experimental data. The value $T_f = \mu c^2/k$ coincides with the indications previously got basing on the analysis of different experimental data (shower composition [8], energy spectrum [4] (+)).

(*) It is necessary to note that since we neglect some influence of the hydrodynamical transverse components the cited values of T_f are, strictly speaking, the maximum values of T_f.

(+) Here it is necessary to point out particularly Koba's calculation of the value T_f by the percentage of heavy nuclei in showers [8]. The theoretical value of this characteristic is also independent of the collision conditions. However its experimental value, obtained with the help of photographic emulsion, contains some indefinite factor- (the number of recoil nucleons, some uncertainty in the selection of the radiation lenght unit [9], etc.).

3) Since the temperature value T_f is directly connected with the interaction cross-section value of secondary particles [10] (substantially, π-mesons), we conclude that this value by its order is equal to the geometrical nucleon cross-section $(h/\mu c)^2$.

REFERENCES

[1] L. D. LANDAU: *Izv. Akad. Nauk SSSR, Ser. Fiz.*, **17**, 51 (1953).
[2] E. FERMI: *Progr. Theor. Phys.*, **5**, 570 (1950).
[3] I. L. ROZENTAL' and D. S. ČERNAVSKIJ, *Usp. Fiz. Nauk*, **52**, 185 (1954).
[4] I. L. ROZENTAL': *Žu. Èksper. Teor. Fiz.*, **31**, 278 (1956).
[5] I. M. HALATNIKOV: *Žu. Èksper. Teor. Fiz.*, **27**, 529 (1954).
[6] A. DEBENEDETTI, C. M. GARELLI, L. TALLONE and M. VIGONE: *Nuovo Cimento*, **4**, 1142 (1956).
[7] I. M. GRAMENIZKIJ, G. B. ŽDANOV, E. A. ZAMČALOVA and M. A. ŠČEERBAKOVA, in press.
[8] Z. KOBA: *Progr. Theor. Phys.*, **15**, 461 (1956).
[9] I. L. ROZENTAL', M. L. TER-MIKAELJAN and E. L. FEINBERG: *Dokl. Akad. Nauk SSSR*, **103**, 581 (1955).
[10] S. Z. BELEN'KIJ: *Dokl. Akad. Nauk SSSR*, **99**, 523 (1954).

SUPPLEMENTO AL VOLUME VIII, SERIE X
DEL NUOVO CIMENTO

N. 2, 1958
2° Triemestre

Multiple Production of Particles in Jets.

D. S. ČERNAVSKIJ

P. N. Lebedev Institute of Physics of the USSR Academy of Sciences - Moscow

1. – Introduction.

Jets observed in photoemulsion arise due to interaction of nucleons of high energy ($E_l > 10^{10}$ eV) with substance. The following cases are possible:

1) Interaction of a nucleon with internal parts of a heavy nucleus;

2) Head-on interaction of a nucleon with one of the surface nucleons of the nucleus, or with a nucleus of hydrogen (nucleon-nucleon interaction);

3) Peripheric interaction of a nucleon with a nucleon, taking place when the nucleon passes at a distance $b > \hbar/\mu c$ from the edge of the nucleus.

The numbers of such cases [1] in photoemulsion relate to each other as $103 : 56 : 31 \approx 3 : 2 : 1$.

2. – Collision of a nucleon with an internal part of a nucleus.

The first two cases were treated in detail in ref. [1]. When a collision of a nucleon with a nucleus occurs, the nucleon cuts a tunnel in the nucleus and interacts only with it. To interpret such cases, it is necessary to determine two values: *A*) the length of the tunnel n (i.e. the number of nucleons in it) and *B*) the energy E_l of the nucleon in the laboratory system (below designated as the L.S.). Using the statistical theory, both of these values may be found on the basis of two experimental figures, they are the number of shower particles in the jet, N_s, and its angular spread in the L.S.

In the center of mass system of nucleons jets have a symmetric angular distribution (which at low energies is even isotropic). Thus, the velocity v

of the center of mass system (C.S.) relative to the L.S. may be found from

$$\frac{1}{\operatorname{tg} \vartheta_{l\frac{1}{2}}} \simeq \frac{1}{\sqrt{1-v^2}} = \gamma \tag{1}$$

$\vartheta_{l\frac{1}{2}}$ is the angle in the L.S. which contains half of the total number of particles.

The dependence of the number of particles N_s on γ and on the length of the tunnel may be found using the statistical theory. For high energies, $E_l \gtrsim 10^{12}$ eV when thermodynamics is used (*),

$$N_s = 2(n+1)^{\frac{1}{4}} n^{\frac{3}{4}} \gamma^{\frac{1}{4}} + \frac{n+1}{2}. \tag{2}$$

For low energy, $E_l \leqslant 10^{11}$ eV, when it was necessary to use the statistical weight [3], the values for N_s were found in [1]. The formula is complicated and it is much simpler to use the curves that were given there. This method was applied to the analysis of the jets of ref. [4]. It turned out that two classes of cases (class A, large number of particles and large angle $\vartheta_{l\frac{1}{2}}$, and class B, small number of particles with a small angle $\vartheta_{l\frac{1}{2}}$) in which the authors classify their showers correspond as to class A, to collisions of nucleons producing tunnels and as to class B, to nucleon-nucleon collisions.

It was also shown that the determination of the coefficients of inelasticity K according [5] to the formula

$$K = \frac{1{,}5\, N_s \gamma \cdot \sin \vartheta_{l\,\max}}{2(\gamma-1)M}$$

is not adequate. It may be correct only if the number of particles in the shower is $N_s \gtrsim 100$ (which is practically unrealistic).

3. – Peripherical collisions.

Earlier [6], it was shown that classical treatment of peripheric interactions of two nucleons is not adequate, and that it is necessary to take into account the quantum structure of the field. For this aim, it is suitable to apply the method of Weizsäcker-Williams. According to this method, in the C.S. of colliding nucleons the field of each nucleon $\varphi(r)$ is developed in series

(*) The factor $2^{\frac{3}{4}}$ is introduced to secure an accordance with the Landau formula [2]. Of course, it should not be taken too literally. All figures are correct within a factor ~ 1.5.

over plane waves. The coefficients (or, to be more exact, their squares) give probability of a collision of a nucleon with a meson of given energy, this meson belonging to another nucleon (recoil of the emitting nucleon should be disregarded).

Therefore, the problem of peripheric interaction of two nucleons is reduced to the problem of head-on interaction of a nucleon with a meson: the nucleons flying past each other exchange mesons. The energies (and meson momenta) which are exchanged by the nucleons may vary within the limits of the spectrum which is determined by the development of $q(r)$ in a Fourier series.

The following cases are possible when mesons are exchanged:

a) Nucleons exchange mesons having approximately equal energies. In this case the observed pattern in C.S. will be symmetric.

b) The energies of transmitted mesons differ from each other.

c) Just one nucleon gives away its meson and another one receives it.

Then only one of the colliding nucleons is excited and emits mesons. The pattern in C.S. is definitely asymmetric .

a) *Symmetrical collisions.* – Let the function of the meson field in the proper system be given by the Yukawa potential:

$$\varphi(r) = \frac{\exp[-r]}{r}. \qquad (\hbar = \mu = c = 1). \tag{3}$$

Developing this function in C.S. of colliding nucleons (below referred to as the nucleon-system) (N.S.) over plane waves, we shall receive for the probability density

$$\varrho(\varepsilon, \gamma_N, b) = \frac{2}{\gamma_N} K_0^2\left(b \cdot \sqrt{1 + \left(\frac{\varepsilon}{\gamma_N}\right)^2}\right). \tag{4}$$

where $\varrho(\varepsilon, \gamma_N, b)$ is the probability of impinging a unit surface for a meson having the energy ε, $\varepsilon + d\varepsilon$; b the collision parameter (the distance from the path of the nucleon to the center of the unit surface), and

$$\gamma_N = (1 - v_N^2)^{-\frac{1}{2}},$$

v_N being the nucleon velocity in the N.S. Neglection of the emitting nucleon recoil means that we may consider collisions only with $\varepsilon \ll E_N$. Since the upper limit is, $\varepsilon \sim \gamma_N \sim E_N/M$, this leads to the condition of the validity of our calculations: $1/M \ll 1$.

The properties of the function $\varrho(\varepsilon, \gamma_N, b)$, are:

1) ϱ is normalized per total nucleon energy in the N.S. *i.e.*

$$\int_0^\infty 2\pi b \, \mathrm{d}b \int_0^\infty \varepsilon \, \mathrm{d}\varepsilon \varrho(\varepsilon, \gamma_N, b) = E_N = M\gamma_N \,. \tag{5}$$

2) At short distances from the nucleon, $b < 1$, the number of particles hitting the unit surface is large and nucleons collisions with $b < 1$ do not differ from head-on collisions.

3) For large collision parameters, $b \gtrsim 1$, the density of mesons is small. The energy of a meson passing beyond the distance $b = 1$ may have any value from 0 to γ_N. The average energy is $\bar{\varepsilon} = 0.5\gamma_N$. Let us take, for the beginning, energies of mesons in the N.S. to equal each other and ε. Each of the nucleons is excited and then emits mesons. (Such a model was examined earlier [7, 8] but not in sufficient details). The total number of produced particles according to the statistical theory is

$$N_s \sim \Omega_c^{\frac{1}{4}} E_c^{\frac{3}{4}} \,, \tag{6}$$

where Ω_c and E_c is the volume of the excited nucleon and its energy in this rest system, i.e. in the C.S. of the colliding nucleon and the meson; below, we shall refer to this system as to the CS.

The velocity of the C.S. with respect to the N.S. we shall designate by v_c. We have

$$\gamma_c = (1 - v_c)^{-\frac{1}{2}} = \frac{E_N}{2\sqrt{\varepsilon \cdot E_N}} \,. \tag{7}$$

The energy of the excidet nucleon in its proper system (C.S. is

$$E_c = 2\sqrt{\varepsilon \cdot E_N} \,. \tag{8}$$

In order to determine Ω_c, it is necessary to find the velocity of the C.S. with respect to the system in which the nucleon before the collision was at rest and had a volume of $\Omega_0 = \frac{4}{3}\pi$. The nucleon energy prior to the collision, in the C.S., is:

$$E_c^{(n)} = \tfrac{1}{2} E_c = \sqrt{\varepsilon \cdot E_N} \,. \tag{9}$$

Therefore the contracted volume will be equal to $\Omega_c = \frac{4}{3}\pi(M/\sqrt{\varepsilon \cdot E_N})$, and

the number of particles will be

$$N_s \approx (\varepsilon \cdot E_N)^{\frac{1}{4}} . \tag{10}$$

The proportionality coefficient (equal to 1) is determined in such a way, that for $\varepsilon = \frac{1}{2} E_N$ (which formally corresponds to the head-on collision) equation (10) goes over into the equation for the number of particles for a head-on collision $N_s \simeq 2(E_N/M)^{\frac{1}{4}}$.

Therefore, for $\varepsilon < E_N$ the number of produced particles may be considerably smaller than for head-on collision.

Angular distribution. – We are primarily interested in the case (see above) $\varepsilon \ll E_N$, $\gamma_c \gg 1$, when the particles produced by two different nucleons give in the N-system two independent narrow cones near 0 and π.

Let us assume that the emission of produced particles in each of the rest systems of excited nucleons takes place in accordance with the Landau theory [2] let us study one of the excited nucleons. Its angular distribution in its C.S. will be

$$\mathrm{d}N = \exp\left[\sqrt{L^2 - \lambda_c^2}\right] \mathrm{d}\lambda_c , \tag{11}$$

where

$$\lambda_c = -\ln \operatorname{tg} \frac{\vartheta_c}{2} , \qquad L = \ln \frac{\sqrt{\varepsilon \cdot E_N}}{M} .$$

This distribution over λ_c has a maximum $\mathrm{d}N/\mathrm{d}\lambda_c$ for $\lambda_c = 0$ ($\vartheta_c = \pi/2$). In order to receive the angular distribution of these particles in the N.S., we may simply « shift » the distribution given by the eq. (11) by $\Delta\lambda = \ln 2\gamma_c$.

Thus, in the N.S. the angular distribution of this cone will be

$$\mathrm{d}N = \exp\left[\sqrt{L^2 - (\lambda_N - \ln 2\gamma_c)^2}\right] \mathrm{d}\lambda_N , \tag{12}$$

where

$$\lambda_N = -\ln \operatorname{tg} \frac{\vartheta_N}{2} .$$

Another excited nucleon will give a reverse cone in the N.S. Due to the symmetry of the whole pattern, its angular distribution may be received from eq. (12) by reflecting it at the point $\lambda_N = 0$ ($\vartheta_N = \pi/2$).

That means that the total angular distribution is:

$$\mathrm{d}N = \left\{\exp\left[\sqrt{L^2 - (\lambda_N - \ln 2\gamma_c)^2}\right] + \exp\left[\sqrt{L^2 - (\lambda_N + \ln 2\gamma_c)^2}\right]\right\} \mathrm{d}\lambda_N . \tag{13}$$

The transition to the L.S. is performed quite similarly, i.e. by shifting the whole pattern by $\lambda = \ln 2\gamma_N$.

Thus, in the L. S. we have:

$$(14) \qquad \mathrm{d}N = \{\exp[\sqrt{L^2 - (\lambda_l - \ln 2\gamma_c - \ln 2\gamma_N)^2}] + \exp[\sqrt{L^2 - (\lambda_l + \ln 2\gamma_c - \ln 2\gamma_N)^2}]\}\,\mathrm{d}\lambda_l .$$

This angular distribution has two maxima. As a rule, all the angles in the L. S. are rather small, and

$$\lambda_l \simeq -\ln\frac{\vartheta_l}{2}; \qquad \mathrm{d}\lambda_l = -\frac{\mathrm{d}\vartheta_l}{\vartheta_l} .$$

Using the above formulas, we may perform some estimations. For example, let the observed star to have in co-ordinates $\mathrm{d}N/\mathrm{d}\lambda_l$, λ_l a symmetrical double-humped distribution. Let the number of charged particles in it be N_s. Then the energy may easily be determined from the formula which is true for all symmetrical stars, $E_N = M\gamma_N = M(1/\mathrm{tg}\,\vartheta_{l\frac{1}{2}})$.

Now, from (10) we may determine ε using E_N and N_s. After determining γ_c from (7), we may construct a complete angular distribution and compare it with the experiment. The comparison will serve as a check of the above theory.

b) Asymmetrical collision. – If the energies of the exchanged mesons are different (and equal to ε_1 and ε_2), then the angular distribution in the N.S. will be asymmetrical: the narrow cone will contain less particles while the wide cone will contain more particles (*). The number of particles in the first and the second cone will be equal respectively to:

$$(15) \qquad N_{s1} = 0.5(\varepsilon_1 E_N)^{\frac{1}{4}} ,$$

$$(16) \qquad N_{s2} = 0.5(\varepsilon_2 E_N)^{\frac{1}{4}} .$$

In practice, it is possible to observe the asymmetry only if the difference $N_{s1} - N_{s2}$ is greater than the statistical fluctuation, i.e. if it exceeds $\Delta N_s \simeq \sqrt{N_{s1}}$ Thus, asymmetry will be observable if

$$(17) \qquad E_N^{\frac{1}{4}}(\varepsilon_1^{\frac{1}{4}} - \varepsilon_2^{\frac{1}{4}}) \gtrsim E_N^{\frac{1}{4}}\varepsilon_1^{\frac{1}{4}} ,$$

or

$$\frac{\varepsilon_2}{\varepsilon_1} \gtrsim [1 - (E_N\varepsilon_1)^{-\frac{1}{2}}]^4 .$$

(Here we neglect the factor $\sqrt{0.5}$).

(*) In this case, it is not permitted to use eq. (1) for determination of γ_N, i.e. of the velocity of the N.S. with respect to the L.S.

In order to calculate the probability that the collision will be asymmetric, we shall approximate the spectrum ε by a function

$$\varrho(\varepsilon, \gamma_N) = \begin{cases} \dfrac{1}{\gamma_N}, & \varepsilon < \gamma_N, \\ 0, & \varepsilon > \gamma_N, \end{cases}$$

The probability that the collision will be asymmetrical is equal to the probability that ε_2 will be less than

$$\varepsilon_1 [1 - (\varepsilon_N \varepsilon_1)^{-\frac{1}{3}}]^4 .$$

This gives

$$\frac{\varepsilon_1}{\gamma_N} [1 - (E_N \varepsilon_1)^{-\frac{1}{3}}]^4 .$$

Therefore, the complete relative probability that the collision will be asymmetrical is:

$$(18) \qquad W = 2 \int_0^{\gamma_N} \frac{\varepsilon_1 \, d\varepsilon_1}{\gamma_N^2} [1 - (E_N \varepsilon_1)^{-\frac{1}{3}}]^4 =$$

$$= 2 \left\{ \frac{1}{2} - \frac{32}{15} \left(\frac{2}{E_l} \right)^{\frac{1}{3}} + \frac{24}{7} \left(\frac{2}{E_l} \right)^{\frac{2}{3}} - \frac{32}{13} \left(\frac{2}{E_l} \right)^{\frac{3}{3}} + \frac{2}{3} \left(\frac{2}{E_l} \right)^{\frac{4}{3}} \right\} .$$

The probability increases as E_l increases and when $E_l \to \infty$ the probability approaches 1. However, it approaches this value very slowly: even when the energy of the nucleon in the L.S. is $E_l \sim 2 \cdot 10^{12}$ eV; $W = 0.16$; if $E_l \sim 10^{14}$ eV; $W = 0.4$; and if $E_l \sim 10^{16}$ eV, $W = 0.6$.

c) Single-meson interaction. – When the collision parameter exceeds unity, $b > 1$, the probability for a nucleon to interact with a meson of another nucleon is

$$W'(b) = \int_0^{\gamma_N} d\varepsilon \, \varrho(\varepsilon, \gamma_N, b) \sigma_0 .$$

Here σ_0 is the cross-section for interaction of a nucleon and a meson. The probability for another nucleon to not interact with the meson is $W'' = 1 - W'$. Thus, the probability of a single meson interaction when the collision parameter is b, equals to $W_1' = W' \cdot W''$. The total probability of a single meson interaction is

$$W_1 = \int_{b_{cr}}^{\infty} W_1 \, 2\pi b \, db .$$

On the other hand, the probability of an exchange of two mesons is

$$W_2 = \int_{b_{cr}}^{\infty} (W')^2 \, 2\pi b \, \mathrm{d}b \, .$$

These quantities depend severely on the choice of σ_0, of the function $\varphi(r)$ and of the values of b_{cr} (b_{cr} is the smallest value of b for which the above calculations hold, $b_{cr} \sim \hbar/\mu c$). If $\varphi(r)$ is chosen (as above) in the form of the Yukawa potential, and we assume $\sigma_0 = 0.56_{geom}$, $b_{cr} = 1$ then the ratio of the two probabilities is $W_1/W_2 \sim 2$. However, this figure is extremely sensitive to the accepted values of $\varphi(r)$, b_{cr} and σ_0.

In the previous paragraph, the probability of an asymmetrical distribution was calculated under the condition that there was an exchange of two mesons. If only one meson was involved in the exchange, then the distribution in the N.S. is certainly asymmetrical. Thus, the ratio of numbers of asymmetrical cases and symmetrical ones (when the encounter is already known to be peripheral) is $(W_1 + W_2 W)/W_2 = (W_1/W_2) + W$.

If only one of the nucleons is excited and emits mesons, then the angular distribution of the produced particles will be symmetrical not in the N.S., but in the rest system of the excited state (C.S.). If the primary fast nucleon is excited, then such a case in the L.S. will imitate a « jet » of a very high energy, however containing few particles.

In order to determine experimentally the energy of the primary particle in the L.S., it is necessary to find

$$\tilde{\gamma} = \frac{1}{\operatorname{tg} \vartheta_{l\frac{1}{2}}} = \frac{1}{\sqrt{1 - \tilde{v}^2}} ,$$

where $\tilde{v}$ is the velocity of the excited nucleon in the L.S. Starting from the observed number of particles N_s, we find the energy of excitation E_{ex}. This may be done by using formula:

$$N_s \simeq 2 \left(\frac{E_{ex}}{2M} \right)^{\frac{1}{2}},$$

if the number N_s is large enough (thermodynamical theory), or according to the curves in [1] for $N_s < 10$.

The energy of the primary nucleon in the L.S. will be $E_l = E_{ex} \tilde{\gamma}$.

4. – Processes accompanying the interaction of a nucleon with a nucleus.

a) Excitation of the nucleus. – At large energy the primary nucleon does not interact with the whole nucleus, but only with the substance that is on its path (it cuts a tunnel). HEITLER and TERRAUX [9] calculated the excitation

energy of such a nucleus and found that the main contribution is due to the surface energy of the tunnel, which is approximately (150 ÷ 200) MeV. In such a case, it emits few (approximately 2, 3) slow heavy particles. This explains the fact that among the stars that are observed in the photoemulsion, we often find cases that are accompanied with a small number of « black » tracks, although produced as a result of central nucleon collision with a heavy nucleus.

However, there are often cases when the shower is accompanied by a large number of « black » tracks. The Heitler-Terraux theory does not explain these cases.

It is possible to point out another mechanism of high excitation of the nucleus. If a meson is present in the meson field which surrounds the nucleon and if it is beyond the limit $b > 1(\hbar/\mu c)$, then it will interact with the nucleus independently of its nucleon, since during the time of interaction they will not be able to connect themselves by a signal. The probability of finding such a meson beyond the limit $\hbar/\mu c = 1$ is equal to 0.8 (if $\varphi(r) = e^{-r}/r$).

We may consider two cases:

1) The meson has high energy. Then, similarly to the nucleon itself, it cuts a « tunnel » in the nucleus and forms an accompanying shower (this case will be discussed below).

2) The meson has low energy and is « caught » in the nucleus, highly exciting it. The energy of such a meson (in the nucleus rest system) should not exceed a certain critical energy ε_{cr} (in case of collision with a heavy nucleus $\varepsilon_{cr} \sim 5$ GeV). The probability of excitation of the nucleus will be approximately equal to

$$W_{ex} = \int_1^\infty 2\pi b \, db \int_0^{\varepsilon_{cr}} d\varepsilon \, \varrho(\varepsilon, \gamma, b) \,,$$

where $\gamma = (1 - v^2)^{-\frac{1}{2}}$, v is the nucleon velocity in the nucleon rest system.

If the nucleon energy is high, $E_i \leqslant 100$ MeV we have $W_{ex} \simeq 36/\gamma$, i.e. the probability of excitation of the nucleus decreases, when the energy increases. This conclusion practically does not depend on the choice of the function $\varphi(r)$, since it is a result of the fact, that the meson spectrum is flat (4).

It would be interesting to compare this result with the experimental data which unfortunately are not complete at the present moment.

b) *Accompanying collisions*, – If the meson energy is sufficiently high then an accompanying shower is produced besides the main one, which is a result of the collision of a meson having an energy ε, with the nucleus « tunnel ». The size of the second tunnel should be near to the size of the first one. The energy emitted in accompanying collisions, as well as the number of gene-

rated particles should be smaller than in the main shower, but the angular distribution in the L.S. is much wider. Therefore, in the C.S. of the impinging nucleon and the tunnel, the accompanying shower will be directed « backwards », i.e. the particles will be limited in the direction that is opposite to the motion of the initial nucleon (*). Thus, in this case, the angular distribution will be asymmetrical but in contrast with the previous cases, the surplus of particles in all showers will be directed in one and the same direction—backwards in the C.S.

Let us carry out some estimations:

1) The probability of accompanying collisions will be equal to $W_{acc} = W_0 - W_{ex}(\gamma)$, where W_0 is the probability that there are mesons beyond the distance $\hbar/\mu c = 1$, W_{ex} is the probability that this meson has energy lower than the critical one.

Both of these quantities depend on the choice of the function of the meson field. For example, for a function of the type of the Yukawa potential $W_{acc} = 0.8 - (36/\gamma)$, if $\varepsilon_{cr} \sim 5$ GeV.

2) The number of particles may be determined by the statistical theory formula:

$$N_s \simeq n^{\frac{1}{4}}(n+1)^{\frac{1}{4}}\varepsilon^{\frac{1}{4}},$$

where n is the number of nucleons in the tunnel. ε is the meson energy in the L.S. (nucleus rest system). Average energy is: $\bar{\varepsilon} = 0{,}5\gamma$.

Therefore, the average number of particles in the accompanying shower is $\sqrt[4]{M/0.5} \sim 2$ times smaller than in the primary one.

3) Supposing that the distribution of particles in the C.S. of the colliding meson and the secondary tunnel are symmetrical, we may estimate the half angle in the L.S. $\operatorname{tg}\vartheta_{l\frac{1}{2}} = \sqrt{2M_n/\varepsilon}$.

The mean value of ε is $\bar{\varepsilon} = 0.5\gamma$. Therefore, on the average the angle $\vartheta_{l\frac{1}{2}}$ (to be more exact, its tangent) in the accompanying shower will be $\sqrt{M/0.5} \sim 4$ times wider than in the primary one.

It should be emphasized that, since the spectrum ε is flat, it is very probable that collisions may occur with characteristics substantially different from the average ones.

Events as those considered above seem to have been observed by TAKIBAJEV

(*) Due to the asymmetry of angular distribution, the determination of the C.S. based on using the magnitude of the angles in this case is untrue. A preliminary symmetrization of the shower, i.e. the elimination of the accompanying collision shower, is necessary.

(USSR), who tried to perform a symmetrization of asymmetrical jets. However, the study has not yet been completed.

The above results in the essential part were obtained in close co-operation with Y. A. Romanov and Y. F. Strokov.

* * *

The author offers hearty thanks to Dr. E. L. Feinberg for many helpful discussions.

REFERENCES

[1] I. A. Ivanovskaja and D. S. Černavskij: *Nucl. Phys.*, **3** (1957).
[2] L. D. Landau: *Izv. Akad. Nauk SSSR. Ser. Fiz.*, **17**, 51 (1953).
[3] V. M. Maksimenko and I. L. Rozental': *Žu. Èksper. Teor. Fiz.*, **32**, 32 (1956).
[4] T. F. Hoang: *Journ. de Phys.*, **14**, 395 (1953); C. C. Dilworth, S. I. Goldsack, T. F. Hoang and L. Scarsi: *Nuovo Cimento*, **10**, 1261 (1953); **11**, 424 (1954); C. Castagnoli, G. Cortini, C. Franzinetti, A. Manfredini and D. Moreno: *Nuovo Cimento*, **10**, 1539 (1953); G. Bertolino and D. Pescetti: *Nuovo Cimento*, **12**, 630 (1954); **3**, 141 (1956).
[5] C. Peyrou, B. D'Espagnat and L. Leprince-Ringuet: *Compt. Rend. Acad. Sci.*, **228**, 1777 (1949).
[6] E. L. Feinberg and D. S. Černavskij: *Dokl. Akad. Nauk, SSSR*, **91**, 511 (1953).
[7] E. L. Feinberg and D. S. Černavskij: *Dokl. Akad. Nauk, SSSR*, **81**, 795 (1951).
[8] I. L. Rozental' and D. S. Černavskij: *Usp. Fiz. Nauk*, **52**, 185 (1955); *Fortschritte d. Phys.* (Berlin), **4**, 560 (1956).
[9] W. Heitler and Ch. Terraux: *Proc. Phys. Soc.*, A **66**, 929 (1953).

SUPPLEMENTO AL VOLUME VIII, SERIE X
DEL NUOVO CIMENTO

N. 2, 1958
2° Trimestre

Explosive Showers Produced by High-Energy Cosmic-Ray Particles.

I. I. Gurevič, A. P. Mišakova, B. A. Nikol'skij and L. V. Surkova

Academy of Sciences - Moscow

In the present work a pellicle stack technique was used to study showers produced by high energy cosmic-ray particles. Preliminary results obtained with 29 showers have been reported previously [1]. The purpose of the work reported here was to determine the energy dependence of shower characteristics in the $(10^{10} \div 10^{1})$ eV energy range.

The pellicle stack had a 4.5 cm thickness and a 10 cm diameter. It consisted of 100 NIKFI «type *R*» emulsion layers. The stack was exposed in the stratosphere during 7 h at a 27 km height in May 1956. The emulsion was processed by D. M. Samojlovič.

In the course of pellicle scanning explosive showers consisting of more than 5 relativistic tracks all laying inside a sufficiently narrow cone were selected and registered. The preliminary shower selection did not include any discrimination respective to the number of black and grey prongs. During scanning we also registered relativistic-particle jets consisting of more than 5 tracks. Later the jets were retraced through several pellicles and only 5 of them were found to represent explosive showers, the remaining 200 being electron-photon showers which are of no interest in the present work.

For each explosive shower found in the emulsion we determined the charge of the primary particle (single-, double-, or multiply charged particle) and measured the angular distribution of the shower particles relative to the shower axis.

To determine theshower energy we assume that the shower-particle angular distribution was symmetric in respect to $\theta = \pi/2$ in the centre of mass sys-

tem (C.S.) (*). Starting with this assumption the quantity

$$\gamma' = \frac{1}{\sqrt{1-\beta_c^2}}$$

(where β_c represents the velocity of the C.S.) can be determined by one of the three methods:

1) as $\gamma_c = \operatorname{ctg} \vartheta_{\frac{1}{2}}$; where $\vartheta_{\frac{1}{2}}$ is the angle containing a half of the shower particles;

2) from $\ln \gamma_c = -\ln \operatorname{tg} \vartheta_{\frac{1}{2}}$;

3) from the condition

$$\ln \frac{F(\lambda)}{1-F(\lambda)} = 0 ,$$

where $\lambda = \ln \operatorname{tg} \vartheta$ and F represents the number of shower particles with λ not exceeding a given value.

As can be seen from Table I the three methods of γ_c determination mentioned above give γ_c values differing on the average by $(20 \div 30)\%$.

BELEN'KIJ and LANDAU [2] have calculated the multiple-particle production using a hydrodynamical model and assuming the primary nucleon to interact with the nucleus as a whole, i.e. with a « tube » of it. They obtained the following expression for the angular distribution of particles in the C.S.:

$$(1) \qquad \begin{cases} \mathrm{d}N \sim \exp\left[\sqrt{L^2 - \Lambda^2}\right] \mathrm{d}\Lambda , \\ \Lambda = \ln \operatorname{tg} \dfrac{\theta}{2} , \qquad L = \ln \dfrac{1+l}{4\gamma_c} , \end{cases}$$

vhere l represents the « tube length », i.e. the number of nuclear nucleons along the ntersection of the primary particle trajectory with the volume of the target nucleus. Since the distribution (1) is symmetric in respect to $\theta = \pi/2$ it follows immediately that — in case the theory is correct — γ_c for nucleon-« nuclear tube » collisions can be determined in the same way as for single nucleon-nucleon collisions.

Table I summarizes the main results of the analysis of 43 showers produced by nucleons and 20 showers produced by α-particles and heavier nuclei.

(*) Here and in subsequent equations θ stands for the shower-particle emission angle in the C.S., while ϑ represents the corresponding angle in thelaboratory system. (L.S.).

TABLE I.

No.	Primary	n_s+n_g	n_s	$\vartheta_{\frac{1}{2}}$ (degrees)	γ			$\bar{\gamma}_c$	E_0 (eV)
					$(\vartheta_{\frac{1}{2}})$	(λ)	(F)		
				$E = (10^{10} \div 10^{11})$ eV					
1	p	14+ 6	23	11.5	4.9	4.8	6.0	5.2	$5.3\cdot10^{10}$
2	p	15+ 5	24	10	5.6	4.6	7.6	5.9	$6.9\cdot10^{10}$
3	p	4+ 2	8	11	5.1	4.7	—	4.9	$4.7\cdot10^{10}$
4	n	7+ 3	13	26	2.0	2.1	2.9	2.3	$1.0\cdot10^{10}$
5	p	13+ 3	14	16.5	3.4	2.8	3.6	3.3	$2.1\cdot10^{10}$
6	p	8+ 8	8	18	3.1	2.0	3.5	2.9	$1.6\cdot10^{10}$
7	p	9+ 3	12	11	5.1	3.6	5.1	4.6	$4.1\cdot10^{10}$
8	n	11+ 2	23	18	3.1	2.5	3.2	2.9	$1.6\cdot10^{10}$
9	p	10+ 7	25	16	3.5	—	—	—	$4.0\cdot10^{10}$
10	n	6+ 6	15	16.5	3.4	—	—	—	$2.2\cdot10^{10}$
11	n	6+ 9	22	14.5	3.9	—	—	—	$2.9\cdot10^{10}$
12	p or n	14+ 6	21	16.5	3.4	—	—	—	$2.2\cdot10^{10}$
13	p	5+ 3	22	11	3.3	—	—	—	$2.1\cdot10^{10}$
14	α	1+ 2	35	10.7	5.3	4.7	6.4	5.5	$6.0\cdot10^{10}$
15	α	12+ 3	42	10.6	5.3	5.9	8.3	6.5	$8.4\cdot10^{10}$
16	α	17+ 9	36	9.0	6.3	5.1	6.5	5.6	$6.2\cdot10^{10}$
17	α	9+ 4	17	8.0	7.1	5.0	7.9	6.6	$8.6\cdot10^{10}$
18	Z	8+26	87	12.2	4.6	—	—	—	$4.1\cdot10^{10}$
19	α	12+ 3	20	13.0	4.3	4.3	5.0	4.9	$4.4\cdot10^{10}$
20	α	16+ 8	45	23.5	2.2	1.9	2.3	2.1	$0.9\cdot10^{10}$
21	α	16+15	35	19.5	2.7	2.4	3.0	2.7	$1.4\cdot10^{10}$
22	Z	17+ 6	74	10.5	5.3	5.7	7.2	6.0	$7.0\cdot10^{10}$
23	α	16+ 8	26	23.0	2.3	2.3	2.5	2.4	$1.1\cdot10^{10}$
24	α	10+ 6	16	15.0	3.7	3.6	4.2	3.8	$2.8\cdot10^{10}$
25	α	15+10	28	9.5	5.9	5.7	6.8	6.1	$7.1\cdot10^{10}$
26	Z	12+ 8	41	15.0	3.7	3.2	3.8	3.6	$2.4\cdot10^{10}$
27	α	9+ 3	13	20.0	2.7	3.2	3.6	3.2	$1.9\cdot10^{10}$
28	α	13+ 5	29	17.0	3.3	3.4	4.0	3.6	$2.4\cdot10^{10}$
				$E_0 = (10^{11} \div 10^{12})$ eV					
1	p	5+ 2	23	3.3	17.1	16.6	13.6	15.8	$5.0\cdot10^{11}$
2	p	3+ 4	15	3.5	17.1	13.9	20.0	17.0	$5.9\cdot10^{11}$
3	p	5+ 3	14	4.7	12.3	10.4	14.1	12.5	$3.1\cdot10^{11}$
4	p	3+ 2	18	6.5	11.9	11.0	15.1	12.7	$3.2\cdot10^{11}$
5	p	5+ 3	15	5.5	10.4	7.0	12.6	10.0	$2.0\cdot10^{11}$
6	p	12+ 7	24	6.9	8.3	6.1	8.0	7.5	$1.1\cdot10^{11}$
7	p	9+ 7	14	5.1	11.2	11.2	15.1	12.5	$3.1\cdot10^{11}$
8	p	13+10	19	2.5	22.9	12.2	15.8	17.0	$5.7\cdot10^{11}$
9	p	1+ 2	29	6.5	8.8	7.1	8.7	8.2	$1.3\cdot10^{11}$
10	p	1+ 1	12	8.1	7.0	5.9	8.3	7.1	$1.0\cdot10^{11}$
11	p	13+ 2	30	7.5	7.5	7.6	7.2	7.4	$1.1\cdot10^{11}$
12	n	10+ 1	23	7.0	8.1	5.1	8.5	7.2	$1.0\cdot10^{11}$
13	p	3+ 0	8	6.5	8.8	6.9	9.1	7.9	$1.2\cdot10^{11}$
14	n	4+ 1	7	3.5	16.3	9.1	12.0	12.3	$3.0\cdot10^{11}$

TABLE I (*continued*).

No.	Primary	n_s+n_g	n_g	$\vartheta_{\frac{1}{2}}$ (degrees)	γ_c			$\bar{\gamma}_c$	E_0 (eV)
					$(\vartheta_{\frac{1}{2}})$	(λ)	(F)		
15	p	10+ 6	35	6.7	8.3	8.4	15.0	10.6	$2.2\cdot10^{11}$
16	n	7+ 5	32	5.4	10.6	9.9	15.0	11.8	$2.8\cdot10^{11}$
17	p	1+ 1	20	2.0	28.6	15.8	19.5	21.3	$9.1\cdot10^{11}$
18	n	1+ 0	10	3.2	17.5	12.6	20.0	16.7	$5.6\cdot10^{11}$
19	p	1+ 2	19	6.5	8.8	9.2	11.0	9.7	$1.9\cdot10^{11}$
20	p	10+ 1	29	5.4	10.5	10.5	13.2	11.4	$2.6\cdot10^{11}$
21	p	12+ 3	11	5.7	9.5	6.3	9.6	8.5	$1.4\cdot10^{11}$
22	Z	1+ 1	22	6.8	8.4	7.3	10.0	8.6	$1.5\cdot10^{11}$
23	α	3+ 1	27	4.0	14.3	11.1	12.6	12.5	$3.2\cdot10^{11}$
24	α	0+ 2	29	6.5	8.8	9.2	10.0	9.2	$1.7\cdot10^{11}$
25	Z	4+ 0	57	3.7	15.4	—	—	—	$4.7\cdot10^{11}$
		$E_0 = (10^{12} \div 10^{13})$ eV							
1	n	5+ 8	35	1.0	55	20	53	43	$3.7\cdot10^{12}$
2	p	2+ 3	27	2.1	27	32	32	30	$1.8\cdot10^{12}$
3	p	0+ 0	9	1.7	34	27	37	33	$2.1\cdot10^{12}$
4	p	5+ 3	27	2.4	24	17	25	22	$9.6\cdot10^{11}$
5	p	2+ 4	27	1.0	57	36	50	48	$4.6\cdot10^{12}$
6	p	6+ 4	20	2.6	22	20	25	22	$1.0\cdot10^{12}$
7	p	1+ 2	43	1.3	43	36	40	40	$3.2\cdot10^{12}$
8	α	7+ 3	33	2.3	24	21	30	25	$1.3\cdot10^{12}$
		$E_0 = (10^{13} \div 10^{14})$ eV							
1	p	11+13	16	0.70	82	50	120	84	$1.4\cdot10^{13}$
2	p	5+ 4	9	0.25	227	141	300	222	$9.9\cdot10^{13}$

The L.S. shower energy E_0 indicated in column 10 was calculated under the assumption of the single nucleon-nucleon collision mechanism.

In the case of the nucleon-« nuclear tube » collision mechanism:

$$\gamma = 2l\gamma_c^2 .$$

1. – Angular distribution of particles in the centre of mass system.

The exit angle of a shower particle in the C.S. and the corresponding angle in the L.S. are correlated in the extremely relativistic case according to the equation:

$$\operatorname{ctg}\vartheta = \gamma_c \operatorname{ctg}\frac{\theta}{2} . \tag{2}$$

For every shower the angular distribution of particles in the C.S. has been found using equation (2). In order to obtain statistically more signi-

ficant angular distributions total angular distributions of shower particles were computed, each total distribution representing a whole interval of shower energy values.

These distributions are shown in tables II, II *a* and in Fig. 1. The

TABLE II. – *C.S. angular distributions of particles in nucleon-produced showers. The table indicates relative numbers of particles per steradian.*

E_0 \ θ	0°-30°	30°-60°	60°-90°	90°-120°	120°-150°	150°-180°
10^{10} - 10^{11}	5.56±0.92	2.15±0.35	2.17±0.30	1.75±0.27	2.67±0.39	5.25±0.91
10^{11} - 10^{12}	3.28±0.56	2.72±0.31	2.30±0.24	1.78±0.21	2.01±0.26	7.22±0.83
10^{12} - 10^{14}	3.47±0.80	2.87±0.44	2.00±0.31	1.61±0.28	2.07±0.37	8.19±1.2

TABLE II *a*. – *Angular distributions of particles in showers produced by primaries having* $Z \geqslant 2$. *The table indicates relative numbers of particles per steradian.*

E_0 \ θ	0°-30°	30°-60°	60°-90°	90°-120°	120°-150°	150°-180°
10^{10} - 10^{11}	3.40±0.50	2.73±0.27	2.28±0.21	2.08±0.20	2.66±0.27	4.29±0.56
10^{11} - 10^{14}	4.13±0.97	2.94±0.50	1.85±0.34	2.09±0.36	2.19±0.43	5.75±1.2

errors indicated in the tables are statistical deviations calculated as $\sqrt{\mathcal{N}_i}$, $\mathcal{N}_i$ representing the number of particles in a given angular interval.

Tables II and II*a* show that $f(\theta)$ is in general substantially non-isotropic while for showers produced by $(10^{11} \div 10^{14})$ eV nucleons the distribution is in addition non-symmetric in respect to $\theta = \pi/2$. The angular distributions in C.S. presented in the tables were obtained using equation (2), γ_c being determined as $\gamma_c = \operatorname{ctg} \vartheta_{\frac{1}{2}}$. In order to determine γ_c by this equation we presupposed the numbers of particles in the angular intervals $0 - \pi/2$ and $\pi/2 - \pi$ to

Fig. 1. – Shower-particle angular distributions in the centre of mass system. The full line represents showers in the $(10^{10} \div 10^{11})$ eV energy range. The interrupted line corresponds to the $(10^{11} \div 10^{12})$ eV energy range, the dotted-interrupted line corresponds to the $(10^{12} \div 10^{14})$ eV energy range. All the distributions shown represent showers produced by single nucleons.

be equal. Therefore the lack of symmetry of the angular distribution for such a value of γ_c means that $f(\theta)$ cannot be made symmetric by any other choice of γ_c.

It is interesting to note that the above mentioned asymmetry does not appear for showers in the energy range of $(10^{10} \div 10^{11})$ eV and seems much weaker for showers produced by heavy particles. This conclusion, however, is not quite definitive because of scarcity of data in the $(10^{11} \div 10^{14})$ eV energy range.

The observed asymmetry might be supposed to result from secondary interactions of shower particles with nucleons inside the same nucleus. It turned out, however, that this asymmetry does not depend on the number $n_h - n_g$. This fact clearly indicates that secondary interactions are not responsible for the asymmetry of the angular distribution of the shower particles in respect to $\theta = \pi/2$.

The asymmetry observed could arise if each shower were produced as a result of several interactions of the primary particle with nucleons of the target nucleous. If such were the case the asymmetry would obviously increase for higher shower multiplicities. Experimental results, however, discard such a supposition.

We are thus led to assume that the asymmetry of $f(\theta)$ in respect to $\theta = \pi/2$ is not the result of subsidiary processes but rather arises from the very nature of shower production in nuclear interactions of nucleons.

This result contradicts the conclusions of the «hydrodynamical» theory of shower production in knock-on collisions according to which the angular distribution of the shower particles should be symmetric relative to $\theta = \pi/2$ in the C.S. (see equation (1)).

2. – Relation between the number of shower particles and shower energy.

Table III presents average multiplicities of showers for different energy intervals of primary nucleons.

TABLE III. – *Average numbers of shower particles in nucleon-produced showers.*

E_0 (eV)	$\vartheta_{\frac{1}{2}}$	$\bar{n}_s$	$\bar{n}_s(n_h + n_g < 3)$	$\bar{n}\ (n_h + n_g > 3)$	$\bar{n}\ (\vartheta_{\frac{1}{2}} < \bar{\vartheta}_{\frac{1}{2}})$	$\bar{n}\ (\vartheta_{\frac{1}{2}} > \bar{\vartheta}_{\frac{1}{2}})$
10^{10} - 10^{11}	15.3	17.7	—	17.7	19.0	16.6
10^{11} - 10^{12}	5.34	19.4	16.3	20.6	15.3	21.9
10^{12} - 10^{14}	1.45	23.8	26.0	23.1	26.2	20.8
10^{11} - 10^{14}	4.17	20.7	18.8	21.4	20.5	20.9

One can readily see from Table III that the number of shower particles n_s is a very weak function of the angle $\vartheta_{\frac{1}{2}}$. Accordingly, if the method of shower

energy determination from the angular distribution of shower particles described above does indeed give a reasonable evaluation of E_0, it can be concluded that the experimental dependence $n_s = f(E_0)$ is substantially different from that predicted by theory: $(\bar{n}_s)_{\text{theor}} \sim \sqrt[4]{E_0}$. In addition Table III illustrates the weak dependence of n_s on the angle $\vartheta_{\frac{1}{2}}$ and on the number of black and grey tracks associated with the shower. This fact suggests that secondary interactions of shower particles with nucleons inside the nucleus play no prominent role in the shower production mechanism. It must be noted, however, that a more careful analysis of this effect requires a more accurate determination of E_0 with due account of the « nuclear-tube » mechanism of shower production. The result of such an analysis will be reported by the authors in a detailed paper in the *Žu. Éksper. Teor. Fiz.*

In showers produced by particles with $Z > 2$ the number of shower particles substantially exceeds the value $\bar{n}_s$ obtained for nucleon-produced showers. This may be naturally explained by supposing each such shower to be produced in a simultaneous interaction of several nucleons.

REFERENCES

[1] V. V. Alpers, I. I. Gurevič, V. M. Kutukova, A. P. Mišakova, B. A. Nikol'skij and L. V. Surkova: *Dokl. Akad. Nauk SSSR*, **112**, 33 (1957).
[2] S. Z. Belen'ky and L. D. Landau: *Usp. Fiz. Nauk*, **6**, 309 (1955).

SUPPLEMENTO AL VOLUME VIII, SERIE X
DEL NUOVO CIMENTO

N. 2, 1958
2° Trimestre

Theoretical Interpretation of Multiple Production of Particles in High Energy Collisions.

G. WATAGHIN

Istituto di Fisica dell'Università - Torino

The purpose of the following remarks is to outline a theoretical approach to the interpretation of the multiple production of particles on the basis of a non local field theory proposed by the author [1]. It will be shown also that the main experimental data on multiple production can be understood if one introduces a convenient interaction-hamiltonian.

The theory must explain following experimental data on nuclear collisions concerning jets of energies in the laboratory system (L.S.) from 10^{10} eV to 10^{16} eV:

1) cross-sections, which are of the order of geometrical values;

2) anelasticity coefficient K, defined as the ratio of the total energy of created particles after the collision and the total energy of colliding particles (both measured in the C.S.); in most cases one finds $0.2 \lesssim K \leqslant 1$;

3) the spectrum of transverse momenta, which does not depend on the reference system; in most cases of high energy jets the average value of the transverse momentum is: $\lesssim 0.5$ GeV; the average longitudinal components in the C.S. apparently increase with the primary energy as $\sim E_{\mathrm{CM}}^{\frac{1}{4}}$; in the observed jets sometimes they have values ~ 10 GeV;

4) the angular distribution shows large fluctuations: it is nearly isotropic for low energy jets; in the cases of jets with $E_{\mathrm{L.S.}} > 10^{13}$ eV one finds marked anisotropy;

5) the variation of the multiplicity with energy is not well known; it depends on the anelasticity coefficient and apparently it increases slowly with the primary energy in the center of mass system (approximately as $E_{\mathrm{C.S.}}^{\frac{1}{4}}$).

In this report only some features of the theory will be briefly mentioned. The most important assumption, we introduce, concerns the existence of small domains of uncertainty in every interaction process depending on a unique universal length l.

In order to take into account this fundamental uncertainty we introduce new internal parameters η_ν by a method similar to the one proposed by M. MARKOV and H. YUKAWA, and then proceed to define the S-matrix substituting new co-ordinates $X_\nu = x_\nu + \eta_\nu$ instead of usual ones x_ν, where x_ν are the variables appearing in the free-field equations, whereas η_ν are parameters, conveniently defined, which express the uncertainty in our knowledge of the co-ordinates during the interaction. The term of n-th order of the S-matrix

$$S_n = \frac{(-i)^n}{n!} \int F\left(\eta_{\lambda\nu}, \frac{\partial}{\partial x^+_{\lambda\nu}}, \ldots\right) P[H(x_1) H'(x_2) \ldots H(x_n)] \, \mathrm{d}^4 x_1 \ldots \mathrm{d}^4 \eta_1 \ldots \mathrm{d}^4 \eta_n ,$$

contains a universal form-operator F defined in the previous paper [1]. The interaction-hamiltonian densities H' are here used only as operators determining the amplitudes of probability of transitions between certain states of fields which are eigen-states of the energy and momentum. The elimination of η_ν from the expression of the S-matrix gives us in the momentum space the cut-off factors satisfying the claim of macroscopic causality. These are of two types being functions respectively of two invariants I_s, I_t defined in the following manner. In the momentum space only some Fourier components of S_n are needed to represent a given collision process. Let $P_\nu = p'_\nu + p''_\nu$ be the total energy-momentum 4-vector of the incoming colliding particles and let u_ν be the velocity vector of the C.S., of these particles: $u_\mu = (1/m) P_\mu$, where $m^2 = P_\nu P^\nu > 0$. The two invariants are: $I_t = k_\nu U^\nu, = \sqrt{I_t^2 - k_\nu k^\nu}$. We call them respectively the « projection » on the time axis and on the space of the C.S., because in the C.S., one has $I_t = k_0$; $I_s = |k|$.

The first kind of a cut-off operator G_s is a function of $I_s(lk_\nu)$, where l is chosen to be the Compton-wave length of the nucleon. The second kind G_t is a function od $I_t(lk_\nu)$. G_s^2 is interpreted as giving the statistical weight of the state k_ν relative to the considered collision process. The cut-off factor G_t is applied only to the intermediate virtual states and gives an extension in time of the elementary domain of interaction and a life time $\sim l$ of a virtual state. Making a convenient choice (*) of $G(t)$ one obtains a rapid convergency of the perturbation series.

In order to derive a field-theory of multiple production, we assume that a non-linear interaction hamiltonian, e.g. of the type considered by GLAUBER:

$$\bar{\psi} \psi f (g \gamma_5 \varphi) , \tag{1}$$

(*) This choice is discussed in detail in a forthcoming note in *Nuovo Cimento*.

where, for example, $f(\alpha) = e^{\alpha} - 1$, or of the type:

$$\chi(\bar{\psi}, \psi) f(g \Gamma_r v_\nu \partial_\nu \varphi^r) , \tag{2}$$

where χ is another non-linear function of ψ and ψ, and Γ_r are matrices in generalised isospin space, describes the interaction of barions (ψ) and π- and K-mesons (φ_r) in high energy collisions.

In order to obtain the observed angular distribution of particles in high energy jets we make use in (2) of a new invariant operator defined as a scalar product of the 4-vector $i\partial_\nu$ and of the following vector:

$$v_\nu = \frac{p'_\nu - p''_\nu}{|p'_\nu - p''_\nu|} \tag{3}$$

where p'_ν and p''_ν are the momenta of the incident particles. This v_ν can be put into the interaction hamiltonian by the mathematical formalism previously suggested [1].

The main purpose of the foregoing remarks is to state, that even without knowing the exact form of non-linear interaction hamiltonians and of the correct cut-off operators, one can see that an S-matrix formalism of the above type will give rise to several terms containing matrix elements of the type: $\langle p', p' | O | p'_f p''_f k_1 \dots k_n \rangle$ representing a given set of incoming and outgoing particles. The competition between various possibilities is based on the combined probabilities of transitions and on the densities and statistical weights of final states. In the transition probabilities, factors containing $K_\nu U^\nu$ can explain the angular distributions, whereas $G_s(lk_\nu)$ enter in the determination of the expected momentum spectra of final states [2].

It seems to us that one has in the above sketched formalism the necessary tools for a field theoretical interpretation of the multiple production.

REFERENCES

[1] G. Wataghin: *Nuovo Cimento*, **5**, 689 (1957).
[2] G. Wataghin: *Acad. Brasil. de Ciencias Symposium on Cosmic Rays*, (Rio de Janeiro, 1941), p. 129.

SUPPLEMENTO AL VOLUME VIII, SERIE X
DEL NUOVO CIMENTO

N. 2, 1958
2° Trimestre

Cosmic Ray Neutron Studies (*).

S. A. KORFF

New York University - University Heights - N. Y.

1. – Neutron measurements in Alaska.

1·1. *Introduction.* – In connection with our IGY program we installed a neutron monitor in Alaska. The monitor is of the standard Simpson type, using 12 counters in a paraffin and lead pile. Two identical but independent scaling circuits record the counts, and the sum is also recorded by an Esterline-Angus pen recorder. The monitor is located at Ballaine's Lake, which is about 1 mile NW of College or 6 miles NW from Fairbanks, Alaska. The geographic latitude is 65° north, the longitude 148° west. The geomagnetic latitude is about 66° north. The altitude is about 300 feet above sea level. The counts and barometer are photographed at intervals of 15 min and the barometer coefficient is calculated and applied in the usual manner.

1·2. *The observations.* – The instrument started producing data and a number of interesting fluctuations were noted. These occurred on the dates listed in Table I, and in the amounts and magnitudes shown on that table. This list must not be considered complete, for trouble has been had with the device photographing the counter registers, resulting in occasional interruptions of the record, and occasional cases in which the Esterline-Angus recorder showed a fluctuation but in which it was not possible to verify it by observing the two sets of counters. To improve the reliability of the device, automatic printers are being installed but the printers were not in operation in time for their data to be included in this paper.

Only the largest fluctuations are presented. These are so large that they

(*) Assisted by the USNC-IGY Program, by the joint program of the ONR-AEC and in part by the Air Force Research and Development Command.

far outweigh the pressure variations, and hence it does not matter whether the pressure coefficient is applied or not.

1·3. *Remarks about the fluctuations.* – One interesting one is a decrease of the order of 15 or 20%, in the interval of January 21 to 27. This is apparently a world-wide effect for it has been reported by several other observers. It also correlates with magnetic and ionospheric disturbances.

A curious double spike occurred at 0922 and 1003 U. T. on February 13, and again at the same times on the following night, although the ones the second night were about half the amplitude of the first. On these we do not have both E-A recorder totals and independent counts from each set of counters. Each spike appeared to have a very abrupt start and then an exponential decline to normal.

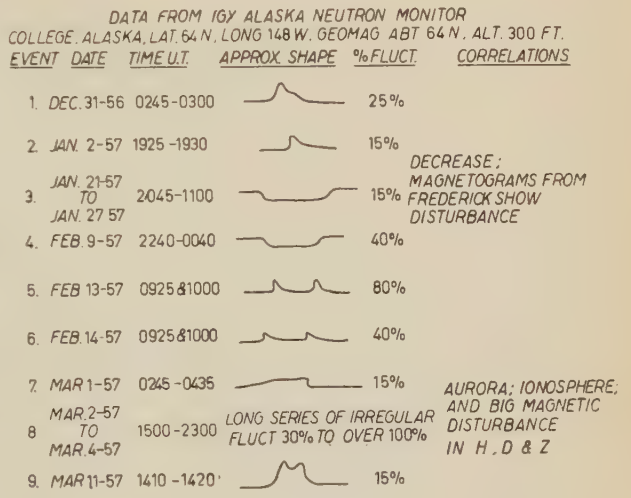
DATA FROM IGY ALASKA NEUTRON MONITOR
COLLEGE, ALASKA, LAT. 64 N, LONG 148 W, GEOMAG ABT 64 N, ALT. 300 FT.
EVENT DATE TIME U.T. APPROX. SHAPE % FLUCT. CORRELATIONS
1. DEC. 31-56 0245-0300 25%
2. JAN. 2-57 1925-1930 15%
3. JAN. 21-57 TO JAN. 27 57 2045-1100 15% DECREASE; MAGNETOGRAMS FROM FREDERICK SHOW DISTURBANCE
4. FEB. 9-57 2240-0040 40%
5. FEB 13-57 0925 & 1000 80%
6. FEB. 14-57 0925 & 1000 40%
7. MAR 1-57 0245-0435 15%
8. MAR. 2-57 TO MAR. 4-57 1500-2300 LONG SERIES OF IRREGULAR FLUCT 30% TO OVER 100% AURORA; IONOSPHERE; AND BIG MAGNETIC DISTURBANCE IN H, D & Z
9. MAR 11-57 1410-1420 15%

Fig. 1

An increase of the order of 25% in the radiation was observed starting on December 30, 1956 at 1650 local time (0250 on December 31, U.T.) which returned to normal, exponentially, in about 20 minutes.

A series of large irregularities started on March 2 to 4, 1957, in which irregular increases of the order of 50% to 100% occurred over a period of several days, gradually becoming normal. The usual exponential return was not observed. This correlates with strong geomagnetic and ionospheric disturbances, and auroral displays.

Several other less spectacular fluctuations were noted. Fig. 1 shows the several variations.

2. – The neutron balance in the atmosphere.

2·1. *Introduction.* – A number of persons have discussed the problem of the number of neutrons being produced and disappearing in the atmosphere. As knowledge of the subject has increased, it has become apparent that the

subject is quite complicated, and that neutrons both are produced and disappear by a number of mechanisms in competitive equilibrium. We shall briefly review some of these here. As will be seen the accuracy of the data varies quite widely, and some of the processes are known with precision while others are not.

2·2. *The mechanisms.* – Neutrons are produced by several processes. First, primary cosmic rays produce high energy disintegrations. Some neutrons result directly from this, and are slowed down by collisions and survive to become slow neutrons. Then, through the well-known nucleonic cascade, fast neutrons and other particles formed in the fast disintegrations may produce evaporation stars, nuclear disintegrations involving much less energy per event. These stars in turn result in the production of evaporation neutrons formed in such stars. Other products formed in such stars which complicate the analysis are tritium and helium three. Second, in any cascade process there are numerous photons, which may form photoneutrons. This process obviously is in competitive equilibrium with the cascade process, and has a substantially smaller cross-section. Nonetheless, some neutrons are added by this process. Finally we must consider primary neutrons arriving from the sun.

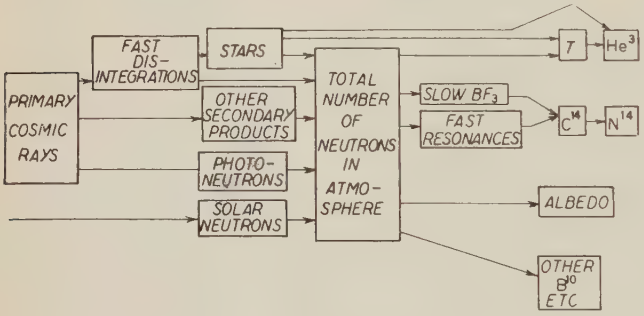

Fig. 2.

Processes by which the neutrons disappear are, first the formation of tritium and radiocarbon upon interaction with nitrogen, second the escape or loss of neutrons to the earth by albedo, and then a few neutrons enter into other reactions, such as the formation of less abundant isotopes in the earth's crust and atmosphere. We shall estimate these several effects. Fig. 2 shows the relationship of the several processes.

2·3. *Available data on each process.* – The primary intensity we shall take as about 610 peters [1] (particles $m^{-2}\,sr^{-1}\,s^{-1}$). Multiplied by 2π, this corresponds to flux of 0.3 particles per cm^2 and per s from all directions in the upward hemisphere. This is the flux which gives rise to the neutrons. Each of these particles will produce, on the average about one per cm^2 fast disintegration, and each of these about 3 stars, the star production rate according to PUPPI [2] being around 3 per cm^2 and per s. Stars in nitrogen consist, ac-

cording to ORTEL [3] of on the average 1.5 neutrons, the rest being other fragments with which we are not concerned. Hence this source gives rise to a rate of production of 4.5 neutrons per cm^2 column per s in the atmosphere.

The actual rates at the top of the atmosphere presumably exceed these rates somewhat. We must include fast neutrons slowed down and neutrons produced by other processes. The most difficult problem is estimating the number of stars in which only a neutron emerges. The above figure is then a lower limit.

FIREMAN [4], basing on experimental measurements of the rates of production of neutrons and tritons by beams in large machines, argues that the total production of neutrons by all processes is around 4.3 per cm^2, and that of this, about 1.1 escapes by albedo, 2.2 goes into radiocarbon and 1 is left over for tritium and all other processes. The figure for the albedo is obtained by noting that the curve of neutrons as a function of altitude has a maximum, but the stars are produced all the way to the top. He takes the difference between the star curve and the neutron curve as albedo. Actually as SIMPSON has pointed out, the neutron curve is for slow neutrons, and if one measures neutrons with higher energies, then the maximum is higher in the atmosphere.

The rate of production of photoneutrons in the cascade process, $q(\gamma, n)$ will be related to the rate of production of electrons in the ratio of the photoneutron cross-section to that of the cascade electron production. This latter we may estimate, recalling that on the average a radiation length in nitrogen is 312 meters according to ROSSI [5]. A path of 312 meters corresponds to a cross-section of 1.2 barns. If the photoneutron cross-section is of the order of 12 mb, then the production of photoneutrons in cascade events will be by about one percent of the photons. Since the large cascade events which contain many photons are not numerous, and since they decrease in number faster than they increase in energy, we can only ascribe some 0.1 neutrons to this mechanism.

As to primary neutrons from the sun, it has not yet been proved that these exist at all. While it would indeed be strange if the sun did not emit some neutrons, for there must be some charge exchange scattering high in the solar atmosphere, the evidence today seems to indicate that such emission is only significant at the times of large flares or other disturbances. The point is being studied further. Provisionally however, we omit solar neutrons from the total.

As a result of albedo, the earth will seem to be a source of neutrons if viewed from outside. Therefore measurements of neutrons in rockets and satellites will be of importance. It is also suggested that extra-atmospheric vehicles may give a good measure of neutron lifetimes. Certainly the amount and energy distribution of albedo neutrons should be measured.

Turning next to the processes whereby neutrons disappear, we have the estimates from the radiocarbon measurements of LIBBY [6], KULP and others,

of between 2.2 and 1.8 neutrons per cm^2 column per s. This is the total production needed to account for the observed radiocarbon. The data from the BF_3 counters in the atmosphere give, according to SOBERMAN [7] (after correcting an obvious numerical error in this paper) about 1.4 neutrons which have slowed down enough for the counters to measure them. By subtraction we get 0.4 neutrons as being captured while fast by the resonances. Unfortunately radiocarbon decays with a 5720 year period [9] into ordinary already abundant nitrogen, so that the rate of accumulation of this substance is not a useful measuring tool.

Tritium production has been measured in both wine and water by von GROSSE, LIBBY, KAUFMAN and others [8]. The values obtained are around 0.12 per column. FIREMAN [4] suggests a larger value, namely 0.1 to 0.2 from neutrons and 0.3 to 0.7 from stars.

The amount of helium three will exceed the amount of tritium decaying since helium three can be produced directly in stars. The amount of ^3He has been calculated and measured by various persons but is not a subject for this paper.

All other processes whereby neutrons disappear are small compared to the above. The rates of production of such rare isotopes as ^{10}Be or ^7Be have been estimated by PETERS [10] and by BENIOFF [11], to cite a few. The orders of magnitude are 0.1 per column. That there are many such processes, not all of which have yet been discussed in the literature seems certain. That the total contribution of these is small seems also estabished.

REFERENCES

[1] W. R. WEBBER: *Nuovo Cimento*, **4**, 1285 (1956).

[2] G. PUPPI: in *Progress in Cosmic Ray Physics*, Vol. **3** (Amsterdam, 1956).

[3] W. G. C. ORTEL: *Phys. Rev.*, **93**, 561 (1954).

[4] E. L. FIREMAN: *Phys. Rev.*, **91**, 922 (1953); E. L. FIREMAN and D. SCHWARZER: *Phys. Rev.*, **94**, 385 (1954).

[5] B. ROSSI: *High Energy Particles* (New York, 1952).

[6] W. F. LIBBY: *Radiocarbon Dating* (Chicago, 1955); J. R. ARNOLD and W. F. LIBBY: *Science*, **110**, 678 (1949).

[7] R. SOBERMAN: *Phys. Rev.*, **102**, 1399 (1956).

[8] A. V. GROSSE, A. D. KIRSHENBAUM, J. L. KULP and W. S. BROECKER: *Phys. Rev.*, **93**, 250 (1954); S. KAUFMAN and W. F. LIBBY: *Phys. Rev.*, **93**, 1337 (1954); V. FALTINGS and P. HARTRICK: *Zeits. f. Naturfor.*, **5**, 438 (1950); A. V. GROSSE, W. M. JOHNSTON, R. L. WOLFGANG and W. F. LIBBY: *Science*, **113**, 1 (1951).

[9] A. G. ENGELKEMEIR, W. H. HAMILL, M. G. INGHRAM and W. F. LIBBY: *Phys. Rev.*, **75**, 1825 (1949).

[10] B. PETERS: mimeographed notes (1956).

[11] P. A. BENIOFF: *Phys. Rev.*, **104**, 1122 (1956).

SUPPLEMENTO AL VOLUME VIII, SERIE X
DEL NUOVO CIMENTO

N. 2, 1958
2° Trimestre

Prehistoric Cosmic Ray Intensity.

P. S. Goel, D. P. Kharkar, D. Lal, N. Narsappaya,
B. Peters and V. Yatirajam

Tata Institute for Fundamental Research - Bombay

A method for determining prehistoric cosmic ray intensity is to study the isotopic changes produced by cosmic rays. The isotopic changes produced can be studied at two places: on the earth and in the meteorites. On the earth, the isotopic changes are brought about in the atmosphere and in the surface crust.

So far the only determination of past cosmic ray intensity was based on studies of the cosmic ray produced radio-isotope ^{14}C. Its studies have shown that up to $(10 \div 15) \cdot 10^3$ years, the cosmic ray intensity was the same within $\pm 10\%$. The measurements of Kulp and Volchok [1] on ^{14}C concentration in sections of ocean sediments, whose age was determined by the ionium method, showed that the cosmic ray intensity remained substantially constant in the last 30000 years. These results, however, depend on the validity of the ionium age determination method, and have recently been criticized.

Two years ago, it was pointed out by one of us [2] that the 2.7 million year half-life radio-isotope, ^{10}Be, which is produced mainly in interactions of cosmic rays with atmospheric nitrogen and oxygen nuclei, may finally accumulate in deep sea sediments and should be detectable in regions of small sedimentation rates. If such sediments can be found which have remained undisturbed in the past, both physically and chemically, its studies should yield the cosmic ray intensity up to 10 million years in the past.

^{10}Be has now been detected in the deep sea Pacific sediments by Arnold [3] and in our laboratory [4]. We have analyzed its concentrations in the upper and lower ends of a 14 metre long sediment core. The results of Arnold are confined to upper sediment layers and are consistent with ours. The experimental procedure and the results of our experiments are described here briefly; for details see reference [4] and [5].

The beryllium activity was extracted chemically from the sediment by a procedure which is specific for beryllium. The chemical efficiencies were determined by pilot tests using artificial ^{7}Be in about the same concentrations as that expected for ^{10}Be in the core. The samples were counted on a stable low-level β-counting unit, which employed a small end window counter of diameter 6 mm. The background was ≈ 8 counts per hour. The samples counted had a net counting rate of $(3 \div 5)$ c.p.h. above the background. That the activity extracted is due to ^{10}Be, was ascertained by two independent checks.

a) The samples obtained after the first series of chemical purification were combined and subjected to two additional chemical purifications by a procedure which is highly specific for beryllium. The specific activity of the sample remained unchanged after the additional chemical purification cycles.

b) The emitted radiation was identified by absorption measurements. It corresponds to a β-radiation of maximum energy (0.68 ± 0.20) MeV which is consistent with the value of 0.55 reported for ^{10}Be β-radiation in the literature.

These checks proved that the measured activity is due to ^{10}Be.

The concentration of ^{10}Be nuclei was measured at a depth of 31.2 g cm^{-2} and found to be $(1.56 \pm 0.43) \cdot 10^{10}$ nuclei per g of dry sediment. The ratio of the activities between depths 8.5 and 350 g cm^{-2} depths was also determined and found to be 1.75 ± 0.75.

Apart from the fact that the activity seems to be smaller in the lower portion of the core compared to that in the upper portion, we have no other indications that the core represents an undisturbed sedimentation. However, if we assume that the core has remained undisturbed both physically and chemically, i.e. the ^{10}Be nuclei have remained attached to their appropriate layers since deposition and if we further assume that the deposition of ^{10}Be in the analysed core corresponds reasonably well to the average global deposition of ^{10}Be over the earth's surface, we can derive some information from these measurements.

In an undisturbed core, the concentrations of ^{10}Be nuclei at a particular depth are only a function of the sedimentation rate, and the cosmic ray intensity. At first, we try the hypothesis that the sedimentation rate and the cosmic ray intensity have remained constant up to a time period corresponding to the lower end of the core. We then find for the rate of ^{10}Be deposition, a value of $2.55 \cdot 10^{6}$ nuclei cm^{-2} year^{-1}, and for the sedimentation rate, a value of 0.155 mg/1000 years (5.5 mm/1000 years). The lower limits still consistent with our measurements are for the deposition rate of ^{10}Be, $1.1 \cdot 10^{6}$ nucleic m^{-2} year^{-1} and for the sedimentation rate, 3.4 mm/1000 years; the errors are as yet too large to permit an upper estimate.

The present day global deposition rate of ^{10}Be has been calculated from the available cosmic ray and accelerator data [2, 6], and also has been estimated from the observed deposition rate of another cosmic ray produced isotope, ^{7}Be [5]. The two estimates agree closely and we find a present day deposition rate of $2.3 \cdot 10^6$ ^{10}Be nuclei cm $^{-2}$ year $^{-1}$. This value agrees well with that obtained from the core analysis on the assumption of a constant cosmic ray intensity and sedimentation rate. The results are therefore consistent with a constant cosmic ray intensity up to ~ 2 million years.

We then try the hypothesis that the rate of sedimentation has remained constant, but the cosmic ray intensity has been varying; its variation being represented by a function varying linearly with time. Assumption of a linear variation should be adequate since the transit time of the average cosmic ray particles before reaching the earth's surface must be at least 120 000 years as shown by Morrison, Olbert and Rossi [7], in order to account for the observed spatial isotropy of the incident radiation. Therefore, even sudden changes in the cosmic ray production must manifest themselves only as gradual intensity changes on the earth.

It can be easly shown that the integrated concentration of ^{10}Be in an infinitely long undisturbed core is only a function of the past cosmic ray intensity, and does not depend on the sedimentation rate [5]. The underlying basic assumption of an undisturbed core and an average rate of deposition of ^{10}Be on the ocean bed, can therefore be checked by measuring the integrated ^{10}Be concentration per unit area in different regions of the ocean.

If these assumptions are proved by experiments and if the assumption of a linear variation of cosmic ray intensity in the past is justified, one can determine both the intensity of cosmic radiation and sedimentation rate in the past.

Since our measurements are not exhaustive at present, we have assumed a constant rate of sedimentation and a linear variation of the cosmic ray intensity in the past. Using the present day deposition rate of $2.3 \cdot 10^6$ atoms cm^{-2} year $^{-1}$, we then find for the sedimentation rate 5.1 mm/1000 years and that 2.45 million years ago, the cosmic ray intensity was 5% higher than it is to-day. Within the errors of measurements, it could have been either 10% lower than to-day 3.2 million years ago, or 55% higher 1.7 million years ago. The upper limit on the cosmic ray intensity arises due to the fact that within the errors of measurements, the activity in the lower end of the core could be the same as that in the upper section.

These results should be considered tentative at present since they are based on few measurements which have small stastistical accuracy and are subject to the correctness of underlying assumptions which must await confirmation by future experiments.

It must be pointed out here that the cosmic ray intensity as determined by the ^{10}Be method is that incident on the earth's surface and therefore includes

the effects due to any variations in the earth's magnetic field and the transparency of the interplanetary space during prehistoric periods.

* * *

The authors wish to express their gratitude to Professor H. PETTERSON, retired director of the Swedish Oceanographic Institute at Goteborg and its present director Dr. B. KULLENBERG for supplying the ocean core samples. They are also indebted to Drs. J. SHANKAR and U. T. ATHAVALE of the Department of Atomic Energy for advice in chemical problems, and to Mr. M. S. VARDE for co-operation in the fluorometric measurements.

REFERENCES

[1] J. L. KULP and H. L. VOLCHOK: *Phys. Rev.*, **90**, 713 (1953).
[2] B. PETERS: *Proc. Ind. Acad. Sci.*, **41**, 67 (1955).
[3] J. R. ARNOLD: *Science*, **124**, 584 (1956).
[4] P. S. GOEL, D. P. KHARKAR, D. LAL, N. NARSAPPAYA, B. PETERS and V. YATIRAJAM: *Deep Sea Research*, **4**, 202 (1957).
[5] B. PETERS: *Zeits. f. Phys.*, **148**, 93 (1957).
[6] D. LAL, P. K. MALHOTRA and B. PETERS: to be published.
[7] P. MORRISON, S. OLBERT and B. ROSSI: *Phys. Rev.*, **94**, 440 (1954).

INDICE DEL SUPPLEMENTO

AL VOLUME VIII, SERIE X, DEL
NUOVO CIMENTO
Anno 1958

R. G. Glasser and G. A. Snow – Tables of the kinematics of the processes, $K^- + p \to \Sigma^\pm + \pi^\mp$ and $K^\mp + p \to K^\mp + p$ . . . . . pag. 1

Convegno Internazionale sui Raggi Cosmici - Varenna, sul Lago di Como, Villa Monastero, 21-26 Giugno 1957 . . . . . » 125

Fine del *Supplemento* al Vol. VIII, Serie X
del *Nuovo Cimento*, 1958

PROPRIETÀ LETTERARIA RISERVATA

Direttore responsabile: G. POLVANI

Tipografia Compositori - Bologna

Questo fascicolo del *Supplemento* è stato licenziato dai torchi il 23-X-1958

19/50
2